The North Atlantic Igneous Province: Stratigraphy, Tectonic, Volcanic and Magmatic Processes

edited by D. W. Jolley and B. R. Bell

Geological Society
Special Publication
No. 197

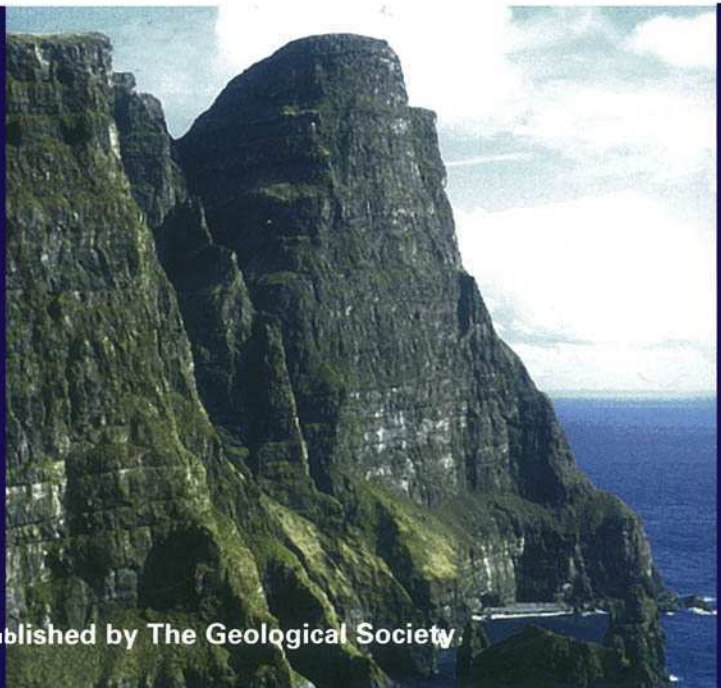

Published by The Geological Society

The North Atlantic Igneous Province: Stratigraphy, Tectonic, Volcanic and Magmatic Processes

Society Publication reviewing procedures

The Society makes every effort to ensure that the scientific and production quality of its books matches that of its journals. Since 1997, all book proposals have been refereed by specialist reviewers as well as by the Society's Books Editorial Committee. If the referees identify weaknesses in the proposal, these must be addressed before the proposal is accepted.

Once the book is accepted, the Society has a team of Book Editors (listed above) who ensure that the volume editors follow strict guidelines on refereeing and quality control. We insist that individual papers can only be accepted after satisfactory review by two independent referees. The questions on the review forms are similar to those for *Journal of the Geological Society*. The referees' forms and comments must be available to the Society's Book Editors on request.

Although many of the books result from meetings, the editors are expected to commission papers that were not presented at the meeting to ensure that the book provides a balanced coverage of the subject. Being accepted for presentation at the meeting does not guarantee inclusion in the book.

Geological Society Publications are included in the ISI Index of Scientific Book Contents, but they do not have an impact factor, the latter being applicable only to journals.

More information about submitting a proposal and producing Society Publications can be found on the Society's web site: www.geolsoc.org.uk.

GEOLOGICAL SOCIETY SPECIAL PUBLICATION NO. 197

The North Atlantic Igneous Province: Stratigraphy, Tectonic, Volcanic and Magmatic Processes

EDITED BY

D. W. JOLLEY
University of Sheffield, UK

B. R. BELL
University of Glasgow, UK

2002

Published by

The Geological Society

London

THE GEOLOGICAL SOCIETY

The Geological Society of London (GSL) was founded in 1807. It is the oldest national geological society in the world and the largest in Europe. It was incorporated under Royal Charter in 1825 and is Registered Charity 210161.

The Society is the UK national learned and professional society for geology with a worldwide Fellowship (FGS) of 9000. The Society has the power to confer Chartered status on suitably qualified Fellows, and about 2000 of the Fellowship carry the title (CGeol). Chartered Geologists may also obtain the equivalent European title, European Geologist (EurGeol). One fifth of the Society's fellowship resides outside the UK. To find out more about the Society, log on to *www.geolsoc.org.uk*.

The Geological Society Publishing House (Bath, UK) produces the Society's international journals and books, and acts as European distributor for selected publications of the American Association of Petroleum Geologists (AAPG), the American Geological Institute (AGI), the Indonesian Petroleum Association (IPA), the Geological Society of America (GSA), the Society for Sedimentary Geology (SEPM) and the Geologists' Association (GA). Joint marketing agreements ensure that GSL Fellows may purchase these societies' publications at a discount. The Society's online bookshop (accessible from *www.geolsoc.org.uk*) offers secure book purchasing with your credit or debit card.

To find out about joining the Society and benefiting from substantial discounts on publications of GSL and other societies world-wide, consult *www.geolsoc.org.uk*, or contact the Fellowship Department at: The Geological Society, Burlington House, Piccadilly, London W1J 0BG: Tel. +44 (0)20 7434 9944; Fax +44 (0)20 7439 8975; Email: *enquiries@geolsoc.org.uk*.

Published by The Geological Society from:
The Geological Society Publishing House
Unit 7, Brassmill Enterprise Centre
Brassmill Lane
Bath BA1 3JN, UK

(*Orders*: Tel. +44 (0)1225 445046
Fax +44 (0)1225 442836)
Online bookshop: *http://bookshop.geolsoc.org.uk*

British Library Cataloguing in Publication Data
A catalogue record for this book is available from the British Library.

ISBN 1-86239-108-4
ISSN 0305-8719

Typeset by Aarontype Ltd, Bristol, UK

Printed by Alden Press, Oxford, UK

Distributors

USA
AAPG Bookstore
PO Box 979
Tulsa
OK 74101-0979
USA
Orders: Tel. +1 918 584-2555
Fax +1 918 560-2652
E-mail: *bookstore@aapg.org*

India
Affiliated East-West Press PVT Ltd
G-1/16 Ansari Road, Daryaganj,
New Delhi 110 002
India
Orders: Tel. +91 11 327-9113
Fax +91 11 326-0538
E-mail: *affiliat@nda.vsnl.net.in*

Japan
Kanda Book Trading Co.
Cityhouse Tama 204
Tsurumaki 1-3-10
Tama-shi
Tokyo 206-0034
Japan
Orders: Tel. +81 (0)423 57-7650
Fax +81 (0)423 57-7651

Contents

It is recommended that reference to all or part of this book should be made in one of the following ways:

JOLLEY, D. W. & BELL, B. R. 2002. *The North Atlantic Igneous Province: Stratigraphy, Tectonic, Volcanic and Magmatic Processes*. Geological Society, London, Special Publications, **197**.

NØHR-HANSEN, H., SHELDON, E. & DAM, G. 2002. A new biostratigraphic scheme for the Paleocene onshore West Greenland and its implications for the timing of the pre-volcanic evolution. *In*: JOLLEY, D. W. & BELL, B. R. (eds) *The North Atlantic Igneous Province: Stratigraphy, Tectonic, Volcanic and Magmatic Processes*. Geological Society, London, Special Publications, **197**, 111–156.

The evolution of the North Atlantic Igneous Province and the opening of the NE Atlantic rift

DAVID W. JOLLEY[1] & BRIAN R. BELL[2]

[1] *Department of Animal and Plant Sciences, University of Sheffield, Alfred Denny Building, Western Bank, Sheffield S10 2TN, UK (e-mail: d.jolley@sheffield.ac.uk)*

[2] *Division of Earth Sciences, University of Glasgow, Lilybank Gardens, Glasgow G12 8QQ, UK (e-mail: bbell@earthsci.gla.ac.uk)*

The papers in this volume represent a step forward in our knowledge of the geological evolution of the North Atlantic from the Cretaceous–Palaeogene boundary through to the early Eocene. With the increase in hydrocarbon exploration activities in the Faroe–Shetland Basin (Fig. 1), new interpretations of the regional geology have become increasingly important, and the accuracy of the time frame for this work is vital to our understanding of the sequence of volcanic and sedimentary events.

The synthesis of data relating to Palaeogene volcanism and sedimentation along the Norwegian Margin by **Eldholm *et al.*** emphasizes the importance of transfer zones, possibly inherited from the Proterozoic basement, in the distribution of sediments and volcanic products during rifting (Fig. 2). Furthermore, subsequent uplift and the development of marginal highs are invoked as factors which affected water circulation within the basins, leading to a deterioration in the Eocene climate. This work identifies the relevance of the North Atlantic Igneous Province (NAIP) as an influence on environmental systems on a global scale.

Ar–Ar and Pb–U isotopic age data show that the main period of continental flood basalt volcanism in the NAIP extended from *c.* 60.5 Ma through to *c.* 54.5 Ma (Table 1). Biostratigraphical analysis of these volcanic–sedimentary sections (Jolley *et al.* 2002) shows that the onset of this interval equates to the Late Paleocene Thermal Maximum (LPTM). New isotopic dating of the oldest part of the volcanic sequence on the Faroe Islands, the Lower Formation, by **Waagstein *et al.*** has further confirmed the age for the interval around the LPTM (Fig. 3). However, problems remain with regard to the identification of normal polarity events within these lavas, recognized as Chrons 25n and 26n. Stratigraphy within the Faroe–Shetland Basin has benefited from the identification of genetic depositional sequences by Ebdon *et al.* (1995), based on the BP interpretation of geophysical and biostratigraphical information (Fig. 3). This approach subdivides the sediments of the basin into a number of depositional sequences (T10–T60). Palynofloras (**Ellis *et al.***; Jolley *et al.* 2002) attributable to the upper part of Sequence T40 (Ebdon *et al.* 1995) are recovered from the exposed Lower Formation of the Faroe Islands, confirming that the two normal polarity events present in the Lower Formation are cryptochrons.

From: JOLLEY, D. W. & BELL, B. R. (eds) *The North Atlantic Igneous Province: Stratigraphy, Tectonic, Volcanic and Magmatic Processes*. Geological Society, London, Special Publications, **197**, 1–13. 0305-8719/02/$15.00

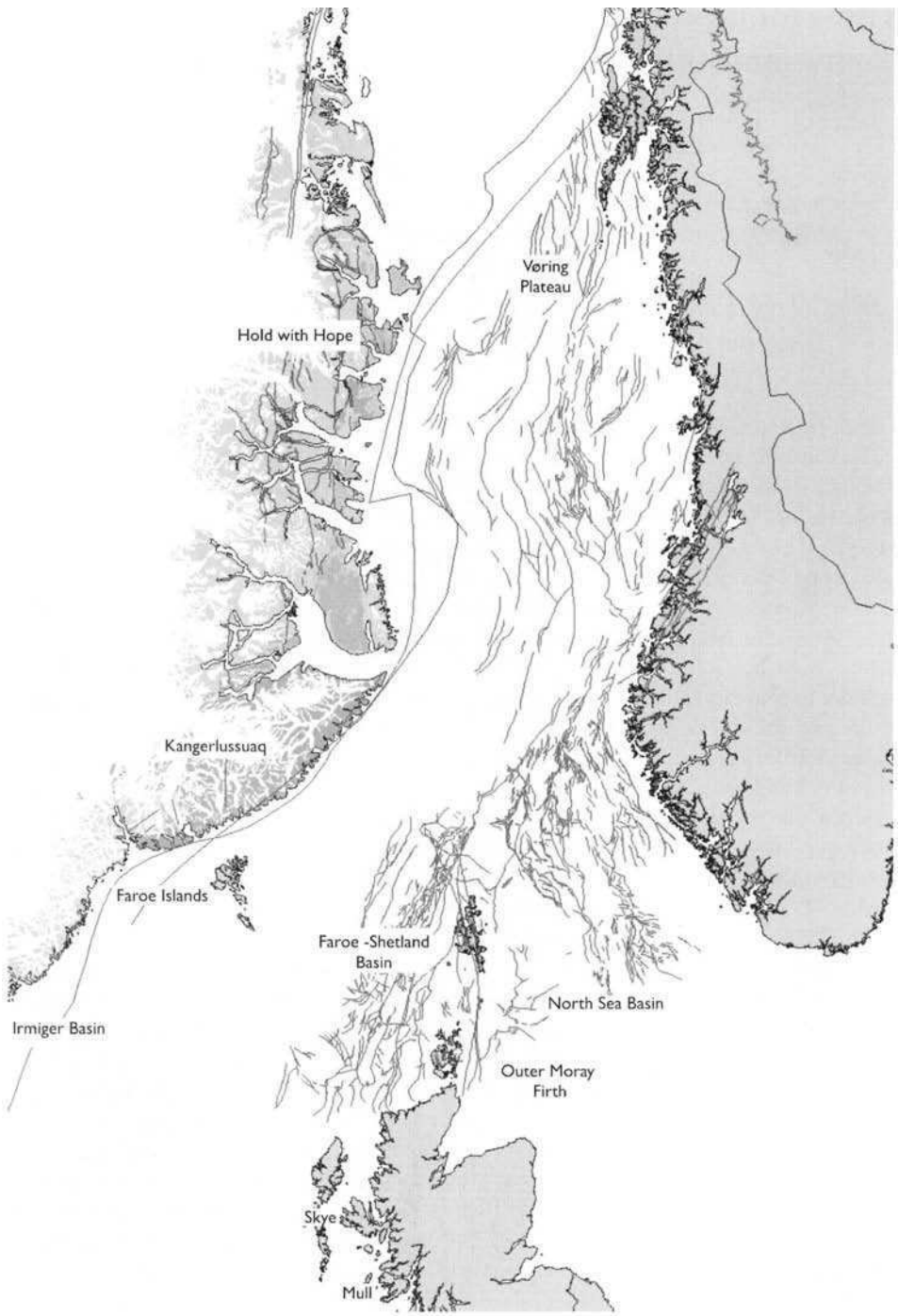

Fig. 1. Location map of the NE Atlantic Margin restored to pre-rift geography.

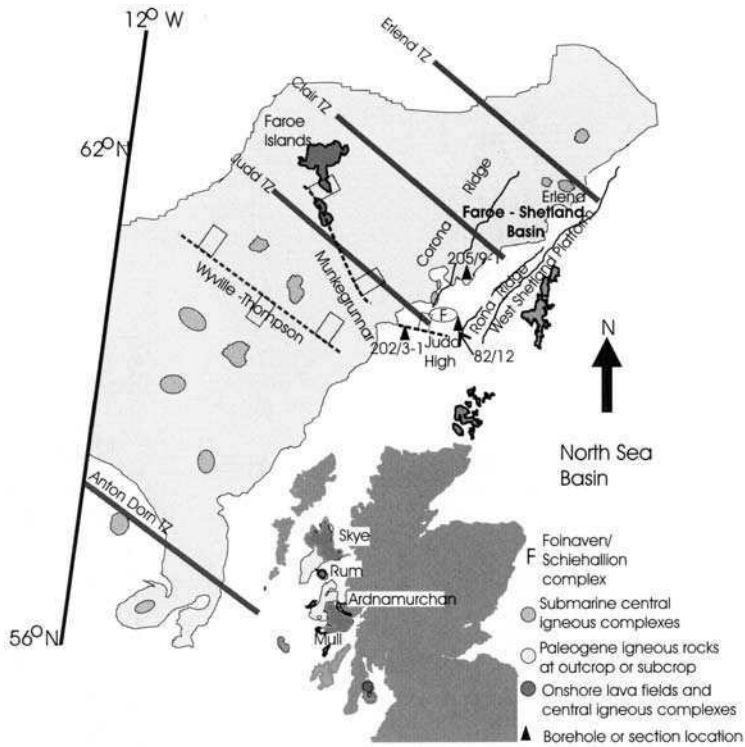

Fig. 2. Location and major structural map of the Faroe–Shetland Basin and adjoining areas.

Cryptochrons of this age are recorded in equivalent Chron 25n sedimentary rocks of the London Basin by Ali & Jolley (1996) and in the Mull Lava Field by Chambers & Pringle (2002; Fig. 3).

Correlation of the lavas on the Faroe Islands with those from Kangerlussuaq in East Greenland has been achieved using geochemical data (Larsen *et al.* 1999). Additional biostratigraphical information from the underlying sedimentary rocks in East Greenland has shown that the oldest lavas, those of the Nansen Fjord Formation (Fig. 3), were erupted in the latter part of Sequence T40 times (Jolley & Whitham 2001). A large unconformity separates the sub basaltic Lower Eocene sedimentary rocks from those of the underlying Upper Cretaceous. Although approximate ages, based around isotopic dates, were given by Larsen *et al.* (1999), **Hansen *et al.*** have analysed the oldest lavas in the Nansen Fjord Formation and other younger flows. These Nansen Fjord Formation Ar–Ar dates were given to 2σ, and consequently have greater experimental errors. Despite this they are consistent with the 57.5–60.56 Ma range of isotopic dates recorded from the Sequence T40 interval within the NAIP (Jolley *et al.* 2002), including the age data presented here by **Wagstein *et al.***, for the Faroes Lower Formation. Of equal significance, is the recognition of lavas erupted in East Greenland during the interval represented by sedimentary sequences T45 and T50 (Ebdon *et al.* 1995). In their analysis of Milne Land Formation lavas, **Hansen *et al.*** present dates within the envelope of 57.0 Ma to 53.5 Ma already recorded from

Table 1. *Summary table of recently published North Atlantic Igneous Province isotopic dates*

Location	Age	Method	Author
Faroe Islands			
Lower formation lava	56.5 ± 1.3 to 58.9 ± 1.3	K/Ar	**Waagstein *et al.***
Lower FM lava, Lopra	60.0 ± 2.1 to 63.1 ± 1.8	Ar/Ar	**Waagstein *et al.***
Lower formation lava	55.7 ± 0.9	Ar/Ar	**Waagstein *et al.***
Skye			
Coire Uagneich granite	59.3	Rb–Sr	Dickin 1981
Loch Ainort granite	58.58 + 0.13	Ar/Ar	Chambers & Pringle 2001
Cuillins centre	58.91 + 0.7	U/Pb	Hamilton *et al.* 1998
Main lava series	59.83 + 0.12	Ar/Ar	Chambers & Pringle 2001
Mull			
Dykes	58.12 + 0.13	Ar/Ar	Chambers & Pringle 2001
Loch Ba ring dyke	58.48 + 0.18	Ar/Ar	Chambers & Pringle 2001
Loch Ba ring dyke	58.7 + 0.1	Pb/U	Hamilton, pers. comm. in Jolley *et al.* 2002
Central group lavas	59.05 + 0.27	Ar/Ar	Chambers & Pringle 2001
Staffa group lava	60.56 + 0.29	Ar/Ar	Chambers & Pringle 2001
Plateau group lava	58.66 + 0.25	Ar/Ar	Chambers & Fitton 2000
Muck			
Eigg lava FM	62.8 + 0.6	Ar/Ar	Pearson *et al.* 1996
Eigg lava FM	62.4 + 0.6	Ar/Ar	Pearson *et al.* 1996
Rum			
Layered Igneous complex	60.53 + 0.08	U/Pb	Hamilton *et al.* 1998
Hebrides terrace			
Borehole 85/5B lava	56.4 + 0.7	Ar/Ar	Sinton *et al.* 1998
West Greenland			
Maligat FM	60.1 + 2.2	Ar/Ar	Storey *et al.* 1998
	60.5 + 0.9	Ar/Ar	Storey *et al.* 1998
	61.0 + 1.2	Ar/Ar	Storey *et al.* 1998
Vaigat FM	60.3 + 1.3	Ar/Ar	Storey *et al.* 1998
	60.3 + 1.0	Ar/Ar	Storey *et al.* 1998
	60.4 + 0.8	Ar/Ar	Storey *et al.* 1998
Voring Plateau			
Lower series lava	54.3 + 0.5	Ar/Ar	Sinton *et al.* 1998
Lower series lava	57.9 + 1.0	Ar/Ar	Sinton *et al.* 1998
Lower series lava	55.6 + 2.0	Ar/Ar	Sinton *et al.* 1998
Irmiger Basin			
ODP152-917A 52R-1 46CM	61.7 + 0.5	Ar/Ar	Sinton & Duncan 1998
Continental succession	60.5 + 0.2	Ar/Ar	Werner *et al.* 1998
Continental succession	60.3 + 0.2	Ar/Ar	Werner *et al.* 1998
Oceanic succession	54.7 + 1.8	Ar/Ar	Werner *et al.* 1998
East Greenland lava	58.7 + 1.4	Ar/Ar	Upton *et al.* 1995
Kangerlussuq Sill	56.3 + 0.9	Ar/Ar	Tegner *et al.* 1998
Kangerlussuq Sill	56.0 + 0.4	Ar/Ar	Tegner *et al.* 1998
Tephra	53.8 + 0.3	Ar/Ar	Heister *et al.* 2001
North Sea			
Sele FM-17 ash	54.0 + 0.53	Ar/Ar	Berggren *et al.* 1995
Sele FM-17 ash	54.04 + 0.33	Ar/Ar	Berggren *et al.* 1995
Sele FM-17 ash	54.51 + 0.05	Ar/Ar	Berggren *et al.* 1995
Sele FM-17 ash	54.56 + 0.14	Ar/Ar	Berggren *et al.* 1995

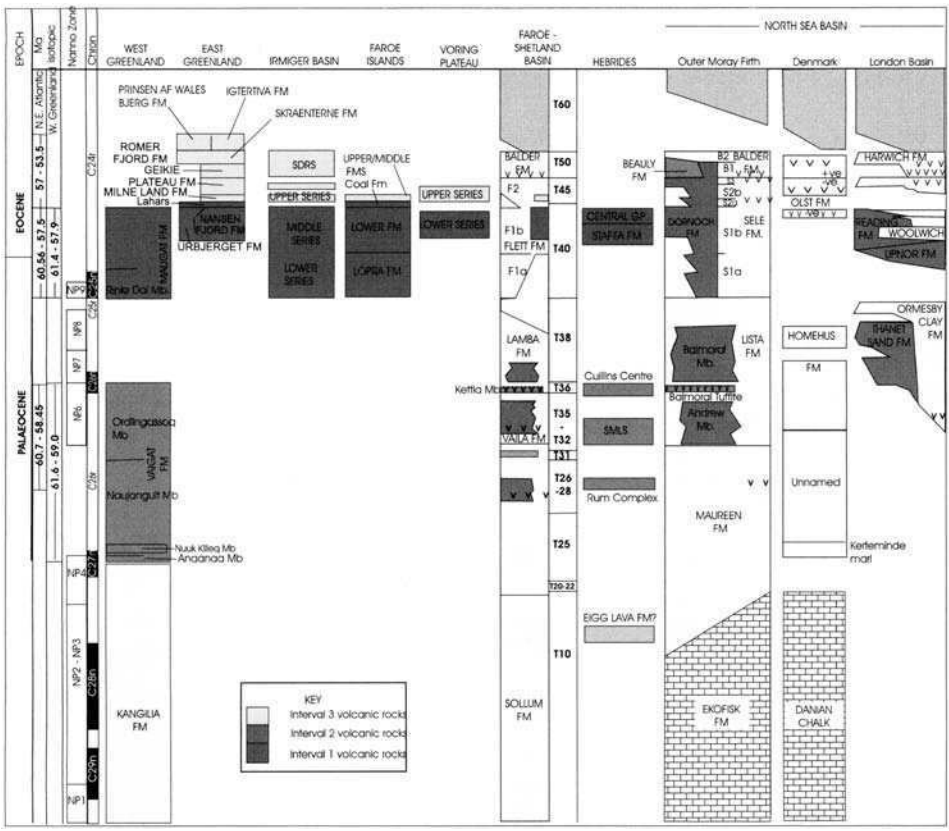

Fig. 3. Stratigraphical panel showing the correlation of rocks within the North Atlantic Igneous Province. Isotopic dates derived from rocks in the northeast Atlantic Margin and west Greenland are shown on the left alongside nannofossil zones identified from sections within the province.

volcanic rocks within this interval (Jolley *et al.* 2002). These data, provide further evidence for the slow-down in both eruption and sedimentation rates at the onset of Sequence T45 sedimentation.

The biostratigraphical analysis of the pre-volcanic Danian–Selandian Kangilia Formation of West Greenland (**Nøhr-Hansen *et al.***) provides a valuable building block in our stratigraphical knowledge of the North Atlantic region. This analysis identifies the existence of calcareous nannofossil zones NP1 to NP4 within the formation. Combined with the isotopic dating of the overlying volcanic rocks of the Vaigat Formation by Storey *et al.* (1998), and the additional biostratigraphical analysis of Piaseki *et al.* (1992), these nannofossil zones help to clarify aspects of NAIP Early Paleocene depositional history. Overlying these nannofossil-dated sediments, the lavas and hyaloclastites of the Vaigat Formation in West Greenland yield isochron ages ranging from 61.6 to 59.0 Ma. Dinoflagellate cyst floras recovered by Piaseki *et al.* (1992), from the lower Ordlingassoq Member, Vaigat Formation (Fig. 3), included *Isabelladinium viborgense*, a taxon which became extinct within

Sequence T31 times in the Faroe–Shetland Basin. Similarly, the occurrences of *Alisocysta margarita* in the basal sedimentary units of the Vaigat Formation demonstrate an age no older than the first appearance of this taxon in intra-Sequence T25 deposits of the Faroe–Shetland Basin.

Whereas it remains difficult to constrain the upper age limit of the Vaigat Formation, the presence of a normal polarity zone in the upper flows suggests cessation of volcanic activity during Chron 26n (Fig. 3). Identification of the duration of eruption of the Vaigat Formation as spanning the intra T25 to intra T36 interval highlights its co-occurrence with tuffaceous deposits in the Vaila Formation of the Faroe–Shetland Basin. Common occurrences of the dinoflagellate cyst *Palaeocystodinium bulliforme* in preparations made by us from tuffaceous claystones in BGS borehole 82/12 (Morton *et al.* 1988), demonstrate the widespread nature (Fig. 2) of the earliest of these Selandian ashes in Vaila Formation units 2 and 3, and equivalent sedimentary units (Fig. 3). While Morton *et al.* (1988) discounted the British Tertiary Igneous Province as a source of these ashes on the basis of geochemical evidence, an east Greenland–Faroe Islands origin was regarded as plausible. However, the age of the onshore Faroe Islands and East Greenland lava fields discounts them as a source for these ashes, suggesting an as yet unidentified igneous centre in the offshore NE Atlantic.

Somewhat younger than these Vaila Fm Unit 2 ashes are the thick volcaniclastic sandstones of the Kettla Member (Lamba Formation), also in the Faroe–Shetland Basin (Fig. 2). These are probably coeval with the last stages of Vaigat Formation (Ordlingassoq Member) volcanism in west Greenland, but again a direct link with that source remains unproven. The Kettla Member is a widespread unit of siliciclastic and volcaniclastic sandstones, composed of quartz, degraded feldspars, lithoclasts of reworked basaltic debris and basaltic ash. This deposit represent the contemporaneous re-sedimentation of volcanic debris and silicicalstic sediment derived from an area of active pyroclastic eruption. These mixed, immature sediments were transported from the neritic zone where they accumulated, into a deep water environment as density flows.

Overlying the Vaigat Formation volcanic rocks are those of the Maligat Formation. Isotopic dating by Storey *et al.* (1998) identified a range of isochron ages, from 61.4 Ma through to 57.9 Ma. Some dinoflagellate cysts were reported by Piaseki *et al.* (1992) from sedimentary rocks at the base of the Rinks Dal Member (Fig. 3), including *Deflandrea oebsifeldensis, Cerodinium glabrum* and *Glaphyrocysta* species. Of these, *D. oebisfeldensis* first appears at the base of Sequence T40, a period which also sees a bloom in numbers of *C. glabrum* and *Glaphyrocysta* species in the Faroe–Shetland Basin. Although Piaseki *et al.* (1992) commented on the absence of *Apectodinium* species from this assemblage, elsewhere *Apectodinium* does not occur commonly until post-LPTM assemblages are encountered (i.e. in mid-Sequence T40 times; Fig. 3). Given the age of the underlying Vaigat Formation, and the normal magnetisation of the basal units of the Rinks Dal Member, the Maligat Formation phase of volcanism can be interpreted as commencing in early Sequence T40 times. Active eruption appears to have been shortlived, the isotopic dates of Storey *et al.* (1998) indicating a cessation in Maligat Fm eruption at the top of the T40 interval. This eruption is coeval with the Faroes Lopra-1 and Lower Formation eruptions, and with other centres in the east, for example, Erlend (**Jolley & Bell**).

Development of the NAIP volcanic sequences and the initiation of the NE Atlantic rift

The stratigraphical correlation presented in Figure 3 demonstrates several distinct intervals of igneous activity. There are constraints placed on the descriptive terminology of these intervals by previous attempts to quantify the stratigraphy of ash deposition (e.g. Knox & Morton 1988). Apparently the earliest evidence for impact of the proto-Icelandic plume beneath the Paleocene NE Atlantic lithosphere is provided by Danian basaltic lavas and trachytic tuffs of the Eigg Lava Formation, Inner Hebrides, NW Scotland (Pearson *et al.* 1996). We are unaware of any other contemporaneous volcanic activity in the NAIP, and the Eigg Lava Formation activity was localized and small scale. At this time, the majority of the Faroe–Shetland Basin was receiving relatively minor amounts of clastic sediment during the deposition of the Sullom Formation (Fig. 3).

Interval 1: Sequence T25 to Sequence T36 (nannofossil zones NP4–NP6)

This interval marks the onset of widespread and voluminous volcanism. The first major volcanic sequence developed in central West Greenland, with the eruption of hyaloclastites and lavas of the Vaigat Formation. Tephra from these eruptions may have been transported downwind to the coastal margins of East Greenland where it accumulated in unstable coastal deposits before being remobilized and transported via sedimentary conduits into the deep basin. However, the presence of volcanic lithoclasts in these turbidite sandstones mitigates against this.

The question of magma production rate in the Vaigat Formation is addressed in this volume by **Pedersen *et al.*** Detailed consideration of a sequence of basin margin lavas and hyaloclastites within the Naujánguit Member of the Vaigat Formation, central West Greenland, erupted during the geomagnetic polarity transition, C27n to C26r, indicates a production rate of *c.* 0.042 $km^3 a^{-1}$, with hyaloclastites aggrading at a rate of *c.* 33 $m ka^{-1}$ into the basin. Extrapolated for the entire Vaigat Formation, this would suggest eruption in only 70 ka. However, it is likely that non-depositional events within the formation lasted for considerably longer periods.

Offshore, in the south of the Faroe–Shetland Basin (Fig. 2), wells on the Judd High (e.g. 202/3-1) show evidence for the abrupt termination of marine sedimentation in early T20 times. It appears probably that the uplift and subsequent erosion of this area, which is coincident with the onset of Interval 1 volcanism, was in response to thermal uplift associated with the arrival of the Iceland Plume in this area.

To the southeast, in the Inner Hebrides of Scotland, the Rum Central Complex testifies to early intrusive activity. The rapid unroofing of this central complex and the eruption of the Skye Lava Field (Hamilton *et al.* 1998) suggests continuation of punctuated volcanism on the southeastern NAIP margin, contemporaneous with central West Greenland volcanism. From this evidence, it is apparent that Interval 1 activity was concentrated at the west and southeastern margins of the NAIP. The perceived lack of Interval 1 volcanism around the later position of the North East Atlantic rift is somewhat surprising. If volcanic activity was concentrated at the eastern and western margins of the NAIP, it may reflect on the initial shape of the proto-Iceland Plume. However, our understanding of the distribution of the volcanism

with time may be limited by our lack of knowledge with respect to early volcanism in the Faroes area. Evidence of Interval 1 volcanism within the Faroes area, may be mantled by the extensive Interval 2 (late Paleocene to early Eocene) volcanic sequences. Unfortunately, seismic and gravity survey data cannot currently differentiate between Eocene lavas and potentially underlying, Selandian volcanic rocks in the Faroes area. The occurrence of mixed siliciclastic and volcaniclastic sediments in Sequence T28 and the Kettla Member (Sequence T36), hints at a volcanic source more proximal to the Faroe–Shetland Basin than the lava fields of West Greenland.

Above Sequence T36, there is currently no evidence for the continuation of Interval 1 volcanism in the Faroe–Shetland area. This termination of volcanic activity appears to have had fundamental consequences to the sedimentary supply into the Faroe–Shetland Basin. The thick developments of basin floor fan sands seen in the Vaila Formation are coincident with the uplift and erosion of areas such as the Judd High. The termination of this thermally supported uplift with the cessation of activity in Sequence T36 times, could have caused the switch in sedimentary sources recognised in the Foinaven/Schiehallion field area (**Morton *et al.***).

Interval 2: Sequence T40 (nannofossil zone NP9)

Interval 1 was followed by a short period of quiescence, with no volcanism recorded in the NAIP. Normal deep marine sedimentation occurred within the Faroe–Shetland Basin, although in late Sequence T38 times, a significant unconformity was formed. In deeper basin areas, this is limited to the non-deposition of the upper parts of Sequence T38, but in more proximal settings it can result in a hiatus that spans the upper Sequence T38 to upper Sequence T40 period. Such a widespread unconformity may be attributed to thermal uplift at the initiation of Interval 2 volcanism. The first evidence for volcanism in this interval is seen in disparate locations, around the Erlend Volcano (**Jolley & Bell**), in thick volcaniclastic sequences in the Faroe Islands area (**Ellis *et al.***) and in West Greenland, where isotopic dating (Storey *et al.* 1998) and biostratigraphy (Piaseki *et al.* 1992) suggest Rinks Dal Member volcanism in early Sequence T40 times (Fig. 3).

The apparent switch from localized lava field activity to the eruption of more widespread volcanic sequences, commenced in mid Sequence T40 times, and was coincident with the Late Paleocene Thermal Maximum (LPTM). A causal linkage between high latitude increased heat flow, ocean water mass warming and resultant oceanic perturbations and clathrate release, may explain the coincidence (Hesselbo *et al.* 2000; Jolley *et al.* 2002). Whatever the mechanism of initiation, the relationship between the onset of vigorous Interval 2 NAIP igneous activity, the release of ocean floor clathrates and their atmospheric oxidation to CO_2, suggests that the NAIP was a factor in creating the LPTM global greenhouse climate.

The LPTM greenhouse climate, although gradually cooling for 2 Ma, persisted to the end of Sequence T40 times (Winkler & Gawenda 1999; Jolley *et al.* 2002), during which the warm and humid climate would have accelerated the weathering of exposed lava fields. Furthermore, the increase in plant diversity and biomass associated with the favourable high pCO_2 atmospheric conditions of the LPTM would have impacted on the clastic sedimentary system by increasing the volume of humic acids in regional groundwater, thus further accelerating weathering processes. Red

boles are consequently a characteristic feature of Interval 2 lava fields. During the height of the volcanic activity in Interval 2, basaltic sequences were erupted in (approximately from west to east): West Greenland, the Irmiger Basin, the Faroe Islands area, the Vøring Plateau, the Faroe–Shetland Basin, the Rockall Basin, the Inner Hebrides, and Antrim.

Interval 3: uppermost Sequence T40–Sequence 50 (nannofossil zone NP9-10)

Near the upper limit of Sequence T40, the vigorous volcanism of the basaltic lava fields of Interval 2 ceased. A widespread unconformity developed, which was exploited by sedimentary drainage systems. Examples of these systems are seen around Rockall, as the Coal-bearing Formation of the Faroe Islands, and as the lahars and other sedimentary deposits recorded by Larsen *et al.* (1999) from Kangerlussuaq, East Greenland. At the southeastern and western extremes of the NAIP, igneous activity ceased at this point, with no evidence for volcanism being seen in West Greenland or the Inner Hebrides.

Evidence for the resumption of volcanism is concentrated on the margins of the proto-North Atlantic rift zone, seen now in the Irmiger Basin, the Faroe Islands, East Greenland and the Vøring Plateau. Rapid eruption of the Middle Lava Formation in the Faroe Islands area (**Ellis *et al.***) was matched and may be correlated with the eruption of the Milne Land Formation in East Greenland (Larsen *et al.* 1999). This correlation is further strengthened by a significant (although not abrupt) change in lava geochemistry towards the top of these formations, continuing into the overlying lavas sequences. While it is currently difficult to identify the exact timing of, and any possible tectonic linkage to, this change in lava geochemistry, the seaward dipping reflectors (SDRS) in the Irmiger Basin appear to have been emplaced during this period, with the switch to the Oceanic Succession, detailed by Larsen & Saunders (1998), having occurred at the start of Interval 3. The nature of the link between the geochemical change in lava composition, the widespread unconformity and the onset of SDRS emplacement still requires resolution.

In the closing stages of Interval 3, increased volcanic activity at the site of ocean floor spreading, and a marine incursion associated with the early Eocene Sequence T50 eustatic rise in relative sea level (Fig. 3; Haq *et al.* 1987) caused widespread phreatomagmatic eruptions. These produced large volumes of basaltic tephra which were distributed downwind in excess of 2000 km into northwestern continental Europe, forming the distinctive ashy claystones of the Balder Formation in the North Sea and Faroe–Shetland Basin.

Interval 4: Sequence T60–present

From the end of the phreatomagmatic eruptions of Sequence T50 times, submarine seaward dipping reflector emplacement along the North Atlantic rift became the major expression of Iceland Plume activity. Some late stage volcanism in East Greenland also occurred, but the dating constraints on the Skraeterne Formation, and the alkaline extrusive rocks of the Prinsen af Wales Bjerg and Igtertiva formations need tightening before they can be integrated into the picture of rift evolution.

The establishment of widespread fully marine sedimentation conditions took around 1.5–2 Ma after the cessation of the Sequence T50 phreatomagmatic eruptions, evidence being provided for this by glauconitic sandstones and siltstones in the Irmiger Basin. The duration of the break between these sedimentary deposits and the underlying SDRS lavas is of importance in assessing the earliest developments of this part of the rift zone (see **Smallwood & White**), but evidence is currently sparse. A thin basalt bed in the oldest sandstone units of ODP Hole 918, which overlie the main SDRS basalts, yielded an age of 52.1 ± 0.8 Ma, younger than the nannofossil zonation for the host sediment (Wei 1998). Larsen & Saunders (1998) used these data to suggest an intrusive relationship for the thin basalt unit with relatively continuous sedimentation from cessation of SDRS eruption. This interpretation appears to overemphasize the accuracy of calibration of isotopic ages to the bio- and magnetostratigraphical timescale, and a nannofossil age determination based on fossil absence data. A re-interpretation of this section can be made which takes into account the evidence for a prolonged period of basalt erosion prior to marine deposition (Holmes 1998) and the palynofloral zonation based on diverse assemblages. These suggest a near time equivalence for the basalt and host sandstones, indicating an invasive flow into recently deposited sands. This thin basalt unit in ODP Hole 918 therefore represents an example of Interval 4 extrusive activity. The dating of the Prinsen af Wales Bjerg Formation in East Greenland as having been erupted at around 53 Ma (**Hansen *et al.***) confines Interval 4 volcanism to the immediate Northeast Atlantic rift area.

Although older Chron 24r sedimentary rocks are seen in the south around Rockall (Beling *et al.* 2001), from the Irmiger Basin to the Erlend Volcano in the north, the glauconitic, and frequently tuffaceous, sediments of late Chron 24r and Chron 24n rest unconformably on older eroded Paleocene or Sequence T50 sedimentary and volcanic rocks (Fig. 3). This regional unconformity demonstrates that a period of subaerial conditions lasting for nearly 2 Ma occurred in the area away from the immediate rift zone. Because of this hiatus, eruption products were only preserved away from the rift, with thin ashes derived from east Greenland preserved in the Rosnaes Clay Formation of Denmark.

Sill complexes

The linkage of sill complexes within the Faroe–Shetland Basin to phases of eruption in the region has been problematical, and previously reliant mainly on isotopic dating. The two papers contained in this volume take us closer to a more sophisticated interpretation of their genesis and linkage.

Smallwood & Maresh discuss the methodology for imaging sill geometries by seismic reflection techniques and determining their physical properties from wireline log measurements. A variety of sill 'shapes' have been recognized, similar to the sills from the northern part of the Faroe–Shetland Basin described by **Bell & Butcher**. **Smallwood & Maresh** also used seismic data to estimate sill volumes and likely depths of emplacement, suggesting that these intrusive events were on the same scale as the voluminous volcanic eruptions within the basin. The shallow emplacement of magma into sections of the basin, resulting in dense crystalline doleritic sills, appears to have influenced subsequent sedimentation events. **Smallwood & Maresh** suggest that reservoir quality sands may have been preferentially deposited within 'lows' flanking

areas on the basin floor, which have been inflated due to sill intrusion. Such differential compaction 'domes' are also discussed by **Bell & Butcher**, who also presented seismic data which indicated that eruption of sill magmas onto the basin floor lead to the development of vents, most likely composed of hyaloclastite and associated fragmental volcanic products.

Conclusions

The collection of studies in this volume mark a further advancement towards the state of knowledge of the geological evolution of the NE Atlantic over a critical period in the early Tertiary. With exploration for hydrocarbon reserves now extended into Faroese waters, new geological information will provide challenges to accepted interpretations of NAIP geology. These, and continued work on the exposed remnants of NAIP volcanism, may help us to resolve some of the continuing problems alluded to above. Increasing refinement in the chronostratigraphy of the various lava fields of the NAIP will impact on interpretations of igneous underplating and its relationship to sedimentation and basin dynamics. An increased understanding of sedimentary provenance, together with the appreciation of sedimentary and igneous rock interaction will aid exploration programmes in determining reservoir quality and likely location.

As this research progresses, as in the papers of this volume, additional questions regarding the evolution of the sedimentary and igneous sequences of the NAIP and their wider environmental effects will be raised. The papers presented here are a further step in resolving some of these problems, and help in identifying those still remaining unresolved.

References

ALI, J. R. & JOLLEY, D. W. 1996. Biostratigraphically constrained magnetostratigraphy of the Late Paleocene and Early Eocene of the Anglo–Belgium–Paris Basin. *In*: KNOX, R. W.O'B., CORFIELD, R. & DUNAY, R. E. (eds) *Correlation of the Early Paleogene in Northwest Europe*. Geological Society, London, Special Publications, **101**, 129–144.

BELING, M., JOLLEY, D. W. & SCOTCHMAN, I. 2001. Eocene fan development in the Rockall Basin. *In*: *Programme & Abstracts Palaeogene Stratigraphy, Tectonics and Petroleum Geology of North West Europe*. Abstracts Volume, Geological Society, London.

BERGGREN, W. A., KENT., D. V., SWISHER, C. C. & AUBREY, M.-P 1995. A revised Cenozoic geochronology and chronostratigraphy. *In*: Berggren, W. A. *ET AL.* (eds) *Geochronology, time scales and global stratigraphic correlations*. SEPM, Special Publication, **54**, 129–212.

CHAMBERS, L. M. & FITTON, J. G. 2000. Geochemical transitions in the ancestral Iceland plume: Evidence from the Isle of Mull Tertiary Volcano, Scotland: *Journal of the Geological Society, London*, **157**, 261–263.

CHAMBERS, L. M. & PRINGLE, M. S. 2001. Age and duration of activity at the Isle of Mull Tertiary igneous centre, Scotland, and confirmation of the existence of subchrons during Anomaly 26r. *Earth and Planetary Science Letters*, **193**, 333–345.

DICKIN, A. P. 1981. Isotope geochemistry of Tertiary Igneous rocks from the Isle of Skye, N.W. Scotland. *Journal of Petrology*, **22**, 155–189.

EBDON, C. C., GRANGER, P. J., JOHNSON, H. D. & EVANS, A. M. 1995. Early Tertiary evolution and stratigraphy of the Faroe–Shetland Basin: Implications for hydrocarbon prospectivity. *In*: SCRUTTON, R. A. *ET AL.* (eds) *Sedimentation and Palaeoceanography of the North Atlantic Region*. Geological Society, London, Special Publications, **90**, 51–69.

HAMILTON, M. A., PEARSON, D. G., THOMPSON, R. N., KELLEY, S. P. & EMELEUS, C. H. 1998. Rapid eruption of Skye lavas inferred from precise U–Pb and Ar–Ar dating on the Rum and Cuillin plutonic complexes. *Nature*, **394**, 260–262.

HAQ, B. U., HARDENBOL, J. & VAIL, P. R. 1987. Chronology of fluctuating sea levels since the Triassic. *Science*, **235**, 1156–1166.

HEISTER, L. E., O'DAY, P. A., BROOKS, C. K., NEUHOFF, P. S. & BIRD, D. K. 2001. Pyroclastic deposits within the East Greenland Tertiary flood basalts. *Journal of the Geological Society, London*, **158**, 269–284.

HESSELBO, S. P., GRÖCKE, D. R., JENKYNS, H. C., BJERRUM, C. J., FARRIMOND, P. L., MORGANS-BELL, H. S. & GREEN, O. 2000. Massive dissociation of gas hydrates during a Jurassic Oceanic Anoxic Event. *Nature*, **406**, 392–395.

HOLMES, M. A. 1998. Alteration of uppermost lavas and volcaniclastics recovered during Leg 152 to the East Greenland Margin. *In*: SAUNDERS, A. D. *ET AL.* (eds) *Proceedings of the Ocean Drilling Program, Scientific results*. Ocean Drilling Program, College Station, Texas, **152**, 115–128.

HESSELBO, S. P., GRÖCKE, D. R., JENKYNS, H. C., BJERRUM, C. J., FARRIMOND, P. L., MORGANS-BELL, H. S. & GREEN, O. 2000. Massive dissociation of gas hydrates during a Jurassic Oceanic Anoxic Event. *Nature*, **406**, 392–395.

JOLLEY, D. W., CLARKE, B. & KELLEY, S. 2002. Paleogene time scale miscalibration: evidence from the dating of the North Atlantic Igneous Province. *Geology*, **30**, 7–10.

JOLLEY , D. W. & WHITHAM, A. G. 2001. A stratigraphical and palaeoenvironmental analysis of the sub-basaltic Paleogene sediments of East Greenland. *In*: *Programme and Abstracts Palaeogene Stratigraphy, Tectonics and Petroleum Geology of North West Europe*. Abstracts volume, Geological Society of London.

JOLLEY, D. W. 1998, Early Eocene palynofloras from Holes 915A, 916A, 917A and 918D, East Greenland. *In*: SAUNDERS, A. D. *ET AL.* (eds) *Proceedings of the Ocean Drilling Program, Scientific Results*. Ocean Drilling Program, College Station, Texas, **152**, 221–231.

KNOX, R. W. O. & MORTON, A. C. 1988. The record of early Tertiary N Atlantic volcanism in sediments of the North Sea Basin. *In*: MORTON, A. C. & PARSON, L. M. (eds) *Early Tertiary Opening of the NE Atlantic*. Geological Society, London, Special Publications, **39**, 407–419.

LARSEN, H. C. & SAUNDERS, A. D. 1998, Tectonism and volcanism at the southeast Greenland rifted margin: a record of plume impact and later continental rupture. *In*: SAUNDERS, A. D. *ET AL.* (eds) *Proceedings of the Ocean Drilling Program, Scientific Results*. Ocean Drilling Program, College Station, Texas, **152**, 503–533.

LARSEN, M. L., WAAGSTEIN, R., PEDERSEN, A. K. M. & STOREY, M. 1999. Trans-Atlantic correlation of the Palaeogene volcanic successions in the Faroe Islands and East Greenland. *Journal of Geological Society, London*, **156**, 1081–1095.

MORTON, A. C. EVANS, D., HARLAND, R., KING, C. & RITCHIE, D. K. 1988. Volcanic ash in a cored borehole W of the Shetland Islands: evidence for Selandian (Late Palaeocene) volcanism in the Faroes region. *In*: MORTON, A. C. & PARSON, L. M. (eds) *Early Tertiary Opening of the NE Atlantic*. Geological Society, London, Special Publications, **39**, 263–269.

PEARSON, D. G., EMELEUS, C. H. & KELLEY, S. P. 1996. Precise $^{40}Ar/^{39}Ar$ dating for the initiation of Palaeogene volcanism in the Inner Hebrides and its regional significance. *Journal of the Geological Society, London*, **153**, 815–818

PIASEKI, S., LARSEN, L. M., PEDERSEN, A. K. & PEDERSEN, G. K. 1992. Palynostratigraphy of the Lower Tertiary volcanics and marine clastic sediments in the southern part of the West Greenland Basin: implications for the timing and duration of the volcanism. *Rapports Gronlands Geologiske Undersolgelse*, **154**, 13–31.

SINTON, C. W. & DUNCAN, R. A. 1998. ^{40}Ar–^{39}Ar ages of lavas from southeast Greenland Margin, ODP Leg 152, and the Rockall Plateau, DSDP Leg 81. *In*: SAUNDERS, A. D. *ET AL.* (eds) *Proceedings of the Ocean Drilling Program, Scientific Results*. Ocean Drilling Program, College Station, Texas, **152**, 387–402.

SINTON, C. W., HITCHEN, K. & DUNCAN, R. A. 1998. ^{40}Ar–^{39}Ar geochronology of silicic and basic volcanic rocks on the margins of the North Atlantic. *Geological Magazine*, **135**, 161–170.

STOREY, M., DUNCAN, R. A., PEDERSEN, A. K. LARSEN, L. M. & LARSEN, H. C. 1998. $^{40}Ar/^{39}Ar$ geochronology of the West Greenland Tertiary volcanic province. *Earth and Planetary Science Letters*, **160**, 569–586.

TEGNER, C., DUNCAN, R. A., BERSTIEN, S., BROOKS, C. K., BIRD, D. K. & STOREY, M. 1998. $^{40}Ar/^{39}Ar$ geochronology of Tertiary mafic intrusions along the East Greenland rifted margin: Relation to flood basalts and the Iceland hotspot track. *Earth and Planetary Science Letters*, **156**, 75–88.

UPTON, B. G. J., EMELEUS, C. H., REX, D. C. & THIRWALL, M. F. 1995. Early Tertiary magmatism in NE Greenland. *Journal of the Geological Society, London*, **152**, 959–964.

WERNER, R, VAN DEN BOGAARD, P., LACASSE, C. & SCHMINCKE, H-U. 1998. Chemical composition, age and sources of volcaniclastic sediments from Sites 917 and 918. *In*: SAUNDERS, A. D., *ET AL.* (eds) *Proceedings of the Ocean Drilling Program Scientific Results*. Ocean Drilling Program, College Station, Texas, **152**, 93–113.

WEI, W. 1998. Calcareous nannofossils from the southeast Greenland margin: biostratigraphy and paleoceanography. *In*: SAUNDERS, A. D. *ET AL.* (eds) *Proceedings of the Ocean Drilling Program, Scientific Results*. Ocean Drilling Program, College Station, Texas, **152**, 147–157.

WINKLER, W. & GAWENDA, P. 1999. Distinguishing climate and tectonic forcing of turbidite sedimentation and the bearing on turbidite bed scaling: Palaeocene Eocene of northern Spain. *Journal of the Geological Society, London*, **156**, 791–800.

This page intentionally left blank

Ridge–plume interaction in the North Atlantic and its influence on continental breakup and seafloor spreading

J. R. SMALLWOOD[1] & R. S. WHITE[2]

[1] *Amerada Hess Limited, 33 Grosvenor Place, London SW1X 7HY, UK*

[2] *Bullard Laboratories, University of Cambridge, Madingley Road, Cambridge CB3 0EZ, UK (e-mail: rwhite@esc.cam.ac.uk)*

Abstract: Development of the rifted continental margins and subsequent seafloor spreading in the North Atlantic was dominated by interaction between the Iceland mantle plume and the continental and oceanic rifts. There is evidence that at the time of breakup a thin sheet of particularly hot asthenospheric mantle propagated beneath the lithosphere across a 2500 km diameter region. This event caused transient uplift, massive volcanism and intrusive magmatism, and a rapid transition from continental stretching to seafloor spreading. Subsequently, the initial plume instability developed to an axisymmetric shape, with the *c.* 100 km diameter central core of the Iceland plume generating 30–40 km thick crust along the Greenland–Iceland–Faroes Ridge. The surrounding 2000 km diameter region received the lateral outflow from the plume, causing regional elevation and the generation of thicker and shallower than normal oceanic crust. We document both long-term (10–20 Ma) and short-term (3–5 Ma) fluctuations in the temperature and/or flow rate of the mantle plume by their prominent effects on the oceanic crust formed south of Iceland. Lateral ridge jumps in the locus of rifting are frequent above the regions of hottest asthenospheric mantle, occurring in both the early history of seafloor spreading, when the mantle was particularly hot, and throughout the generation of the Greenland–Iceland–Faroes Ridge.

The northern North Atlantic is a classic example of continental breakup above a thermal anomaly in the mantle created by a mantle plume. The most obvious consequence of this was the generation of huge volumes of basaltic magmas by partial melting of the mantle at the time of continental breakup (White & McKenzie 1989). Most of this magma bled up to the crust, where the majority (perhaps 60–80%) was frozen in the lower crust, while the rest was extruded as lava flows and pyroclastic deposits, often after undergoing fractionation in crustal magma chambers. If the extrusion rates are sufficiently high, lava flows may form extensive, sub-horizontal flood basalts extending across the continental hinterland. On rifted continental margins, the extrusive lavas are typically expressed as seaward dipping reflector sequences that are readily identifiable on seismic reflection profiles. All these features have been found along more than 2500 km of the rifted continental margins in the northern

From: JOLLEY, D. W. & BELL, B. R. (eds) *The North Atlantic Igneous Province: Stratigraphy, Tectonic, Volcanic and Magmatic Processes*. Geological Society, London, Special Publications, **197**, 15–37. 0305-8719/02/$15.00

North Atlantic, on both the European and the Greenland sides. Furthermore, the mantle plume that gave rise to the thermal anomaly in the mantle is still going strong, lying beneath Iceland at the present day.

The northern North Atlantic is therefore an excellent 'natural laboratory' in which to investigate the interplay between rifting and magmatism, because the history of rifting is well recorded from the time of continental breakup in the early Tertiary to the seafloor spreading at the present day. Magnetic anomaly field reversals during the Tertiary were frequent, and south of Iceland there are few large fracture zones in the oceanic crust, so the seafloor spreading magnetic anomalies contain a clear record of the rifting history throughout the ocean basin. There have also been several well-constrained wide-angle seismic surveys of the continental margins on both sides of the Atlantic (Barton & White 1997*b*; Smallwood *et al.* 1999; Korenaga *et al.* 2000), often with coincident drilling penetrating the volcanic rocks, so both the structure of the rifted margins and the timing of the igneous activity are well known.

In this paper we examine the interaction between the mantle plume and rifting, first of the continental lithosphere to form the present continental margins, and subsequently of the oceanic lithosphere to form the mid-ocean ridge and the land mass of Iceland.

Continental breakup

There are two striking features of the magmatism accompanying continental breakup in the North Atlantic region. The first is its relatively short duration (White & McKenzie 1989; Saunders *et al.* 1997). The second is the extremely widespread and almost simultaneous onset of voluminous volcanism across a huge region (Fig. 1): extending from Baffin Island and west Greenland in the west, to the northern portion of Norway in the north, and as far as the southern tips of east Greenland and the Rockall Plateau in the south. Since there is no indication of the presence of a mantle plume immediately prior to the widespread onset of volcanism, this provides strong constraints on the initiation of the mantle thermal anomaly under this region.

Throughout the area, the onset of volcanism was consistently at 62–61 Ma (Saunders *et al.* 1997). Frequently, picritic basalts were amongst the first volcanic units erupted, indicative of high temperature mantle sources: perhaps the most striking example of this is on Disko Island, west Greenland, where the most magnesium-rich extrusive rocks have been found, despite being on the periphery of the North Atlantic Igneous Province (NAIP) (Fig. 1). Many of these early volcanic units show signs of limited contamination by continental lithosphere, indicative of passage of the magmas through continental lithosphere, and indeed most of them are emplaced onto unequivocal continental crust. There is a general indication of only limited continental rifting during this earliest phase of volcanism (Larsen & Saunders 1998).

Following the first, and widespread magmatic outburst, there appears to have been a hiatus in volcanism lasting up to *c.* three million years, before a second, more sustained period of volcanism during 56–53 Ma which accompanied the start of seafloor spreading in the North Atlantic (Saunders *et al.* 1997). This hiatus is documented off east Greenland (Larsen & Saunders 1998), and in the Faroe Islands, where thin coal deposits developed between the Lower and Middle Lava formations (Larsen *et al.* 1999). Both the rate of volcanic production and the total melt generation during

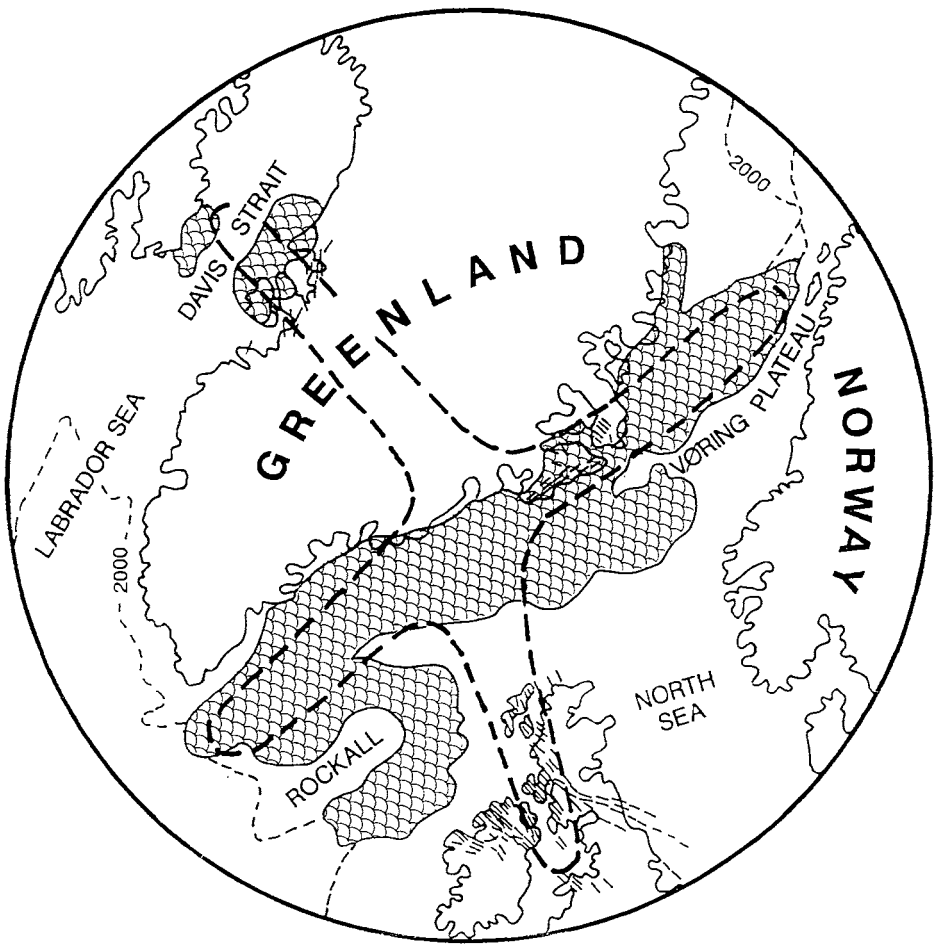

Fig. 1. Reconstruction of the northern North Atlantic at 55 Ma, shortly after the onset of seafloor spreading (after White 1992). Shaded area shows known extent of lava flows and sills emplaced during continental breakup with dykes shown as thin lines. Note that the extent of any dykes emplaced beneath mainland Greenland is unknown due to the ice cover, although an approximately east–west track of circular magnetic anomalies across central Greenland (Brozena 1995; Roest *et al.* 1995) may represent a line of igneous centres. The configuration of a possible set of rising hot sheets of asthenospheric mantle at the time of breakup is outlined by heavy broken lines. The reconstruction uses an equal area Lambert stereographic projection centred on the core of the mantle plume, and encompasses an area with a radius of 1500 km.

the second phase of activity were much larger than during the first phase, and the volcanism accompanied a rapid thinning of the continental lithosphere. It was during this second phase that the main series of seaward dipping reflector sequences, up to 150 km wide on both sides of the Atlantic, were generated on the margins, in addition to massive basaltic lava flows which extended into the sedimentary basins adjacent to the rifted margins (Richardson *et al.* 1999). The total igneous thickness on the rifted margins reached 25–35 km (Reid *et al.* 1997; White & Barton 1997*b*), and the seaward dipping reflector sequences were erupted near to, or above sea level.

What can be learnt about the initial mantle thermal anomaly under the North Atlantic region from the distribution and timing of the magmatism?

There are three main indicators of mantle temperature, though each may also be affected by factors other than solely the temperature: (i) the total volume of melt produced; (ii) the uplift and subsidence history that resulted, in part, from the addition of new igneous material to the crust, and in part from dynamic support by the underlying plume (Bown & White 1995; Barton & White 1997*b*); and (iii) the geophysical, geochemical and petrological characteristics of the igneous rocks themselves (White & McKenzie 1995). The surprising observation from the North Atlantic region is that abnormally hot mantle arrived simultaneously, or at least within the limits of resolution of our measurements of about one million years, across the entire region, at points more than 2000 km apart in the pre-rift reconstruction (Fig. 1) (Saunders *et al.* 1997; Larsen & Saunders 1998; Larsen *et al.* 1999). The main phase of volcanism produced igneous sections along the rifted margins of the North Atlantic that vary little in thickness along a 2000 km length from south Rockall Plateau to northern Norway (Barton & White 1997*b*), and along the east coast of Greenland from its southern tip to the Greenland–Iceland–Faroe Ridge. It is also apparent that the oceanic crust that was formed adjacent to the rifted margins within a few million years of continental breakup, with exception to the area directly above the core of the plume (that lay beneath the Greenland–Iceland–Faroe Ridge), reduced rapidly in thickness compared to the igneous thickness on the rifted margins. Thereafter, the distribution of crustal thickness along the Mid-Atlantic rift remained similar to that found today around the present-day mantle plume centred beneath Iceland, suggesting a broadly similar regional distribution of mantle temperatures since shortly after the onset of seafloor spreading (White *et al.* 1995).

Care must be taken when inferring the mantle temperature directly from the crustal thickness. Where the mantle decompresses passively beneath a rift, and there is no lateral flow of the melt away from the rift, then the crustal thickness provides a direct measure of the mantle temperature (White & McKenzie 1989). Apart from directly above the mantle plume under Iceland, this is the situation that we believe pertains at the present day along the northern North Atlantic spreading centres. However, where there is active convection-driven flow of the mantle through the melting region, as in the narrow (*c.* 100 km diameter) central core of the Iceland plume, then even modest temperature anomalies in the mantle can build large crustal thicknesses. The more active the flow, the smaller the temperature anomaly required to generate a given thickness of igneous crust. In present-day Iceland, the crustal thickness of 40 km directly above the mantle plume (Darbyshire *et al.* 2000), is due in part to the excess temperature of the mantle plume and in part to active convection. Geochemical characteristics of the igneous rocks can assist in determining the parent mantle temperature, and even within 150 km of the Iceland plume, geochemical- and seismic-based measurements of the crustal thickness suggest that the mantle decompresses passively beneath the rift and therefore lies outside the central rising core of the mantle plume (White *et al.* 1995; Weir *et al.* 2001).

If the mantle decompression under the nascent rifted margins was passive at the time of continental breakup, then the large igneous thicknesses found along the entire length of the rift are indicative of a thermal anomaly in the asthenospheric mantle of *c.* 150°C (Clift *et al.* 1995). The decrease in crustal thickness after the onset of seafloor spreading would then indicate a rapid drop in the mantle thermal anomaly to *c.* 50°C

in the distal areas, though it remained high directly over the plume core (Barton & White 1997*b*). These inferred temperatures are probably upper limits: if there was a component of active convection under the rifts at breakup time, then the mantle temperature anomaly would have been smaller. However, if a significant amount of melt flowed laterally away from the rift zones, either on the surface as flows, or at depth as dykes and sills, then our temperature estimates would be on the low side.

While the timing and extent of the volcanism provides control on the magnitude and extent of the abnormally hot mantle underlying the region at breakup time, the uplift and subsidence history provides further information on the dynamic support from the mantle plume, which is proportional to the product of the size of the mantle thermal anomaly and its thickness. Transient dynamic support of a few hundred metres, unaccompanied by any rifting or magmatism, has been reported by Nadin *et al.* (1995) during the early Tertiary in the northern North Sea. This area is well removed from the line of continental breakup, showing that abnormally hot mantle flowed widely beneath the region. Furthermore, subsidence modelling of data from DSDP holes in the Edoras Bank region of the Rockall margin shows that the abnormally hot asthenospheric mantle in this distal region of the plume anomaly was only a few tens of kilometres thick, and that the thermal anomaly and associated dynamic support decayed rapidly over a period of 5–10 million years from *c.* 150°C above normal to only *c.* 50°C above normal shortly after continental breakup (Barton & White 1997*b*).

From these observations a picture emerges of the extremely rapid propagation of a thin sheet of mantle a few tens of kilometres thick and *c.* 150°C hotter than normal beneath the unrifted continental lithosphere at around 62 Ma. This gave rise to volcanism across a large area, including eastern and western Greenland, the Faroes, Ireland and the British Tertiary Province. This early phase of volcanism was succeeded by a much larger volume of magmatism as the continental lithosphere stretched and thinned during the process of continental breakup, allowing decompression melting of the hot mantle beneath the rift. The rapid drop of mantle temperature following this phase of volcanism suggests that the widespread sheet of abnormally hot sub-lithospheric mantle intruded prior to continental breakup was absorbed into the melting beneath the rift, and not subsequently replenished (Barton & White 1997; Saunders *et al.* 1997). Thereafter, the pattern of thermal anomalies in the mantle continued in a more axisymmetric shape, as the narrow hot plume beneath Iceland, which generated the Greenland–Iceland–Faroes Ridge as the Greenland and European plates moved apart, and a surrounding region of moderately hot material fed laterally from the central plume.

Several different models have been suggested to explain the widespread occurrence of this early Tertiary magmatism. One is that there was a long period of incubation of hot asthenospheric mantle plume material prior to the onset of rifting and volcanism (Kent *et al.* 1992; Saunders *et al.* 1992), however, the simultaneous and widespread onset of volcanism across the entire region and the absence of earlier evidence of uplift or magmatism suggests that such a long period of incubation did not occur in the North Atlantic region (White & McKenzie 1989; Saunders *et al.* 1997).

A second set of models assumes that the onset of volcanism was associated with the arrival of a new mantle plume, which itself had arisen as a boundary layer instability from much deeper in the mantle: such boundary layer instabilities commonly exhibit enhanced temperatures and larger rates of flow in the initial phase, and both

these are consistent with the observations (White & McKenzie, 1989). The precise shape of the thermal anomaly is less clear. One possibility to explain the distribution of initial volcanism is that the mantle instability originated as either three or four rising sheets of abnormally hot mantle, which subsequently developed into a more conventional axisymmetric plume centred at the meeting point of the sheets beneath where Iceland now sits. Using this explanation Barton & White (1997*b*) suggested a tripartite system of hot mantle sheets, with one sheet extending south between Rockall Plateau and southern Greenland, another northeastwards between eastern Greenland and Norway, and a third westward beneath central Greenland to Baffin Island. The first two mantle sheet upwellings lay along the line of subsequent continental breakup, coincident with the locations of maximum igneous thickness. The third sheet, crossing central Greenland, explains the simultaneous, high-temperature melts extruded on both Disko Island, west Greenland, and the east Greenland margin at *c.* 62 Ma. Although the thick ice cover prevents direct mapping of the geology beneath central Greenland, lineations of marked magnetic (Roest *et al.* 1995) and gravity anomalies along the line of the postulated mantle sheet beneath Greenland have been interpreted by Brozena (1995) as being due to igneous intrusions into the crust. N. J. White (pers. comm. 2001) has drawn attention to a possible fourth lineation of mantle melts extending southeastward to the Irish sea (Fig. 1); the evidence for this is in the abundance of early Tertiary magmatism along this lineation, together with the evidence for marked uplift which caused *c.* 2.5 km of denudation in the east Irish Sea region between 62 and 54 Ma (Lewis *et al.* 1992; Rowley & White 1998). An alternative way to explain the short-lived burst of volcanism in the west Greenland area is that it was caused either by a completely separate mantle plume, or by a blob of hot mantle that detached itself from the main plume beneath the North Atlantic. Lawver & Müller (1994) explained the west Greenland and Atlantic magmatism by postulating that an axisymmetric plume was located beneath central Greenland at the time of breakup, and that only subsequently did it migrate eastward to cross the east Greenland coast at about 35 Ma. We think that this explanation is unlikely, since it cannot explain the continuous formation of the thick crust of the Greenland–Iceland–Faroes Ridge, which we attribute to a mantle plume that lay close to the rift beneath eastern Greenland at the time of breakup (at the centre of the projection in Figure 1) and continued to sit beneath the North Atlantic ridge axis as the ocean opened, as postulated by White & McKenzie (1989).

On the evidence for an extensive thin horizontal sheet of anomalously hot mantle beneath the lithosphere required to explain the uplift and subsidence patterns, the most likely explanation seems to be that the initial widespread thermal anomaly

Fig. 2. Bathymetry, free air gravity anomaly and magnetic anomaly in the NE Atlantic. Panels **b** and **c** include flowlines back to anomaly 24 time centred on the present spreading axis. (**a**) Bathymetry, 1000 m interval contours. Location of FIRE profile shown in Figure 5, and magnetic anomaly flowline profiles recorded by Charles Darwin 70 (Profile A) and Charles Darwin 87 (Profile B) shown in Figure 6 are marked. Present active rift axes are shown in red, and selected extinct rifts are shown by dashed red lines: S, Skagi; V, Vestfirdir; NVZ, EVZ, WVZ, northern, eastern and western volcanic zones; KR, Kolbeinsey Ridge; RR, Reykjanes Ridge; GIR, Greenland–Iceland Ridge; FIR, Faroe–Iceland Ridge; IrB, Irminger Basin; IB, Iceland Basin; LS, Labrador Sea; ICE, Iceland; GB, Great Britain; RP, Rockall Plateau; FI, Faroe Islands. (**b**) Free air gravity anomaly (Sandwell & Smith 1997). Zone of ephemeral fracture zones outlined by broken white line. (**c**) Magnetic anomaly (Macnab *et al.* 1995).

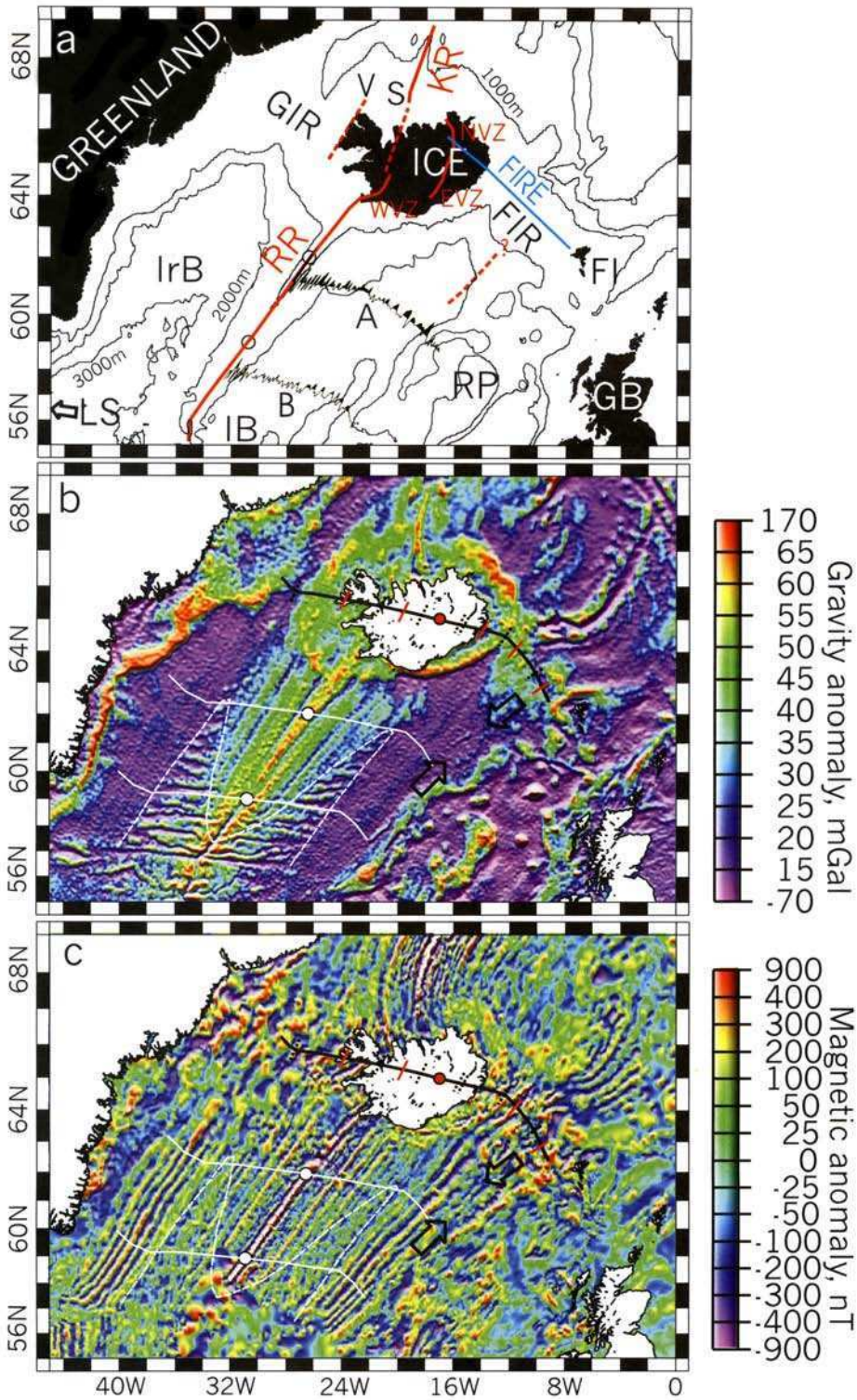
a
GREENLAND
GIR
V S
KR
1000m
ICE
NVZ
WVZ
EVZ
FIRE
FIR
FI
RR
IrB
2000m
A
3000m
LS
IB
B
RP
GB
68N
64N
60N
56N
b
Gravity anomaly, mGal
170
65
60
55
50
45
40
35
30
25
20
15
-70
c
Magnetic anomaly, nT
900
400
300
200
100
50
25
0
-25
-50
-100
-200
-300
-400
-900
40W
32W
24W
16W
8W
0

resulted from the lateral injection just beneath the lithospheric lid of a thin (a few tens of kilometres thick) sheet of abnormally hot asthenospheric mantle from a central plume feeder. The high temperature and low viscosity of such a thin sheet would allow it to be injected rapidly with little conductive heat loss (Larsen *et al.* 1999), and would explain the transient uplift without accompanying volcanism seen, for example, in the northern North Sea, far from the location of eventual breakup (Nadin *et al.* 1995; Barton & White 1997*b*). Volcanism only occurred where the mantle could decompress, either beneath a pre-existing region of thin lithosphere, or in an area where rifting was actively thinning the lithosphere (Saunders *et al.* 1997). The subsequent rapid cooling of the thin sheet would occur partly in response to decompression and associated partial melting, and partly as a result of conductive heat loss into the adjacent colder mantle that lay both above and below the thin sheet of hot mantle.

Seafloor spreading

Continent–ocean transition

Compared to typical non-volcanic margins, the interval between the beginning of continental stretching and the onset of full seafloor spreading was extremely short in the North Atlantic, lasting perhaps 4–6 Ma, and the width of the continent–ocean transition zone is narrow, reaching only a few tens of kilometres. This compares with the long periods of pre-breakup stretching, perhaps lasting 25 Ma or more, and the great widths of stretched lithosphere, extending across 150 km or more, found on many non-volcanic margins. The reason is probably because the injection of huge volumes of melt into the stretching continental lithosphere weakened it greatly, allowing rapid thinning and progress to seafloor spreading, and because the added gravitational potential provided by the mantle plume in a region predisposed to extension throughout the Mesozoic may have encouraged continental breakup.

Flowlines

Prior to making reconstructions of the seafloor spreading in the North Atlantic, we calculated flowlines that reproduce the rotations between the Greenland and Eurasian plates (Fig. 2). We restrict our discussion primarily to the region south of Iceland (the Irminger and Iceland Basins, Fig. 1), because to the north the picture is complicated by major ridge jumps which isolated the continental fragment of Jan Mayen in the mid-Tertiary.

Seafloor spreading magnetic anomalies 20–23 are easy to recognize in the North Atlantic, forming linear, unbroken anomalies with no major offsets south of Iceland (Fig. 2c). The most landward anomaly is usually part of anomaly 24, though due to the multiplicity of magnetic reversals between chrons 24 and 25 (Cande & Kent 1995), it is not always possible to be certain which of these, or what combination of them, generated the main magnetic anomaly stripe. The continent–ocean boundary (COB) itself is unlikely to be a precise line, instead representing a continent–ocean transition from highly stretched and intruded continental crust to dominantly new igneous crust. Figure 3 shows the approximate location of the COB based on wide-angle seismic surveys extrapolated by the gravity maps along the margins. Pre-breakup

reconstructions would close to a position somewhat landward of the COB, to account for the stretching of the continental crust prior to breakup. On the western margin of the Rockall Plateau we estimate this pre-breakup stretching to be of the order of 25–35 km from wide-angle seismic experiments.

Several authors have published reconstruction poles between Greenland and Eurasia back to anomaly 24 (Srivastava & Tapscott 1986; Müller & Roest 1992; Wold 1995). In Figure 4 we show a comparison of flowlines calculated using different authors' finite rotations. The flowlines calculated using Srivastava & Tapscott's (1986) rotations fit the present-day azimuth of spreading at the Reykjanes Ridge well, but the slow change of azimuth with time means that they are not parallel to the fracture zones formed during the period between chrons 18 and 5 when the ridge was morphologically segmented on a 30–80 km scale. Flowlines calculated using Müller & Roest's (1992) finite rotations also strike obliquely to the fracture zone traces between chrons 18 and 13. The finite rotations of Wold (1995) produce a pronounced kink in the flowline at chron 21 (Fig. 4), we believe this may be because he has included in his rotation calculations identifications of magnetic anomalies 7 (from the north) and 20, 21, 22 and 24 (from the south) over the Faroe–Iceland Ridge. Identification of seafloor spreading anomalies from lavas erupted subaerially, as were those on the Faroe–Iceland Ridge, is likely to be extremely uncertain. Factors leading to uncertainty include: the long flow lengths of lava flows, and their complex interaction with topography; the subsequent erosion of 1–2 km of the uppermost crust of the Faroes–Iceland Ridge; and the likelihood of small-scale shifting rift zones and possible multiple rifts such as are observed today in Iceland over the mantle plume in a similar setting to that which generated the Faroe–Iceland Ridge.

Here we use a combination of Helman's (1989) North America–Eurasia rotations and Roest & Srivastava's (1989) North America–Greenland rotations to obtain finite rotation poles for Greenland–Eurasia (Table 1). Helman's (1989) rotations are based on magnetic anomalies both in the region south of Iceland that we are investigating, and in the Atlantic south of the Charlie Gibbs fracture zones: they give synthetic fracture zone traces (flowlines) that match well the trends of the Charlie Gibbs fracture zones. Seafloor spreading at the Ran Ridge in the Labrador Sea ceased prior to anomaly 13 time (Kristofferson & Talwani 1977). Detailed study of the final spreading episode of the Ran Ridge suggests that the spreading slowed between chrons 21 and 13 (47–33 Ma) (Louden *et al.* 1996). We assume that the slowing occurred linearly between chrons 21 and 13. The resultant rotations produce flowlines that match the fracture zone traces well (Fig. 2), with a fairly smooth angular change as spreading slowed down and stopped in the Labrador Sea (solid line, Fig. 4).

Reconstructions

Finite rotations are used here to reconstruct the opening of the North Atlantic south of Iceland from shortly after breakup time to the present day, rotating some of the most prominent seafloor spreading magnetic anomalies to illustrate major changes in the style of seafloor spreading and ridge segmentation (Figs 3a–e). The oceanic crust formed during seafloor spreading falls into four main regimes. These changes are probably directly related to changes in the flow pattern or temperature of the Iceland mantle plume.

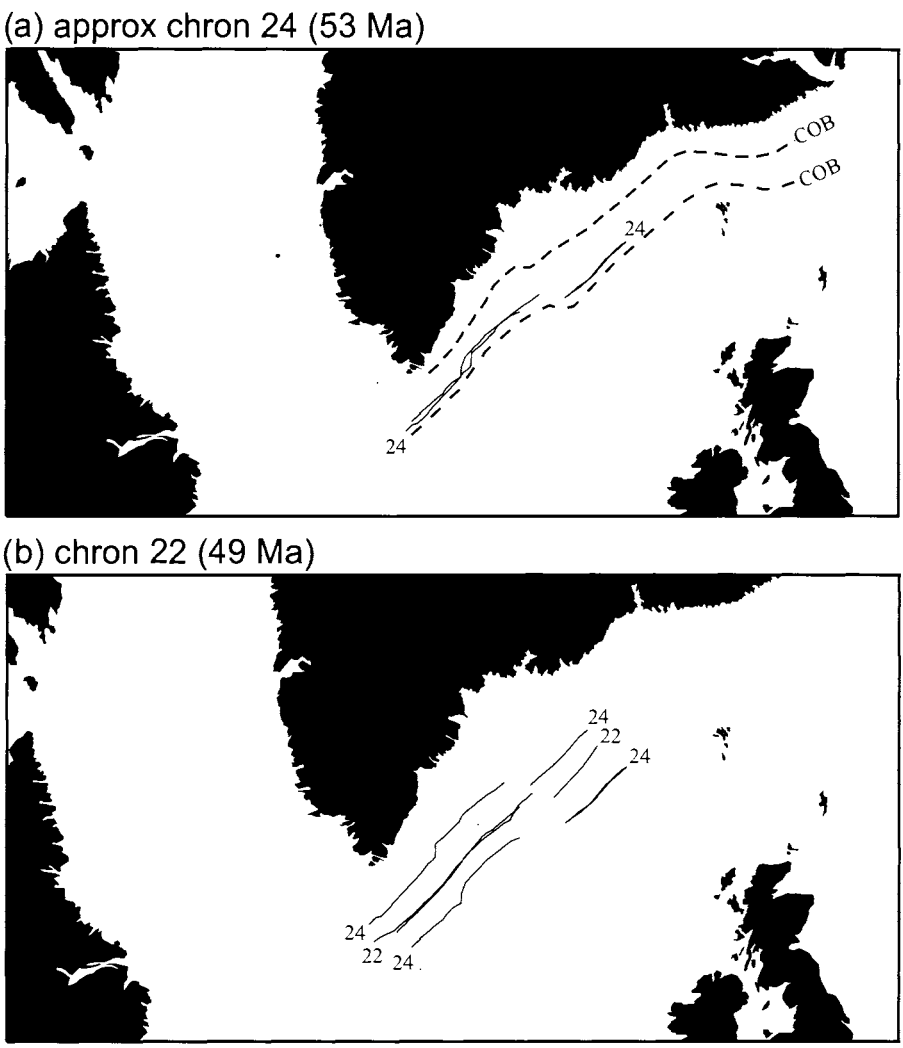

Fig. 3. Reconstruction of seafloor spreading in the Irminger and Iceland Basins, with present land-masses shown shaded, based on finite rotations with Eurasian plate held fixed. (**a**) Shortly after the onset of seafloor spreading, at 54 Ma. The landward-most magnetic lineations (anomaly 24) in the Irminger and Iceland Basins are superposed. The approximate continent–ocean boundaries (COB) on the conjugate rifted margins are shown by broken lines: the region between the COB and the magnetic lineations are occupied by seaward dipping reflector sequences. The ridge crest was offset about 50 km dextrally. (**b**) Early unsegmented axis, chron 22 (49 Ma). Between chron 22 and chron 21 a ridge jump in the northern part of the ocean removed the dextral offset to give a continuous ridge axis by chron 21. (**c**) Transition from segmented to continuous ridge axis, chron 9 (27.5 Ma). The 30–80 km ridge segmentation formed around 40 Ma is now being combined into an unsegmented axis propagating from the north, with associated oblique spreading. (**d**) Chron 6 (20 Ma). Continued southward propagation of the unsegmented ridge axis has removed all but the southernmost ridge segmentation. (**e**) Present day, with oblique spreading along a continuous 750 km length of ridge crest with no major offsets. Fine line shows 2000 m contour, and broken lines show approximate location of COB.

(c) chron 9 (27.5 Ma)

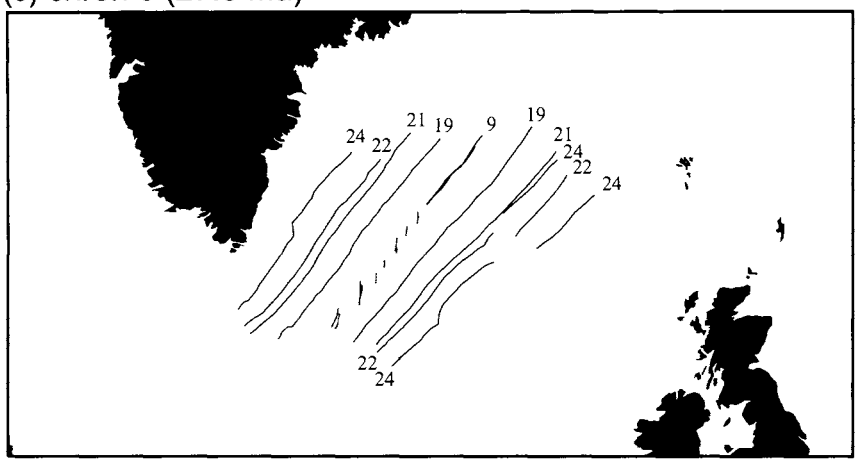

(d) chron 6 (20 Ma)

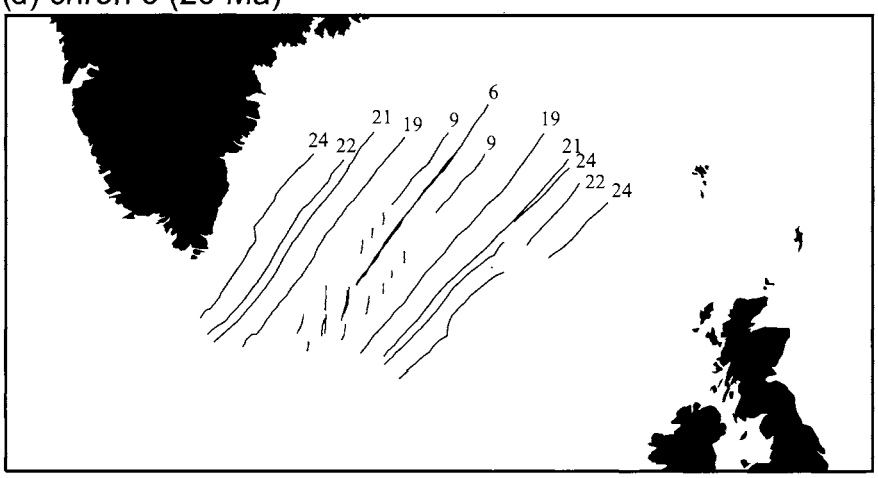

(e) Present day

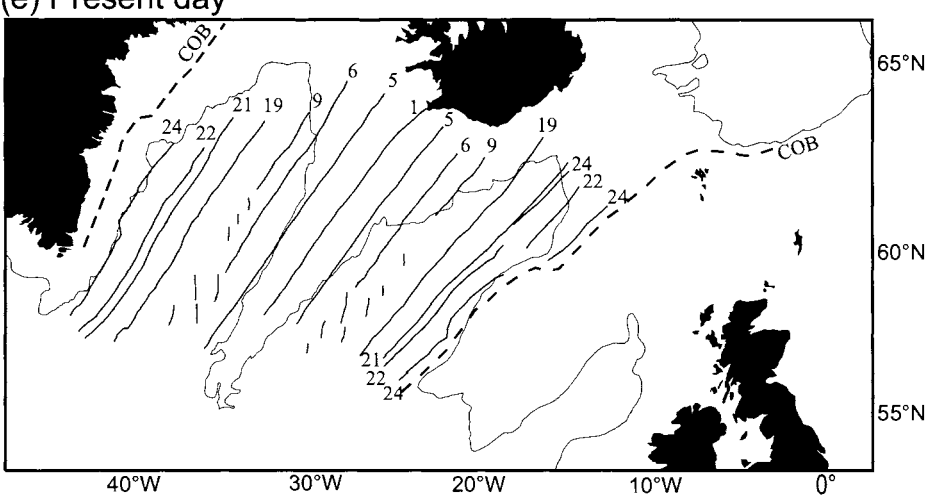

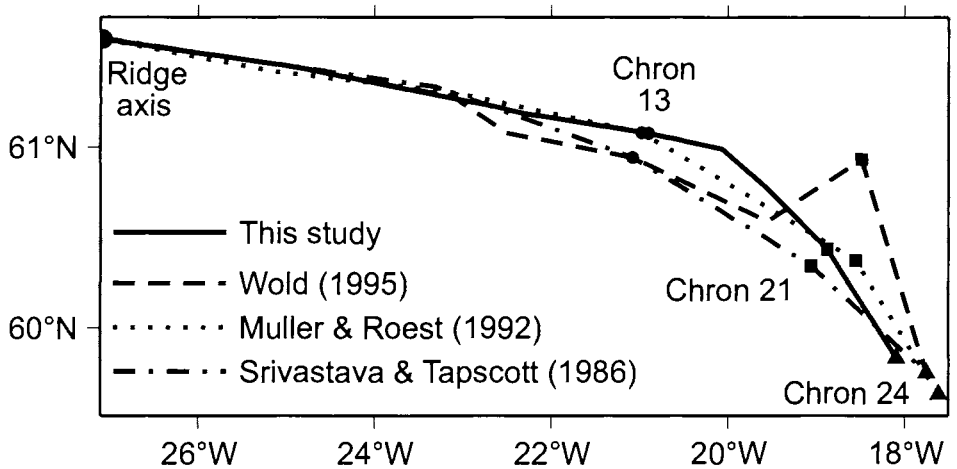

Fig. 4. Flowlines calculated for the Iceland Basin from a point on the Reykjanes Ridge, using a variety of published Greenland–Eurasia reconstruction poles. Points corresponding to magnetic chrons 13, 21 and 24 are shown as circles, squares and triangles respectively. Previously published reconstruction poles (Srivastava & Tapscott 1986; Muller & Roest 1992; Wold 1995) give flowlines that strike oblique to the fracture zones from chron 13, or later. The preferred flowline from this study is shown as a solid line (see text for details).

Table 1. *Greenland–Eurasia closure poles*

Chron	${}^{0}_{NAm}ROT^{t}_{Grn}$			${}^{0}_{Eur}ROT^{t}_{NAm}$			${}^{0}_{Eur}ROT^{t}_{Grn}$		
	Lat, °N	Lon, °E	Angle, °	Lat, °N	Lon, °E	Angle, °	Lat, °N	Lon, °E	Angle, °
5A				68.00	137.00	3.01	68.00	137.00	3.01
8				66.85	135.46	5.97	66.85	135.46	5.97
13				62.50	138.50	7.30	62.50	138.50	7.30
17	62.80	−91.95	−0.21	62.50	138.50	7.83	61.41	137.50	7.69
18	62.80	−91.95	−0.48	62.50	141.50	8.39	60.17	139.32	8.08
20	62.80	−91.95	−1.33	62.50	141.50	9.29	56.25	136.41	8.47
21	62.80	−91.95	−2.61	55.70	143.25	9.81	42.20	135.83	8.54
24	55.86	−104.55	−4.44	61.10	144.90	12.04	43.17	128.30	9.87

Greenland–Eurasia closure poles, from the Eurasia–North America poles of Helman (1989) and the Greenland–North America poles of Roest & Srivastava (1989), assuming a linear slowing of spreading in the Labrador Sea from anomaly 21 to anomaly 13 time. Subscripts NAm, Grn & Eur refer to North American, Greenland and Eurasian plates respectively.

The very oldest oceanic crust comprises a zone of seaward dipping reflectors, up to 150 km wide at its greatest width, generated between breakup time and chron 24 (i.e. between approximately 56–53 Ma). Because they were extruded sub-aerially, clear seafloor spreading magnetic anomalies were not always developed, although fine lineations perpendicular to the spreading direction have been recognized off the east Greenland margin (Larsen & Saunders 1998). This zone is bounded at the seaward end by the prominent magnetic anomaly 24. Although an oceanward zone of seaward dipping reflectors is developed on both sides of the Atlantic basin (Larsen &

Jakobsdóttir 1988; Mutter & Zehnder 1988; Barton & White 1997*a*), there appears to be a gross asymmetry, with anomaly 24 lying some 100–150 km off the COB on the Greenland margin, but lying close to the COB on the Rockall Plateau margin (Fig. 3a). This asymmetry was probably removed by one or more minor eastward ridge jumps prior to anomaly 24, after which the seafloor spreading in the bulk of the region was broadly symmetric on both sides of the spreading axis. We return in a later section to discuss the rate of seafloor spreading during formation of this oldest oceanic crust.

The second main phase of seafloor spreading occurred between chrons 24 and 21 (53–46 Ma). This generated prominent seafloor spreading anomalies, with the direction of spreading perpendicular to the spreading axis (see flowline on Fig. 2c). The spreading axis was unbroken by any fracture zones other than a 50 km dextral offset between the northern and southern parts of the ridge axis south of Iceland (Fig. 3b). Oceanic crust was somewhat thicker than normal (9–11 km, compared to *c.* 6 km for normal ocean basins), indicative of asthenospheric mantle temperatures in the region being some 50°C above normal (White 1997). In tectonic style, this interval of spreading most closely resembles the fast-spreading ridges such as the East Pacific Rise at the present day. We suggest that the similarity arises because the enhanced melt production and thicker than normal crust produced in the North Atlantic produces a rheologically weak spreading axis. On the East Pacific Rise, although the crust is thinner, the frequent crustal melt injection episodes produced by the fast spreading rate maintain the spreading axis at a hotter temperature, on average, than that of a normal slow-spreading ridge. So either fast spreading or enhanced melt production on a slow-spreading ridge may have a similar effect of producing a weak spreading axis. Between anomalies 22 and 21 the dextral offset in the central part of the spreading axis was removed by a westward ridge jump, producing an unbroken, linear axis at anomaly 21 time (see Fig. 3c). The ridge jump has left two sections of anomaly 24 on the eastern side of the basin south of the Faroe–Iceland Ridge (Voppel *et al.* 1979). The extinct ridge axis (dashed line on Fig. 2a and arrowed on Fig. 2b), has been previously recognized in gravity anomaly data (Roest *et al.* 1995).

A major change of spreading style accompanied a marked change in spreading direction after chron 20 (43 Ma). Reorientation of the azimuths of the spreading axes produced a third phase of seafloor spreading style, with a zone of short (30–80 km long) spreading segments offset by small transform faults. The spreading segments strike approximately perpendicular to the new spreading direction, and the transform faults lay approximately parallel to the spreading direction, although like small-offset transforms found elsewhere, locally they may deviate from it considerably. This change in style can be seen in both the gravity and magnetic maps in Figure 2, and can also be seen in the sediment distribution mapped using seismic reflection profiles (Ruddiman 1972). This style of spreading, typical of slow-spreading ridges formed away from the influence of mantle plumes, occurred diachronously in the North Atlantic, as shown by the region outlined by broken white lines in Figures 2b & c. The reduced residual depth anomalies in this region suggests that the mantle was less hot than during the preceding and succeeding intervals (White 1997), which is consistent with reversion to normal seafloor spreading. The diachronous onset is consistent with the mantle thermal anomaly generated by the Iceland plume withdrawing slowly northward, associated with a cooling of the plume material fed southward from the plume core.

The fourth and final change of spreading style in the North Atlantic saw a gradual reversion to an unsegmented, but now obliquely spreading axis on the Reykjanes Ridge. This propagated from the north, starting at approximately chron 9 (27 Ma), (Figs 3c–e). We suggest that this is indicative of somewhat higher temperature mantle feeding southward from the plume core beneath Iceland, allowing the development of abnormally thick crust in the northern part of the Reykjanes Ridge. South of 57°N on the Reykjanes Ridge, the crustal thickness drops toward a more normal 7 km, and a median valley reappears (White 1997).

These gross changes in seafloor spreading style on timescales of 10–20 Ma are probably related to large-scale changes either in the temperature and/or the flow rate of the mantle plume, or in the relationship between the narrow rising core of the mantle plume and the spreading axis. As we show later, superimposed on these major changes are shorter term fluctuations in the plume on timescales of 1–3 Ma, which generated prominent 'V-shaped' ridges on the Reykjanes Ridge (Vogt 1971).

Ridge jumps

We have already discussed the likelihood of small ridge jumps during the initial few million years of seafloor spreading. However, in the Irminger and Iceland basins there is little indication of resolvable ridge jumps thereafter, apart from the small changes in the spreading axis that must have occurred as the spreading regime reoriented from linear to segmented and back again.

There is a long history of major ridge jumps in the region close to the core of the Iceland plume, in the Greenland–Iceland–Faroes Ridge itself. This was produced above the region of hottest mantle, with temperature anomalies of perhaps 150°C above normal. So it may be no coincidence that the most frequent ridge jumps elsewhere in the Iceland and Irminger basins are recorded from the first few million years of seafloor spreading, when we infer that the mantle beneath the rifting continental margins and the newly-formed oceanic crust was hotter than in the succeeding period of seafloor spreading (Barton & White 1997*b*).

The best documented ridge jumps on Iceland are those which have moved the rift axes eastward so as to keep them centred approximately above the core of the mantle plume, as the plume has drifted eastward with respect to the spreading axis. Two major eastward ridge jumps have been documented in northern Iceland, one at *c.* 16 Ma from Vestfirdir to the Skagi Peninsula, and another during 7–3 Ma from the Skagi Peninsula to the present Northern Volcanic Zone (NVZ) (Saemundsson 1974, 1979; Helgason 1985; Hardarson *et al.* 1997) (see Fig. 2a for locations). Similar ridge jumps toward the east have occurred in south Iceland (Krisjánsson & Jónsson 1998), producing at the present day a *c.* 150 km eastward offset of the rift zones on Iceland compared to the offshore spreading centres of Reykjanes Ridge to the south and Kolbeinsey Ridge to the north (Fig. 2a). The ridge jumps do not occur as instantaneous transfers of spreading from the old rift axis to the new one, but rather occur over a period (estimated as *c.* 4 million years for the most recent ridge jumps of the NVZ), during which spreading is distributed across both the old and the new rift zones.

There are also several other more tentative identifications of ridge jumps on the portions of the Greenland–Iceland–Faroes Ridge that are now underwater. Smallwood

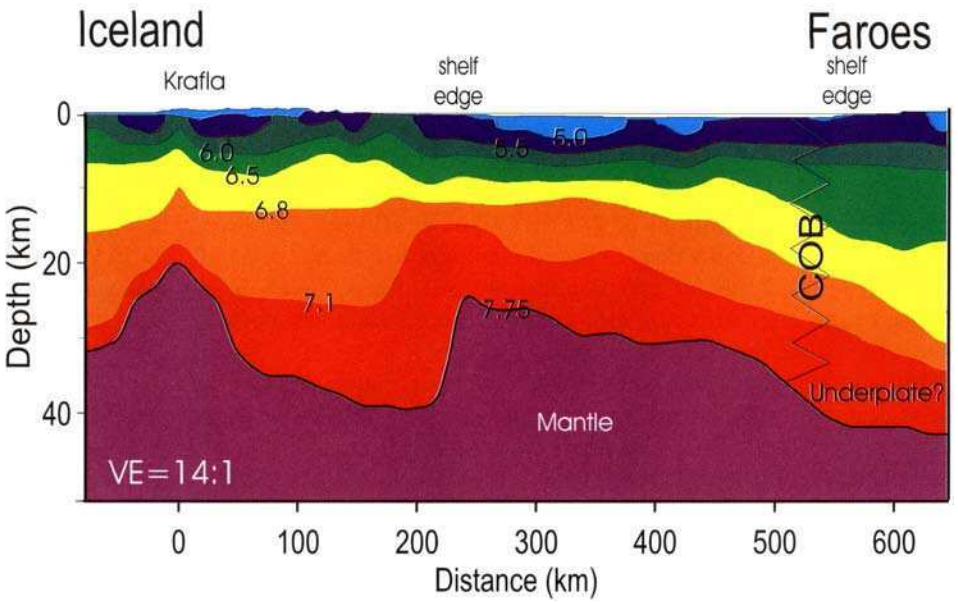

Fig. 5. Interpretation of crustal structure from seismic profile along FIRE line on the Faroes–Iceland Ridge (see Figure 2a for location and Smallwood *et al.* 1999 for details). Note the abrupt crustal thickness changes associated with ridge jumps, particularly near the Iceland shelf edge and the present Northern Volcanic Zone at Krafla. COB marks continent–ocean boundary offshore the Faroe Islands. Inferred region of underplating below the Faroes continental block is from Richardson *et al.* (1998). Zero on the distance scale is at the present rift axis under Krafla.

et al. (1999) have postulated at least two westward ridge jumps from the Faroes–Iceland Ridge, one of which is marked by a change in basement structure, and the other (at *c.* 40 Ma) at the position of the abrupt change in crustal thickness that lies beneath the present Icelandic shelf edge (Fig. 5). On the western side of Iceland, Larsen & Jakobsdóttir (1988) have identified a ridge jump on the Greenland–Iceland Ridge from an angular unconformity in the lavas.

This multiplicity of ridge jumps directly above the track of the core of the mantle plume is not mirrored in the regions to the north and south of the plume. This means that the thickened crust of the Greenland–Iceland–Faroes Ridge which formed above the plume core, is often bounded by transform faults of variable offset (Nunns 1983). At the present day, for example, the Tjörnes Fracture Zone off northern Iceland connects the Northern Volcanic Zone to the Kolbeinsey Ridge. Another consequence of the frequent ridge jumps is that they may cause abrupt changes in crustal thickness along the plume track. Where the rift zone lies directly above the narrow plume core, igneous crust of up to 40 km thickness may be generated, as is currently the case in Iceland (Darbyshire *et al.* 1998). Thus, the crustal thickness changes along the Greenland–Iceland–Faroes Ridge probably reflect both variations in the precise location of the rift axis with respect to the narrow core of the mantle plume, as well as long-term variations in the temperature or flow rate of the plume which, as discussed in the previous section, also affect the oceanic crust formed much further from the centre.

Short term plume fluctuations

A characteristic feature of the oceanic crust generated south of Iceland is that it exhibits prominent 'V-shaped' ridges in the bathymetry and gravity signatures (Fig. 2). These were first recognized by Vogt (1971). They propagate away from the plume core with apparent velocities of 75–150 mm a^{-1}, some 4–8 times faster than the full spreading rate. Geochemical and seismic data suggest that they are generated by crustal thickness variations of 1–2 km (White *et al.* 1995; Smallwood & White 1998; Weir *et al.* 2001), equivalent to mantle temperature fluctuations of *c.* 30°C, on timescales of 3–5 Ma. Similar gravity lineations can also be discerned in the oceanic crust formed soon after breakup, although the thicker sediment cover on the older crust tends to reduce their prominence.

Indirect effects of the short-term temperature fluctuations in the mantle can also be seen in two other ways. First, around breakup time in the Paleocene, the mantle temperature fluctuations produced rapid changes in uplift and subsidence in the regions bordering the rift zone, which have been used to explain pulses of sedimentation recorded particularly in fan deposits (White & Lovell 1997). Second, during the Neogene, regional variations in uplift associated with changes in the buoyancy flux of the Iceland plume have been invoked to explain changes in the amount of Northern Component water fed southward into the ocean basin south of Iceland (Wright & Miller 1996): the Greenland–Iceland–Faroes Ridge acted as a barrier to this oceanographic flow during periods of uplift associated with high buoyancy flux from the Iceland plume, but was lowered and thus allowed passage of the Northern Component water during periods of reduced mantle buoyancy flux.

It therefore seems that small-scale, relatively short-term fluctuations in the mantle temperature have been a consistent feature of the Iceland plume throughout its history. It is likely that similar fluctuations occur in all mantle plumes, but that they can be detected well in the North Atlantic because the plume has lain for a long period directly beneath the seafloor spreading centre: in this configuration the passive mantle decompression that occurs in the spreading axis is an extremely sensitive measure of small temperature changes.

Seafloor spreading rates

There have been suggestions that not only was the duration of the breakup stage very short, but that the initial rate of seafloor spreading was extremely high, reaching 88 mm a^{-1} full rate for a period of three million years immediately following breakup (from *c.* 55.3–52.3 Ma), before dropping back to the full spreading rate of *c.* 22 mm a^{-1} found regionally in the northern North Atlantic for the interval between chrons 23n and 20n (Larsen & Saunders 1998). This short-lived, extremely high spreading rate episode is determined only from an aeromagnetic survey off the east Greenland margin, based on lineations seen in the aeromagnetic map and on radiometric age determinations from basalts drilled in ODP sites 915, 917 and 918.

We discuss here an alternative explanation of the magnetic and other data that suggest that spreading rates immediately after breakup reached only 25–30 mm a^{-1} full rate, decreasing only slightly after chron 21 (47 Ma) to an average of *c.* 20 mm a^{-1}.

We calculate half-spreading rates from two magnetic anomaly profiles recorded along flowlines which extend from the continental margin to the present seafloor spreading axis in the Iceland Basin. Profile A is from *RRS Charles Darwin* cruise 70

and Profile B from *RRS Charles Darwin* cruise 87 (for location see Fig. 2a). We also use identifications from the regional magnetic anomaly maps (Fig. 2c) (MacNab *et al.* 1995), and from a detailed aeromagnetic survey in the Irminger Basin (Mercuriev *et al.* 1994).

Anomaly identifications were aided by first constructing a synthetic magnetic anomaly profile, including an appropriate skewness for the magnetic latitude at which the crust was generated (Fig. 6). Our identifications of the anomaly peaks are shown above profiles A and B in Figure 6. Note that the anomaly picks on the oldest oceanic crust closest to the COB have some uncertainty, due to them being close to

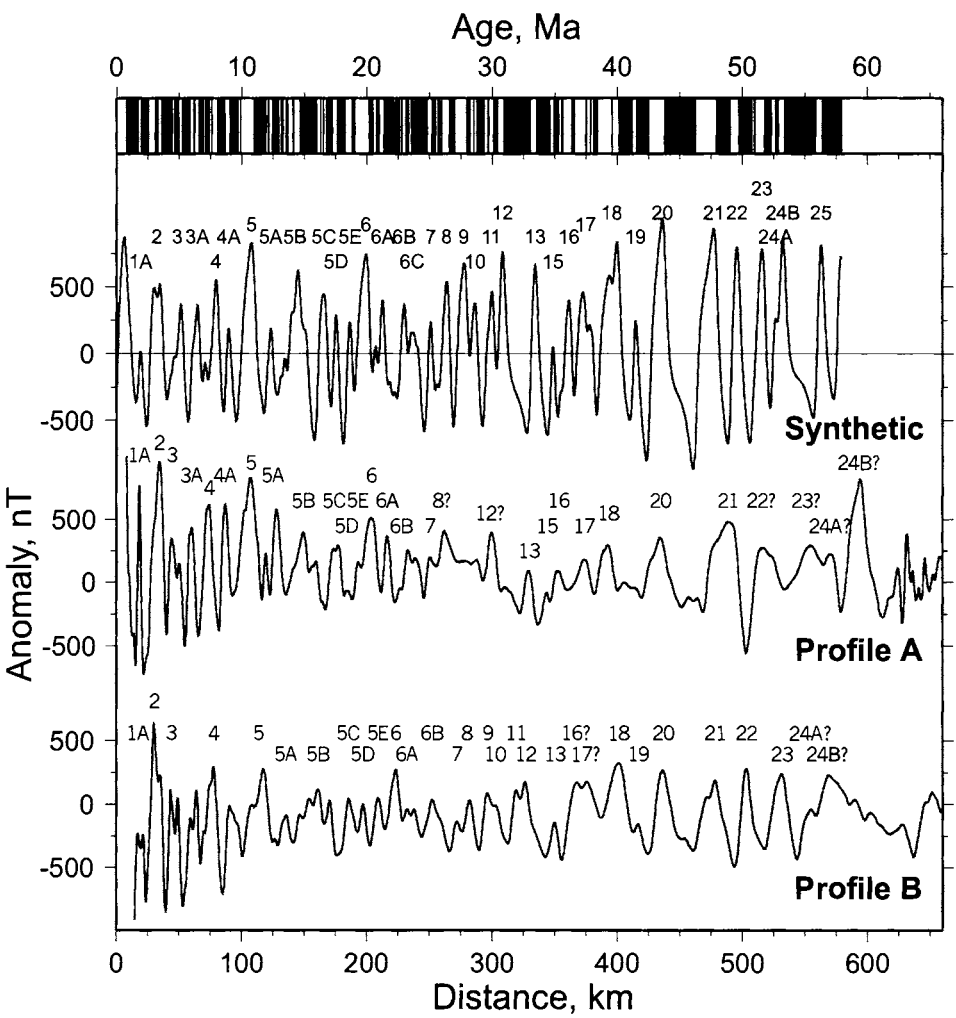

Fig. 6. Magnetic anomaly flowline profiles. Top curve shows synthetic for a constant spreading half-rate of 10 mm a^{-1} using the reversal timescale from Cande & Kent (1995), with a constant thickness and uniform magnetization source layer and with a skewness of 42° to allow for the latitude at which the anomalies were formed. Bottom two curves show magnetic anomalies across the Iceland Basin along profiles A and B; see Figure 2a for locations. Anomaly identifications are annotated above each profile.

the end of the seafloor spreading anomalies, and to the possible 'smearing' by lateral lava flow in the seaward dipping reflectors, together with possible diffuse spreading or minor ridge jumps in the earliest stage of seafloor spreading. Spreading rates from the two flowline magnetic anomaly profiles are compared in Figure 7 with the rates calculated at the same latitudes from the Greenland–Eurasian rotation poles used to make the reconstructions in Figure 3.

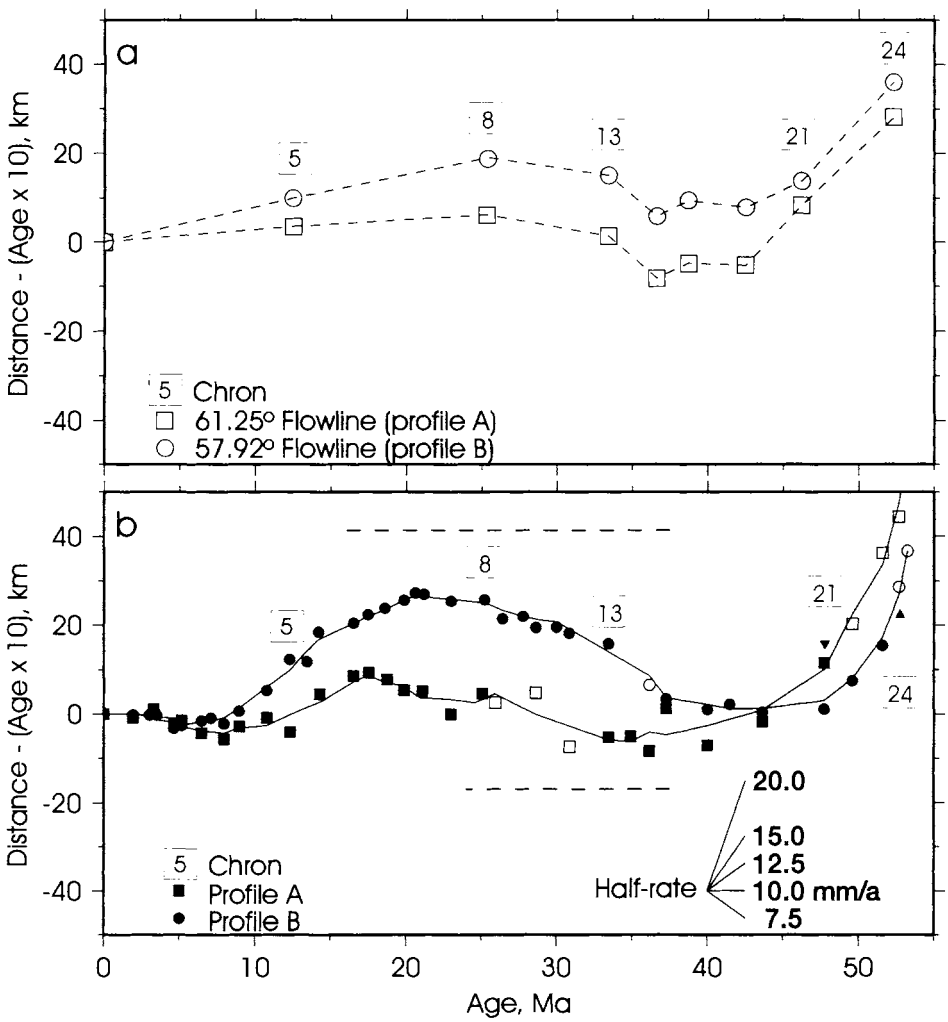

Fig. 7. Distance along flowline v. magnetic chron age (Cande & Kent 1995 timescale modified by Shackleton *et al.* 2000) for two flowlines across the Iceland Basin. In both plots the distance is reduced at $10\,mm\,a^{-1}$, and the gradient gives spreading rate (see key). (**a**) Calculated rates from our rotation poles (see text for details); (**b**) Observed rates from anomaly identifications on profiles A and B. Tentative anomaly identifications are shown with open symbols. The lines show a 3-point smoothing filter fit to the data points. Estimated error on points is ±2 km. The thick dashed line indicates the period when the spreading centre was segmented for the profile A (below) and profile B (above).

Half-spreading rates along our magnetic anomaly flowlines stabilise after anomaly 21 (47 Ma) to *c.* 10 mm a^{-1}. Similar rates are found from both sides of the ocean, showing that spreading about the axis was symmetric. However, during the initial period of seafloor spreading the half-rates were appreciably higher. Over the period between anomalies 24 and 21, we deduce half-rates of about 15 mm a^{-1} from our magnetic profiles (Fig. 7). We suggest that during the period from continental breakup at about 55 Ma to anomaly 23n (52 Ma), the spreading rate was only half of the rate of 88 mm a^{-1} suggested by Larsen & Saunders (1998), because they failed to recognize a ridge jump that occurred in the middle of generating the seafloor magnetic lineations that they report from off the east Greenland margin. Such a ridge jump is necessary to explain the production of *c.* 100 km of oceanic crust between the Greenland COB and the end of the flowlines at anomaly 24 time off the Greenland margin, since on the Eurasian side the end of the flowlines lie close to the Eurasian COB (Fig. 2). With the identification of this ridge jump all along the east Greenland margin, the observed half-spreading rate during this early interval, using the same ages as Larsen & Saunders (1998), drops to 22 mm a^{-1}. This is just a little higher than the half rate of 15 mm a^{-1} we find for the period immediately succeeding it. As we noted in an earlier section, ridge jumps apparently occur more readily above the hottest mantle, such as beneath Iceland at the present day, so the ridge jumps off the Greenland margin are consistent with our observation that transient abnormally hot mantle lay beneath the line of continental breakup in the early Tertiary.

There is also some evidence in the seismic reflection profiles off Greenland (Larsen *et al.* 1998) for this ridge jump during anomaly 24r. In the central part of the 100 km portion of oceanic crust seaward of the Greenland COB containing seaward dipping reflectors is a zone of diffuse reflectivity which Larsen *et al.* (1998) interpret as a period when the seafloor spreading axis may have been submarine. They suggest that the remainder of the seaward dipping reflector sequence was generated with the seafloor at or above sea level. Consequently, this central diffuse zone may correspond to our postulated ridge jump, since the dying rift axis would sink below sea level as the magma productivity decreased. The new rift axis further to the east would then produce more voluminous lavas and seaward dipping reflectors that would flow across and overwrite the reflections from the older oceanic crust beneath them formed prior to the ridge jump. If the ridge jump did not occur as an instantaneous transfer from the old to the new rift axis, but rather went through an interval of simultaneous spreading as the old rift died down and the new one started up, there is a high likelihood of generating a diffuse zone of confused reflectivity in the region of the now extinct rift axis. Such a zone of confused reflectivity is observed off east Greenland.

Discussion

Interaction between the Iceland mantle plume and rifting, first of continental lithosphere, and subsequently of oceanic lithosphere, in the northern North Atlantic region allows us to investigate the long-term behaviour of a mantle plume.

At the time of initiation of the Iceland plume at *c.* 62 Ma, the asthenospheric mantle fed by the plume was much more extensive and hotter than the subsequent plume flow that characterized its behaviour throughout the rest of the Tertiary. This is a feature of boundary layer instabilities, with both the flow rate and the

temperature of the initial instability being much greater than the subsequent flow. However, from the existing data we cannot determine whether the plume instability arose from the upper/lower mantle boundary or from the core/mantle boundary.

The initial anomalously hot plume material spread widely across the region: its geometry may have comprised rising sheets of hot mantle, or separate blobs. However, within a relatively short period of less than 10 Ma, the initial disturbance had collapsed to the axisymmetric shape typical of the present day configuration. This has a narrow (*c.* 100 km diameter) central core of mantle probably *c.* 100–150°C hotter than normal, with a wide surrounding region of plume-fed asthenospheric mantle that is still hotter than normal mantle, but only by a few tens of degrees Celsius.

Several temporal scales of fluctuation can be recognised in the Iceland plume by their effects on the region. Long term fluctuations on the order of tens of millions of years produced regional changes in the structure of the oceanic crust. Shorter term fluctuations of temperature and flow-rate on 3–5 million years timescales can be recognized throughout the history of the Iceland plume and are probably characteristic of all such mantle plumes.

Where rifting has occurred directly above the mantle plume, ridge jumps are a common feature as the active rift migrates in an attempt to remain above the hottest upwelling mantle. This effect has been documented along extensive portions of the continental margin during continental breakup and during the early seafloor spreading history. Subsequently, it has been restricted to the crust formed directly above the upwelling plume core (which has produced the thickened crust of the Greenland–Iceland–Faroes Ridge). It is presumably a result of the higher gravitational potential and weaker lithosphere found directly above the plume core, which makes rifting in that location easiest. The prevalence of ridge jumps during the earliest phase of seafloor spreading is consistent with the widespread extent of abnormally hot mantle during and immediately following continental breakup.

The reconstructions in this contribution were made using the ATLAS computer program developed by Cambridge Paleomap Services. We are grateful to those who sailed on *RRS Charles Darwin* legs 70 and 87 for collecting the magnetic anomaly data. We thank Andy Saunders for his comments on an earlier draft of this paper, which led to significant improvement. The opinions and interpretations expressed herein are those of the authors and not necessarily those of Amerada Hess Ltd., Department of Earth Sciences, Cambridge contribution number 6382.

References

BARTON, A. J. & WHITE, R. S. 1997*a*. Volcanism on the Rockall continental margin. *Journal of the Geological Society, London*, **154**, 531–536.

BARTON, A. J. & WHITE, R. S. 1997*b*. Crustal structure of the Edoras Bank continental margin and mantle thermal anomalies beneath the North Atlantic. *Journal of Geophysical Research*, **102**, 3109–3129.

BOWN, J. W. & WHITE, R. S. 1995. Effect of finite extension rate on melt generation at rifted continental margins. *Journal of Geophysical Research*, **100**, 18 011–18 029.

BROZENA, J. M. 1995. *Kinematic GPS and aerogeophysical measurement: gravity, topography and magnetics*. PhD thesis, University of Cambridge.

CANDE, S. C. & KENT, D. V. 1995. Revised calibration of the geomagnetic polarity timescale for the Late Cretaceous and Cenozoic. *Journal of Geophysical Research*, **100**, 6093–6095.

CLIFT, P. D., TURNER, J. & OCEAN DRILLING PROGRAM LEG 152 SCIENTIFIC PARTY 1995. Dynamic support by the Icelandic plume and vertical tectonics of the northeast Atlantic continental margins. *Journal of Geophysical Research*, **100**, 24 473–24 486.

DARBYSHIRE, F. A., BJARNASON, I. TH., WHITE, R. S. & FLÓVENZ, Ó. G. 1998. Crustal structure above the Iceland mantle plume imaged by the ICEMELT refraction profile. *Geophysical Journal International*, **135**, 1131–1149.

DARBYSHIRE, F. A., WHITE, R. S. & PRIESTLEY, K. P. 2000. Structure of the crust and uppermost mantle of Iceland from a combined seismic and gravity study. *Earth and Planetary Science Letters*, **181**, 409–428.

HARDARSON, B. S., FITTON, J. G., ELLAM, R. M. & PRINGLE, M. S. 1997. Rift relocation – a geochemical and geochronological investigation of a palaeo-rift in NW Iceland. *Earth and Planetary Science Letters*, **153**, 181–195.

HELGASON, J. 1985. Shifts of the plate boundary in Iceland: some aspects of Tertiary volcanism. *Journal of Geophysical Research*, **90**, 10 084–10 092.

HELMAN, M. 1989. *Tectonics of the western Mediterranean*. D.Phil dissertation, Oxford University.

KENT, R. W., STOREY, M. & SAUNDERS, A. D. 1992. Large igneous provinces: sites of plume impact or plume incubation. *Geology*, **22**, 891–894.

KORENAGA, J., HOLBROOK, W. S., KENT, G. M., KELEMEN, P. B., DETRICK, R. S., LARSEN, H.-C., HOPPER, J. R. & DAHL-JENSEN, T. 2000. Crustal structure of the southeast Greenland margin from joint refraction and reflection seismic tomography. *Journal of Geophysical Research*, **105**, 21 591–21 614.

KRISJÁNSSON, L. & JÓNSSON, G. 1998. Aeromagnetic results and the presence of an extinct rift zone in western Iceland. *Journal of Geodynamics*, **25**, 99–108.

KRISTOFFERSEN, Y. & TALWANI, M. 1977. Extinct triple junction south of Greenland and the Tertiary motion of Greenland relative to North America. *Geological Society of America Bulletin*, **88**, 1037–1049.

LARSEN, H. C. & JAKOBSDÓTTIR, S. 1988. Distribution, crustal properties and significance of seaward dipping subbasement reflectors off East Greenland. *In*: MORTON, A. C. & PARSON, L. M. (eds) *Early Tertiary Volcanism and the Opening of the NE Atlantic*. Geological Society, London, Special Publications, **39**, 95–114.

LARSEN, H. C. & SAUNDERS, A. D. 1998. Tectonism and volcanism at the southeast Greenland rifted margin: A record of plume impact and later continental rupture. *In*: SAUNDERS, A. D., LARSEN, H. C. & WISE, S. W. JR. (eds) *Proceedings of the Ocean Drilling Program, Scientific Results*. College Station, Texas (Ocean Drilling Program), **152**, 503–533.

LARSEN, H. C., DAHL-JENSEN, T. & HOPPER, J. R. 1998. Crustal structure along the leg 152 drilling transect. *In*: SAUNDERS, A. D., LARSEN, H. C. & WISE, S. W. JR. (eds) *Proceedings of the Ocean Drilling Program, Scientific Results*. College Station, Texas (Ocean Drilling Program), **152**, 463–474.

LARSEN, L. M. WAAGSTEIN, R., PEDERSEN, A. K. & STOREY, M. 1999. Trans-Atlantic correlation of the Palaeogene volcanic successions in the Faroe Islands and East Greenland. *Journal of the Geological Society, London*, **156**, 1081–1095.

LARSEN, T. B., YUEN, D. A. & STOREY, M. 1999. Ultrafast mantle plumes and implications for flood basalt volcanism in the northern Atlantic region. *Tectonophysics*, **311**, 31–43.

LAWVER, L. A. & MÜLLER, R. D 1994. Iceland hotspot track. *Geology*, **22**, 311–314.

LEWIS, C. L. E., GREEN, P. F., CARTER, A. & HURFORD, A. J. 1992. Elevated K/T palaeotemperatures throughout northwest England: three kilometres of Tertiary erosion? *Earth and Planetary Science Letters*, **112**, 131–145.

LOUDEN, K. E., OSLER, J. C., SRIVASTAVA, S. P. & KEEN, C. E. 1996. Formation of oceanic crust at slow spreading rates: New constraints from an extinct spreading centre in the Labrador Sea. *Geology*, **24**, 771–774.

MACNAB, R., VERHOEF, J., ROEST, W. & ARKANI-HAMED, J. 1995. New database documents the magnetic character of the Arctic and North Atlantic. *EOS, Transactions, American Geophysical Union*, **76**, 449 and 458.

MERCURIEV, S. A., SOTCHEVANOVA, N. A., MACNAB, R., LÉVESQUE, S. & OAKEY, G. 1994. Evidence for a propagating rift in Irminger Basin near Reykjanes Ridge: detailed magnetic

and bathymetric investigations (abstract). *EOS, Transactions, American Geophysical Union*, **75**, suppl. no. 16, 131.

MÜLLER, R. D. & ROEST, W. R. 1992. Fracture zones in the North Atlantic from combined Geosat and Seasat data. *Journal of Geophysical Research*, **97**, 3337–3350.

MUTTER, J. C. & ZEHNDER, C. M. 1988. Deep crustal structure and magmatic processes: the inception of seafloor spreading in the Norwegian–Greenland sea. *In*: MORTON, A. C. & PARSON, L. M. (eds) *Early Tertiary Volcanism and the Opening of the NE Atlantic*. Geological Society, London, Special Publications, **39**, 35–48.

NADIN, P. A., KUSZNIR, N. I. & TOTH, J. 1995. Transient regional uplift in the Early Tertiary of the northern North Sea and the development of the Iceland plume. *Journal of the Geological Society, London*, **152**, 935–948.

NUNNS, A. G. 1983. Plate tectonic evolution of the Greenland–Scotland Ridge and surrounding regions. *In*: BOTT, M. H. P., SAXOV, S., TALWANI, M. & THIEDE, J. (eds) *Structure and Development of the Greenland–Scotland Ridge*. Plenum Press, New York, 11–30.

REID, I. D., DAHL-JENSEN, T., HOLBROOK, W. S., LARSEN, H. C., KELEMEN, P. H., HOPPER, P. R., KORENAGA, J., DETRICK, R. & KENT, G. 1997. 32–38 km thick mafic igneous crust beneath the Greenland–Iceland Ridge. *EOS, Transactions, American Geophysical Union*, **78**, 656.

RICHARDSON, K. R., SMALLWOOD, J. R., WHITE, R. S., SNYDER, D. & MAGUIRE, P. K. H. 1998. Crustal structure beneath the Faroe Islands and the Faroe–Iceland Ridge. *Tectonophysics*, **300**, 159–180.

RICHARDSON, K. R., WHITE, R. S., ENGLAND, R. W. & FRUEHN, J. 1999. Crustal structure east of the Faroe Islands. *Petroleum Geoscience*, **5**, 161–172.

ROEST, W. R. & SRIVASTAVA, S. P. 1989. Sea-floor spreading in the Labrador Sea: A new reconstruction. *Geology*, **17**, 1000–1003.

ROEST, W. R., VERHOEF, J. & MACNAB, R. 1995. Regional tectonics of the Arctic and North Atlantic oceans and adjacent land areas, as seen in new maps of compiled magnetic observations (abstract). *EOS, Transactions, American Geophysical Union*, **76**, 46 suppl., 74.

ROWLEY, E. WHITE, N. 1988. Inverse modelling of extension and denudation in the east Irish sea and surrounding areas. *Earth and Planetary Science Letters*, **161**, 57–71.

RUDDIMAN, W. F. 1972. Sediment redistribution on the Reykjanes Ridge: Seismic evidence. *Geological Society of America Bulletin*, **83**, 2039–2062.

SAEMUNDSSON, K. 1974. Evolution of the axial rifting zone in northern Iceland and the Tjörnes Fracture Zone. *Geological Society of America Bulletin*, **85**, 495–504.

SAEMUNDSSON, K. 1979. Outline of the geology of Iceland. *Jökull*, **2**, 7–28.

SANDWELL, D. T. & SMITH, W. H. F. 1997. Marine gravity anomaly from Geosat and ERS 1 satellite altimetry. *Journal of Geophysical Research*, **102**, 10039–10054.

SAUNDERS, A. D., FITTON, J. G., KERR, A. C., NORRY, M. J. & KENT, R. W. 1997. *In*: MAHONEY, J. J. & COFFIN, M. F. (eds). The North Atlantic Igneous Province. *American Geophysical Union*, Geophysical Monograph, **100**, 45–93.

SAUNDERS, A. D., STOREY, M., KENT, R. W. & NORRY, M. J. 1992. Consequences of plume-lithosphere interactions. *In*: STOREY, B. C., ALABASTER, T. & PANKHURST, R. J. (eds) *Magmatism and the Causes of Continental Break-up*. Geological Society, London, Special Publications, **68**, 41–60.

SMALLWOOD, J. R. & WHITE, R. S. 1998. Crustal accretion at the Reykjanes Ridge, 61–62°N. *Journal of Geophysical Research*, **103**, 5185–5201.

SMALLWOOD, J. R., STAPLES, R. K., RICHARDSON, K. R., WHITE, R. S. & FIRE WORKING GROUP. 1999. Crust generated above the Iceland mantle plume: from continental rift to oceanic spreading center. *Journal of Geophysical Research*, **104**, 22885–22902.

SMALLWOOD, J. R., WHITE, R. S. & STAPLES, R. K. 1998. Deep crustal reflectors under Reydarfjördur, eastern Iceland: Crustal accretion above the Iceland mantle plume. *Geophysical Journal International*, **134**, 277–290.

SHACKLETON, N. J., HALL, M. A., RAFFI, I., TAUXE, L. & ZACHOS, J. 2000. Astronomical calibration age for the Oligocene–Miocene boundary. *Geology*, **28**, 447–450.

SRIVASTAVA, S. P. & TAPSCOTT, C. R. 1986. Plate kinematics of the North Atlantic. *In*: VOGT, P. R. & TUCHOLKE, B. E. (eds) *The Geology of North America, M, The Western North Atlantic Region*. Geological Society of America, Boulder, 379–404.

STAPLES, R. K., WHITE, R. S., BRANDSDÓTTIR, B., MENKE, W., MAGUIRE, P. K. H. & MCBRIDE, J. H. 1997. Färoe–Iceland Ridge Experiment, 1. Crustal structure of northeastern Iceland. *Journal of Geophysical Research*, **102**, 7849–7866.

VOGT, P. R. 1971. Asthenospheric motion recorded by the ocean floor south of Iceland. *Earth and Planetary Science Letters*, **13**, 153–160.

VOPPEL, D., SRIVASTAVA, S. P. & FLEISCHER, U. 1979. Detailed magnetic measurements south of the Iceland–Faroe Ridge. *Deutschland Hydrograph Zeit*, **32**, 154–172.

WEIR, N. R. W., WHITE, R. S., BRANDSDÓTTIR, B., EINARSSON, P., SHIMAMURA, H. & SHIOBARA, H. 2001. Crustal structure of the northern Reykjanes Ridge and Reykjanes peninsula, south-west Iceland. *Journal of Geophysical Research*, **106**, 6347–6368.

WHITE, N. J. & LOVELL, B. 1997. Measuring the pulse of a plume with the sedimentary record. *Nature*, **387**, 888–891.

WHITE, R. S. 1992. Crustal structure and magmatism of North Atlantic continental margins. *Journal of the Geological Society, London*, **149**, 841–854.

WHITE, R. S. 1997. Rift-plume interaction in the North Atlantic. *Philosophical Transactions of the Royal Society, London*, Series A, **355**, 319–339.

WHITE, R. & MCKENZIE, D. 1989. Magmatism at rift zones: The generation of volcanic continental margins and flood basalts. *Journal of Geophysical Research*, **94**, 7685–7729.

WHITE, R. S. & MCKENZIE, D. 1995. Mantle plumes and flood basalts. *Journal of Geophysical Research*, **100**, 17 543–17 585.

WHITE, R. S., BOWN, J. W. & SMALLWOOD, J. R. 1995. The temperature of the Iceland plume and origin of outward propagating V-shaped ridges. *Journal of the Geological Society, London*, **152**, 1039–1045.

WOLD, C. N. 1995. Palaeobathymetric reconstruction on a gridded database: the northern North Atlantic and southern Greenland–Iceland–Norwegian sea. *In*: SCRUTTON, R. A., STOKER, M. S., SHIMIELD, G. B & TUDHOPE, A. W. (eds) *The Tectonics, Sedimentation and Palaeoceanography of the North Atlantic Region*. Geological Society, London, Special Publications, **90**, 270–302.

WRIGHT, J. D. & MILLER, K. G. 1996. Control of North Atlantic deep water circulation by the Greenland–Scotland Ridge. *Palaeoceanography*, **11**, 157–170.

This page intentionally left blank

Continental margin off Norway 62–75°N: Palaeogene tectono-magmatic segmentation and sedimentation

O. ELDHOLM[1,2], F. TSIKALAS[1] & J. I. FALEIDE[1]

[1] *Department of Geology, University of Oslo, PO Box 1047 Blindern, N-0316 Oslo, Norway (e-mail: olav.eldholm@geologi.uio.no)*
[2] *Institute of Solid Earth Physics, University of Bergen, Allegt 41, N-5007 Bergen, Norway*

Abstract: The development of rifted and sheared segments on the Norwegian continental margin between 62 and 75°N is spatially related to a distinct along-margin segmentation which is governed by transfer zones formed during the Late Jurassic–Early Cretaceous rift episode. In fact, these structures may represent a repeated structural inheritance going back to the Proterozoic. Complete lithospheric breakup near the Paleocene–Eocene transition was preceded by a rift episode which was probably initiated in the early to middle Campanian. It culminated with a massive, regional magmatic event during breakup characterized by eruption of thick lava sequences covering large areas along the continent–ocean transition. The Norwegian volcanic margin belongs to the North Atlantic Large Igneous Province formed by impingement of the Iceland plume on a lithosphere under extension. Offsets in the initial plate boundary, combined with late rift uplift and subsequent construction of emerged marginal highs during breakup, provide key constraints on the Palaeogene water mass circulation, basin evolution and sedimentation during a period of progressive environmental deterioration following early Eocene greenhouse conditions.

Early studies of the continental margin off Norway (Figs 1 & 2) revealed a first-order tectono-magmatic segmentation, apparently linking old crustal sutures and weakness zones with offsets in the initial Eurasia–Greenland plate boundary, and a structural division of the passive margin into rifted and sheared segments (Talwani & Eldholm 1972, 1977). Later, the margin has become the target of extensive geophysical surveying, both by research institutions and industry. Scientific holes have been drilled on the outer margin, and commercial wells on the shelf and in the Vøring Basin.

Within the study area, 62–75°N, we divide the margin into four main rifted segments: Møre, Vøring, Lofoten-Vesterålen and Vestbakken margins separated by the Jan Mayen, Bivrost and Senja fracture zones and their landward prolongations (Fig. 2). During chron 24r, near the Paleocene–Eocene transition, Late Cretaceous–Paleocene rifting culminated with onset of sea floor spreading between Norway and Greenland accompanied by massive, regional igneous activity. Subsequently, the passive margin evolved in response to subsidence and sediment loading during the post-Paleocene widening and deepening of the Norwegian–Greenland Sea. The combined pre- and post-opening histories have governed the present margin physiography, crustal structure, tectono-magmatic segmentation and sedimentation.

From: JOLLEY, D. W. & BELL, B. R. (eds) *The North Atlantic Igneous Province: Stratigraphy, Tectonic, Volcanic and Magmatic Processes*. Geological Society, London, Special Publications, **197**, 39–68. 0305-8719/02/$15.00

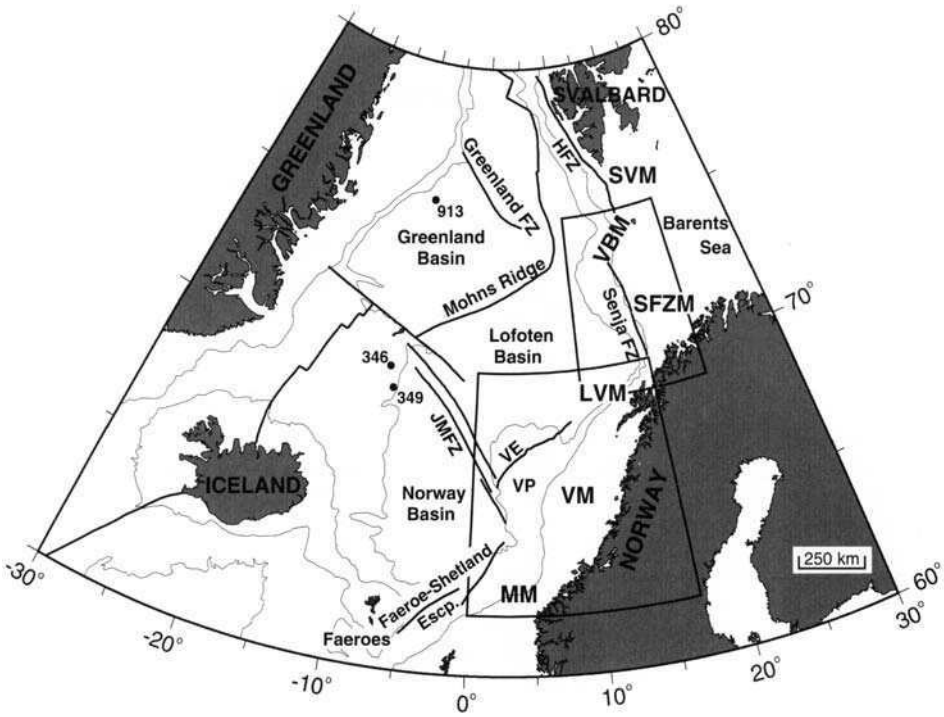

Fig. 1. Norwegian–Greenland Sea and continental margins, outlined by selected 500 and 2000 m contours, and conjugate DSDP/ODP drill sites sampling Palaeogene rocks. Study area (Figs 2 & 3) within boxes. MM, VM, LVM, SFZM, VBM, SVM, Møre, Vøring, Lofoten–Vesterålen, Senja Fracture Zone, Vestbakken and Svalbard margins, respectively; JMFZ, Jan Mayen Fracture Zone; VE, Vøring Escarpment; VP, Vøring Plateau; HFZ, Hornsund Fault Zone.

Physiographically, the high-latitude continental shelf is relatively deep, with numerous banks and depressions reflecting glacial influence. The width of the shelf, and the width and steepness of the continental slope varies considerably (Fig. 2). The shelf edge and the foot of the slope are well defined by bathymetric gradient changes except in areas of large glacial drainage systems. Off central Norway, the slope is broken by the large Vøring marginal plateau at 1000–1500 m water depth. The relatively young age of the Norwegian–Greenland Sea and the plate geometry explain the poorly developed abyssal plains and the absence of a continental rise in the adjacent Norway and Lofoten basins (e.g. Myhre *et al.* 1992).

Here, we first describe the crustal structure exemplified by crustal transects across main margin segments. Then, we discuss the pre-breakup basin formation history,

Fig. 2. Norwegian continental margin 62–75°N: main physiography, tectono-magmatic features, segmentation; and selected sea floor spreading magnetic anomalies in Norway and Lofoten basins. Abbreviations in Tables 1 and 3. FSE, Faroe–Shetland Escarpment; VE, Vøring Escarpment; GR, Gjallar Ridge; NH, Nyk High; HG, Hel Graben; LR, Lofoten Ridge; SH, Stappen High; FFC, Fles Fault Complex; OLD, Ormen Lange Dome; HHA, Helland Hansen Arch; VD, Vema Dome; ND, Naglfar Dome; VVP, Vestbakken Volcanic Province.

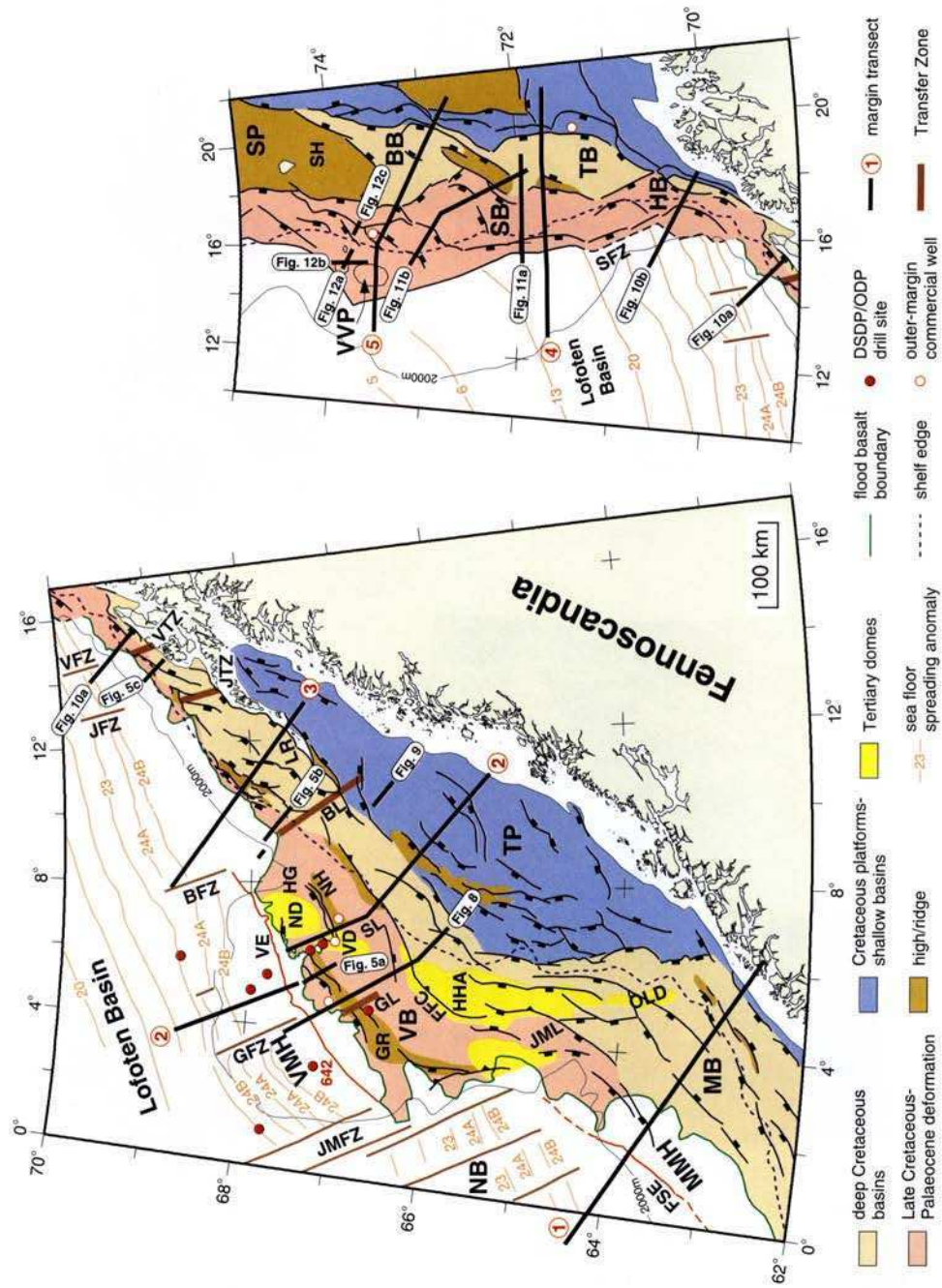
Fennoscandia
100 km
Lofoten Basin
VFZ
JFZ
BFZ
GFZ
JMFZ
VZ
JTZ
LR
BL
HG
NH
ND
VE
VD
SL
GL
GR
VB
FFC
HHA
VMH
642
TP
OLD
JML
MB
NB
MMH
FSE
SP
SH
BB
SB
TB
HB
SFZ
VVP
Fig. 5a
Fig. 5b
Fig. 5c
Fig. 8
Fig. 9
Fig. 10a
Fig. 10b
Fig. 11a
Fig. 11b
Fig. 12a
Fig. 12b
Fig. 12c
deep Cretaceous basins
Late Cretaceous-Palaeocene deformation
Cretaceous platforms-shallow basins
high/ridge
Tertiary domes
sea floor spreading anomaly
flood basalt boundary
shelf edge
DSDP/ODP drill site
outer-margin commercial well
margin transect
Transfer Zone

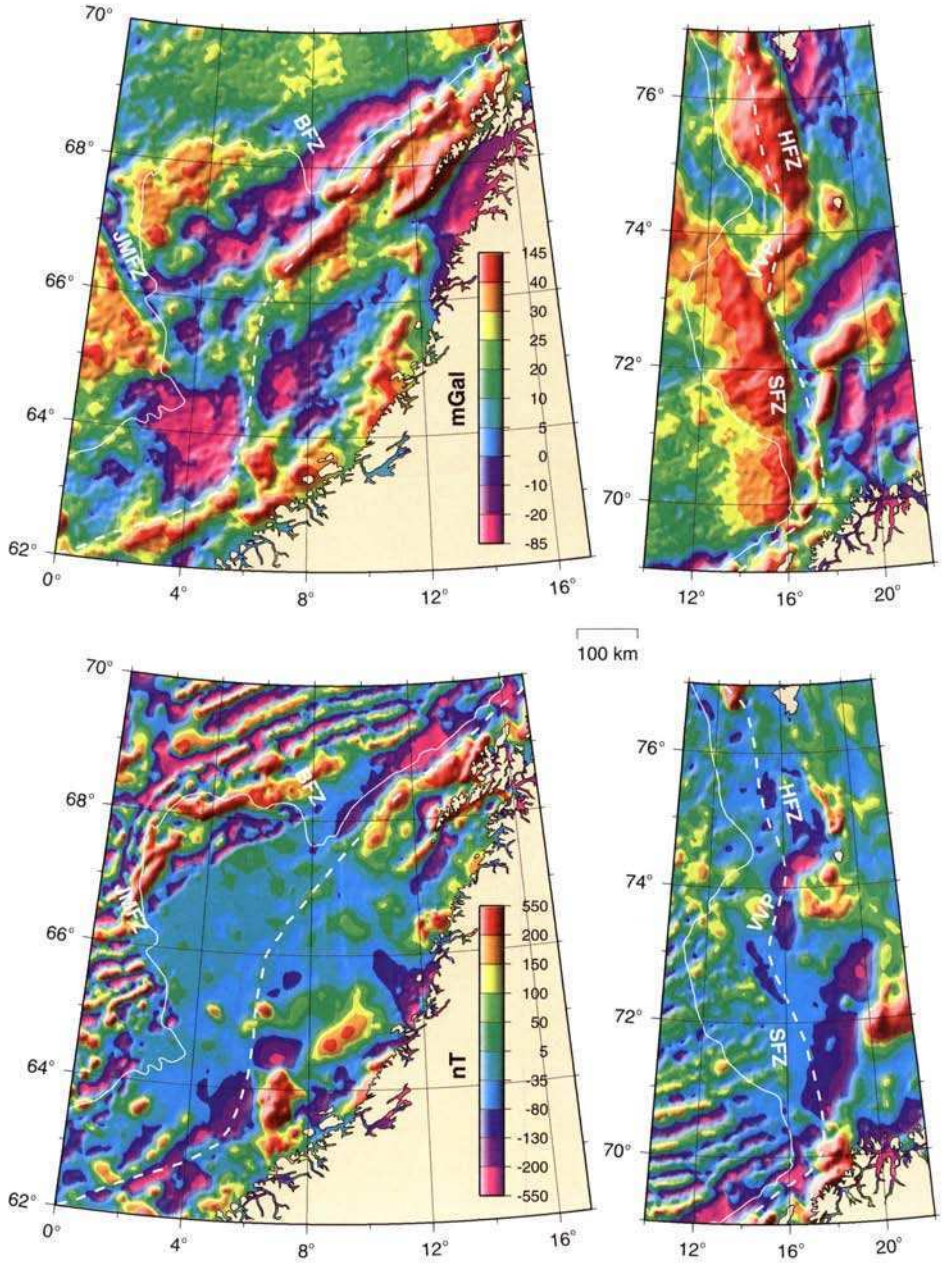

Fig. 3. $1 \times 1'$ grid free-air gravity south of 72°N (Sandwell & Smith 1997 V9.2) and $2 \times 2'$ grid north of 72°N (Andersen & Knudsen 1998) (top); and 5×5 km gridded magnetic (Verhoef *et al.* 1996) (bottom) anomaly fields. Note the maps extend to 77°N to outline the trend of the Hornsund Fault Zone, HFZ, along the Svalbard margin. The margin is outlined by the shelf edge and 2000 m contour in white. Abbreviations in Table 3. VVP, Vestbakken Volcanic Province.

and typical breakup-related tectono-magmatic features and events. Finally, we consider the post-opening margin evolution with an emphasis on the Palaeogene period. The analysis is based on a large amount of seismic and geological data, gravity and magnetic data (Fig. 3), and heat flow data (Sundvor *et al.* 2000). Although many papers cover these objectives in whole, or in part, we also refer to previous summary papers with a focus on: (1) regional aspects (Myhre *et al.* 1992; Blystad *et al.* 1995; Doré *et al.* 1999; Brekke 2000; Skogseid *et al.* 2000); (2) volcanic margin features and evolution (Eldholm *et al.* 1989, 1995); (3) sheared margins (Faleide *et al.* 1991, 1993*a*, *b*); and (4) environmental aspects (Eldholm *et al.* 1994). We apply the timescales of Gradstein *et al.* (1994) and Cande & Kent (1995).

Crustal structure

The five crustal transects across the main margin segments in Figure 4 are constructed from a comprehensive base of deep multichannel seismic (MCS) profiles and wide-angle seismic velocity-depth profiles combined with standard, depth-converted MCS profiles to obtain the upper crustal configuration. Figures 2 and 4 show that the continental margin segments are composed of different geological province types constituting distinct crustal blocks (Table 1).

The 6–10 km thick crystalline normal oceanic crust in the Norway and Lofoten basins (Eldholm & Mutter 1986; Jackson *et al.* 1990; Olafsson *et al.* 1992; Kodaira *et al.* 1995; Mjelde *et al.* 1996) approximates the 7.1 km world average of White *et al.* (1992), whereas the thickness near the coastline is about 30 km (Kinck *et al.* 1993). These end-members bound a continental margin where the crustal thickness is primarily governed by extensional deformation, magmatism and sediment loading. In particular, the voluminous igneous activity during breakup has left a distinct imprint on the rifted margin segments. Passive, rifted margins are commonly classified as volcanic margins if there is evidence of excessive, transient magmatic activity during final continental breakup and initial sea floor spreading. A lower crustal body (LCB) characterized by high seismic velocity, 7.1–7.7 km s^{-1} (Eldholm & Grue 1994; Mjelde *et al.* 1997, 1998) is characteristic for the outer parts of the volcanic margins. The top of the LCB has been imaged in deep MCS profiles (Skogseid & Eldholm 1995), whereas the Moho is determined from wide-angle profiles. Elsewhere the base of the crust is commonly recorded both by wide-angle profiles and MCS images. The

Table 1. *Main crustal province types (Figs 2 & 4) on the Norwegian margin, 62–75°N*

Crustal province type	Moho depth range, km	Geological province
Oceanic crust	12–15	Norway (NB) & Lofoten (LB) basins
Marginal High	22–25	Møre (MMH) & Vøring (VMH)
Cretaceous Basin	18–23	Møre (MB),Vøring (VB), Harstad (HB), Tromsø (TB), Bjørnøya (BB) & Sørvestsnaget (SB)
Pre-Cretaceous Platform	26–28	Trøndelag (TP) & Svalbard (SP)
Exposed continental basement	>30	Fennoscandia
	c. 20	Lofoten–Vesterålen Islands

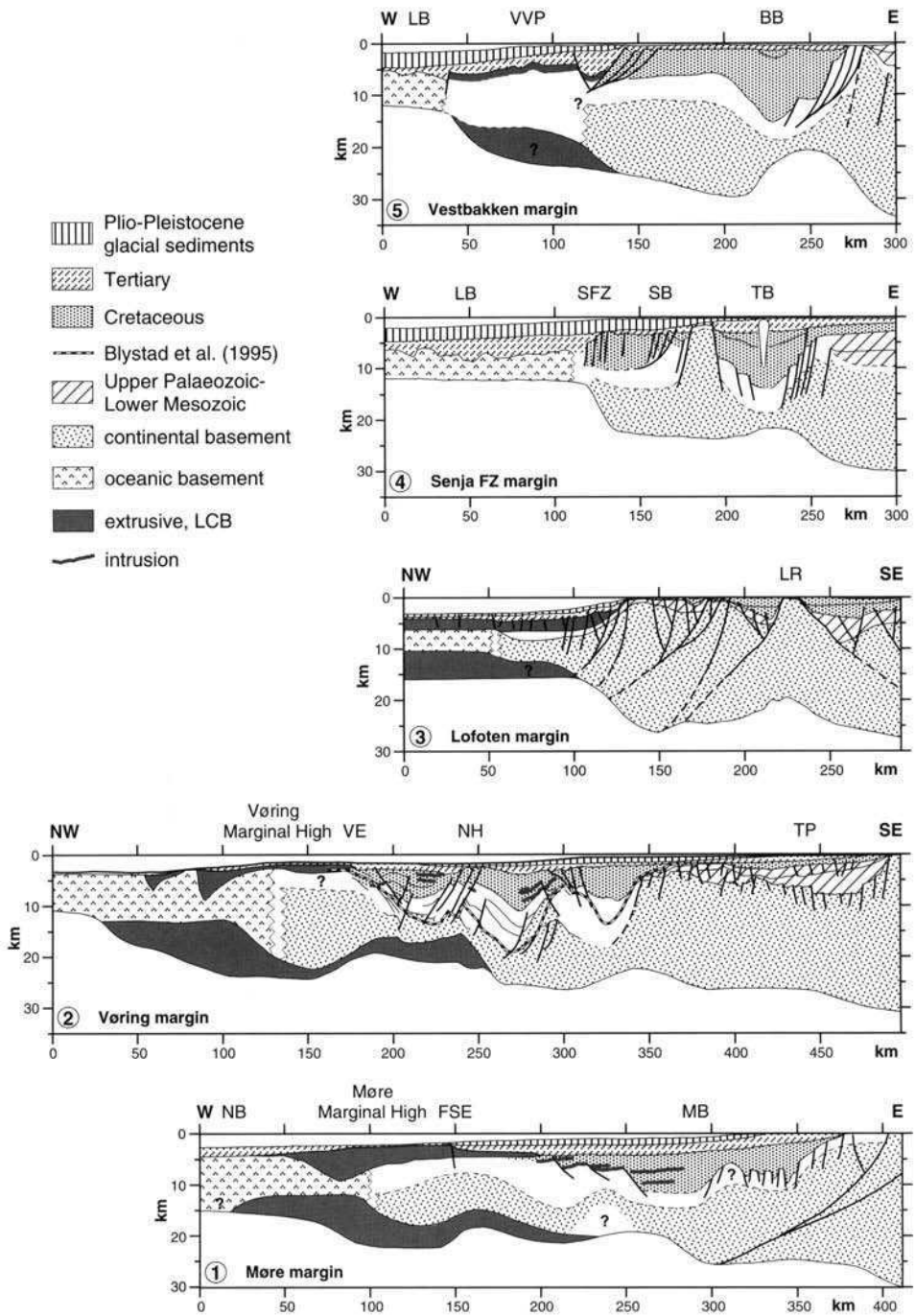

Fig. 4. Margin transects representative of typical rifted (Møre, Vøring, Lofoten, Vestbakken) and sheared (Senja Fracture Zone) margin segments (Figs 1 & 2). In the Vøring Basin we show both the base Cretaceous level of Skogseid *et al.* (1995) and Blystad *et al.* (1995). The base crust in the two northern transects is in part from gravity modeling (Breivik *et al.* 1998, 1999). Abbreviations in Figures 1 and 2.

LCB is best developed on the Møre and Vøring segments where it forms the lower part of the thickened crust beneath the marginal highs, continuing east below the crust that was extended and thinned prior to breakup (Fig. 4).

The transition from oceanic to continental crust differs considerably between the rifted and sheared margin segments. The change from the top of oceanic to continental crystalline basement, the continent–ocean boundary (COB), is restricted to 5–10 km wide zone along the sheared Barents Sea margin (Faleide *et al.* 1993*a*, *b*). It is underlain by a distinct zone of steeply dipping Moho between oceanic and continental levels, i.e. the continent–ocean transition (COT) (Jackson *et al.* 1990; Faleide *et al.* 1991, 1993*b*). On the rifted segments, the lava-covered COB is commonly placed landward of anomaly 24 at the seaward termination of a base reflector below the inner parts of typical seaward dipping wedges of basalt flows. The position is less clear in the Vestbakken Volcanic Province where seaward dipping wedges and sea floor spreading anomalies have not yet been identified at the marginal high (Faleide *et al.* 1991, Jebsen 1998) (Figs 2 & 4). The COT on the rifted segments includes both the thickened oldest oceanic crust and the pervasively intruded continental crust landward of the COB (Fig. 4) (Eldholm *et al.* 1995).

Pre-breakup basin formation

The margin evolved within a region which has undergone successive periods of regional lithospheric extension since the post-Caledonian orogenic backsliding and collapse in Devonian times. These periods were followed by subsidence and basin formation leading to a series of pre-opening sedimentary basins within the North Atlantic–Arctic region (Doré *et al.* 1999; Roberts *et al.* 1999).

The pre-opening, structural margin framework is dominated by the prominent NE Atlantic–Arctic Late Jurassic–Early Cretaceous rift episode setting the stage for the development of major Cretaceous basins such as the Møre and Vøring basins off Norway, and the Harstad, Tromsø, Sørvestsnaget and Bjørnøya basins in the SW Barents Sea (Fig. 2). However, the seismic and well control in these basins becomes less substantive in the Lower Cretaceous, particularly on the outer margin. There is yet no consensus about the base Cretaceous level in the central and western Møre and Vøring basins. In fact, Vøring Basin models vary by several kilometers in depth as shown in Figure 4 (cf. Ren *et al.* 1998). Thus, large uncertainties may exist in pre-Cretaceous sediment thickness estimates and in the depth to crystalline basement which in most cases is inferred from the seismic velocity-depth distribution (Eldholm & Mutter 1986; Jackson *et al.* 1990; Olafsson *et al.* 1992; Mjelde *et al.* 1998).

Regional rift episodes off Norway have also been interpreted as being of Late Carboniferous to Permian times, and of Triassic to Jurassic age (Bukovics *et al.* 1984; Brekke & Riis 1987; Blystad *et al.* 1995). Moreover, the definition and the timing of the late Middle Jurassic to Early Cretaceous tectonism are under discussion. Late Middle Jurassic to earliest Cretaceous rifting is recognized by most authors (Blystad *et al.* 1995; Brekke *et al.* 1999; Brekke 2000), but there is less consensus on how far into Early Cretaceous time the extension continued. For example, Lundin & Doré (1997) and Doré *et al.* (1999) divide this episode into separate Late Jurassic and Early Cretaceous tectonic phases, suggesting that the Vøring Basin was mainly formed by subsidence following the latter phase. A similar tectonic evolution is recognized in

the Barents Sea, where Faleide *et al.* (1993*a*) also separate the main episode into Middle/Late Jurassic and Early Cretaceous phases.

In the North Atlantic realm, there is evidence for modest mid-Cretaceous extension in the Vøring Basin (Lundin & Doré 1997; Doré *et al.* 1999; Ren *et al.* in press), Lofoten–Vesterålen margin (Tsikalas *et al.* 2001), onshore East Greenland (Surlyk *et al.* 1981; Surlyk 1990), and SW Barents Sea (Faleide *et al.* 1993*a*). In particular, biostratigraphic data from the Vøring margin reveal a change from neritic to bathyal conditions and increase in sediment accommodation space change in the Aptian–Albian, attributed to eustatic sea-level rise and regional tectonism (Gradstein *et al.* 1999). Considerable quantities of sands were deposited on the basin flanks and around structural highs, particularly after a hiatus emanating from a mid-Cenomanian tectonic pulse. However, the regional character and the inter-relationships of the tectonism need further studies.

Breakup-related tectonism and magmatism

At the onset of the Late Cretaceous rifting, the area between Norway and Greenland was an epicontinental sea covering a region in which the crust had been attenuated by the multiple post-Caledonian rift events (Doré 1991). The Late Jurassic–Early Cretaceous rift, in particular, is characterized by considerable crustal extension and thinning (Faleide *et al.* 1993*a*; Skogseid 1994). Thus, the next major rift episode took place within a region of greatly accentuated lithospheric relief.

There is little direct tectono-stratigraphic evidence to precisely date the onset of the Late Cretaceous–Paleocene rift episode leading to complete lithospheric breakup. However, in the northern Vøring Basin Ren *et al.* (1998) and Skogseid *et al.* (2000) inferred that rifting occurred for a *c.* 20 Ma period prior to breakup at *c.* 55 Ma. Additional seismic interpretation and commercial drilling results on structural highs in the outer Vøring Basin (Fig. 2) made Ren *et al.* (in press) suggest onset of rifting at about 81 Ma and that the main period of brittle faulting, observed in the seismic data, occurred in the Campanian followed by smaller-scale activity towards breakup. On the other hand, Paleocene focussing of the extension toward the initial plate boundary may imply that part of the Paleocene brittle deformation is hidden beneath the breakup lavas (Fig. 2) as documented by local, rotated fault-blocks protruding the lava surface on the Lofoten–Vesterålen slope (Fig. 5) (Tsikalas *et al.* 2001). The Campanian rifting resulted in low-angle detachment structures that updome thick Cretaceous sequences and sole out at medium to deep intra-crustal levels on the Vøring and Lofoten–Vesterålen margins (Fig. 5), locally accompanied by core complex development near the Gjallar Ridge (Lundin & Doré 1997; Ren *et al.* 1998) and on the Lofoten–Vesterålen shelf (Tsikalas *et al.* 2001).

The extent of the breakup-related rifting north of Jan Mayen Fracture Zone is shown in Figure 2. Although similar features have not yet been documented in the outer Møre Basin, we now continue the extension into the basin (Fig. 2). We also predict that it continues farther southward below the lavas, noting that the distance between the landward lava boundary and the COB is larger than on the Vøring margin.

Fig. 5. Interpreted seismic profiles (Fig. 2) illustrating Late Cretaceous low-angle detachment systems beneath the Gjallar Ridge in the outer Vøring Basin (**a**) (Ren *et al.* in press); and on the Lofoten–Vesterålen margin (**b** and **c**) (Tsikalas *et al.* 2001).

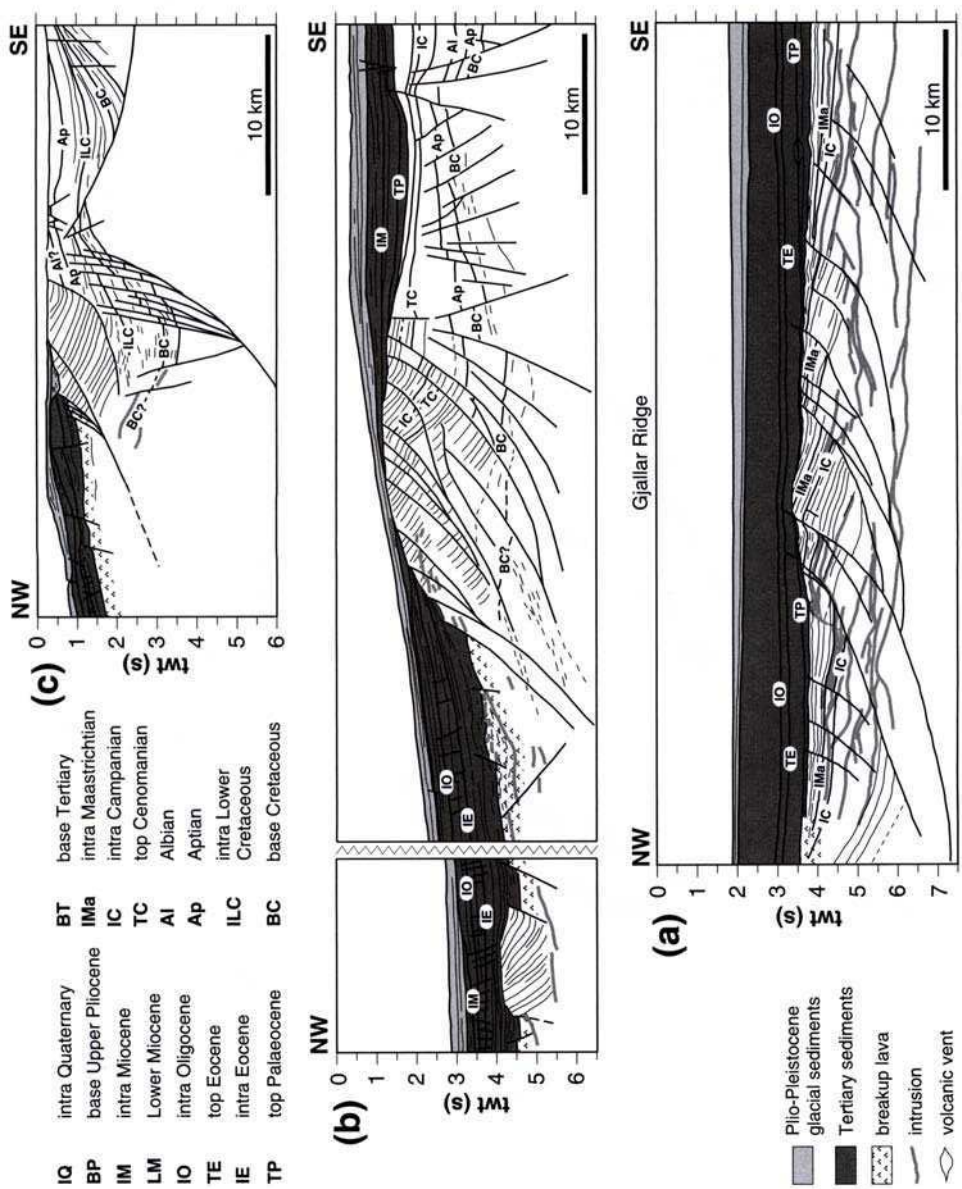
IQ intra Quaternary
BP base Upper Pliocene
IM intra Miocene
LM Lower Miocene
IO intra Oligocene
TE top Eocene
IE intra Eocene
TP top Palaeocene
BT base Tertiary
IMa intra Maastrichtian
IC intra Campanian
TC top Cenomanian
Al Albian
Ap Aptian
ILC intra Lower Cretaceous
BC base Cretaceous
(c)
NW
SE
twt (s)
10 km
(b)
(a)
Gjallar Ridge
Plio-Pleistocene glacial sediments
Tertiary sediments
breakup lava
intrusion
volcanic vent

South of 70°N, the Late Cretaceous–Paleocene rift obliquely cuts the Late Jurassic–Early Cretaceous rift zone. The nascent plate boundary constituted two mega-lineaments; the rifted Reykjanes–Mohn Lineament in the south and the transcurrent De Geer Lineament between the Barents Sea–Svalbard and NE Greenland farther north (Fig. 6). Subsidence and sediment deposition within the growing rift continued into Paleocene time when the Iceland Plume approached the base of the lithosphere (Skogseid *et al.* 1992; Saunders *et al.* 1997) inducing dynamic and thermal uplift of the rift basins. When the plume head material preferentially migrated into the pre-existing region of thinned lithosphere, decompressional partial melting accelerated, and culminated with massive subaerial volcanism during breakup and early sea floor spreading (Fig. 6). The change in thermal regime in the continental lithosphere caused by the approaching and impinging plume may have affected the rheology of the continental crust (Buck *et al.* 1988; Pedersen & Skogseid 1989), thus contributing to a change from brittle to more ductile extensional deformation from Campanian to Paleocene times.

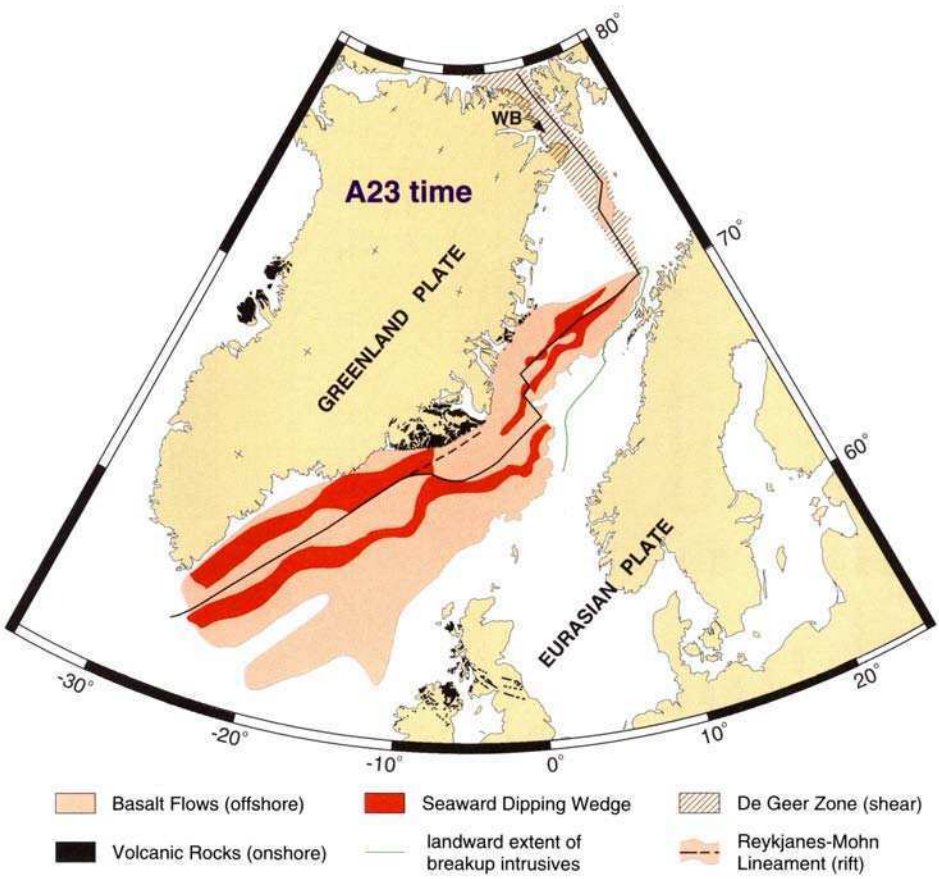

Fig. 6. North Atlantic Large Igneous Province extrusive cover shown in an anomaly 23 plate reconstruction, *c.* 3.5 Ma after breakup, modified from Eldholm & Grue (1994). Eastern limit of sill and low-angle dyke province off Norway from Berndt *et al.* (2001) and Tsikalas *et al.* (2001). WB, Wandel Sea Basin.

Table 2. *Manifestations of Early Tertiary igneous breakup activity on the Norwegian margin*

- Continental flood basalts
  - associated intrusives
- Extrusive complexes along COT
  - seaward dipping wedges, subhorizontal units
  - associated intrusives
- Sills and low-angle dykes in pre-Eocene basin sediments
- Regional tephra horizons
  - vents
- Thick initial oceanic crust
- High-velocity lower crustal bodies

Onshore and offshore studies combined with scientific drilling show that the rifted volcanic margins in Figure 2 belong to the North Atlantic Large Igneous Province (cf. Eldholm *et al.* 1989; White & McKenzie 1989). The magmatism was initiated at about 62–60 Ma by sporadic, and small volume melting of variable compositions (Saunders *et al.* 1997), followed by an intense, breakup phase producing voluminous mafic melts lasting 1–1.5 million years, gradually changing into waning, small-volume melting of variable compositions. About three million years after breakup the system returned to relatively normal mid-oceanic ridge production rates and the injection center had subsided to the NE Atlantic mid-oceanic ridge depth. The igneous breakup activity is manifested by a number of features (Table 2) of which the extrusive constructions, including huge wedges of seaward dipping lava flows, are among the most spectacular in the seismic records (Figs 4 & 6). The present remains of the basaltic lavas cover an area of at least 1.6×10^6 km^2 (Eldholm & Grue 1994). Spatially, there appears to be a correlation of pre-breakup rift structures, intrusive distribution and the LCB. Note that the LCB is part of both the oceanic crust formed during the intense breakup phase and the pre-existing, thinned continental crust (Fig. 4) where it is commonly interpreted as an underplated layer (White & McKenzie 1989), i.e. melts ponded at the base of the continental crust. Alternatively, the LCB may represent a body of layered intrusions (Handy & Strait 1999; Berndt *et al.* 2000).

Margin segmentation

The first-order rifted and sheared margin framework in Figures 2–4, defined by offsets in the early Eocene plate boundary, is complemented by cross-margin structural features or lineaments separating margin segments of different along-margin tectono-magmatic style and sediment distribution. Most of these features appear to be associated with pre-opening transfer or accommodation zones demarcating transverse or oblique structural elements in extensional terrains (Lister *et al.* 1986, 1991; Rosendahl 1987). The transfer zones within extended continental crust are commonly spatially connected to early opening, small-offset fracture zones (Table 3). Following Tsikalas *et al.* (2001) we use the term transfer system to include both the transfer zone and the fracture zone. We stress that the fracture zone trend may represent a different stress regime; thus it may differ from that of the transfer zone while the initial fracture zone location is governed by the older zone of weakness.

Table 3. *Main cross-margin features associated with along-margin segmentation*

Fracture zone	Transfer zone	Main deformation period
Jan Mayen (JMFZ)	Jan Mayen Lineament (JML)	Late Jur.–Early Cr.
Gleipne (GFZ)	Gleipne Lineament (GL)	Late Cr.–Paleocene
	Surt Lineament (SL)	Late Cr.–Paleocene
Bivrost (BFZ)	Bivrost Lineament (BL)	Late Jur.–Early Cr.
Jennegga (JFZ)	Jennegga (JTZ)	Late Jur.–Early Cr.
Vesterålen (VFZ)	Vesterålen (VTZ)	Late Jur.–Early Cr.
Senja (SFZ)	De Geer Zone	Pre-Tertiary, Eocene
Hornsund Fault Zone (HFZ)	De Geer Zone	Pre-Tertiary, Eocene–Miocene

In the south, complete continental separation along the Jan Mayen Fracture Zone (Skogseid & Eldholm 1987) was achieved in the early middle Eocene, *c.* 48 Ma. Its landward prolongation, the Jan Mayen Lineament (Blystad *et al.* 1995), offsets large, positive gravity and magnetic anomaly belts more than 200 km in a left-lateral sense (Figs 2 & 3) probably reflecting Palaeozoic or older crustal lineaments (Talwani & Eldholm 1972). Similarly, the Mesozoic basin axes are shifted westward and Torske & Prestvik (1991) suggested that the lineament represents a transfer zone separating opposing, pre-opening, simple-shear detachment systems in the Møre and Vøring basins.

The landward prolongation of the Gleipne Fracture Zone is described as a diffuse Late Cretaceous–Paleocene structural lineament, whereas the coeval Surt Lineament farther north (Fig. 2, Table 3) marks a change in fault polarities between the Gjallar Ridge and the Hel Graben, offsetting the Gjallar Ridge and Nyk High fault complexes (Ren *et al.* in press). The Surt Lineament coincides with a change in magnetic signature (Doré *et al.* 1997) and it may be a basement-controlled feature (Brekke *et al.* 1999).

The Vøring and Lofoten-Vesterålen margins are separated by the Bivrost transfer system. Structurally, the fracture zone marks the northern termination of the Vøring Plateau and the Vøring Marginal High, and thus also the Vøring Escarpment. The Bivrost Lineament represents a dextral shift in main structural elements which may have been rejuvenated during several tectonic episodes (Blystad *et al.* 1995).

The Lofoten–Vesterålen margin contrasts with the adjacent margins in terms of physiography, crustal structure, sediment distribution and history of vertical motion (Talwani & Eldholm 1972; Eldholm *et al.* 1979; Løseth & Tveten 1996), making it a separate tectono-magmatic entity. However, analysis of seismic and potential field data by Tsikalas *et al.* (2001) shows that it consists of three separate segments, the Lofoten, Vesterålen, and Andøya segments, defined by pre-opening NNW-trending, Late Jurassic–Early Cretaceous transfer zones (Fig. 2). The normal fault polarity changes from seaward- to landward-dipping across the Jennegga transfer zone, accompanied by a decrease in fault intensity; whereas the Vesterålen transfer zone marks a change in polarity to seaward-dipping and a further decrease in fault intensity. The transfer zones correspond to the small-offset, early opening Jennegga (Mokhtari & Pegrum 1992) and Vesterålen (Tsikalas *et al.* 2001) fracture zones (Fig. 2, Table 3).

The Senja Fracture Zone lies within the De Geer Zone (Harland 1969; Faleide *et al.* 1993*a*), a mega-shear system linking the North Atlantic and Arctic prior to breakup (Fig. 6). The fracture zone was first mapped beneath an elongate isostatic gravity high on the continental slope in a conjugate position to the oceanic Greenland Fracture Zone (Fig. 1) (Talwani & Eldholm 1977). Seismic data have later defined the COB at the landward flank of the anomaly (Faleide *et al.* 1991). Nonetheless, the regional shear zone may be composed of several segments offset by small rift segments forming a series of pull-apart basins east of the COB (Faleide *et al.* 1993*a*, *b*). Southwest of Bjørnøya, the COB is shifted to the east by a rifted margin segment, the Vestbakken Volcanic Province (Figs 2–4), characterized by smooth, opaque basement interpreted as lavas extruded during breakup (Faleide *et al.* 1988, 1991). Farther north, the westernmost fault block of the Hornsund Fault Zone has been interpreted as the COB. The fault zone was a shear zone during the Eocene, but later developed into a series of NNW-trending normal faults east of the COB in response to the change in relative plate motion in the earliest Oligocene (Myhre & Eldholm 1988).

Except for the Gleipne and Surt lineaments, there is little evidence for major deformation along the transfer zones in Late Cretaceous–Paleocene time. Hence, the present margin segmentation is largely inherited from the Late Jurassic–Early Cretaceous structural patterns. Nonetheless, the combined offshore and onshore data indicate that the structural inheritance may extend much farther back in time. For example, the prominent elongate gravity and magnetic shelf edge anomalies offset by the Jan Mayen Lineament (Figs 2 & 3) may reflect intra-basement high-density bodies of probable Precambrian age and/or basement relief (Talwani & Eldholm 1972). Moreover, the Senja Fracture Zone has been considered as the prolongation of the Bothnian–Senja fault complex, an Early Proterozoic shear zone across the Baltic Shield (Henkel 1991; Zwaan 1995); and most other transfer zones have gravity and/or magnetic signatures that may suggest some basement relief (Olesen *et al.* 1997; Fichler *et al.* 1999; Tsikalas *et al.* 2001).

Palaeogene margin evolution, environment and sedimentation

Although a continental margin is a post-opening feature, we also include the preceding rift episode for consistency. Following some general inferences, we discuss the rift- and shear-dominated margins, i.e. the margins off Norway and the Barents Sea, separately.

The initial and early, i.e. Palaeogene, margin history and segmentation is dependent on both the state of the lithosphere prior to the onset of the Late Cretaceous extension and the tectono-magmatic events during rifting and breakup. In addition, the plate boundary configuration during the early opening and the sediment supply are important parameters. However, the history of the Norwegian margin must also take into account that the complex interaction of tectono-magmatic, erosional and depositional processes took place during a period of major climatic change. The Cenozoic depositional margin history comprises three main stages (Hjelstuen *et al.* 1999*a*): (1) Paleocene–early Eocene rift province uplift, breakup volcanism and restricted basin sedimentation during a climatic maximum culminating during the early Eocene greenhouse; (2) middle Eocene–Early Pliocene margin subsidence and relatively modest sedimentation during a period of climatic decline;

and (3) Late Pliocene–Pleistocene Northern Hemisphere glaciation resulting in deep continental erosion, and very high sedimentation rates and large-scale sedimentary fan construction.

The plate tectonic evolution provides first-order boundary conditions for palaeoceanography and sedimentation in the Norwegian–Greenland Sea and its continental margins (Eldholm *et al.* 1994). The Palaeogene water mass circulation was governed by a pronounced *along-margin* ocean basin segmentation caused by offsets in the initial plate boundary, the change in relative plate motion near the Eocene–Oligocene transition, local migration of the mid-ocean ridge axis, and the subsidence of the Greenland–Faroe Ridge. In addition, the regional uplift along the initial plate boundary and the subsequent formation of emerged marginal highs along several of the rifted segments created important *across-margin* barriers (Fig. 7). This system of across- and along-margin barriers affected Palaeogene sediment sources, water mass circulation and sediment deposition.

The pronounced Late Cretaceous transgression resulted in a fine-grained depositional mode within the seaway between Norway and Greenland (Doré *et al.* 1999). However, the period of passive basin infill was followed by the Campanian–Early Maastrichtian extension and basin fragmentation creating depositional environments ranging from marginal to deep marine on the Møre–Vøring margins changing to shallow marine conditions farther north (Gradstein *et al.* 1999; Roberts *et al.* 1999). This regional basin setting may have persisted into the Paleocene when the

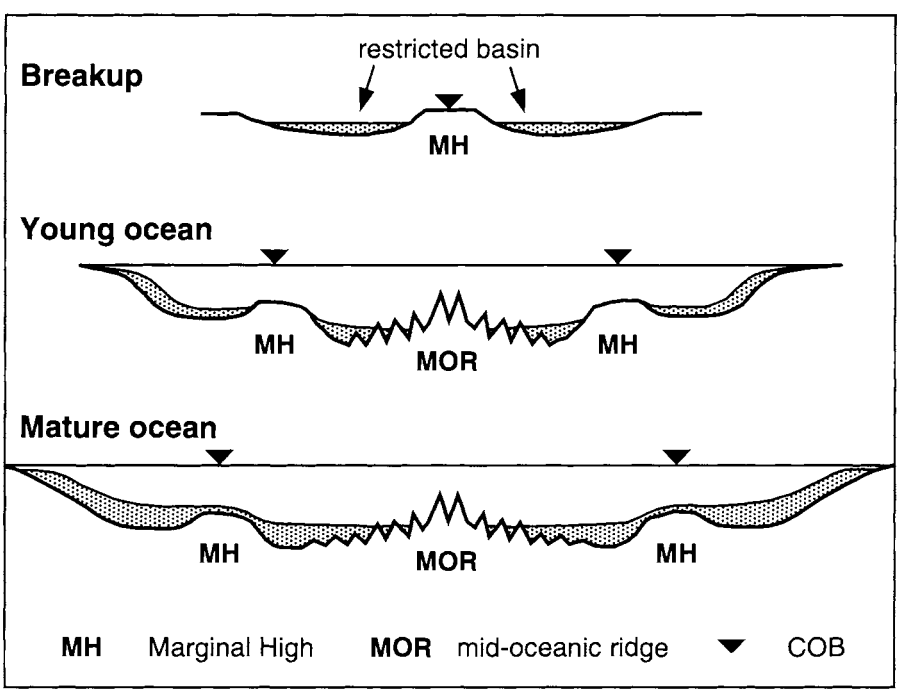

Fig. 7. Schematic illustration of volcanic margin basin segmentation creating across-margin barriers for water mass circulation caused by late rift uplift and construction of extrusive edifices along the continent–ocean boundary (COB).

arrival of the Iceland plume within the region under lithospheric extension led to thermal and dynamic uplift of the rift zone, part of which may have been emergent from latest Paleocene until a few million years after opening.

The margin segmentation implies that the understanding of the Palaeogene history in space and time is critically dependent on seismic well-ties in the various geological provinces. Despite the many commercial wells on the Møre, Vøring and SW Barents Sea shelves, there is yet only sparse well information from the middle and lower continental slope (e.g. Brekke *et al.* 1999; Martinsen *et al.* 1999; Spencer *et al.* 1999). In addition to some pre-glacial samples obtained by shallow coring and drilling, the three recent industry wells exist on structural highs in the outer Vøring Basin (Granholm 1999; Ren *et al.* in press). However only one well on the Nyk High has yet been described in the literature (Kittilsen *et al.* 1999). In addition, DSDP sites 338–340, 342, 346, and 349 (Talwani *et al.* 1976) and ODP sites 642–643 (Eldholm *et al.* 1987) and 913 (Myhre *et al.* 1995) (Figs 1 & 2) have sampled Palaeogene sediments and/or lavas erupted during breakup on the conjugate margins and the Jan Mayen Ridge microcontinent. These sites (Figs 1 & 2), in particular, provide important biostratigraphic and environmental data (Goll 1989; Goll & Hansen 1992). Together with the biostratigraphy and palaeobathymetry inferred from commercial wells on the shelf (Gradstein & Backstrøm 1996), regional geologic considerations, and sequence stratigraphic relations in the seismic data, we summarize a margin history which predicts some aspects of relative motions and sedimentation, noting that parameters such as absolute uplift and subsidence, and in particular palaeowater depths, are still poorly constrained.

Norwegian margin

In the Late Cretaceous, pulses of coarse clastic input with an East Greenland provenance appear in the Vøring Basin from early Cenomanian to at least early Campanian (Roberts *et al.* 1999; Kittelsen *et al.* 1999). A western source was maintained during the Paleocene leaving thick coarse clastic sequences thinning eastward on the outer margin west of Shetland and in the Møre-Vøring basins (Fig. 8) (Hitchen & Ritchie 1987; Skogseid *et al.* 1992; Doré *et al.* 1999; Skogseid *et al.* 2000). The source for most these sequences is probably the uplifted Late Cretaceous–Early Paleocene rift.

On the Møre and Vøring shelves, the Paleocene epoch was characterized by shallow water conditions dominated by channel and deltaic sedimentation creating a regional, coast-parallel and asymmetric Paleocene depocentre (Brekke & Riis 1987; Blystad *et al.* 1995) extending from the North Sea (Ghazi 1992; Kyrkjebø *et al.* 2001) to the western Barents Sea (Faleide *et al.* 1993; Nagy *et al.* 1997). Its origin is not obvious, but it is probably related to a modest regional uplift of the mainland source area. Skogseid *et al.* (2000) have indicated a link to plume impingement which may induce rapid subsidence and subsequent rapid rebound along the plume circumference where the plume head thickness is small relative to the lithosphere.

ODP Site 642 on the Vøring Marginal High (Fig. 2), which terminated almost 1 km below acoustic basement (Eldholm *et al.* 1987), provides key information of the composition and vertical motion history of a marginal high. The basement rocks consist of two different lava series and interbedded volcanoclastic sediments. The

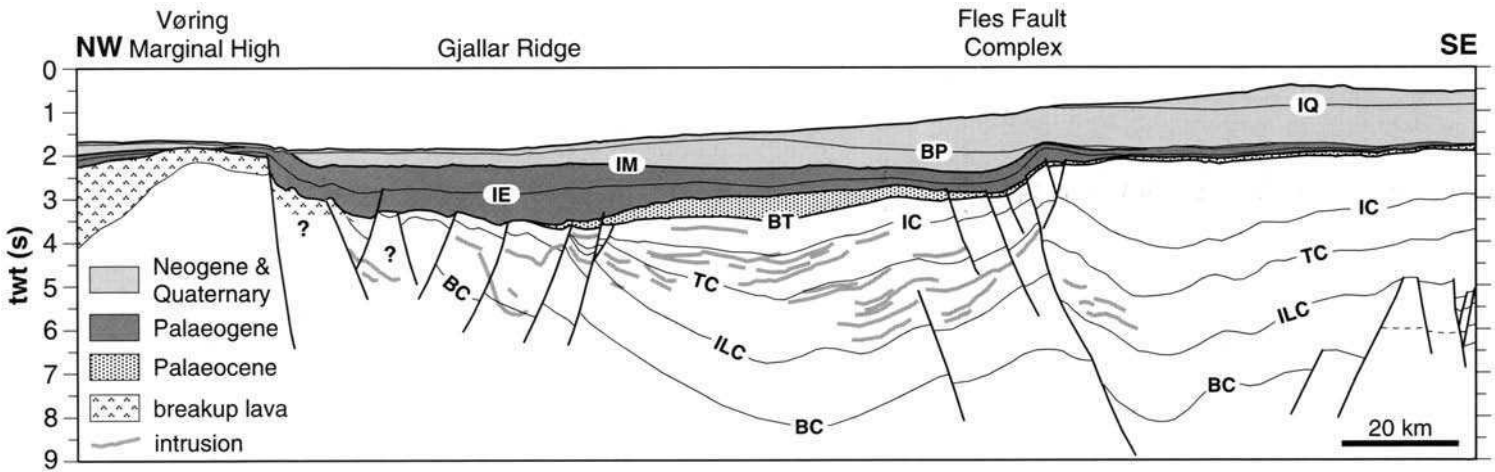

Fig. 8. Seismic interpretation of a profile across the outer Vøring margin (Blystad *et al.* 1995) (Fig. 2) illustrating tectono-magmatic style and the Paleocene–early Eocene western sediment source area (East Greenland–Vøring Marginal High–Jan Mayen Ridge). Legend in Figure 5.

lower series is andesitic to dacitic in composition, emplaced by infrequent eruptions of crustal melts during the late rift stage, and interbedded sediments indicate fluvial or shallow-water deposition. The upper series has been dated radiometrically to 55 Ma, whereas the lower series is not more than one million years older (Sinton *et al.* 1998). The *c.* 800 m thick upper lavas consist of transitional, mid-oceanic tholeiitic basalts and altered, interbedded, basaltic vitric tuffs. Subaerial and neritic environments are inferred during and after breakup, when the lavas erupted during an intense phase of explosive, subaerial basaltic volcanism.

After breakup, the oldest 'Icelandic'-type oceanic crust accreted above or near sea level. The intense volcanism abated in 2–3 million years, and the injection center submerged to mid-oceanic ridge levels. The change in production volume and emplacement mode left the marginal highs trailing behind new crust accreted at the mid-oceanic ridge (Fig. 7). As the ocean basin widened and deepened, the highs subsided at rates similar to oceanic crust, maintaining the basement relief (Eldholm *et al.* 1989). Thus, across-margin circulation barriers, induced by regional uplift along the initial plate boundary and the subsequent formation of marginal highs, were maintained also after breakup.

The elevated plate boundary region, which probably had an accentuated along-plate boundary relief, was rapidly denuded. Thus, a major early Palaeogene sedimentary source region existed first in the central epicontinental sea between Greenland and Eurasia and later on the young margins, dominating the sediment supply and deposition in the Møre and Vøring basins (Fig. 7). Sediments from the east reached the marginal high in middle Eocene. Later, the relief of the outer margin was gradually smoothed and the high became sediment-covered during the middle Oligocene to early Miocene. This model is consistent with recovered basal sediments on the high derived from continental soils formed under a hot, seasonably humid, climate followed by an initially restricted marine depositional regime (Thiede *et al.* 1989).

Widespread volcanic ashes and bentonite beds in uppermost Paleocene to lowermost Eocene in and around the North Sea Basin (Knox & Morton 1988) indicate that the subaerial volcanic activity was unusually violent probably reflecting local magma-water interaction. The most abundant ash layers occur in the lower Balder Formation where a regional seismic marker has been attributed to the intensive breakup volcanism (e.g. Eldholm *et al.* 1989; Skogseid & Eldholm 1989). The widespread marker horizon documents that the igneous breakup activity (Fig. 6) had a significant regional environmental impact (Eldholm & Thomas 1993).

The Eocene and Oligocene epochs reflect the early margin history, governed by differential subsidence caused by thermal cooling and contraction of the lithosphere and by sediment loading and compaction. Several sea level falls are recorded by unconformities and onlapping seismic patterns, and the Norwegian land mass and the inner shelf gradually became dominant source areas. The sediment supply may have decreased during the Eocene, but early Oligocene outbuilding on the inner shelf indicates a regional, moderate uplift of Fennoscandia (Fig. 9). The continental relief may, however, have been rapidly smoothed. Relatively modest sedimentation prevailed through the late Oligocene, possibly creating the peneplain that existed prior to the late Neogene Fennoscandian epeirogenic uplift (Stuevold & Eldholm 1996).

The Bivrost Lineament represents a hinge line between the Vøring Basin and the structurally elevated Lofoten–Vesterålen shelf (Brekke 2000). The latter has only a thin Cenozoic cover south of the Jennegga transfer zone, whereas a Cenozoic wedge

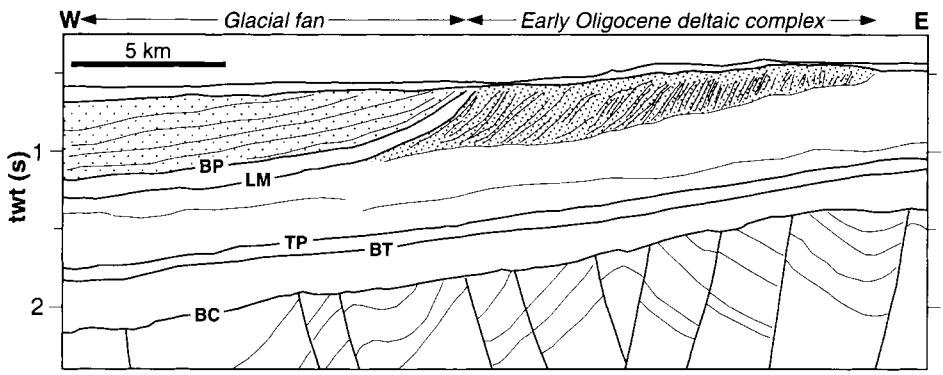

Fig. 9. Example of Oligocene and post-late Pliocene outbuilding on the Vøring shelf (Hjelstuen *et al.* 1999*a*) (Fig. 2). Legend in Figure 5.

increasing in thickness seaward is developed farther north. The breakup lavas extend far up the slope (Figs 2 & 4), locally bounded by shallow basement ridges along the shelf edge (Tsikalas *et al.* 2001). It appears that the opening occurred on the east flank of the main Mesozoic basin, i.e the equivalent to the Møre and Vøring basins, lies on the conjugate, wide East Greenland margin (Figs 1 & 6).

On both the middle and lower Lofoten–Vesterålen and the southernmost Barents Sea slopes normal faults locally offset the lavas and part of the overlying pre-glacial sediments (Fig. 10). We believe this syn- and post-breakup tectonism is the response of rapid post-breakup subsidence to the level of oceanic crust, contrasting significantly with the region south of Bivrost transfer system. After breakup the subsiding margin, and the Vøring Basin, received sediments from the Lofoten–Vesterålen shelf and adjacent islands. However, the steep slope allowed a major portion of the sediments to be deposited on oceanic crust in the Lofoten Basin (Figs 4 & 10).

SW Barents Sea margin

The Late Cretaceous rift basins terminated at the De Geer Zone along which dextral oblique shear movements produced the Harstad and Sørvestsnaget pull-apart basins in the SW Barents Sea and the Wandel Basin in NE Greenland (Figs 2 & 6) (Håkansson & Stemmerik 1989; Faleide *et al.* 1993*a*). The Harstad, Sørvestsnaget and Tromsø basins continued to subside in Late Cretaceous while the coeval sequences are condensed or misssing farther east. The extension is recorded by numerous normal faults, but minor wrench components are mapped locally. A hiatus spanning the Cretaceous–Paleocene transition is overlain by a relatively uniform and widespread late Paleocene marine sequence. However the hiatus is absent in the Vestbakken Volcanic Province (Knutsen & Larsen 1997). Biostratigraphic data from well 7119/9-1 in the Tromsø Basin (Fig. 2) suggest a deepening of the depositional environment, culminating near the end of the Paleocene, followed by shallower conditions (Nagy *et al.* 1997).

Fig. 10. Interpretations of seismic profiles at either side of the regional rift-shear intersection (Fig. 2) illustrating volcanic build-ups during breakup, and syn- and post-breakup tectonic activity (Tsikalas *et al.* 2001). SDR, seaward dipping reflector sequence.

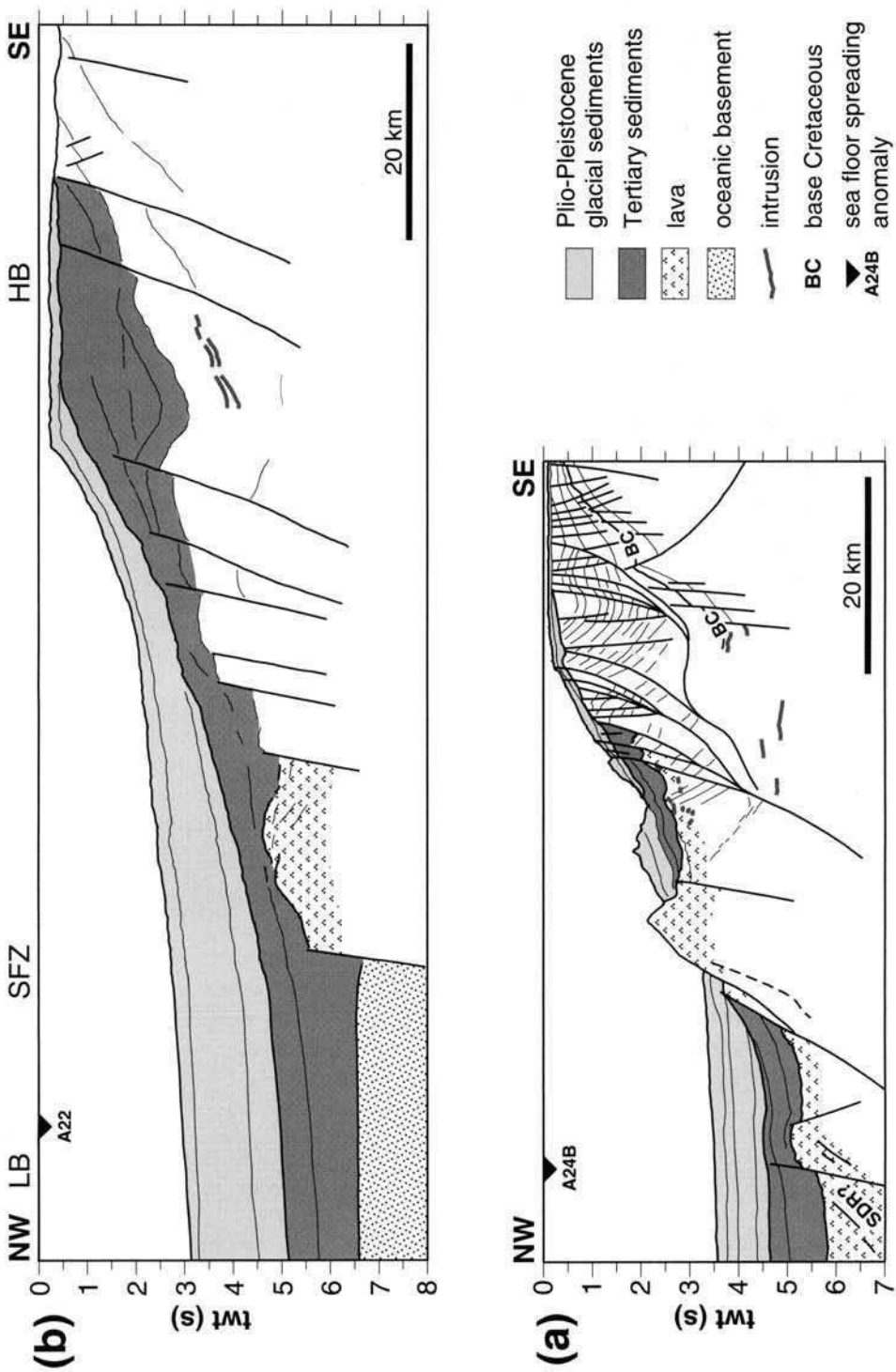
(b)
NW
LB
A22
SFZ
HB
SE
20 km
twt (s)
0
1
2
3
4
5
6
7
8
(a)
NW
A24B
SDR?
BC
BC
SE
20 km
twt (s)
0
1
2
3
4
5
6
7
Plio-Pleistocene glacial sediments
Tertiary sediments
lava
oceanic basement
intrusion
BC base Cretaceous
A24B sea floor spreading anomaly

After breakup the margin south of the Vestbakken Volcanic Province evolved as a progressively lengthening sheared margin within the De Geer Zone until the end of Eocene. The direction of Eocene plate motion was at a small angle with the Senja Fracture Zone yielding transform motion with a transtensional component.

The Harstad Basin, located close to the regional rift-shear corner, experienced early Eocene downfaulting and differential subsidence in a pull-apart setting. Sill intrusions are observed within Cretaceous strata and a fault block just landward of the COB is probably covered by lavas (Fig. 10). Local uplift and erosion in the southern Sørvestsnaget Basin during this period is compatible with the predicted response of a thermo-mechanically coupled COT as the northeastern end of the proto-Mohns Ridge passed along the margin (Vågnes 1997). Sediments from the uplifted areas prograded eastward into the Tromsø Basin, while sediments sourced from the uplifted Stappen High and the Vestbakken Volcanic Province were deposited in the northern Sørvestsnaget Basin (Fig. 11).

The Vestbakken Volcanic Province underwent rifting and volcanism followed by down-faulting in a pull-apart setting (Fig. 12). The Tertiary stratigraphy is constrained by exploration well 7316/5-1 near the Vestbakken Volcanic Province (Fig. 2) and several shallow cores which sample the most complete succession drilled in the western Barents Sea (Eidvin *et al.* 1994; Sættem *et al.* 1994; Knutsen & Larsen 1997). Repeated tectono-magmatic activity in the Vestbakken Volcanic Province, comprising as much as eight tectonic events (Jebsen 1998) and renewed magmatism near the Eocene–Oligocene transition (Faleide *et al.* 1988) and in late Pliocene (Mørk & Duncan 1993), is probably related to the complex plate tectonic evolution of the Greenland Sea. The breakup-related structuring pre-dates, and is partly masked by lavas. Subsequently, regional subsidence led to sedimentation over the entire province but with local, minor faulting within the Eocene basin fill.

At the beginning of the Oligocene the entire length of the present Senja Fracture Zone margin had developed. Increased westward progradation probably reflects a regional uplift event coeval with that off Norway. The Oligocene sequence blankets the entire margin as well as the oceanic crust in the adjacent Lofoten Basin (Fig. 11a). Early Oligocene rifting related to the change in relative plate motion reactivated faults in the Vestbakken Volcanic Province, in particular those with a NE–SW trend. This phase was also associated with renewed volcanism, which partly overprinted the breakup structures (Fig. 12) (Faleide *et al.* 1988; Jebsen 1998).

Intra-basin deformation

After breakup the margin became part of a regional compressive regime giving rise to a number of intra-basin inversion features off Norway and on the margin farther south (Doré & Lundin 1996; Roberts *et al.* 1999; Doré *et al.* 1999). Off Norway large domes and arches are the most common expression of the deformation (Fig. 2), but reverse faulting is also observed. For example, a Cretaceous normal fault beneath the outer flank of the Helland–Hansen Arch (Fig. 2) is reversely reactivated (Skogseid & Eldholm 1989; Doré & Lundin 1996). In addition, Stuevold *et al.* (1992) and Hjelstuen *et al.* (1997) point out that differential sediment loading has also to be considered when evaluating dome geometry and location, and doming mechanisms.

Many features show a multiphase inversion, in some cases reactivating older rift structures, and there are indications that the timing becomes younger to the north.

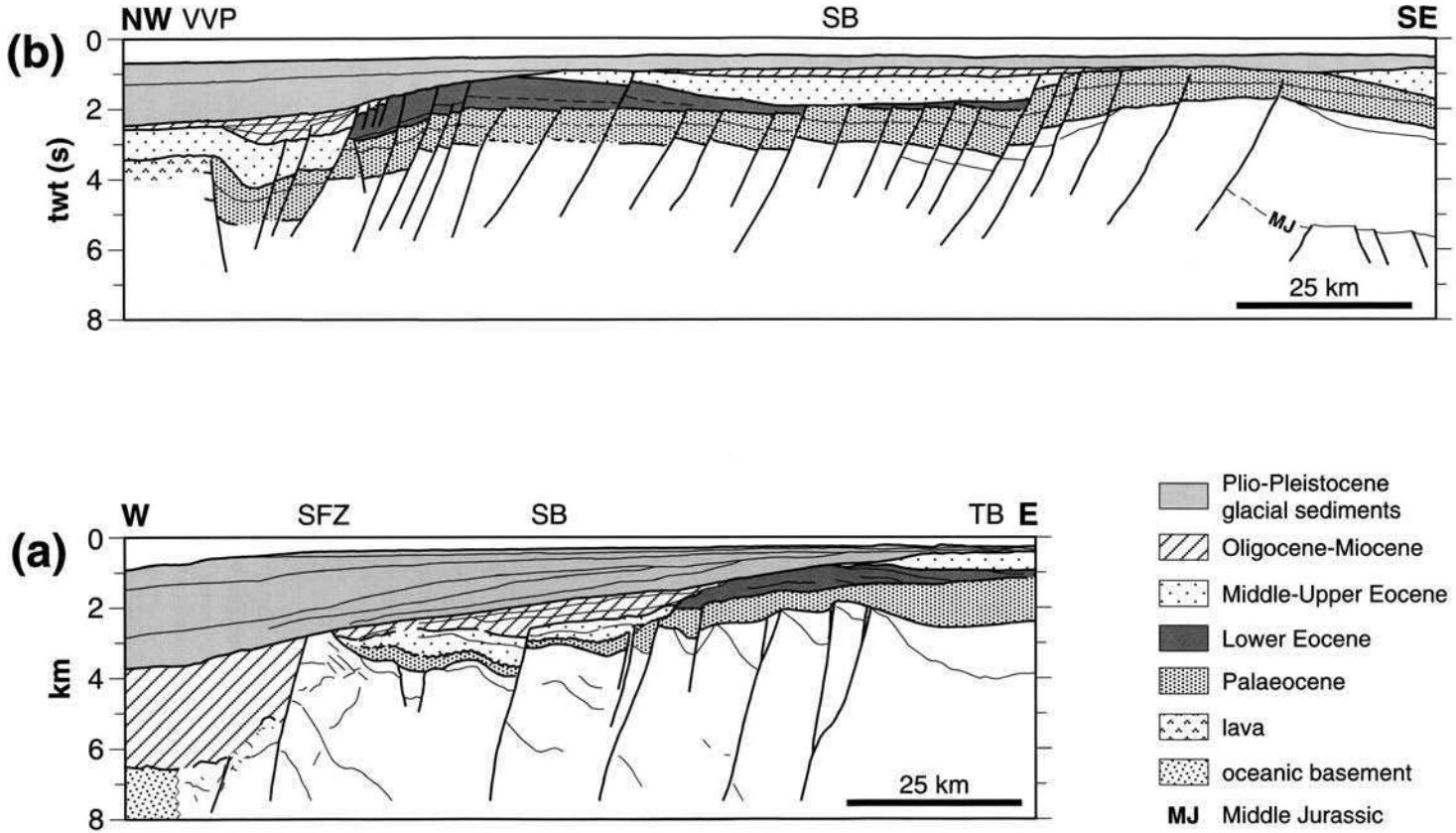

Fig. 11. Interpretation of seismic profiles on the Senja Fracture Zone margin (Fig. 2) illustrating Cenozoic sediment sequences and structural elements: (**a**) development of a lower Eocene sequence in response to thermo-mechanical uplift of the continent–ocean boundary (Vågnes 1997); (**b**) development of a lower Eocene sequence in response to post-breakup uplift of the Vestbakken Volcanic Province.

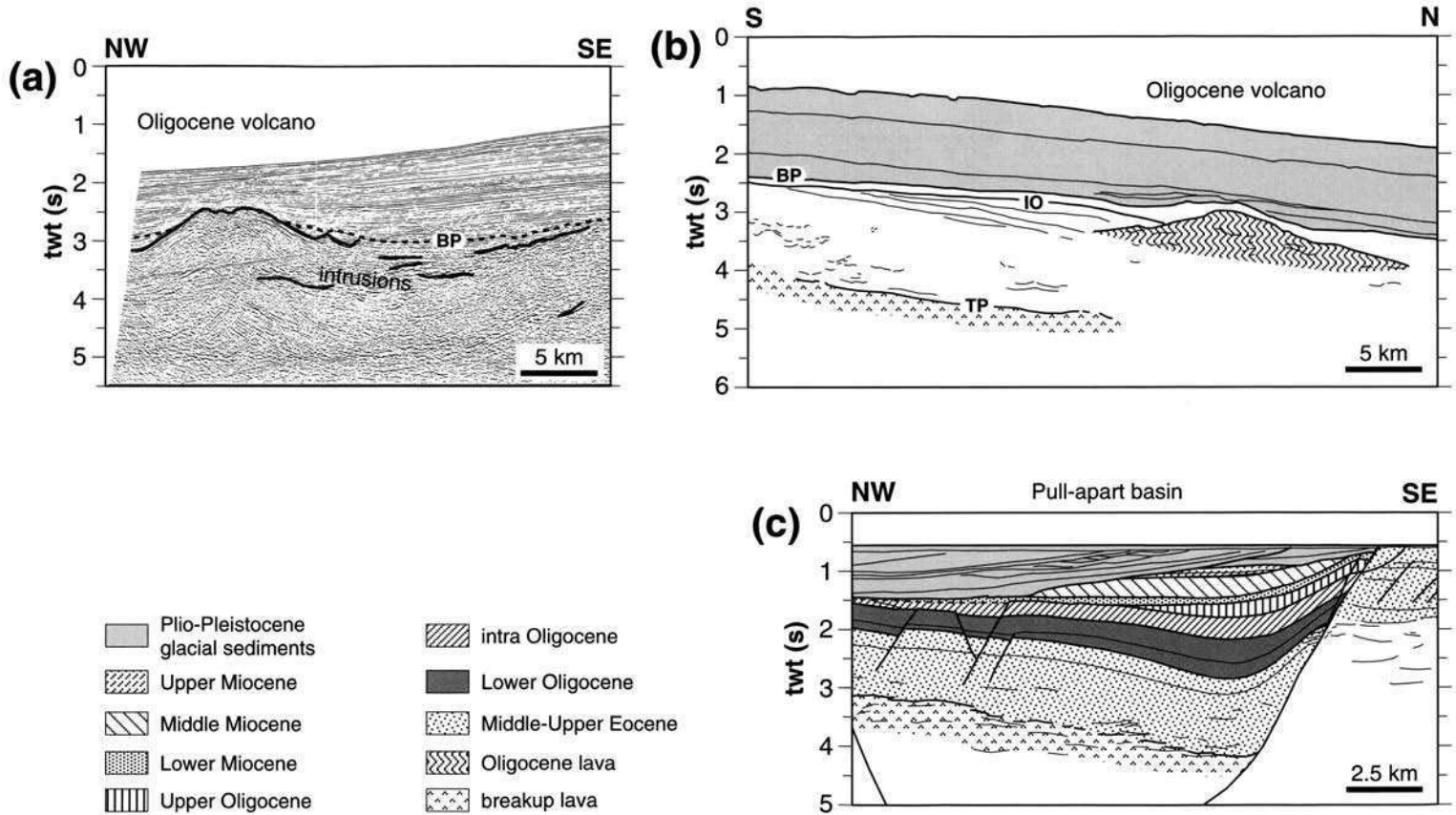

Fig. 12. Interpretations and seismic example from the Vestbakken Volcanic Province (Fig. 2) illustrating faulting and magmatism related to plate tectonic reorganization at the Eocene Oligocene transition (Jebsen 1998). See key in Figure 5.

The main inversion of the domes in Figure 2 is dated as late Eocene–early Oligocene on the Ormen Lange Dome, late Eocene–early Miocene on the Helland–Hansen Arch, and early–middle Miocene on the Naglfar Dome by Doré *et al.* (1999), whereas Hjelstuen *et al.* (1997) suggest a late Oligocene–Miocene age for both Vema and Naglfar domes. We also note that a detailed study of the Ormen Lange Dome reveals only moderate, <2–3%, contraction and that it has been growing continuously from Eocene to Present (Vågnes *et al.* 1998).

There has been much speculation as to far-field events that may induce changes in the regional stress pattern, thus potentially trigger doming. In particular, events in the Norwegian–Greenland Sea such as the change in relative plate motion near the Eocene–Oligocene transition, shift in the position of spreading ridge segments, and changes in relative plate speed have commonly been suggested (Hjelstuen *et al.* 1997; Doré *et al.* 1999). However, no in-depth cause-and-effect analysis have yet been convincingly documented.

Neogene and Quaternary summary

For completeness, we briefly note some important margin features and events. The domes and arches controlled the sedimentation on the Vøring margin in post-middle Miocene times when Late Miocene muds and oozes filled in and buried the existing relief (Brekke *et al.* 1999). Sedimentation continued into the Pliocene interspersed with ice-rafted debris signifying regional cooling and formation of mountain glaciers (Thiede *et al.* 1989; Stuevold & Eldholm 1996). Over the entire shelf there is a distinct unconformity, which changes on the slope to a downlap surface for huge prograding wedges of sandy muds sourced on the mainland and the shelf (Fig. 9). This horizon marks the transition to glacial sediment deposition during the Northern Hemisphere Glaciation since about 2.6 Ma. In terms of total post-opening sediment volume the glacial component constitutes as much as about 70 and 50% on the margins off the western Barents Sea and Norway, respectively (Figs 8–12). The high-density glacial load on sediments of lower density and higher water content may, in part, explain recent margin deformation such as large-scale sliding (Fig. 10) (Bugge *et al.* 1987), mud volcanoes and extensive provinces of mud diapirism (Vogt *et al.* 1997; Hjelstuen *et al.* 1999*a*, *b*), and possibly rejuvenation of older faults triggering earthquakes (Byrkjeland *et al.* 2000).

The morphology of Fennoscandia and the almost complete absence of onshore Mesozoic and Cenozoic sediments have for more than a century been interpreted in terms of epeirogenic uplift. In particular, a lower to middle Miocene hiatus on the Norwegian shelf (Gradstein & Backstrøm 1996; Brekke 2000) may be related to renewed tectonic uplift of the eroded landmass in late Oligocene or early Miocene time, later amplified by the isostatic response to the numerous glacials and interglacials since the late Pliocene. This induced large-scale glacial erosion of the shelf and mainland sourcing the voluminous wedges of glacial sediments centered near the present shelf edge (Stuevold & Eldholm 1996; Faleide *et al.* 1996).

Summary and conclusions

The continental margin off mainland Norway and SW Barents Sea, 62–75°N, evolved after opening of the Norwegian–Greenland Sea near the Paleocene–Eocene

transition. The lithospheric breakup was accompanied by massive, regional magmatic activity forming marginal highs and covering the initial oceanic crust, and large parts of the adjacent continental crust, with thick lava sequence, resulting in rifted volcanic margin segments. The magmatism is related to the impingement of the Iceland plume on lithosphere under extension, thus the volcanic margins belong to the North Atlantic Large Igneous Province. The breakup was preceded by a rift episode, clearly recognized by low-angle normal faulting on the outer margin during the Campanian. The fault activity continued toward breakup but appears to have been less frequent during the Paleocene. This is ascribed to focussing toward the incipient plate boundary, an area now covered by lavas, as well as to a more ductile lithospheric response when the thermal regime changed during plume arrival.

The margin exhibits a distinct along-margin segmentation comprising four main rifted segments: Møre, Vøring, Lofoten–Vesterålen and Vestbakken margins separated by the East Jan Mayen, Bivrost and Senja fracture zones and their landward prolongations. We also document a further segmentation of the Vøring and Lofoten–Vesterålen margins. The present margin segmentation is mainly related to Late Jurassic–Early Cretaceous transfer zones which have pre-determined the location of early opening fracture zones. However, many indicators point towards a much longer history of structural inheritance, extending back to pre-Mesozoic times.

After breakup, the passive margin evolved in response to subsidence and sediment loading during the widening and deepening of the Norwegian–Greenland Sea. The complex interaction of tectono-magmatic, erosional and depositional processes which occurred during a period of climatic deterioration have governed the present, and in particular the Palaeogene, margin physiography, crustal structure, tectono-magmatic segmentation and sedimentation. In addition to the along-margin constraints on Palaeogene palaeoceanography and sedimentation caused by offsets in the initial plate boundary, the water mass circulation was also governed by a pronounced across-margin basin segmentation caused by regional uplift along the initial plate boundary and the subsequent formation of emerged marginal highs along several of the rifted margin segments. The Palaeogene sedimentation on the outer margin was dominated by western source areas in the Paleocene and early–middle Eocene, whereas shelf sedimentation reflected a modest uplift of the mainland. In late Eocene and Oligocene, the mainland and shelf areas became progressively more dominant, and most of the marginal high and fracture zone relief was buried by the end of the period. Sediment volumes were relatively modest, except for a pulse of rapid progradation from the mainland in the early Oligocene. The setting was maintained, superimposed by intra-basinal doming on the Vøring margin, until the Late Pliocene when the Northern Hemisphere Glaciation led to rapid progradation and greatly increased sedimentation rates forming a huge, regional depocentre near the shelf edge along the entire margin.

This study is in part based on work by many colleagues and students associated with the University of Oslo Passive Margin Research Group (PMRG), and was completed while the senior author was on sabbatical leave at the University of Bergen. In particular, we recognize contributions from Shicun Ren and Jakob Skogseid. Funding of PMRG by Statoil a.s is gratefully acknowledged, and we thank Vidar B. Larsen and Erik Lundin for valuable insight and assistance.

References

ANDERSEN, O. A. & KNUDSEN, P. 1998. Global marine gravity field fro the ERS-1 and Geosat geodetic mission. *Journal of Geoooophysical Research*, **103**, 8129–8138.

BERNDT, C., SKOGLY, O. P., PLANKE, S., ELDHOLM, O. & MJELDE, R. 2000. High-velocity breakup-related sills in the Vøring Basin, off Norway. *Journal of Geophysical Research*, **105**, 28 441–28 454.

BERNDT, C., PLANKE, S., ALVESTAD, E., TSIKALAS, F. & RASMUSSEN, T. 2001. Seismic volcanostratigraphy of the Norwegian Margin: constraints on tectonomagmatic break-up processes. *Journal of the Geological Society, London*, **158**, 413–426.

BLYSTAD, P., BREKKE, H. & FÆRSETH, R. B., LARSEN, B. T., SKOGSEID, J. & TØRUDBAKKEN, B. 1995. Structural elements of the Norwegian continental shelf. Part II: the Norwegian Sea region. *Norwegian Petroleum Directorate Bulletin*, **8**.

BREIVIK, A. J., FALEIDE, J. I. & GUDLAUGSSON, S. T. 1998. Southwestern Barents Sea margin: late Mesozoic sedimentary basins and crustal extension. *Tectonophysics*, **293**, 21–44.

BREIVIK, A. J., VERHOEF, J. & FALEIDE, J. I. 1999. Effect of thermal contrasts on gravity modeling at passive margins: results fro the western Barents Sea. *Journal of Geophysical Research*, **104**, 15 293–15 312.

BREKKE, H. 2000. The tectonic evolution of the Norwegian Sea continental margin with emphasis on the Vøring and Møre basins. *In*: NØTTVEDT, A. (ed.) *Dynamics of the Norwegian Margin*. Geological Society, London, Special Publications, **167**, 327–378.

BREKKE, H. & RISS, F. 1987. Tectonics and basin evolution of the Norwegian shelf between 62°N and 72°N. *Norsk Geologisk Tidsskrift*, **67**, 295–322.

BREKKE, H., DAHLGREN, S., NYLAND, B. & MAGNUS, C. 1999. The prospectivity of the Vøring and Møre basins on the Norwegian continental margin. *In*: FLEET, A. J. & BOLDY, S. A. R. (eds) *Petroleum Geology of Northwest Europe: Proceedings of the 5th Conference*. Geological Society, London, 231–246.

BUCK, W. R., MARTINEZ, F., STECKLER, M. S. & COCHRAN, J. R. 1988. Thermal consequences of lithospheric extension: pure and simple. *Tectonics*, **7**, 213–234.

BUGGE, T., BEFRING, S., BELDERSON, R. H., EIDVIN, T., JANSEN, E., KENYON, N. H., HOLTEDAHL, H. & SEJRUP, H. P. 1987. A giant three-stage submarine slide off Norway. *Geo-Marine Letters*, **7**, 191–198.

BUKOVICS, C., CARTIER, E. G., SHAW, N. D. & ZIEGLER, P. A. 1984. Structure and development of the Mid-Norway Continental margin. *In*: SPENCER, A. M. *ET AL.* (eds) *Petroleum Geology of the North European Margin*. Graham & Trotman, London, 407–424.

BYRKJELAND, U., BUNGUM, H. & ELDHOLM, O. 2000. Seismotectonics of the Norwegian continental margin. *Journal of Geophysical Research*, **105**, 6221–6236.

CANDE, S. C. & KENT, D. V. 1995. Revised calibration of the geomagnetic polarity timescale for the Late Cretaceous and Cenozoic. *Journal of Geophysical Research*, **100**, 6093–6095.

DORÉ, A. G. 1991. The structural foundation and evolution of Mesozoic seaways between Europe and the Arctic. *Palaeogeography Palaeoclimatology Palaeoecology*, **87**, 441–492.

DORÉ, A. G. & LUNDIN, E. R. 1996. Cenozoic compressional structures on the NE Atlantic margin: nature, origin and potential significance for hydrocarbon exploration. *Petroleum Geoscience*, **2**, 299–311.

DORÉ, A. G., LUNDIN, E. R., FICHLER, C. & OLESEN, O. 1997. Patterns of basement structure and reactivation along the NE Atlantic margin. *Journal of the Geological Society, London*, **154**, 85–92.

DORÉ, A. G., LUNDIN, E. R., JENSEN, L. N., BIRKELAND, Ø., ELIASSEN, P. E. & FICHLER, C. 1999. Principal tectonic events in the evolution of the northwest European Atlantic margin. *In*: FLEET, A. J. & BOLDY, S. A. R. (eds) *Petroleum Geology of Northwest Europe: Proceedings of the 5th Conference*. Geological Society, London, 41–61.

EIDVIN, T., GOLL, R. M., GROGAN, P., SMELROR, M. & ULLEBERG, K. 1994. En stratigrafisk undersøkelse av øvre del av brønn 7316/5-1 (Bjørnøya Vest). *NPD Contribution* **38**.

ELDHOLM, O. & GRUE, K. 1994. North Atlantic volcanic margins: Dimensions and Production Rates. *Journal of Geophysical Research*, **99**, 2955–2968.

ELDHOLM, O. & MUTTER, J. C. 1986. Basin structure on the Norwegian margin from analysis of digitally recorded sonobuoys. *Journal of Geophysical Research*, **91**, 3763–3783.

ELDHOLM, O. & THOMAS, E. 1993. Environmental impact of volcanic margin formation. *Earth and Planetary Science Letters*, **117**, 319–329.

ELDHOLM, O., SUNDVOR, E. & MYHRE, A. M. 1979. Continental margin off Lofoten–Vesterålen, northern Norway. *Marine Geophysical Researches*, **4**, 3–35.

ELDHOLM, O., MYHRE, A. M. & THIEDE, J. 1994. Cenozoic tectono-magmatic events in the North Atlantic: potential paleoenvironmental implications. *In*: BOULTER, M. C. & FISCHER, H. C. (eds) *Cenozoic Plants and Climates of the Arctic, NATO ASI Series*, **127**. Springer-Verlag, Heidelberg, 35–55.

ELDHOLM, O., THIEDE, J. & TAYLOR, E. 1989. Evolution of the Vøring Volcanic Margin. *In*: ELDHOLM, O., THIEDE, J., TAYLOR, E. *ET AL.* (eds) *Proceedings of the Ocean Drilling Program, Scientific Results*. College Station, TX (Ocean Drilling Program), **104**, 1033–1065.

ELDHOLM, O., SKOGSEID, J., PLANKE, S. & GLADCZENKO, T. P. 1995. Volcanic margin concepts. *In*: BANDA, E., TALWANI, M. & TORNÉ, M. (eds) *Rifted Ocean–Continent Boundaries*. NATO ASI Series Volume, Kluwer Academic, Dordrecht, 1–16.

ELDHOLM, O., THIEDE, J., TAYLOR, E. *ET AL.* 1987. *Proceedings Ocean Drilling Program, Initial Reports*, College Station, TX (Ocean Drilling Program) **104**.

FALEIDE, J. I., MYHRE, A. M. & ELDHOLM, O. 1988. Early Tertiary volcanism at the western Barents Sea margin. *In*: MORTON, A. C. & PARSON, L. M. (eds) *Early Tertiary Volcanism and the Opening of the NE Atlantic*. Geological Society, London, Special Publications, **39**, 135–146.

FALEIDE, J. I., VÅGNES, E. & GUDLAUGSSON, S. T. 1993*a*. Late Mesozoic–Cenozoic evolution of the southwestern Barents Sea in a regional rift-shear tectonic setting. *Marine and Petroleum Geology*, **10**, 186–214.

FALEIDE, J. I., VÅGNES, E. & GUDLAUGSSON, S. T. 1993*b*. Late Mesozoic–Cenozoic evolution of the southwestern Barents Sea. *In*: PARKER, J. R. (ed.) *Petroleum Geology of Northwest Europe: Proceedings of the 4th Conference*. Geological Society, London, 933–950.

FALEIDE, J. I., GUDLAUGSSON, S. T., ELDHOLM, O., MYHRE, A. M. & JACKSON, H. R. 1991. Deep seismic transects across the western Barents Sea continental margin. *Tectonophysics*, **189**, 73–89.

FALEIDE, J. I., SOLHEIM, A., FIEDLER, A., HJELSTUEN, B. O., ANDERSEN, E. S. & VANNESTE, K. 1996. Late Cenozoic evolution of the western Barents Sea–Svalbard continental margin. *Global and Planetary Change*, **12**, 53–74.

FICHLER, C, RUNDHOVDE, E., OLESEN, O., SÆTHER, B. M., RUESLÅTTEN, H., LUNDIN, E. & DORÉ, A. G. 1999. Regional tectonic interpretation of image enhanced gravity and magnetic data covering the mid-Norwegian shelf and adjacent mainland. *Tectonophysics*, **306**, 183–197.

GHAZI, S. A. 1992. Cenozoic uplift in the Stord Basin area and its consequences for exploration. *Norsk Geologisk Tidskrift*, **72**, 285–290.

GOLL, R. M. 1989. A synthesis of Norwegian Sea biostratigraphies: ODP Leg 104 on the Vøring Plateau. *In*: ELDHOLM, O., THIEDE, J., TAYLOR, E. *ET AL.* (eds) *Proceedings of the Ocean Drilling Program, Scientific Results*. College Station, TX (Ocean Drilling Program), **104**, 777–826.

GOLL, R. M. & HANSEN, J. W. 1992. The Cenozoic sequence stratigraphy of the Halten Terrace and outer Vøring Plateau based on seismic and biostratigraphic data. *Norsk Geologisk Tidskrift*, **72**, 295–299.

GRADSTEIN, F. M. & BACKSTRØM, S. 1996. Cainozoic biostratigraphy and paleobathymetry, northern North Sea and Haltenbanken. *Norsk Geologisk Tidskrift*, **76**, 3–32.

GRADSTEIN, F. M., KAMINSKI, M. A. & AGTERBERG, F. P. 1999. Biostratigraphy and paleoceanography of the Cretaceous seaway between Norway and Greenland. *Earth Science Reviews*, **46**, 27–98.

GRADSTEIN, F. M., AGTERBERG, F. P., OGG, J. G., HARDENBOL, J., VAN VEEN, P., THIERRY, J. & HUANG, Z. 1994. A Mesozoic time scale. *Journal of Geophysical Research*, **99**, 24 051–24 074.

GRANHOLM, P. G. 1999. Gjallar mest spennende boring i 1999. *Geo*, **2**(2), 2–3.

HANDY, M. & STRAIT, J. 1999. Mechanics and mechanisms of magmatic underplating: inferences from mafic veins in deep crustal mylonite. *Earth and Planetary Science Letters*, **165**, 271–286.

HARLAND, W. B. 1969. Contribution of Spitsbergen to understanding of tectonic evolution of North Atlantic region. *In*: KAY, M. (ed.) *North Atlantic; geology and continental drift*. American Association of Petroleum Geologists, Memoirs, **12**, 817–851.

HENKEL, H. 1991. Magnetic crustal structures in Northern Fennoscandia. *Tectonophysics*, **192**, 57–79.

HITCHEN, K. & RITCHIE, J. D. 1987. Geological review of the west Shetland area. *In*: BROOKS, J. & GLENNIE, K. (eds) *Petroleum Geology of North West Europe*. Graham & Trotman, London, 737–749.

HJELSTUEN, B. O., ELDHOLM, O. & SKOGSEID, J. 1997. Vøring Plateau diapirs and their structural and depositional settings. *Marine Geology*, **144**, 33–57.

HJELSTUEN, B. O., ELDHOLM, O. & SKOGSEID, J. 1999*a*. Cenozoic evolution of the northern Vøring margin. *Geological Society of America Bulletin*, **111**, 1792–1807.

HJELSTUEN, B. O., ELDHOLM, O. & VOGT, P. R. 1999*b*. Ein 'aktiv' passiv kontinentalmargin. *Geology*, **2**(4), 22–25.

HÅKANSSON, E. & STEMMERIK, L. 1989. Wandel Sea basin – a new synthesis of the late Paleozoic to Tertiary accumulation in North Greenland. *Geology*, **17**, 683–686.

JACKSON, H. R., FALEIDE, J. I. & ELDHOLM, O. 1990. Crustal structure of the sheared southwestern Barents Sea continental margin. *Marine Geology*, **93**, 119–146.

JEBSEN, C. 1998. *Kenozoisk utvikling av Vestbakkvulkanittprovinsen på den vestlige Barentshavmarginen*. MSc thesis, University of Oslo.

KINCK, J. J., HUSEBYE, E. S. & LARSSON, F. R. 1993. The Moho depth distribution in Fennoscandia and the regional tectonic evolution from Archean to Permian times. *Precambrian Research*, **64**, 23–51.

KITTELSEN, J. E., OLSEN, R. R., MARTEN, R. F., HANSEN, E. K. & HOLLINGSWORTH, R. R. 1999. The first deepwater well in Norway and its implications for the Upper Cretaceous play, Vøring Basin. *In*: FLEET, A. J. & BOLDY, S. A. R. (eds) *Petroleum Geology of Northwest Europe: Proceedings of the 5th Conference*. Geological Society, London, 275–280.

KNOX, R. W. O'B. & MORTON, A. C. 1988. The record of early Tertiary N Atlantic volcanism in sediments of the North Sea Basin. *In*: MORTON, A. C. & PARSON, L. M. (eds) *Early Tertiary Volcanism and the Opening of the NE Atlantic*. Geological Society, London, Special Publications, **39**, 407–419.

KNUTSEN, S.-M. & LARSEN, K. I. 1997. The late Mesozoic and Cenozoic evolution of the Sørvestsnaget Basin: a tectonostratigraphic mirror for regional events along the southwestern Barents Sea margin? *Marine and Petroleum Geology*, **14**, 27–54.

KODAIRA, S., GOLDSCHMIDT-ROKITA, A., HARTMANN, J. M., HIRSCHLEBER, H. B., IWASAKI, T., KANZAWA, T., KRAHN, H., TOMITA, S. & SHIMAMURA, H. 1995. Crustal structure of the Lofoten continental margin, off northern Norway, from ocean-bottom seismographic studies. *Geophysical Journal International*, **121**, 907–924.

KYRKJEBØ, R., KJENNERUD, T., GILLMORE, G. K., FALEIDE, J. I. & GABRIELSEN, R. H. 2001. Cretaceous–Tertiary palaeo-bathymetry in the northern North Sea; integration of palaeo-water depth estimates obtained by structural restoration and micropalaentological analysis. *In*: MARTINSEN, O. & DREYER, T. (eds) *Sedimentary Environments Offshore Norway: Palaeozoic to Recent*. Norwegian Petroleum Society, Special Publication, **10**, 321–345.

LISTER, G. S., ETHERIDGE, M. A. & SYMONDS, P. A. 1986. Detachment faulting and the evolution of passive continental margins. *Geology*, **14**, 246–250.

LISTER, G. S., ETHERIDGE, M. A. & SYMONDS, P. A. 1991. Detachment models for the formation of passive continental margins. *Tectonics*, **10**, 1038–1064.

LUNDIN, E. R. & DORÉ, A. G. 1997. A tectonic model for the Norwegian passive margin with implications for the NE Atlantic: Early Cretaceous to break-up. *Journal of the Geological Society, London*, **154**, 545–550.

LØSETH, H. & TVETEN, E. 1996. Post-Caledonian structural evolution of the Lofoten and Vesterålen offshore and onshore areas. *Norsk Geologisk Tidsskrift*, **76**, 215–230.

MARTINSEN, O. J., BØEN, F., CHARNOCK, M. A., MANGERUD, G. & NØTTVEDT, A. 1999. Cenozoic development of the Norwegian margin 60–64°N: sequences and sedimentary response to variable basin physiography and tectonic setting. *In*: FLEET, A. J. & BOLDY,

S. A. R. (eds) *Petroleum Geology of Northwest Europe: Proceedings of the 5th Conference*. Geological Society, London, 293–304.

MJELDE, R., KODAIRA, S., SHIMAMURA, H., KANAZAWA, T., SHIOBARA, H., BERG, E. W. & RIISE, O. 1997. Crustal structure of the central part of the Vøring Basin, mid-Norway margin, from ocean bottom seismographs. *Tectonophysics*, **277**, 235–257.

MJELDE, R., DIGRANES, P., SHINAMURA, H., SHIOBARA, H., KODAIRA, S., BREKKE, H., EGEBJERG, T., SØRENES, N. & THORBJØRNSEN, S. 1998. Crustal structure of the northern part of the Vøring Basin, mid-Norway margin, from wide-angle seismic and gravity data. *Tectonophysics*, **293**, 175–205.

MJELDE, R., KODAIRA, S., HASSAN, R. K., GOLDSCHMIDT-ROKITA, A., TOMITA, N., SELLEVOLL, M. A., HIRSCHLEBER, H. B., SHIMAMURA, H., IWASAKI, T. & KANAZAWA, T. 1996. The continent/ocean transition of the Lofoten volcanic margin, N. Norway. *Journal of Geodynamics*, **22**, 189–206.

MOKHTARI, M. & PEGRUM, R. M. 1992. Structure and evolution of the Lofoten continental margin, offshore Norway. *Norsk Geologisk Tidskrift*, **72**, 339–355.

MYHRE, A. M. & ELDHOLM, O. 1988. The western Svalbard margin (74–80°N). *Marine and Petroleum Geology*, **5**, 134–146.

MYHRE, A. M. & ELDHOLM, O., SKOGSEID, J., FALEIDE, J. I., GUDLAUGSSON, S. T., PLANKE, S., STUEVOLD, L. M. & VÅGNES, E. 1992. The Norwegian continental margin. *In*: POAG, C. W. & GRACIANSKY, P. C. (eds) *Geologic Evolution of Atlantic Continental Rises*. Van Nostrand Reinhold, New York, 157–185.

MYHRE, A. M., THIEDE, J., FIRTH, J. V. *ET AL.* 1995. *Proceedings Ocean Drilling Project, Initial Reports*. College Station, TX (Ocean Drilling Program), **151**.

MØRK, M. B. E. & DUNCAN, R. A. 1993. Late Pliocene basaltic volcanism on the western Barents shelf margin implications from petrology and ^{40}Ar–^{39}Ar dating of volcaniclastic debris from a shallow drill-core. *Norsk Geologisk Tidskrift*, **73**, 209–225.

NAGY, J., KAMINSKI, M. A., JOHNSEN, K. & MITLEHNER, A. G. 1997. Foraminiferal, palynomorph, and diatom biostratigraphy and paleoenvironments of the Torsk Formation: a reerence section for the Paleocene–Eocene transition in the western Barents Sea. *In*: HASS, C. & KAMINSKI, M. A. (eds) *Micropaleontology and Paleoceanography of the northern North Atlantic*. Grzybowski Foundation, Special Publication, **5**, 15–38.

OLAFSSON, I., SUNDVOR, E., ELDHOLM, O. & GRUE, K. 1992. Crustal structure from analysis of Expanded Spread Profiles. *Marine Geophysical Researches*, **14**, 137–162.

OLESEN, O., TORSVIK, T. H., TVETEN, E., ZWAAN, K. B., LØSETH, H. & HENNINGSEN, T. 1997. Basement structure of the continental margin in the Lofoten–Lopphavet area, northern Norway: constraints from potential field data, on-land structural mapping and palaeomagnetic data. *Norsk Geologisk Tidskrift*, **77**, 15–30.

PEDERSEN, T. & SKOGSEID, J. 1989. Vøring Plateau volcanic margin: extension, melting and rifting. *In*: ELDHOLM, O., THIEDE, J., TAYLOR, E. *ET AL.* (eds) *Proceedings of the Ocean Drilling Program, Scientific Results*. College Station, TX (Ocean Drilling Program), **104**, 985–991.

REN, S., SKOGSEID, J. & ELDHOLM, O. 1998. Late Creataceous–Paleocene extension on the Vøring volcanic margin. *Marine Geophysical Research*, **20**, 343–369.

REN, S., FALEIDE, J. I., ELDHOLM, O., SKOGSEID, J. & GRADSTEIN, F. in press. Late Cretaceous–Early Tertiary tectonic development of the NW Vøring Basin. *Marine and Petroleum Geology*.

ROBERTS, D. G., THOMPSON, M., MITCHENER, B., HOSSACK, J., CARMICHAEL, S. & BJØRNSETH, H.-M. 1999. Palaeozoic to Tertiary rift and basin dynamics: mid-Norway to the Bay of Biscay – a new context for hydrocarbon prospectivity in the deep water frontier. *In*: FLEET, A. J. & BOLDY, S. A. R. (eds) *Petroleum Geology of Northwest Europe: Proceedings of the 5th Conference*. Geological Society, London, 7–40.

ROSENDAHL, B. R. 1987. Architecture of continental rifts with special reference to East Africa. *Annual Review Earth and Planetary Sciences*, **15**, 445–503.

SANDWELL, D. T. & SMITH, W. H. F. 1997 (V9.2). Marine gravity anomaly from Geosat and ERS-1 altimetry. *Journal of Geophysical Research*, **102**, 10 039–10 054.

SAUNDERS, A. D., FITTON, J. G., KERR, A. C., NORRY, M. J. & KENT, R. W. 1997. The North Atlantic Igneous Province. *Geophysical Monograph 100*, American Geophysical Union, 45–93.

SINTON, C. W., HITCHEN, K. & DUNCAN, R. A. 1998. ^{40}Ar–^{39}Ar geochronology of silic and basic volcanic rocks on the margins of the North Atlantic. *Geological Magazine*, **135**, 161–170.

SKOGSEID, J. 1994. Dimensions of the Late Cretaceous–Paleocene Northeast Atlantic rift derived from Cenozoic subsidence. *Tectonophysics*, **240**, 225–247.

SKOGSEID, J. & ELDHOLM, O. 1987. Early Cenozoic crust at the Norwegian continental margin and the conjugate Jan Mayen Ridge, *Journal of Geophysical Research*, **92**, 11 471–11 491.

SKOGSEID, J. & ELDHOLM, O. 1989. Vøring Plateau continental margin: seismic interpretation, stratigraphy and vertical movements. *In*: ELDHOLM, O., THIEDE, J., TAYLOR, E. *ET AL.* (eds) *Proceedings of the Ocean Drilling Program, Scientific Results*. College Station, TX (Ocean Drilling Program), **104**, 993–1030.

SKOGSEID, J. & ELDHOLM, O. 1995. Rifted continental margin off mid-Norway. *In*: BANDA, E., TALWANI, M. & TORNÉ, M. (eds) *Rifted Ocean–Continent Boundaries*, NATO ASI Series Volume. Kluwer Academic Publications, Dordrecht, 147–153.

SKOGSEID, J., PEDERSEN, T., ELDHOLM, O. & LARSEN, B. T. 1992. Tectonism and magmatism during NE Atlantic continental break-up: the Vøring margin. *In*: STOREY, B. C., ALABASTER, T. & PANKHURST, R. J. (eds) *Magmatism and the causes of continental break-up*. Geological Society, London, Special Publications, **68**, 305–320.

SKOGSEID, J., PLANKE, S., FALEIDE, J. I., PEDERSEN, T., ELDHOLM, O. & NEVERDAL, F. 2000. NE Atlantic continental rifting and volcanic margin formation. *In*: NØTTVEDT, A. (ed.) *Dynamics of the Norwegian Margin*. Geological Society, London, Special Publications, **167**, 295–326.

SPENCER, A. M., BIRKELAND, Ø., KNAG, G. Ø. & FREDSTED, R. 1999. Petroleum systems of the Atlantic margin of northwest Europe. *In*: FLEET, A. J. & BOLDY, S. A. R. (eds) *Petroleum Geology of Northwest Europe: Proceedings of the 5th Conference*. Geological Society, London, 231–246.

STUEVOLD, L. M. & ELDHOLM, O. 1996. Cenozoic uplift of Fennoscandia inferred from a study of the mid-Norwegian margin. *Global and Planetary Change*, **12**, 359–386.

STUEVOLD, L. M., SKOGSEID, J. & ELDHOLM, O. 1992. Post-Cretaceous uplift events on the Vøring continental margin. *Geology*, **20**, 919–922.

SUNDVOR, E., ELDHOLM, O., GLADCZENKO, T. P & PLANKE, S. 2000. Norwegian–Greenland Sea thermal field. *In*: NØTTVEDT, A. (ed.) *Dynamics of the Norwegian Margin*. Geological Society, London, Special Publications, **167**, 397–410.

SURLYK, F. 1990. Timing, style and sedimentary evolution of Late Paleozoic–Mesozoic extensional basins of East Greenland. *In*: HARDMAN, R. P. F. & BROOKS, J. (eds) *Tectonic events responsible for Britain's oil and gas reserves*. Geological Society, London, Special Publications, **55**, 107–125.

SURLYK, F., CLEMMENSEN, L. B. & LARSEN, H. C. 1981. Post-Paleozoic evolution of the East Greenland continental margin. *In*: KERR, J. W. & FERGUSSON, A. J. (eds) *Geology of the North Atlantic Borderlands*. Canadian Society of Petroleum Geologists, Memoirs, **7**, 611–645.

SÆTTEM, J., BUGGE, T., FANAVOLL, S., GOLL, R. M., MØRK, A., MØRK, M. B. E., SMELROR, M. & VERDENIUS, J. G. 1994. Cenozoic margin development and erosion of the Barents Sea: Core evidence from southwest of Bjørnøya. *Marine Geology*, **118**, 389–449.

TALWANI, M. & ELDHOLM, O. 1972. The continental margin off Norway: A geophysical study. *Geological Society of America Bulletin*, **83**, 3573–3606.

TALWANI, M. & ELDHOLM, O. 1977. Evolution of the Norwegian–Greenland Sea. *Geological Society of America Bulletin*, **83**, 3573–3606.

TALWANI, M., UDINTSEV, G. *ET AL.* 1976. *Initial Reports Deep Sea Drilling Project*. Leg 38 (US Government Printing Office).

THIEDE, J., ELDHOLM, O. & TAYLOR, E. 1989. Variability of Cenozoic Norwegian–Greenland Sea paleoceanography and northern hemisphere paleoclimate. *In*: ELDHOLM, O., THIEDE, J. TAYLOR, E. *ET AL.* (eds) *Proceedings of the Ocean Drilling Program, Scientific Results*. College Station, TX (Ocean Drilling Program), **104**, 1067–1118.

TORSKE, T. & PRESTVIK, T. 1991. Mesozoic detachment faulting between Greenland and Norway: inferences from Jan Mayen Fracture Zone system and associated alkalic volcanic rocks. *Geology*, **19**, 481–484.

TSIKALAS, F., FALEIDE, J. I. & ELDHOLM, O. 2001. Lateral variations in tectono-magmatic style along the Lofoten–Vesterålen volcanic margin off Norway. *Marine and Petroleum Geology*, **18**, 807–832.

VERHOEF, J., ROEST, W. R., MACNAB, R., ARKANI-HAMED, J. & MEMBERS OF THE PROJECT TEAM 1996. *Magnetic anomalies of the Arctic and North Atlantic Oceans and adjacent land areas*. Geological Survey of Canada, Dartmouth NS, Open File **3125**.

VOGT, P. R., CHERKASHEV, G., GINSBURG, G., IBANOV, G., MILKOV, A., CRANE, K., LEIN, A., SUNDVOR, E., PIMENOV, N. & EGOROV, A. 1997. Haakon Mosby mud volcano provides unusual example of venting. *Eos*, **78**, 549–557.

VÅGNES, E. 1997. Uplift at thermo-mechanically coupled ocean–continent transforms: modeled at the Senja Fracture Zone, southwestern Barents Sea. *Geo-Marine Letters*, **17**, 100–109.

VÅGNES E., GABRIELSEN, R. H. & HAREMO, P. 1998. Late Cretaceous–Cenozoic intraplate contractional deformation at the Norwegian continental shelf: timing, magnitude and regional implications. *Tectonophysics*, **300**, 29–46.

WHITE, R. S. & MCKENZIE, D. 1989. Magmatism at rift zones: the generation of volcanic continental margins and flood basalts. *Journal of Geophysical Research*, **94**, 7685–7729.

WHITE, R. S., MCKENZIE, D. & O'NIONS, K. R. 1992. Oceanic crustal thickness from seismic measurements and rare earth element inversions. *Journal of Geophysical Research*, **97**, 19 683–19 715.

ZWAAN, K. B. 1995. Geology of the West Troms Basement Complex, northern Norway, with emphasis on the Senja Shear Belt: a preliminary account. *Geological Survey of Norway Bulletin*, **427**, 33–36.

Evolution of Paleocene sediment dispersal systems in the Foinaven Sub-basin, west of Shetland

ANDREW C. MORTON[1,2], J. DOUGLAS BOYD[3] & DAVID F. EWEN[3]

[1] *HM Research Associates, 100 Main Street, Woodhouse Eaves, Leicestershire LE12 8RZ, UK*
[2] *Department of Geology and Petroleum Geology, University of Aberdeen, Aberdeen AB24 3UE, UK*
[3] *BP Exploration, Farburn Industrial Estate, Dyce, Aberdeen AB21 7PB, UK*

Abstract: Heavy mineral assemblages in deepwater Paleocene sandstones of the Foinaven Sub-basin (west of Shetland) reflect the influence of three main provenance and dispersal systems. The Schiehallion system has relatively uniform characteristics and persisted through much of the early-mid Paleocene. Its sphere of influence was centred on the Schiehallion Field, but it progressively encroached into the Foinaven area with time. Its main source was the Triassic Foula Formation, with minor supply from Lewisian and Moine basement rocks. The Foinaven system shows marked changes in character, related to evolution of the source area. The earliest sands were derived from a heavily weathered late Cretaceous regolith, and represent the onset of uplift and exhumation of the Shetland Platform. Progressive unroofing led to the incorporation of increasing amounts of Lewisian- and Moine-sourced detritus. Following deposition of the main reservoir sandstones in Foinaven and Schiehallion, there was a progressive change in provenance, with a gradual increase in the amount of sediment shed directly from metamorphic basement. Pulsing of the proto-Icelandic plume has been proposed as the mechanism for repeated influx of sand to the basins around Scotland. However, on the basis of available geochronological data, there does not appear to be a direct link between events in the British Tertiary Igneous Province (BTIP) and changes in provenance in the Foinaven Sub-basin. The initial influx of sediment from a weathered land surface may have been coeval with the onset of magmatism in the BTIP, but the cessation of supply through the Foinaven system at *c.* 59 Ma does not appear to be related to magmatic events in the BTIP. The waning of magmatism in the BTIP around 58 Ma is broadly coincident with a gradual increase of first-cycle basement detritus.

The Paleocene of the Faroe–Shetland Basin (Fig. 1) has been the object of much oil industry attention since the discovery of the Foinaven and Schiehallion fields in the early 1990s (Hanna *et al.* 1996). Together with the more recently discovered Loyal and Suilven fields and near-field satellites, total reserves are estimated to be close to one billion barrels (Lamers & Carmichael 1999). Although a number of gas discoveries have been made in Paleocene sandstones in the Flett Sub-basin, which lies in

From: JOLLEY, D. W. & BELL, B. R. (eds) *The North Atlantic Igneous Province: Stratigraphy, Tectonic, Volcanic and Magmatic Processes.* Geological Society, London, Special Publications, **197**, 69–93. 0305-8719/02/$15.00

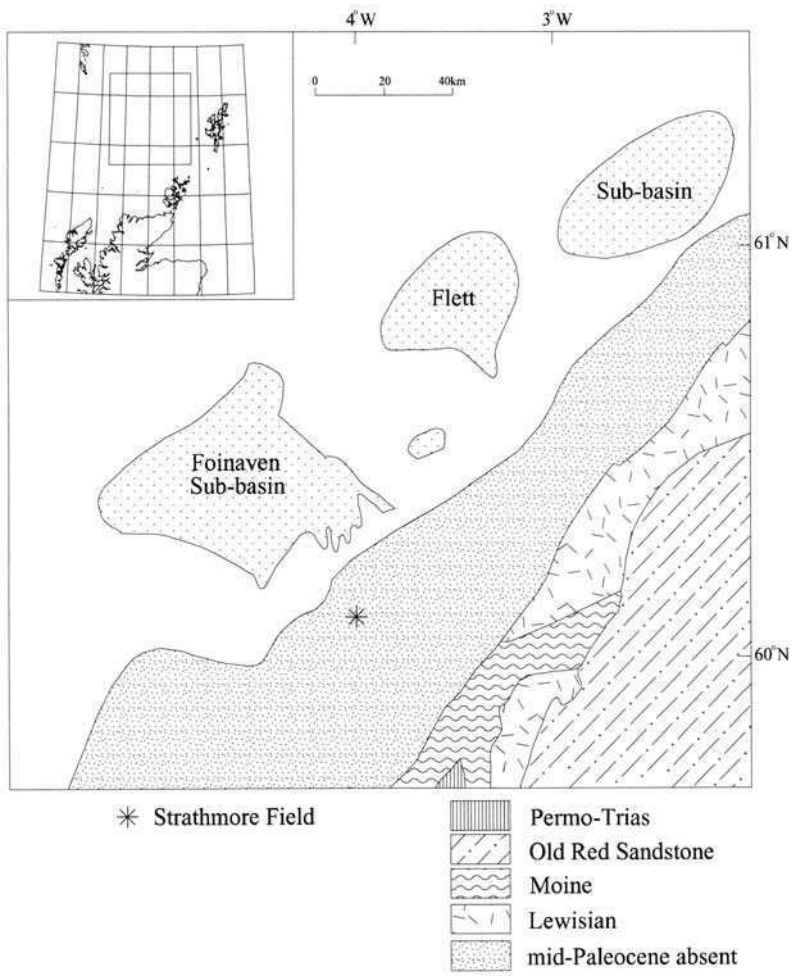

Fig. 1. The Foinaven and Flett sub-basins, west of Shetland, UK continental shelf, showing distribution of potential source rock lithologies in the provenance, together with the location of the Strathmore Field. Adapted from Lamers and Carmichael (1999).

the northeastern part of the Faroe–Shetland Basin, the greatest attention has focussed on the Foinaven Sub-basin, in the southwest, where the only oil accumulations have been found.

The reservoir sandstones in the Foinaven Sub-basin are of Late Paleocene (Thanetian) age, and are deepwater in origin, deposited within or related to channelized submarine slope systems (Cooper *et al.* 1999; Leach *et al.* 1999). Similar deepwater sands are found at older stratigraphic levels as far back as Early Paleocene (Ebdon *et al.* 1995), but these have not yet been proved to be hydrocarbon-bearing. During the Late Paleocene, a large prograding shelf system built out from the SE (Ebdon *et al.* 1995; Lamers & Carmichael 1999), and a non-marine, paralic environment was established across the whole area by the Early Eocene.

Ebdon *et al.* (1995) drew attention to the question of sediment provenance in the Foinaven Sub-basin, recognizing that lateral and stratigraphic variations in sand

input were a key element in reservoir presence, and possibly in reservoir quality. This paper documents variations in composition of the lower to mid-Paleocene sands of the Foinaven and Schiehallion areas, and discusses the implications of these mineralogical variations in terms of the lateral extent of sediment dispersal systems, the evolution of sand provenance and its implications for uplift and exhumation, the relationship with reservoir quality and the recognition of multiple phases of oil migration. The study utilizes heavy mineral data from 10 wells (204/19-3A, 204/20-1; -1Z, 204/23-1; 204/24a-1; 204/24a-2; -2Y, 204/24a-3; 204/24a-5; 204/24a-6; 204/24a-7; 204/25b-5 and 205/16-2) and is based on over 340 conventional heavy mineral analyses of core and sidewall core samples augmented by microprobe analysis of garnet populations from over 110 samples (50 garnets per sample).

Heavy mineral analysis

Heavy minerals are sensitive indicators of provenance because many of the detrital minerals found in sediments have restricted parageneses. However, in addition to provenance, a variety of processes operative during the sedimentation cycle influence the composition of heavy mineral suites. These include weathering at source, mechanical abrasion during transport, weathering during alluvial storage, hydrodynamic conditions at the time of deposition, and diagenesis during burial (Morton & Hallsworth 1999). Consequently, it is important that the heavy mineral criteria used to differentiate sand provenance and to delineate sand body distribution are not influenced by these overprinting processes.

Two methods are used to establish sand provenance from heavy mineral data. The first approach uses ratios of the abundance of minerals that have similar hydraulic behaviour and are stable within the diagenetic regime affecting the sample set. Such ratios are not affected by variations in the hydraulic regime or by burial diagenesis (Morton & Hallsworth 1994). Ratios routinely used for provenance discrimination are garnet/zircon (GZi), apatite/tourmaline (ATi), rutile/zircon (RuZi), monazite/zircon (MZi) and chrome spinel/zircon (CZi). They were determined during optical analysis of the heavy-mineral residues, and are expressed as index values as shown in Table 1. Of these ratios, the only two that show significant variations in the Foinaven Sub-basin are GZi and ATi. In some circumstances, GZi values may not be representative of depositional characteristics because of diagenetic dissolution of garnet during deep burial (Morton & Grant 1998). However, in the Foinaven Sub-basin there is no evidence for development of corrosion textures on grain surfaces, indicating that garnet dissolution has not occurred to any appreciable extent (Morton *et al.* 1989). Consequently, variations in GZi are considered to be unaffected by diagenetic

Table 1. *Definition of provenance-sensitive mineral indices (from Morton & Hallsworth 1994)*

Index	Mineral pair	Determination
ATi	Apatite, tourmaline	100 × apatite count/(total apatite plus tourmaline)
GZi	Garnet, zircon	100 × garnet count/(total garnet plus zircon)
RuZi	Rutile, zircon	100 × rutile count/(total rutile plus zircon)
CZi	Chrome spinel, zircon	100 × chrome spinel count/(total chrome spinel plus zircon)
MZi	Monazite, zircon	100 × monazite count/(total monazite plus zircon)

processes. It is not possible to alter the ATi value during diagenesis given the stability of both apatite and tourmaline during deep burial. However, ATi may be lowered by weathering processes that act at source, during periods of alluvial storage during transport, and at the final site of deposition. In the deep-water environment of the early-mid Paleocene of the Foinaven Sub-basin, weathering processes cannot have lowered ATi at the depositional site. Nevertheless, ATi values may at least in part reflect the overall weathering history of the sediment (both during the present sedimentary cycle and in previous cycles).

The second approach to establishing sand provenance concentrates on variations shown by an individual mineral species. Such varietal studies include analysis of attributes observed during optical analysis, such as colour or grain shape. In this study, emphasis was placed on geochemical variations shown by detrital garnet populations, as described by Morton (1985). Previous studies (Morton 1987; Morton *et al.* 1993) have demonstrated that garnet geochemical data provide a high degree of resolution in distinguishing Paleocene sand provenances in the North Sea.

Geochemical studies of garnets derived from different Scottish basement terrains provide a basis for linking garnet assemblages to their original source. Garnets derived from low- to moderate grade metasedimentary terrains (such as the Moine and Dalradian) are virtually exclusively low in pyrope, and have variable grossular and spessartine (Fig. 2). By contrast, garnet populations derived from the high-grade Lewisian orthogneiss terrain contain abundant high-pyrope, high-grossular garnets ($py > 10\%$, $gr > 10\%$). Both Lewisian and Moine basement rocks were exposed along the western margin of the Shetland Platform during the Paleocene (Fig. 1). Neither type of basement rock provide appreciable quantities of high-pyrope, low-grossular garnets ($py > 20\%$, $gr > 10\%$). These garnets are frequently found in UK sandstones, including the Paleocene of the North Sea (Morton 1987; Morton *et al.* 1993), and form a significant component of the garnet populations in the Paleocene of the Foinaven Sub-basin. They are, however, found in high abundances in Triassic Foula Formation sandstones in the Strathmore area (Herries *et al.* 1999), in the immediate vicinity of the Foinaven Sub-basin (Fig. 1), and are considered to have an exotic source consisting of high-grade (granulite facies) metasediments or charnockites. Thus, in the Foinaven Sub-basin, the relative abundance of (i) high-pyrope, low-grossular garnets; (ii) high-pyrope, high-grossular garnets; and (iii) low-pyrope, variable grossular, variable spessartine garnets can be used to indicate the relative amounts of sediment ultimately supplied from the Foula Formation, from Lewisian-type basement, and from Moine/Dalradian-type basement respectively.

Both optical (including ratio determinations) and geochemical heavy mineral studies were conducted on the 63–125 μm fraction, following Morton & Hallsworth (1994). Analytical methods are as described by Morton & Berge (1995).

Paleocene stratigraphy

Paleocene sediments in the Foinaven Sub-basin have been subdivided using both a lithostratigraphic scheme (Knox *et al.* 1997) and a sequence stratigraphic framework (Ebdon *et al.* 1995). The sequence stratigraphic scheme uses a series of packages (T10-T50) bounded by maximum flooding surfaces, formulated using a combination of well, seismic, log and biostratigraphic data. Lamers & Carmichael (1999) have introduced greater sophistication to the T-sequence scheme in the Faroe–Shetland

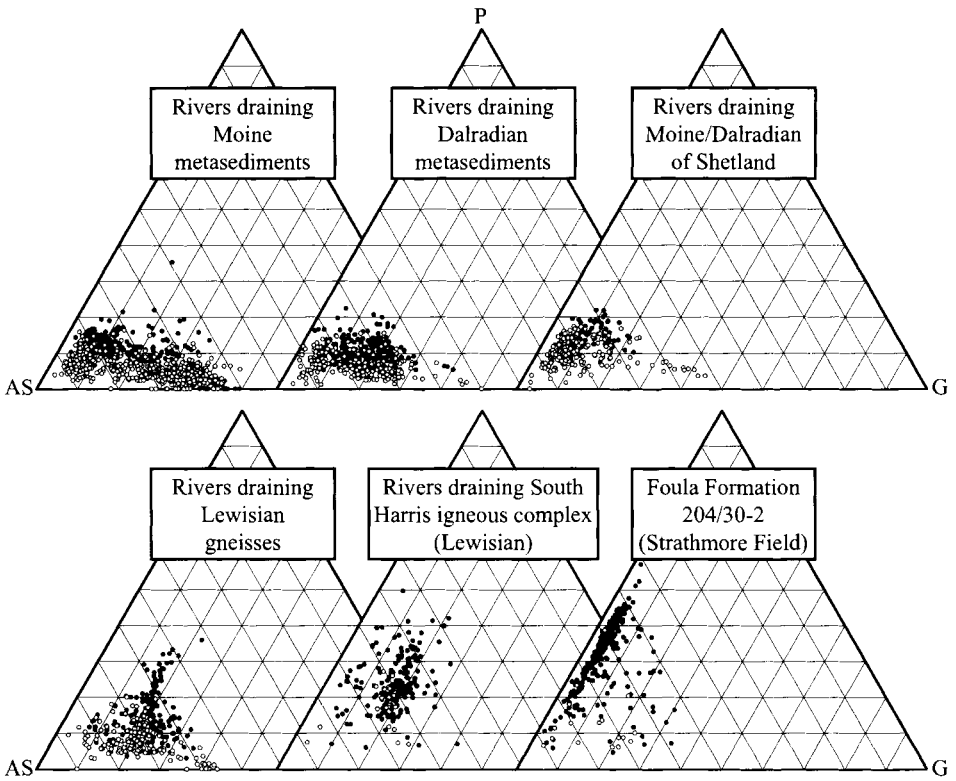

Fig. 2. Garnets from river sediments draining the low- to moderate grade metasedimentary terrains (Moine and Dalradian) of northern Scotland, compared with those from rivers draining high-grade Lewisian gneisses and from the Foula Formation (Triassic) in the Strathmore Field. AS, almandine plus spessartine; P, pyrope; G, grossular.

Basin, with the subdivision of T20-T30 into nine packages (T22, T25, T28, T31, T32, T34, T35, T36 and T38). The relationship between the T-sequences and the lithostratigraphic framework is shown in Figure 3.

For the purposes of this study, sandstones have been grouped into six stratigraphic packages (T10-22, T25, T31-32, T34, T35-36L and T36U). The subdivision of T36 sandstones into lower and upper is made on the basis of their position below or above a regional volcaniclastic marker, the Kettla Member, which forms the basal part of the Lamba Formation (Knox *et al.* 1997).

Evolution of sand provenance

Lateral and stratigraphic changes in mineralogy are illustrated using three plots for each time-slice, linked to a map identifying which wells have particular mineralogies. The three plots are:

(1) ATi (apatite/tourmaline index) v. GZi (garnet/zircon index).
(2) ATi v. proportion of high-pyrope, low-grossular (py > 20%; gr < 10%) garnets (recycled from the Foula Formation).

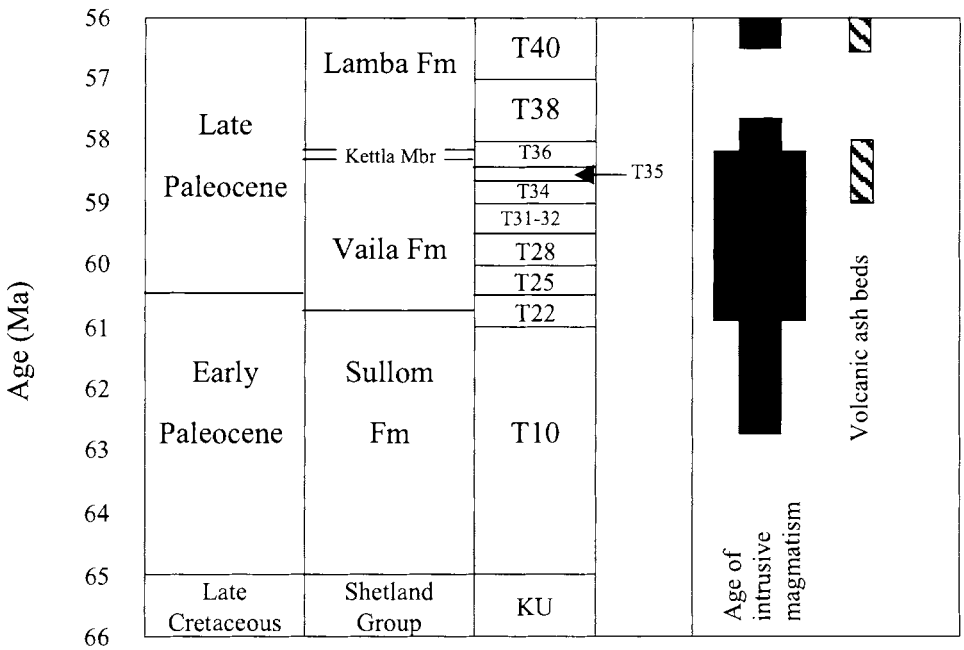

Fig. 3. Paleocene stratigraphy in the Foinaven Sub-basin, from Lamers and Carmichael (1999). Time scale is that of Berggren *et al.* (1995). Ages of intrusive magmatism and stratigraphic distribution of volcanic ash beds simplified from White & Lovell (1998), with the onset of magmatism taken at 62.8 Ma following Pearson *et al.* (1996).

(3) Ternary diagram showing relative abundance of high-pyrope, low-grossular ($py > 20\%$; $gr < 10\%$) garnets (Foula Formation source), high-pyrope, high-grossular ($alm + spe < 70\%$, $py > 10\%$, $gr > 10\%$) garnets (Lewisian source), and low-pyrope, variable grossular garnets (Moine source).

T10-T22 (Fig. 4)

Two distinct supply systems can be distinguished on the basis of the heavy mineral data during T10-T22. One of these supplied sediment to the eastern part of the

Figs 4–9. Key heavy mineral characteristics of T10-T22, T25, T31-32, T34, T35-36L and T36U sandstones in the Foinaven sub-basin, shown using:

(i) a crossplot of garnet-zircon index (GZi) against apatite–tourmaline index (ATi);
(ii) apatite–tourmaline index (ATi) against abundance of high-pyrope ($py > 20\%$), low grossular ($gr < 10\%$) garnet (as a component of the detrital garnet population); and
(iii) ternary diagram showing the relative abundances of high-pyrope, low-grossular garnet ($py > 20\%$, $gr < 10\%$), high-pyrope, high-grossular garnet ($py > 10\%$, $gr > 10\%$), and low-pyrope, variable grossular garnet. Compositions of garnet assemblages from Moine and Dalradian metasediments, Lewisian gneisses and Foula Formation sandstones (from Fig. 2) are shown for comparison.

Maps identify wells where sandstones of contrasting mineralogies have been found, together with inferred sediment entry points.

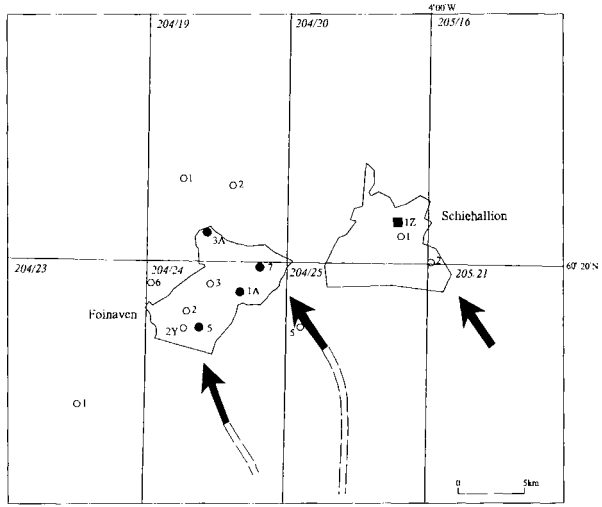

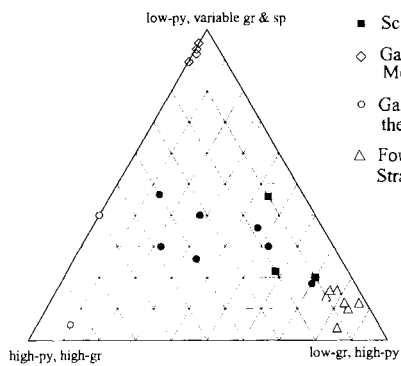

- ● Foinaven System
- ■ Schichallion System
- ◇ Garnets from rivers draining Moine and Dalradian
- ○ Garnets from rivers draining the Lewisian
- △ Foula Formation (Triassic), Strathmore field

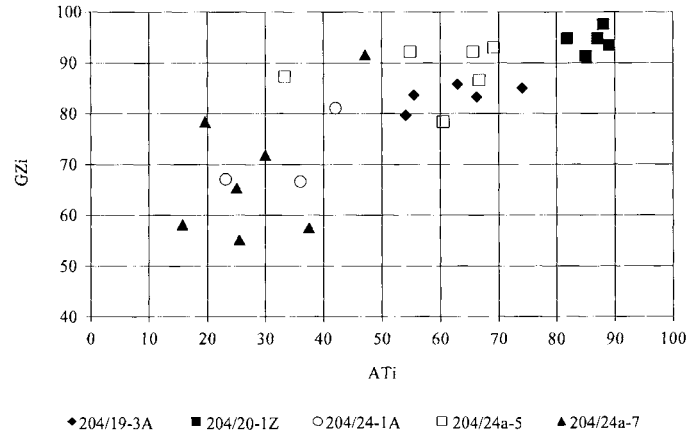

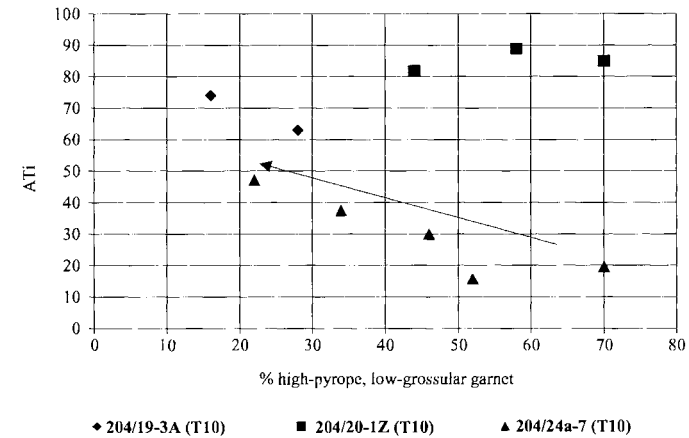

T10-22

Fig. 4.

sub-basin (the Schiehallion area), identified in Well 204/20-1Z. The sediment supplied by this system is characterized by uniformly high ATi and GZi values (>80 and >90 respectively), and by garnet assemblages with moderate to high abundances of high-pyrope, low-grossular garnets. These parameters indicate that the provenance of this system was dominated by Foula-type sediment, with minor amounts of material ultimately derived from Moine/Lewisian basement rocks. The high ATi and high GZi suggests that the source material had undergone relatively limited weathering.

In the wells from the western part of the study area (204/19-3A, 204/24-1A, 204/24a-5 and 204/24a-7) the sandstone mineralogy shows a clear evolution with time. ATi and GZi values are at their lowest in the earliest T10 sandstones, increasing stratigraphically upwards in all wells to a maximum ATi of *c.* 70 and GZi of *c.* 90. This trend is accompanied by an evolution in garnet composition, beginning with assemblages dominated by high-pyrope, low-grossular types (sourced from the Foula Formation) and progressing to assemblages with a stronger basement (predominantly Lewisian) component. The full evolutionary pattern is shown by 204/24a-7 and 204/24-1A, whereas only the later stages of the pattern are seen in 204/19-3A and 204/24a-5. It therefore appears that 204/24a-7 and 204/24-1A are more proximal to the entry point supplying this material, and that the mineralogical data may provide useful constraints on correlation in the T10-22 interval in the Foinaven area. The source of the sediment supplying the Foinaven area at this time initially comprised intensely weathered Triassic and basement rocks, presumably representing a Late Cretaceous regolith, with unroofing causing the rapid introduction of unweathered material. BGS boreholes along the western margin of the UKCS have found evidence for deep weathering profiles, most notably BGS borehole 77/7, located on the Solan Bank High to the south of the Foinaven Sub-basin in Block 202/16 (Evans *et al.* 1997). This borehole found a kaolinitic regolith some 18.5 m thick overlying Lewisian basement. Evans *et al.* (1997) suggested that the regolith development was most likely to have taken place in the early Eocene, but Cretaceous was also considered a possibility.

There is evidence, therefore, for the operation of at least two distinct feeder systems to the Foinaven Sub-basin from the very start of Paleocene sedimentation. One of these (the Schiehallion system) supplied sediment mostly derived from the Foula Formation to the Schiehallion area, with no evidence for the existence of a Late Cretaceous weathering profile. The other (the Foinaven system) supplied the Foinaven area with detritus from a combination of basement and Foula material, with evidence for the progressive removal of deeply-weathered material from the Late Cretaceous land surface. The fact that the evolutionary trend terminates with detritus that has an ATi value of *c.* 70 indicates that weathered material remains a component of the Foinaven provenance. This component may be recycled (i.e. weathered during previous sedimentation cycles); a possible candidate for this is the Jurassic Rona Formation (Verstralen *et al.* 1995; Herries *et al.* 1999). The presence of the complete T10–22 evolutionary trend in 204/24a-7 and 204/24-1A suggests that the entry point for the sediment was to the SE of the Foinaven Field, in Block 204/25, as shown by Cooper *et al.* (1999). Ebdon *et al.* (1995) suggested that there may have been further entry points to supply postulated depocentres in the unlicensed area in the Foinaven Sub-basin ('White Zone') to the NW, but as yet mineralogical data are not available for comparison.

T25 (Fig. 5)

Relatively few T25 sandstones have been analysed, but the limited data available indicate that the two different dispersal systems identified at the T10-22 level continued to operate. However, the area influenced by the Schiehallion system appears to have expanded at the expense of the Foinaven system. The samples from 204/20-1Z, 204/24a-7 and one from 204/19-3A have similar parameters to those from the T10-22 in 204/20-1Z, with high ATi, high GZi and abundant high-pyrope, low-grossular garnets. These sediments were evidently supplied from similar sources to those supplying the Schiehallion area in T10–22 (dominantly Foula-type material). It seems likely, however, that this material entered the basin through both the Schiehallion entry point and the entry point SE of Foinaven. This implies a change in the nature of sediment supplied through the SE Foinaven entry point.

The T25 sequence in 204/19–3A also includes sands with mineralogies akin to those supplying the Foinaven area during the later part of the T10-22 interval, with generally lower ATi values and higher abundances of garnets derived from Lewisian- and Moine-type basement. These sands, which appear to be volumetrically relatively insignificant, represent continuation of supply from the Foinaven system, but it seems likely that this was fed through the entry point identified to the south of Foinaven (Cooper *et al.* 1999).

T31-32 (Fig. 6)

The T31-32 sands, together with those in the succeeding T34 interval, host the majority of hydrocarbons discovered to date in the Foinaven Sub-basin. Heavy mineral data from this interval show that two distinct sources continued to supply sediment to the area through a number of separate entry points. This has clear and important implications for the understanding of reservoir sand distribution in the area.

Sandstones from the Schiehallion Field (204/20-1 & -1Z, 205/16-2) and the northeastern part of the Foinaven Field (204/19-3A, 204/24a-7) have high ATi and GZi, together with common to abundant high-pyrope, low-grossular garnets. The range of parameters found in these samples is virtually identical to that shown by sand supplied earlier (T10-20) through the Schiehallion system. They are interpreted as having been sourced by the same system, fed through at least two entry points, one S of Schiehallion and one SE of Foinaven. The provenance of this material is identical to that of material fed through the same system in T10-20.

Sandstones in the western part of the Foinaven area (204/23-1, 204/24a-2 & -2Y, 204/24a-3, 204/24a-5 and 204/24a-6) have lower ATi, lower GZi and higher abundances of Lewisian- and Moine-type basement-sourced garnets. On the ATi-high pyrope, low grossular garnet crossplot and the garnet ternary diagram, the range of parameters shown by this group of sandstones does not overlap with that supplied through the Schiehallion system. On the ATi–GZi crossplot, the two groups are also well-defined, although there is a small degree of overlap. The sands in the western part of the Foinaven Field represent sediment supplied through the Foinaven system, fed through the entry point in the S of the field (Cooper *et al.* 1999).

The mineralogy of sediment fed through the Foinaven system during T31-32 shows further evolution compared with that supplied during T10-20. ATi and GZi

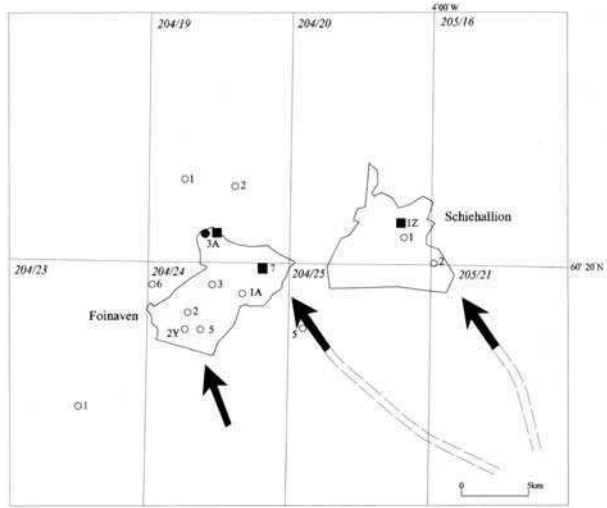
4°00 W
204/19
204/20
205/16
204/23
204/24
204/25
205/21
60° 20 N
Foinaven
Schiehallion
3A
7
1A
1Z
2Y
5
0
5km

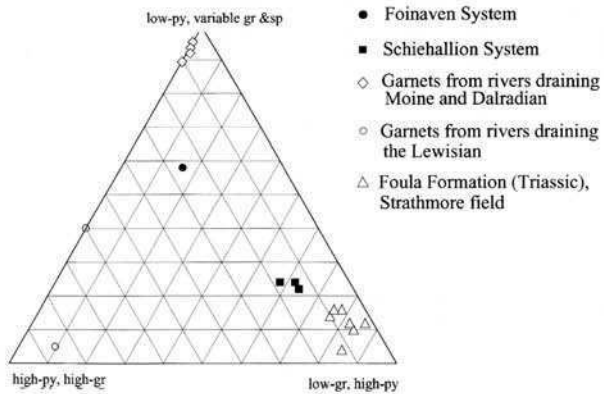
low-py, variable gr &sp
high-py, high-gr
low-gr, high-py
Foinaven System
Schiehallion System
Garnets from rivers draining Moine and Dalradian
Garnets from rivers draining the Lewisian
Foula Formation (Triassic), Strathmore field

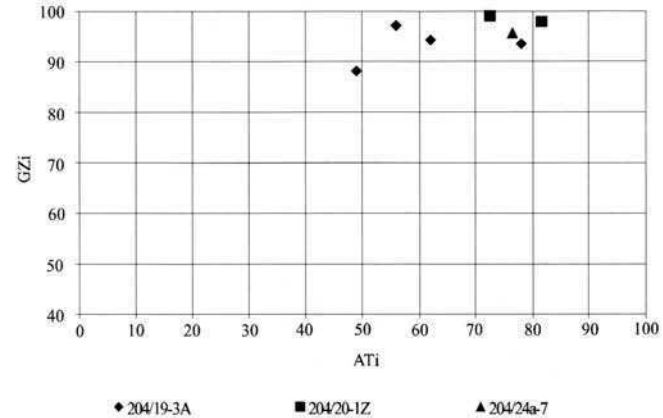
GZi
ATi
204/19-3A
204/20-1Z
204/24a-7

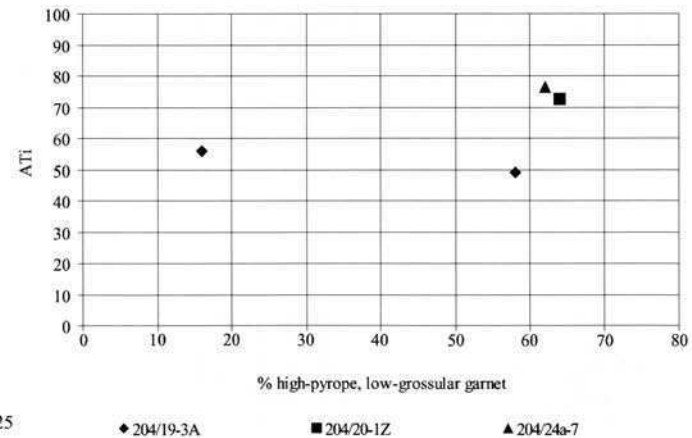
ATi
% high-pyrope, low-grossular garnet
204/19-3A
204/20-1Z
204/24a-7

T25

Fig. 5.

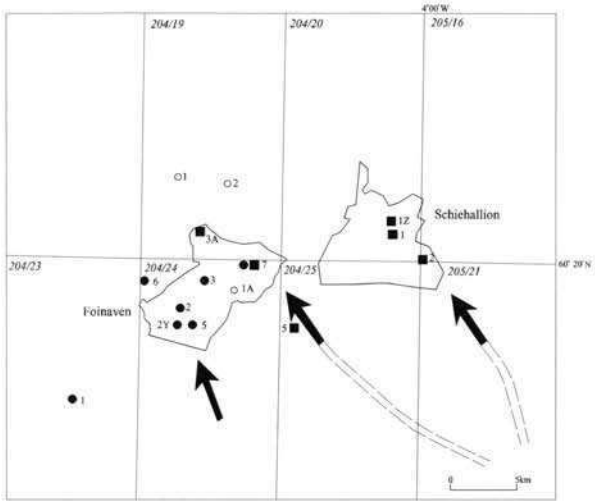

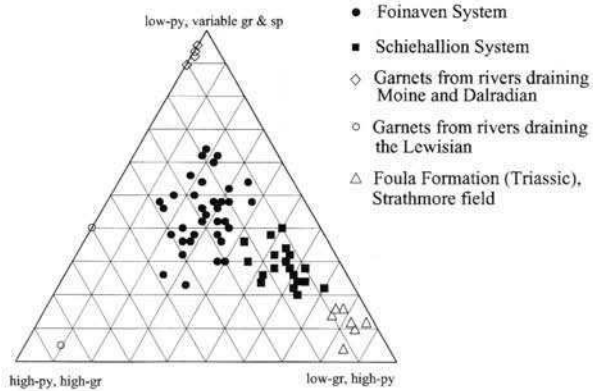

- Foinaven System
- Schiehallion System
- Garnets from rivers draining Moine and Dalradian
- Garnets from rivers draining the Lewisian
- Foula Formation (Triassic), Strathmore field

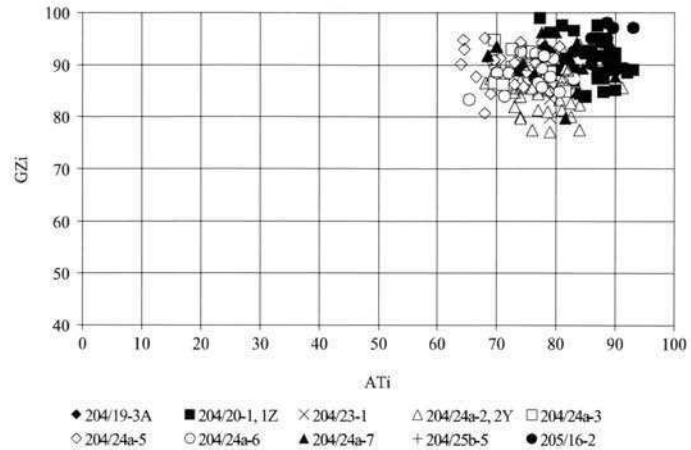

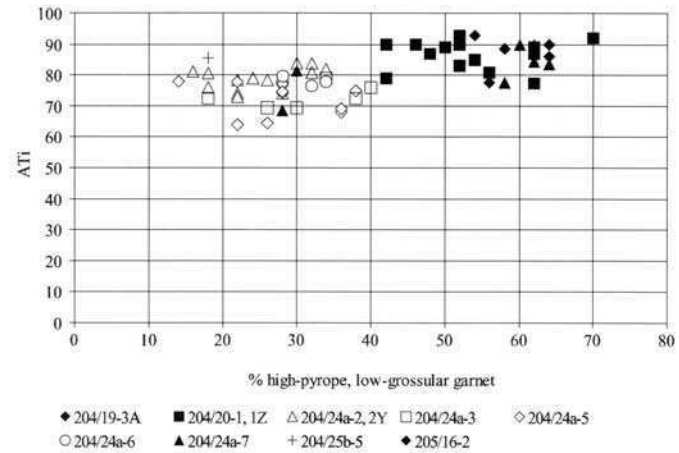

T31-T32

Fig. 6.

values are generally higher, and show greater affinities to sand fed through the Schiehallion system. Garnet assemblages include generally higher numbers of high-pyrope, low-grossular garnets. The Foinaven system therefore appears to have incorporated greater amounts of Foula-type material than during T10-20, with lower proportions of Lewisian- and Moine-type basement. The mineralogical data indicate a greater degree of homogenization of provenance at this time, with the provenance of the Foinaven system becoming more akin to that of the Schiehallion system.

By mapping seismic reflection terminations, Cooper *et al.* (1999) interpret the T32 reservoirs in Foinaven as comprising a series of offlapping channel complexes, one linked to the SE entry point and the other three with the S entry point. The heavy mineral data are generally consistent with the channel distribution as mapped seismically, with the exception of 204/24a-3. This well is interpreted by Cooper *et al.* (1999) to lie at the southern limit of the channel linked to the SE entry point, but heavy mineral data indicate it is strongly influenced by the system fed through the S entry point. Evidently, linking provenance data with detailed seismic mapping adds sophistication to the understanding of channel distribution.

Although most of the sands in well 204/24a-7 have Schiehallion-type mineralogy, fed through the SE entry point to Foinaven, some samples have clear affinities with sediment fed through the S entry point. This dual affinity is manifested by interbedding of Schiehallion- and Foinaven-type mineralogies. It is not clear at this stage how this interbedding was achieved. It is possible that the pattern resulted from the interfingering of two systems operating simultaneously. Alternatively, it is possible that Foinaven-type material was fed through the SE entry point periodically during T31. This could also account for the anomalous mineralogy shown by two samples from 204/25b-5, located within the channel near to the SE entry point; these samples have the high ATi and GZi associated with the Schiehallion source, but have garnet compositions akin to those of the Foinaven system.

T34 (Fig. 7)

There was a significant change in sediment provenance between T31-32 and T34, since all the T34 sands in Foinaven and Schiehallion have heavy mineral characteristics comparable with those previously associated with the Schiehallion disperal system (high ATi, high GZi and garnet assemblages rich in the high-pyrope, low-grossular component). It therefore appears that across the entire area, T34 sands represent continued input from the Schiehallion system, sourced predominantly from material with Foula Formation characteristics with small amounts supplied from other sources. The Foinaven-type source appears to have been cut off, and does not reappear during T36. Sediment input is likely to have occurred via the entry point south of Schiehallion and through the SE entry point in Foinaven.

T35-lower T36 (Fig. 8)

Coverage of the T35-lower T36 interval is less comprehensive than with T31-32 and T34, but the data show that provenance and dispersal patterns continued to change. In fact, one of the most fundamental changes in Paleocene provenance took place between T34 and T35.

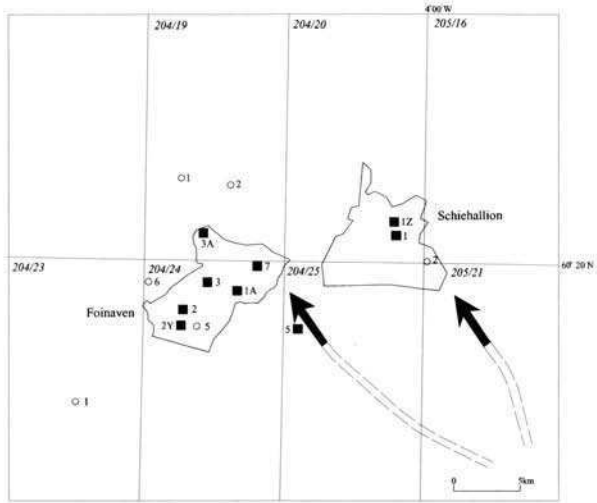

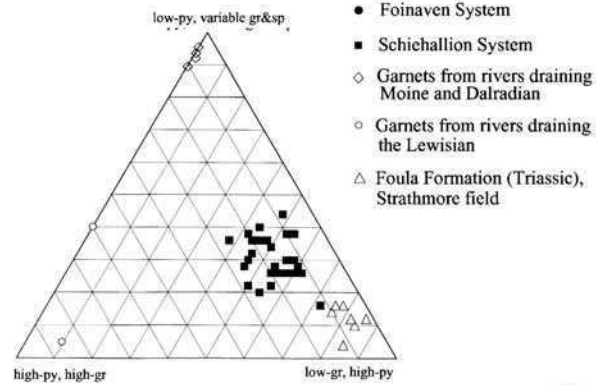

- Foinaven System
- Schiehallion System
- ◇ Garnets from rivers draining Moine and Dalradian
- ○ Garnets from rivers draining the Lewisian
- △ Foula Formation (Triassic), Strathmore field

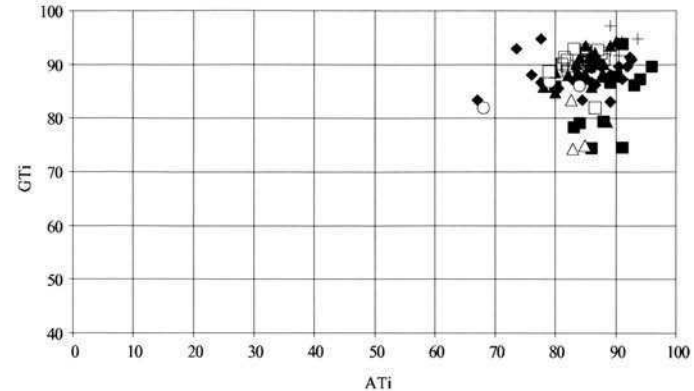

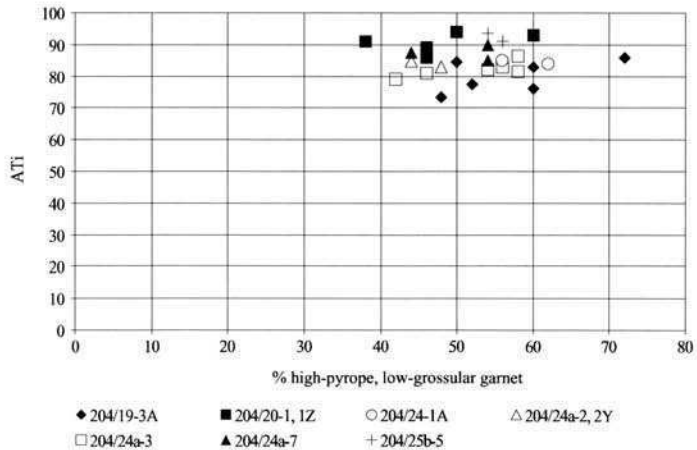

T34

Fig. 7.

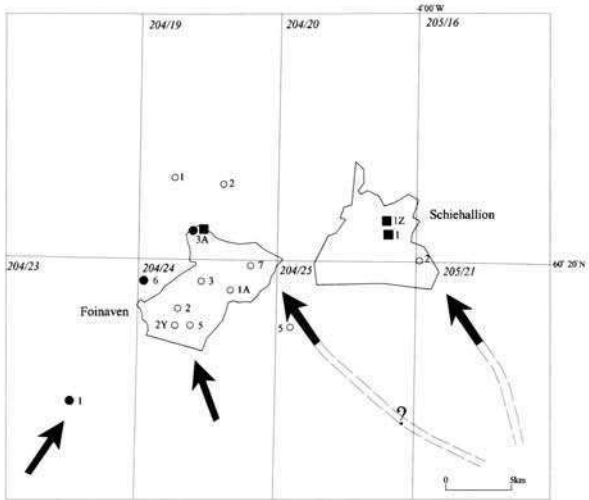
4°00'W
204/19
204/20
205/16
204/23
204/24
204/25
205/21
60° 20'N
Foinaven
Schiehallion
3A
1Z
1
1A
2Y
5
?
0
5km

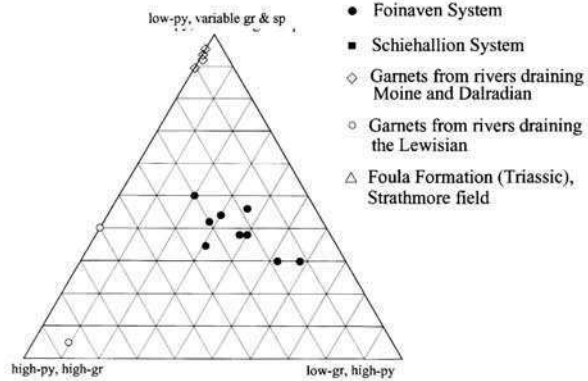
low-py, variable gr & sp
high-py, high-gr
low-gr, high-py
Foinaven System
Schiehallion System
Garnets from rivers draining Moine and Dalradian
Garnets from rivers draining the Lewisian
Foula Formation (Triassic), Strathmore field

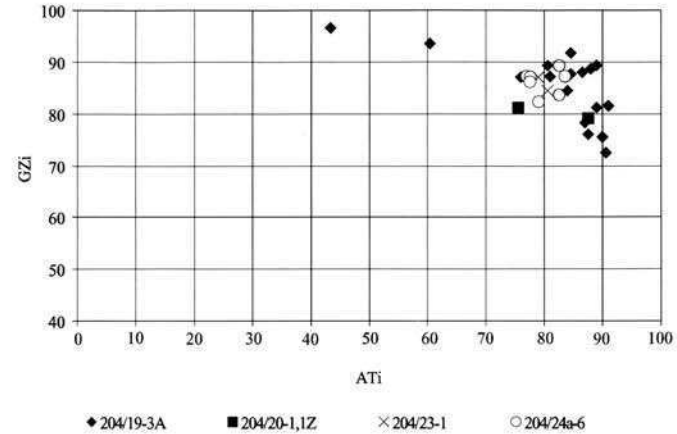
GZi
ATi
204/19-3A
204/20-1,1Z
204/23-1
204/24a-6

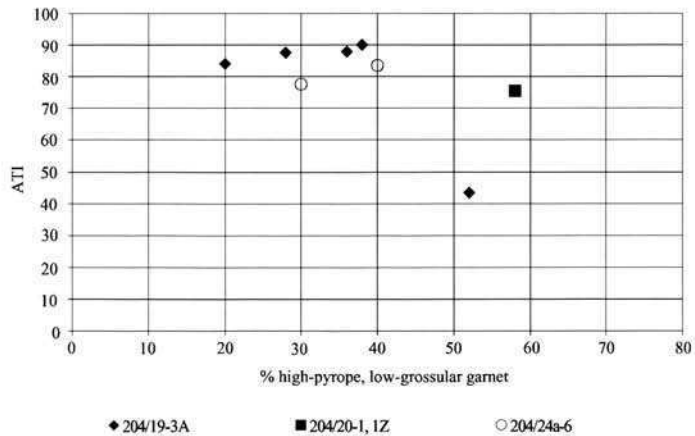
ATI
% high-pyrope, low-grossular garnet
204/19-3A
204/20-1, 1Z
204/24a-6

T35-36L

Fig. 8.

The long-lived and mineralogically consistent Schiehallion dispersal system continued to supply sand to the Schiehallion area, but only one sample (from 204/20-1Z) has the typical characteristics of this source (high ATi, high GZi and abundant high-pyrope, low-grossular garnets). Samples from 204/23-1, 204/24a-6 and most of those from 204/19-3A have high ATi and high GZi, similar to Schiehallion-type sands, but are distinctive in that garnet assemblages are relatively poor in high-pyrope, low-grossular (Foula-type) garnets (Fig. 8). A relatively large number of samples have GZi values between 70 and 80, lower than those typically linked with the Schiehallion system, but these have higher ATi values than those associated with the Foinaven system. Where mineral dissolution is not advanced (in 204/23-1 and the upper part of 204/19-3A), epidote and amphibole abundances are unusually high (in the context of the Foinaven Sub-basin data set).

These characteristics suggest that most of the sediment was sourced directly from basement rocks (including Lewisian and Moine). Recycling is of lesser importance than previously, although there is continued evidence for a Foula component. The tendency for relatively low garnet abundances in some samples is interpreted as a reflection of the involvement of intermediate-acidic Lewisian gneisses, which are garnet-poor. This change in provenance is not clearly identifiable using mineral ratio data alone, but is obvious when garnet data are available. Ebdon *et al.* (1995) noted a marked decline in Mesozoic reworking in the post-T34 section, which was attributed to an increase in proportion of sediment supplied directly from basement rocks. The basement-sourced sediments of T35-lower T36 are interpreted to have been fed through an entry point in the vicinity of 204/23-1 (Ebdon *et al.* 1995).

Within the lower T36 sequence of 204/19-3A, dominated by largely basement-derived sediment, there is thin sand unit (*c.* 4 m) with low ATi, high GZi and abundant Foula-type garnets. This represents a short-lived incursion of sediment from a different source. In most respects, this has the characteristics of the Schiehallion dispersal system, but the markedly lower ATi value indicates it has undergone more prolonged weathering. This suggests derivation from similar source rocks, but through a different transport system to that still operating in the Schiehallion area. In this instance, it seems unlikely that the low ATi values reflect a weathered land surface, and it is considered more likely that the sediment was subjected to weathering during alluvial storage prior to entering the marine system.

Upper T36 (Fig. 9)

The only well with coverage of upper T36 (post-Kettla Member) sandstones is 204/19-3A. GZi and ATi values remain high, with considerable overlap on the GZi-ATi crossplot between T36 upper and T35-T36 lower. The garnet data, however, show continued evolution towards basement-dominated assemblages. Foula-type (high pyrope, low grossular) garnets form less than 15% of the garnet assemblage. The majority of the basement garnets have Lewisian affinities but there is evidence for continued involvement of Moine-type material. Unstable mineral (epidote and amphibole) abundances are very high, consistent with a predominantly first-cycle basement source.

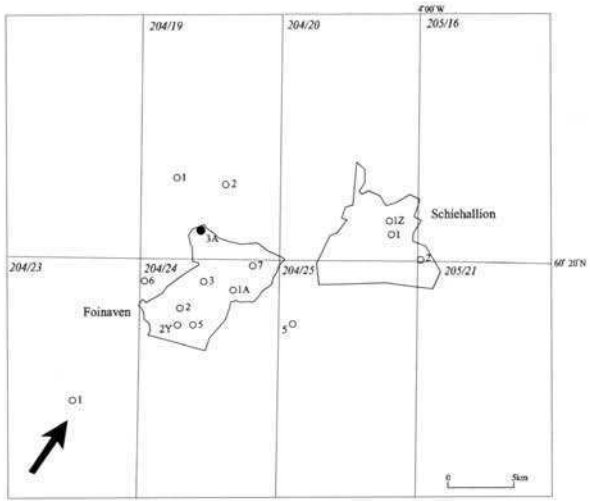
204/19
204/20
205/16
204/23
204/24
204/25
205/21
Foinaven
Schiehallion
0 5km

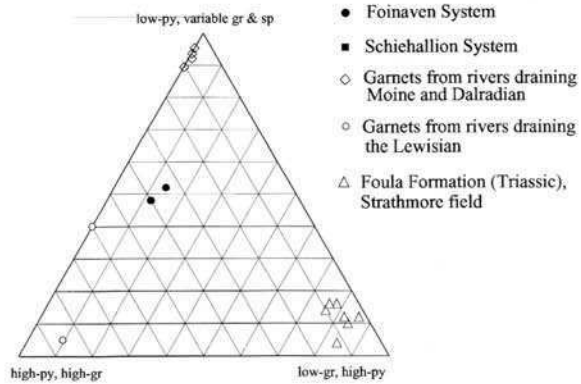
low-py, variable gr & sp
high-py, high-gr
low-gr, high-py
Foinaven System
Schiehallion System
Garnets from rivers draining Moine and Dalradian
Garnets from rivers draining the Lewisian
Foula Formation (Triassic), Strathmore field
T36U

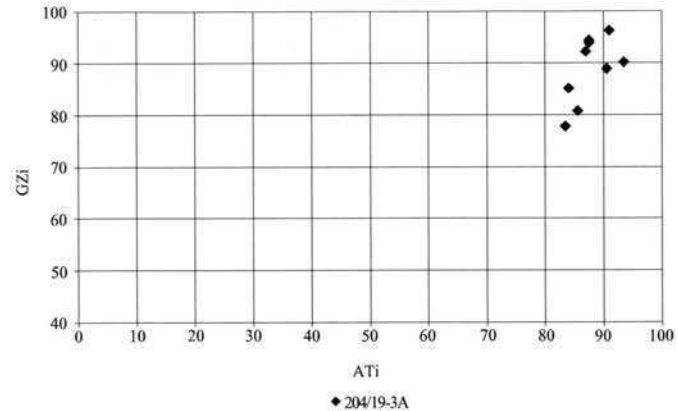
GZi
ATi
204/19-3A

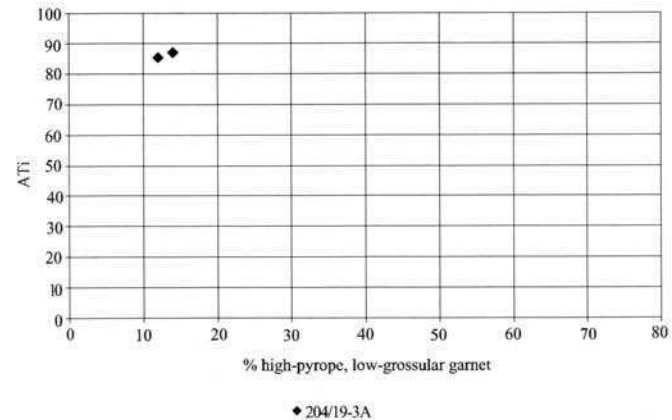
ATi
% high-pyrope, low-grossular garnet
204/19-3A

Fig. 9.

Upper T36 sandstones are considered to represent the products of the same dispersal system to that operating in T35 and lower T36, with continued evolution in source characteristics related to an increased input directly from Lewisian and Moine basement.

Relationship with magmatic activity

The major change in depositional regime from carbonate-dominated to clastic-dominated in the Early Paleocene of the North Sea has been widely ascribed to the onset of magmatic activity along the northwestern margin of the UK landmass and adjacent continental shelf (Parker 1975; Rochow 1981). Uplift of the British Isles during the early Tertiary has been demonstrated by apatite fission track studies, which have suggested denudation of at least 1 km may have taken place (Rowley & White 1998; Thomson *et al.* 1999). This concept was developed by White & Lovell (1997), who suggested that pulsing of the proto-Icelandic plume may have been responsible for the repeated influx of coarse clastics that form the various submarine fan complexes comprising North Sea formations such as Maureen, Andrew and Forties.

The detailed picture of evolution in provenance in the Foinaven Sub-basin described above enables us to compare the timings of significant events in the basin with those in the British Tertiary Igneous Province. In provenance terms, three significant events can be recognized in the early–mid Paleocene sequence of the Foinaven Sub-basin. The first of these was responsible for the influx of coarse clastics in T10, the second for the change in source between T31/32 and T34, and the third for the progressive change in source beginning in T35 and extending through T36.

Of these, the most significant is the T10 event, which records erosion of a highly weathered land surface. The presence of apatite- and garnet-depleted detritus at the base of the T10 sandstone sequence is a strong indication that this represents the first phase of exhumation of the Shetland Platform, because if had there been earlier phases of erosion these would have removed such highly weathered material. The influx of coarse clastic sediments into the Foinaven Sub-basin during T10 is therefore considered to mark the earliest phase of uplift and exhumation of the Shetland Platform.

Reliable radiometric data from the British Tertiary Igneous Province (BTIP) cluster in the 58–61 Ma bracket (Mussett *et al.* 1988; White & Lovell 1997), corresponding to T22-T36 (Fig. 3). Much of the magmatism therefore appears to post-date the main uplift event on the Shetland Platform. However, it appears that some magmatism took place before 61 Ma. Although the dates of 62.4 ± 0.6 Ma and 62.8 ± 0.6 Ma from tephras at the base of the extrusive lava pile on the Isle of Muck, Inner Hebrides (Pearson *et al.* 1996) are presently being re-evaluated (Pearson pers. comm.), they are consistent with the earlier work of Mussett *et al.* (1988), who showed that the earliest lavas on Muck and Eigg are extruded at *c.* 63 Ma. This places the onset of igneous activity during deposition of the T10 sequence. It is therefore considered likely that the onset of igneous activity at *c.* 62.5 Ma is coeval with the uplift event on the Shetland Platform responsible for the T10 sandstones in the Foinaven Sub-basin.

On the basis of available evidence, it is less easy to identify convincing relationships between magmatic activity and the other two provenance events in the Foinaven Sub-basin. The cessation of input through the Foinaven system took place between

deposition of the T31/T32 and T34 sequences, at approximately 59 Ma, in the middle of the maximum pulse of BTIP magmatism which took place over an approximate three million years period. It is therefore difficult to ascribe this event to pulsing of the proto-Icelandic plume. By contrast, it may be significant that the progressive increase in supply from metamorphic basement relative to recycled sediment, beginning with the T35 sequence and extending through T36, broadly coincides with the waning of BTIP magmatism at *c.* 58 Ma (White & Lovell 1997). Alternatively, it could be argued that this change could be simply the result of progressive denudation, which gradually removed the Mesozoic and Paleozoic cover from the metamorphic basement.

Therefore, it would appear that there is a first-order relationship between the initial uplift of the Shetland Platform and the arrival of the proto-Icelandic plume, although even this still remains to be proven by further geochronological studies of the BTIP and adjacent areas. The evidence relating subsequent provenance changes with events in the BTIP are, however, far from convincing, and the concept of a 'pulsing' proto-Icelandic plume causing repeated sediment influx remains to be proven. Other factors, such as eustatic sea-level fluctuations, climate change or progressive denudation, could have been responsible for some, or all, of the changes in provenance observed in the basin. It is also possible that there is a lag between the pulsing of the plume and timing of the sedimentary response. However, it is difficult to argue for a significant time lag between the arrival of the plume and the initial uplift, since the record of magmatism in the BTIP is scanty prior to 61 Ma, and there is still doubt over the timing of events on Muck and Eigg, which represent the earliest manifestations of BTIP magmatism.

Relationship between provenance and reservoir properties

The differences in provenance detected from heavy minerals at the T31-T32 level, described above, are also reflected in detrital mineralogy, in particular in the abundance of ductile rock fragments. Figure 10 plots mean values of the major detrital categories for T31-T32 sandstones in Foinaven wells. Data are restricted to upper fine and lower medium grained massive (structureless) sandstones to minimize mineralogical variations related to facies and texture. The results show a clear distinction in ductile rock fragment abundance between those wells sourced through the entry point SE of Foinaven (204/19-3A, 204/24a-7) and those sourced from the entry point to the S. These rock fragments comprise mudstone, siltstone and altered volcanic material.

Detrital mineralogy also influences reservoir quality. Figure 11 plots porosity against permeability for massive sandstones (again, to minimize facies-related variation) from wells 204/24a-7 (SE entry point) and 204/24a-5 (S entry point). The difference in reservoir quality between the two wells can be attributed largely to their different ductile grain abundances. Sandstones from 204/24a-7 support approximately twice the permeability, for a given porosity, as the more ductile-rich sandstones from 204/24a-5. This reflects greater compaction of the 204/24a-5 rock fabric, with deformed ductile grains constricting pore throats and thus reducing permeability. Mercury injection data confirm that a much higher proportion of the pore system in 204/24a-5 comprises non-effective microporosity compared with 204/24a-7, largely because of the intragranular microporosity within the more abundant ductile grains in 204/25a-5.

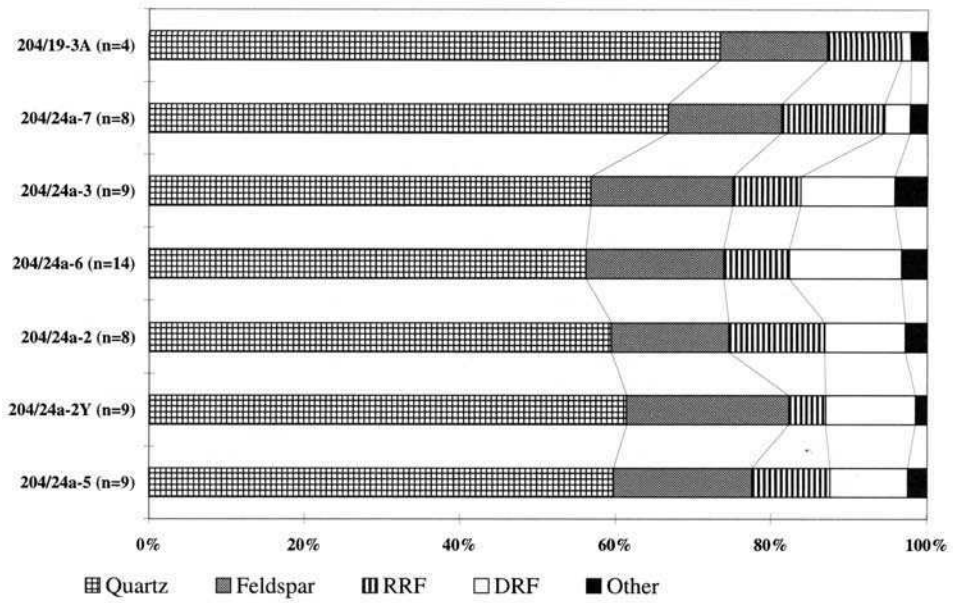

Fig. 10. Summary of the detrital mineralogy found in T31-T32 massive (structureless) upper fine and lower medium grained sandstones, Foinaven Field. DRF, ductile rock fragments; RRF, rigid rock fragments.

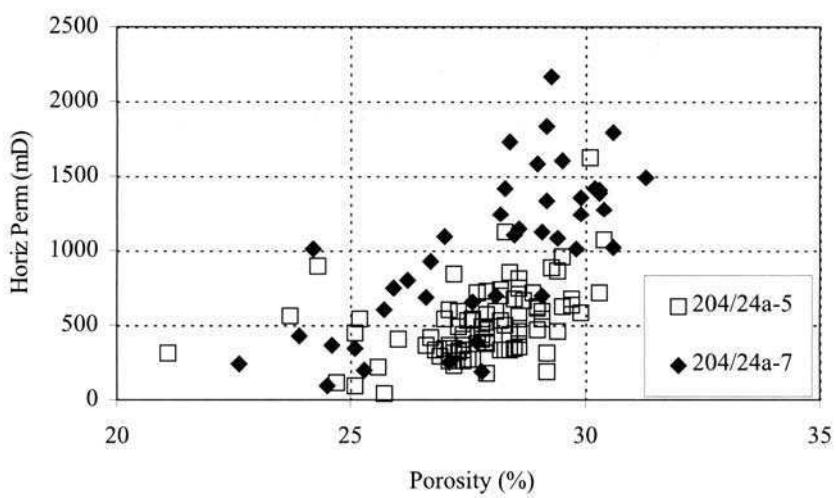

Fig. 11. Porosity–permeability crossplot for T31-T32 massive (structureless) sandstones, wells 204/24a-5 and 204/24a-7, Foinaven Field.

Heavy mineral dissolution

Heavy mineral assemblages generally show a decrease in diversity with increasing depth of burial (Morton & Hallsworth 1999). This change in diversity is the result of progressive dissolution of unstable species as pore fluid temperatures increase.

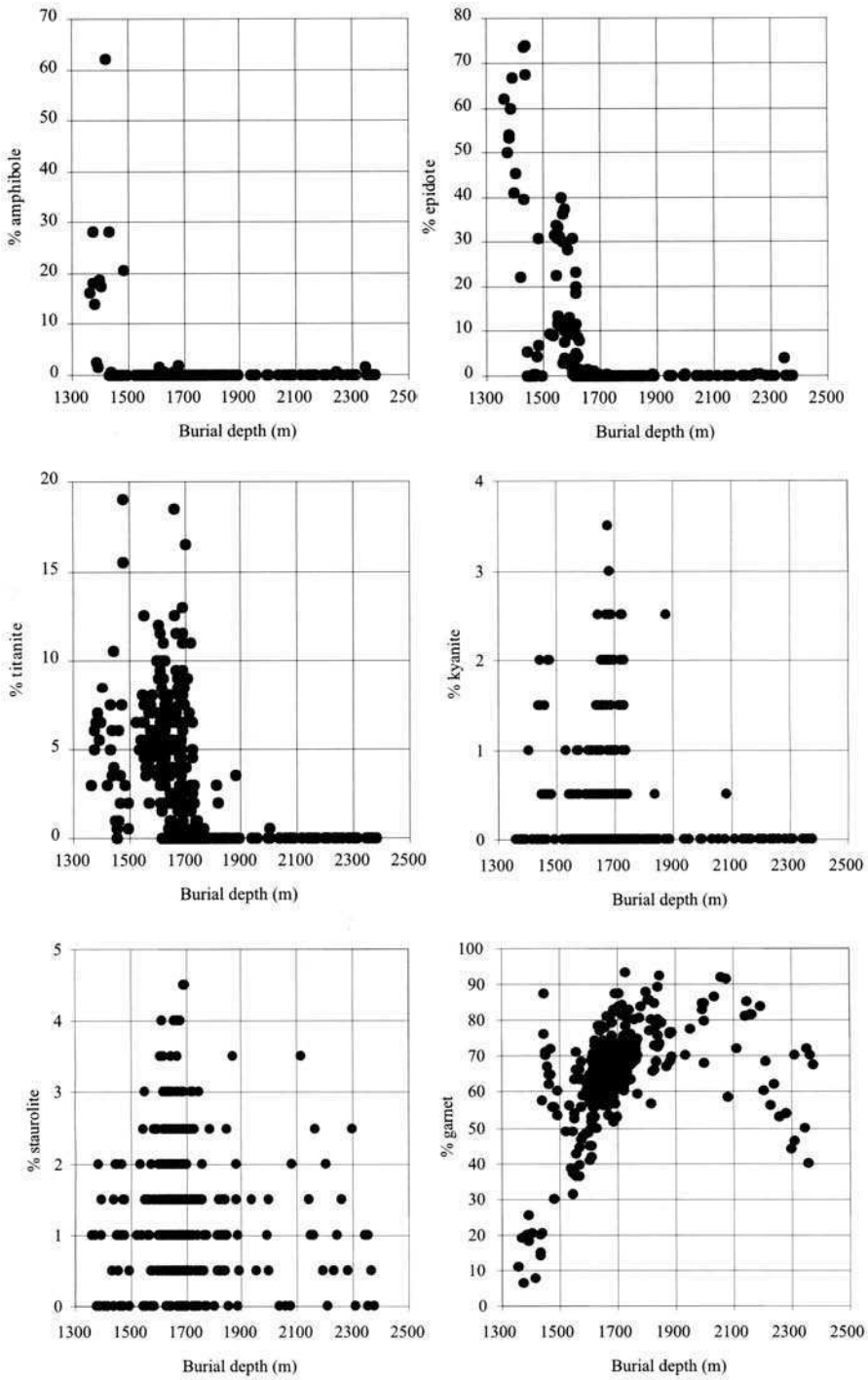

Fig. 12. Plots of mineral abundance against burial depth (true vertical depth, sub-sea floor) for T10-T36 sandstones of the Foinaven Sub-basin, showing progressive depletion of unstable minerals (amphibole, epidote, titanite, kyanite) with increasing burial.

Comparison of dissolution patterns from a number of sedimentary basins suggests that a consistent order of mineral stability applies worldwide. The dataset from the Foinaven Sub-basin offers a further opportunity to examine mineral stability during deep burial.

The relationships between burial depth and mineral abundances are shown in Figure 12. Amphibole is the first to be eliminated, being absent from virtually all samples over 1500 m below sea bed. Epidote disappears at about 1620 m, titanite at about 1700 m and kyanite at about 1760 m. Staurolite is present throughout (maximum burial depth is *c.* 2400 m). Similarly, garnet shows no evidence for elimination through burial diagenesis. Relative abundances of this mineral become greater with increased burial between *c.* 1400 m–1800 m burial, principally due to the removal of amphibole, epidote and titanite. Some samples below 2200 m have relatively low garnet abundances, but this is considered to be a provenance effect related to deep weathering of the Cretaceous land surface. This pattern of mineral depletion matches precisely those seen elsewhere (as summarized by Morton & Hallsworth 1999) and confirms that minerals appear to have consistent relative stabilities in different basins, despite inevitable differences in pore fluid composition.

The depths at which amphibole, epidote, titanite and kyanite are eliminated in the Foinaven Sub-basin are relatively closely spaced compared with other basins where this effect has been documented. In the Foinaven Sub-basin, the depth difference between amphibole depletion and kyanite depletion is only *c.* 260 m, whereas in the Paleocene of the central North Sea, amphibole depletion occurs at 600 m and kyanite at 1800 m (Morton 1984). Moreover, mineral depletion in the Foinaven Sub-basin takes place at greater burial depths than in the North Sea. The difference in mineral dissolution patterns between the two areas is probably the result of oil migration, since the dissolution pattern in the central North Sea was established using water-wet sandstones, whereas many of the samples analysed from the Foinaven area are oil-bearing.

In detail, the downhole distribution of heavy minerals shows evidence for at least two phases of hydrocarbon migration. In the lower T36 section of 204/19-3A (Fig. 13), the upper three samples are epidote-rich, with epidote group minerals forming over 70% of the assemblages. Below 2005.8 m, epidote is scarce or absent. This suggests that the assemblages in the upper part of the lower T36 section were protected from dissolution by early migration of hydrocarbons. However, the present oil-water contact is lower down, at *c.* 2018 m. The heavy mineral evidence therefore suggests that the oil-water contact has changed, presumably through a later phase of hydrocarbon migration. This is consistent with the findings of Parnell *et al.* (1999), who deduced two phases of hydrocarbon migration in the Tertiary on the basis of apatite fission track analysis and fluid inclusion studies, and with the remigration model for hydrocarbon fill along the NE Atlantic margin proposed by Doré *et al.* (1997).

Conclusions

Heavy mineral assemblages in deepwater Paleocene sandstones of the Foinaven Sub-basin are the result of a complex interplay between variations in provenance (both laterally and stratigraphically) and overprinting factors, the most significant being

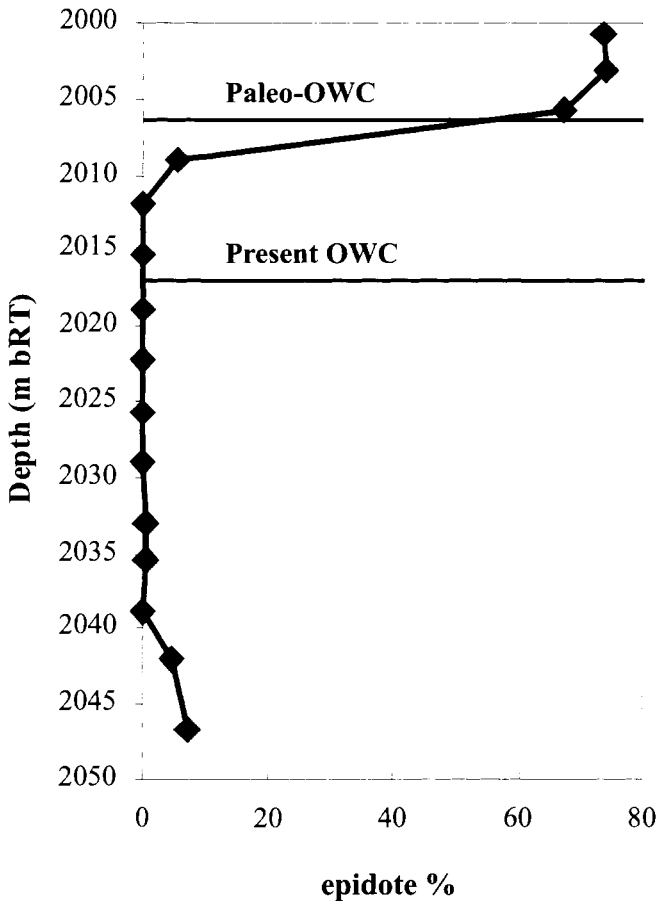

Fig. 13. Downhole variation in abundance of epidote in the T36L section of 204/19-3A, showing sudden depletion in epidote at *c.* 2008 m (measured depth), taken to be the location of a paleo-oil–water contact.

burial diagenesis. The variations in provenance are relatively subtle and can be detected only by using provenance-sensitive aspects of the heavy mineral assemblages (cf. Morton & Hallsworth 1994), namely ratios of minerals with similar hydraulic and diagenetic behaviour and geochemical attributes of individual mineral populations. The distribution of minerals such as amphibole, epidote, titanite and kyanite is heavily influenced by burial diagenesis, the pattern of mineral depletion being directly comparable to that seen in other deep basins worldwide.

Three main provenance and dispersal systems have been detected in the T10-T36 interval. One system, the Schiehallion system, has relatively uniform characteristics and is long-lived, its products being recognized from T10 through to lower T36. The sphere of influence of this system is centred on the Schiehallion Field, but encroaches into the eastern and northern parts of Foinaven during T25 and T31-32, and covers the entire Foinaven Field during T34. The main source component of this system is the Triassic Foula Formation, with minor supply from Lewisian and Moine

basement rocks. There is no evidence for involvement of deeply-weathered material in the source area.

The Foinaven system, by contrast, shows marked changes in character, related to evolution of the source area. The earliest T10 sands were derived from a heavily weathered late Cretaceous regolith developed on Foula Formation and basement rocks. This represents the onset of uplift and exhumation of the Shetland Platform and is likely to have been coeval with the onset of magmatism in the British Tertiary Igneous Province.

Unroofing during later T10-22 and T25 caused the weathered material to be stripped off and the incorporation of increasing amounts of detritus sourced from Lewisian and Moine rocks. The detritus supplied by the Foinaven system in T31-32 was similar to that in T10-25, but with a slightly greater Foula Formation component. As a result, the Foinaven system characteristics approach those of the Schiehallion system, although there is still little or no overlap of the most diagnostic parameters. The Foinaven system appears to have ceased to operate at the end of T32.

In T35, there was a distinct change in provenance, with an increase in the amount of sediment shed directly from Lewisian and Moine basement. This change was progressive, with the latest T36 sediments having the greatest amount of first-cycle basement material, and coincides with a decrease in reworking of Mesozoic palynomorphs (Ebdon *et al.* 1995), consistent with the heavy mineral evidence for greater first-cycle input. The gradational increase in first-cycle basement detritus is broadly coincident with the waning of magmatism in the BTIP (White & Lovell 1997), but a convincing link between this change in sediment source and magmatic activity has yet to be proven.

The heavy mineral data therefore provide important evidence for the operation of different sediment supply systems whose spheres of influence vary as the basin developed. This information has been crucial in constraining sand (i.e. potential reservoir) distribution in the basin. When linked with petrographic and porosity/permeability data, there is evidence that differences in provenance are also responsible for differences in reservoir quality.

The fact that different dispersal systems can be recognized in the Foinaven and Schiehallion areas over the T10-T32 interval suggests that the shelf systems which fed the deepwater deposits were not homogenized through longshore drift processes. It is possible that greater homogenization was achieved during T31-32, with the Foinaven system characteristics approaching those of the Schiehallion system. The disappearance of Foinaven-type sands during T34 may indicate more thorough homogenization. However, it is considered more likely that the Foinaven source was cut off at this time, since the T34 sands have identical characteristics to those of the T31-32 sands derived through the Schiehallion system, rather than having features intermediate between those of the earlier Foinaven and Schiehallion systems.

We are grateful to BP Exploration for permission to present the data used in this paper.

References

BERGGREN, W. A., KENT, D. V., SWISHER, C. C. III & AUBRY, M.-P. 1995. A revised Cenozoic geochronology and chronostratigraphy. *In*: BERGGREN, W. A., KENT, D. V., AUBRY, M.-P. & HARDENBOL, J. (eds) *Geochronology, time scales and stratigraphic correlation: framework for an historical geology*. SEPM, Special Publication, **54**, 129–212.

COOPER, M. M., EVANS, A. C., LYNCH, D. J., NEVILLE, G. & NEWLEY, T. 1999. The Foinaven Field: managing reservoir development uncertainty prior to start-up. *In*: FLEET, A. J. & BOLDY, S. A. R. (eds) *Petroleum Geology of Northwest Europe: Proceedings of the 5th Conference*. Geological Society, London, 675–682.

DORÉ, A. G., LUNDIN, E. R., BIRKELAND, Ø., ELIASSEN, P. E. & JENSEN, L. N. 1997. The NE Atlantic margin: implications of late Mesozoic and Cenozoic events for hydrocarbon prospectivity. *Petroleum Geoscience*, **3**, 117–131.

EBDON, C. C., GRANGER, P. J., JOHNSON, H. D. EVANS, A. M. 1995. Early Tertiary evolution and sequence stratigraphy of the Faroe–Shetland Basin: implications for hydrocarbon prospectivity. *In*: SCRUTTON, R. A., STOKER, M. S., SHIMMIELD, G. B. & TUDHOPE, A. W. (eds), *The tectonics, sedimentation and palaeoceanography of the North Atlantic region*. Geological Society, London, Special Publications, **90**, 51–69.

EVANS, D., MORTON, A. C., WILSON, S., JOLLEY, D. & BARREIRO, B. A. 1997. Palaeoenvironmental significance of marine and terrestrial Tertiary sediments on the NW Scottish shelf in BGS borehole 77/7. *Scottish Journal of Geology*, **33**, 31–42.

HANNA, R. W., CURRIE, M. T., CONNOLLY, P., COWPER, D. R., SMITH, R. L. & LINSKAILL, C. J. 1996. Multiple hypothesis reservoir description utilising advanced 3D seismic west of Shetland. *Offshore Technology Conference* **OTC 7962**, Houston, 91–98.

HERRIES, R., PODDUBIUK, R. & WILCOCKSON, P. 1999. Solan, Strathmore and the back basin play, west of Shetland. *In*: FLEET, A. J. & BOLDY, S. A. R. (eds) *Petroleum Geology of Northwest Europe: Proceedings of the 5th Conference*. Geological Society, London, 693–712.

KNOX, R. W. O'B., HOLLOWAY, S., KIRBY, G. A. & BAILY, H. E. 1997. *Stratigraphic nomenclature of the UK North West Margin. 2. Early Paleogene Lithostratigraphy and Sequence Stratigraphy*. British Geological Survey, Nottingham.

LAMERS, E. & CARMICHAEL, S. M. M. 1999. The Paleocene deepwater sandstone play west of Shetland. *In*: FLEET, A. J. & BOLDY, S. A. R. (eds) *Petroleum Geology of Northwest Europe: Proceedings of the 5th Conference*. Geological Society, London, 645–659.

LEACH, H. M., HERBERT, N., LOS, A. & SMITH, R. L. 1999. The Schiehallion development. *In*: FLEET, A. J. & BOLDY, S. A. R. (eds) *Petroleum Geology of Northwest Europe: Proceedings of the 5th Conference*. Geological Society, London, 683–692.

MORTON, A. C. 1984. Stability of detrital heavy minerals in Tertiary sandstones of the North Sea Basin. *Clay Minerals*, **19**, 287–308.

MORTON, A. C. 1985. A new approach to provenance studies: electron microprobe analysis of detrital garnets from Middle Jurassic sandstones of the northern North Sea. *Sedimentology*, **32**, 553–566.

MORTON, A. C. 1987. Influences of provenance and diagenesis on detrital garnet suites in the Forties sandstone, Paleocene, central North Sea. *Journal of Sedimentary Petrology*, **57**, 1027–1032.

MORTON, A. C. & BERGE, C. 1995. Heavy mineral suites in the Statfjord and Nansen Formations of the Brent Field, North Sea: a new tool for reservoir subdivision and correlation. *Petroleum Geoscience*, **1**, 355–364.

MORTON, A. C., BORG, G., HANSLEY, P. L., HAUGHTON, P. D. W., KRINSLEY, D. H. & TRUSTY, P. 1989. The origin of faceted garnets in sandstones: dissolution or overgrowth. *Sedimentology*, **36**, 927–942.

MORTON, A. C. & GRANT, S. 1998. Cretaceous depositional systems in the Norwegian Sea: heavy mineral constraints. *Bulletin of the American Association of Petroleum Geologists*, **82**, 274–290.

MORTON, A. C. & HALLSWORTH, C. R. 1994. Identifying provenance-specific features of detrital heavy mineral assemblages in sandstones. *Sedimentary Geology*, **90**, 241–256.

MORTON, A. C. & HALLSWORTH, C. R. 1999. Processes controlling the composition of heavy mineral assemblages in sandstones. *Sedimentary Geology*, **124**, 3–29.

MORTON, A. C., HALLSWORTH, C. R. & WILKINSON, G. C. 1993. Evolution of sand provenance during Paleocene deposition in the Northern North Sea. *In*: PARKER, J. R. (ed.) *Petroleum Geology of Northwest Europe: Proceedings of the 4th Conference*. Geological Society, London, 73–84.

MUSSETT, A. E., DAGLEY, P. & SKELHORN, R. R. 1988. Time and duration of igneous activity in the British Tertiary Igneous Province. *In*: MORTON, A. C. & PARSON, L. M. (eds) *Early Tertiary volcanism and the opening of the NE Atlantic*. Geological Society, London, Special Publications, **39**, 271–281.

PARKER, J. R. 1975. Lower Tertiary sand development in the central North Sea. *In*: WOODLAND, A. W. (ed.) *Petroleum and the Continental Shelf of Northwest Europe*. Applied Science Publishers, London, 447–453.

PARNELL, J., CAREY, P. F., GREEN, P. & DUNCAN, W. 1999. Hydrocarbon migration history, West of Shetland: integrated fluid inclusion and fission track studies. *In*: FLEET, A. J. & BOLDY, S. A. R. (eds) *Petroleum Geology of Northwest Europe: Proceedings of the 5th Conference*. Geological Society, London, 613–625.

PEARSON, D. G., EMELEUS, C. H. & KELLEY, S. P. 1996. Precise $^{40}Ar/^{39}Ar$ age for the initiation of Palaeogene volcanism in the Inner Hebrides and its regional significance. *Journal of the Geological Society, London*, **153**, 815–818.

ROCHOW, K. A. 1981. Seismic stratigraphy of the North Sea 'Palaeocene' deposits. *In*: ILLING, L. V. & HOBSON, G. D. (eds) *Petroleum Geology of the Continental Shelf of Northwest Europe*. Heyden & Son, London, 255–266.

ROWLEY, E. & WHITE, N. J. 1998. Inverse modelling of extension and denudation in the East Irish Sea Basin. *Earth and Planetary Science Letters*, **161**, 57–71.

STOKER, M. S., HITCHEN, K. & GRAHAM, C. C. 1993. *The geology of the Hebrides and West Shetland shelves, and adjacent deep-water areas*. HMSO, London.

THOMSON, K., UNDERHILL, J. R., GREEN, P. F., BRAY, R. J. & GIBSON, H. J. 1999. Evidence from apatite fission track analysis for the post-Devonian burial and exhumation history of the northern Highlands, Scotland. *Marine and Petroleum Geology*, **16**, 27–39.

VERSTRALEN, I., HARTLEY, A. & HURST, A. 1995. The sedimentological record of a late Jurassic transgression: Rona Member (Kimmeridge Clay Formation equivalent), West Shetland Basin, UKCS. *In*: HARTLEY, A. J. & PROSSER, D. J. (eds), *Characterisation of Deep Marine Clastic Systems*. Geological Society, London, Special Publications, **94**, 155–176.

WHITE, N. & LOVELL, B. 1997. Measuring the pulse of a plume with the sedimentary record. *Nature, London*, **387**, 888–891.

This page intentionally left blank

Genesis and age of the Erlend Volcano, NE Atlantic Margin

DAVID W. JOLLEY[1] & BRIAN R. BELL[2]

[1] *Department of Animal and Plant Science, University of Sheffield, Alfred Denny Building, Western Bank, Sheffield S10 2TN, UK (e-mail: d.jolley@sheffield.ac.uk)*

[2] *Division of Earth Sciences, University of Glasgow, Gregory Building, Glasgow G12 8QQ, UK (e-mail: b.bell@earthsci.gla.ac.uk)*

Abstract: The Palaeogene Erlend Volcano subcrops in the Faroe–Shetland Basin on the NE Atlantic Margin and was first recognized on the basis of its pronounced positive gravity and magnetic anomalies. Three hydrocarbon exploration wells (209/3-1; 209/4-1A; 209/9-1) have penetrated thick sequences of subaerial facies basaltic lavas and subaqueous volcanic breccias (the 'Basaltic Suite'), overlying Palaeogene (Thanetian) and Cretaceous (Maastrichtian and Campanian) sedimentary rocks interbedded with medium to fine-grained silicic igneous rocks (the 'Acidic Suite'). Detailed palynological and petrological analysis indicates that the basaltic rocks were contemporaneous with the Faroes Lower Lava Formation at *c.* 56.6–55 Ma, and were erupted into environments ranging between dry land and brackish to freshwater lagoons at the margin of a marine channel separating the Erlend Volcano from the Brendan's Volcano to the north. The subjacent Acidic Suite is interpreted as a series of sills emplaced approximately contemporaneously with the volcanic rocks on the basis of their diachronous relationship with interbedded sedimentary rocks, together with high Thermal Alteration Index values of *in situ* fossils.

The Erlend Volcano is located offshore of NW Scotland in the Faroe–Shetland Basin at 61°50′N, 00°30′W, within the north of UK Quadrants 208 and 209 (Fig. 1) and was first recognized by the pronounced gravity and magnetic signatures of its subjacent (intrusive) central complex during a regional survey by the British Geological Survey in 1977 (Chalmers & Western 1979). It was named by Ridd (1983), and it is one of a number of subcrop Palaeogene volcanic structures which developed in the NE Atlantic prior to the onset of ocean floor spreading between the Faroe Islands and East Greenland at *c.* 55 Ma. Unlike the related onshore central complexes on Skye, Rum and Mull, where the associated volcanic superstructure has been removed by erosion, the Erlend Volcano retains a reasonably complete succession of volcanic lithologies. This contribution considers lithological and palynological evidence for the depositional environment and age of the strata of the Erlend Volcano.

From: JOLLEY, D. W. & BELL, B. R. (eds) *The North Atlantic Igneous Province: Stratigraphy, Tectonic, Volcanic and Magmatic Processes.* Geological Society, London, Special Publications, **197**, 95–110. 0305-8719/02/$15.00

History of research

Regional offshore gravity and magnetic surveys, combined with 2D and 3D seismic surveys, indicate that the onshore Palaeogene volcanic/intrusive centres of the Hebridean Volcanic Province also occur within the Faroe–Shetland Basin and the Rockall Trough. One of the first offshore volcanic centres to be identified was Erlend. Chalmers & Western (1979) provided a simple model which interpreted the Erlend gravity and magnetic anomaly in terms of a dense cylindrical body of igneous material *c.* 14 km in diameter, extending downwards from a depth of *c.* 2 km, and akin to the eroded remnants of intrusive centres such as Skye and Mull.

Other apparently similar central complexes within the Faroe–Shetland Basin, including Brendan, Westray and Judd, lack well penetration. In contrast, Erlend has been drilled at three different locations by hydrocarbon exploration wells. The wells 209/3-1, 209/4-1A and 209/9-1 have provided sample material, mainly ditch cuttings, with some sidewall cores for this study (Fig. 1).

Ridd (1983) provided a brief account of the igneous lithologies encountered in Well 209/9-1, comprising a succession over 400 m in thickness. Basaltic rocks overlie acidic igneous rocks, the latter intercalated with Cretaceous (Campanian; cf. Ridd 1983) sedimentary rocks dated by their foraminiferal content. The precise age of the overlying basaltic rocks was not determined. Gatliff *et al.* (1984) provided a more detailed account of the internal structure of the Erlend Volcano. Analysis of gravity data led them to conclude that there are two (possibly overlapping) volcanic centres, which they named Erlend and West Erlend, the latter producing a smaller gravity anomaly. The central complex below the Erlend Volcano was interpreted to be of gabbroic composition and to have a diameter of 14 km, with a base at a depth of 15 km, whereas the West Erlend Central Complex was modelled on the basis of a downward-tapering mass of similar material.

Detailed mapping of *c.* 6000 km of commercial multichannel seismic data at a scale of 1:50 000 indicated to Gatliff *et al.* (1984) that the edge of the strongly reflective lavas varied between a feather edge and a more obvious scarp, with a relief of up to 250 m. The lava escarpment is best developed around the SW and NE margins of the volcanic sequence and is interpreted in this study as a hyaloclastite deltaic sequence which formed as lavas entered the basin, chilled and fragmented, producing a prograding sequence of bedded volcanic breccias (cf. Wood *et al.* 1988; Pedersen *et al.* 1993). Where the volcanic sequence is thick, subvolcanic imaging is poor. Sills which form obvious reflections beyond the edge of the volcanic rocks, are not easily recognized below the main volcanic sequence.

Gatliff *et al.* (1984) recognized a depression, *c.* 2000 m across and 300–400 m deep, on the top volcanic surface above the Erlend Central Complex, which they interpreted as a vent. Around the vent, internal reflectors within the volcanic sequence dip radially, outwards. The uppermost part of the volcanic sequence appears to have been eroded prior to deposition of the overlying sediments.

No precise age for the volcano was presented by Gatliff *et al.* (1984), although comparisons with the onshore Palaeogene volcanic sequences of the Inner Hebrides were made. Of significance, the Balder Formation onlaps the volcanic sequence on the SE flank of the volcano, a clear indication that the Erlend Volcano is stratigraphically older.

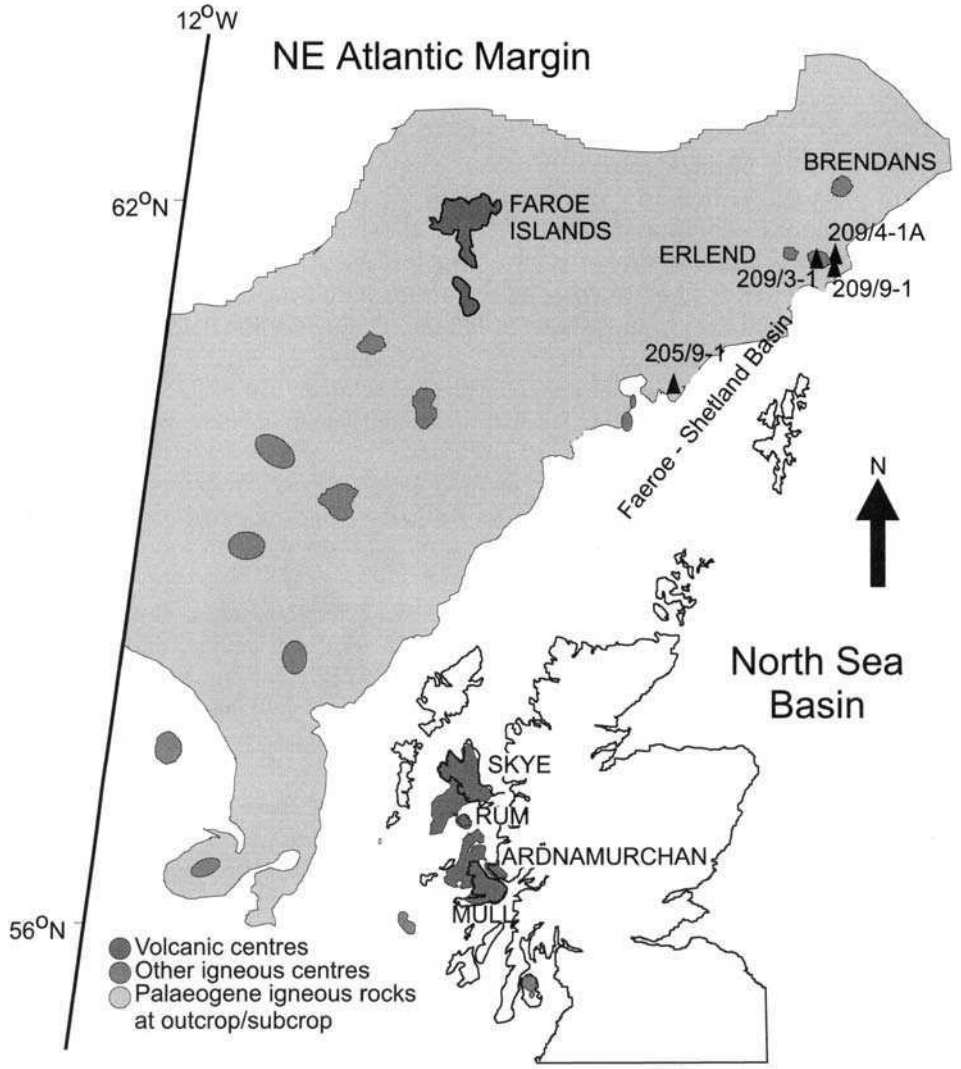

Fig. 1. Location map showing gravity anomaly, extent of lavas, well locations, quadrants, latitudes and longitudes, and lava escarpments.

Kanaris-Sotiriou *et al.* (1993) described the petrography and geochemistry of basalts and cordierite-bearing dacites from Well 209/3-1, located west of the gravity/magnetic maximum (Fig. 1). The basalts were determined as being of N- to T-type MORB affinity. The geochemistry of the dacites suggests an origin by partial melting of aluminous sedimentary or metasedimentary lithologies. Kanaris-Sotiriou *et al.* (1993) did not make the assumption that the dacites are extrusive units and suggested that an intrusive origin is equally likely. An age of 58 ± 3 to 55 ± 4 Ma (whole rock; K–Ar) for the dacites in Well 209/4-1A was reported by Mitchell & Euwe (1988), which appears to be at variance with the late Cretaceous age suggested by Ridd

(1983) and the age reported by Hitchen & Ritchie (1987) of 64.8 ± 0.8 (whole rock; Ar–Ar) for acidic igneous rocks in Well 209/9-1.

Basaltic suite lithologies

Detailed analysis of ditch cuttings, sidewall cores and downhole wireline log data (rate of progress, gamma ray; resistivity) from the three Erlend Wells (Fig. 1), together with published seismic data (Gatliff *et al.* 1984) indicate a variety of lithologies in the igneous-prone intervals of each of the three wells. These lithologies, listed below, are shown in Figure 2 as complex depositional units between the Campanian/Maastrichtian Shetland Group sediments and the siltstones of the Balder Formation.

Well 209/3-1. 823 m of basalts and interbedded sedimentary rocks, underlain by siltstones and limestones interbedded with basic and acidic igneous rocks;

Well 209/4-1A. 475 m of hyaloclastites and basaltic lavas, together with interbedded siltstones and sandstones, underlain by claystones and shales interbedded with basic and acidic igneous rocks;

Well 209/9-1. 170 m of interbedded basalts and hyaloclastites, together with siltstones and sandstones, underlain by *c.* 270 m of dominant acidic non-fragmental and fragmental rocks (possibly with some interbedded claystones), in turn underlain by *c.* 930 m of claystones and shales interbedded with basic and acidic igneous rocks, with a basement of Caledonian (Late Silurian–Early Devonian) granite (the Rendle Granite).

To analyse the age and environment of deposition of these lithologies, palynological analysis was undertaken on a suite of samples from each of the three wells. Evidence from dinoflagellate cysts, other algae, pollen and spores preserved in the sedimentary inter- and intra-basaltic sediments in the volcanic sequence (Fig. 3) was compared to a standard pollen and spore profile and microplankton event scheme for the 65–52 Ma period, derived from regional Faroe–Shetland Basin well data.

Ditch cuttings were available for all three wells, together with sidewall cores from Well 209/3–1. Material was analysed from throughout the entire volcanic sequence. Sample depths were chosen on the basis of the gamma ray log, which allows the rapid identification of the depths of the sedimentary intercalations. In addition, boles were targeted for their potential palynomorph contents, in a manner similar to that applied to the onshore volcanic sequences of Skye, Mull and Antrim (Bell & Jolley 1997; Jolley 1997).

Preparation of samples for palynological analysis involved dissolution of silicates in hydrofluoric acid, and a brief oxidation in nitric acid to remove any pyrite. Samples were processed quantitatively, using a weighed sediment fraction; a known proportion of the residue remaining at the end of processing was mounted as strew mounts at a known dilution, ensuring consistency of quantitative data. The quantitative nature of the analysis, involving the counting of up to three hundred specimens and a subsequent scan of other material allowed the preparation of the data matrices presented here (Fig. 3). The implications of these data are discussed below in downhole order. In all cases, the nature of the sample material necessitates the use of first downhole occurrence (FDO) datums.

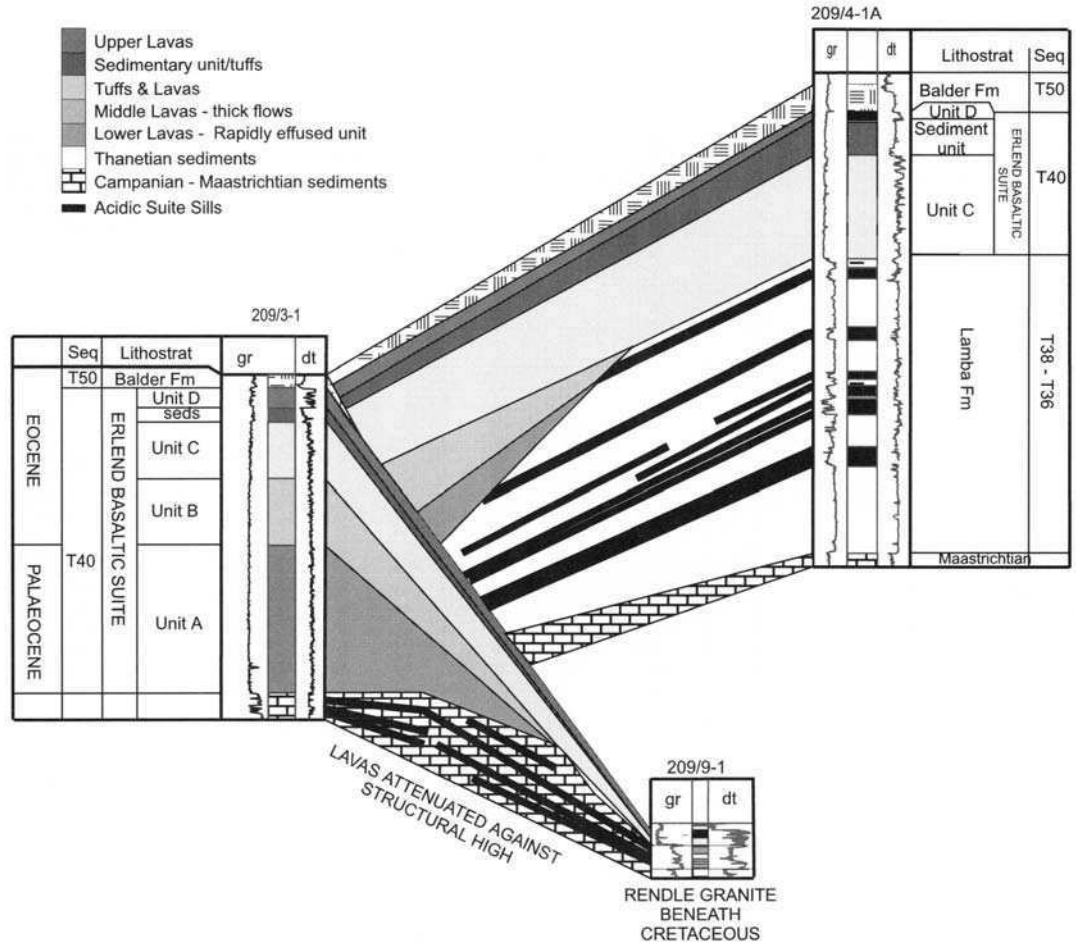

Fig. 2. Fence diagram showing the correlation of the three wells drilled on the Erlend Volcano.

Taxon/Sample depth	1151	1157	1160	1172	1181	1190	1202	1205	1220	1235	1241	1247	1265	1268	1283	1286	1349	1352	1460	1490	1496	1508	1661	1664
Dinocysts and Algae																								
Areoligera cf. coronata	10	0	0	0	0	0	0	0	0	0	0	0	0	0	0	0	0	0	0	0	0	0	0	0
Areoligera cf. medusettiformis	14	0	3	0	0	0	0	0	0	0	0	0	0	0	0	0	0	0	0	0	0	0	0	0
Areosphaeridium diktyoplokus	0	3	0	0	0	0	0	0	0	0	0	0	0	0	0	0	0	0	0	0	0	0	0	0
Areosphaeridium michoidii	0	8	0	0	0	0	0	0	0	0	0	0	0	0	0	0	0	0	0	0	0	0	0	0
Botryococcus spp.	1	0	0	1	0	0	0	0	1	1	0	0	0	0	0	0	0	0	0	0	0	0	0	0
Chatangiella sp. (spiny form)	0	0	0	0	0	0	0	0	0	0	0	0	0	0	0	0	0	0	0	0	12	3	0	4
Chatangiella spp.	0	0	0	0	0	0	0	0	0	0	0	0	0	0	0	0	0	0	3	3	23	4	11	3
Chatangiella tripartita	0	0	0	0	0	0	0	0	0	0	0	0	0	0	0	0	0	0	3	0	0	1	4	0
Chatangiilla ditissima	0	0	0	0	0	0	0	0	0	0	0	0	0	0	0	0	0	0	1	1	6	11	2	2
Cleistosphaeridium spp.	0	0	0	0	0	0	0	0	0	0	0	0	0	0	0	0	0	0	1	1	0	0	0	0
Cordosphaeridium gracile	2	0	0	0	0	0	0	0	0	0	0	0	0	0	0	0	0	0	0	0	0	0	0	0
Deflandrea phosphoritica	4	0	1	0	0	0	0	0	0	0	0	0	0	0	0	0	0	0	0	0	0	0	0	0
Diphyes ficusoides	0	0	1	0	0	0	0	0	0	0	0	0	0	0	0	0	0	0	0	0	0	0	0	0
Eatonicysta ursulae	7	0	1	-2	0	0	0	0	0	0	0	0	0	0	0	0	0	0	0	0	0	0	0	0
Florentinia radiculata	0	0	0	0	0	0	0	0	0	0	0	0	0	0	0	0	0	0	0	0	0	0	0	2
Fromea fragilis	4	0	2	0	0	0	0	0	0	0	0	0	0	0	0	0	0	0	0	0	0	0	2	2
Hapsocysta sp. Davey	0	0	0	0	0	0	0	0	0	0	0	0	0	0	0	0	0	0	0	0	0	0	1	1
Heterosphaeridium heteracanthum	0	0	0	0	0	0	0	0	0	0	0	0	0	0	0	0	0	0	4	2	1	1	9	10
Homotryblium oceanicum	4	0	0	0	0	0	0	0	0	0	0	0	0	0	0	0	0	0	0	0	0	0	0	0
Homotryblium tenuispinosum	153	0	18	0	0	0	0	0	0	0	0	0	0	0	0	0	0	0	0	0	0	0	0	0
Isabelladinium cooksoniae	0	0	0	0	0	0	0	0	0	0	0	0	0	0	0	0	0	0	4	1	12	10	13	1
Laciniidinium biconicum	0	0	0	0	0	0	0	0	0	0	0	0	0	0	0	0	0	0	0	4	30	30	9	18
Lentinia wetzelii	2	0	0	0	0	0	0	0	0	0	0	0	0	0	0	0	0	0	0	0	0	0	0	0
Odontochitina costata	0	0	0	0	0	0	0	0	0	0	0	0	0	0	0	0	0	0	0	0	1	0	1	3
Oligosphaeridium complex	0	0	0	0	0	0	0	0	0	0	0	0	0	0	0	0	0	0	5	2	6	1	3	14
Palaeohystrichophora infusorioides	0	0	0	0	0	0	0	0	0	0	0	0	0	0	0	0	0	0	0	1	9	20	2	0
Palaeoperidinium cretaceum	0	0	0	0	0	0	0	0	0	0	0	0	0	0	0	0	0	0	0	3	4	1	1	0
Palaeoperidinium pyrophorum	0	0	0	0	0	0	0	0	0	0	0	0	0	0	0	0	0	0	20	19	12	2	14	19
Phthanoperidinium echinatum	13	0	2	0	0	0	0	0	0	0	0	0	0	0	0	0	0	0	0	0	0	0	0	0
Spinidinium densispinosum	0	0	0	0	0	0	0	0	0	0	0	0	0	0	0	0	0	0	0	3	3	1	0	0
Spiniferites ramosus subsp ramosus	7	0	8	0	0	0	0	0	1	0	0	0	0	0	0	0	0	0	4	0	5	3	12	15
Subtilisphaera pallida	6	0	2	0	0	0	0	0	0	0	0	0	0	0	0	0	0	0	0	0	0	0	0	0
Systematophora placacantha	10	0	2	0	0	0	0	0	0	0	0	0	0	0	0	0	0	0	0	0	0	0	0	0
Trithyrodinium suspectum	0	0	0	0	0	0	0	0	0	0	0	0	0	0	0	0	0	0	0	2	6	1	0	0
Wetzeliella sp	3	0	1	0	0	0	0	0	0	0	0	0	0	0	0	0	0	0	0	0	0	0	0	0
Wetzelliela articulata sensu J de C	5	0	0	0	0	0	0	0	0	0	0	0	0	0	0	0	0	0	0	0	0	0	0	0

Pollen and Spores																									
Alnipollenites verus	1	1	1	0	0	1	1	0	1	2	0	0	1	0	1	1	0	0	0	1	0	0	1
Aquilapollenites spinulosus	0	0	0	0	0	0	0	0	0	0	0	0	0	0	0	0	0	0	6	6	9	1	18
Arecipites spp.	1	1	0	0	0	1	0	0	0	0	0	0	0	0	0	0	0	0	0	0	0	0	0
Azolla massulae	1	0	0	2	0	0	0	0	0	0	0	0	0	0	1	2	0	0	0	0	0	0	0
Baculatisporites primarius	0	0	0	0	0	0	2	0	2	0	0	0	0	0	0	0	0	0	0	0	0	0	1
Caryapollenites circulus	2	2	1	1	0	2	0	0	0	0	0	0	2	3	0	4	0	0	0	0	0	0	0
Caryapollenites triangulus	0	0	1	0	0	0	0	0	0	0	0	0	0	0	0	0	0	0	0	0	0	0	0
Caryapollenites veripites	3	1	7	0	0	1	9	3	5	0	2	1	15	13	13	26	4	8	0	2	0	0	0
Cupuliferoidaepollenites lib liblarensis	0	0	0	2	0	0	0	0	0	0	0	0	1	1	0	0	0	0	0	0	1	0	0
Cupuliferoipollenites cingulum fusus	0	0	1	1	0	0	0	0	0	0	1	0	1	2	1	3	1	2	0	0	1	0	0
Cupuliferoipollenites cingulum oviformis	0	0	0	0	0	0	1	0	0	0	0	0	0	1	0	0	0	0	0	0	0	0	0
Cupuliferoipollenites cingulum pusillus	0	0	1	0	0	0	0	0	0	0	0	0	1	0	0	1	0	0	0	0	0	0	0
Deltoidospora adriennis	3	1	2	2	0	1	3	3	1	1	0	0	2	2	3	3	1	5	0	0	0	0	1
Deltoidospora maxoides	0	0	0	1	0	0	0	0	0	0	0	0	0	1	1	1	0	0	0	0	0	0	0
Deltoidospora wolfii	0	0	0	1	0	0	0	0	0	0	0	0	0	0	0	0	0	0	0	0	0	0	0
Ilexpollenites iliacus	0	0	2	0	0	0	0	0	0	0	0	0	0	0	0	0	0	0	0	0	0	0	0
Inaperturopollenites distichiforme	0	1	2	0	0	1	0	6	2	3	1	0	11	9	6	6	5	3	0	0	3	0	1
Inaperturopollenites hiatus	16	4	21	19	0	4	46	36	18	21	11	11	98	125	86	123	0	75	14	8	35	14	23
Intratriporopollenites microreticulatus	2	1	3	1	0	1	6	5	2	1	2	0	2	5	7	6	3	4	0	0	0	0	0
Kurtzipites sp?	0	0	0	0	0	0	0	0	0	0	0	0	0	0	0	0	0	0	0	0	0	0	2
Laevigatosporites haardtii	4	1	6	6	0	1	8	5	2	4	2	0	10	18	21	30	5	12	2	4	2	3	9
Milfordia hungarica	0	0	1	0	0	0	0	0	1	0	0	0	0	4	0	0	0	1	0	0	0	0	0
Momipites anellus	0	0	0	0	0	0	0	0	0	0	0	0	0	0	0	1	0	0	0	0	0	0	0
Momipites spp.	0	0	6	1	0	0	3	0	0	0	0	0	0	1	0	1	2	0	0	0	0	0	0
Momipites triradiatus	0	0	0	0	0	0	0	0	0	0	0	0	0	0	1	0	0	0	0	0	0	0	1
Monocolpopollenites tranquilis	3	3	0	0	0	3	2	1	0	0	0	2	2	2	3	4	0	0	1	1	2	0	2
Nyssapollenites kruschi analepticus	3	3	9	6	0	3	8	8	9	14	7	3	21	30	30	40	6	14	3	1	9	2	5
Pityosporites spp.	38	5	23	0	0	5	27	45	12	19	9	0	53	75	61	70	38	1	42	40	65	0	36
Platycaryapollenites platycaryoides	1	1	0	0	0	1	0	1	0	0	0	1	3	6	5	9	1	1	0	1	1	0	0
Platycaryapollenites swastacoidus	0	0	1	0	0	0	0	0	0	0	0	0	0	0	0	0	0	0	0	0	0	0	0
Plicapollis pseudoexcelsus	0	0	0	1	0	0	2	0	1	0	0	0	2	1	1	2	2	0	0	1	0	0	0
Plicatapollis plicatus	0	0	0	0	0	0	0	0	0	0	0	0	0	2	0	2	2	0	0	0	0	0	0
Polypodiaceoisporites marxheimensis	0	0	0	0	0	0	0	0	0	0	0	1	0	0	0	0	0	0	0	0	0	0	0
Pseudointegricorpus spp.	0	0	0	0	0	0	0	0	0	0	0	0	0	0	0	0	0	0	4	3	1	1	6
Retitricolpites retiformis	1	0	1	0	0	0	3	2	2	1	0	0	5	6	4	7	4	2	0	2	0	1	0
Salixpollenites discolorpites	0	0	1	0	0	0	0	0	0	0	0	0	0	0	0	0	0	0	0	0	0	0	0
Sequoiapollenites polyformosus	0	0	0	0	0	0	2	0	1	0	0	0	0	2	0	1	0	0	0	0	0	0	0
Sparganiaceaepollenites magnoides	0	0	0	0	0	0	0	0	0	0	0	0	0	0	0	1	0	0	0	0	0	0	0
Stereisporites (D.) germanicus	0	0	0	0	0	0	0	0	0	0	0	0	0	1	0	0	0	0	1	0	0	0	0
Stereisporites (Distgranisporis) spp.	0	1	1	1	0	1	0	0	0	0	0	0	0	0	1	0	0	0	0	0	1	0	0
Stereisporites (Stereisporits) steroides	1	1	1	1	0	1	0	0	0	0	0	0	0	1	4	3	0	0	0	0	2	0	2
Triatiopollenites subtriangulus	0	0	0	0	0	0	0	0	0	1	1	0	0	0	1	2	1	1	0	0	0	0	0
Tricolpites cf hians	1	1	0	3	0	1	1	3	0	0	0	0	2	8	7	13	2	4	1	0	2	0	0
Tricolpites hians	1	4	1	1	0	4	3	1	4	1	0	0	2	0	1	1	0	0	0	0	0	1	0
Triporopollenites coryloides	4	0	0	0	0	0	0	0	0	0	0	0	0	1	0	0	0	0	0	1	1	0	0
Triporopollenites robustus	0	0	3	0	0	0	0	4	2	1	0	0	2	5	2	1	0	0	0	0	0	0	0

Fig. 3. Selective palynological dataset for Well 209/9-1. Datasets for 209/3-1 and 209/4-1A are stored in the Geological Society data repository.

Post volcanism sedimentation

Samples from the claystones immediately overlying the volcanic rocks of the Erlend Volcano contain a dinoflagellate cyst-dominated palynoflora typical of the early Eocene. The occurrence of abundant *Homotryblium tenuispinosum* and *Eatonicysta ursulae* indicates a late Early Eocene age of *c.* 52.5 Ma, and corresponds to similar strata found over the seaward dipping reflector series in the Irmiger Basin and Voring Plateau (Jolley, 1998), representing a period of significant relative sea level rise. In wells 209/3-1 and 209/4-1, the Balder Formation onlaps the volcanic sequence, providing a minimum age of 54.26 Ma (Cande & Kent 1995 timescale) for the termination of volcanism around the fringes of the Erlend Volcano.

Volcanic sequence

Cavings from the overlying claystones occur in all ditch cuttings from the volcanic interval of the Erlend Volcano; however, the composition of the pollen and spore assemblage from the volcanic interval is highly distinctive. It contains abundant *Inaperturopollenites hiatus* and *Pityosporites* spp., together with common *Caryapollenites veripites, Platycaryapollenites platycaryoides, Laevigatosporites haardtii* and *Nyssapollenites kruschii* subsp. *analepticus,* all characteristic of the palynofloras seen in the latest Paleocene and earliest Eocene interval, referred to Sequence T40 by Ebdon *et al.* (1995). This age is confirmed by occurrences of *Cicatricosisporites dorogensis* and *Monocolpopollenites tranquilus,* taxa which occur frequently in uppermost Sequence T40 assemblages in southern England, the North Sea and Faroe–Shetland basins. Further evidence for a late Paleocene age is provided by the occurrence of *Azolla cretaceae* massulae in wells 209/3-1 and 209/9-1. Occurrences of this taxon are typical of the middle part of the Flett Formation in the Faroe–Shetland Basin. This characteristic palynoflora is regularly recorded from the upper part of Sequence T40 in the Faroe–Shetland Basin, and has a wider occurrence documented in Jolley *et al.* (2002), where it is referred to as the 'Staffa Flora', after its occurrence in the Staffa Group of Mull.

At the base of the volcanic interval in Well 209/9–1, recovery is lower, but contains palynofloras of a contrasting association typical of the late Thanetian. The low diversity of these palynofloras, and the occurrence of *Momipites* species strongly suggests this siltstone interval is attributable to the latest Paleocene, Sequence T38, or Lamba Formation. Similar material has caved into the uppermost part of the subjacent Acidic Suite depth interval. This assemblage occurs beneath the lowermost basaltic lavas, and defines a maximum age for the lavas.

In summary, the sediments within the volcanic sequence, together with the associated boles, indicate a late Paleocene age, also confirmed by the occurrence of *Apectodinium* species in the volcanic succession of Well 209/4–1A. Equivalent palynofloras in the Faroe–Shetland Basin occur in upper Sequence T40. Within the uppermost part of this interval is the Faroes Lower Lava Formation, suggesting contemporaneous volcanism on the Faroes Block and the Erlend Platform.

Both the 'Staffa Flora' and the influx of *Apectodinium* in the upper part of the Erlend lava sequence are biological events driven by the late Paleocene thermal maximum (LPTM), factors already documented by Bujak & Brinkhuis (1999) and Jolley *et al.* (2002). The global process controlling their occurrence ensure a short-term

widespread event sequence ideal for correlation across terrestrial to marine facies, and place the Erlend Basaltic Suite into the immediately post-LPTM period, which it is recommended, will fall into the earliest part of the Eocene.

Evidence from lithologies in this sequence of volcanic rocks supports a terrestrial to shallow marine environment. The two dominant lithologies may be summarized as follows:

(a) Subaerial facies basaltic lava flows (simple and/or compound) which are typically <20 m thick, with occasional interbeds of fluvial/alluvial sediment (sands, silts, muds) which are typically <5 m thick. By comparison with onshore sequences such as Skye, these thicknesses are within the expected or typical range (Williamson & Bell 1994). Amygdaloidal textures are common, with composite infills involving chlorite, calcite and zeolite group minerals. Olivine and plagioclase porphyritic varieties are recognized, although typically the olivine is replaced by secondary iddingsite and/or chlorite (Kanaris-Sotiriou *et al.* 1993). Ophitic-textured groundmasses are common.

(b) Subaqueous facies basaltic hyaloclastites (volcanic breccias), a coarse-grained clastic rock composed of angular lithoclasts of basaltic material set in a glassy matrix. Olivine and plagioclase porphyritic varieties are recognized, although typically the olivine is replaced by secondary iddingsite and/or chlorite.

Subdivision of the volcanic sequence

The uppermost portions of the volcanic sequences in the Erlend wells comprise a relatively thin unit (Erlend D) which, in wells 209/3-1 and 209/4-1A, overlies a relatively thick sequence of siltstones and sandstones, the latter with relatively higher gamma ray log responses and lower densities than the volcanic rocks (Fig. 2). This sedimentary sequence does not occur in Well 209/9-1, which is condensed and may have suffered more extensive post-depositional erosion. In Well 209/4-1A, the dominant volcanic lithology is hyaloclastite, indicative of eruption into a subaqueous environment, confirmed by the occurrences of dinoflagellate cysts including *Apectodinium*. Conversely, in wells 209/3-1 and 209/9-1 the unit consists of lavas with boles containing pollen and spores, typical of eruption into a subaerial environment.

Below the main intrabasaltic unit in wells 209/3-1 and 209/4-1A is Erlend Unit C (Fig. 2). In Well 209/9-1, Unit C lies directly below Unit D, with no intervening main intrabasaltic unit. Unit C is dominated by hyaloclastites in Well 209/4-1A and by subaerial facies lava flows characterized by abundant lateritized material (boles) in wells 209/3-1 and 209/9-1. Within all three wells are thin tuffaceous layers representing some form of pyroclastic material, possibly reworked.

In Well 209/3-1, which contains the thickest volcanic sequence, the Erlend Unit B and the Erlend Unit A constitute in excess of 600 m of section. Unit B takes the form of relatively thick (up to 10 m) simple subaerial facies flows, whereas Unit A comprises a sequence of relatively rapidly erupted thinner subaerial facies flow units, as suggested by the overall lower recovery of organic debris and presence of fewer boles.

The acidic suite

The acidic igneous rocks are referred to as forming an Acidic (Volcanic) Suite (Well 209/4-1A, North Sea Sun Offshore Composite Well Log, 1986), consisting of

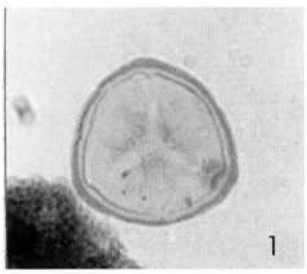
1

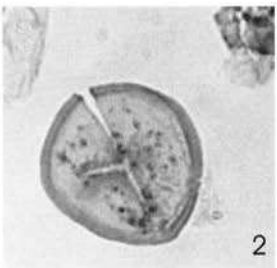
2

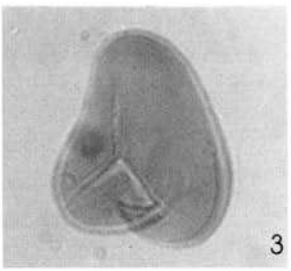
3

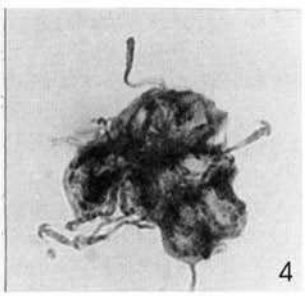
4

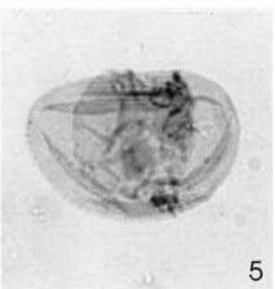
5

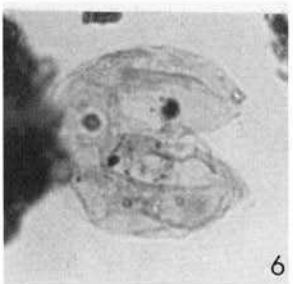
6

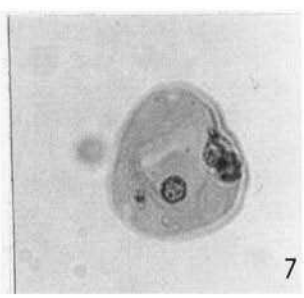
7

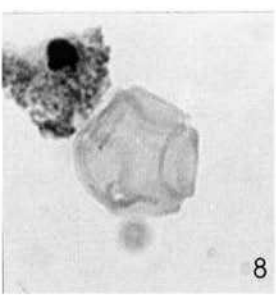
8

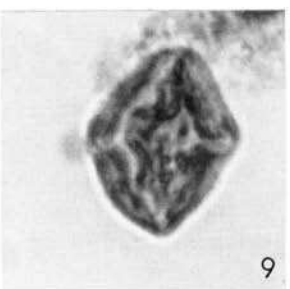
9

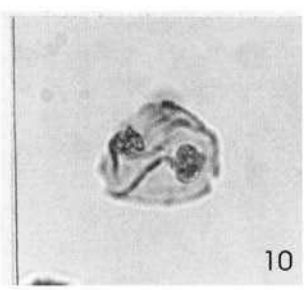
10

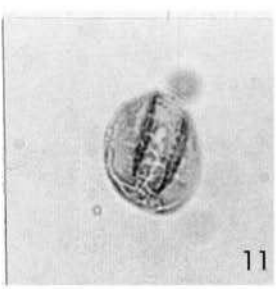
11

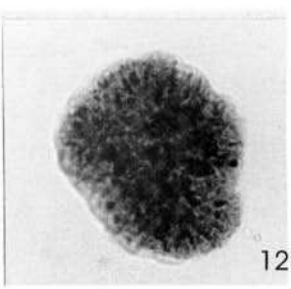
12

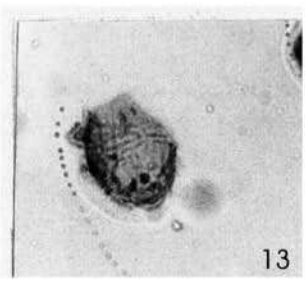
13

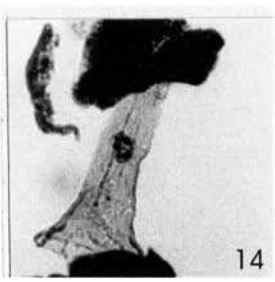
14

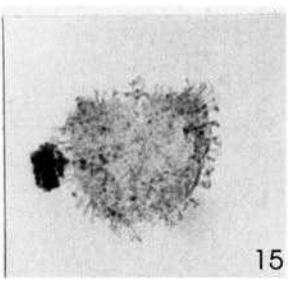
15

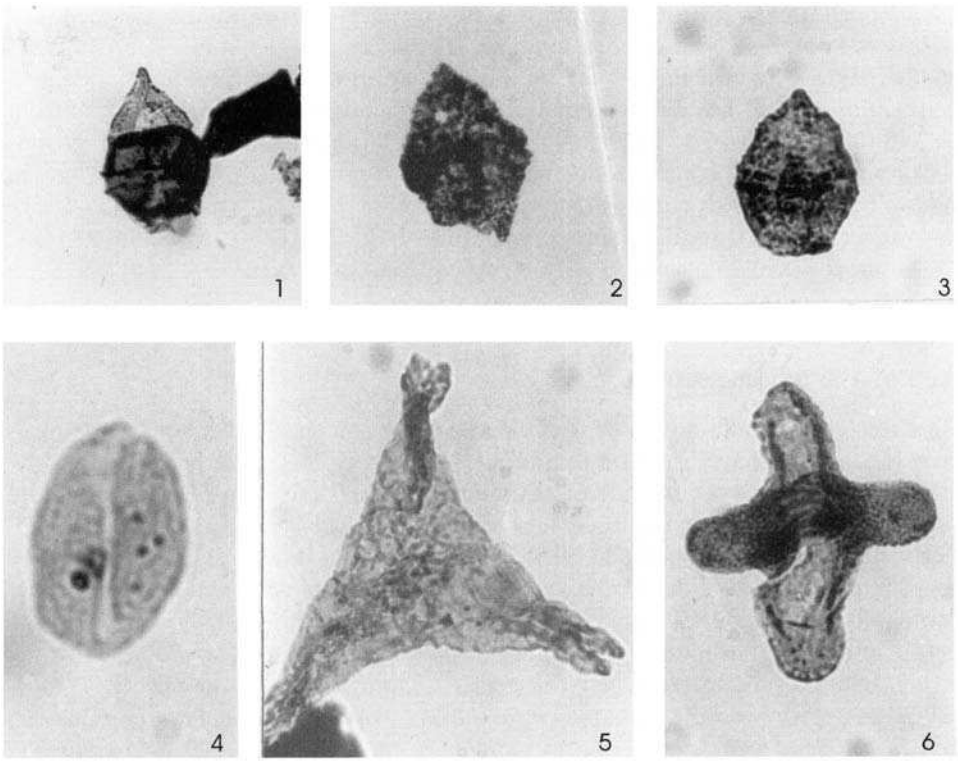

Fig. 5. Photomicrographs of palynomorphs from the Shetland Group equivalent, acidic suite, 1, *Chatangiella* spp. (209/9-1, 1496′); 2, *Palaeoperidinium pyrophorum* (209/9-1, 1490′); 3, *Chatangiella* spp. (209/9-1, 1496′). 2 and 3 show thermally mature specimens from sediments adjacent to acidic igneous sheets. Pollen from the Basaltic Suite 4, *Monocolpopollenites tranquilus* (209/9-1, 1268′), and the Acidic Suite, Shetland Group equivalent; 5, *Pseudointegricorpus* spp. (209/9-1, 1460′) and 6, *Aquilapollenites spinulosus* (209/9-1, 1460′).

microgranite through to rhyolite, pitchstone and obsidian. Similar material from Well 209/9-1 comprise a variety of textural types, ranging from micro-crystalline rhyolite and dacite through to rhyolitic and dacitic glass, together with pitchstone and vesiculated material (pumice). Ridd (1983) reported peperitic textures which appear to have developed along the interfaces between igneous material and sediment.

Fig. 4. Photomicrographs of spores of the Erlend Basaltic Suite interbasaltic sediments: 1, *Stereisporites (Distancoraesporis) germanicus* (209/3-1, 4780′swc); 2, *Stereisporites (Distgranisporis)* spp. (209/4-1, 5520′); 3, *Deltoidospora adriennis* (209/3-1, 4780′swc); 4, *Azolla cretaceae* massulae (209/3-1, 4500′); 5, *Laevigatosporites haardtii* (209/4-1, 6420′) characteristic pollen; 6, *Inaperturopollenites hiatus* (209/4-1, 5520′); 7, *Caryapollenites veripites* (209/3-1, 4780′swc); 8, *Alnipollenites verus* (209/3-1, 5020′swc); 9, *Nyssapollenites kruschii* (209/9-1, 1268′); 10, *Platycaryapollenites platycaryoides* ((209/3-1, 5020′swc); 11, *Cupuliferoidaepollenites liblarensis* (209/4-1, 5520′); and algae 12, *Botryococcus braunii* (209/9-1, 1235′). Dinocyst from the Acidic Suite (Lamba Fm); 13, *Alisocysta margarita* (209/4-1, 7020'), and Shetland Group equivalent; 14, *Odontochitina costata* (operculum 209/9-1, 1496′); and 15, *Tenua hystrix* (209/3-1, 1460′).

Compositional data are relatively sparse; however, rhyolitic and dacitic compositions appear to be the most common. The most detailed study is of the Well 209/3-1 cordierite-bearing dacites by Kanaris-Sotiriou *et al.* (1993), involving a petro- graphic and geochemical analysis of these corundum-normative rocks from Core 3 (2310.4–2316.5 m; 7580–7600′). Contact relationships between these igneous rocks and the interbedded sedimentary rocks are not constrained by the limited sidewall core and ditch cuttings dataset available for this study (but see Ridd 1983); however, evidence from the Thermal Alteration Index (TAI) is used below to argue for an intrusive relationship.

Age of the acidic suite

Ridd (1983) originally suggested that the rocks in this interval where of Late Cretaceous (Campanian) age based on foraminifera, an interpretation largely dismissed by later authors because of the Paleocene radiometric ages derived from the Acidic Suite rocks and the perception that these igneous rocks were lavas. Our new evidence supports the interpretation of Ridd (1983). Palynofloras recovered from the sedimentary rocks interbedded with the Acidic Suite are of a completely different character when compared to the material within the overlying volcanic sequence (Figs 4 & 5). In the depth interval 1460–1508 m in Well 209/9-1, the palynofloras are dominated by dinoflagellate cysts, in particular the genus *Chatangiella,* and the species *Palaeoperidinium pyrophorum, Laciniidinium biconicum, Palaeohystrichophora infusorioides* and *Isabellidinium cooksoniae* occur abundantly. In addition, species of *Aquilapollenites* and *Pseudointegricorpus* occur commonly. These are typical of latest Campanian marine sediments in the Boreal Realm, and show similarity to palynofloras reported from the Campanian of Greenland (Nøhr-Hansen 1996). Below a depth of 1496 m, the occurrence of *Odontochitina costata* suggests a late Campanian age. Significantly, no older palynofloras are detected, to the lowermost analysed sample at 1664 m.

The palynological record of the Acidic Suite in wells 209/3-1 and 209/4-1A is different, with occurrences of *Alisocysta margarita* in a low diversity microplankton and pollen and spore palynoflora. This suggests an age no younger than the late Thanetian Sequence T38. In Well 209/4-1, these strata are underlain by Late Cretaceous palynofloras encountered in the mudstones underlying the Acidic Suite at a depth of *c.* 3100 m (10 130′), where an assemblage, most likely of late Campanian age and dominated by *Heterosphaeridium spp.*, is encountered. A similar sequence is encountered in Well 209/3-1, which has possible Maastrichtian palynofloras in the mudstones underlying the bulk of the Acidic Suite. In this well, acidic igneous bodies of identical composition are also identified in the underlying Campanian sedimentary sequence (Fig. 2).

There is no noticeable change in the abundance of pollen upsection in the Campanian and Maastrichtian sedimentary rocks interbedded with the Acidic Suite. This is strongly suggestive of an environment of continuous deposition, and does not indicate emergence or shallowing of the shelf sea at any time during the Cretaceous. In samples examined from this interval in all three wells, a mixture of low and high Thermal Alteration Index *in situ* fossils are recorded, highly suggestive of thermal alteration of marine palynofloras by igneous activity. Thermal alteration of this

character is not a characteristic of palynofloral assemblages preserved within sedimentary intercalations within proven volcanic sequences such as Skye and Mull, where TAI is usually low. The variable, and often high, TAI values recorded from material interbedded with the Acidic Suite are highly suggestive of significant heatflow, of the type generated by intrusive bodies of magma. Furthermore, an extrusive scenario is unlikely in a shelfal marine setting, as the continuous marine record negates the possibility of rapid oscillations in sea level. Instead, the Acidic Suite of the Erlend area represents a spatially- and genetically-associated intrusive phase of acidic magmatism typical of central complex activity, such as is seen in the eroded Palaeogene central complexes exposed in NW Scotland.

Furthermore, elsewhere in the Faroe–Shetland Basin, intrusive bodies ranging in composition from basic types (dolerite and gabbro) are relatively common (Gibb & Kanaris-Sotiriou 1988; Naylor *et al.* 1999). However, it is in close proximity to central intrusive complexes that acidic intrusions become dominant.

Radiometric dates for members of the Acidic Suite in Well 209/9-1, determined by Hitchen & Ritchie (1987), indicate an age of 64.8 ± 0.8 Ma and therefore a period of sill emplacement in Campanian to Danian times, with the sills of Well 209/9-1 belonging to the last phase of this activity. However, the age of the interbedded sediments determined by palynological analysis reported here does not support this interpretation in view of the Thanetian palynofloras recovered from two of the wells (209/4-1A and 209/9-1).

Although the sills in the Erlend wells were obviously injected into the host rocks after the Campanian, their presence in Thanetian sediments is strongly suggestive of a period of intrusive activity closer to that of the extrusion of the Erlend volcanic sequence, i.e. in the late Paleocene. Given our current understanding of the relatively fast evolutionary histories of the volcanoes responsible for the volcanic sequences and associated central complexes (Chambers & Fitton 2000), it is possible that the extrusive and intrusive activity recorded by the Erlend volcanic sequence and the Acidic Suite, respectively, were essentially synchronous and genetically related.

Palaeoenvironments of the Erlend area in Cretaceous and Palaeogene times

Within the marine dinoflagellate cyst palynofloras of the late Campanian strata are terrestrial assemblages, dominated by species of *Aquilapollenites* and *Pseudointegricorpus*, both genera characteristic of the Campanian–Maastrichtian in the Northern Hemisphere (Batten 1981). Although *Aquilapollenites spinulosus* is recorded from strata within the earliest Eocene of the Faroe–Shetland Basin, this is a diverse series of assemblages of Cretaceous character. The abundance of these pollen grains, together with the diversity of the marine dinoflagellate cysts, suggests that the sedimentary rocks interbedded with the Acidic Suite were deposited in a marine shelf environment during the late Campanian.

From the limited amount of information contained in the three wells, it appears that the Erlend area became a platform towards the end of the Cretaceous, resulting in truncation of the Cretaceous record. Thanetian sedimentary rocks are interbedded with the Acidic Suite in wells 209/4-1A and 209/9-1 on the flanks of the Erlend Volcano (Fig. 1) and are of shelf marine character. However, in the more central

209/3-1 area these sediments are absent, suggesting that uplift occurred here first, most likely in response to uplift caused by the arrival of magma at relatively shallow depths. This occured at around 56 Ma (new date from this study), a time when the eruption of tholeiitic basalt magmas was widespread throughout the NE Atlantic, for example in the Palaeogene Hebridean Volcanic Province (Bell & Jolley 1997; Jolley 1997), as well as along the NW flank of the Faroe–Shetland Basin, on the Faroe Islands (Waagstein 1988; Ritchie & Hitchen 1996).

The palynofloras preserved in the boles of the volcanic sequence, together with the interbedded fluvial sediments, are derived from an angiosperm lowland swamp forest which grew on the flanks of the volcano. The occurrence of *Azolla* massulae in several localities across the Faroe–Shetland Basin during this period points to a raised watertable, with standing water bodies on the lava field present around the location of wells 209/3-1 and 209/9-1. Further to the NE, in the Well 209/4-1A area, the occurrence of comparable palynofloras in the volcanic sequence containing dinoflagellate cysts of the genus *Apectodinium* marks a transition to a marine environment. These taxa are known to favour lower salinity, high ecological stress conditions, which, when taken with the high pollen content and lack of other dinoflagellate cysts in these samples, suggests a littoral environment. It appears, therefore, that the volcanic rocks were erupted into brackish to freshwater at the margin of the marine channel that separated the Erlend Volcano from the Brendan Volcano to the north. The recognition of hyaloclastites within the Erlend C and D units in Well 209/4-1A provides a useful lithological corollary to the palynological evidence that the eruption environment was subaqueous in the NE quadrant of the volcano.

We thank our many colleagues in Statoil (UK) Ltd., Shell UK Ltd, Exxon-Mobil and the British Geological Survey for sample material and useful discussions on the evolution of the Faroe–Shetland Basin.

References

BATTEN, D. J. 1981. Stratigraphy, palaeogeographic and evolutionary significance of Late Cretaceous and early Tertiary Normapolles pollen. *Review of Palaeobotany and Palynology*, **35**, 125–138.

BELL, B. R. & JOLLEY, D. W. 1997. Application of palynological data to the chronology of the Palaeogene lava fields of the British Province: implications for magmatic stratigraphy. *Journal of the Geological Society, London*, **154,** 701–708.

BUJAK, J. & BRINKHUIS, H. 1998. Global warming and dinocyst changes across the Paleocene/Eocene Epoch boundary. *In*: AUBRY, M-P, LUCAS, S. & BERGGREN, W. A. (eds) *Late Paleocene–Early Eocene Climatic and Biotic Evolution*. Columbia University Press, New York, 277–295.

CANDE, S. C. KENT, D. V. 1995. Revised calibration of the geomagnetic time scale for the Late Cretaceous and Cenozoic. *Journal of Geophysical Research*, **100,** 6,093–6,095.

CHALMERS, J. A. & WESTERN, P. G. 1979. A Tertiary igneous centre north of the Shetland Isles. *Scottish Journal of Geology*, **15**, 333–342.

CHAMBERS, L. M. & FITTON, J. G. 2000. Geochemical transitions in the ancestral Iceland plume: evidence from the Isle of Mull Tertiary volcano, Scotland. *Journal of the Geological Society, London*, **157**, 261–263.

EBDON, C. C., GRANGER, P. J., JOHNSON, H. D. & EVANS, A. M. 1995, Early Tertiary evolution and stratigraphy of the Faroe–Shetland Basin: Implications for hydrocarbon prospectivity. *In*: SCRUTTON, R. A. *et al.* (eds) *Sedimentation and Palaeoceanography of the North Atlantic Region*. Geological Society, London, Special Publications, **90**, 51–69.

GATLIFF, R. W., HITCHEN, K., RITCHIE, J. D. & SMYTHE, D. K. 1984. Internal structure of the Erland Tertiary volcanic complex, north of Shetland, revealed by seismic reflection. *Journal of the Geological Society, London*, **141**, 555–562.

GIBB, F. G. F. & KANARIS-SOTIRIOU, R. 1988. The geochemistry and origin of the Faroe–Shetland Sill Complex. *In*: MORTON, A. C. & PARSON, L. M. (eds) *Early Tertiary Volcanism and the opening of the NE Atlantic*. Geological Society, London, Special Publications, **39**, 241–252.

HITCHEN, K. & RITCHIE, J. D. 1987. Geological review of the West Shetland area. *In*: BROOKS, J. & GLENNIE, K. (eds) *Petroleum Geology of North West Europe*. Graham and Trotman, London, 737–749.

JACQUE, M. & THOUVENIN, J. 1975. Lower Tertiary tuffs and volcanic activity in the North Sea. *In:* WOODLAND, A. W. (ed.) *Petroleum and the Continental Shelf of North-West Europe. 1, Geology*. Applied Science Publishers, Barking, Essex, 455–66.

JOLLEY, D. W. 1997. Palaeosurface palynofloras of the Skye lava field and the age of the British Tertiary volcanic province. *In*: WIDDOWSON, M. (ed.) *Palaeosurfaces: Recognition, Reconstruction and Palaeoenvironmental Interpretation*. Geological Society, London, Special Publications, **120**, 67–94.

JOLLEY, D. W. 1998. Early Eocene palynofloras from Holes 915A, 916A, 917A and 918D, East Greenland. *In*: SAUNDERS, A. D., LARSEN, H. C. & WISE, S. W. (eds) *Proceedings of the Ocean Drilling Programme, Scientific Results*. College Station, Texas, **152**, 221–231

JOLLEY, D. W., CLARKE, B. & KELLEY, S. 2002. Evidence for the association between rifting of the North Atlantic and the Late Paleocene Thermal Maximum. *Geology*, **30**, 7–10.

KANARIS-SOTIRIOU, R., MORTON, A. C. & TAYLOR, P. N. 1993. Palaeogeneperaluminous magmatism, crustal melting and continental break-up: the Erlend complex, Faroe-Shetland Basin, NE Atlantic. *Journal of the Geological Society, London*, **150**, 903–914.

MITCHELL, J. G. & EUWE, M. G. 1988. A model of single-stage concomitant potasium-argon exchange in acidic lavas from the Erlend volcanic complex, north Shetland Islsnds. *Chemical Geology (Isotope Geoscience Section)*, **72**, 95–109.

NAYLOR, P. H., BELL, B. R., JOLLEY, D. W., DURNALL, P. & FREDSTED, R. 1999. Palaeogene magmatism in the Faroe–Shetland Basin: Influences on uplift history and sedimentation. *In*: FLEET, A. J. & BOLDY, S. A. R. (eds) *Petroleum Geology of Northwest Europe: Proceedings of the 5th Conference*. Geological Society, London, 545–558.

NØHR-HANSEN, H. 1996. *Upper Cretaceous dinoflagellate cyst stratigraphy, onshore west Greenland*. Bulletin Grønlands Geologiske Undersølgelse **170**.

PEDERSEN, A. K., LARSEN, L. M. & DUEHOLM, A. K. 1993. *Geological section along the south coast of Nuussuaq, central West Greenland. 1:20 000 coloured geological sheet*. The Geological Survey of Greenland, Copenhagen.

RIDD, M. F. 1983. Aspects of the Tertiary geology of the Faroe–Shetland Channel. *In*: BOTT, M. H. P., SAXOV, S., TALWANI, M. & THIEDE, J. (eds) *Structure and Development of the Greenland–Scotland Ridge*. Plenum Press, New York, 91–108.

RITCHIE, J. D. & HITCHEN, K. 1996. Early Paleogene offshore igneous activity to the northwest of the UK and its relationship to the North Atlantic Igneous Province. *In*: KNOX, R. W.O'B., CORFIELD, R. M. & DUNAY, R. E. (eds) *Correlation of the Early Paleogene in Northwest Europe*. Geological Society, London, Special Publications, **101**, 63–78.

WAAGSTEIN, R. 1988. Structure, composition and age of the Faroe basalt plateau. *In*: MORTON, A. C. & PARSON, L. M. (eds) *Early Tertiary Volcanism and the opening of the NE Atlantic*. Geological Society, London, Special Publications, **39**, 225–238.

WILLIAMSON, I. T. & BELL, B. R. 1994. The Palaeocene lava field of west-central Skye, Scotland: stratigraphy, palaeogeography and structure. *Transactions of the Royal Society of Edinburgh: Earth Sciences*, **85**, 39–75.

WOOD, M. V., HALL, J. DOODY, J. J. 1988. Distribution of early Tertiary lavas in the NE Rockall Trough. *In*: MORTON, A. C. & PARSON, L. M. (eds) *Early Tertiary Volcanism and the opening of the NE Atlantic*. Geological Society, London, Special Publications, **39**, 283–292.

This page intentionally left blank

A new biostratigraphic scheme for the Paleocene onshore West Greenland and its implications for the timing of the pre-volcanic evolution

H. NØHR-HANSEN, E. SHELDON & G. DAM[1]

The Geological Survey of Denmark and Greenland (GEUS), Øster Voldgarde 10, DK-1350 Copenhagen K, Denmark (e-mail: hnh@geus.dk; es@geus.dk; gda@dong.dk)
[1] *Present address: DONG E & P, Agern Alle 24–26, DK-2970 Hørsholm, Denmark*

Abstract: Based upon dinoflagellate cyst and nannofossil data, a detailed zonation of the Lower Paleocene succession in the Nuussuaq Basin, onshore West Greenland has been established. The succession is divided into the five dinoflagellate cyst zones: *Trithyrodinium evittii*, *Cerodinium pannuceum*, *Senegalinium iterlaaense*, *Palaeocystodinium bulliforme* and *Alisocysta margarita*. The dinoflagellate cyst zones are correlated with nannoplankton zones. The stratigraphically most important nannofossils recorded include *Chiasmolithus* cf. *bidens*, *Neochiastozygus modestus*, *N. perfectus*, *N. saepes*, *Prinsius martinii* and *Zeugrhabdotus sigmoides*. A new zonal scheme has been erected and resolves previous problems relating biostratigraphic and $^{40}Ar/^{39}Ar$ data in the region.

The Upper Maastrichtian–Lower Paleocene succession records faulting and valley/submarine canyon incision resulting from pre-volcanic rifting and regional uplift of the basin. Two Early Paleocene tectonic phases have been recognized during NP1–NP3. These uplift phases were followed by rapid subsidence during NP4. Initiation of volcanism onshore West Greenland is broadly concurrent with the *Alisocysta margarita* Zone indicating that volcanism began during late NP4, in accordance with recent palaeomagnetic results and $^{40}Ar/^{39}Ar$ dating of the volcanics. On the basis of the first occurrence datum of the dinoflagellate cyst species *Cerodinium kangiliense* and *Alisocysta margarita*, it is possible to correlate the lowermost volcanic Anaanaa Member hyaloclastites from the southwestern part of Nuussuaq with sediments of the Eqalulik Formation from the northern coast of Nuussuaq.

Biostratigraphy of sediments which predate the early Paleocene volcanism and integration of palynostratigraphic and radiometric dating have, in recent years, caused problems in the North Atlantic Igneous Province (Storey *et al.* 1998). Palynomorphs from the Cape Seale Formation, underlying the volcanic strata on Baffin Island, Northwest Territories, Canada comprise sparse corroded and unidentifiable dinoflagellate cysts, but contain a distinctive palynomorph assemblage suggesting an Early and mid Paleocene age for the sediments (Burden & Langille 1990, 1991).

In West Greenland, Hansen (1980) dated the marine mudstones underlying the onshore Paleocene volcanics as mid Paleocene based upon dinoflagellate cysts, and correlated the upper part with nannoplankton zones NP5 and NP6 (Martini 1971).

From: JOLLEY, D. W. & BELL, B. R. (eds) *The North Atlantic Igneous Province: Stratigraphy, Tectonic, Volcanic and Magmatic Processes*. Geological Society, London, Special Publications, **197**, 111–156. 0305-8719/02/$15.00

This was in conflict with the NP3 dating of the same succession by Jürgensen & Mikkelsen (1974). Piasecki *et al.* (1992) dated the dinoflagellate cyst assemblages from intrabasaltic sediments as late Danian to Thanetian and suggested a correlation to NP zones 4–8. Nøhr-Hansen (1997*a*, *b*) and Christiansen *et al.* (1997) suggested a Selandian (NP5–NP6) age for the upper part of the mudstones underlying the volcanics. However, these biostratigraphic datings are not consistent with recent radiometric dating and palaeomagnetic results of Storey *et al.* (1998) and Riisager & Abrahamsen (1999).

In East Greenland a sparse dinoflagellate cyst flora including *Wetzeliella* spp. suggests an Early Eocene age (Soper *et al.* 1976) for the lowermost volcanics. This is in conflict with a spore and pollen assemblage associated with the first volcanic deposits at Kulhøje in East Greenland, which can be correlated to the Lamba and Flett formations in the Faroe–Shetland Basin, suggesting a Late Paleocene age (Hjortkjær & Jolley 1999), and radiometric dating from the Leg 152 ODP cruise, suggesting that volcanism started at 61–62 Ma (latest Early Paleocene; Larsen & Saunders 1998).

Because of their terrestrial origin, it has been impossible to assign an age to the palynomorph assemblages recorded from the Palaeogene lava fields of the British province (Bell & Jolley 1997). Jolley (1997) presented a regional study of miospores from the West Shetland Basin, which can be used as a regional standard for terrestrial palynoflora and shows a broad differentiation into several palynofloral types. On the basis of similarities with the record from the North Sea and SE England, it has been possible to compare the West Shetland Basin events to chronostratigraphically dated sections (Ali & Jolley 1996). However, the radiometric ages often conflict with observable stratigraphic and field relationships (Bell & Jolley 1997).

The aim of the present paper is to present new dinoflagellate cyst and nannofossil data from West Greenland. The integration of these data allows a precise biostratigraphic dating of the initiation of volcanism in West Greenland. The results are in accordance with the radiometric dating and the palaeomagnetic results of Storey *et al.* (1998) and Riisager & Abrahamsen (1999) and are probably the most well-documented and successful integration of biostratigraphic data with radiometric and palaeomagnetic data from the North Atlantic Igneous Province. Moreover, the sedimentary evolution preluding volcanism in the Nuussuaq Basin is described.

Geological setting

The margin of West Greenland was formed by extensional opening of the Labrador Sea in Late Mesozoic–Early Cenozoic time. A complex of linked rift basins were present from the Labrador Sea to northern Baffin Bay (e.g. Rolle 1985; Chalmers *et al.* 1993; Chalmers *et al.* 1999). Cretaceous–Paleocene sediments outcrop onshore on Cape Dyer on Baffin Island and in the Nuussuaq Basin in the Disko–Svartenhuk Halvø region (69°–72°N), where they are overlain by Palaeogene basalts (Fig. 1; Clarke & Pedersen 1976; Henderson *et al.* 1976; Burden & Langille 1990). Although now bounded to the east by an extensional fault system, the sediments in the Nuussuaq Basin may originally have extended both east and south of their present area of outcrop (Chalmers *et al.* 1999). The maximum thickness of the sediments in the basin exceeds 8 km (Christiansen *et al.* 1995; Chalmers *et al.* 1999), but the age and the character of the deepest sediments are not known.

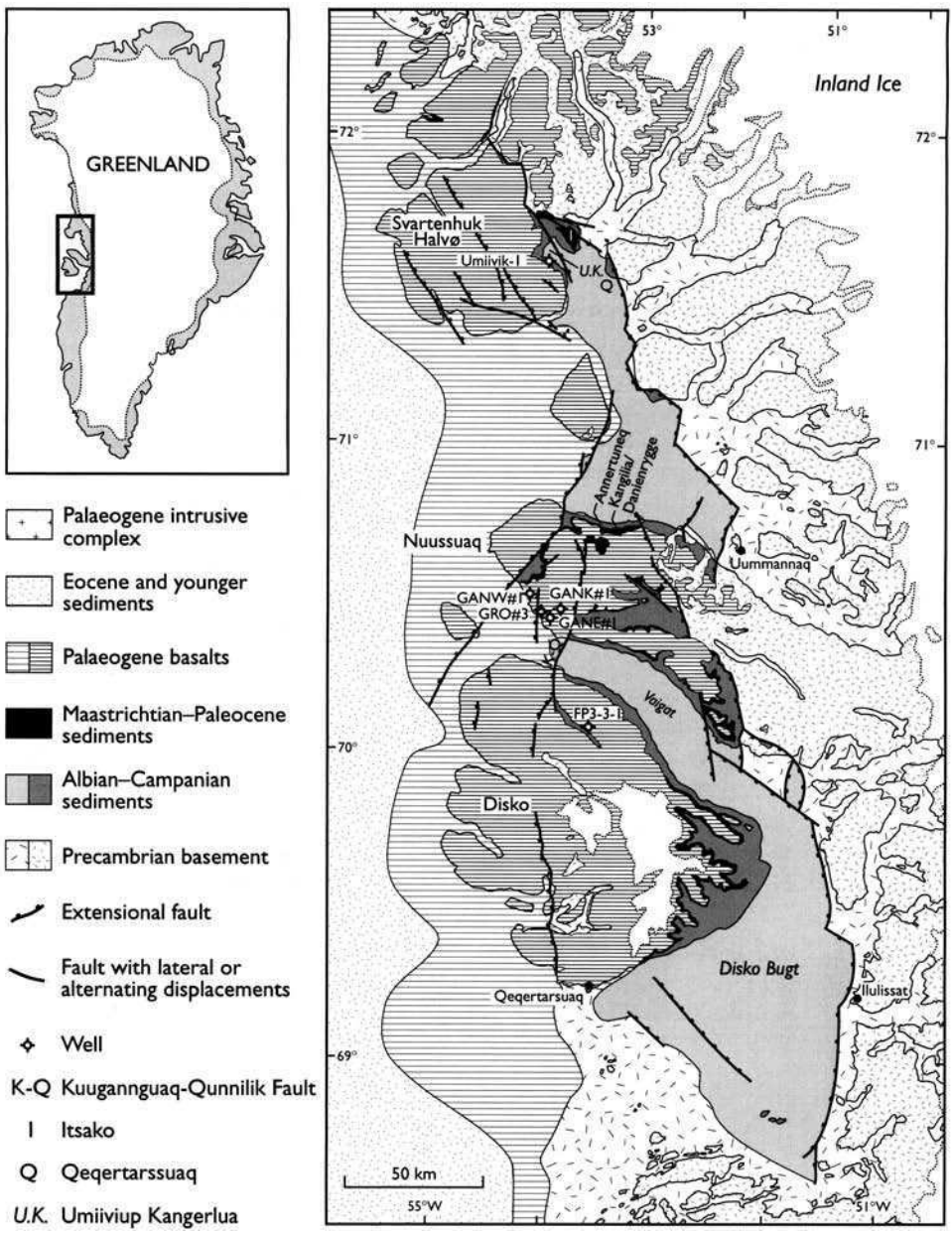

Fig. 1. Geological map of the Nuussuaq Basin showing off- and onshore geology, localities and wells mentioned in the text. Based on Chalmers *et al.* (1999).

The oldest known Cretaceous syn-rift to early post-rift sediments in the Nuussuaq Basin, which are of Albian age (Henderson *et al.* 1976), consists of fan-delta, fluvio-deltaic and shallow marine deposits that onlap the basement on the north coast of Nuussuaq, on Disko (well FP93-3-1) and on Itsako (Figs 1 & 2). These sediments constitute the Kome Formation (Fig. 2; see Henderson *et al.* 1976; Nøhr-Hansen 1992; Midtgaard 1996*a*, *b*; Larsen & Pulvertaft 2000).

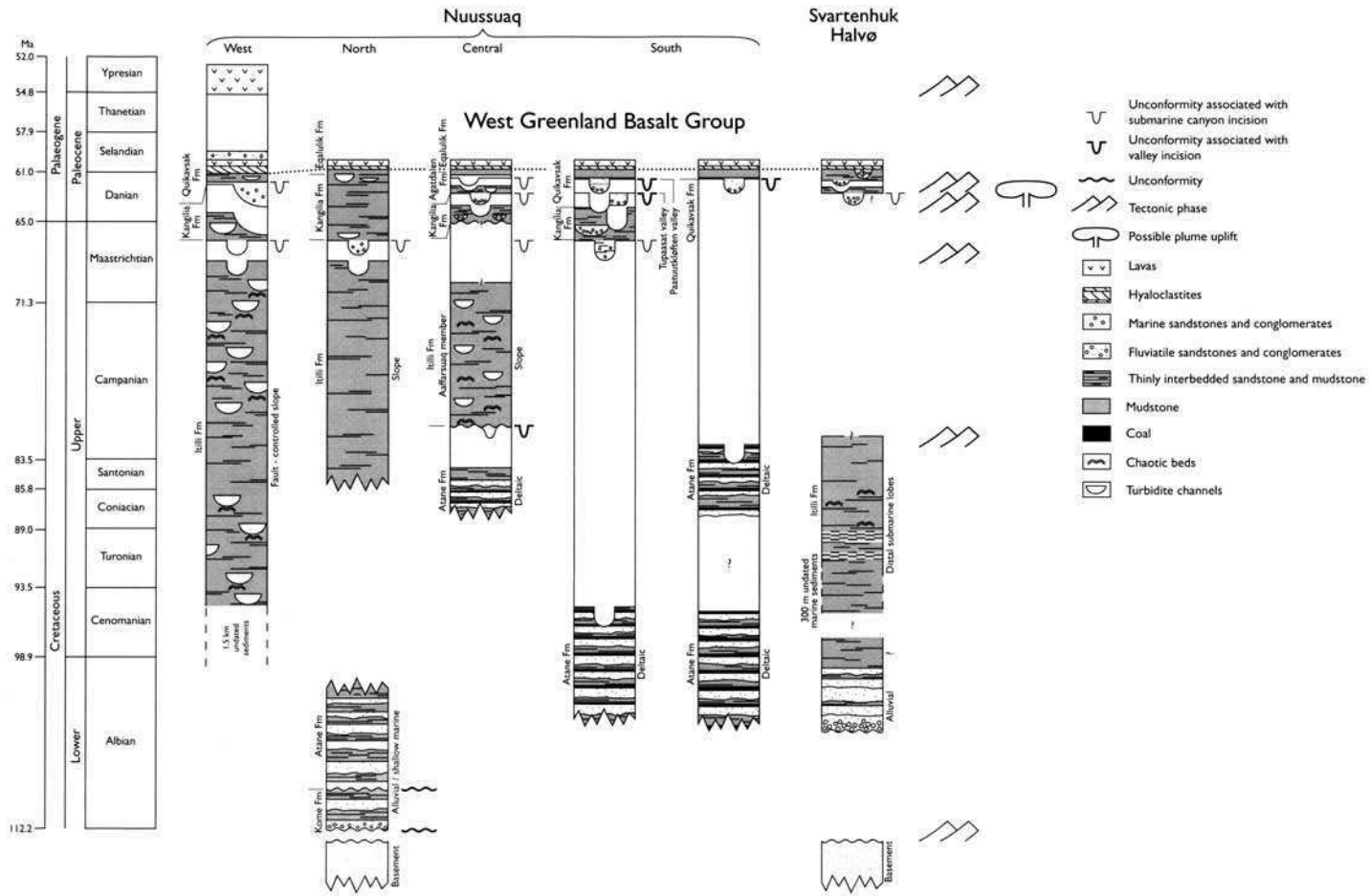

Fig. 2. Generalized stratigraphy of the Cretaceous–Palaeogene sediments on Nuussuaq and Svartenhuk Halvø, West Greenland. Note that the heights of the stratigraphic columns relate to the chronostratigraphic divisions on the left and not to thicknesses of the sedimentary successions.

The Kome Formation is overlain unconformably by Albian to Lower Campanian post-rift sediments of the Atane Formation which were deposited in a fluvial- and wave-dominated delta environment (Fig. 2; Johannessen & Nielsen 1982; Pedersen & Pulvertaft 1992; Olsen 1993; Midtgaard 1996*a*). The youngest Early Campanian strata of the Atane Formation are only present along the south coast of Nuussuaq and in central Nuussuaq (e.g., Lanstorp 1999; Dam *et al.* 2000). The Atane delta fanned to the west and north-west from a point east of Disko island (Schiener 1975; Pedersen & Pulvertaft 1992), with deeper-water turbidite environments west of the Kuugannguaq-Qunnilik Fault (Figs 1 & 2; Dam & Sønderholm 1994; Dam 1997; Kristensen & Dam 1997). The sediments deposited in the deep-water marine environment are referred to as the Itilli Formation (Fig. 2).

In the northern part of the basin Upper Albian–Lower Cenomanian fluvial deposits outcrop on Qeqertarssuaq (Croxton 1978; Larsen & Pulvertaft 2000) grading into fluvio-deltaic mudstones and sandstones at Itsako. Turonian–Early Campanian distal marine slope mudstones and thinly interbedded sandstones and mudstones are exposed in stream gullies in the eastern part of Svartenhuk Halvø and also in low coastal outcrops around Umiiviup Kangerlua Bay and in the Umiivik-1 well drilled on the south coast of this bay (Fig. 1; Dam *et al.* 1998*b*; Larsen & Pulvertaft 2000).

In the Late Santonian there is evidence of increased subsidence in the shallower part of the basin, possibly due to tensional sagging preceding a new rift phase that took place in Early Campanian times (Fig. 2; Dam *et al.* 2000). Shelf delta deposition was replaced by the catastrophic deposition of the Aaffarsuaq Member. These sediments were deposited from gravity flows in a fully marine environment.

Prior to Early Paleocene volcanism in West Greenland, the Nuussuaq Basin underwent major rifting in the Late Maastrichtian–Early Paleocene; at least three tectonic phases can be recognized (Fig. 2; Dam *et al.* 1998*a*; Dam & Sønderholm 1998). Rifting was associated with substantial uplift and repeated erosion and infilling of incised subaerial valleys and submarine canyons resulting in basin-wide unconformities at the base of the Kangilia, Quikavsak and Agatdalen Formations (see Fig. 2). The incision and trend of the valleys seem to have been governed by NW–SE-trending transverse faults. In western Nuussuaq the Paleocene incised valleys pass into a submarine canyon system along a fault-controlled slope. Uplift was followed by a phase of rapid subsidence shortly before extrusion of picritic hyaloclastic breccias. In the interval between subsidence and volcanism, a regional marine mudstone blanket was deposited.

Between the active Paleocene volcanic province and the crystalline Precambrian basement, lacustrine mudstones and sandstones, and hyaloclastite breccias, accumulated in low-lying areas inundated by fresh water and sealed off from marine connections by a broad subaerial volcanic terrain (e.g. Pedersen *et al.* 1998). $^{40}Ar/^{39}Ar$ dating shows that volcanism commenced in West Greenland between 60.9 and 61.3 Ma and that *c.* 80% of the Paleocene lava pile was erupted in one million years or less (Storey *et al.* 1998).

Previous biostratigraphy

The dinoflagellate cysts from the pre-volcanic marine mudstone succession and the intrabasaltic Paleocene sediments at Nuussuaq were described by Hansen (1980), Piasecki *et al.* (1992), Nøhr-Hansen (1996, 1997*a*,*b*), Nøhr-Hansen & Dam (1997)

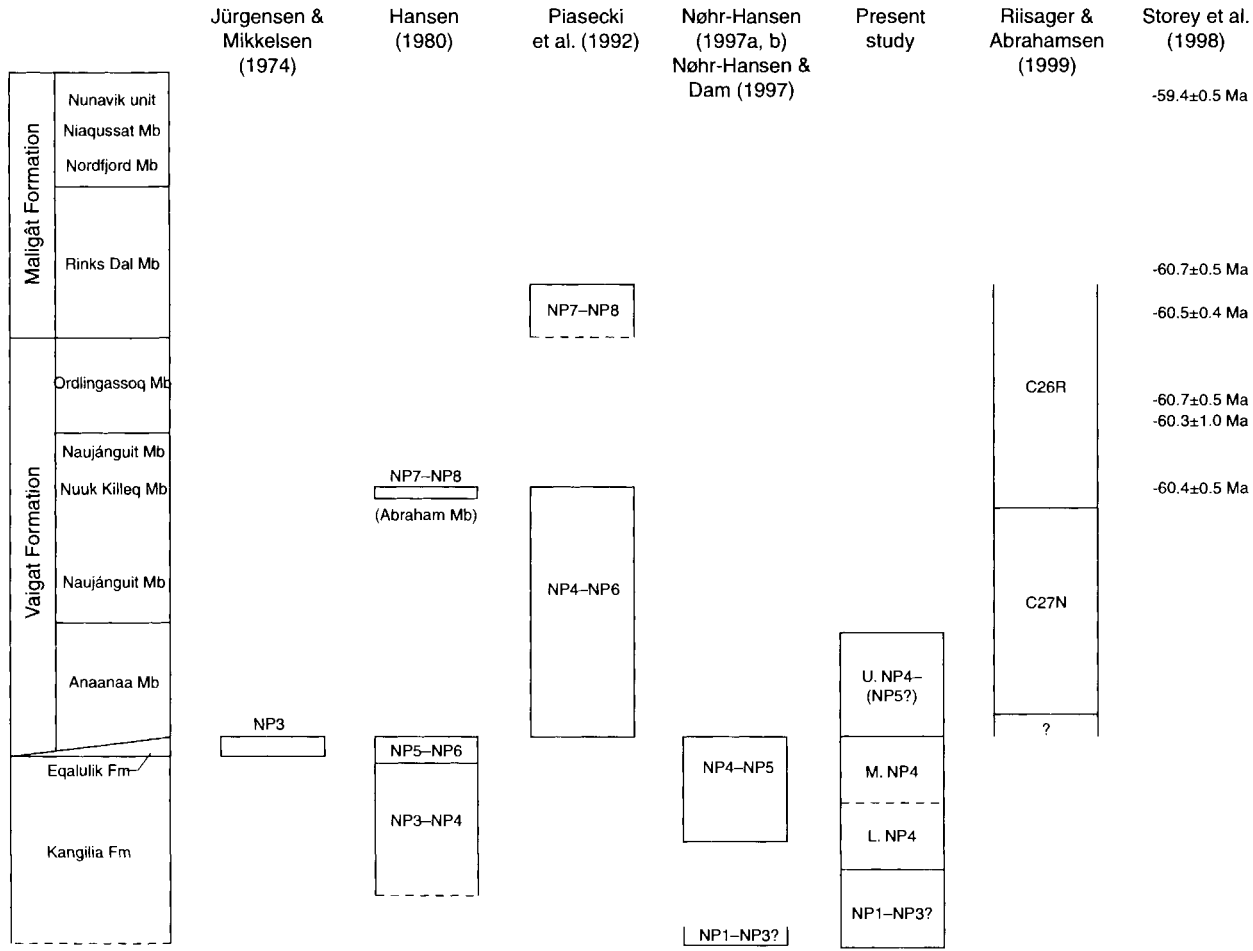

Fig. 3. Previous biostratigraphic, magnetostratigraphic and radiometric dating of the lower Palaeogene succession in West Greenland compared with the results of the present study.

and Nøhr-Hansen & Heilmann-Clausen (2000). Nannoplankton assemblages have been described from isolated sections from the Paleocene succession on Nuussuaq by Perch-Nielsen (1973), Jürgensen & Mikkelsen (1974) and Nøhr-Hansen & Sheldon (2000).

Hansen (1980) dated the lower and upper part of the marine Paleocene mudstone succession at Nuussuaq as Early and mid Paleocene based upon dinoflagellate cysts and correlated it with nannoplankton zones NP3–NP4 (lower part) and NP5–NP6 (upper part) (Martini 1971) (Fig. 3). This is in conflict with the NP3 dating of the upper part of the succession by Jürgensen & Mikkelsen (1974). Jürgensen & Mikkelsen (1974) described the nannoflora from the volcaniclastic sediments in the upper part of the Kangilia Formation (now the Eqalulik Formation) on the north coast of Nuussuaq and Marraat Killiit on the south-western coast (Figs 1 & 3) and assigned them to the late Danian *Chiasmolithus danicus* Zone (NP3). This appears to be based on the presence of several species of *Neochiastozygus*, including *N.* cf. *N. saepes* and *N. modestus*.

Recent examination of the nannoplankton from the Eqalulik Formation (Nøhr-Hansen & Sheldon 2000) revealed a poorly preserved late Danian assemblage represented by *Neochiastozygus eosaepes*, *Prinsius dimorphosus*, *P. martinii* and *Thoracosphaera* spp. The presence of *Neochiastozygus eosaepes* indicates the upper part of NP3 and the lower part of NP4; a slightly younger and more constrained age for the sediments than suggested by Jürgensen & Mikkelsen (1974).

Piasecki *et al.* (1992) dated the dinoflagellate cyst assemblage from intrabasaltic sediments as late Danian to Thanetian and suggested a correlation with NP zones 4–8 (Fig. 3). Nøhr-Hansen (1997*a*, *b*) and Christiansen *et al.* (1997) dated the dinoflagellate cyst assemblages from the Paleocene sediments of wells GANE#1, GANK#1, GANW#1 and GRO#3 and suggested a Selandian age (NP5–NP6) for the upper part of the succession (Fig. 3), and an early Danian age (NP1–NP3?) was suggested for the oldest Paleocene on Nuussuaq (Fig. 3; Nøhr-Hansen & Dam 1997). These previous biostratigraphic datings did not correlate with the recent palaeomagnetic results for the Anaanaa Member or the $^{40}Ar/^{39}Ar$ dating of the volcanic Nuuk Killeq Member. Riisager & Abrahamsen (1999) determined the lowermost volcanic Anaanaa Member in the Nuussuaq Basin to be formed during the normally magnetized part of chron 27 (C27n). C27n correlates with the late Danian (60.92–61.27 Ma) according to Berggren *et al.* (1995; Fig. 3). An $^{40}Ar/^{39}Ar$ dating of 60.4 ± 0.5 Ma was assigned to the younger Nuuk Killeq Member by Storey *et al.* (1998; Fig. 3). Piasecki *et al.* (1992), Nøhr-Hansen (1997*a*, *b*) and Christiansen *et al.* (1997) based their correlation to NP5–NP6 on the presence of a dinoflagellate cyst species similar to the Selandian marker species *Isabelidinium viborgense*, previously only recorded from NP5 and NP6 (Heilmann-Clausen 1985; Powell 1992). However, later examination proved the species similar to *I. viborgense* to be a new species. This new species, *Senegalinium iterlaaense* was described by Nøhr-Hansen & Heilmann-Clausen (2000). They correlated its first occurrence in the upper part of NP3 (mid Danian), based upon observations from the Hvalløse borehole in Denmark.

Material and methods

Palynological and nannofossil preparation and studies of the samples were carried out at the Geological Survey of Denmark and Greenland (GEUS).

Palynomorphs were extracted from 20 g of sediment from each sample by modified standard preparation techniques including treatment with hydrochloric (HCl) and hydrofluoric (HF) acids, sieving using a 20 μm nylon mesh and oxidation (3–10 minutes) with concentrated nitric acid (HNO_3). Finally, palynomorphs were separated from coal particles and woody material in most samples, using the separation method described by Hansen & Gudmundsson (1978) or by swirling. After each of the steps mentioned above the organic residues were mounted in a solid medium (Eukitt®) or in glycerine gel. The palynological slides were studied with transmitted light using a Leitz Dialux 22 microscope (No. 512 742/057691). Dinoflagellate cysts, acritarchs and selected stratigraphically important pollen species were recorded from the sieved, oxidized or gravity-separated slides. Approximately 100 specimens were counted when possible.

The dinoflagellate cyst zones herein are based on the study of 158 samples from the three outcrop successions at Kangilia, Danienrygge, Annertuneq and the four wells GANW#1, GRO#3, GANE#1 and GANK#1 (Fig. 1). The samples from the wells are conventional core samples except for samples from the GRO#3 well which are all ditch cuttings samples. The majority of the nannofossil samples were prepared by crushing approximately 1 cm^3 of sediment and adding it to a 10% potassium hydroxide solution to remove humic material. The sample was then centrifuged and decanted and added to a small amount of ethanol in order to avoid formation of sulphuric acid which would dissolve any calcareous component. After the suspension was shaken and allowed to settle, a few drops were pipetted from the middle of the liquid fraction, placed on a glass coverslip, spread evenly and allowed to dry. The coverslip was mounted, smear side down using *Norland Optical Adhesive*® and was allowed to cure in daylight for 24 hours. The nannofossil slides were studied with transmitted light using a Leitz Orthoplan microscope (No. 851318). The zones herein are based on the study of 107 samples from the outcrop and well successions mentioned in the section above. It is important to note that the low abundance of nannofossils in the samples prevents an accurate dating from being carried out. The illustrations of dinoflagellate cysts and nannofossils recorded from the transmitted light microscope are marked with sample number, slide number, England Finder index (EF), data base number (MicroImage; MI) and laser-video-record number (LVR) for later identification. The illustrated dinoflagellate cysts are also marked with MGUH numbers and are stored in the type collection of the Geological Museum of the University of Copenhagen, Øster Voldgade 5–7, DK 1350, Copenhagen K, Denmark.

Organic material and nannofossil content

The organic material which dominates the samples mainly comprises terrestrially derived black to brownish woody material. Amorphous organic material, dinoflagellate cysts, spores and pollen only constitute a minor proportion. Low species density and diversity prevented counting a minimum of 100 specimens in several samples. The preservation of the dinoflagellate cyst assemblages is variable; samples with well preserved specimens are rare. Thermal Alteration Index (TAI) evaluation has not been carried out systematically, but the organic material in most of the samples revealed TAI values of between −2 and 3, indicating that the organic material is thermally immature to mature with respect to oil generation. Reworked

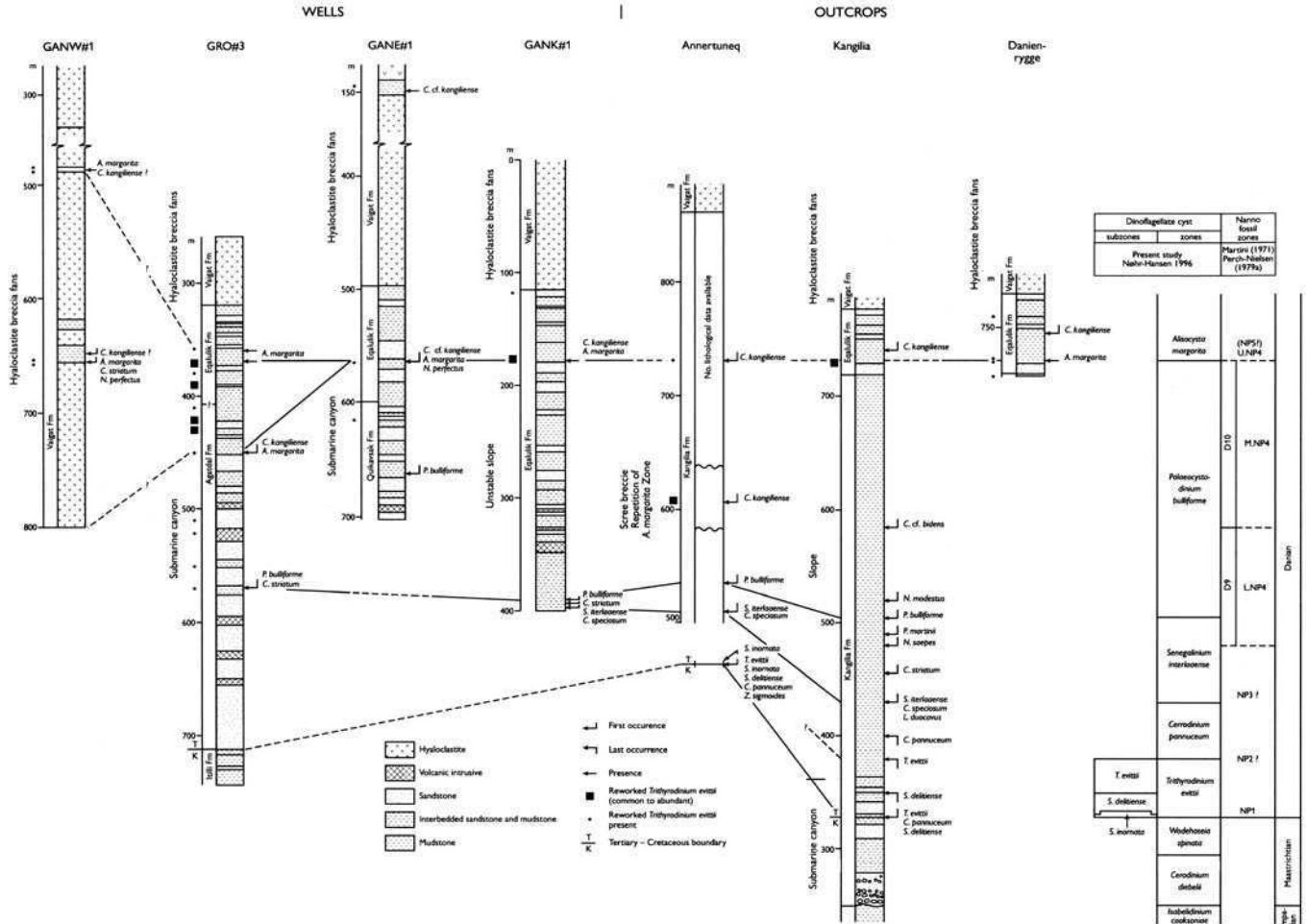

Fig. 4. Biostratigraphic correlation, dating and lithostratigraphy of the studied outcrops sections and wells, based on dinoflagellate cysts and nannofossils.

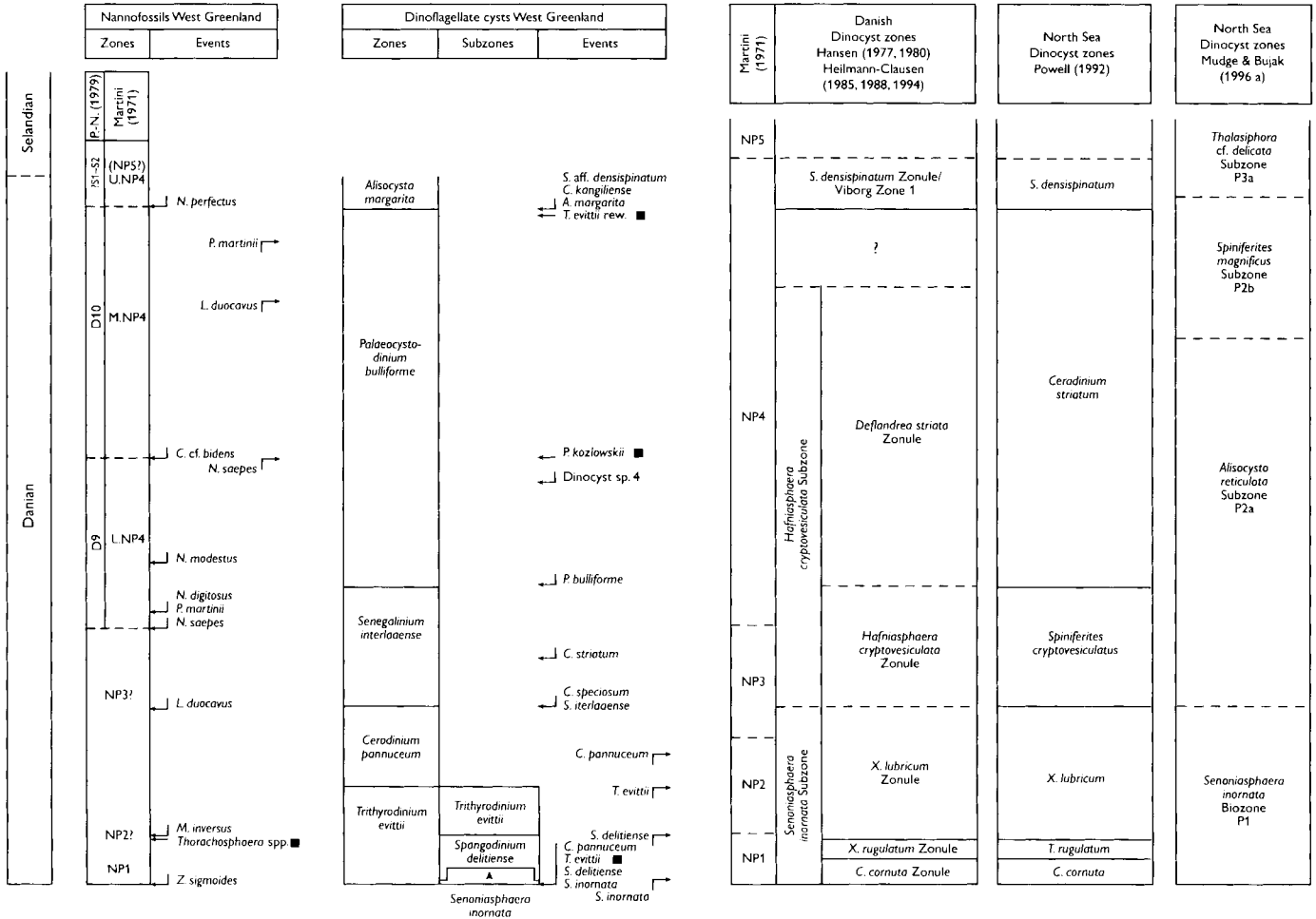

Fig. 5. Dinoflagellate cysts and nannofossils zonation of the Danian succession onshore West Greenland, compared with dinoflagellate cysts zonations from Denmark and the North Sea.

Late Cretaceous and earliest Paleocene species were observed, especially in the late Danian where specimens from the earliest Danian can be used as a marker horizon, especially *Trithyrodinium evittii* (Fig. 4).

The nannofossil samples yielded a poorly preserved, low abundance and low diversity floras. Whole coccolith specimens were rarely encountered, often only outer cycles, or remnants remained. When whole specimens were present, they were usually obscured by organic material.

Palynological zonation

The lower Paleocene succession on Nuussuaq has been divided into five dinoflagellate cyst zones of which the lowermost *Trithyrodinium evittii* Zone is subdivided into three subzones. The bases and tops of the five zones *Trithyrodinium evittii*, *Cerodinium pannuceum*, *Senegalinium iterlaaense*, *Palaeocystodinium bulliforme* and *Alisocysta margarita* (Fig. 5) are defined on the first and last occurrences of stratigraphically important species. Important marker species are shown in Figures 6–8.

Trithyrodinium evittii *Zone*

Age. Early Danian, Early Paleocene.

Correlation. Correlation with Martini's (1971) nannoplankton zones NP1 (pars) and NP2 (pars) is suggested.

Definition. The base of the zone is defined by the first occurrences of *Senoniasphaera inornata* and *Trithyrodinium evittii*, and the top by the last occurrence of *T. evittii* (Fig. 5).

Subdivision. The *Trithyrodinium evittii* Zone is divided into three subzones, the *Senoniaphaera inornata* Subzone, the *Spongodinium delitiense* Subzone and the *Trithyrodinium evittii* Subzone.

Thickness and distribution. The entire zone is recorded from the lower part of the Kangilia section, where it is represented by approximately 60 m of the Kangilia Formation. The lower part of the zone is also recorded from the K/T boundary section at Annertuneq, described in detail by Nøhr-Hansen & Dam (1997).

Comments. The *Trithyrodinium evittii* Zone may correlate with the Early Paleocene *Trithyrodinium evittii* Zone described from Australia by Stover & Partridge (1973) and from New Zealand by Strong *et al.* (1995).

Senoniasphaera inornata *Subzone*

Age. Earliest Danian, Early Paleocene.

Correlation. Correlation with Martini's (1971) nannoplankton zone NP1 (pars) is suggested.

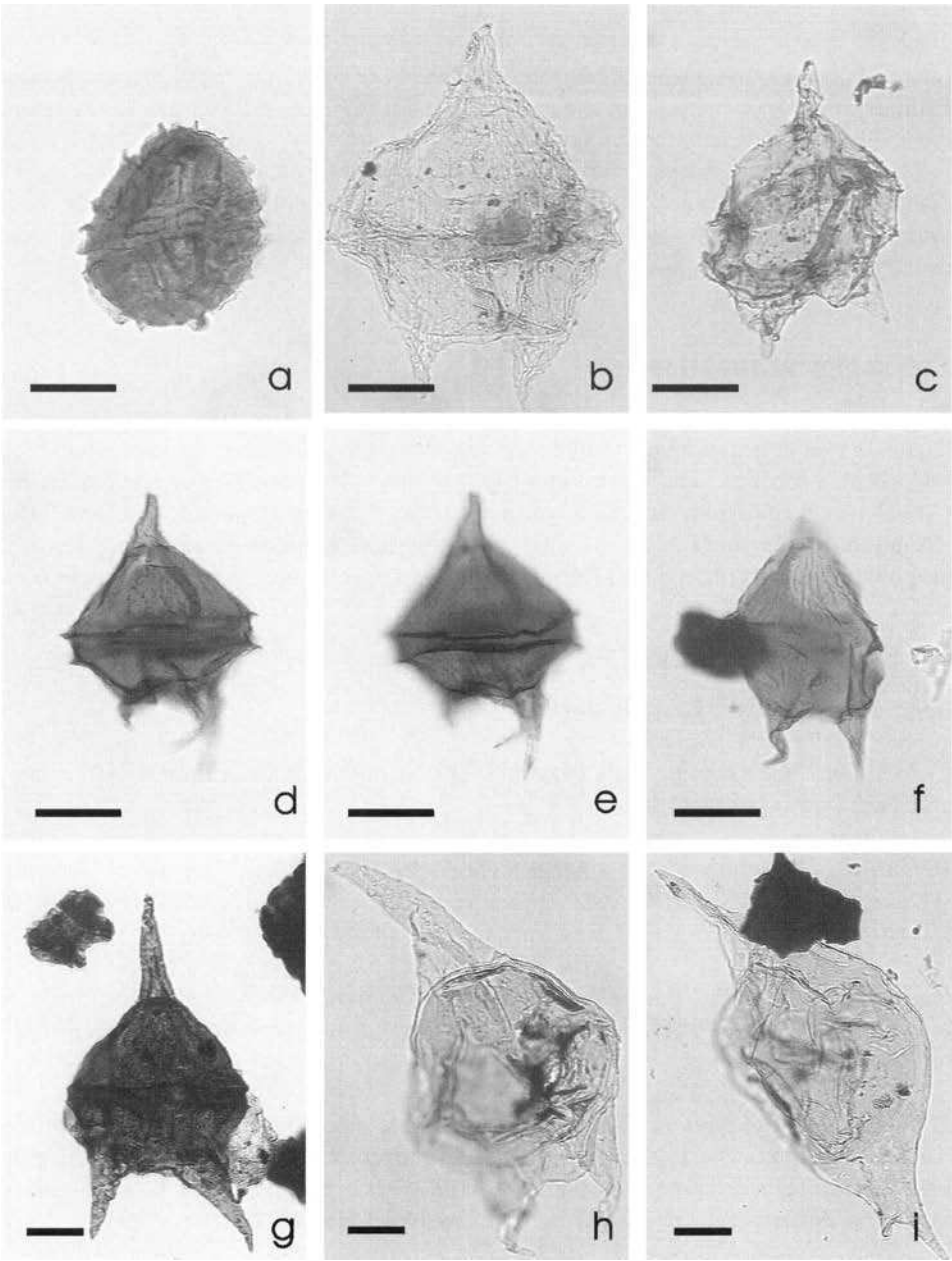

Fig. 6. Stratigraphically important dinoflagellate cysts, scale bars 20 µm. (**a**) *Alisocysta margarita*, GANE#1 well 564.7 m, GGU no. 439001-514-4, EF J22-4, MI 7473, LVR 1.10999, MGUH 26436. (**b**) *Cerodinium pannuceum*, Kangilia 400 m, GGU no. 369696-4, EF P19-1, MI 7481, LVR 1.11009, MGUH 26437. (**c**) *Cerodinium kangiliense*, Annertuneq 608 m, GGU no. 366599-3, EF Y32-1, MI 7478, LVR 1.11005, MGUH 26438. (**d**) *Cerodinium* aff. *granulostriatum*, GANE#1 well 146.9 m, GGU no. 439001-1155-3, EF T38-2, MI 7476, LVR 1.11002, MGUH 26439. (**e**) *Cerodinium* aff. *granulostriatum*, GANE#1 well 146.9 m, GGU no. 439001-1155-3, EF T38-2, MI 7476, LVR 1.11003, MGUH 26439. (**f**) *Cerodinium* aff. *granulostriatum*, GANE#1 well 146.9 m, GGU no. 439001-1155-3, EF T32-4, MI 7477, LVR 1.11004, MGUH 26440. (**g**) *Cerodinium striatum*, (164 µm) GANE#1 well 615.9 m, GGU no. 439001-515-4, EF P33-3, MI 7474, LVR 1.11000, MGUH 26441. (**h**) *Cerodinium speciosum*, Kangilia 505 m, GGU no. 369702-8, EF H25-4, MI 7484, LVR 1.11012, MGUH 26442. (**i**) *Palaeocystodinium bulliforme*, (220 µm) GANK#1 well 174.7 m, GGU no. 439201-48-3, EF E37-4, MI 7480, LVR 1.11007, MGUH 26443.

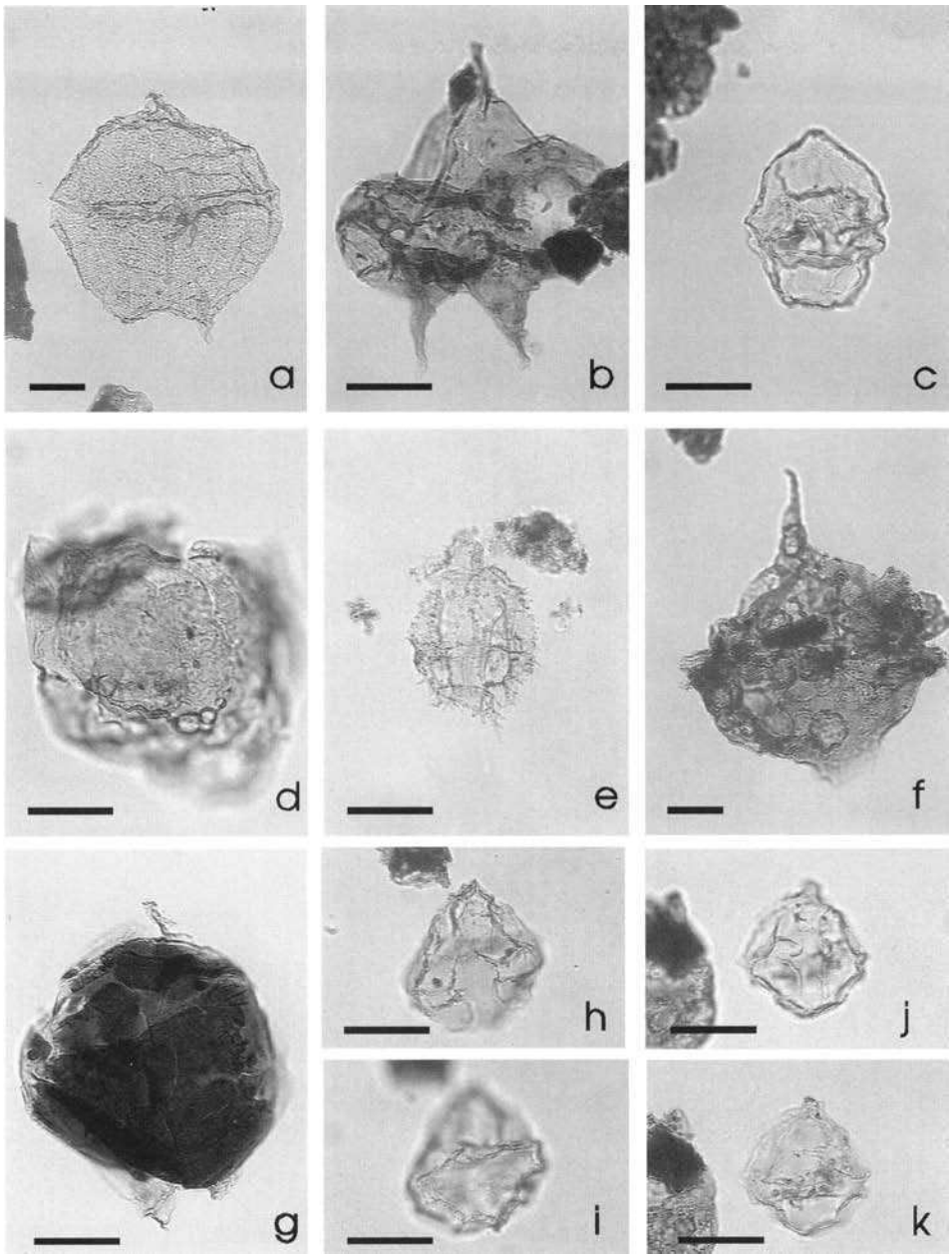

Fig. 7. Stratigraphically important dinoflagellate cysts, scale bars 20 µm. (**a**) *Palaeoperidinium pyrophorum*, (118 µm) Kangilia 390 m, GGU no. 369695-4, EF O35-2, MI 7482, LVR 1.11010, MGUH 26444. (**b**) *Phelodinium kozlowski* Kangilia 585 m, GGU no. 369710-4, EF Q16-1, MI 7488, LVR 1.11020, MGUH 26445. (**c**) *Senegalinium iterlaaense*, Kangilia 460 m, GGU no. 369698-3, EF G55-2, MI 7479, LVR 1.11006, MGUH 26446. (**d**) *Senoniasphaera inornata*, Annertuneq K/T boundary section 452.1 m, GGU no. 405305-7, 46.4-106.4, MI 5799, LVR 1.8030, MGUH 26447. (**e**) *Spinidinium* cf. *densispinatum*, Danienrygge 720 m, GGU no. 456943-3, EF W13-4, MI 7486, LVR 1.11014, MGUH 26448. (**f**) *Spongodinium delitiense*, (144 µm) Kangilia 350 m, GGU no. 369691-5, EF E29-2, MI 7483, LVR 1.11011, MGUH 26449. (**g**) *Trithyrodinium evittii*, Annertuneq K/T boundary section 452.9 m, GGU no. 405313-3, 43.4-105.2, MI 6972, LVR 1.9765, MGUH 25288. (**h**) & (**i**) Dinocyst sp 1 HNH 1997, Kangilia 595 m, GGU no. 369711-4, EF W49-3, MI 7487, LVR 1.11016-17, MGUH 26450. (**j**) & (**k**) Dinocyst sp. 1 HNH 1997, Danienrygge 722 m, GGU no. 456945-4, EF E18-1, MI 7218, LVR 1.11018-19, MGUH 26451.

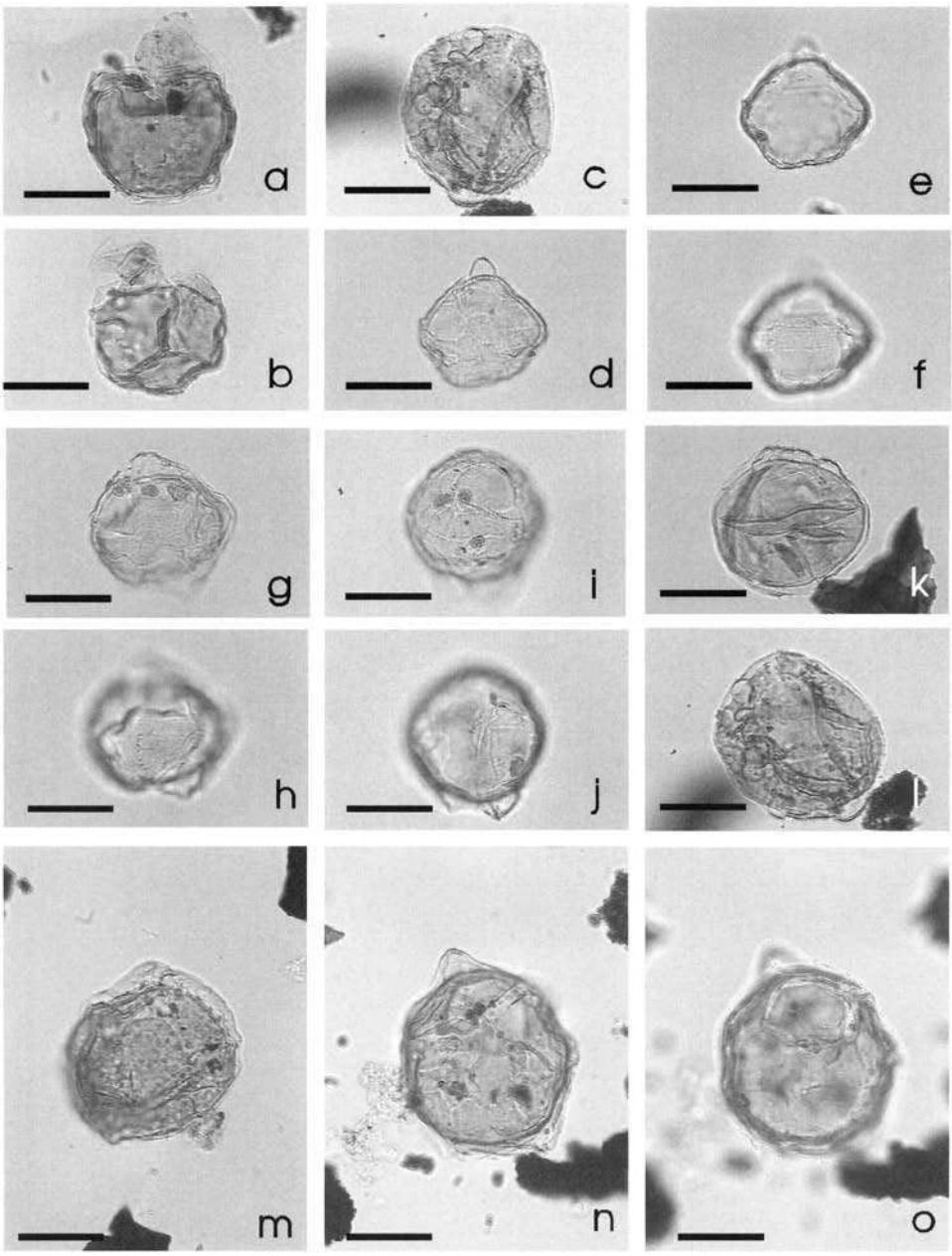

Fig. 8. Stratigraphically important dinoflagellate cysts, scale bars 20 µm. (**a**) Dinocyst sp. 2 HNH 1997, Kangilia 430 m, GGU no. 369697-4, EF U25-4, MI 7489, LVR 1.11021, MGUH 26452. (**b**) Dinocyst sp. 2 HNH 1997, Kangilia 430 m, GGU no. 369697-3, EF E13-3, MI 7490, LVR 1.11022, MGUH 26453. (**c**) Dinocyst sp. 2 HNH 1997, Kangilia 430 m, GGU no. 369697-3, EF L33-3, MI 7491, LVR 1.11023, MGUH 26454. (**d–f**) Dinocyst sp. 3 HNH 1997, Kangilia 762 m, GGU no. 369733-8, EF L44-1, MI 7492, LVR 1.11024–26, MGUH 26455. (**g**) & (**h**) Dinocyst sp. 3 HNH 1997, Kangilia 762 m, GGU no. 369733-4, EF J27-3, MI 7493, LVR 1.11027–28, MGUH 26456. (**i**) & (**j**) Dinocyst sp. 3 HNH 1997, Kangilia 762 m, GGU no. 369733-4, EF K52-1, MI 7494, LVR 1.11029–30, MGUH 26457. (**k**) Dinocyst sp. 4 HNH 1997, Kangilia 585 m, GGU no. 369710-3, EF F27.3, MI 7495, LVR 1.11031, MGUH 26458. (**l**) Dinocyst sp. 4 HNH 1997, Kangilia 430 m, GGU no. 369697-3, EF L33-3, MI 7038, LVR 1.9883, MGUH 26459. (**m**) Dinocyst sp. 4 HNH 1997, Danienrygge 710 m, GGU no. 456942-3, EF O18-3, MI 7026, LVR 1.9863, MGUH 26460. (**n**) & (**o**) Dinocyst sp. 4 HNH 1997, Danienrygge 720 m, GGU no. 456943-3, EF Q21-4, MI 7213, LVR 1.10216–18, MGUH 26461.

Definition. The base of the subzone is defined by the first occurrences of *Senoniasphaera inornata* and *Trithyrodinium evittii*, and the top by the last occurrence of *Senoniasphaera inornata* (Fig. 5).

Thickness and distribution. The subzone is only recorded from the lowermost part of the K/T boundary section at Annertuneq (Fig. 9), where it is represented by 20 cm of sediment just above the K/T boundary.

Characteristic species. The base of the subzone is characterized by the first occurrence of *Cerodinium pannuceum*, *S. inornata*, *Spongodinium delitiense* and *T. evittii*. *Spongodinium delitiense* and *T. evittii* are common to abundant within the zone.

Comments. The palynological assemblages across the K/T boundary at Annertuneq have previously been described by Nøhr-Hansen & Dam (1997). The first occurrence of *S. inornata* has been recorded immediately above the K/T boundary e.g. in Denmark (Hansen 1977), Alabama and Georgia (Moshkovitz & Habib 1993), the Netherlands (Smit & Brinkhuis 1996) and in Tunisia (Brinkhuis & Schiøler 1996). The first occurrence of *T. evittii* seems to vary from low to high palaeolatitudes, however, Nøhr-Hansen & Dam (1999) illustrated that *T. evittii* has its first occurrence immediately above the K/T boundary in middle to high latitudes (30–80°). The *Senoniasphaera inornata* Subzone defined herein from the lowermost Paleocene succession (NP1 pars) in West Greenland differs in age from the *S. inornata* Subzone described from Denmark (Hansen 1977) and the *S. inornata* Biozone described from the North Sea (Mudge & Bujak 1996*a*, *b*; Fig. 5). These represent the majority of the Danian, NP1 to middle NP3 and NP1 to middle NP4, respectively. None of the diagnostic events defining the *Carpartella cornuta* Zonule (Fig. 5) have been recorded in West Greenland.

Spongodinium delitiense *Subzone*

Age. Early Danian, Early Paleocene.

Correlation. Correlation with Martini's (1971) nannoplankton zones NP1 and NP2 (pars) is suggested.

Definition. The base of the subzone is defined by the last occurrence of *Senoniasphaera inornata*, and the top by the last occurrence of *Spongodiniun delitiense* (Fig. 5).

Thickness and distribution. The entire subzone is only recorded from the lower part of the Kangilia section (Fig. 10), where it is represented by approximately 23 m of sediment above the K/T boundary. The lower part of the subzone is also recorded from the K/T boundary section at Annertuneq (Fig. 9).

Characteristic species. The subzone is characterized by abundant *Cerodinium pannuceum*, *Spongodiniun delitiense* and *T. evittii* and by the ocurrence of *Alterbidinium ulloriaq* in the lower part.

Comments. According to Williams *et al.* (1993) and Hardenbol *et al.* (1998), *S. delitiense* has a last occurrence in the early mid Danian (correlating with the top of NP2

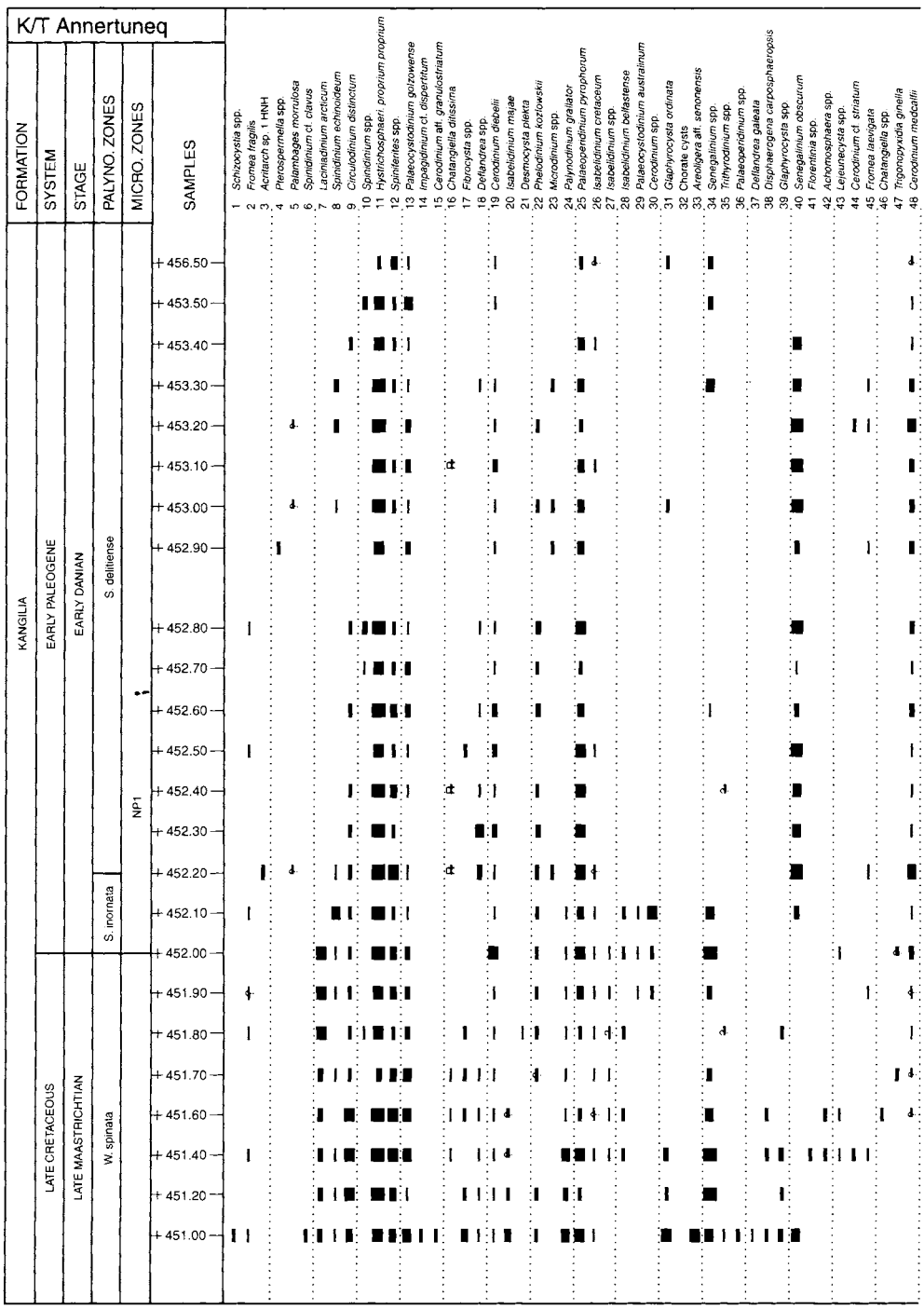

Fig. 9. Range chart showing the recorded palynomorphs and nannofossils from the K/T boundary section at Annertuneq on the north coast on Nuussuaq.

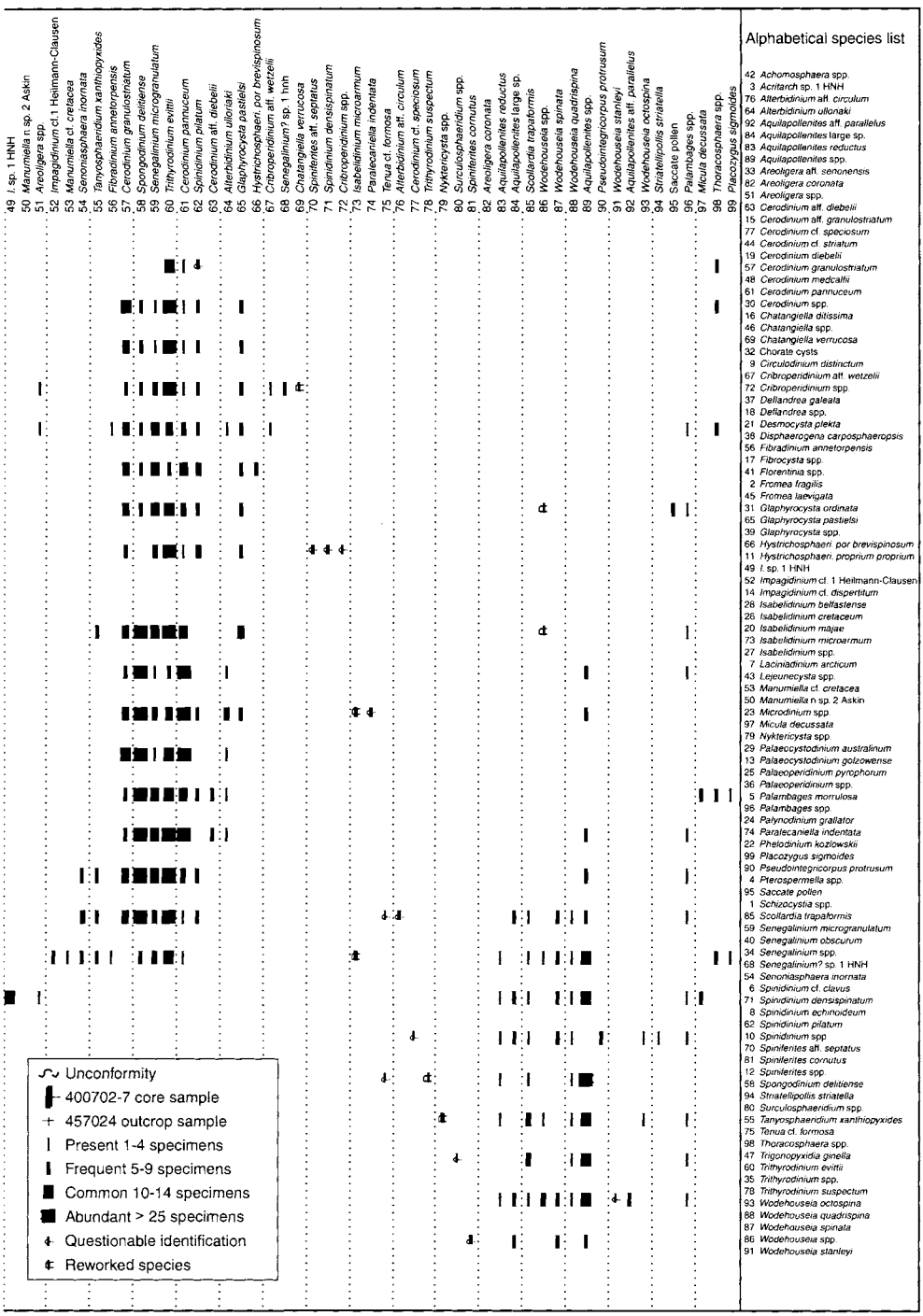
Alphabetical species list
42 Achomosphaera spp.
3 Acritarch sp. 1 HNH
76 Alterbidinium aff. circulum
64 Alterbidinium ulloriaki
92 Aquilapollenites aff. parallelus
84 Aquilapollenites large sp.
83 Aquilapollenites reductus
89 Aquilapollenites spp.
33 Areoligera aff. senonensis
82 Areoligera coronata
51 Areoligera spp.
63 Cerodinium aff. diebelii
15 Cerodinium aff. granulostriatum
77 Cerodinium cf. speciosum
44 Cerodinium cf. striatum
19 Cerodinium diebelii
57 Cerodinium granulostriatum
48 Cerodinium medcalfii
61 Cerodinium pannuceum
30 Cerodinium spp.
16 Chatangiella ditissima
46 Chatangiella spp.
69 Chatangiella verrucosa
32 Chorate cysts
9 Circulodinium distinctum
67 Cribroperidinium aff. wetzelii
72 Cribroperidinium spp.
37 Dellandrea galeata
18 Dellandrea spp.
21 Desmocysta plekta
38 Disphaerogena carposphaeropsis
56 Fibradinium annetorpensis
17 Fibrocysta spp.
41 Florentinia spp.
2 Fromea fragilis
45 Fromea laevigata
31 Glaphyrocysta ordinata
65 Glaphyrocysta pastielsi
39 Glaphyrocysta spp.
66 Hystrichosphaeri. por brevispinosum
11 Hystrichosphaeri. proprium proprium
49 I. sp. 1 HNH
52 Impagidinium cf. 1 Heilmann-Clausen
14 Impagidinium cf. dispertitum
28 Isabelidinium belfastense
26 Isabelidinium cretaceum
20 Isabelidinium majae
73 Isabelidinium microarmum
27 Isabelidinium spp.
7 Laciniadinium arcticum
43 Lejeunecysta spp.
53 Manumiella cf. cretacea
50 Manumiella n. sp. 2 Askin
23 Microdinium spp.
97 Micula decussata
79 Nyktericysta spp.
29 Palaeocystodinium australinum
13 Palaeocystodinium golzowense
25 Palaeoperidinium pyrophorum
36 Palaeoperidinium spp.
5 Palambages morrulosa
96 Palambages spp.
24 Palynodinium grallator
74 Paralecaniella indentata
22 Phelodinium kozlowskii
99 Placozygus sigmoides
90 Pseudointegricorpus protrusum
4 Pterospermella spp.
95 Saccate pollen
1 Schizocystia spp.
85 Scollardia trapaformis
59 Senegalinium microgranulatum
40 Senegalinium obscurum
34 Senegalinium spp.
68 Senegalinium? sp. 1 HNH
54 Senoniasphaera inornata
6 Spinidinium cf. clavus
71 Spinidinium densispinatum
8 Spinidinium echinoideum
62 Spinidinium pilatum
10 Spinidinium spp
70 Spiniferites aff. septatus
81 Spiniferites cornutus
12 Spiniferites spp.
58 Spongodinium delitiense
94 Striatellipollis striatella
80 Surculosphaeridium spp.
55 Tanyosphaeridium xanthiopyxides
75 Tenua cf. formosa
98 Thoracosphaera spp.
47 Trigonopyxidia ginella
60 Trithyrodinium evittii
35 Trithyrodinium spp.
78 Trithyrodinium suspectum
93 Wodehouseia octospina
88 Wodehouseia quadrispina
87 Wodehouseia spinata
86 Wodehouseia spp.
91 Wodehouseia stanleyi
Unconformity
400702-7 core sample
457024 outcrop sample
Present 1-4 specimens
Frequent 5-9 specimens
Common 10-14 specimens
Abundant > 25 specimens
Questionable identification
Reworked species

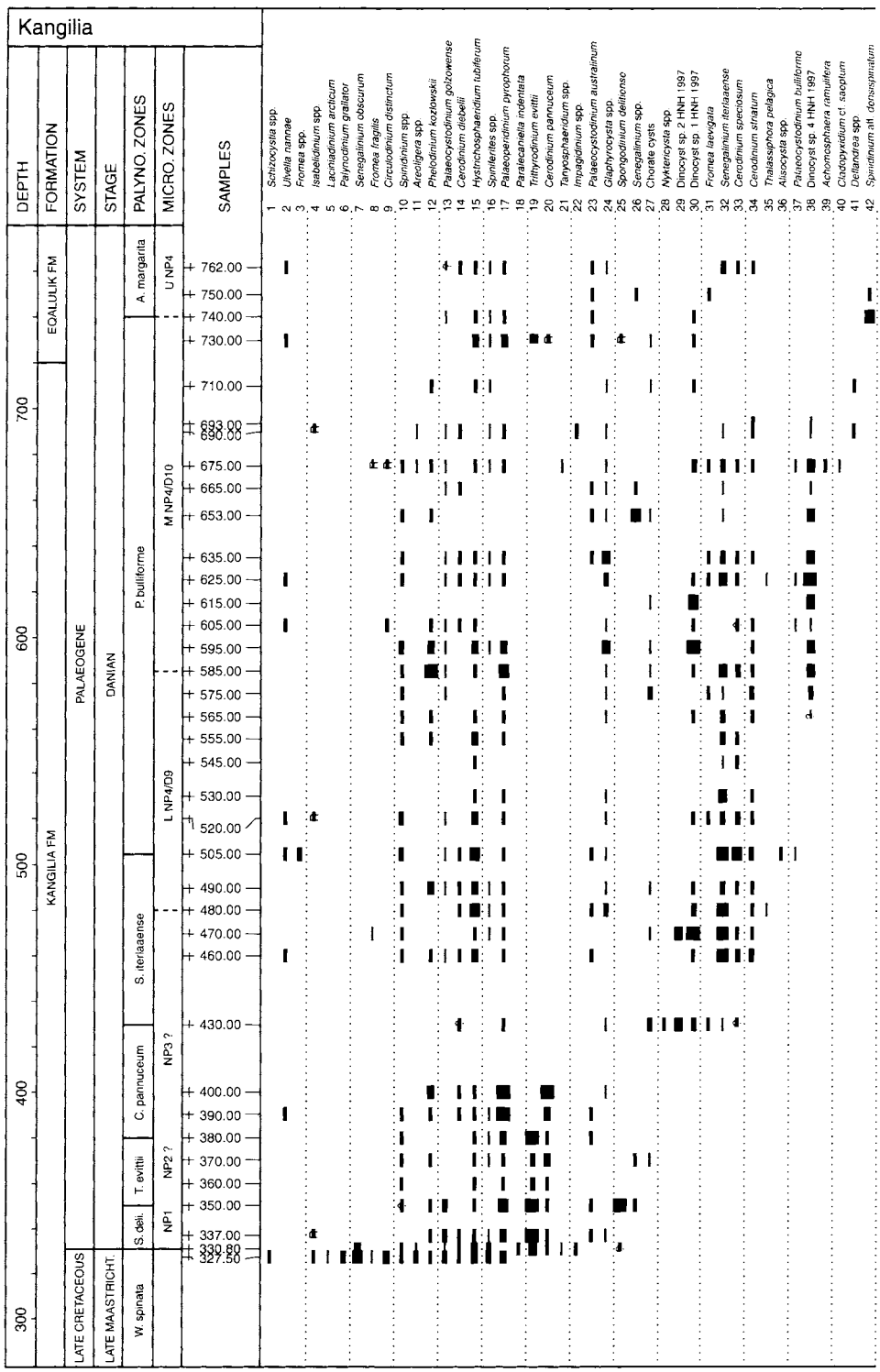

Fig. 10. Range chart showing the recorded palynomorphs and nannofossils from the Kangilia section on the north coast on Nuussuaq.

Alphabetical species list

39 *Achomosphaera ramulifera*
36 *Alisocysta* spp.
54 *Aquilapollenites* cf. *conatus*
51 *Aquilapollenites* spp.
11 *Areoligera* spp.
72 *Arkhangelskiella cymbiformis*
14 *Cerodinium diebelii*
43 *Cerodinium kangiliense*
20 *Cerodinium pannuceum*
33 *Cerodinium speciosum*
34 *Cerodinium striatum*
47 *Chatangiella ditissima*
46 *Chatangiella granulifera*
49 *Chatangiella* spp.
70 *Chiasmolithus* cf. *bidens*
68 *Chiasmolithus* spp.
27 Chorate cysts
9 *Circulodinium distinctum*
40 *Cladopyxidium* cf. *saeptum*
67 *Cruciplacolithus asymmetricus*
41 *Deflandrea* spp.
30 Dinocyst sp. 1 HNH 1997
29 Dinocyst sp. 2 HNH 1997
44 Dinocyst sp. 3 HNH 1997
38 Dinocyst sp. 4 HNH 1997
8 *Fromea fragilis*
31 *Fromea laevigata*
3 *Fromea* spp.
24 *Glaphyrocysta* spp.
15 *Hystrichosphaeridium tubiferum*
22 *Impagidinium* spp.
45 *Isabelidinium microarmum*
4 *Isabelidinium* spp.
5 *Laciniadinium arcticum*
63 *Lanternithus duocavus*
61 *Markalius inversus*
59 *Micula decussata*
65 *Neochiastozygus digitosus*
69 *Neochiastozygus modestus*
64 *Neochiastozygus saepes*
62 *Neochiastozygus* spp.
73 *Nephrolithus frequens*
28 *Nyktericysta* spp.
23 *Palaeocystodinium australinum*
37 *Palaeocystodinium bulliforme*
13 *Palaeocystodinium golzowense*
48 *Palaeohystrichophora infusorioides*
17 *Palaeoperidinium pyrophorum*
56 *Palambages* spp.
6 *Palynodinium grallator*
18 *Paralecaniella indentata*
12 *Phelodinium kozlowskii*
57 *Placozygus sigmoides*
74 *Prediscosphaera cretacea*
71 *Prinsiosphaera* spp.
66 *Prinsius martinii*
1 *Schizocystia* spp.
32 *Senegalinium iterlaaense*
7 *Senegalinium obscurum*
26 *Senegalinium* spp.
42 *Spinidinium* aff. *densispinatum*
10 *Spinidinium* spp.
16 *Spiniferites* spp.
25 *Spongodinium delitiense*
21 *Tanyosphaeridium* spp.
35 *Thalassiphora pelagica*
58 *Thoracosphaera operculata*
60 *Thoracosphaera* spp.
19 *Trithyrodinium evittii*
2 *Ulvella nannae*
50 *Vesperopsis* spp.
55 *Wodehouseia octospina*
52 *Wodehouseia spinata*
53 *Wodehouseia* spp.

or lowermost NP3) in the northern hemisphere. The records of Hansen (1977) from Denmark show that *S. delitiense* last occurs at the top of the *Xenicodinium lubricum* Zonule (Fig. 5).

Trithyrodinium evittii *Subzone*

Age. Early Danian, Early Paleocene.

Correlation. Correlation with Martini's (1971) nannoplankton zones NP2 and NP3? is suggested.

Definition. The base of the subzone is defined by the last occurrence of *Spongodiniun delitiense*, and the top by the last occurrence of *Trithyrodinium evittii* (Fig. 5).

Thickness and distribution. The entire subzone is only recorded from the lower part of the Kangilia section (Fig. 10), where it is represented by approximately 30 m of sediment.

Characteristic species. The subzone is characterized by the abundance of *Cerodinium pannuceum* and *T. evittii.*

Comments. Trithyrodinium evittii was described from the early part of the Danian in California (Drugg 1967) and later from the lowermost part of NP1 to the lower part of NP2 in Alabama (Moshkovitz & Habib 1993). The *Trithyrodinium evittii* Subzone may correlate with the upper part of the Early Paleocene *Trithyrodinium evittii* Zone described from Australia by Stover & Partridge (1973) and from New Zealand by Strong *et al.* (1995).

Cerodinium pannuceum *Zone*

Age. Early Danian, Early Paleocene.

Correlation. Correlation with Martini's (1971) nannoplankton zones NP2 and NP3? is suggested.

Definition. The base of the zone is defined by the last occurrence of *Trithyrodinium evittii*, and the top by the first occurrence of *Senegalinium iterlaaense*. The last occurrence of *C. pannuceum* is recorded in the middle of the zone (Fig. 5).

Thickness and distribution. The zone is only recorded from the lower part of the Kangilia section (Fig. 10), where it is represented by approximately 50 m of sediment.

Characteristic species. The zone is characterized by the abundance of *Cerodinium pannuceum* and *Palaeoperidinium pyrophorum* in the lower half of the zone.

Comments. Cerodinium pannuceum was described from the Early Paleocene in South Dakota (Stanley 1965) and from the latest Maastrichtian to the early Danian Zone NP2 in Alabama (Moshkovitz & Habib 1993).

Senegalinium iterlaaense *Zone*

Age. Mid to late Danian, Early Paleocene.

Correlation. Correlation with Martini's (1971) nannoplankton zones NP3? and the lower part of NP4 is suggested.

Definition. The base of the zone is defined by the first occurrence of *Senegalinium iterlaaense*, and the top by the first occurrence of *Palaeocystodinium bulliforme* (Fig. 5).

Thickness and distribution. The entire zone is recorded from the lower part of the Kangilia section (Fig. 10), where it is represented by approximately 75 m of sediment. Part of the zone is also recorded from the lower part of the Annertuneq section (Fig. 11) and the lower part of the GANK#1 well core (Fig. 12).

Characteristic species. The zone is characterized by common to abundant *Senegalinium iterlaaense* throughout and by the first occurrence of *Cerodinium speciosum* and *C. striatum* in the lower part.

Comments. *Senegalinium iterlaaense* has recently been described by Nøhr-Hansen & Heilmann-Clausen (2000), who reported the species to have a first occurrence in the mid Danian, NP3 Zone (*Neochiastozygus modestus* Subzone, Thomsen & Heilmann-Clausen 1985), in the Hvalløse borehole, Denmark, correlating with the lower part of the *Hafniasphaera cryptovesiculata* Subzone (Fig. 5). *Senegalinium iterlaaense* has not been recorded from Selandian deposits in Denmark (C. Heilmann-Clausen pers. comm. 2000). Thomsen & Heilmann-Clausen (1985) also found the first occurrence of *Cerodinium striatum* in the *Neochiastozygus modestus* Subzone in the Hvalløse borehole, Denmark, whereas others (e.g. G. L. Williams pers. comm. 1999) consider *C. striatum* to range into the Late Maastrichtian.

Palaeocystodinium bulliforme *Zone*

Age. Mid to late Danian, Early Paleocene.

Correlation. Correlation with lower and middle nannoplankton Zone NP4 (Martini 1971) is suggested.

Definition. The base of the zone is defined by the first occurrence of *Palaeocystodinium bulliforme*, and the top by the first occurrence of *Alisocysta margarita* (Fig. 5).

Thickness and distribution. The zone is recorded from the upper part of the Kangilia section (Fig. 10), where it is represented by approximately 235 m of sediment. The zone is also recorded from the lower Annertuneq section (Fig. 11), the lower part of the GANK#1 well (Fig. 12), the lower part of the GANE#1 well (Fig. 13) and the middle part of the GRO#3 well (Fig. 14).

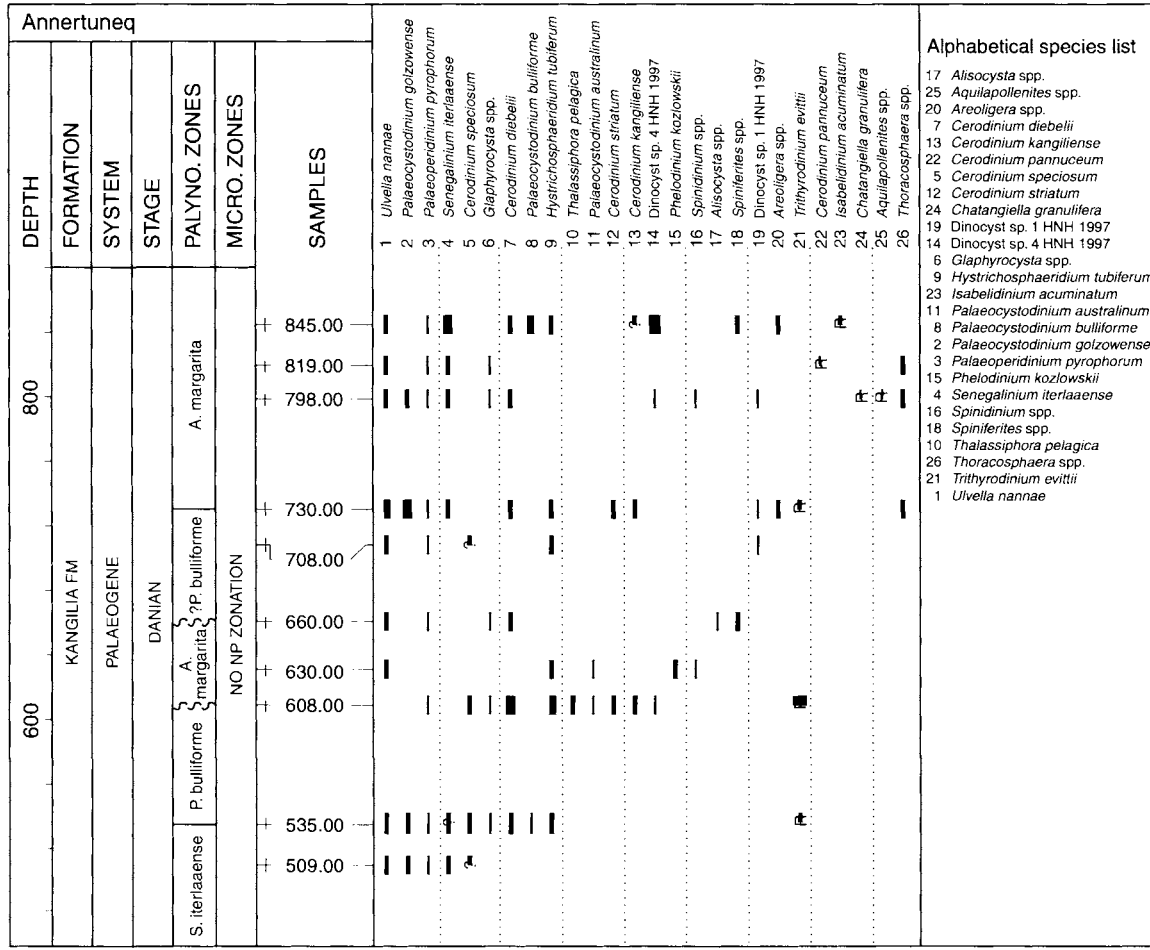

Fig. 11. Range chart showing the recorded palynomorphs and nannofossils from the Annertuneq section on the north coast on Nuussuaq.

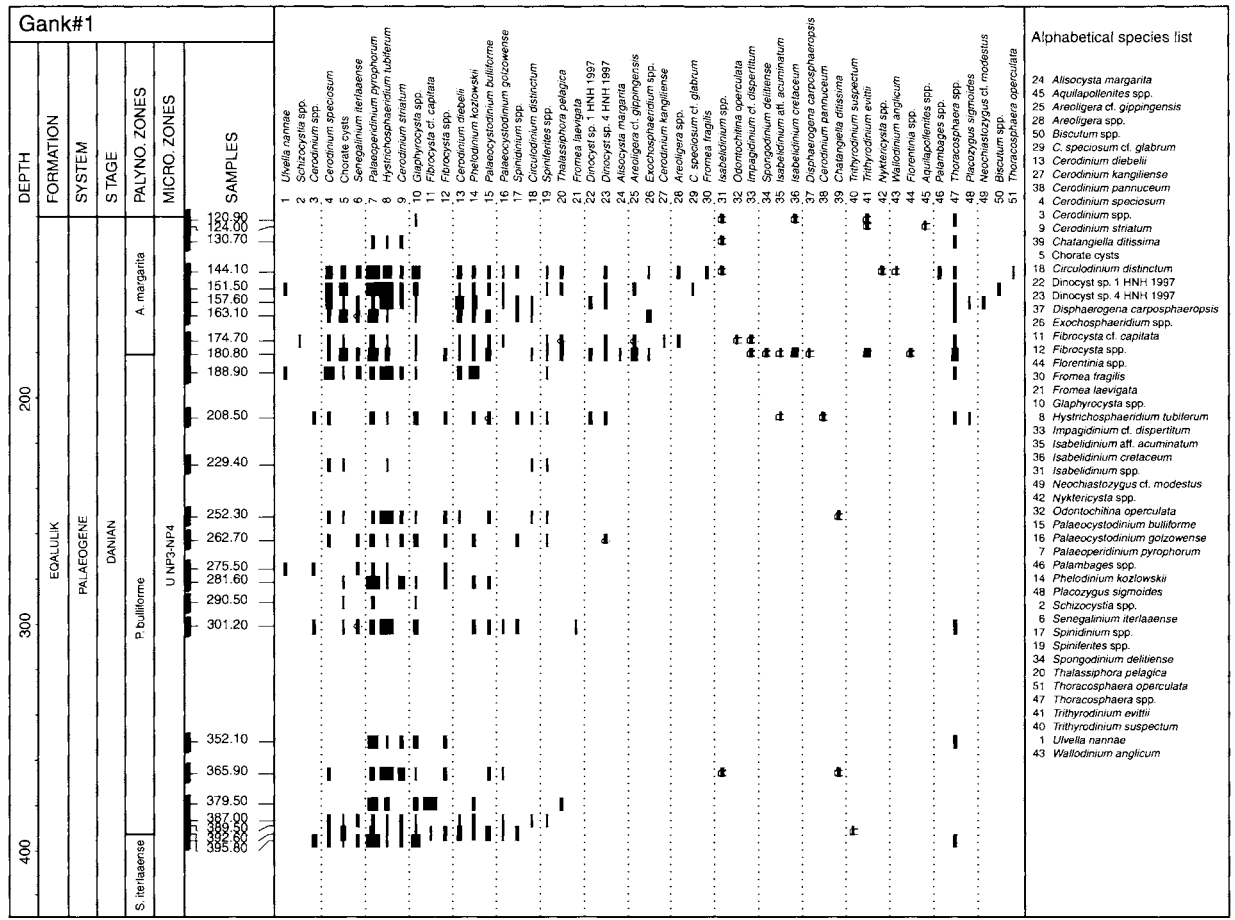

Fig. 12. Range chart showing the recorded palynomorphs and nannofossils from the GANK#1 well on the south western part of Nuussuaq.

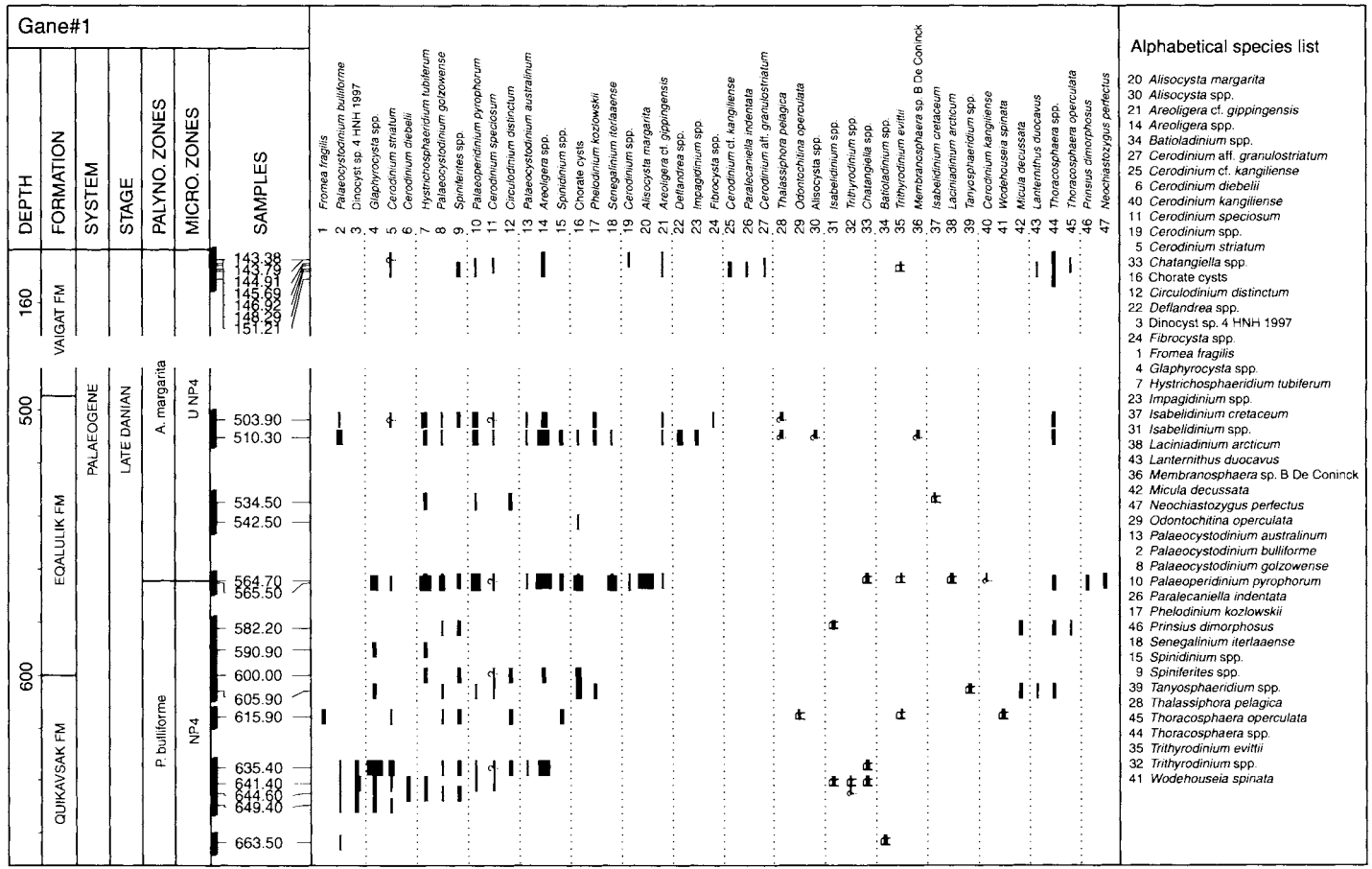

Fig. 13. Range chart showing the recorded palynomorphs and nannofossils from the GANE#1 well on the south western part of Nuussuaq.

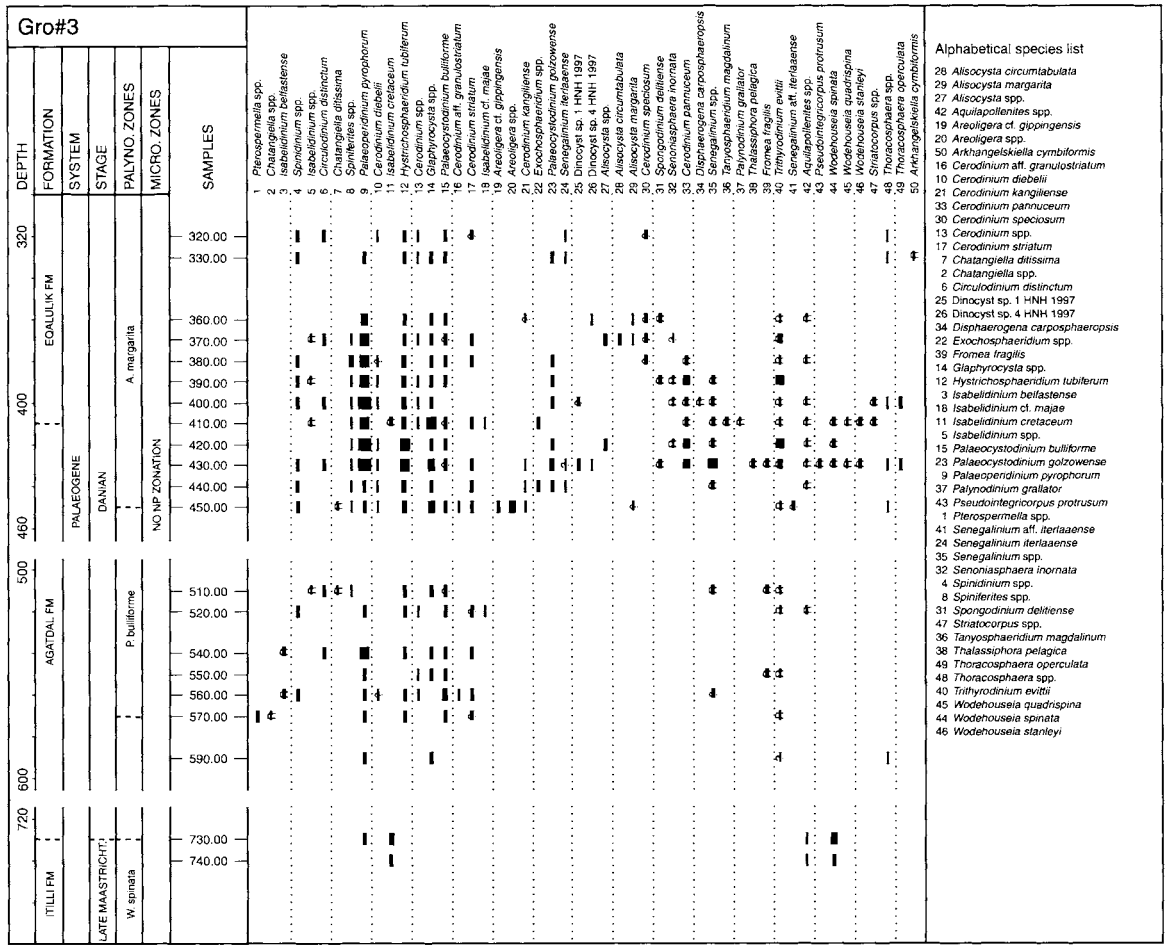

Fig. 14. Range chart showing the recorded palynomorphs and nannofossils from the GRO#3 well on the south western part of Nuussuaq.

Characteristic species. The base of the zone is characterized by the first occurrence of *Palaeocystodinium bulliforme* and the middle part by common to abundant Dinocyst sp. 4 (Nøhr-Hansen 1997*a*). A high abundance of *Phelodinium kozlowskii* has been recorded from the lower part of the zone in the Kangilia section (Fig 10).

Comments. *Palaeocystodinium bulliforme* was described from the Early Paleocene on Bylot Island, Canada (Ioannides 1986). The first occurrence of *P. bulliforme* has previously been recorded (as *Palaeocystodinium australinum*) from the late Danian (lower NP4, middle *Neochiastozygus saepes* Zone) in the Hvalløse borehole, Denmark (Thomsen & Heilmann-Clausen 1985) correlating with the *Deflandrea striata* Zonule (upper part of the *Hafniasphaera cryptovesiculata* Subzone) (Heilmann-Clausen 1988; Fig. 5). Powell (1992) used the first occurrence of *Palaeocystodinium australinum* to define his *Cerodinium striatum* Interval Biozone (Fig. 5).

In the following paragraph, and in Figure 5, an attempt has been made to clarify some confusion in the literature as concerns the *Hafniasphaera cryptovesiculata* and *Deflandrea striata* zones and some species of *Palaeocystodinium*. In the definition of the *Hafniasphaera cryptovesiculata* Subzone Hansen (1977, pp. 7–8) remarked: 'At Klintholm and Hvalløse localities, belonging to the uppermost part of this subzone, species of *Palaeocystodinium* Alberti, 1961 occur. Yet these species have not been found in other parts of the Danian indicating the presence of very young Danian deposits at Klintholm and Hvalløse'. Later Hansen (1980) in his unpublished PhD thesis proposes a subdivision of his *Hafniasphaera cryptovesiculata* Subzone into two zonules: a lower *Hafniasphaera cryptovesiculata* Zonule and an upper *Deflandrea striata* Zonule (now *Cerodinium striatum*). The upper *Deflandrea striata* Zonule was defined by sediments containing *Cerodinium striatum* but excluded sediments containing *Deflandrea speciosa* (now *Cerodinium speciosum*) and *Spinidinium densispinatum*. Within the *Deflandrea striata* Zonule Hansen (1980) recorded abundant specimens of the informal '*Palaeocystodinium klintholmense*' later descibed as *Palaeocystodinium bulliforme* by Ioannides (1986). Later Heilmann-Clausen (1988, p. 339 and fig. 172) published Hansen's (1980) zonal scheme with the new *Hafniasphaera cryptovesiculata* Subzone, *Hafniasphaera cryptovesiculata* Zonule and the *Deflandrea striata* Zonule. Heilmann-Clausen (1988, p. 339) also mentioned that the *Deflandrea striata* Zonule is defined by the first occurrence of *Deflandrea striata* and *Palaeocystodinium australinum* (shown as the invalid species name *klintholmense* in the range chart of Heilmann-Clausen, 1988).

Later Powell (1992) established the *Spiniferites cryptovesiculata* Interval Biozone based on the old *Hafniasphaera cryptovesiculata* Subzone of Hansen (1977) and the *Cerodinium striatum* Interval Biozone based on an emendation of the *Deflandrea striata* Zonule of Heilmann-Clausen (1988). The confusion is thus mainly due to the *Hafniasphaera cryptovesiculata* Subzone of Hansen (1977) being different from the *Hafniasphaera cryptovesiculata* Zonule of Heilmann-Clausen (1988) ex Hansen (1980).

Alisocysta margarita *Zone*

Age. Mid to late Danian, Early Paleocene.

Correlation. Correlation with the upper part of Martini's (1971) nannoplankton Zone NP4 is suggested.

Definition. The base of the zone is defined by the first occurrence of *Alisocysta margarita*. The top of the zone is not defined, as the clastic sediments are terminated by a thick hyaloclastic succession (Fig. 5).

Thickness and distribution. The zone is recorded from all the sections studied (Figs 9–16). The sedimentary thicknesses vary between 22 and 130 m representing the major part of the Eqalulik Formation (Fig. 3). A repetition of the *Alisocysta margarita* Zone occurs in the Annertuneq main section resulting from a downthrown landslide block. The *A. margarita* Zone is also recognized in intrabasaltic sediments in the volcanic Anaanaa Member in the GANW#1 (Fig. 15) and GANE#1 wells (Fig. 13).

Characteristic species. The lower part of the zone is characterized by the first occurrences of *Alisocysta margarita* and *Cerodinium kangiliense*. Both *A. margarita* and *C. kangiliense* are recorded from intrabasaltic mudstones within the Anaanaa Member in the GANW#1 and GANE#1 wells. The first occurrence of *Spinidinium* cf. *densispinatum* and common to abundant *Palaeoperidinium pyrophorum* are also recorded within this zone. Another character useful for the recognition of the base of the zone, are common to abundant occurrences of reworked specimens of the earliest Danian *Trithyrodinium evittii*, just below or coincident with the first occurrence of *A. margarita*. The high abundance of reworked *T. evittii* is concentrated in a narrow interval at Kangilia, Annertuneq and in the GANK#1 well, whereas the interval expands to approximately 60 m in the GRO#3 well. The first occurrence of *Spinidinium* cf. *densispinatum* and common to abundant *Palaeoperidinium pyrophorum* are also recorded within this zone.

Comments. The first occurrence of *Alisocysta margarita* (Fig. 4) suggests a mid to late Selandian age according to Heilmann-Clausen (1994) and Powell *et al.* (1996). However, an earlier occurrence of *Alisocysta margarita* has been reported from the late Danian (61.58 Ma) in California by Hardenbol *et al.* (1998). In his study of the Thanetian (Late Paleocene) in southeastern England, Jolley (1998) observed that *A. margarita* apparently favoured outer neritic and basinal settings, reaching an abundance peak in these depositional environments. In Nuussuaq *A. margarita* appears in low numbers in narrow intervals. However, it is abundant in a narrow interval in GANE#1, and in the GANW#1 and GRO#3 wells it occurs in low abundances but with a wide stratigraphic range (Fig. 4). The occurrence of *A. margarita* in more than one interval in the GANW#1 and GRO#3 wells in the south-western part of Nuussuaq, is suggested as indicating an expansion of the event due to rapid sedimentation in that area. Jolley's (1998) assumption that the presence and high abundance of *A. margarita* indicates a change to deeper marine depositional conditions supports the sedimentological interpretation of the Eqalulik Formation.

Nøhr-Hansen & Heilmann-Clausen (2000) recently described the species *Cerodinium kangiliense* and recorded its stratigraphic range as mid Danian to earliest Selandian (upper NP3 to lower NP5) in Denmark. In Nuussuaq both *A. margarita* and *C. kangiliense* continue into the intrabasaltic mudstone within the Anaanaa Member in the GANW#1 and GANE#1 wells (Fig. 4), suggesting that the Anaanaa Member is of latest Danian or earliest Selandian age.

The first occurrence of *Spinidinium* cf. *densispinatum* within the *Alisocysta margarita* Zone suggests correlation with the *Spinidinium densispinatum* Interval Biozone of

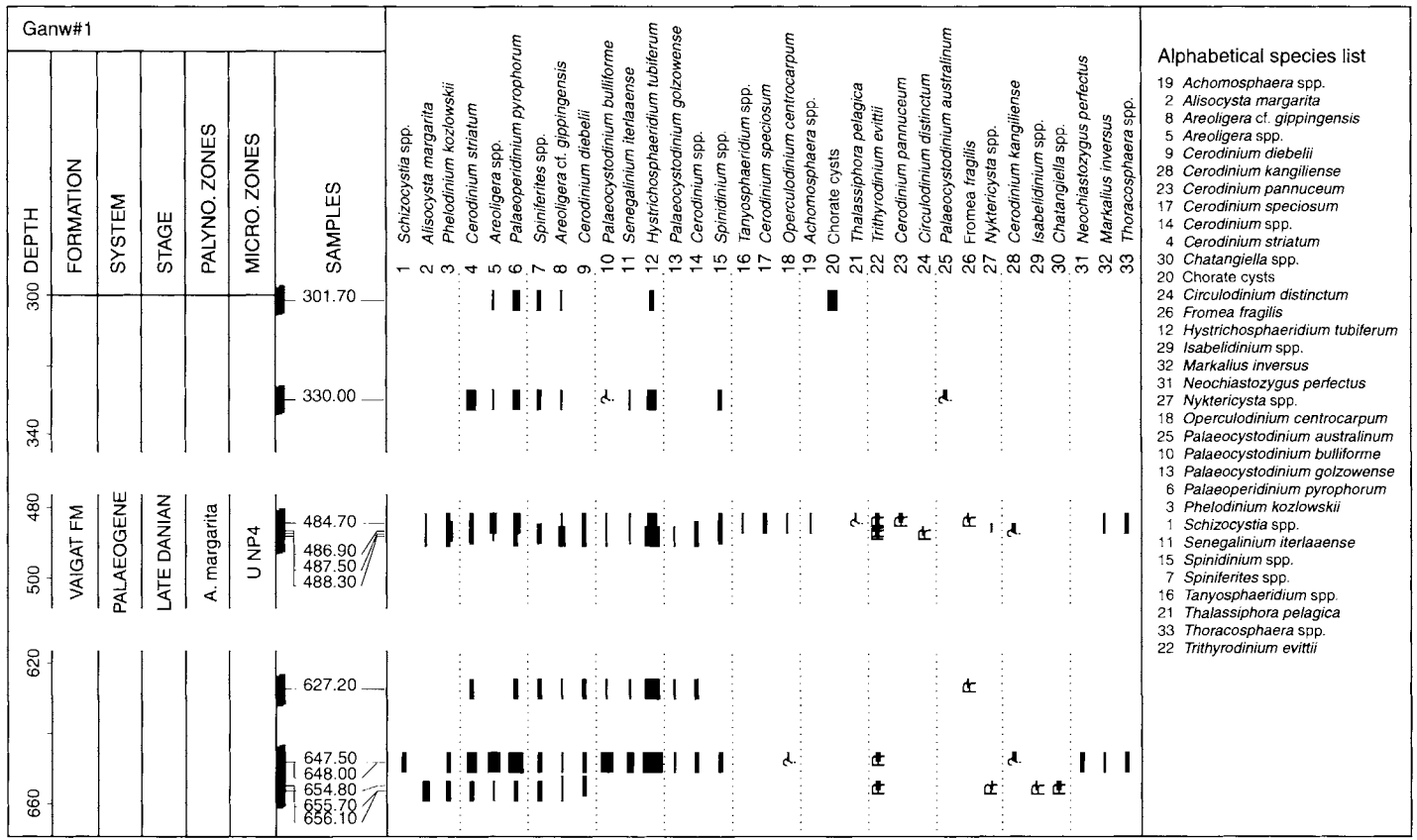

Fig. 15. Range chart showing the recorded palynomorphs and nannofossils from the GANW#1 well on the south western part of Nuussuaq.

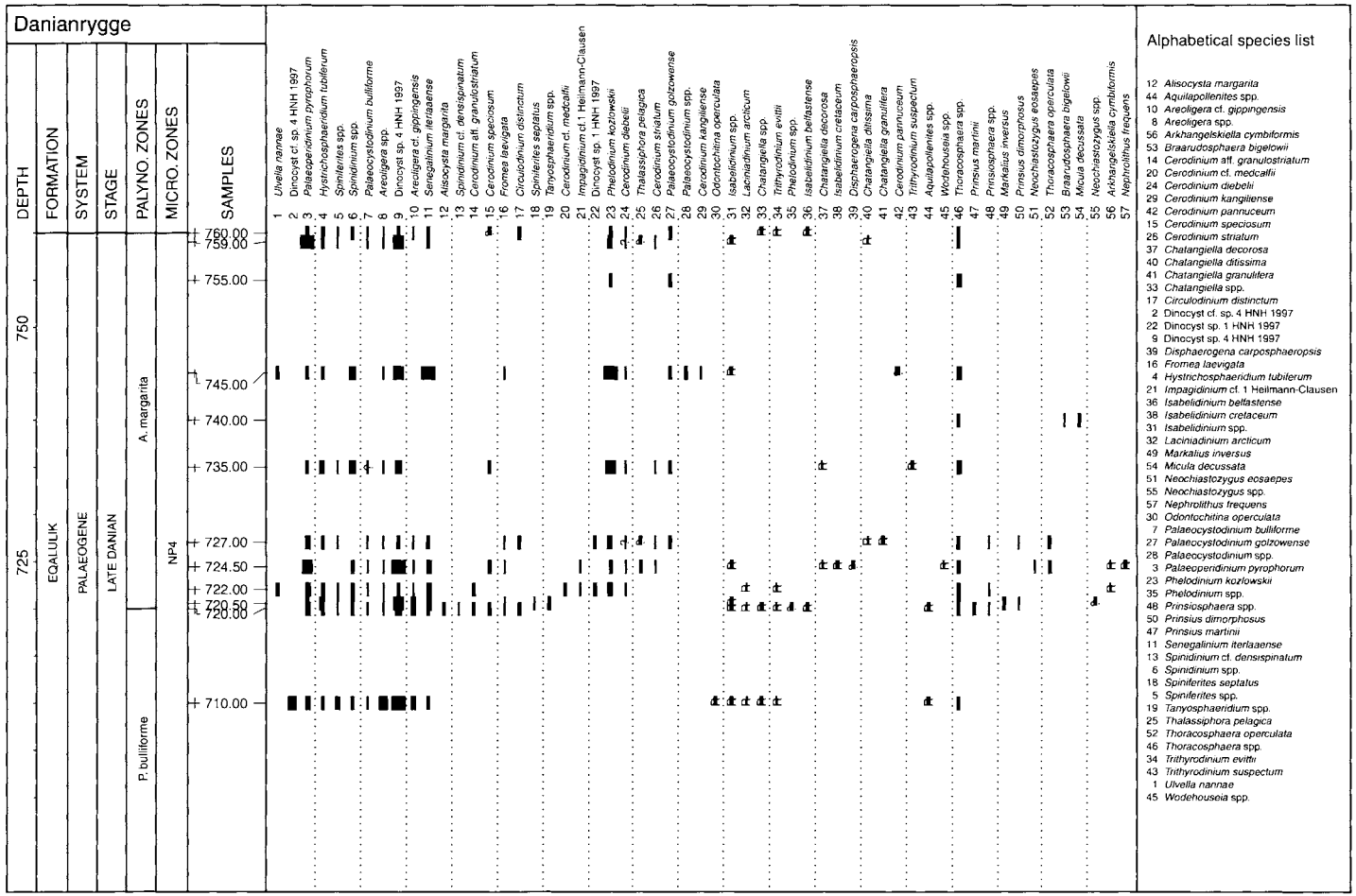

Fig. 16. Range chart showing the recorded palynomorphs and nannofossils from the Danienrygge section on the north coast on Nuussuaq.

Powell (1992), this zone was based on the *Spinidinium densispinatum* Zonule of Heilmann Clausen (1988) and the Viborg Zone 1 of Heilmann-Clausen (1985). Powell (1992) calibrated the *Spinidinium densispinatum* Interval Biozone with NP 5 (pars) and dated it as Thanetian (pars). This is in disagreement with Heilmann-Clausen (1994), who stated that the *Spinidinium densispinatum* Interval Biozone is defined in the Danian Limestone and should therefore be placed in the latest Danian. Heilmann-Clausen (1994) also mentioned that the *Spinidinium densispinatum* Interval Biozone was not recorded in NP5 but rather in the local Danish S1 + S2 nannofossil zones of Thomsen & Heilmann-Clausen (1985). The presence of common to abundant *Palaeoperidinium pyrophorum* in the *Alisocysta margarita* Zone may suggest correlation with the *Spiniferites magnificus* Subzone (P2b) or the *Thalassiphora* cf. *delicata* Subzone (P3a) of Mudge & Bujak (1996*a*, *b*).

Nannofossils

The Lower Paleocene succession on Nuussuaq is divided into Martini's global NP zones (Martini 1971), and correlated with the zonation schemes of Perch-Nielsen (1979), Thomsen (1995) and the current scheme for the North Sea (Varol 1998). The zones are based upon the first and last occurrences of stratigraphically significant species. Important marker species are shown in Figure 17.

NP1–NP2?

Age. Early Danian, Early Paleocene.

Correlation. The interval correlates tentatively with zones D1–D4 (Perch-Nielsen 1979), 1–4 (Thomsen 1995) and NNTp1A–NNTp2E (Varol 1998).

Definition. Assemblages comprise species common to the Early Paleocene. The base of the overlying zone is tentatively based upon the first occurrence of the dinoflagellate cyst *Senegalinium iterlaaense* (Fig. 5). At the Kangilia locality the zones

Fig. 17. Nannofossil illustrations compare poorly preserved nannofossils from the West Greenland material with well preserved specimens from the Danish Chalk (Danish specimens taken from material described in Stouge *et al.* (2000). (**a**) *Lanternithus duocavus*, Kangilia 605 m, GGU no. 369712-C775, EF Q36-4, MI 7470, LVR 1.10988, MGUH 26462. (**b**) *Lanternithus duocavus*, Kangilia 605 m, GGU no. 369712-C775, EF Q36-4, MI 7470, LVR 1.10989, MGUH 26462. (**c**) *Lanternithus duocavus*, Gemmas Allé (90 cm above base of Lellinge Grøn sand Formation), DGU no. Amager Vandtårn 13, EF (no number), MI 7261, LVR 1.10315, MGUH 26463. (**d**) *Biscutum* spp., GANK#1 well 151.1 m, GGU no. 439201-40, EF S47-2, MI 7466, LVR 1.10978, MGUH 26464. (**e**) *Biscutum* spp., GANK#1 well 151.1 m, GGU no. 439201-40, EF S47-2, MI 7466, LVR 1.10976, MGUH 26464. (**f**) *Biscutum* spp., Gemmas Allé (260 cm below base of Lellinge Grønsand Formation), DGU no. Amager Vandtårn 3, EF O48-4, MI 7472, LVR 1.10998, MGUH 26465. (**g**) *Neochiastozygus perfectus*, GANE#1 well 564.7 m, GGU no. E604, EF O36-1, MI 7465, LVR 1.10970, MGUH 26466. (**h**) *Neochiastozygus perfectus*, GANE#1 well 564.7 m, GGU no. E604, EF O36-1, MI 7465, LVR 1.10973, MGUH 26466. (**i**) *Neochiastozygus perfectus*, Gemmas Allé (90 cm above base of Lellinge Grønsand Formation), DGU no. Amager Vandtårn 13, EF (no number), MI 7260, LVR 1.10312, MGUH 26467. (**j**) *Chiasmolihus/Cruciplacolithus* spp., Kangilia 762 m, GGU no. 369733-C780, EF O52-4, MI 7471, LVR 1.10991, MGUH 26468. (**k**) *Chiasmolihus/Cruciplacolithus* spp., Kangilia 762 m, GGU no. 369733-C780, EF O52-4, MI 7471, LVR 1.10992, MGUH 26468. (**l**) *Chiasmolithus bidens*, Gemmas Allé (90 cm above base of Lellinge Grønsand Formation), DGU no. Amager Vandtårn 13, EF (no number), MI 7255, LVR 1.10300, MGUH 26469.

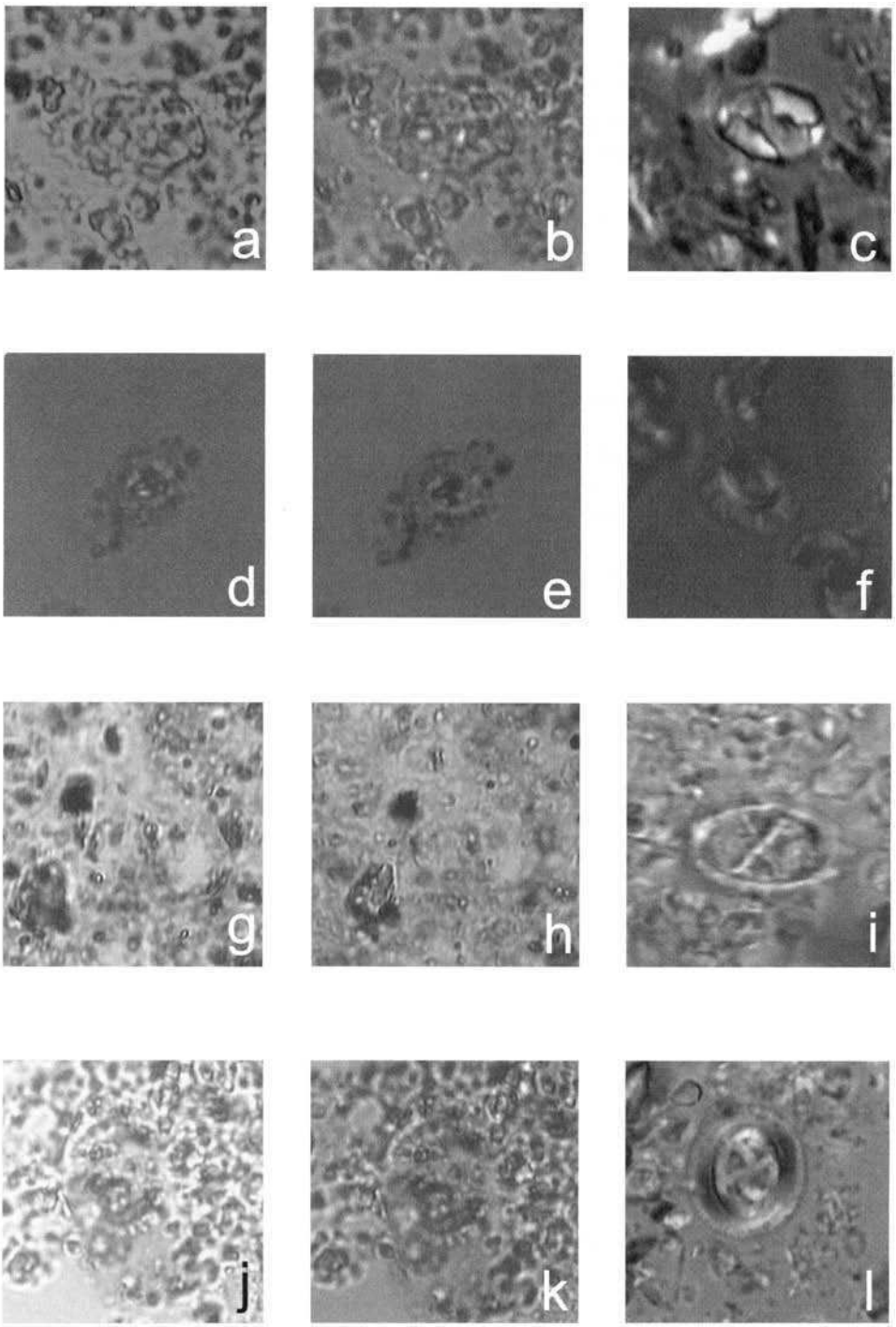
a
b
c
d
e
f
g
h
i
j
k
l

cannot be further sub-divided due to a very low abundance and diversity assemblage of nannofossils, and absence of marker species.

Characteristic species. The early Danian is indicated by the presence, especially in the Kangilia section, of *Thoracosphaera* spp. (common), *Markalius inversus*, *Zeugrhabdotus sigmoides*, *Thoracosphaera operculata* and specimens of reworked *Arkangelskiella cymbiformis* and *Micula decussata*.

Comments. The ubiquitous *Thoracosphaera* spp. is known to occur as 'blooms' in the Early Paleocene (NP1–4). It is thought that these 'blooms' are a result of opportunistic species occupying an environment when there is a lack of competition, i.e. after the K/T boundary event (Perch-Nielsen, 1985). *Zeugrhabdotus sigmoides* (Annertuneq, Kangilia, GANK#1) and *Markalius inversus* (Danienrygge, Kangilia, GANW#1) are species which survived into the Early Paleocene from the Late Cretaceous. According to Perch-Nielsen (1979), *Z. sigmoides* is absent or extremely rare in the lowermost part of NP1 (D1). Nannofossils reworked from the Late Cretaceous were observed in several samples. Robust forms such as *Arkhangelskiella cymbiformis* (GRO#3, Danienrygge), *Micula decussata* (Danienrygge, Annertuneq, Kangilia, GANE#1), *Prediscosphaera cretacea* (Kangilia) and the Late Maastrichtian marker *Nephrolithus frequens* (Danienrygge, Kangilia) are examples found in Nuussuaq (Figs 10, 14 & 16).

NP3?

Age. Mid Danian, Early Paleocene.

Correlation. The interval correlates tentatively with zones D5–D8 (Perch-Nielsen 1979), 5–6 (Thomsen 1995) and NNTp2F–NNTp4C (Varol 1998).

Definition. The low abundance and diversity assemblages again prevent accurate dating of this interval. The first occurrence of the dinoflagellate cyst *Senegalinium iterlaaense* may indicate correlation with NP3 (Fig. 5). Negative evidence such as the absence of younger species (e.g. *Chiasmolithus bidens* , *Neochiastozygus perfectus* and *N. saepes* which are recorded from higher stratigraphic intervals), can be used tentatively to suggest this section is older than NP4.

Characteristic species. The interval described as NP3? is devoid of useful marker species. Only specimens of *Lanternithus duocavus*, *Markalius inversus*, *Micula decussata*, *Thoracosphaera operculata* and *Thoracosphaera* spp. were present.

Comments. The low abundance and diversity assemblages in this interval make it almost impossible to date using nannoplankton alone. The dinoflagellate cyst *Senegalinium iterlaaense* has been described from the Hvalløse borehole in Denmark (Nøhr-Hansen & Heilmann-Clausen 2000) and was correlated with Zone NP3 (mid Danian). The presence of this species in the GANK#1 well, and Annertuneq and Kangilia sections suggests a similar correlation.

NP4

The presence of several late Danian marker species at this level allows for a speculative subdivision of NP4.

Lower NP4

Age. Late Danian, Early Paleocene.

Correlation. The interval correlates with Zone D9 (Perch-Nielsen 1979), Zone 7 (Thomsen 1995) and NNTp4D–E (Varol 1998).

Definition. The base of Zone NP4 (corresponding with the base of D9) is characterized by the first occurrence of *Neochiastozygus saepes* (Fig. 5). The middle part of NP4 (corresponding with the base of the overlying Zone D10) is indicated by the first occurrence of *Chiasmolithus* cf. *bidens.*

Characteristic species. The assemblage is characterized by *Cruciplacolithus asymmetricus*, *Lanternithus duocavus*, *Markalius inversus*, *Neochiastozygus modestus*, *N. saepes*, *Prinsius martinii* and *Thoracosphaera operculata* (all present in the Kangilia section).

Comments. The first occurrence of the dinoflagellate cyst *Palaeocystodinium bulliforme* was recorded just above the first occurrence of *Neochiastozygus saepes* in the Kangilia section. The first occurrence of *P. bulliforme* (previously recorded as *Palaeocystodinium australinum*) in the Hvalløse borehole, Denmark (Thomsen & Heilmann-Clausen 1985) was correlated with the lower part of Zone NP4.

Middle NP4

Age. Late Danian, Early Paleocene.

Correlation. The interval correlates with Zone D10 (Perch-Nielsen 1979), Zone 8 (Thomsen 1995) and NNTp4E–NNTp5A (Varol 1998).

Definition. The middle part of NP4 (corresponding with the base of the overlying Zone D10) is indicated by the first occurrence of *Chiasmolithus* cf. *bidens* and the upper part of NP4 (corresponding with the base of the overlying Zone S1 of Perch-Nielsen 1979) is indicated by the first occurrence of *Neochiastozygus perfectus* (Fig. 5).

Characteristic species. An assemblage comprising *Chiasmolithus* cf. *bidens*, *Neochiastozygus modestus*, *N. saepes*, and *Lanternithus duocavus* (all present in the Kangilia section) characterizes this interval. Reworked and survivor species from the Late Cretaceous continue to occur.

Comments. Chiasmolithus bidens sensu stricto is characterized by a central cross with two straight and two curved bars and 'teeth-like' projections into the central area, and according to van Heck & Prins (1987), does not occur in the Danian of the

North Sea. They erected a new species; *Chiasmolithus edentulus* to accommodate those specimens lacking the central projections. The first occurrence of *Chiasmolithus edentulus* marks the base of the *Chiasmolithus inconspicuus* Zone (van Heck & Prins 1987) and this equates to the base of Zone D10 (Perch-Nielsen 1979) and the first occurrence of *Chiasmolithus bidens*.

The poor preservation of the material from West Greenland prevented precise identification of the specimens in the Kangilia section, hence their referral to *Chiasmolithus* cf. *bidens*.

Upper NP4 (–NP5?)

Age. Late Danian–?early Selandian, Early–?middle Paleocene.

Correlation. The interval correlates with zones S1–S2 (Perch-Nielsen 1979), Zone 9 (Thomsen 1995) and NNTp5b–?NNTp10 (Varol 1998).

Definition. The base of this interval is characterized by the first occurrence of *Neochistozygus perfectus*. The sedimentary succession is succeeded abruptly by volcanics and the top of the interval is thus not seen (Fig. 5).

Characteristic species. The interval is characterized by specimens of *Neochiastozygus perfectus* (GANE#1, GANW#1), *Chiasmolithus* cf. *bidens* (Kangilia), *Neochiastozygus* cf. *modestus* (GANK#1) and *Prinsius dimorphosus* (GANE#1), along with the continued presence of reworked and survivor species from the Late Cretaceous.

Comments. In Europe, *Neochiastozygus perfectus* first appears in the latest Danian (uppermost NP4); at the base of Zone S1 (Perch-Nielsen 1979), the base of Zone 9 (Thomsen 1994) and the base of NNTp5B (Varol 1998). Therefore a late Danian age (equivalent to upper Zone NP4) is suggested for this interval in West Greenland. However, as *Neochiastozygus perfectus* ranges up into the Selandian, a younger age, possibly of NP5, cannot be totally ruled out.

Early Paleocene depositional evolution

Prior to Early Paleocene volcanism in West Greenland, the Nuussuaq Basin underwent major rifting in the Late Maastrichtian–Early Paleocene, and at least three tectonic phases have been recognized (Figs 2 & 18; Dam *et al.* 1998*a*). Rifting was associated with substantial uplift and repeated erosion and infilling of incised subaerial valleys and submarine canyons resulting in basin-wide unconformities (Figs 2 & 18). A new lithostratigraphy based upon recognition of major unconformities is currently undertaken for the Nuussuaq Basin and a stratigraphic scheme of the Early Paleocene post-volcanic and syn-volcanic marine sediments is shown in Figures 2 & 18. Late Maastrichtian–Early Paleocene marine sediments are bounded by a major latest Maastrichtian unconformity associated with submarine canyon incision and are referred to as the Kangilia Formation (Fig. 19). This unconformity marks the first phase of Late Maastrichtian–Early Paleocene rifting. The submarine canyons are at least 105 m deep and the deposits are referred to as the Conglomerate Member

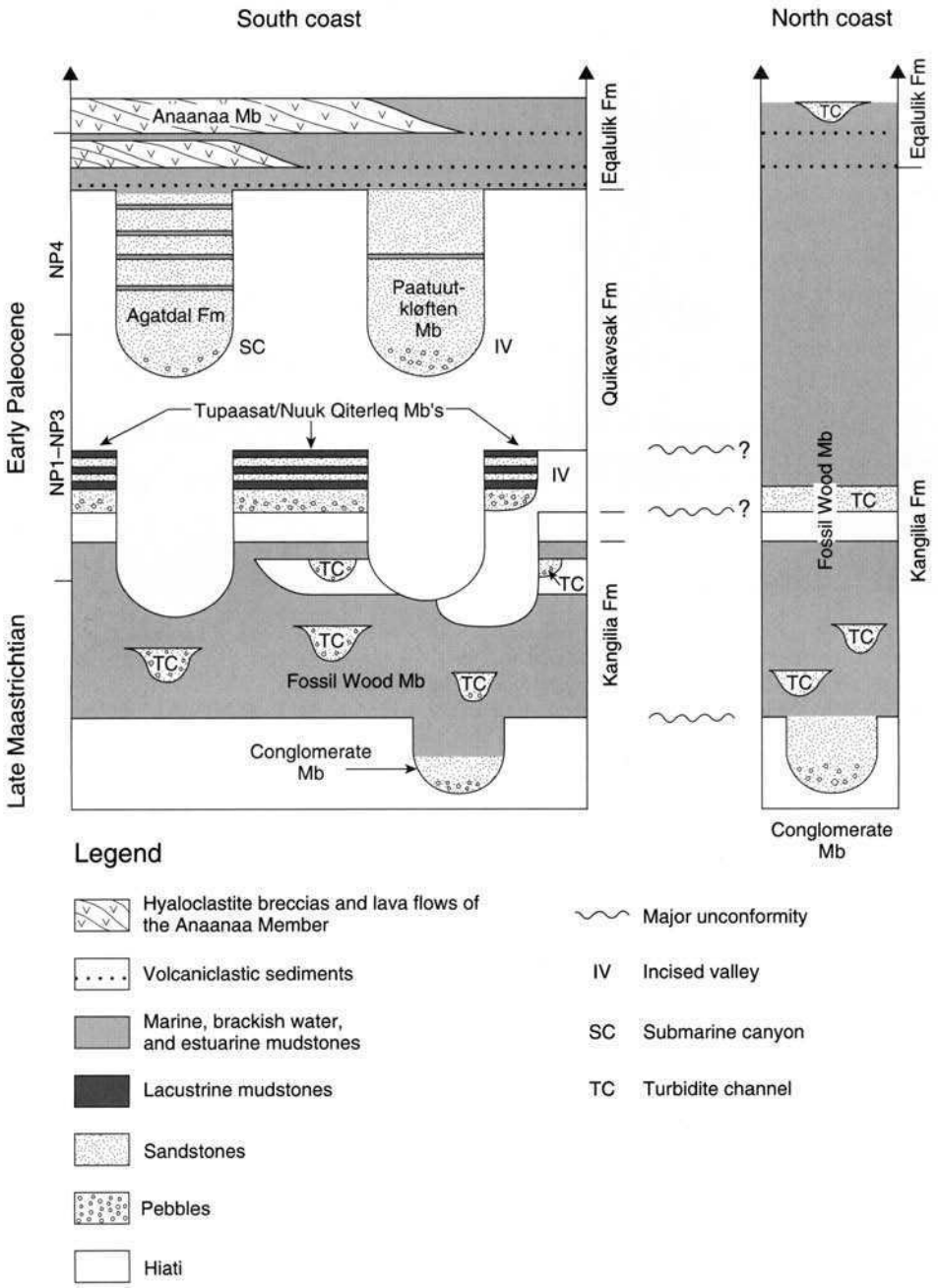

Fig. 18. Generalized stratigraphy of the Paleocene sediments and lowermost volcanics on the north and south coast of Nuussuaq. It should be emphasized that the figure is schematical, thus there are no relations between the heights of the columns and the thicknesses of lithostratigraphical units, and the event are only related to the NP zones they took place in, not to the duration of these events.

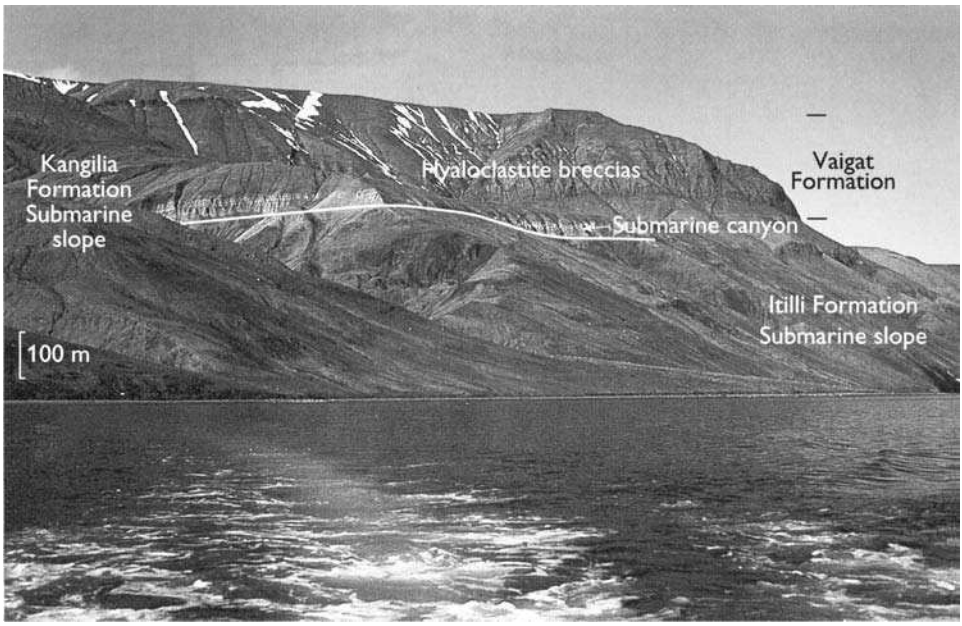

Fig. 19. Exposure of the Cretaceous–Paleogene sedimentary and volcanic succession at Annertuneq on the north coast of Nuussuaq (see Fig. 1 for location). Below the conglomerate are upper Campanian turbidite slope mudstones of the Itilli Formation. They are unconformably succeeded by Maastrichtian–Paleocene submarine canyon conglomerates and turbidite slope mudstones of the Kangilia Formation. The succession is topped by the Eqalulik Formation succeeded by hyaloclastites of the Vaigat Formation. The mountain is about 1.3 km high.

and consist of conglomerates, sandstones and mudstones deposited from turbidite currents and debris flows.

Following a new episode of Early Paleocene faulting, two valley systems were incised along the south coast of Nuussuaq (Figs 18 & 20; Dam & Sønderholm 1998; Dam *et al.* 1998*a*). The deposits of these valleys are referred to as the Tupaasat/Nuuk Qiterleq and Paatuutkløften Members of the Quikavsak Formation respectively (Fig. 18). The valleys cut deeply into Early Paleocene NW–SE trending normal faults, clearly showing the structural control of the valley relief and trend of the valleys. In western Nuussuaq the Paleocene incised valleys pass into a submarine canyon system traversing a fault-controlled slope along the Kuugannguaq–Qunnilik Fault. This canyon system was drilled in the GRO#3 well and the uppermost part of the canyon system was cored in the GANE#1 well. These, and contemporaneous canyon deposits in central Nuussuaq are referred to as the Agatdal Formation (Figs 4 & 18).

The Tupaasat Member valley is up to 120 m deep and the fill consists of pebbly sandstones and conglomerates deposited from high-density turbidity currents (Fig. 18). Deposition took place during a single drainage event associated with catastrophic drainage of large dammed water masses. Catastrophic deposition was followed by a rapid decrease in flow discharge and the establishment of a lacustrine environment within the valley. The lacustrine deposits, consisting of heterolithic sediments are referred to as the Nuuk Qiterleq Member, and were deposited by repeat progradation of shoreface or bayhead deltas into a lacustrine environment.

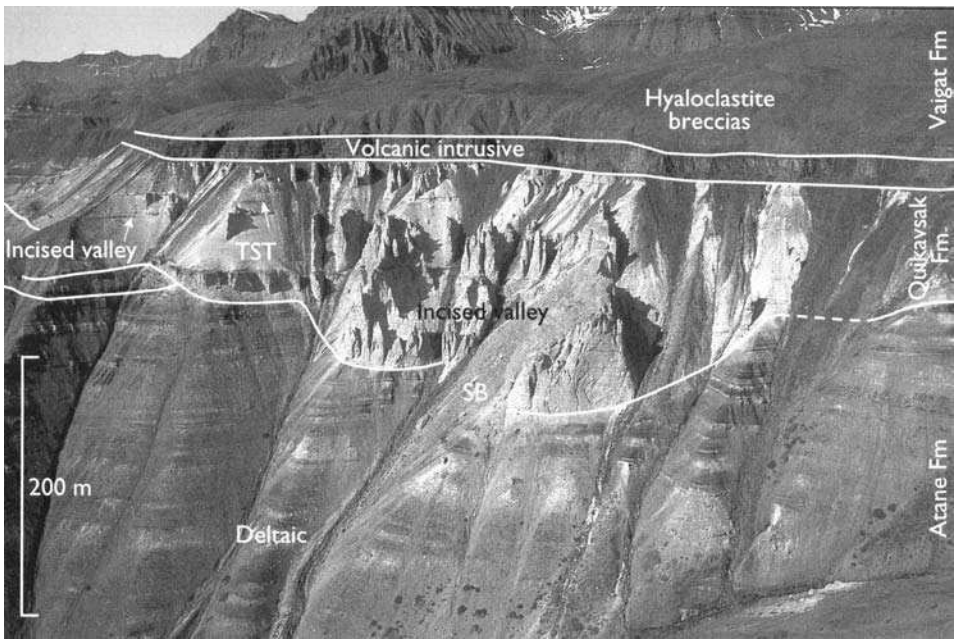

Fig. 20. The Quikavsak Formation incised valleys underlying the volcanics of the Vaigat Formation. The valley is 190 m deep and is incised into middle Cretaceous deltaic deposits of the Atane Formation. From Ippigaarsukkløften (see Fig. 1 for location).

The Paatuutkløften Member valley is up to 190 m deep and cuts into the Tupaasat valley which in many places is completely or almost completely eroded and probably marks renewed tectonic activity and uplift of the basin (Fig. 20). The fill consists of a homogeneous succession of fluvial and tidal-estuarine sandstones, arranged in an overall fining-upward succession (Dam & Sønderholm 1998). The valley fill is succeeded by offshore mudstones.

The Agatdal/Eqalulik Formation submarine canyon was drilled in the GRO#3 well and cored in the GANE#1 well (Fig. 4). The fill is up to 395 m thick (including Early Paleocene volcanic intrusives) and is arranged in an overall fining-upward succession. The lowermost 250 m of the fill is dominated by coarse-grained sandstones. The uppermost part of the coarse-grained sandstones was drilled in the GANE#1 well and is dominated by graded beds deposited from high-density turbidity currents. The coarse-grained sandstones are succeeded by heterolithic deposits. Most of these sediments are arranged in small fining-upward successions deposited from small turbidite channels situated within the submarine canyon. At the top of the canyon–fill, reworked volcaniclastic sandstones and pebbles are present. The boundary between the Agatdal and Eqalulik Formations and the Kangilia Formation and the Eqalulik Formation is placed at the first appearance of volcaniclastic material (Fig. 18). The introduction of volcaniclastic material is generally associated with the occurrence of debris flow and slump deposits indicating unstable slope conditions during the initial phase of volcanism in the area.

The Paatuutkløften Member valley fill testifies to a very rapid rise in relative sea-level and was followed by deposition of a regional cover of offshore mudstones,

before eruption of picritic hyaloclastite breccias. The breccias form giant-scale Gilbert-type delta structures with foresets up to 700 m high (e.g. Pedersen 1993), indicating continued subsidence after valley filling, before prograding hyaloclastite fans reached the area (Dam *et al.* 1998*a*).

Biostratigraphic dating of geological events preluding volcanism in central West Greenland

The present study provides a biostratigraphic constraint on the initial Early Paleocene volcanism onshore West Greenland and some of the geological events preluding volcanism. The first indication of Late Maastrichtian–Early Paleocene tectonic activity in the Nuussuaq Basin is provided by incision of the Conglomerate Member submarine canyons that are exposed on both the north and south coasts of Nuussuaq and have been cored in the GANT#1 well (Figs 18 & 19). On both the north and south coasts, the biostratigraphic dating of the mudstones above the conglomerate suggest a Late Maastrichtian age (McIntyre 1993; Nøhr-Hansen 1996). In the GANT#1 well the Maastrichtian–Tertiary boundary is placed in the uppermost part of the canyon fill (Nøhr-Hansen 1997*a*), suggesting that the unconformity has a latest Maastrichtian age.

Renewed tectonic activity, uplift and valley and submarine canyon incision occurred in the Early Paleocene. The best exposures of this event are present on the south coast of Nuussuaq, but dating of the mudstones underlying the incised valley sandstones is based upon spores and pollen and suggest an undifferentiated Early Paleocene age (McIntyre 1993). On the basis of the fossil flora, the incised valleys on the south coast of Nuussuaq can be correlated with submarine canyons in Agatdalen in central Nuussuaq (Koch 1963). The nannoplankton assemblage found in the submarine canyon fill was suggested as belonging to Zone NP3 (Perch-Nielsen 1973), however, this assemblage could be younger than NP3 due to the presence of *Neochiastus modestus*. The first occurrences of the dinoflagellate cyst species *P. bulliforme* and *C. striatum* in the lower part of the Agatdal Formation submarine canyon in the GRO#3 well indicate a early to middle NP4 age of the fill, suggesting that the Early Paleocene tectonic events took place during NP1–NP3. These tectonic events are not well recorded on the north coast of Nuussuaq (Fig. 18), but could be associated with some of the sandstones present just above the K/T boundary in the Kangilia section. However, the Kangilia section is poorly exposed above the basal conglomerate prohibiting detailed sedimentological investigations.

Valley and submarine canyon incision was followed by very rapid subsidence preceding initial volcanism in the area (Fig. 18). This event is well-constrained to the *Palaeocystodinium bulliforme* dinoflagellate cyst zone, suggesting a early to middle NP4 age. Subsidence may, however, have begun earlier.

Initial volcanism onshore central West Greenland began in the south-western part of Nuussuaq and is represented by hyaloclastite breccias of the Anaanaa Member. $^{40}Ar/^{39}Ar$ dating shows that volcanism commenced in West Greenland between 60.9 and 61.3 Ma (Storey *et al.* 1998). The basalts of the Vaigat Formation, the lowermost of the two volcanic formations, were extruded during only two polarity zones. $^{40}Ar/^{39}Ar$ dating indicates that the lower normal polarity zone, including hyaloclastites of the Anaana Member, is C27n (Riisager & Abrahamsen 1999).

The volcaniclastic sandstones and pebbles of the Eqalulik Formation in the GRO#3, GANE#1 and GANK#1 wells and at the top of the Kangilia section and Danienrygge probably represent the bottomsets of the hyaloclastite breccia fans or reworked tuffaceous sediments. The first occurrence of volcaniclastic sandstone in the GANE#1 well and in the Kangilia and Danienrygge sections at the base of the Eqalulik Formation is broadly concurrent with the base of the *Alisocysta margarita* Zone (Fig. 4). This zone continues into sediments interbedded with the hyaloclastite foresets in the GANW#1 well and possibly in the upper part of the GANE#1 well (Fig. 4), suggesting a late NP4 age for the initial Early Paleocene volcanism onshore central West Greenland. This is in agreement with the magnetostratigraphic and $^{40}Ar/^{39}Ar$ data of Riisager & Abrahamsen (1999) and Storey *et al.* (1998), respectively.

Discussion of the Danian/Selandian boundary

Published stratigraphic schemes correlating absolute time scales, magneto-chronostratigraphy, standard chronostratigraphy and biozones show large discrepancies across the Danian–Selandian boundary (Fig. 21). Berggren *et al.* (1995, fig. 1) placed the top of the Danian at 61 Ma, almost corresponding to the upper boundary of C27n (Fig. 21; spanning 60.92–61.27 Ma, according to Cande & Kent 1992). Berggren *et al.* (1995, figs 1 & 7) defined the Danian/Selandian boundary as the boundary between the planktonic foraminiferal zones P2 and P3a, and correlated the boundary with the middle part of the NP4 Zone of Martini (1971). According to Thomsen (1994), the base of the Selandian in Denmark occurs within the local nannoplankton Zone S2, correlating wih the upper part of NP4 or lower NP5. However, there is a continued debate upon where exactly between NP4 and NP5 the boundary should be placed in high latitudes as the nannofossils which mark the base of NP5 are rare or absent in these areas (Perch-Nielsen 1985; Thomsen 1994,1995). Ali *et al.* (1994) interpreted preliminary magnetostratigraphic investigations of the upper Danian in the Hvalløse borehole in Denmark, and correlated the upper part of NP3 to lower NP4 with normal polarity, probably representing C27n, therefore suggesting that the S2 Zone of Thomsen 1994 be placed in the overlying C26r. In their study of the Zumaya section in Spain as a possible global stratotype section for the Selandian and Thanetian stages, Schmitz *et al.* (1998) suggested that the Danian/Selandian boundary be placed at the base of NP5 coinciding with the first occurrence of the nannoplankton species *Fasciculithus tympaniformis* (rarely found in high latitudes), approximately 10 m above the boundary between the planktonic foraminiferal zones P2 and P3a. However the first occurrence of the nannoplankton species *Neochiastozygus perfectus* occurs 75cm below the P2–P3a boundary, and in NP4. At this locality it was also suggested that C27n correlates with lower NP4, and the upper part of NP4 and lower part of NP5 be represented by C26r (Fig. 21).

The study from Nuusssuaq, West Greenland differs markedly from the aforementioned studies, by correlating absolute dating, magnetostratigraphic measurements, dinoflagellate cyst and nannoplankton zonations from relatively closely situated sections in a restricted area. It is now possible to correlate the uppermost pre-volcanic marine mudstone succession; dated as latest Danian (late NP4) with the overlying and partly time equivalent volcanics of C27n. These hyaloclastites underlie volcanics of

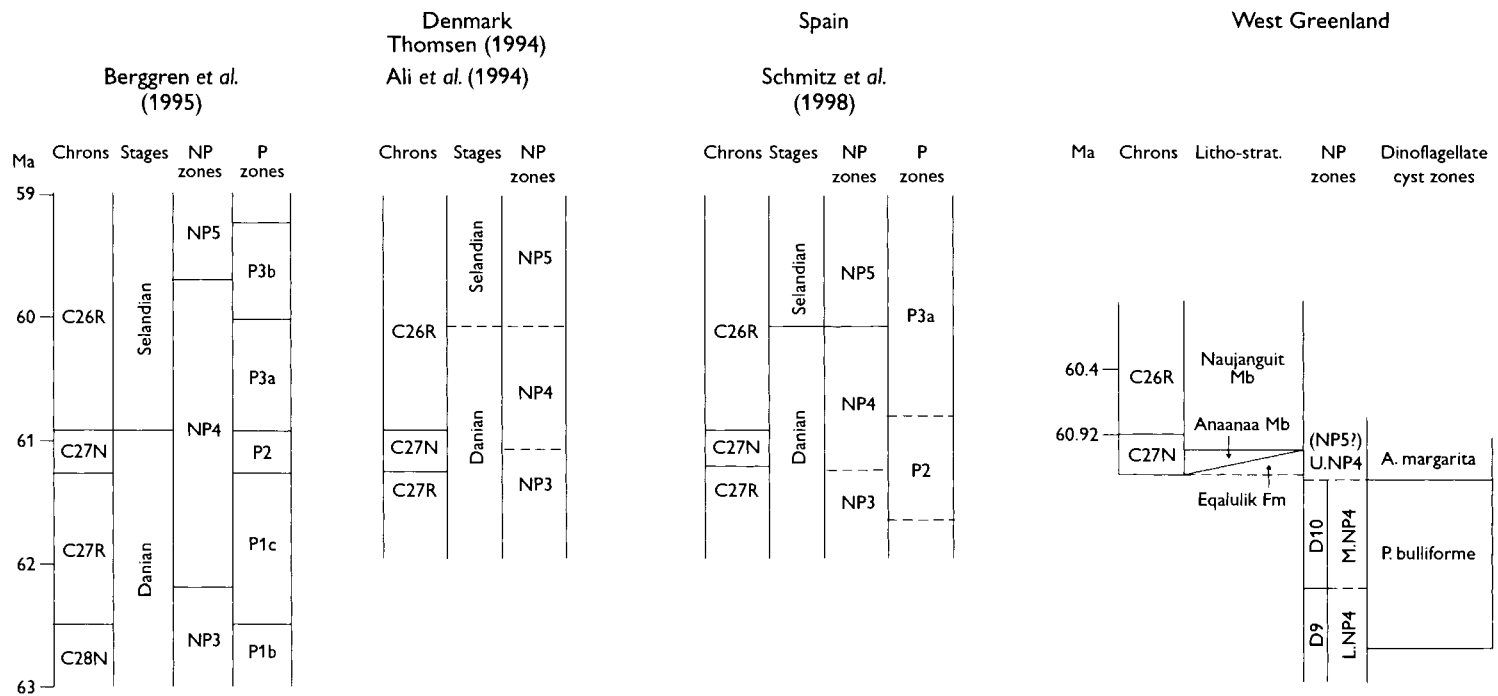

Fig. 21. Published schemes correlating absolute time scale, magneto-chronostratigraphy, standard chronostratigraphy and biochrono zones across the Danian–Selandian boundary, compared with the correlation established in the present study.

chron C26r (Riisager & Abrahamsen 1999), which are dated as 60.9 and 61.3 Ma by $^{40}Ar/^{39}Ar$ measurements (Storey *et al.* 1998). The data from Nuussuaq (Fig. 21) favours the correlating between absolute time scale and magneto-chronostratigraphy arguments of Berggren *et al.* (1995), whereas our correlation of chronostratigraphy and biozones favours the discussions of Thomsen (1994), Heilmann-Clausen (1994) and Schmitz *et al.* (1998).

Conclusions

On the basis of an integration of dinoflagellate cyst and nannofossil data, it has been possible to divide the Lower Paleocene succession on Nuussuaq into five dinoflagellate cyst zones and correlate them with Martini's (1971) global nannoplankton zones and to date the initiation of volcanism onshore West Greenland. The first occurrence of hyaloclastites and reworked volcaniclastic sandstones is broadly concurrent with the base of the *Alisocysta margarita* Zone indicating that volcanism in West Greenland began during upper NP4. This agrees with published $^{40}Ar/^{39}Ar$ and magnetostratigraphic dating of the volcanic rocks. In light of this new biostratigraphic data, it is possible for the first time to provide an agreement between palynostratigraphic, nannostratigraphic and radiometric dating in the North Atlantic Igneous Province. Moreover, it is possible to date the events associated with rifting, tranquil uplift and valley and submarine canyon incision of the basin that occurred immediately prior to the volcanism in West Greenland. Three pre-volcanic tectonic phases have been recognized, all associated with valley and submarine canyon incision. The first phase took place in the Late Maastrichtian and was by followed by two phases in the Early Paleocene. The two Early Paleocene events took place during NP1–NP3, and were followed by rapid subsidence preceding volcanism in NP4. Finally, the study shows that there are large discrepancies in correlating absolute time scales, magneto-chronstratigraphy, standard chronostratigraphy and biochrono zones across the Danian–Selandian boundary.

We thank the Carlsberg Foundation for financial support. Thanks to Asger Ken Pedersen and Lotte Melchior Larsen for providing us with samples and discussion. Thanks also to Claus Heilmann-Clausen, Stefan Piasecki, colleagues in the West Greenland Group and the two referees J. Riding and A. Whitham for discussions and constructive criticism of the manuscript. Y. Desezar, B. Hammerstrøm and K. Villadsen prepared the samples and J. Halskov produced the figures. The paper is published with permission of the Geological Survey of Denmark and Greenland.

References

ALI, J. R. & JOLLEY, D. W. 1996. Chronostratigraphic framework for the Thanetian and lower Ypresian deposits of southern England. *In*: KNOX, R. W. O'B., CORFIELD, R. M. & DUNAY, R. E. (eds) *Correlation of the Early Paleogene in Northwest Europe*. Geological Society, London, Special Publications, **101**, 129–144.

ALI, J. R., HEILMANN-CLAUSEN, C., THOMSEN, E. & ABRAHAMSEN, N. 1994. Magnetostratigraphy of the type Selandian: preliminary results. *Geologiska Föreningens i Stockholm Förhandlingar*, **116**, 43.

BELL, B. R. & JOLLEY, D. W. 1997. Application of palynological data to the chronology of the Palaeogene lava fields of the British Province: Implications for magmatic stratigraphy. *Journal of the Geological Society, London*, **154**, 701–708.

BERGGREN, W. A., KENT, D. V., SWISHER, III, C. C. & AUBRY, M.-P. 1995. A revised Cenozoic geochronology and chronostratigraphy. *In*: BERGGREN, W. A., KENT, D. V., AUBRY, M.-P. & HARDENBOL, J. (eds) *Geochronology, time scales and global stratigraphic correlation*. Society of Economic Paleontologists and Mineralogists, Special Publications, **54**, 129–212.

BRINKHUIS, H., & SCHIØLER, P. 1996. Palynology of the Geulhemmerberg Cretaceous/Tertiary boundary section (Limburg, SE Netherlands). *Geologie en Mijnbouw*, **75**, 193–213.

BURDEN, E. T. & LANGILLE, A. B. 1990. Stratigraphy and sedimentology of Cretaceous and Paleocene strata in half-grabens on the southeast coast of Baffin Island, Northwest Territories. *Canadian Petroleum Geology Bulletin*, **38**, 185–195.

BURDEN, E. T. & LANGILLE, A. B. 1991. Palynology of Cretaceous and Tertiary strata, northeast Baffin Island, Northwest Territories, Canada: Implications for the history of rifting in Baffin Bay. *Palynology*, **15**, 91–114.

CANDE, S. C. & KENT, D. V. 1992. A new geomagnetic polarity time scale for the Late Cretaceous and Cenozoic. *Journal of Geophysical Research*, **97**, 13.917–13.951.

CHALMERS, J. A., PULVERTAFT, T. C. R., CHRISTIANSEN, F. G., LARSEN, H. C., LAURSEN, K. H. & OTTESEN, T. G. 1993. The southern West Greenland continental margin: rifting history, basin development and petroleum potential. *In*: PARKER, J. R. (ed.) *Petroleum Geology of Northwest Europe: Proceedings of the 4th Conference*. The Geological Society, London, 915–931.

CHALMERS, J. A., PULVERTAFT, T. C. R., MARCUSSEN, C. & PEDERSEN, A. K. 1999. New insight into the structure of the Nuussuaq Basin, central West Greenland. *Marine and Petroleum Geology*, **16** 197–224.

CHRISTIANSEN, F. G., MARCUSSEN, C. & CHALMERS, J. A. 1995. Geophysical and petroleum geological activities in the Nuussuaq–Svartenhuk Halvø area 1994: promising results for onshore exploration potential. *Rapport Gronlands Geologiske Undersogelse*, **165**, 30–39.

CHRISTIANSEN, F. G., DAM, G., LARSEN, L. M., NØHR-HANSEN, H., PEDERSEN, A. K., BOSERUP, J., BOJESEN-KOEFOED, J., LAIER, T. & PULVERTAFT, T. C. R. 1997. Stratigraphy, sedimentology and geochemistry of cores and other samples from the GANW#1 well, Nuussuaq, West Greenland. *Danmarks og Gronlands Geologiske Undersogelse Rapport*, **1997/36**.

CLARKE, D. B. & PEDERSEN, A. K. 1976. Tertiary volcanic province of West Greenland. *In*: ESCHER, A. & WATT, W. S. (eds) *Geology of Greenland*. The Geological Survey of Greenland, Copenhagen, 365–387.

CROXTON, C. A. 1978. *Report of field work undertaken between 69° and 72°N, central West Greenland in 1975 with preliminary palynological results*. Grønlands Geologiske Undersøgelse Open File Report, **78-1**, 88.

DAM, G. 1997. *Sedimentology of the Umiivik-1 core, Svartenhuk Halvo, West Greenland*. Danmarks og Grønlands Geologiske Undersøgelse Rapport, **1997/136**.

DAM, G. & SØNDERHOLM, M. 1994. Lowstand slope channels of the Itilli succession (Maastrichtian–Lower Paleocene), Nuussuaq, West Greenland. *Sedimentary Geology*, **94**, 47–71.

DAM, G. & SØNDERHOLM, M. 1998. Sedimentological evolution of a fault-controlled Early Paleocene incised-valley system, Nuussuaq Basin, West Greenland. *In*: SHANLEY, K. W. & MCCABE, P. J. (eds) *Relative role of eustasy, climate, and tectonism in continental rocks*. Society of Economic Paleontologists and Mineralogists, Special Publication, **59**, 109–121.

DAM, G., LARSEN, M. & SØNDERHOLM, M. 1998*a*. Sedimentary response to mantle plumes: Implications from Paleocene onshore successions, West and East Greenland. *Geology*, **26**(3), 207–210.

DAM, G., NØHR-HANSEN, H., CHRISTIANSEN, F. G., BOJESEN-KOFOED, J. A. & LAIER, T. 1998*b*. The oldest marine Cretaceous sediments in West Greenland (Umiivik-1 borehole) – record of the Cenomanian–Turonian Anoxic Event? *Geology of Greenland Survey Bulletin*, **180**, 128–137.

DAM, G., NØHR-HANSEN, H., PEDERSEN, G. K. & SØNDERHOLM, M. 2000. Sedimentary and structural evidence of a new early Campanian rift phase in Central Nuussuaq, West Greenland. *Cretaceous Research*, **21**, 127–154.

DRUGG, W. S. 1967. Palynology of the upper Moreno Formation (Late Cretaceous–Paleocene) Escarpado Canyon, California: *Palaeontographica, Abteilung* **B**, **120**, 1–71.

HANSEN, J. M. 1977. Dinoflagellate stratigraphy and echinoid distribution in Upper Maastrichtian and Danian deposits from Denmark. *Bulletin of the Geological Society of Denmark*, **26**, 1–26.

HANSEN, J. M. 1980. *Stratigraphy and structure of the Paleocene in central West Green land and Denmark*. Unpublished. lic. scient. thesis, Geological Institute, University of Copenhagen.

HANSEN, J. M. & GUDMUNDSSON, L. 1978. A method for separation of acid insoluble microfossils from organic debris. *Micropalaeontology*, **25**, 113–117.

HARDENBOL, J., THIERRY, J., FARLEY, M. B., JACQUIN, T., GRACIANSKY, P.-C. DE & VAIL, P. R. 1998. Mesozoic and Cenozoic sequence chronostratigraphic framework of European Basins. *In*: HARDENBOL, J., THIERRY, J., FARLEY, M. B., JACQUIN, T., GRACIANSKY, P.-C. DE & VAIL, P. R. (eds) *Mesozoic and Cenozoic sequence chronostratigraphic framework of European Basins*. Society of Economic Paleontologists and Mineralogists, Special Publications, **60**, 1–13.

HECK, S. E. VAN & PRINS, B. 1987. A refined nannoplankton zonation for the Danian of the Central North Sea. *Abhandlungen der Geologischen Bundesanstalt*, **39**, 285–303.

HEILMANN-CLAUSEN, C. 1985. Dinoflagellate stratigraphy of the uppermost Danian to Ypresian in the Viborg 1 borehole, central Jylland, Denmark. *Danmarks Geologiske Undersøgelse Serie A*, **7**, 69.

HEILMANN-CLAUSEN, C. 1988: The regional distribution of dinoflagellates; correlation of the interregional zonations with the local zones and with the regional lithostratigraphy. The Danish Sub-basin, Paleogene Dinoflagellates. *In*: VINKEN, R. (ed.) *The Northwest European Tertiary Basin. Results of the International Geological Correlation Programme, Project No. 124*. Geologisches Jahrbuch, Reihe A, **100**, 339–343.

HEILMANN-CLAUSEN, C. 1994. Review of Paleocene dinoflagellates from the North Sea region. *Geologiska Föreningens i Stockholm Förhandlingar*, **116**, 51–53.

HENDERSON, G., ROSENKRANTZ, A. & SCHIENER, E. J. 1976. Cretaceous–Tertiary sedimentary rocks of West Greenland. *In*: ESCHER, A. Watt, W. S. (eds) *Geology of Greenland*. Geological Survey of Greenland, Copenhagen, 341–362.

HJORTKJÆR, B. F. & JOLLEY, D. W. 1999. A spore and pollen assemblage from a late Paleocene sedimentary section at Kulhøje, East Greenland. Implications for the break-up history of the North Atlantic. p. 5. *Programme and Abstracts from the meeting on The North Atlantic Igneous Province: Magmatic Controls on sedimentation*. Geological Society of London, April 20–21, 1999.

IOANNIDES, N. S. 1986. Dinoflagellate cysts from Upper Cretaceous–Lower Tertiary sections, Bylot and Devon Islands, Arctic Archipelago. *Geological Survey of Canada Bulletin*, **371** 1–99.

JOHANNESSEN, P. & NIELSEN, L. H. 1982. Aflejringer fra flettede floder, Atane Formation, Øvre Kridt, Pingo, Øst Disko. *Dansk Geologisk Forening Årsskrift* 1981, 13–27.

JOLLEY, D. W. 1997. Palaeosurface palynofloras of the Skye Lava field, and the age of the British Tertiary Volcanic Province. *In*: WIDDOWSON, M. (ed.) *Palaeosurfaces; Recognition, Reconstruction and Interpretation*. Geological Society, London, Special Publications, **120**, 67–94.

JOLLEY, D. W. 1998. Palynostratigraphy and depositional history of the Palaeocene Ormesby/Thanet depositional sequence set in southeastern England and its correlation with continental West Europe and the Lista Formation, North Sea. *Review of Palaobotany and Palynology*, **99**, 265–315.

JÜRGENSEN, T. & MIKKELSEN, N. 1974. Coccoliths from volcanic sediments (Danian) in Nûgssuaq, West Greenland. *Geological Society of Denmark Bulletin*, **23**, 225–230.

KOCH, B. E. 1963. Fossil plants from the lower Paleocene of the Agatdalen (Angmârtussut) area, central Nûgssuaq peninsula, northwest Greenland. *Grønlands Geologiske Undersøgelse Bulletin* **38**, 120 (also *Meddelelser om Grønland*, **172**).

KRISTENSEN, L. & DAM, G. 1997. Lithological and petrophysical evaluation of the GRO#3 well, Nuussuaq, West Greenland. *Danmarks og Grønlands Geologiske Undersøgelse Rapport*, **1997/136**, 30.

LANSTORP, J. 1999. En palynologisk undersøgelse af Kretassiske og Paleocæne sedimenter fra det sydøstlige Nuussuaq, Vestgrønland. *Geologisk Tidsskrift*, **1999/1**, 13–20.

LARSEN, H. C. & SAUNDERS, A. D. 1998. Tectonism and volcanism at the SE Greenland rifted margin: a record of plume impact and later continental rupture. *In*: SAUNDERS, A. D., LARSEN, H. C. & WIESE, S. (eds) *Proceedings of the Ocean Drilling Program, Scientific Results*. Ocean Drilling Program, College Station, Texas, **152**, 503–536.

LARSEN, J. G. & PULVERTAFT, T. C. R. 2000. The structure of the Cretaceous–Palaeogene sedimentary-volcanic area of Svartenhuk Halvø, central West Greenland. *Geology of Greenland Survey Bulletin*, **188**, 40.

MCINTYRE, D. J. 1993. Palynology of twenty-eight samples from Upper Cretaceous and Paleocene strata at Atâtâ kûa, Nugssuaq, West Greenland. (Map Qutdligssat 70 V.1 Syd). *Geological Survey of Canada*, Paleontological Report, **2-DJM-1993**, 13.

MARTINI, E. 1971. Standard Tertiary and Quaternary calcareous nannoplankton zonation. *Proceedings of the II Planktonic Conference, Roma 1970*, **2**, 739–785.

MIDTGAARD, H. 1996*a*. Inner-shelf to lower-shoreface hummocky sandstone bodies with evidence for geostrophic influenced combined flow, Lower Cretaceous, West Greenland. *Journal of Sedimentary Research*, **66**, 343–353.

MIDTGAARD, H. 1996*b*. *Sedimentology and sequence stratigraphy of coalbearing synrift sediments on Nuussuaq and Upernivik Ø (U. Albian–L. Cenomanian), Central West Greenland*. 175. Unpublished PhD thesis, University of Copenhagen, Copenhagen.

MOSHKOVITZ, S. & HABIB, D. 1993. Calcareous nannofossil and dinoflagellate stratigraphy of the Cretaceous–Tertiary boundary, Alabama and Georgia. *Micropaleontology*, **39**, 167–191.

MUDGE, D. C. & BUJAK, J. P. 1996*a*. Paleocene biostratigraphy and sequence stratigraphy of the UK central North Sea. *Marine and Petroleum Geology*, **13**, 295–312.

MUDGE, D. C. & BUJAK, J. P. 1996*b*. An integrated stratigraphy for the Paleocene and Eocene of the North Sea. *In*: KNOX, R. W. O'B., CORFIELD, R. M. & DUNAY, R. E. (eds) *Correlation of the Early Paleogene in Northwest Europe*. Geological Society, London, Special Publications, **101**, 91–113.

NØHR-HANSEN, H. 1992. Cretaceous marine and brackish(?) dinoflagellate cysts, West Greenland. *8th International Palynological Congress*, Aix-en-Provence, September 6–12, 1992, Program and Abstracts, 107.

NØHR-HANSEN, H. 1996. Upper Cretaceous dinoflagellate cyst stratigraphy onshore West Greenland. *Bulletin Grønlands Geologiske Undersogelse*, **170**, 104.

NØHR-HANSEN, H. 1997*a*. *Palynology of the boreholes GANE#1, GANK#1 and GANT#1, Nuussuaq, West Greenland*. Danmarks og Grønlands Geologiske Undersøgelse Rapport **1997/89**, 22.

NØHR-HANSEN, H. 1997*b*. *Palynology of the GRO#3 well, Nuussuaq, West Greenland*. Danmarks og Grønlands Geologiske Undersøgelse Rapport **1997/151**, 19.

NØHR-HANSEN, H. & DAM, G. 1997. Palynology and sedimentology across a new marine Cretaceous–Tertiary boundary section on Nuussuaq, West Greenland. *Geology*, **25**, 851–854.

NØHR-HANSEN, H & DAM, G. 1999. Emendation of *Trithyrodinium evittii* Drugg 1967 to include the junior synonym *Trithyrodinium fragile* Davey 1969 – The stratigraphic and palaeoenvironmental importance of the dinoflagellate cyst species, previous artificial separated by different processing techniques. *Grana*, **38**, 125–133.

NØHR-HANSEN, H. & HEILMANN-CLAUSEN, C. 2000. *Cerodinium kangiliense* sp. nov. and *Senegalinium iterlaaense* sp. nov. – Two new, stratigraphic important Paleocene species from West Greenland and Denmark. *Neues Jahrbuch für Paläontologie. Abhandlungen*, **219**, 153–170.

NØHR-HANSEN, H. & SHELDON, E. 2000. Palyno- and nannostratigraphic dating of the marine Paleocene succession in the Nuussuaq Basin, West Greenland. *Geologiska Föreningens i Stockholm Förhandlingar*, **122**, 115–116.

OLSEN, T. 1993. Large fluvial systems: the Atane Formation, a fluvio-deltaic example from the Upper Cretaceous of central West Greenland. *In*: FIELDING, C. R. (ed.) *Current research in fluvial sedimentology*. Sedimentary Geology, **85**, 457–473.

PEDERSEN, A. K. 1993. *Geological section along the south coast of Nuussuaq, central West Greenland.* Geological Survey of Greenland, Copenhagen.

PEDERSEN, G. K. & PULVERTAFT, T. C. R. 1992. The nonmarine Cretaceous of the West Greenland Basin, onshore West Greenland. *Cretaceous Research*, **13**, 263–272.

PEDERSEN, G. K., LARSEN, L. M., PEDERSEN, A. K. & HJORTKJÆR, B. F. 1998. The syn-volcanic Naajaat lake, Paleocene of West Greenland. *Palaeogeography, Paleoclimatology, Palaeoecology*, **140**, 271–287.

PERCH-NIELSEN, K. 1973. Danian/Maastrichtian coccoliths from Nûgssuaq, West Greenland. *Bulletin of the Geological Society of Denmark*, **22**, 79–82.

PERCH-NIELSEN, K. 1979. Calcareous nannofossil zonation at the Cretaceous/Tertiary boundary in Denmark. *In*: BIRKELUND, T. & BROMLEY, R. G. (eds) *Cretaceous–Tertiary boundary events. I. Proceedings.* The Maastrichtian and Danian of Denmark, University of Copenhagen, 115–135.

PERCH-NIELSEN, K. 1985. Cenozoic calcareous nannofossils, *In*: BOLLI, H. M., SAUNDERS, J. B. & PERCH NIELSEN, K. (eds) *Plankton Stratigraphy.* Cambridge University Press, Cambridge, 427–554.

PIASECKI, S., LARSEN, L. M., PEDERSEN, A. K. & PEDERSEN, G. K. 1992. Palynostratigraphy of the Lower Tertiary volcanics and marine clastic sediments in the southern part of West Greenland Basin: implications for the timing and duration of the volcanism. *Rapport Grønlands Geologiske Undersøgelse*, **154**, 13–31.

POWELL, A. J. 1992. Dinoflagellate cysts of the Tertiary System. *In*: POWELL, A. J. (ed.) *A stratigraphic Index of Dinoflagellate Cysts.* British Micropalaeontological Society, 155–252.

POWELL, A. J., BRINKHUIS, H. & BUJAK, J. P. 1996. Upper Paleocene–Lower Eocene dinoflagellate cyst sequence biostratigraphy of southeast England. *In*: KNOX, R. W. O' B., CORFIELD, R. M. & DUNAY, R. E. (eds) *Correlation of the Early Paleogene in Northwest Europe.* Geological Society, London, Special Publication, **101**, 145–183.

RIISAGER, P. & ABRAHAMSEN, N. 1999. Magnetostratigraphy of Palaeocene basalts from the Vaigat Formation of West Greenland. *Geophysical Journal International*, **137**, 774–782.

ROLLE, F. 1985. Late Cretaceous–Tertiary sediments offshore central West Greenland: Lithostratigraphy, sedimentary evolution, and petroleum potential. *Canadian Journal of Earth Sciences*, **22**, 1001–1019.

SCHIENER, E. J. 1975. Basin study: central West Greenland onshore Cretaceous–Tertiary sediments **2**, Theme 5. IXme Congrès international de Sedimentologie, Nice 1975, 379–385.

SCHMITZ, B., MOLINA, E. & VON SALIS, K. 1998. The Zumaya section in Spain: A possible global stratotype section for the Selandian and Thanetian stages. *Newsletters on Stratigraphy*, **36**, 35–42.

SMIT, J. & BRINKHUIS, H. 1996. The Geulhemmerberg Cretaceous/Tertiary boundary section Maastrichtian type area, SE Netherlands: Summary of results and a scenario of events: *Geologie en Mijnbouw*, **75**, 283–293.

SOPER, N. J., HIGGINS, A. C., DOWNIE, C., MATTHEWS, D. W. & BROWN, P. E. 1976. Late Cretaceous–early Tertiary stratigraphy of the Kangerdlugssuaq area, east Greenland and the age of opening of the north-east Atlantic. *Journal of the Geological Society, London*, **132**, 85–104.

STANLEY, E. A. 1965. Upper Cretaceous and Paleocene plant microfossils and Paleocene dinoflagellates and hystrichosphaerids from northwestern South Dakota. *Bulletins of American Paleontology*, **49**(222), 175–284.

STOREY, M., DUNCAN, R. A., PEDERSEN, A. K., LARSEN, L. M. & LARSEN, H. C. 1998. $^{40}Ar/^{39}Ar$ geochronology of the West Greenland Tertiary volcanic province. *Earth and Planetary Science Letters*, **160**, 569–586.

STOUGE, S., HJORTKJÆR, B. F., RASMUSSEN, J. A., RONCAGLIA, L. & SHELDON, E. 2000. Micro- and nannofossil biostratigraphy across the Danian/Selandian (Paleocene) Stage boundary at Gemmas Alle', Copenhagen, Denmark. *Geologiska Föreningens i Stockholm Förhandlingar*, **122**, 161–162.

STOVER, L. E. & PARTRIDGE, A. D. 1973. Tertiary and Cretaceous spores and pollen from the Gippsland Basin, Southeastern Australia. *Proceedings of the Royal Society of Victoria*, **85**, 237–286.

STRONG, C. P., HOLLIS, C. J. & WILSON, G. J. 1995. Foraminiferal, radiolarian, and dinoflagellate biostratigraphy of Late Cretaceous to middle Eocene pelagic sediments (Muzzle Group), Mead Stream, Marlborough, New Zealand. *New Zealand Journal of Geology and Geophysics*, **38**, 171–212.

THOMSEN, E. 1994. Calcareous nannofossil stratigraphy across the Danian–Selandian boundary in Denmark. *Geologiska Föreningens i Stockholm Förhandlingar*, **116**, 65–67.

THOMSEN, E. 1995. Kalk og kridt i den danske undergrund. *In*: NIELSEN, O. B. (ed.) *Danmarks geologi fra Kridt til i dag*. Aarhus Geokompendier, Aarhus University, **1**. 31–67.

THOMSEN, E. & HEILMANN-CLAUSEN, C. 1985. The Danian–Selandian Boundary sequence at Svejstrup and remarks on the biostratigraphy of the boundary in western Denmark. *Geological Society of Denmark Bulletin*, **33**, 339–360.

VAROL, O. 1998. Palaeogene. *In*: BOWN, P. R. (ed.) *Calcareous Nannofossil Biostratigraphy*. Chapman & Hall, UK (Cambridge University Press, Cambridge), 200–224.

WILLIAMS, G. L., STOVER, L. E. & KIDSON, E. J. 1993. *Morphology and stratigraphic ranges of selected Mesozoic-Cenozoic dinoflagellate taxa in the Northern Hemisphere*. Geological Survey of Canada, Paper, **92-10**, 137.

Rates of volcanic deposition, facies changes and movements in a dynamic basin: the Nuussuaq Basin, West Greenland, around the C27n–C26r transition

ASGER K. PEDERSEN[1,3], LOTTE M. LARSEN[2,3]
PETER RIISAGER[3] & KELD S. DUEHOLM[4]

[1] *Geological Museum, Øster Voldgade 5–7, DK-1350 Copenhagen K, Denmark (e-mail: akp@savik.geomus.ku.dk)*
[2] *Geological Survey of Denmark and Greenland, Øster Voldgade 10, DK-1350 Copenhagen K, Denmark*
[3] *Danish Lithosphere Centre, Øster Voldgade 10, DK-1350 Copenhagen K, Denmark*
[4] *Informatics and Mathematical Modelling, Technical University of Denmark, Landmålervej 7, DK-2800 Lyngby, Denmark*

Abstract: The initial stages of Palaeogene volcanism in the Nuussuaq Basin in West Greenland were characterized by eruption of basaltic and picritic magmas through sediments of Cretaceous to early Paleocene age into a marine or low-lying coastal environment. Recent magnetostratigraphic work has recognized the C27n–C26r transition (estimated duration less than 10 ka and here assumed to be 5 ka) as a *c.* 170 m thick zone within a succession of thin picritic lava flows. Multi-model photogrammetry combined with chemical and lithological analysis of the volcanic rocks has allowed detailed 3D analysis of the facies variation within this narrow time window. Subaerial lavas flowed eastwards over a more than 40 km wide front. On northern Disko they covered an existing lava plateau and buried a subaerial landscape of dipping Cretaceous sandstones, while on Nuussuaq they flowed into an up to 700 m deep marine embayment and formed prograding hyaloclastite fans passing into fine-clastic mass flows. With a progradation rate of 0.5–1 m a^{-1} the palaeogeography of the basin changed considerably during the short time interval. In addition to substantial basin subsidence, the volcanic facies changes have also preserved a record of synvolcanic differential movement of extensional fault blocks.The following parameters are estimated for the volcanism within the Nuussuaq Basin during the C27n–C26r transition: Production rate *c.* 0.042 km^3 a^{-1}, productivity *c.* 1.2×10^{-3} km^3 a^{-1} km^{-1} (rift), volcanic aggradation *c.* 33 m ka^{-1}, subsidence *c.* 25 m ka^{-1}. If the volcanism evolved continuously at this high aggradation rate, all of the Vaigat Formation could have erupted in 70 ka. However, the complex geological record indicates a much longer total duration, and the volcanism must have had an intermittent character.

In central West Greenland erosion has exposed extensive continuous geological sections through volcanic rocks and sediments deposited during the early phases of the evolution of the Tertiary North Atlantic Igneous Province (NAIP). The voluminous

From: JOLLEY, D. W. & BELL, B. R. (eds) *The North Atlantic Igneous Province: Stratigraphy, Tectonic, Volcanic and Magmatic Processes*. Geological Society, London, Special Publications, **197**, 157–181. 0305-8719/02/$15.00

magmas emplaced in West Greenland were derived at least partly from the proto-icelandic mantle plume and rose into an attenuated continental crust and a thick sedimentary succession in the Nuussuaq Basin (Holm *et al.* 1993; Chalmers *et al.* 1995, 1999; Saunders *et al.* 1997). The earliest Paleocene volcanism in the Nuussuaq Basin gave rise to the volcanic rocks of the Vaigat Formation. This formation records a complicated interplay between the simultaneously developing volcanic pile and sedimentary basin (Rosenkrantz & Pulvertaft 1969; Clarke & Pedersen 1976; Henderson *et al.* 1981; Pedersen 1985*a*; Larsen *et al.* 1992; Pedersen *et al.* 1993; Chalmers *et al.* 1999).

Discovery of widespread migrated oil in vugs and veins in the volcanic rocks of the oldest part of the Vaigat Formation on Nuussuaq and Disko (Christiansen *et al.* 1994, 1999; Bojesen-Koefoed *et al.* 1999), and the fact that the volcanic rocks are underlain by at least 6 km and possibly up to 10 km of Mesozoic sediments (Christiansen *et al.* 1995; Chalmers *et al.* 1999), have led to a great interest in the pre- and syn-volcanic dynamic evolution of the basin. Recent studies have focussed on the sedimentary facies evolution immediately before the onset of volcanism (Dam & Sønderholm 1994, 1998; Dam *et al.* 1998, 2000; Nøhr-Hansen *et al.* 2002) and on the interplay between volcanism and basin evolution during the later stages of deposition of the Vaigat Formation (A. K. Pedersen *et al.* 1993, 1996; G. K. Pedersen *et al.* 1998).

While there is no doubt that the Nuussuaq Basin around the start of volcanism was in a highly dynamic state, it is difficult to derive *quantitative rates* of volcanic deposition and basin movements. This requires knowledge of very precise time slices through the succession which can only rarely be obtained. However, the discovery of a palaeomagnetic polarity transition zone, identified as the C27n–C26r transition and covering a 160–180 m thick succession of subaerial picrite lava flows from the Vaigat Formation on Nuussuaq (Riisager & Abrahamsen 1999, 2000), has provided an extremely narrow time window of only a few thousand years. This represents a time resolution many times better than obtainable by other existing methods for these lithologies.

This paper presents a three-dimensional geological analysis of parts of the volcanic succession in western Nuussuaq and northern Disko, comprising the palaeomagnetic polarity transition zone and the rocks just above and below it. The combination of quantitative chronological and lithological control has enabled us to estimate rates for volcanic progradation and aggradation and the vertical basin movements within the Nuussuaq Basin within a time window of less than 20 ka. The results indicate extremely high rates of volcanic productivity, basin movements and changes in palaeogeography and sedimentary facies during the initial stages of formation of a large igneous province within a sedimentary basin.

Duration of the C27n–C26r transition

The duration of geomagnetic polarity transitions can best be estimated from palaeomagnetic transition zones recorded in rapidly and continuously deposited sediments for which the deposition rates are determined from the polarity stratigraphy or from some other absolute dating technique. Most such studies agree well and indicate durations in the range of 1–8 ka (Merrill & McFadden 1999, and references therein). It is not clear if the variation in durations measured in

different sedimentary sections reflect differences from reversal to reversal at different geographic recording sites, or whether the variation relates to rock magnetic problems such as smoothing of the geomagnetic field variations during recording in the sediments. In contrast, palaeomagnetic recording mechanisms of lavas are better understood but the dating is more difficult. Singer & Pringle (1996) used $^{40}Ar/^{39}Ar$ dating combined with palaeomagnetic data from lava flows from different sites to estimate a maximum duration of 12 ka for the Bruhnes–Matuyama polarity reversal, whereas Mankinen *et al.* (1985) derived a 4.4 ka duration period for the Miocene transition recorded at Steens Mountain plateau lavas using the secular variation record. Recent numerical simulations of polarity reversals using the Glatzmaier–Roberts geodynamo model (Coe *et al.* 2000) corroborate the palaeomagnetic observations of 1–8 ka duration of geomagnetic reversals. In the following, a duration af 5 ka is assigned to the C27n–C26r transition.

Geological setting

The Nuussuaq Basin (Fig. 1) extends onshore from Disko in the south to Svartenhuk Halvø in the north (Henderson *et al.* 1976, 1981) and is part of a series of linked basins extending offshore along the west coast of Greenland (Chalmers *et al.* 1999). The Nuussuaq Basin was a depositional area for clastic sediments for at least 40 Ma from the mid Cretaceous to the Palaeogene.

Vaigat Formation

Volcanism started with the deposition of the Vaigat Formation. $^{40}Ar/^{39}Ar$ dating by Storey *et al.* (1998) has shown that the main phase of volcanism in West Greenland, comprising the Vaigat Formation and the overlying flood basalts of the Maligât Formation, lasted around one million years (*c.* 60.5 Ma to 59.4 Ma). The duration of the Vaigat Formation alone is relatively poorly resolved and may have been around 0.5 Ma. Palaeomagnetic work by Deutsch & Kristjansson (1974), Athavale & Sharma (1975), Hald (1977), Riisager & Abrahamsen (1999, 2000) and Riisager *et al.* (1999) has demonstrated that the lower part of the Vaigat Formation is normally magnetized while its upper part and all of the Paleocene Maligât Formation is reversely magnetized. The two magnetic zones have been identified as C27n and C26r (Fig. 2). The normally magnetized part of the Vaigat Formation can therefore be constrained in duration to less than *c.* 0.35 Ma (the total duration of C27n, Cande & Kent 1995), whereas the duration of the upper part of the formation is poorly constrained due to the very long duration of C26r (*c.* 3 Ma, Cande & Kent 1995).

The volcanic rocks of the Vaigat Formation are dominated by tholeiitic picrites and magnesian basalts (Larsen & Pedersen 2000) which form a widespread succession of greyish-weathering subaerial pahoehoe lava flows and subaqueous hyaloclastite breccias; the total vertical thickness is *c.* 2000 m. Intercalated with the picrites are some units dominated by more evolved basalts and brownish-weathering silica-enriched rocks derived from the reaction between magma and high-level crustal rocks. These units form stratigraphic marker horizons (Pedersen 1985*a*, *b*; Pedersen *et al.* 1996).

The volcanism of the Vaigat Formation occurred in three main cycles, each of which started with olivine-rich magmas and ended with more evolved and often

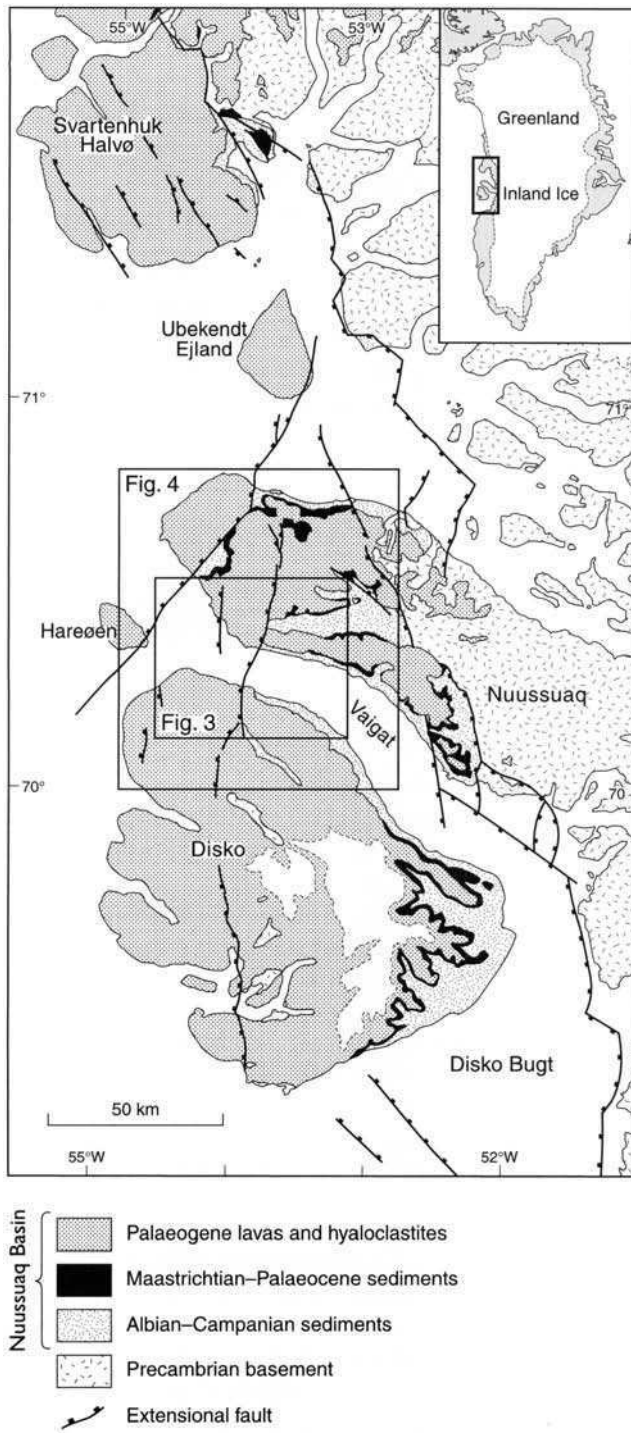

Fig. 1. Geological map showing the Nuussuaq Basin in central West Greenland. Frames show the location of Figures 3 and 4.

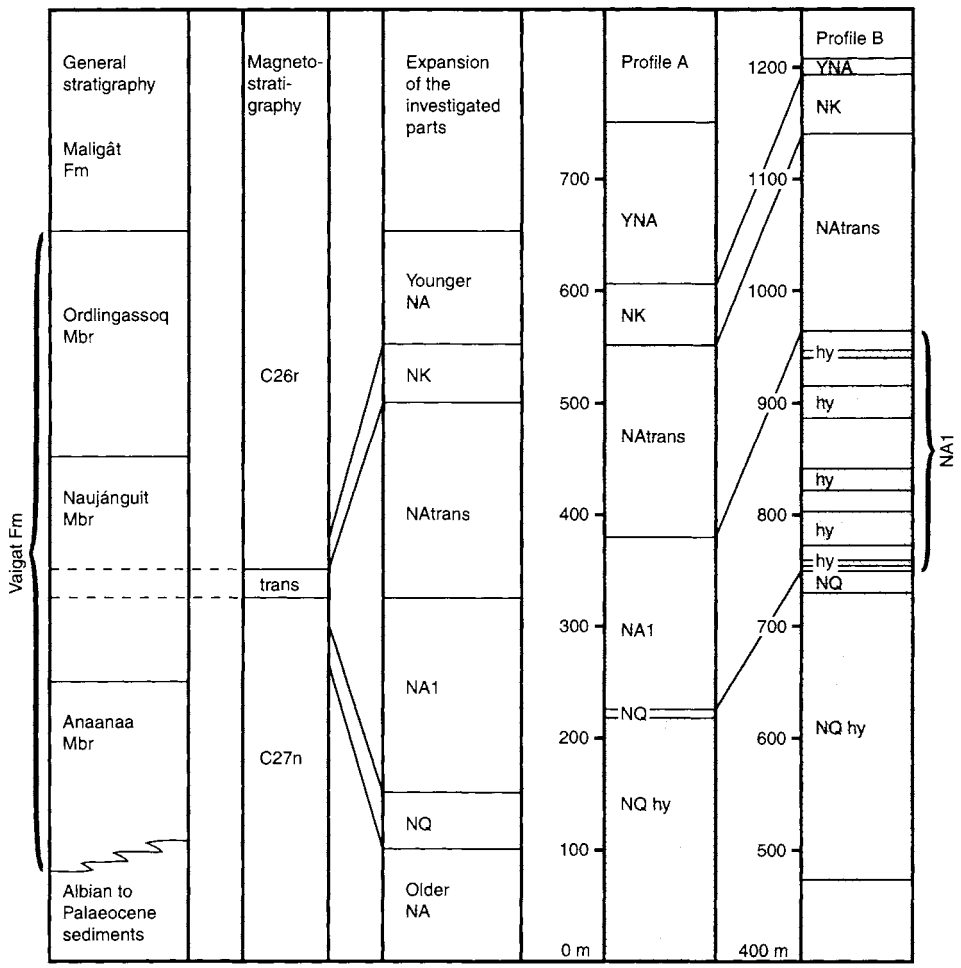

Fig. 2. The stratigraphy of the Vaigat Formation around the magnetic polarity transition C27n–C26r. Two simplified profiles are shown: Profile A at Kuugannguup Innartaa in northern Disko and Profile B at Nuusap Qaqqarsua in western Nuussuaq. NQ, Nuusap Qaqqarsua Member; NA1, Naujánguit Member below the palaeomagnetic transition zone; NAtrans, the palaeomagnetic transition zone within the Naujánguit Member; NK, Nuuk Killeq Member; hy, hyaloclastite breccia.

distinctly crustally contaminated magmas (Larsen & Pedersen 2000). During the eruption of each cycle, and from one cycle to the next, the area of active volcanism expanded as can be seen both from the distribution of lavas and hyaloclastites, as well as from the distribution of located eruption sites and potential feeder dykes. The three cycles gave rise to the three main members which from below are Anaanaa Member, Naujánguit Member and Ordlingassoq Member (Fig. 2). Some of the most important units of evolved, crustally contaminated or alkaline volcanic rocks have been designated independent members which may separate or be enclosed within the main members.

Anaanaa Member. The Anaanaa Member comprises the oldest Paleocene volcanic rocks in West Greenland and is only known from a limited area in western Nuussuaq. All the rocks are normally magnetized. Eruptions onto a sea-covered shelf produced hyaloclastites, mass flows and subaerial lava flows; within the hyaloclastites there are very subordinate clastic sediments including marine limestones. Brief descriptions are given by Henderson (1975), Christiansen *et al.* (1994), and Larsen & Pedersen (1997). This stage was characterized by the formation of rapidly growing volcanic islands. Numerous transitions from hyaloclastite to subaerial lava flows record the position of the palaeo-sea-level, and subaerial flows covered by hundreds of metres of hyaloclastites attest to very substantial crustal movements within the timescale of much less than 350 ka (the total duration of C27n).

Naujánguit Member (Pedersen 1985*a*; Pedersen *et al.* 1996). The Naujánguit Member is known from northern Disko and western and central Nuussuaq. During this cycle the volcanism continued the island building stage, with the formation of hyaloclastites and subaerial lava flows, and soon the lavas also overflowed existing land areas in the south. Large-scale progradation of the volcanic rocks, generally in easterly and northeasterly directions, into a deep marine embayment, caused rapid and substantial palaeogeographical changes within the Nuussuaq Basin, as is particularly well seen on the south coast of Nuussuaq (Pedersen *et al.* 1993). The palaeomagnetic polarity transition zone is located within this member. Naujánguit Member encloses three minor members of distinctly crustally contaminated volcanic rocks, some of which carry native iron. It is overlain by two minor members of contaminated rocks (Tunoqqu and Kûgánguaq Members) produced during the closing stages of this cycle of activity during which the final filling of the large marine basin and the first overspill onto gneiss terrains at the eastern margin of the Nuussuaq Basin took place (Pedersen *et al.* 1996).

Ordlingassoq Member (Pedersen 1985*a*). The Ordlingassog Member is dominated by subaerial lava flows, although hyaloclastites are still common. The member is widespread on northern Disko and Nuussuaq, and time-equivalent picrite lavas may also be present on Ubekendt Ejland and Svartenhuk Halvø. During the third cycle the volcanic migration eastwards continued and large parts of the gneiss terrain at the eastern margin of the Nuussuaq Basin were overlapped by volcanic rocks. The volcanic rocks prograded into and finally filled the large lake complex of the Naujât Member on Nuussuaq (Pedersen *et al.* 1998).

The palaeomagnetic transition zone and its enclosing units

The palaeomagnetic C27n–C26r polarity transition zone has been found in three sections, two on Nuussuaq and one on Disko spaced over a distance of about 30 km, and covers roughly 1000 km^2 including the sea between Disko and Nuussuaq. Within the area, excellent exposures along steep valley walls and coastal cliffs provide detailed geological information, and about 60 km of relevant profiles have been covered by helicopter-borne stereo-photography. Subsequently, the photos have been set up as semicontinuous stereo panels and subjected to multi-model photogrammetrical analysis (Fig. 3; Dueholm 1992; Dueholm *et al.* 1993; Pedersen & Dueholm 1992).

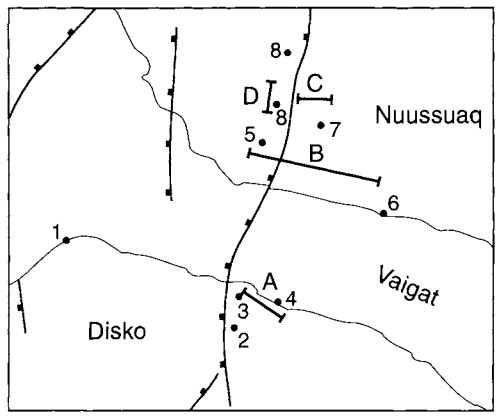

Fig. 3. The location of sections analysed with multi-model photogrammetry. A, northern Disko (Fig. 5); B, Vaigat coast of Nuussuaq (Fig. 6); C, Aaffarsuaq valley in Nuussuaq (Fig. 5); D, Qunnilik valley in Nuussuaq (Fig. 11). Localities mentioned in the text are: 1, Serfarsuit; 2, Kuugannguaq valley; 3, Kuugannguup Innartaa; 4, Naajannguit; 5, Nuusap Qaqqarsua; 6, Nuuk Killeq; 7, Aaffarsuaq valley; 8, Qunnilik valley.

Prior to the palaeomagnetic sampling, selected sections had been sampled for lithological and geochemical analysis, and a lithostratigraphy had been established. The geological analysis within and around the magnetic transition zone presented here is based on quantitative photogrammetrical measurements of lithological boundaries, thicknesses of volcanic units, and orientation of surfaces, also on physically inaccessible near-vertical mountain sides.

The analysis will focus on three WNW to W trending 5–17 km long profiles which cut almost perpendicularly through the palaeo-coastlines at that time (profiles A to C, Figs 5 & 6) and an additional 2 km long N–S trending profile D (Fig. 3).

In western Nuussuaq the palaeomagnetic transition zone lies within a 300–400 m thick series of picritic to olivine-rich basaltic subaerial lava flows from the Naujánguit Member. The series is sandwiched between two members of contaminated volcanic rocks, the Nuusap Qaqqarsua Member and the Nuuk Killeq Member. The rocks of the palaeomagnetic transition zone and the enclosing units can all be followed eastwards along the south coast of Nuussuaq where they change successively into hyaloclastite facies over a horizontal distance of about 16 km (Profile B, cf. Pedersen. *et al.* 1993). This probably represents the best exposed example of volcanic progradation into a marine basin within the NAIP.

The geological analysis covers four main units, from the bottom up (Fig. 2):

(1) Nuusap Qaqqarsua Member (NQ), a series of normally-magnetized (C27n), silica-enriched basaltic lavas and their equivalent hyaloclastites formed by filling of a more than 300 m deep marine basin;
(2) Naujánguit Member below the palaeomagnetic transition zone (NA1) comprising mostly picritic subaerial lavas (*c.* 180 m thick and normally magnetized (top of C27n)), and on Nuussuaq also thin intercalated beds of hyaloclastite;
(3) Naujánguit Member of the transition zone (NAtrans), comprising picritic subaerial lavas (160–180 m thick and represents the C27n–C26r polarity transition), lithologically indistinguishable from the lavas of NA1;

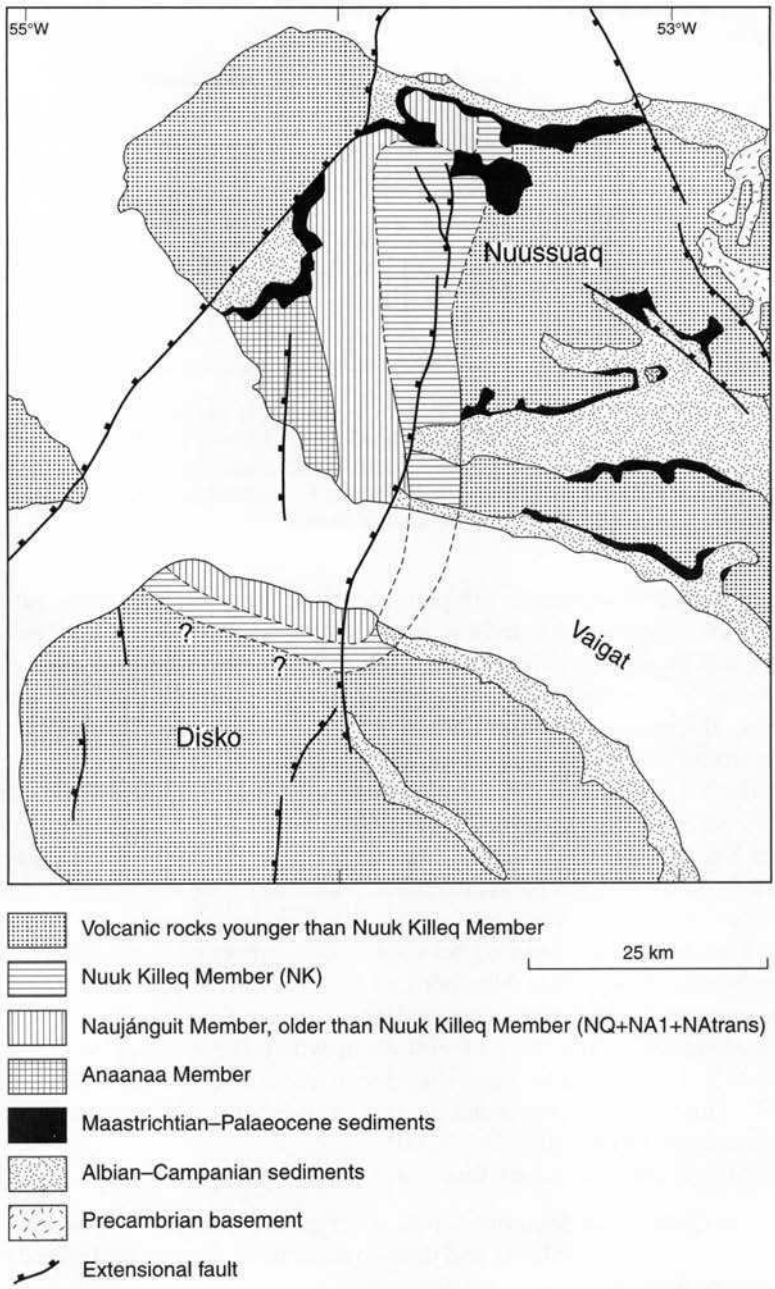

Fig. 4. Simplified geology of northern Disko and Nuussuaq showing the gradual eastwards expansion of the early volcanic rocks of the Vaigat Formation from the Anaanaa to the Nuuk Killeq Member. The western extension of each unit is not shown. The southern extension of the early Vaigat Formation rocks on North West Disko is unconstrained towards the south and west because of later subsidence of the Nuussuaq Basin.

(4) Nuuk Killeq Member (NK), comprising silica-enriched subaerial basaltic lavas (*c.* 50 m thick and reversely magnetized (C26r)),which form a very characteristic lithological marker horizon (see later).

The gradual eastwards expansion of the successive units (NQ + NA1 + NAtrans and NK) is shown in Figure 4.

Pre-volcanic surface

In the area described here, the volcanic rocks transgress a pre-volcanic escarpment which is the site of a N–S trending fault along which the sediment surface was downthrown more than 400 m towards the west. The fault system was reactivated in post Vaigat Formation time as the Kuugannguaq–Qunnilik Fault (Chalmers *et al.* 1999, Foldout 2). East of the fault, tilted blocks of mid-Cretaceous clastic sediments from the Atane Formation (Pedersen & Pulvertaft 1992) now dip 10–20°E to NE. West of the fault the upper part of the sedimentary section is best known from drill holes and consists of Late Cretaceous to Paleocene submarine fan to submarine canyon sediments of the Itilli and Quikavsak Formations (Dam & Sønderholm 1994; Dam 1996; Christiansen *et al.* 1999).

The contact between the hyaloclastites of the NQ to NK units and the underlying sediments in the deep marine basin is exposed at a few localities along the south coast of Nuussuaq (Profile B cf. Pedersen *et al.* 1993) and is important for the assessment of the syn-volcanic subsidence around the transition zone. Here, the clastic sediments of the Cretaceous Atane Formation are separated from the marine hyaloclastites by a thin layer of Paleocene marine mudstone with a sparse assemblage of dinoflagellates (Piasecki *et al.* 1992). The thickness of this layer varies from only a few centimetres to between 5 and 10 m. This lack of sediment suggests a very short pre-volcanic duration of the marine conditions even in the deepest part of the basin overlain by 500 to 700 m of hyaloclastites.

Nuusap Qaqqarsua Member (NQ)

The NQ Member is exposed within a roughly 5 km wide belt extending for 30 km from Kuugannguaq valley on Disko in the south through Nuusap Qaqqarsua to west of Qunnilik valley on Nuussuaq in the north.

On Disko, NQ represents the oldest exposed volcanic rocks and forms a >220 m thick hyaloclastite with continuous foresets indicating a water depth in excess of its exposed thickness. The hyaloclastite foresets indicate filling by lava flow from the west into the marine basin west of the palaeo-escarpment (Fig. 5, Profile A). From the escarpment and eastwards, sandstones of the Atane Formation formed a lowlying plain at the time.

On Nuussuaq, NQ forms a 60 m thick succession of pahoehoe lava flows and associated foreset-bedded hyaloclastites which filled the more than 300 m deep marine basin from the west (Fig. 6). Within the succession a pause in volcanism led to the formation of a 40 m high coastal cliff from which a volcanic conglomerate deposited as a marine talus fan on the hyaloclastite can be followed more than 200 m downslope (Fig. 7).

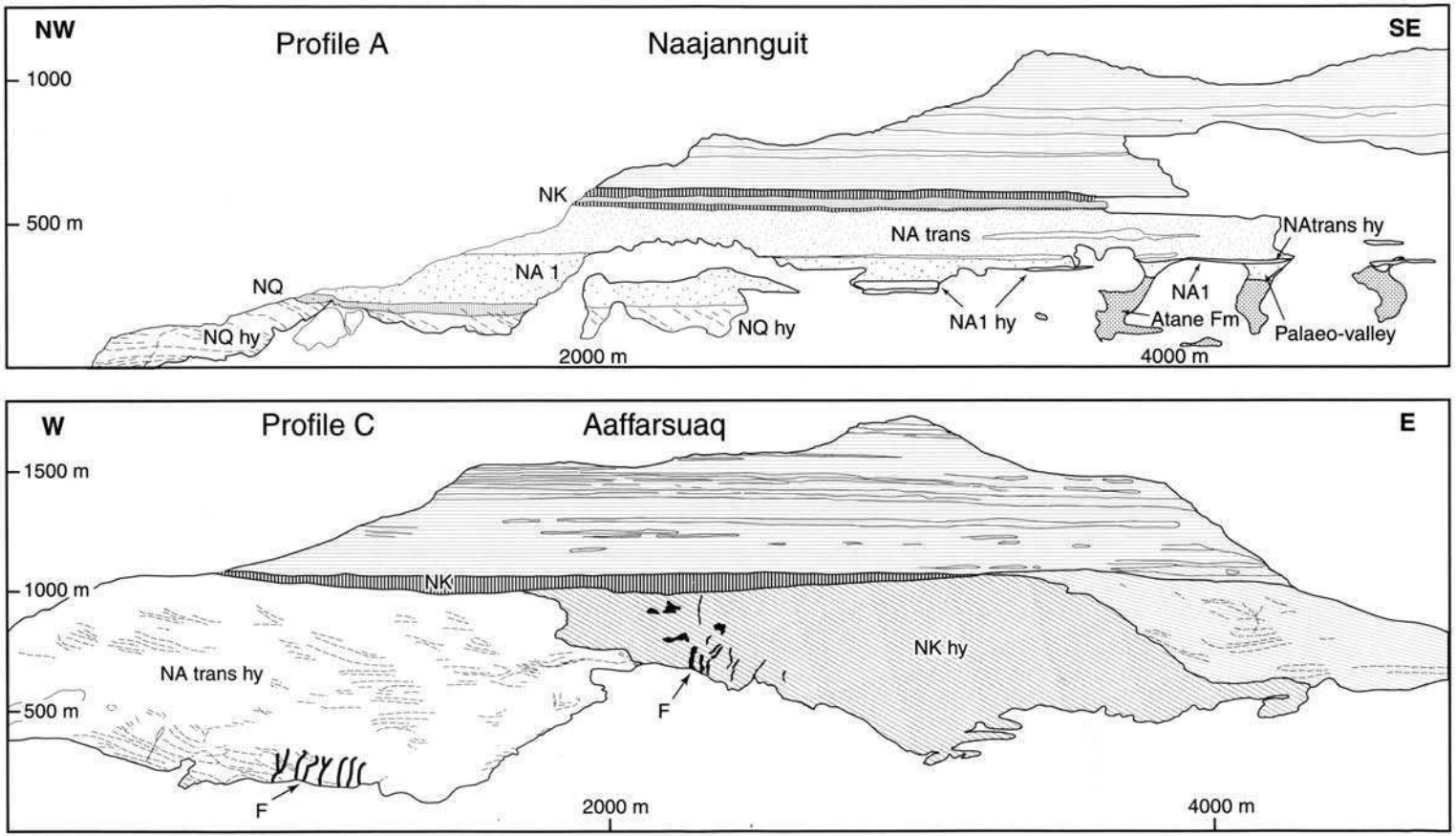

Fig. 5. Profiles A and C (for location, see Fig. 3). Profile A, Naajannguit, shows the oldest exposed rocks of the Vaigat Formation on Disko and illustrates how volcanic rocks of NA1 and NAtrans overlap a palaeo-escarpment at around 3000 to 4000 m at the horizontal axis. The simplified profile A shown in Figure 2 represents the part at 1000 to 2000 m. The palaeo-valley shown in Figure 10 is situated at 4300 m. Profile C, Aaffarsuaq, shows the volcanic rocks of NAtrans and NK from the Aaffarsuaq valley on Nuussuaq and illustrates how Nuuk Killeq Member progrades into the deep marine basin in central Nuussuaq. F, subaquatic feeder dykes; hy, hyaloclastite breccia. At this locality all the volcanic rocks of the magnetic polarity transition zone are in marine facies.

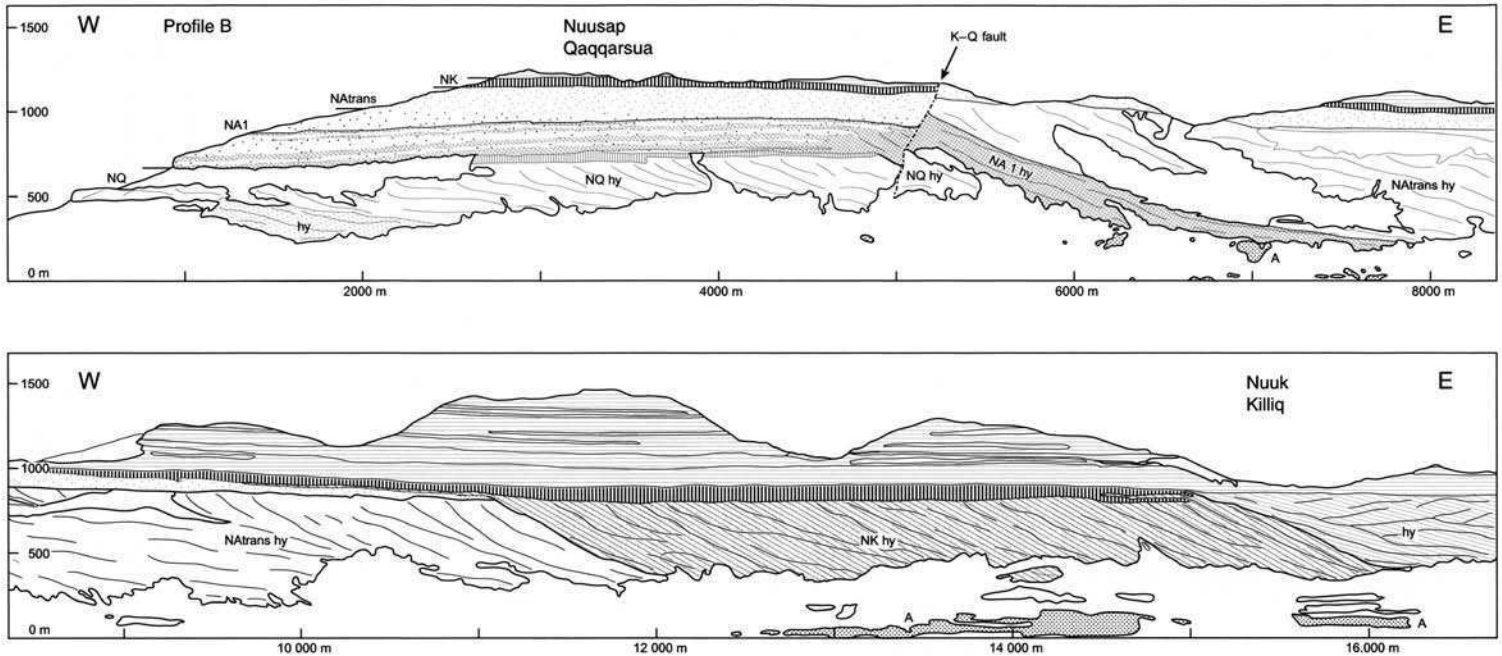

Fig. 6. Profile B, showing the south coast of Nuussuaq between Nuusap Qaqqarsua in the west and Nuuk Killeq in the east. The profile illustrates the progradation of the volcanic rocks and the lateral changes from subaerial into subaquatic facies (hy) from the Nuusap Qaqqarsua Member (NQ) to the Nuuk Killeq Member (NK) and younger. The continuation of hyaloclastite beds from the shore facies to the bottom of the marine basin allows a precise estimation of palaeo water depths. An arrow labelled K–Q fault marks the position of the Kuuganngnuaq–Qunnilik fault. Modified from Pedersen *et al* 1993. The locations of Figs 7, 8 and 9 are all around 3500 to 4400 m on the horizontal scale.

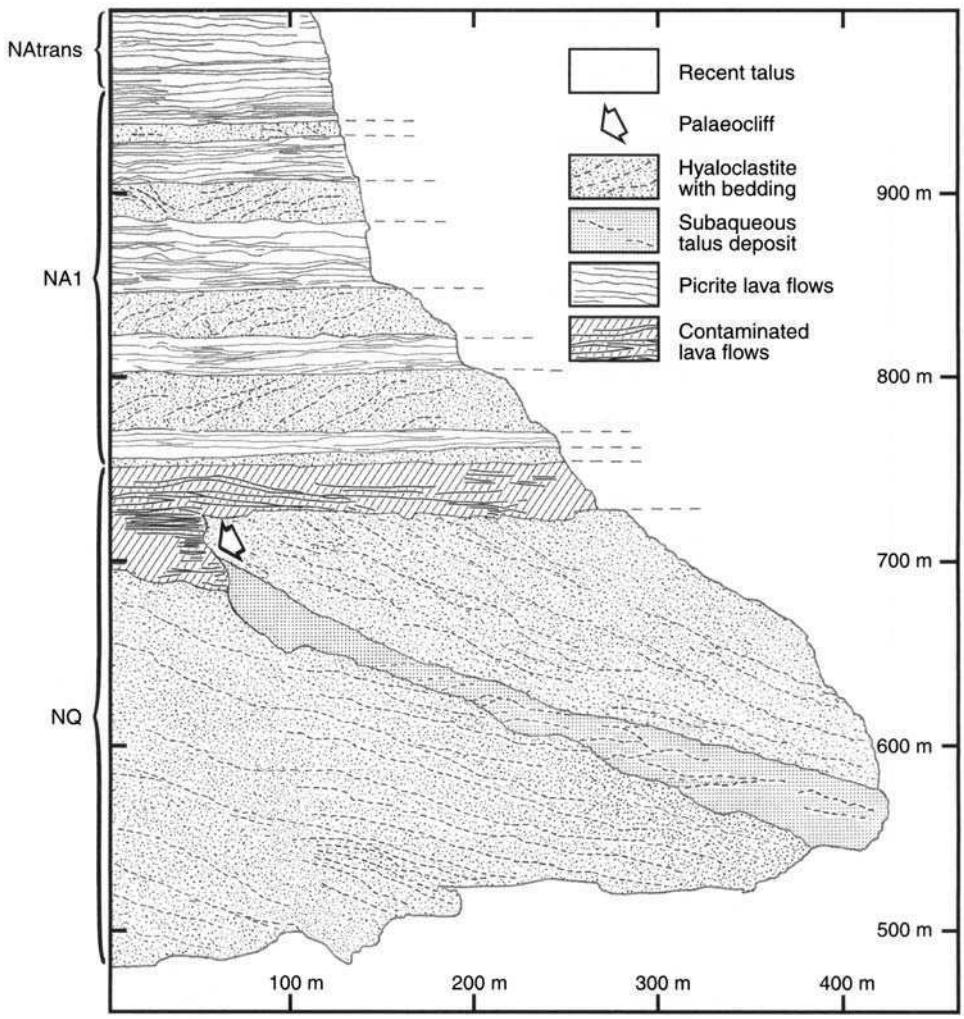

Fig. 7. Detailed multi-model photogrammetrical compilation of the Nuusap Qaqqarsua Member (NQ) and the NA1 unit from the Naujánguit Member in the mountain Nuusap Qaqqarsua (location in Fig. 6 at 3500–4000 m). The palaeo-cliff with a prominent submarine talus fan shows that NQ did not develop at a continuously high eruption rate. Note the five thin hyaloclastite horizons within the NA1 unit, which illustrate an almost perfectly balanced volcanic aggradation and basin subsidence at a high eruption rate. Modified from Pedersen & Dueholm (1992).

At the time of the last eruption of NQ the coast extended N–S for more than 25 km and separated a lava plain in the west from the marine basin in the east. The basin widened from less than 1 km in the south (on Disko) to many kilometres in the north (on Nuussuaq). The northwestern extension of the basin is poorly resolved because of lack of continuous exposures.

The duration of the NQ unit cannot be accurately estimated. The formation of the palaeocliff and conglomerate shows that this phase of volcanism did not evolve continuously.

Naujánguit Member (NA1 and NAtrans)

This part of Naujánguit Member consists of 300–400 m of olivine-rich subaerial lava flows and up to 850 m of lavas and hyaloclastites where the unit prograded into the marine basin. It is partially exposed over a 28 km wide zone in northern Disko and over an up to 15 km wide and up to 35 km long area stretching northwards from the south coast of Nuussuaq. The detailed evolution and facies progression, which is central to our analysis, will be described in a later section.

On Disko, all the exposed parts of NA1 and NAtrans west of Kuugannguaq valley are in subaerial lava facies and record a monotonous lava field. East of Kuugannguaq, the lower part consists both of lavas and intercalated thin hyaloclastite horizons, also where it spills onto the sedimentary land surface, indicating a development very close to sea level.

On Nuussuaq, the lower part of the succession records repeated changes between subaerial and submarine facies in the west, again indicating proximity to sea level, and a general progradation into the deep marine basin eastwards. The upper part of the succession is in purely subaerial facies in the west and gradually progrades into the basin in the east.

Nuuk Killeq Member (NK)

This unit forms one of the most prominent lithological marker horizons within the Vaigat Formation, being quite distinctive in lithology as well as petrography and geochemistry.

On Disko, NK is a succession of lava flows continuously exposed for more than 28 km along the north coast from Serfarsuit in the west to east of Naajannguit, where the member dies out. It is widely present in western Nuussuaq as a lava succession extending from the south coast to the north coast (Fig. 4). Where it occurs in subaerial facies, NK is composed of an up to 50 m thick succession of brown basalt lava flows of either aa- or pahoehoe-type. In some areas the unit encloses a few greyish-weathering picrite lava flows. The wide areal extent of this comparatively thin succession of lava flows shows that the lavas must have flowed over an essentially horizontal lava plain, free of notable depressions or escarpments other than the marine basin bordering the plain towards the east. The basal NK lavas entered the sea along a palaeo-coastline extending for more than 20 km from the south coast of Nuussuaq northwards and across the Qunnilik valley. The foreset-bedded hyaloclastites of this unit record water depths between 450 and 600 m (Fig. 6).

Volcanic rocks of the NK unit filled in a 4–5 km wide part of the marine basin (Fig. 4). Within the younger part of NK, lava flows covered by thin horizons of hyaloclastite demonstrate that continued basin subsidence caused temporary transgressions of the basin shore in a westerly direction, only to be interrupted by the next eruptions.

Eruption frequencies and rates of basin movements derived from the transition zone

The transition zone (NAtrans) has been studied in particular detail on the mountain Nuusap Qaqqarsua, where it has been sampled for stratigraphical, geochemical

and palaeomagnetic studies. The same lithologies have been measured photogrammetrically on the inaccessible near-vertical walls of the south side of the mountain where the best exposures of NAtrans are situated (Fig. 8). NAtrans is here 165 m thick and is composed of 59 picritic pahoehoe lava flows, many of which form small groups of flow tongues. The thickness of individual flows varies from less than 1 m to 10 m, and small lava domes with diameters of less than 15 m are widespread. The number of individual flows encountered in random vertical profiles on the sides of Nuusap Qaqqarsua accordingly varies by a few flows.

The 59 lava flows in NAtrans correspond to a smaller number of eruptive events because each eruption can result in a number of pahoehoe flows. From field appearance and geochemistry at least six eruptive events have been recognized. Based on palaeomagnetic data, Riisager & Abrahamsen (1999, 2000) found at least eight events, each event consisting of several consecutive flows recording the same direction and intensity of the palaeomagnetic field and hence being closely spaced in time. Using features such as soil horizons and lava morphology, colour and oxidation, the photogrammetrical interpretation yields an estimate of 17 eruptive events within

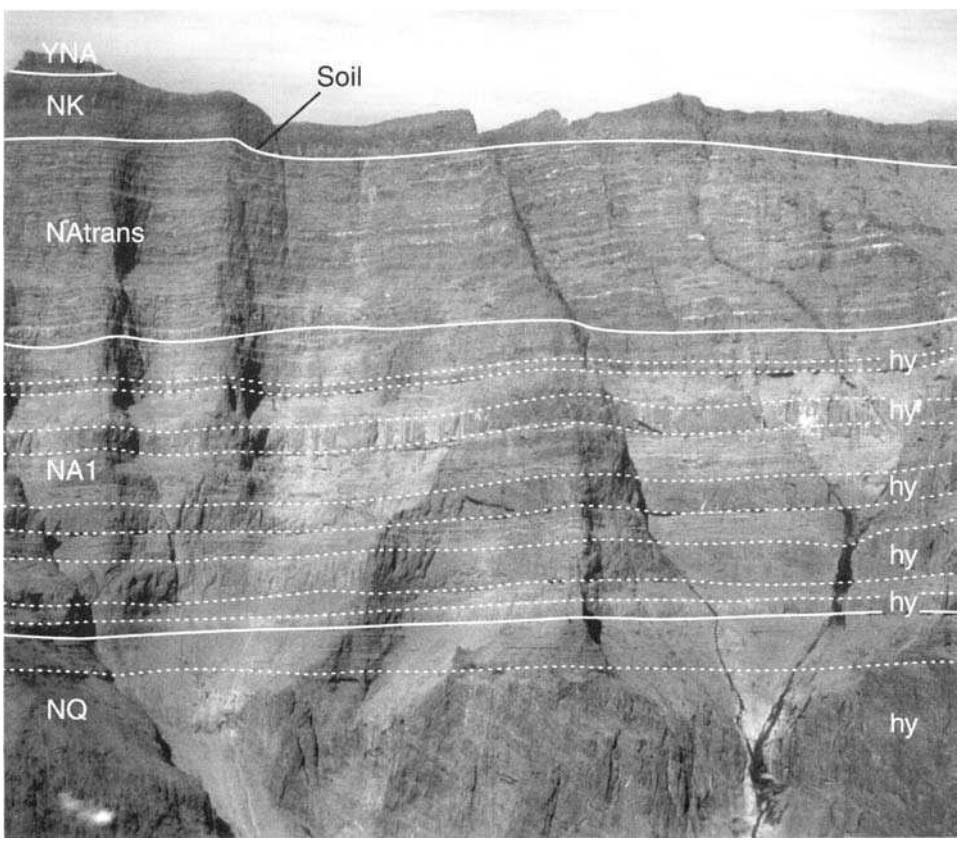

Fig. 8. Photograph showing repeated subaqeous–subaerial facies changes at the near-vertical wall of Nuusap Qaqqarsua on Nuussuaq. hy, hyaloclastite breccia. Height of section is 600–650 m. Location at 3600–4400 m in Figure 6. A detailed photogrammetrical interpretation of the upper part of the succession in the left side of the picture is shown in Figure 9.

NAtrans (Fig. 9). For the Nuusap Qaqqarsua mountain locality we thus arrive at the following values, using a 5 ka estimate for the duration of the C27n–C26r transition: aggradation rate 33 m ka^{-1}; 12 flow tongues per ka; maximum and most probable time separating eruptive events 0.7 and 0.3 ka, respectively. A distinct soil horizon lies between the top of NAtrans and the base of the NK unit and is about 5 to 10 (locally 20) cm thick. It marks a pause in the volcanic activity of some hundred years (see below), but it is not known if it occurred during C27n–C26r trans or C26r.

In profile A at Kuugannguup Innartaa on Disko, which is the stratigraphic type section for the Naujánguit Member (Pedersen 1985*a*; Fig. 5), NAtrans is around 175 m thick and contains a number of flows similar to those on Nuusap Qaqqarsua. Palaeomagnetic work on profile A (J. Riisager pers. comm.) and comparison with the Nuusap Qaqqarsua profile shows the existence of a similar number of different palaeomagnetic directional groups (eruptive events); however, the pole positions cannot be correlated between the two profiles, indicating that the lavas represent different eruptive events and that a typical picrite lava flow has a mean lateral extent of much less than 16 km (the distance between the two profiles). This is in accordance with other observations on picritic lava flows from the Vaigat Formation. It also indicates a similar volcanic aggradation rate over a wide lava plain.

The basal lavas of NAtrans entered the deep marine basin at *c.* 6 km in profile B (Fig. 6) and the youngest NAtrans lava flows entered the marine basin 5 km farther east.This corresponds to a volcanic progradation of about 5 km in 5 ka, yielding a mean progradation rate in the order of 1 m a^{-1}.

Furthermore, the NAtrans subaerial lava succession thins gradually from west to east as the lower flows are successively passed into hyaloclastites, indicating that the basin around the volcanic front was gradually subsiding and that the lavas formed an almost horizontal lava plain which remained very close to but above sea level. Because the lavas in the west remained in subaerial facies the subsidence here was less than the thickness of NAtrans (165 m) but certainly not much less, and a subsidence in the order of 120–150 m in 5 ka, or 25–30 m a^{-1} is considered a reasonable conservative estimate.

A 10–15 m thick horizon of NK hyaloclastite extends for *c.* 1600 m westwards from the point of entry of the youngest NAtrans picrite lavas into the deep basin (Fig. 6, at 10–11 km) increasing to 20 m just before the horizon enters the deep basin, covered by NK lava flows. The marine transgression thus recorded was caused by basin subsidence during the pause in volcanic activity marked by the above mentioned soil horizon at the base of NK at Nuusap Qaqqarsua. If the NAtrans rate of subsidence is assumed for the soil-producing period, this gives a duration of *c.* 0.5 ka for this period. Because it is not resolved whether the pause occurred during C27n–C26r trans or C26r, a further *c.* 10% uncertainty is thus added to the estimates of volcanic productivity and basin movements, but this is trivial compared with the uncertainty of our basic estimate.

Movements recorded in the NA1 zone

The detailed geology of the NA1 zone exemplifies three features of interest here. Firstly, syn-volcanic movements are recorded at the earliest contact between subaerial lava flows and the pre-volcanic sedimentary palaeosurface; secondly, aggradation

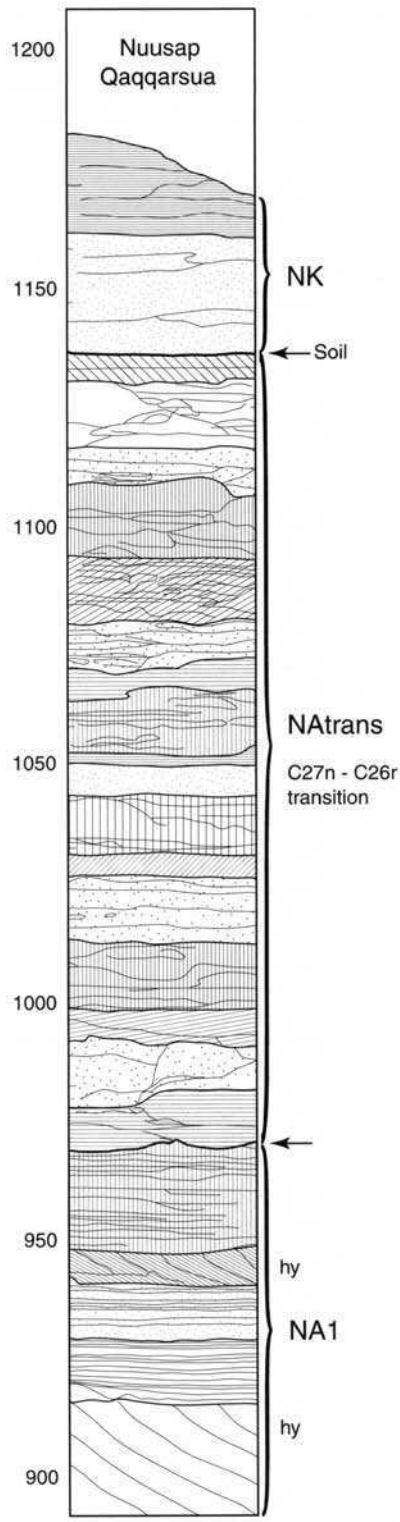
1200
Nuusap
Qaqqarsua
1150
NK
Soil
1100
NAtrans
1050
C27n - C26r
transition
1000
950
hy
NA1
hy
900

and subsidence were very accurately balanced, resulting in oscillations just around sea level; and thirdly, local syn-volcanic extensional differential sagging is seen.

At profile A (Fig. 5) on Disko the NA1 unit is around 150 m thick and is exclusively composed of subaerial pahoehoe lava flows. Interbasaltic soils are very rare, attesting to an almost continuous volcanic activity. The same eruptive frequency and productivity can therefore be assumed for both NA1 and NAtrans which implies a duration of *c.* 5 ka for NA1.

Contact between subaerial lava flows and the pre-volcanic sedimentary surface

Following the NA1 lava succession eastwards on profile A (Fig. 5) its lower parts are concealed under scree but at Naajannguit where the lavas overstep the palaeo-escarpment the lower contact is exposed in several gullies (profile A at 3800–4500 m). Subaerial lava flows from the upper part of NA1 rest on mid-Cretaceous Atane Formation deltaic clastic sediments which dip 15–20°E to NE. The lavas have filled the bottom of a palaeo-valley trending NW–SE and overstep a *c.* 50 m high, steep slope (facing 60 SW) which forms the NE wall of the valley (Fig. 10). The substantial palaeo-topography in the soft sediments strongly suggests that the steep-sided valley was part of a newly created fault scarp and that the Atane Formation sediments were tilted to their subaerial position as the shoulder of an extensional fault block by syn-volcanic extensional tectonism. The first stage of tilting of the sediments could be substantially older. A thin hyaloclastite and pillow lava horizon at the top of the valley, marking the base of NAtrans, indicates that the lavas filled the valley very close to sea-level.

Balanced aggradation and subsidence around sea-level

The NA1 zones on Disko in profile A and on Nuussuaq in profile B (Figs 5 & 6) display a significant difference in volcanic facies. On Disko, the 150 m thick NA1 succession consists entirely of subaerial lava flows. On Nuussuaq, the *c.* 200 m thick NA1 zone consists of subaerial lavas alternating with five horizons of foreset-bedded hyaloclastites between 8 m and 30 m thick (Figs 6, 7 & 8). Only one soil horizon is observed. This succession records an almost perfect balance between aggradation of the lava plateau and subsidence of the basin. Five events are recorded in which subsidence led to submergence of the subaerial lava plain to form a shallow shelf with water depths up to 30 m. Just 1 km farther east the hyaloclastite horizons merge, marking the transition to a deeper basin at the time not yet filled by the advancing volcanic fronts (Profile B at 4800 m). If the NAtrans aggradation rate is applied, the succession indicates a basin subsidence rate close to the volcanic aggradation

Fig. 9. Detailed multi-model photogrammetrical interpretation of the upper part of Nuusap Qaqqarsua including the magnetic polarity transition zone C27n–C26r (NAtrans, base and top marked by arrows) which is estimated to have erupted in *c.* 5 ka. Individual eruptive units are distinguished by different signatures. About 17 eruptive units, most of which consist of several picritic lava flow tongues, can be distinguished within NAtrans. A thin soil horizon separates the NAtrans unit from the overlying contaminated basaltic lavas of the Nuuk Killeq Member (NK). hy, hyaloclastite breccia. Location at 3800 m in Figure 6.

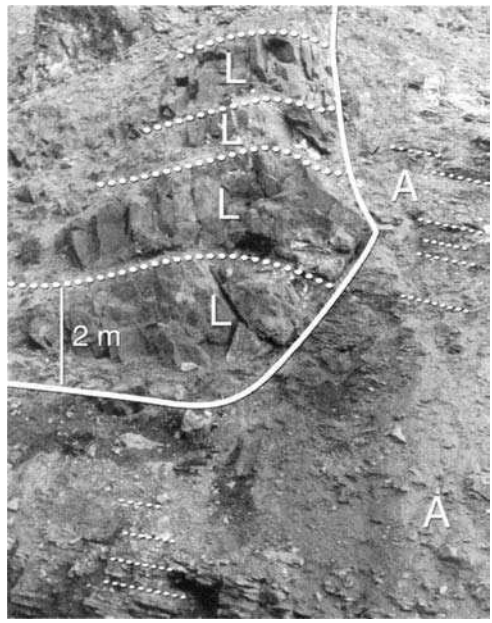

Fig. 10. The steep-walled contact of a palaeo-valley carved into Cretaceous clastic sediments of the Atane Formation (A, bedding planes indicated with stippled lines) has been preserved by the casting effect of a number of subaerial picritic lava flows (L) from the NA1 unit at Naajannguit on northern Disko (Profile A at 4400 m, Fig. 5). The palaeo-valley must have formed at an uplifted fault crest of Atane Formation sediments. The valley is the earliest example of an onlap contact between subaerial lava flows and older sediments within the Nuussuaq Basin.

rate of $30\,m\,ka^{-1}$. The five hyaloclastite deposits then represent periods of volcanic inactivity between 0.3 and 1 ka, which is within the range of periods of volcanic inactivity deduced from the overlying subaerial lavas from NAtrans.

Extension-controlled syn-volcanic differential subsidence

In profile D on the western side of Qunnilik Valley, 12 km due north of profile B, the zones NA1 to NK and younger parts of the Vaigat Formation are well exposed (Fig. 11). The facies development is somewhat similar to that seen in profile B, showing an alternation between subaerial lava flows and hyaloclastites within unit NA1, but the geometry is different. The detailed photogrammetrical analysis (Fig. 11) shows that NA1 is almost exclusively in subaerial facies in the southern part of the valley, but within a distance of less than 1.5 km it develops into a dipping succession of alternating lavas and hyaloclastites, with the hyaloclastite deposits rapidly thickening towards the E to NE. The dips of originally horizontal lava flows and lava to hyaloclastite boundaries gradually decrease up-section from 9° to 4°. The basal *c.* 35 m of NAtrans is a hyaloclastite, and from there up this facies is subaerial with lava flows dipping 3–4°NE. This monotonous dip is probably of post-Vaigat Formation age. The section is interpreted as recording syn-volcanic movement of a slowly tilting, extensional fault block which stopped moving around the time of the start of

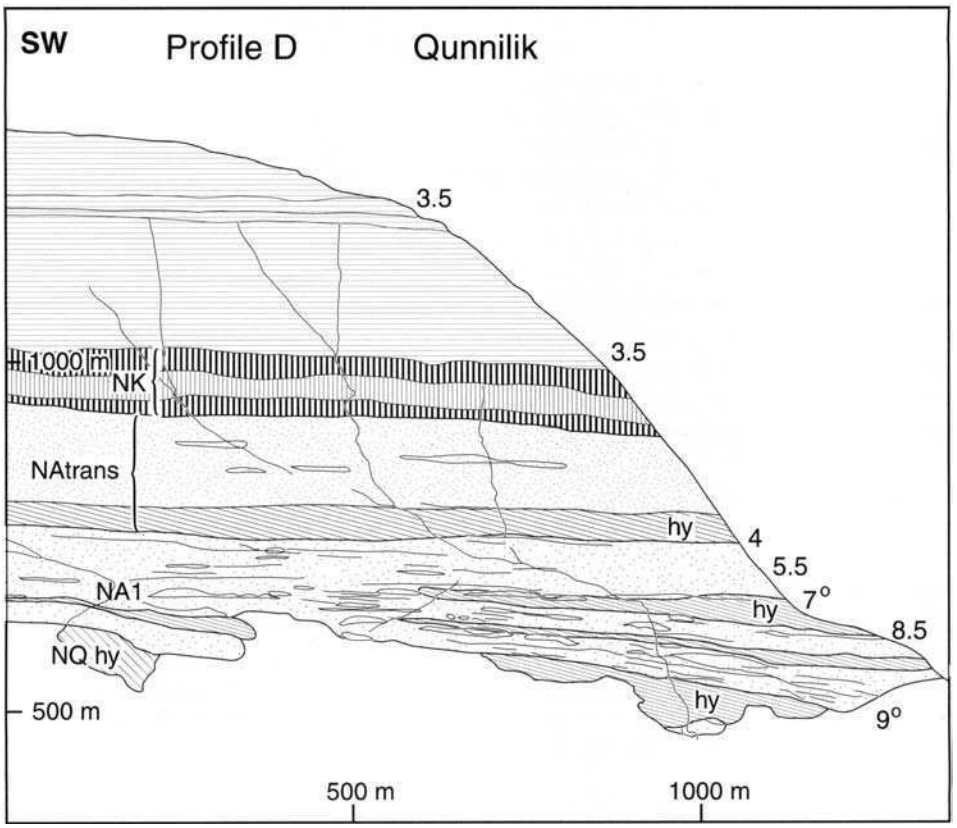

Fig. 11. Profile D showing part of the western wall of the Qunnilik valley. Lava flows and lava to hyaloclastite (hy) contacts show a regularly decreasing dip of 9° to 4° from the base to the top of the NA1 unit while the hyaloclastite horizons decrease in thickness towards the southwest. The volcanic rocks younger than NA1 show a monotonous dip of *c.* 4°. The structure demonstrates the differential movements of a fault block within the *c.* 5 ka time window of NA1 and is preserved in detail because of the very high eruption rates.

NAtrans after a total rotation of at least 5° around a NNW–SSE axis. Subsequent monotonous volcanic aggradation occurred over a rigidly subsiding horizontal lava plain. With an estimate of *c.* 5 ka for NA1, a rate of rotation in the order of $1° ka^{-1}$ is indicated. The differential excess subsidence is around 85 m over 1 km horizontally.

Volcanic productivity during the C27n–C26r transition

A reconstruction of the volcanic province at the beginning of NAtrans shows a horizontal lava plateau extending for roughly 25 km E–W along the north coast of Disko and at least 35 km northwards to central-western Nuussuaq. The western margin of this plateau has now disappeared either through subsidence into the sea west of Disko or due to Quaternary erosion on Nuussuaq. The eastern part of the plateau was the N–S running palaeo-coastline from north of Disko through western Nuussuaq that marked the border of the deep marine basin. The plateau had an

areal extent of at least 875 km^2, and if it was covered by a uniformly 160 m thick succession of NAtrans lavas, the minimum volume of these lavas is 140 km^3. During progradation, NAtrans volcanic rocks filled a 5 km wide and at least 25 km long section of the marine basin with hyaloclastites and covering lavas. With a mean thickness of lavas plus hyaloclastites of 700 m, and applying a factor of 0.75 (conservative estimate) for converting the hyaloclastites into an equivalent magma volume, this sector represents a volume of 10 km^3 lava and *c.* 60 km^3 converted hyaloclastite. The total volume of NAtrans is thus 210 km^3 of lava. The minimum production per year is then 0.042 km^3. This minimum estimate is fairly similar to the magma supply rate of 0.08–0.11 $km^3\,a^{-1}$ estimated for the recent activity of Kilauea volcano, Hawaii (Swanson 1972; Denlinger 1997). In comparisons of rift zones, magma production rates are normally calculated per kilometre of rift length. The rift zone is not well defined in West Greenland, but we assume a rift at this stage with a direction roughly NNW–SSE, as judged from prominent early Vaigat Formation dyke directions and the NNW-directed axis of syn-volcanic fault block rotation noted above. The length is equal to the extension of the volcanic plateau of the time, *c.* 35 km from northern Nuussuaq to northern Disko. The minimum productivity estimate then becomes $1.2 \times 10^{-3}\,km^3\,a^{-1}\,km^{-1}$ (rift). This is an order of magnitude higher than the minimum estimate of $1.3 \times 10^{-4}\,km^3\,a^{-1}\,km^{-1}$ (rift) for the complete Vaigat Formation and early and middle Mâligat Formation given by Storey *et al.* (1998). It is also an order of magnitude higher than the productivity estimate of $1.3 \times 10^{-4}\,km^3\,a^{-1}\,km^{-1}$ for the neo-volcanic rift zones of Iceland (Pálmason 1981). Even with a duration of the transition zone of 10 ka, the productivity would have been greatly in excess of that characterizing recent Iceland.

Discussion and conclusions

Duration of the Vaigat Formation

The combined maximum thickness of all the successive subaerial lava units of the Vaigat Formation is *c.* 2.1 km. To this could be added an unconstrained thickness representing the oldest Anaanaa Member picrites, only known in subaquatic facies. If the Vaigat Formation was erupted continuously with the volcanic aggradation rate of 33 m ka^{-1} established from the C27n–C26r transition, a total duration of just 60–70 ka is implied. Neither existing $^{40}Ar/^{39}Ar$ dating, nor palaeomagnetic nor biostratigraphical work, provide a time resolution which allows discrimination between 70 ka and the crude estimate of 0.5 Ma for the total duration of the Vaigat Formation given earlier. However, a geological assessment can be made.

Those parts of the lava succession composed of olivine-rich rocks have in general only few and thin soil horizons, despite the easily weathering nature of the picrite lavas and the palaeobotanical evidence of a temperate to warm temperate climate (Koch 1963). It is thus likely that the major part of the Vaigat Formation was erupted at a high rate that did not deviate much from that recorded by NAtrans. On the other hand, many geological features make it unlikely that all of the Vaigat Formation was erupted in about 70 ka. The formation evolved in three distinct magmatic cycles, and the boundary between the second and the third cycle is locally a slightly angular erosional unconformity, with eroded lava flows and thin conglomerates (Pedersen 1985*a*, *b*). Soils are common at the bases or tops of the subordinate successions of

evolved basalts or crustally contaminated rocks, most of which represent minor volcanic systems erupted without intermittent picrite volcanism. Some of the contaminated units, such as the Tunoqqu Member (Pedersen *et al.* 1996), record a complicated basin history with several phases of conglomerate formation. Finally, the sedimentary record of at least 140 m of syn-volcanic mudstone deposited in the Naajat Lake contemporaneously with the Vaigat Formation (Pedersen *et al.* 1998) argues against a short duration. All these features add up to a picture of a geological evolution which is extremely unlikely to have lasted only 70 ka. We therefore prefer a scenario in which the Vaigat Formation volcanism evolved under conditions causing high eruption rates over short periods, separated by periods of low activity or even inactivity, over a combined time span much in excess of 70 ka.

Syn-volcanic basin movements

The sea-level record provided by the lava to hyaloclastite transitions allows a firm estimate of subsidence of the basin around the volcanic front in the order of 25 m ka^{-1}. Movements of this size are considerably greater than the eustatic sea level changes around the C27n–C26r transition (Haq *et al.*1987; Neal 1996) and must arise from a combination of loading by the heavy volcanic rocks, sediment compaction (e.g. Reynolds *et al.* 1991) and the tectonic forces of basinal extension. Dam & Sønderholm (1994, 1998), Dam *et al.* (2000), Nøhr-Hansen *et al.* (2002) and Chalmers *et al.* (1999) have demonstrated two late Cretaceous and two pre-volcanic Paleocene tectonic phases within the Nuussuaq Basin, and a late fifth pre-volcanic to syn-volcanic phase of subsidence is evident from the sedimentological record. The syn-volcanic subsidence rate determined here amounts to 25 km Ma^{-1} and is so high that it cannot have been continuous, therefore the main part of the movements must have been short-lived. The sediment-starved contacts between the older Cretaceous basement and the hyaloclastites in the marine basin suggest that the deep basin had only existed for a short period before it was filled with hyaloclastites and that it was undergoing a dramatic deepening within the < 20 ka time interval between the NQ and NK units.

The basin movements of the Vaigat Formation were not exclusively passive load-controlled subsidence. Several examples of short-lived differential basin movements both before and after the eruption of the volcanic rocks of the NAtrans and NA1 units considered here are recorded from the Vaigat Formation on Nuussuaq (Pedersen & Dueholm 1992, figs 10 & 15; Pedersen *et al.* 1993, 24 km, 34 km and 50 km; and unpublished data). Of particular interest are the two cases recorded here in the NA1 volcanic rocks (Figs 10 & 11) which provide proof of extension of the Nuussuaq Basin within or just prior to the narrow time window of this unit. Differential movements of a number of fault blocks at different sites at different times, followed by stabilization of the blocks once a stable subaerial lava plateau had built up on top of them, were apparently characteristic of this stage of development.

Comparison with other parts the North Atlantic Igneous Province

The volcanic rocks of the Vaigat Formation in West Greenland represent one of the first manifestations of volcanism from the proto-Icelandic mantle plume. The

volcanism was very vigorous, even if a 10 ka timespan is assigned to the C27n–C26r transition, and the estimated volcanic production rate of 1.2×10^{-3} km^3 a^{-1} km^{-1} (rift) is similar to the figure of 1.33×10^{-3} km^3 a^{-1} km^{-1} (rift) estimated for the thick seaward-dipping reflector sequences that were produced later, around 56–53 Ma, on the SE Greenland continental margin (Larsen & Saunders 1998). This rate is an order of magnitude higher than the production rate at the present site of the Iceland mantle plume (Pálmason 1981).

Despite the high magma production rates, the total amount of magma produced per year in West Greenland was small because of the limited area of eruption (small hypothetical rift length). Our estimated magma production for the known parts of the C27n–C26r transition zone is a minimum of 0.042 km^3 a^{-1}. The magma production for the whole Baffin Bay region at that time is difficult to estimate. Rocks of the transition zone may be present below sea level on Ubekendt Ejland (Fig. 1), but this is not known. The small lava and hyaloclastite succession on Baffin Island (Clarke & Upton 1971) is normally magnetized (Deutsch *et al.* 1971) and is most likely a time equivalent to the Anaanaa Member of the Vaigat Formation; hence it is older than the magnetic polarity transition zone. Until positive evidence for widespread early Vaigat Formation volcanism offshore West Greenland appears from geophysical data or from oil exploration drilling, the best estimate of the total magma production in and around West Greenland at the C27n–C26r transition is less than 0.1 km^3 a^{-1}. This is considerably less than the rate of eruption later in the history of the NAIP during and after the break-up between Greenland and Europe: for the time interval 57.5–54.5 Ma, Eldholm & Grue (1994) estimated a total production of 2.4 km^3 a^{-1}.

Altogether, a clearer picture is emerging of the early phases of volcanism in West Greenland. We envisage a small but vigorous and rapidly expanding volcanic province developing in a sedimentary basin undergoing extension and rapid subsidence contemporaneously with the progression of the volcanic fronts. With a volcanic productivity comparable to the activity of the present-day Kilauea volcano, the volcanic activity within a timespan of a few tens of ka gave rise to the most substantial palaeo-geographical changes within the Nuussuaq Basin witnessed over its 90 million years of existence.

We are grateful to Ole Mærsk-Møller at the Technical University of Denmark for technical support during the photogrammetrical work. The Geological Survey of Denmark and Greenland's expedition leaders Flemming G. Christiansen and Feiko Kalsbeek provided extensive support during field work in Greenland. Constructive criticism by Chris Pulvertaft and by reviewers Brian Bell and Henry Emeleus are gratefully acknowledged. This paper is published with permission from the Geological Survey of Denmark and Greenland.

References

ATHAVALE, R. N. & SHARMA, P. V. 1975. Paleomagnetic results on Early Tertiary lava flows from West Greenland and their bearing on the evolution history of the Baffin Bay–Labrador Sea region. *Canadian Journal of Earth Sciences*, **12**, 1–18.

BOJESEN-KOEFOED, J. A., CHRISTIANSEN, F. G., NYTOFT, H. P. & PEDERSEN, A. K. 1999. Oil seepage onshore West Greenland: evidence of multiple source rocks and oil mixing. *In*: FLEET, A. J. & BOLDY, S. A. R. (eds) *Petroleum Geology of Northwest Europe: Proceedings of the 5th Conference*. Geological Society, London, 305–314.

CANDE, S. C. & KENT, D. V. 1995. Revised calibration of the geomagnetic polarity time scale for the Late Cretaceous and Cenozoic. *Journal of Geophysical Research*, **100B**, 6093–6095.

CHALMERS, J. A., LARSEN, L. M. & PEDERSEN, A. K. 1995. Widespread Palaeocene volcanism around the northern North Atlantic and Labrador Sea – evidence for a large, hot, early plume head. *Journal of the Geological Society, London*, **152**, 965–969.

CHALMERS, J. A., PULVERTAFT, T. C. R., MARCUSSEN, C. & PEDERSEN, A. K. 1999. New insight into the structure of the Nuussuaq Basin, central West Greenland. *Marine and Petroleum Geology*, **16**, 197–224.

CHRISTIANSEN, F. G., DAM, G. & PEDERSEN, A. K. 1994. Discovery of live oil at Marraat, Nuussuaq, West Greenland – field work, drilling and logging. *Rapport Grønlands Geologiske Undersøgelse*, **160**, 57–63.

CHRISTIANSEN, F. G., MARCUSSEN, C. & CHALMERS, J. A. 1995. Geophysical and petroleum geological activities in the Nuussuaq – Svartenhuk Halvø area 1994: promising results for an onshore exploration potential. *Rapport Grønlands Geologiske Undersøgelse*, **165**, 32–41.

CHRISTIANSEN, F. G., BOESEN, A., BOJESEN-KOEFOED, J. A., CHALMERS, J. A., DALHOFF, F., DAM, G., HJORTKJÆR, B. F., KRISTENSEN, L., LARSEN, L. M., MARCUSSEN, C., MATHIESEN, A., NØHR-HANSEN, H., PEDERSEN, A. K., PEDERSEN, G. K., PULVERTAFT, T. C. R., SKAARUP, N. & SØNDERHOLM, M. 1999. Petroleum geological activities in West Greenland in 1998. *Geology of Greenland Survey Bulletin*, **183**, 46–56.

CLARKE, D. B. & PEDERSEN, A. K. 1976. Tertiary volcanic province of West Greenland. *In*: ESCHER, A. & WATT, W. S. (eds) *Geology of Greenland*. Geological Survey of Greenland, Copenhagen, 364–385.

CLARKE, D. B. & UPTON, B. G. J. 1971. Tertiary basalts of Baffin Bay: field relations and tectonic setting. *Canadian Journal of Earth Sciences*, **8**, 248–258.

COE, R. S., HONGRE, L. & GLATZMAIER, G. A. 2000. An examination of simulated geomagnetic reversals from a palaeomagnetic perspective. *Philosophical Transactions of the Royal Society of London*, A, **358**, 1141–1170.

DAM, G. 1996. Sedimentology of the GANE#1 and GANE#1A cores drilled by grønArctic Energy Inc., Equalulik, Nuussuaq, West Greenland. *Danmarks og Grønlands Geologiske Undersøgelse Rapport* **1996/82**.

DAM, G. & SØNDERHOLM, M. 1994. Lowstand slope channels of the Itilli succession (Maastrichtian–Lower Paleocene), Nuussuaq, West Greenland. *Sedimentary Geology*, **94**, 49–71.

DAM, G. & SØNDERHOLM, M. 1998. Sedimentological evolution of a fault-controlled Early Paleocene incised valley system, Nuussuaq Basin, West Greenland. *In*: SHANLEY, K. W. & MCCABE, P. J. (eds) *Relative role of eustacy, climate, and tectonism in continental rocks*. Society of Economic Palaeontologists and Mineralogists, Special Publications, **59**, 109–121.

DAM, G., LARSEN, M. & SØNDERHOLM, M. 1998. Sedimentary response to mantle plumes: implications from the Paleocene onshore West and East Greenland. *Geology*, **26**, 207–210.

DAM, G., NØHR-HANSEN, H., PEDERSEN, G. K. & SØNDERHOLM, M. 2000. Sedimentary and structural evidence of a new early Campanian rift phase in the Nuussuaq Basin, West Greenland. *Cretaceous Research*, **21**, 127–154.

DENLINGER, R. P. 1997. A dynamic balance between magma supply and eruption rate at Kilauea volcano, Hawaii. *Journal of Geophysical Research*, **102B**, 18 091–18 100.

DEUTSCH, E. R. & KRISTJANSSON, L. G. 1974. Paleomagnetism of Late Cretaceous–Tertiary volcanics from Disko Island, West Greenland. *Geophysical Journal of the Royal Astronomical Society*, **39**, 343–360.

DEUTSCH, E. R., KRISTJANSSON, L. G. & MAY, B. T. 1971. Remanent magnetism of lower Tertiary lavas on Baffin Island. *Canadian Journal of Earth Sciences*, **8**, 1542–1552.

DUEHOLM, K. S. 1992. Geologic photogrammetry using standard small-frame cameras. *Rapport Grønlands Geologiske Undersøgelse*, **156**, 7–17.

DUEHOLM, K. S., GARDE, A. A. & PEDERSEN, A. K. 1993. Preparation of accurate geological and structural maps, cross-sections and block diagrams from colour slides, using multimodel photogrammetry. *Journal of Structural Geology*, **15**, 933–937.

ELDHOLM, O. & GRUE, K. 1994. North Atlantic volcanic margins: dimensions and production rates. *Journal of Geophysical Research*, **99B**, 2955–2968.

HALD, N. 1977. Normally magnetized lower Tertiary lavas on Nûgssuaq, central West Greenland. *Rapport Grønlands Geologiske Undersøgelse*, **79**, 5–7.

HAQ, B. U., HARDENBOL, J. & VAIL, P. R. 1987. Chronology of fluctuating sea levels since the Triassic. *Science*, **235**, 1156–1166.

HENDERSON, G. 1975. Stratigraphy and structure of the Tertiary volcanic rocks of the Marrait Kitlît area, Nûgssuaq. *Rapport Grønlands Geologiske Undersogelse*, **69**, 11–16.

HENDERSON, G., ROSENKRANTZ, A. & SCHIENER, E. J. 1976. Cretaceous–Tertiary sedimentary rocks of West Greenland. *In*: ESCHER, A. & WATT, W. S. (eds) *Geology of Greenland*. Geological Survey of Greenland, Copenhagen, 340–362.

HENDERSON, G., SCHIENER, E. J., RISUM, J. B., CROXTON, C. A. & ANDERSEN, B. B. 1981. The West Greenland Basin. *In*: KERR, J. W. (ed.) *Geology of the North Atlantic Borderlands*. Canadian Society of Petroleum Geologists, Memoirs, **7**, 399–428.

HOLM, P. M., GILL, R. C. O., PEDERSEN, A. K., LARSEN, J. G., HALD, N., NIELSEN, T. F. D. & THIRLWALL, M. F. 1993. The Tertiary picrites of West Greenland: contributions from 'Icelandic' and other sources. *Earth and Planetary Science Letters*, **115**, 227–244.

KOCH, B. E. 1963. Fossil plants from the Lower Paleocene of the Agatdalen (Angmârtussut) area, central Nûgssuaq peninsula, northwest Greenland. *Bulletin Grønlands Geologiske Undersøgelse*, **38** (also *Meddelelser om Grønland* **172**, 5).

LARSEN, H. C. & SAUNDERS, A. D. 1998. Tectonism and volcanism at the Southeast Greenland rifted margin: a record of plume impact and later continental rupture. *In:* SAUNDERS, A. D., LARSEN, H. C. & WISE, S. H. (eds) *Proceedings of the Ocean Drilling Program, Scientific Results*, College Station, TX (Ocean Drilling Program), **152**, 503–534.

LARSEN, L. M. & PEDERSEN, A. K. 1997: The volcanic succession in the West Greenland drill holes GANE-1 and GANK-1, with notes on trapped hydrocarbons. *Danmarks og Grønlands Geologiske Undersøgelse Rapport* **1997/120**.

LARSEN, L. M. & PEDERSEN, A. K. 2000. Processes in high-Mg, high-T magmas: evidence from olivine, chromite and glass in Palaeogene picrites from West Greenland. *Journal of Petrology*, **41**, 1071–1098.

LARSEN, L. M., PEDERSEN, A. K., PEDERSEN, G. K. & PIASECKI, S. 1992. Timing and duration of Early Tertiary volcanism in the North Atlantic: new evidence from West Greenland. *In*: STOREY, B. C., ALABASTER, T. & PANKHURST, R. J. (eds) *Magmatism and the Causes of Continental Break-up*. Geological Society, London, Special Publications, **68**, 321–333.

MANKINEN, E. A., PRÉVOT, M., GROMMÉ, C. S. & COE, R. S. 1985. The Steens Mountain (Oregon) geomagnetic polarity transition. 1. Directional history, duration of episodes, and rock magnetism. *Journal of Geophysical Research*, **90B**, 10 393–10 416.

MERRILL, R. T. & MCFADDEN, P. L. 1999. Geomagnetic polarity transitions. *Reviews of Geophysics*, **37**, 201–226.

NEAL, J. E. 1996. A summary of Palaeogene sequence stratigraphy in northwest Europe and the North Sea. *In*: KNOX, R. W. O'B., CORFIELD, R. M. & DUNAY, R. E. (eds) *Correlation of the Early Paleogene in Northwest Europe*. Geological Society, London, Special Publications, **101**, 15–42.

NØHR-HANSEN, H., SHELDON, E. & DAM, G. [this volume]. Biostratigraphic dating and sedimentary evolution preluding the early Palaeocene volcanism in central West Greenland. *In*: JOLLEY, D. W. & BELL, B. R. (eds) *The North Atlantic Igneous Province: Stratigraphy, tectonics, volcanic and magmatic processes*. Geological Society, London, Special Publications, **197**, 111–156.

PÁLMASON, G. 1981. Crustal rifting, and related thermo-mechanical processes in the lithosphere beneath Iceland. *Geologische Rundschau*, **70**, 244–260.

PEDERSEN, A. K. 1985*a*. *Lithostratigraphy of the Tertiary Vaigat Formation on Disko, central West Greenland*. Rapport Grønlands Geologiske Undersøgelse, **124**.

PEDERSEN, A. K. 1985*b*. Reaction between picrite magma and continental crust: early Tertiary silicic basalts and magnesian andesites from Disko, West Greenland. *Bulletin Gronlands Geologiske Undersøgelse*, **152**.

PEDERSEN, A. K. & DUEHOLM, K. S. 1992. New methods for the geological analysis of Tertiary volcanic formations on Nuussuaq and Disko, central West Greenland, using multi-model photogrammetry. *Rapport Grønlands Geologiske Undersøgelse*, **156**, 19–34.

PEDERSEN, A. K., LARSEN, L. M. & DUEHOLM, K. S. 1993. *Geological section along the south coast of Nuussuaq, central West Greenland.* 1:20 000 Coloured Geological Sheet. Geological Survey of Greenland, Copenhagen.

PEDERSEN, A. K., LARSEN, L. M., PEDERSEN, G. K. & DUEHOLM, K. S. 1996. Filling and plugging of a marine basin by volcanic rocks: the Tunoqqu Member of the Lower Tertiary Vaigat Formation on Nuussuaq, central West Greenland. *Bulletin Grønlands Geologiske Undersøgelse*, **171**, 5–28.

PEDERSEN, G. K. & PULVERTAFT, T. C. R. 1992. The non-marine Cretaceous of the West Greenland Basin, onshore West Greenland. *Cretaceous Research*, **13**, 263–272.

PEDERSEN, G. K., LARSEN, L. M., PEDERSEN, A. K. & HJORTKJÆR, B. F. 1998: The synvolcanic Naajaat lake, Paleocene of West Greenland. *Palaeogeography, Palaeoclimatology, Palaeoecology*, **140**, 271–287.

PIASECKI, S., LARSEN, L. M., PEDERSEN, A. K. & PEDERSEN, G. K. 1992. Palynostratigraphy of the Lower Tertiary volcanics and marine clastic sediments in the southern part of the West Greenland Basin: Implications for the timing and duration of the volcanism. *Rapport Grønlands Geologiske Undersøgelse*, **154**, 13–31.

REYNOLDS, D. J., STECKLER, M. S. & COAKLEY, B. J. 1991. The role of the sediment load in sequence stratigraphy: the influence of flexural isostacy and compaction. *Journal of Geophysical Research*, **96B**, 6931–6949.

RIISAGER, J., RIISAGER, P. & PERRIN, M. 1999. Palaeodirectional and palaeointensity results of Paleocene and Eocene basalts from West Greenland. *Bulletin of the Geological Society of Denmark*, **46**, 69–78.

RIISAGER, P. & ABRAHAMSEN, N. 1999. Magnetostratigraphy of Palaeocene basalts from the Vaigat Formation of West Greenland. *Geophysical Journal International*, **137**, 774–782.

RIISAGER, P. & ABRAHAMSEN, N. 2000. Palaeointensity of West Greenland Palaeocene basalts: asymmetric intensity around the C27n–C26r transition. *Physics of the Earth and Planetary Interiors*, **118**, 53–64.

ROSENKRANTZ, A. & PULVERTAFT, T. C. R. 1969. Cretaceous–Tertiary stratigraphy and tectonics in northern West Greenland. *Memoir of the American Association of Petroleum Geologists*, **12**, 883–898.

SAUNDERS, A. D., FITTON, J. G., KERR, A. C., NORRY, M. J. & KENT, R. W. 1997. The North Atlantic Igneous Province. *In*: MAHONEY, J. J. & COFFIN, M. L. (eds) *Large Igneous Provinces.* American Geophysical Union, Washington, Geophysical Monograph, **100**, 45–93.

SINGER, C. W. & PRINGLE, M. S. 1996. Age and duration of the Matuyama-Bruhnes geomagnetic polarity reversal from $^{40}Ar/^{39}Ar$ incremental heating analysis of lavas. *Earth and Planetary Science Letters*, **139**, 47–61.

STOREY, M., DUNCAN, R. A., PEDERSEN, A. K., LARSEN, L. M. & LARSEN, H. C. 1998. $^{40}Ar/^{39}Ar$ geochronology of the West Greenland Tertiary volcanic province. *Earth and Planetary Science Letters*, **160**, 569–586.

SWANSON, D. E. 1972. Magma supply rate at Kilauea Volcano 1952–1971. *Science*, **175**, 169–170.

This page intentionally left blank

Volcanic stratigraphy of the southern Prinsen af Wales Bjerge region, East Greenland

H. HANSEN [1,2], A. K. PEDERSEN[1,3], R. A. DUNCAN [4], D. K. BIRD[5], C. K. BROOKS[1,6], J. J. FAWCETT[7], J. GITTINS[7], M. GORTON[7] & P. O'DAY[8]

[1] *Danish Lithosphere Centre, Øster Voldgade 10, DK-1350 Copenhagen K, Denmark*
[2] *Presently at: Geological Survey of Denmark and Greenland, Department of Geological Mapping, Øster Voldgade 10, DK-1350 Copenhagen K, Denmark (e-mail: hh@geus.dk)*
[3] *Geological Museum, Øster Voldgade 5–7, DK-1350 Copenhagen K, Denmark*
[4] *College of Oceanic and Atmospheric Sciences, Oregon State University, Corvallis, OR 97331, USA*
[5] *Department of Geological and Environmental Sciences, Stanford University, Stanford, CA 94305–2115, USA*
[6] *Geological Institute, University of Copenhagen, Øster Voldgade 10, DK-1350 Copenhagen K, Denmark*
[7] *Department of Geology, University of Toronto, 22 Russell St., Toronto, M5S 3B1, Ontario, Canada*
[8] *Department of Geological Sciences, Arizona State University, Tempe, AZ 85287–1404, USA. Presently at: Lawrence Livermore National Laboratory, L-219, PO Box 808, Livermore, CA 94550, USA*

Abstract: The volcanic succession in the inland Prinsen af Wales Bjerge contains the oldest known onshore lava flows (61 Ma) of the Palaeogene East Greenland flood basalt province. These flows and interbedded sediments define the Urbjerget Formation and are found in the southernmost part of Prinsen af Wales Bjerge. Flows of the Urbjerget Formation are chemically similar to the coastal Vandfaldsdalen Formation flows and the two formations may be chronostratigraphical equivalents. The Urbjerget Formation is overlain by the <57 Ma tholeiitic basalts of the Milne Land Formation. Four regional volcanic formations are found along the Blosseville Kyst, but the Milne Land Formation is the only one present in the southern Prinsen af Wales Bjerge. Flows of the absent formations (Geikie Plateau, Rømer Fjord and Skrænterne formations) may not have been able to enter the area due to local uplift, more distal located eruption sites or possibly topographic features. A high-Si ($SiO_2 > 52$ wt%) lava flow succession in the Milne Land Formation consists of crustally contaminated magmas which were arrested in crustal chambers as the magma supply rate from the mantle decreased, either due to a

From: JOLLEY, D. W. & BELL, B. R. (eds) *The North Atlantic Igneous Province: Stratigraphy, Tectonic, Volcanic and Magmatic Processes*. Geological Society, London, Special Publications, **197**, 183–218. 0305-8719/02/$15.00

general lowering of potential mantle temperatures or a decrease in the rate of continental rifting. Tholeiitic high-Ti flows (MgO: 10–15 wt%, TiO_2: 5–6 wt%) within the Milne Land Formation are unique to the Prinsen af Wales Bjerge region, and equivalents have not been reported from other flood basalt provinces. Local flow composition variations in the Milne Land Formation can be explained as the result of melting under lithosphere of variable thickness, small-scale variations in mantle composition and mixing in small magma chambers. Unconformably overlying the Milne Land Formation is a succession of *c.* 53 Ma alkaline flows, known as the Prinsen af Wales Bjerge Formation. Several crater sites are known from this flow succession and this suggests that the Prinsen af Wales Formation was only covered locally by later volcanic or sedimentary units. The duration of alkaline volcanic activity in the Prinsen af Wales Bjerge is not well constrained but may have been less than 2.5 Ma. The hiatus between the Urbjerget and Milne Land formations is a regional feature in the North Atlantic as it occurs at a similar stratigraphic level at Nansen Fjord, the Faroe Islands and in the ODP Leg 152 volcanic succession off SE Greenland at *c.* 63°N. It represents a 3–4 Ma long cessation of, or very low frequency of activity in East Greenland/Faroese volcanism and may be explained as the time interval between two pulses in the palaeo-Icelandic plume.

Palaeogene flood basalts are the dominant geological feature of the central East Greenland Blosseville Kyst between *c.* 68° and 70°N (Fig. 1). Geographically the basalts cover an area of *c.* 65 000 km^2 (Pedersen *et al.* 1997), which make them the largest onshore outcrop of Palaeogene flood basalts in the North Atlantic region. The North Atlantic flood basalts are interpreted as the result of palaeo-Icelandic plume activity beneath the rifting Pangaean continent (e.g. Brooks 1973; White & McKenzie 1989; Saunders *et al.* 1997). The increase in potential mantle temperatures caused by presence of the plume led to increased mantle melting and the production of large amounts of mainly tholeiitic basalts with smaller volumes of alkaline volcanics. The distribution of alkaline volcanics relative to tholeiites seems to have been controlled by position relative to the rift axis, lithosphere thickness and the presence of alkali-metal and incompatible element-enriched mantle domains. In East Greenland, the largest volume of alkaline basalts is present in the inland region of Prinsen af Wales Bjerge (Fig. 1). They were formed at a time (*c.* 52 Ma) when active rifting, plate separation and tholeiitic volcanic activity were concentrated close to or off the present coastline of East Greenland (e.g. Larsen & Watt 1985; Brown *et al.* 1996; Storey *et al.* 1996*a*). We also show that some of the first Palaeogene volcanics erupted in East Greenland, and in the North Atlantic region, are present in Prinsen af Wales Bjerge region.

In this paper we present the first formalized volcanic stratigraphy for the southernmost part of the Prinsen af Wales Bjerge region from Urbjerget in the south to 1982 Nunatak in the north (Fig. 2). This is possible through the mapping technique of multimodel photogrammetry (Dueholm & Pedersen 1992) as a basis for determining sampling sites of new lava sections and relating them to previously sampled sections (Hogg *et al.* 1988; Hogg *et al.* 1989; Brooks *et al.* 1996; Hansen *et al.* 1998). By combining photogrammetrical observations with field observations and petrographical, geochemical and geochronological data we have been able to compile the results into a stratigraphic model consistent with that of other Blosseville Kyst flood basalts (Nielsen *et al.* 1981; Larsen *et al.* 1989; Pedersen *et al.* 1997; Larsen *et al.* 1999).

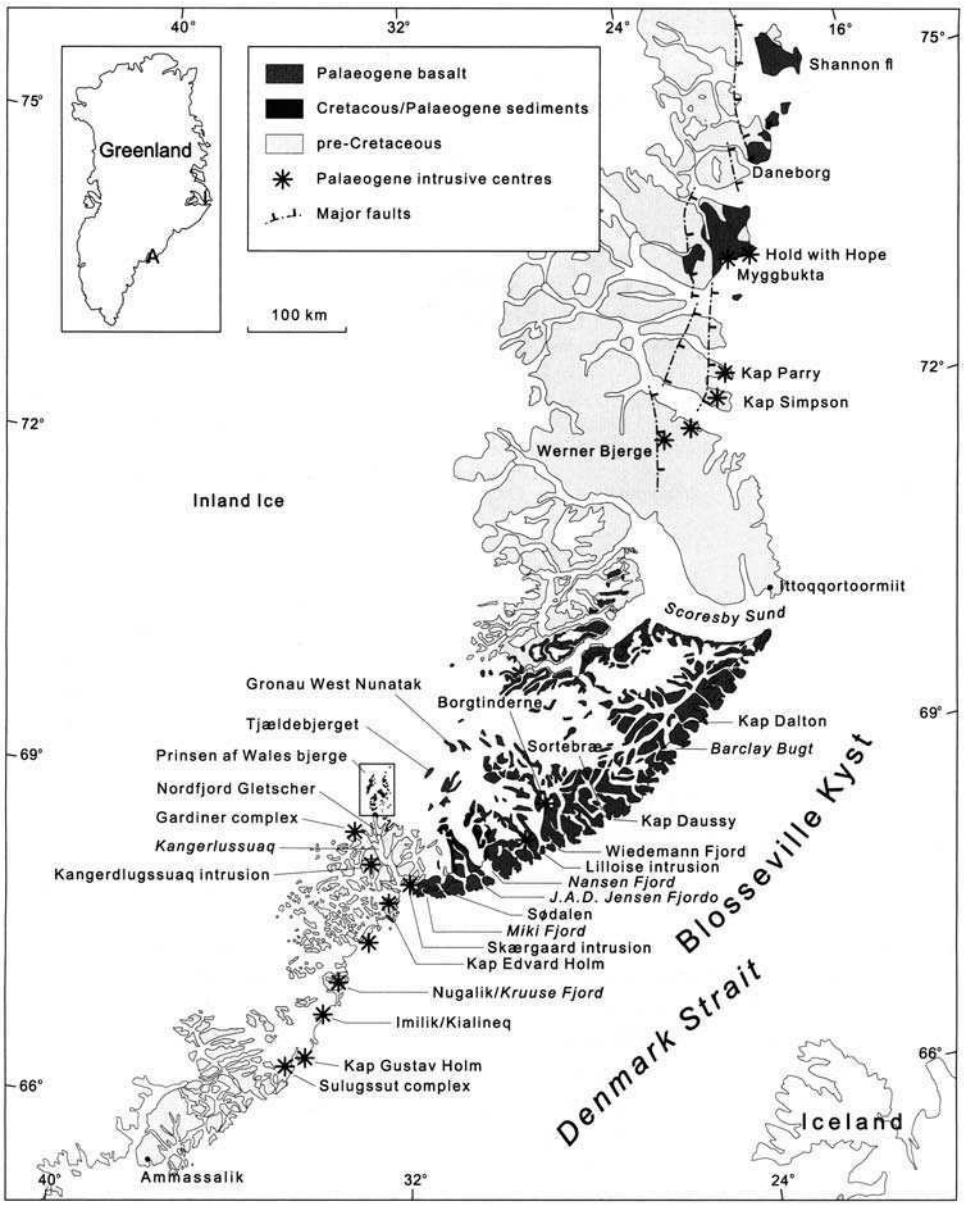

Fig. 1. Map of East Greenland flood basalts. A, Ammassalik; I, Ittoqortoormiit.

Geological and geochronological review of the East Greenland flood basalts

The East Greenland flood basalts were formed as a response to the continental rifting and break-up that lead to the formation of the North Atlantic Ocean. They are closely associated with other igneous activity in the form of dyke, sill and

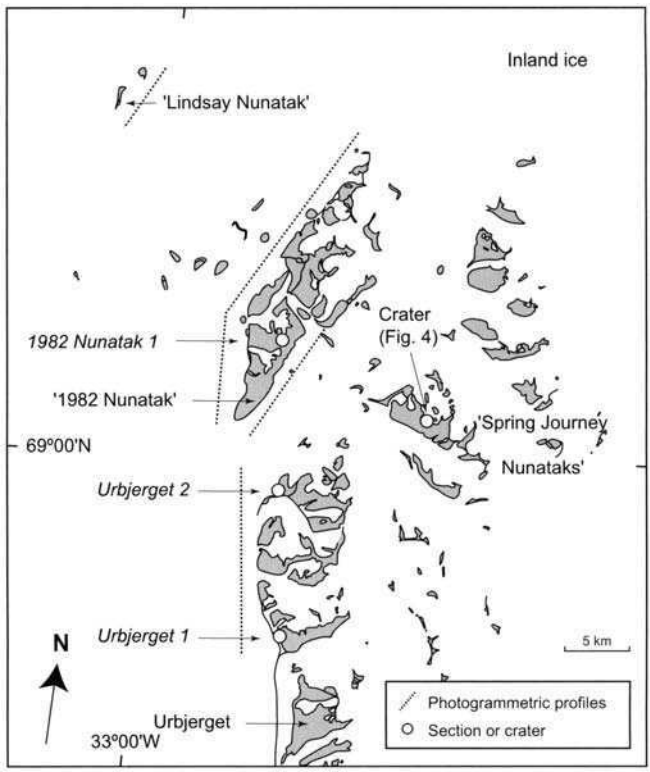

Fig. 2. Exposure map of the Prinsen af Wales Bjerge. Grey, basalt; White, inland ice. Profile names are in italics, place names in regular font. Unofficial place names are in citation marks.

plutonic intrusions, and numerous fault systems related to the evolution of the continental margin (e.g. Karson & Brooks 1999). Age determinations of the flood basalts are summarized in Figure 3. The volcanism occurred in three major phases according to Storey *et al.* (1996*a*) and Tegner *et al.* (1998*a*). Early volcanic rocks were emplaced before 58 Ma, the plateau basalts representing the largest volume of basalts between 56 and 54.5 Ma, and late volcanics mainly later than 54 Ma. The term 'plateau basalts' in this paper is used only as a collective term for the Milne Land, Geikie Plateau, Rømer Fjord and Skrænterne formations (Fig. 3). In the Blosseville Kyst area, the age of the earliest volcanism has not previously been well constrained, but Tegner *et al.* (1998*a*) assumed it to be at approximately 62 Ma. This is the age of early Palaeogene volcanism off the SE Greenland coast (Sinton & Duncan 1998), in West Greenland (Storey *et al.* 1998) and in the British Isles (e.g. Pearson *et al.* 1996). Tegner *et al.* (1998*a*) suggested that the main igneous activity in the third phase took place between 50 and 47 Ma where it was characterized by dyke and pluton intrusions, but at least some volcanism took place later in the Miocene (Storey *et al.* 1996*b*). Saunders *et al.* (1997) suggested that North Atlantic basalts were formed in a two-stage process, the first lasting from 62 to 58 Ma and the second from 56 Ma to the present time. In accordance with Storey *et al.* (1996*a*), Saunders *et al.* (1997) explained the onset of Palaeogene igneous activity as a possible result of

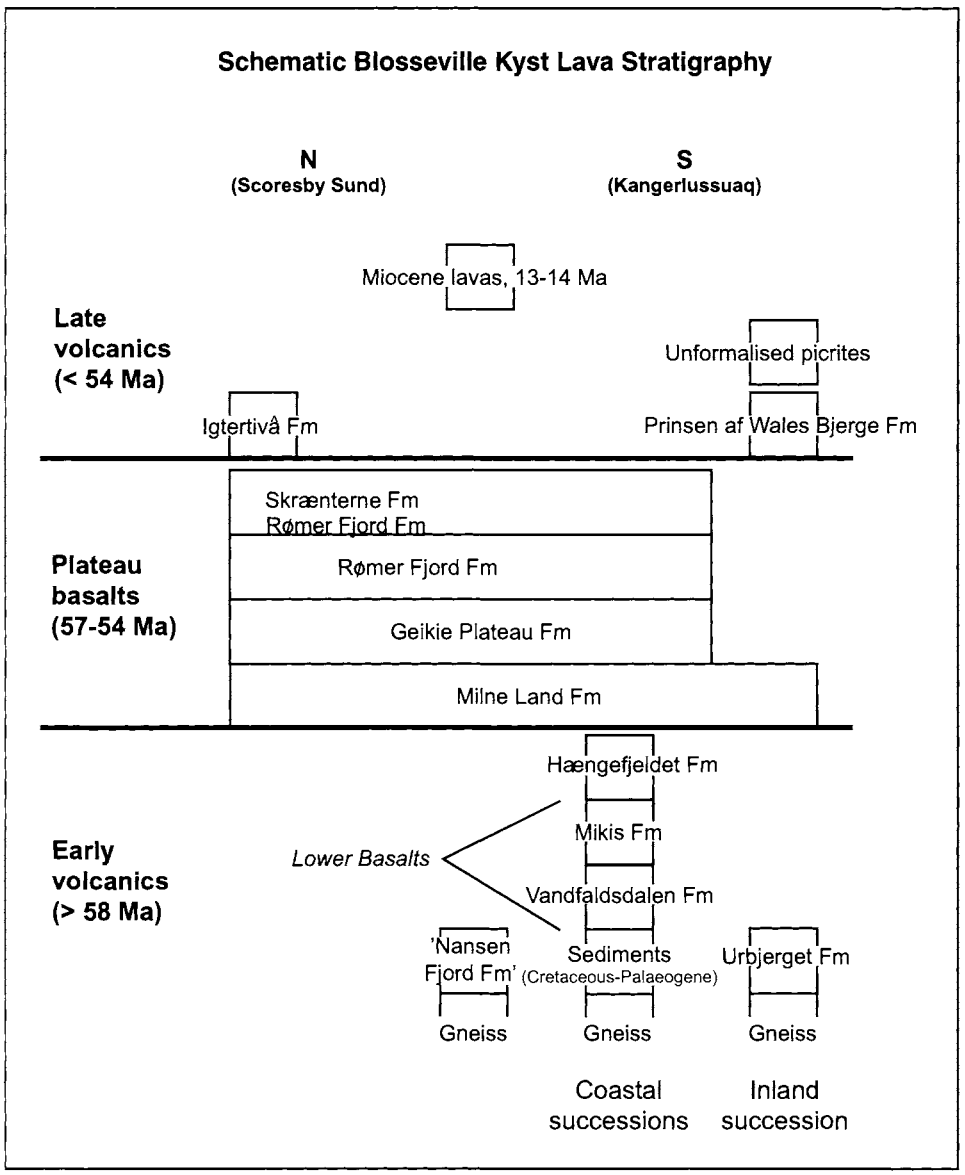

Fig. 3. Volcanic stratigraphy of Blosseville Kyst basalts with data sources in Nielsen *et al.* (1981), Larsen *et al.* (1989), Pedersen *et al.* (1997), Larsen *et al.* (1999). Lava ages from Hansen *et al.* (1995), Storey *et al.* (1996*a*, *b*), Tegner *et al.* (1998*a*), Heister *et al.* (2001) and this study. The Magga Dan Formation of Larsen *et al.* (1989) has been reassigned to the Milne Land Formation (L. M. Larsen pers. comm.). The Urbjerget and Prinsen af Wales Bjerge formations are formalized in this paper, and the Nansen Fjord Formation is not formalized (Larsen *et al.* 1999). Gneiss basement near Kangerlussuaq is probably Archaean (*c.* 2.9 Ga), but was reworked in the Proterozoic (Taylor *et al.* 1992).

mantle plume impact beneath the Pangaean continent at around 62–61 Ma. This is supported by Tegner *et al.* (1998*a*), who interpreted the final two phases of East Greenland igneous activity as reflections of continental break-up and passage of the plume axis beneath the East Greenland margin, respectively.

An overview of the stratigraphy of the central East Greenland Palaeogene flood basalts is also shown in Figure 3. The early volcanics are only exposed in the south-western part of the Blosseville Kyst (Nielsen *et al.* 1981; Larsen *et al.* 1999), roughly between Nansen Fjord and Kangerlussuaq (Fig. 1), and in the Prinsen af Wales Bjerge (this study). The individual formations of the early volcanics are of a relatively limited volumetric and geographic extent compared with the Milne Land, Geikie Plateau, Rømer Fjord and Skrænterne formations of the plateau basalts (Larsen *et al.* 1989; Pedersen *et al.* 1997) (Fig. 3). In the northern area at Kap Dalton (Fig. 1), the plateau basalts are downfaulted and overlain by lavas and tuffs of the Igtertivâ Formation (Larsen *et al.* 1989). In the Prinsen af Wales Bjerge (Fig. 1), alkaline lavas overly the plateau basalts (Wager 1947; Anwar 1955; Hogg 1985; Brown *et al.* 1996; Brooks *et al.* 1996), but the modern (i.e. post-1989) East Greenland flood basalt stratigraphy has not included the Prinsen af Wales Bjerge region. This is mainly because the region consists of scattered outcrops in discrete nunataks that can only be accessed with difficulty. In the southeastern part of Prinsen af Wales Bjerge, Wager (1947) observed two main volcanic suites overlying the metamorphic continental basement: a lower suite of near-horizontal basalt flows, and an upper suite of variably dipping flows, 'The Prinsen af Wales Bjerge Basalts'. The former was associated with the regional plateau basalt succession which dominates the Blosseville Kyst between Kangerlussuaq and Scoresby Sund, the latter with near-vent local volcanism in the Prinsen af Wales Bjerge. Hogg (1985) and Brooks *et al.* (1996) made similar field observations at more westerly locations in the Prinsen af Wales Bjerge, although Brooks *et al.* (1996) suggested that some of the variable dips of 'The Prinsen af Wales Bjerge Basalts' could be due to topographical effects such as draping of the margins of palaeo-river valleys cut into the top of the plateau basalts. Anwar (1955), Hogg (1985) and Brown *et al.* (1996) showed that 'The Prinsen af Wales Bjerge Basalts' are alkaline, whereas the basalts underneath are tholeiitic (Hogg 1985; Hogg *et al.* 1988, 1989).

We present data that enables us to formalize Wager's (1947) 'Prinsen af Wales Bjerge Basalts' to formation status, the Prinsen af Wales Bjerge Formation (Fig. 3). Our new data confirm that most of the near-horizontal basalt flows are related to the 'plateau basalts', more specifically the Milne Land Formation (Fig. 3). We also show that the lowermost part of volcanics in the Prinsen af Wales Bjerge (Urbjerget Formation in Fig. 3) are related to the earliest phase of igneous activity in the Palaeogene of East Greenland.

Geology of the southern Prinsen af Wales Bjerge

The general stratigraphical relationships of the rock successions in the Prinsen af Wales Bjerge have previously been described by Wager (1947), Hogg (1985) and Brooks *et al.* (1996). However, in order to study the detailed stratigraphic and geological relations in the southern Prinsen af Wales Bjerge between Urbjerget and the 1982 Nunatak (Fig. 2), a combination of multimodel photogrammetrical analysis and

geochemical/petrographical sampling of lava flows was used in selected sections. This minimizes the inherent difficulties associated with correlation of widely separated nunatak exposures. Multimodel photogrammetrical analysis is based on interpretation of stereo-photographs of mountainsides taken from Twin Otter airplanes, and details of the method were presented by Dueholm & Pedersen (1992) and Pedersen *et al.* (1997). The photogrammetric lines interpreted in this paper are shown in Figure 2, which also shows the locations of the three sections (Urbjerget 1, Urbjerget 2 and 1982 Nunatak 1) sampled for geochemistry/petrography at Urbjerget and the 1982 Nunatak. Photographs of two of the sections and a crater site east of 1982 Nunatak are shown in Figure 4, and the sections are displayed schematically in Figure 5.

As reported by Wager (1947), towards the south at Urbjerget (Fig. 2, Fig. 4a), gently northward dipping lava flows (identified here as Urbjerget and Milne Land Formations) overly gneisses, probably of Archaean age (Taylor *et al.* 1992). Farther north, continental basement is no longer exposed, but the lava suite continues its slight northerly dip. At the 1982 Nunatak, two morphological flow suites are found (Fig. 4b). The slightly dipping suite is still present (Milne Land Formation in Fig. 4b), but it is overlain discordantly by the variably dipping lava flows (Prinsen af Wales Bjerge Formation in Fig. 4b), which are equivalents to 'The Prinsen af Wales Bjerge

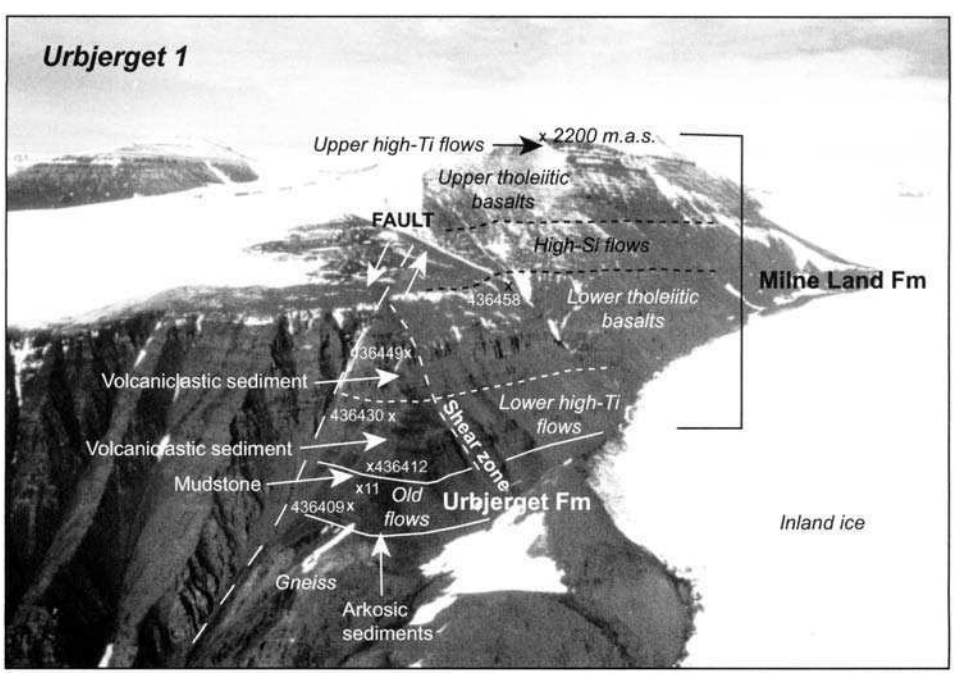

Fig. 4. Photographs of sections (**a**) Urbjerget 1, view towards NE, with the location of dated samples. '11' is an abbreviation of sample no. 436411. (**b**) 1982 Nunatak 1, view towards W, and (**c**) A volcanic crater in the Prinsen af Wales Bjerge Formation. The vertical distance from the flat ground to the peak of the succession of dipping flows in the right side of the photograph is 450 m, and one of the flows has been dated to 52.5 Ma (Peate *et al.* 2000). Locations of sections and crater are marked in Figure 2.

(b)

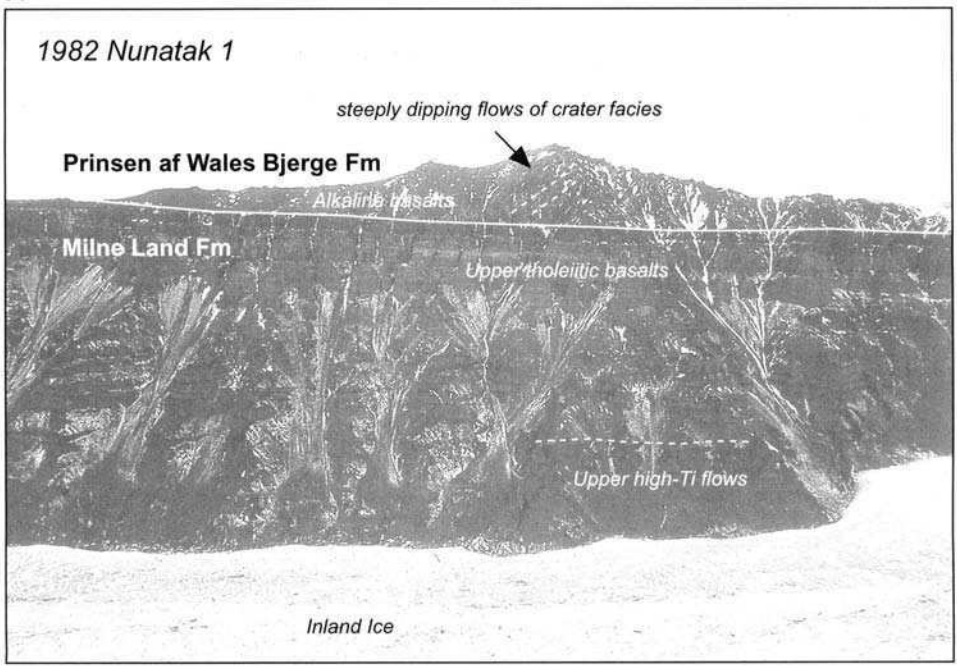

(c)

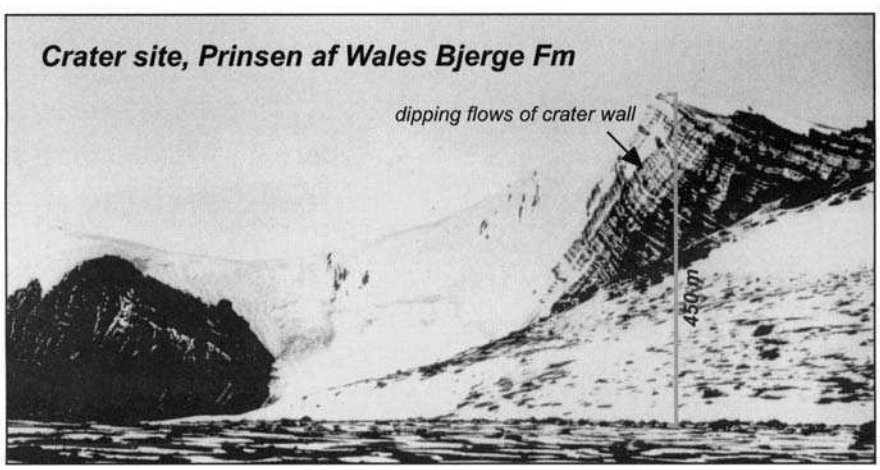

Fig. 4. (*continued*)

Basalts' of Wager (1947). The general structure of the volcanic pile in the region implies that progressively younger flows must be expected when moving from south towards the north. Thus, Urbjerget 1 should contain the oldest part of the succession and 1982 Nunatak 1 the youngest. The Urbjerget and Prinsen af Wales Bjerge formations are formally defined in this paper (see below and Tables 3 & 4), and the presence of the Milne Land Formation in the Prinsen af Wales Bjerge is inferred from the ages, geochemistry and photogrammetrical correlations presented below.

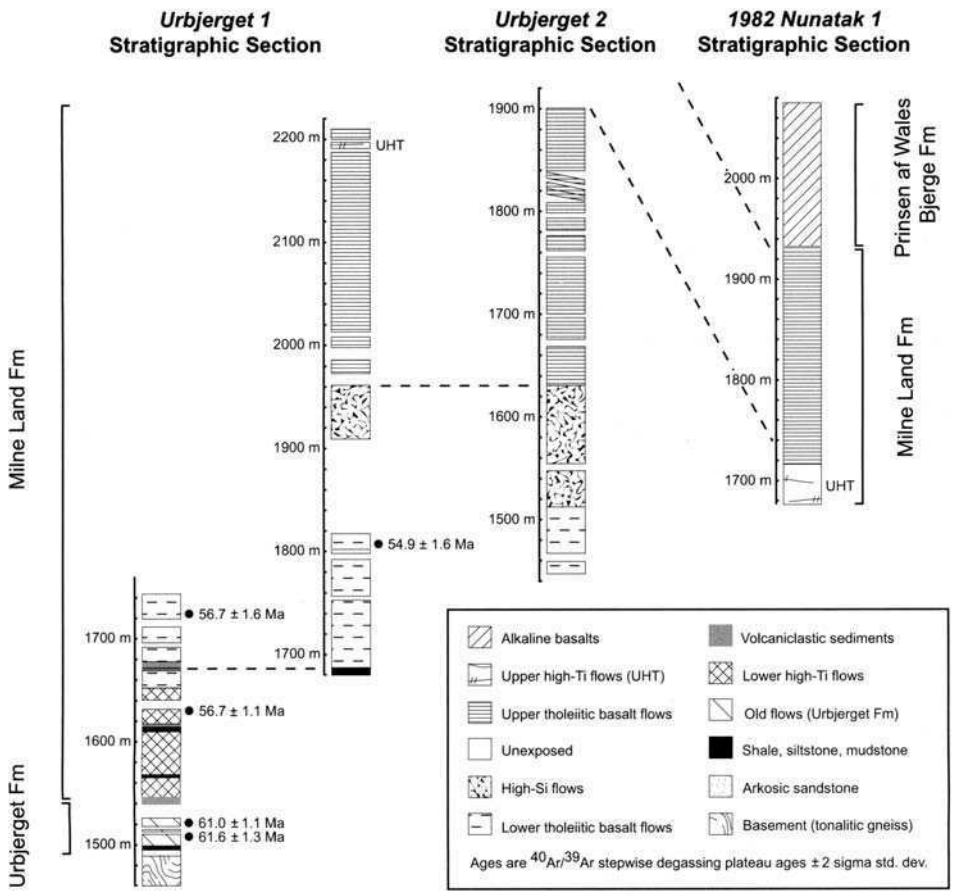

Fig. 5. Stratigraphic sections of Urbjerget 1, Urbjerget 2 and 1982 Nunatak 1 and suggested correlations. Ages with 2σ standard deviations are from Table 1.

There are fewer faults in the Prinsen af Wales Bjerge region than nearer the present-day coast (e.g. Nielsen 1975). An example of this faulting is present at Urbjerget 1 (Fig. 4a). A normal fault with an estimated throw of 450 m cuts through the section in the mid- to left part of the photograph. The faulting most likely took place after emplacement of the whole volcanic succession had taken place.

Many of the steeply and variably dipping flows in the Prinsen af Wales Bjerge are associated with sites of volcanic craters (Wager 1947; Brooks *et al.* 1996). This is the case for the steeply dipping flows at the top of the 1982 Nunatak (Fig. 4b), and Figure 4c shows another example. The field and photogrammetric observations in the northernmost part of Prinsen af Wales Bjerge show that the Prinsen af Wales Bjerge Formation flows in this area tend to have less steep and more uniform dips than in the southern area, reflecting more distal facies relative to exposed eruption sites.

Ages and geochemistry of lavas in the southern Prinsen af Wales Bjerge

$^{40}Ar/^{39}Ar$ ages

Samples from Urbjerget 1 were dated by stepwise $^{40}Ar/^{39}Ar$ degassing method at Oregon State University using AEI MS-10 and MAP 215-50 mass spectrometres for whole rock and plagioclase separates, respectively (Table 1, Fig. 6). The 61.6 ± 1.3 Ma plateau age of sample 436409 from a flow near the base of Urbjerget 1 (Fig. 4a) is the oldest ^{40}Ar–^{39}Ar stepwise degassing age reported from onshore East Greenland lavas (Hansen *et al.* 1995; Storey *et al.* 1996*a*; M. Storey & R. A. Duncan unpubl data). Although the calculated isochron (dashed line in Fig. 6) has an Y-intercept far from the composition of atmospheric argon (near 0.0005 rather than 0.0034), this is mainly due to the highly limited compositional range of plateau steps (black squares in Fig. 6). A slightly less perfectly fitted isochron would intercept the Y-axis in Fig. 6 at or very close to the composition of atmospheric argon ($^{40}Ar/^{36}Ar = 295.5$). Sample 436411 is located above 436409, but still near the base of Urbjerget 1 (Fig. 4a), and its plateau age (61.0 ± 1.1 Ma) is very similar to the age of 436409. Again, the calculated isochron through the plateau steps gives a high value for the initial $^{40}Ar/^{36}Ar$, but the calculated error encompass the value of atmospheric argon. The remaining ages from Urbjerget 1 range between 56.7 and 54.9 ± 1.1 to 1.6 Ma (Table 1, Fig. 4a). These ages are similar to Milne Land Formation age data (Storey *et al.* 1996*a*; Tegner *et al.* 1998*a*; Tegner & Duncan 1999; M. Storey & R. A. Duncan unpubl data).

Geochemistry

Major element compositions were determined on 131 whole rock samples at the Rock Geochemical Laboratory of the Geological Survey of Denmark and Greenland (Kystol & Larsen 1999). Trace element compositions were obtained from inductively coupled mass spectrometry (ICP-MS) on 130 sample solutions prepared using a standard HF-HNO_3 dissolving technique (Turner *et al.* 1999). Sample preparation for ICP-MS analyses took place at Oregon State University, University of Copenhagen,

Table 1. *$^{40}Ar/^{39}Ar$ incremental heating ages for lava flows from the Prinsen af Wales Bjerge region, East Greenland*

Sample no.	Material	Total fusion age (Ma)	Plateau age (Ma ± 2σ)	^{39}Ar % of total	Isochron age (Ma ± 2σ)	MSWD	^{40}Ar-^{36}Ar intercept	J
436409	Plagioclase	65.9	61.59 ± 1.32	69.0	61.19 ± 1.46	1.32	717 ± 325	0.001544
436411	Whole rock	64.1	60.97 ± 1.14	52.0	59.58 ± 1.68	6.95	487 ± 194	0.001618
436412	Whole rock	55.9	56.72 ± 1.01	42.0	None (2-step plateau)			0.001594
436430	Whole rock	64.1	56.74 ± 1.06	57.0	56.93 ± 2.40	2.04	287 ± 92	0.001569
436449	Plagioclase	59.7	56.70 ± 1.65	68.0	56.36 ± 1.77	1.16	316 ± 39	0.001495
436458	Plagioclase	54.8	54.93 ± 1.56	94.0	54.79 ± 2.66	0.62	287 ± 246	0.001579

Ages are reported relative to biotite monitor FCT-3 (28.04 ± 0.12 Ma), which is calibrated against hornblende Mmhb-1 (523.5 Ma, Renne *et al.* 1994). Plateau ages are the mean of concordant step ages, weighted by the inverse of their variances. MSWD is the mean square of weighted deviations and is an F-statistic for the goodness of fit of step ages to the isochron. Calculations use the following decay and reactor interference constants: $\lambda_e = 0.581 \times 10^{-10}\,a^{-1}$, $\lambda_\beta = 4.963 \times 10^{-10}\,a^{-1}$; $(^{36}Ar/^{37}Ar)_{Ca} = 0.000264$, $(^{36}Ar/^{37}Ar)_{Ca} = 0.000673$, $(^{40}Ar/^{39}Ar)_{Ca} = 0.01$. J is the neutron fluence factor, determined from measured monitor $^{40}Ar/^{39}Ar$. Plagioclase separates and whole rock samples were prepared by crushing, sieving and cleaning in deionized water and alcohol. Whole rock samples consisted of 500 μm–2 mm pieces free from secondary alteration, selected by handpicking under a binocular microscope. Plagioclase separates 436449 and 436458 consisted of 500 μm–2 mm plagioclase phenocrysts selected using handpicking under a microscope. 436409 was from the 100–200 μm groundmass plagioclase fraction, magnetically separated and purified by handpicking.

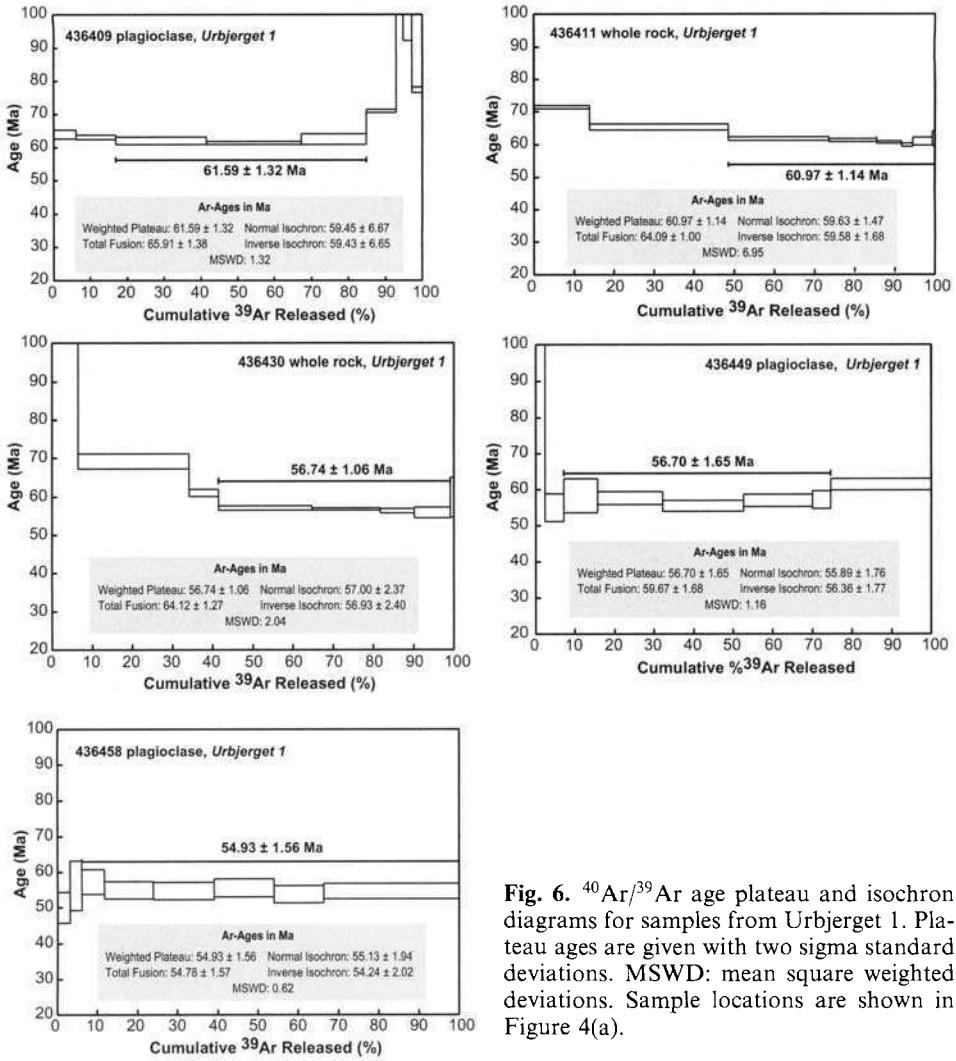

Fig. 6. $^{40}Ar/^{39}Ar$ age plateau and isochron diagrams for samples from Urbjerget 1. Plateau ages are given with two sigma standard deviations. MSWD: mean square weighted deviations. Sample locations are shown in Figure 4(a).

and University of Durham. Samples were analysed at Oregon State University (Pyle *et al.* 1995) and University of Durham (Turner *et al.* 1999). One sample was analysed for trace elements using X-ray fluorescence (XRF) on a pressed sample powder tablet at the Geological Institute, University of Copenhagen (J. Bailey pers. comm.; Norrish & Chappell 1977). Control experiments showed that element concentrations analysed by the XRF and ICP-MS techniques deviate less than 5% for individual samples. Although samples from the 1982 Nunatak have previously been analysed for major and trace element compositions (Hogg 1985; Hogg *et al.* 1989) we reanalysed them using the methods outlined above in order to prevent interlaboratory discrepancies. Representative major and trace element analyses are shown in Table 2, Figure 7 shows some of the major element variations, Figure 8 some trace element ratio variations, and Figure 9 shows trace element spectra normalized to the C1 chondrite of Sun & McDonough (1989).

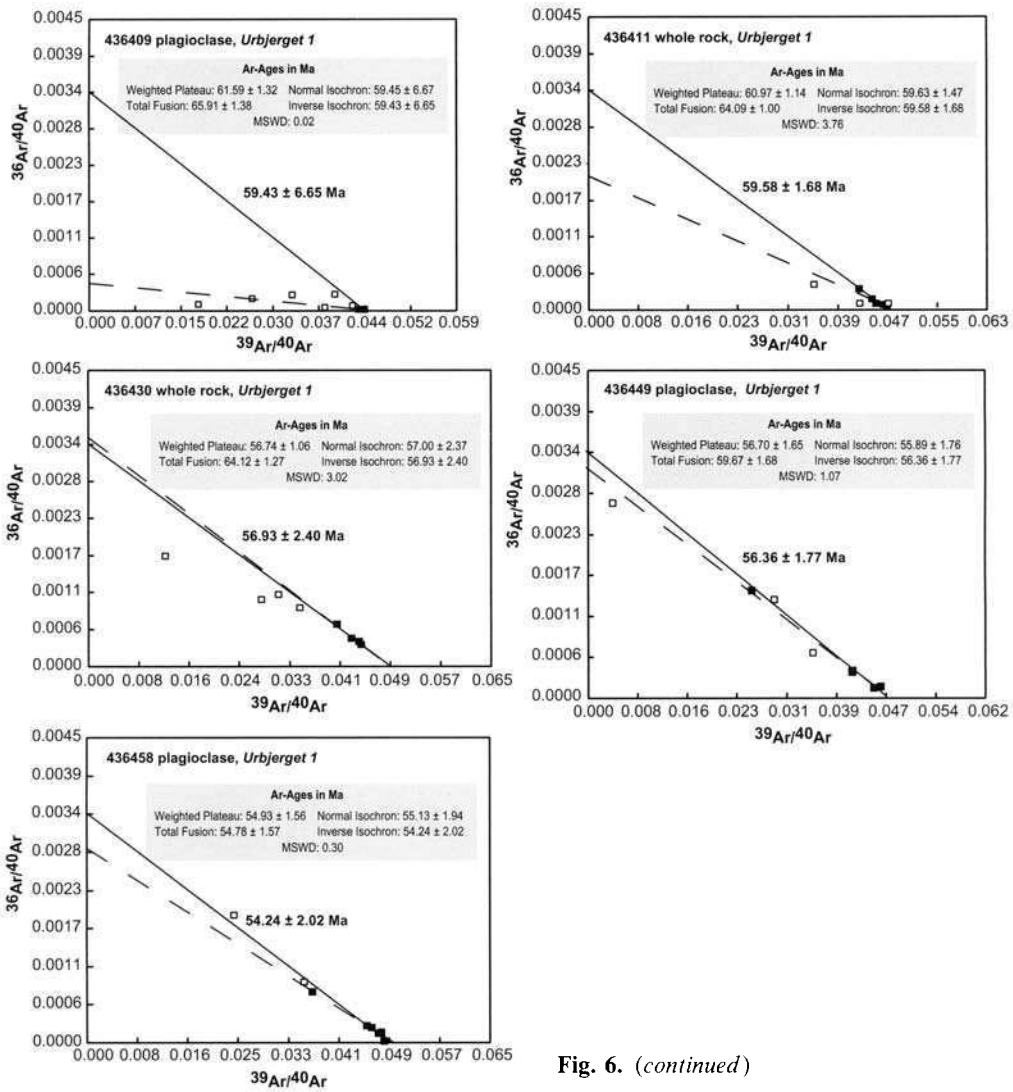

Fig. 6. (*continued*)

$^{87}Sr/^{86}Sr$ isotopic compositions were obtained on 16 samples. Sample powders were cleaned in quartz-distilled water for very finegrained material like clays and zeolites. They were then dissolved and Sr separated following procedures similar to Holm *et al.* (2001). The effect of alteration on Sr-isotopic compositions was evaluated by leaching a couple of very altered flows in 6N HCl following the procedure of Mahoney (1987) before sample dissolution. Analyses were made on the VG5431 mass spectrometre at the Danish Centre for Isotope Geology, University of Copenhagen. $^{87}Sr/^{86}Sr$ compositions of the leached samples were within analytical error of unleached sample values which indicates very little influence from alteration on Sr-isotopic compositions. Results are listed in Table 2.

Fig. 7. Major element variations of flows from the southern Prinsen af Wales Bjerge region. All elements are in weight %. FeO* is all Fe recalculated as FeO.

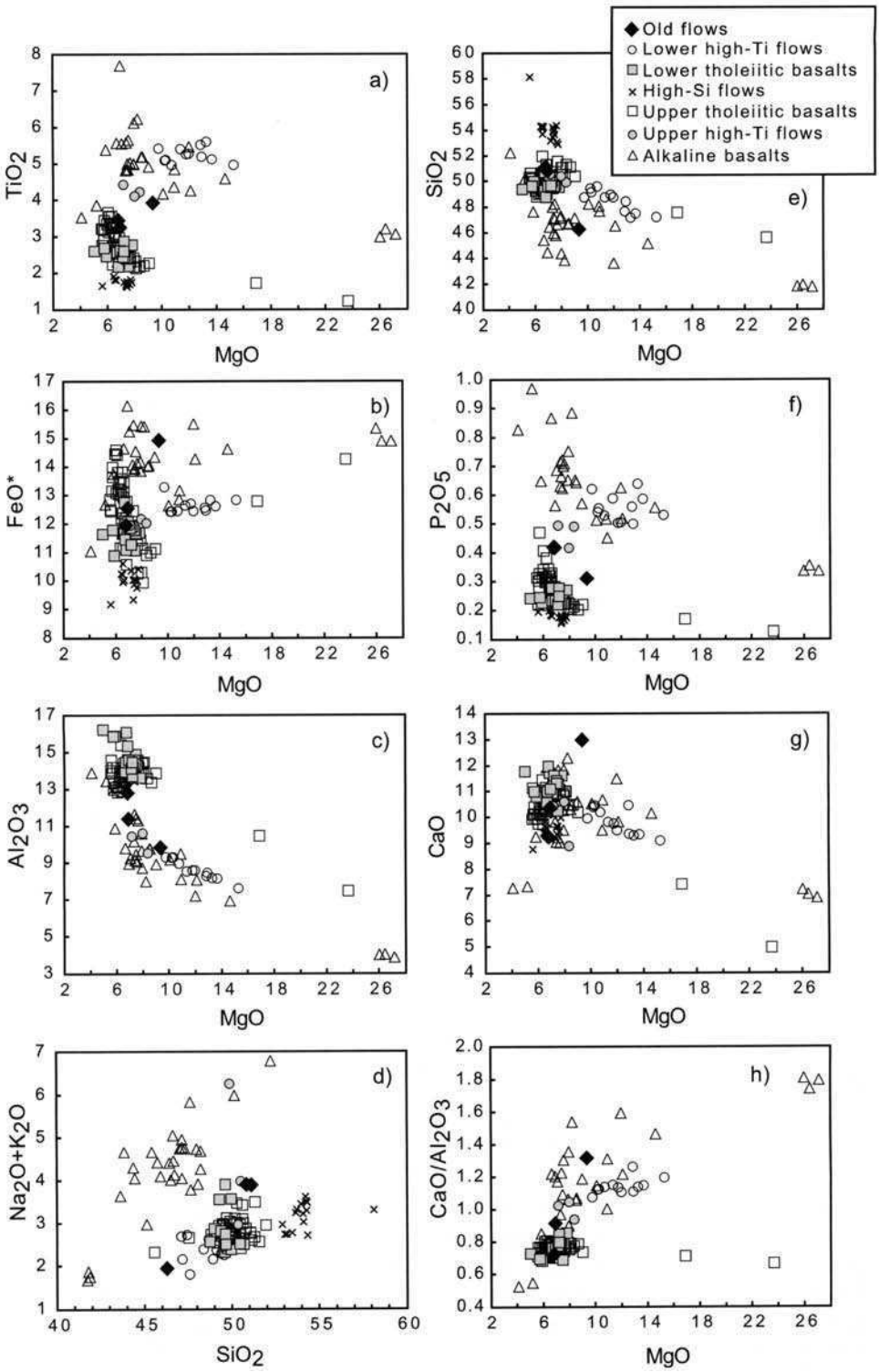
Old flows
Lower high-Ti flows
Lower tholeiitic basalts
High-Si flows
Upper tholeiitic basalts
Upper high-Ti flows
Alkaline basalts
a)
b)
c)
d)
e)
f)
g)
h)
TiO2
FeO*
Al2O3
Na2O+K2O
SiO2
P2O5
CaO
CaO/Al2O3
MgO
SiO2

Table 2. *Major and trace element compositions of selected lava flows*

Sample no.	436409	436410	436411	436412	436437	436439	436441	436446	436452	436459	436460	436464	436466	436468
Stratigraphic position	U1-2	U1-3	U1-4	U1-5	U1-17	U1-18	U1-21	U1-24	U1-32	U1-36	U1-41	U1-44	U1-47	U1-49
Formation	UF	UF	UF	MLF	MLF	MLF	MLF	MLF	MLF	MLF	MLF	MLF	MLF	MLF
Suite	Old flow	Old flow	Old flow	L. High-Ti	L.T. Basalt	L.T. Basalt	L.T. Basalt	L.T. Basalt	L.T. Basalt	L.T. Basalt	High-Si	High-Si	U.T. Basalt	U.T. Basalt
SiO_2	49.58	43.86	49.69	45.67	48.15	47.60	47.41	48.54	48.77	48.81	56.84	53.20	45.62	50.37
TiO2	3.18	3.72	3.34	5.43	2.12	2.19	2.11	2.72	2.37	2.58	1.60	1.66	1.65	2.13
Al_2O_3	11.09	9.32	12.45	7.92	14.43	14.89	15.64	13.36	14.31	14.34	12.65	13.17	10.03	13.32
Fe_2O_3	6.54	6.33	5.91	2.84	5.91	6.41	5.66	4.42	4.55	4.07	6.64	5.75	2.18	4.19
FeO	6.35	8.45	6.30	9.86	5.41	5.30	5.69	7.48	7.41	8.21	2.99	4.66	10.30	6.93
MnO	0.18	0.20	0.16	0.17	0.18	0.16	0.17	0.19	0.18	0.20	0.11	0.16	0.18	0.17
MgO	6.74	8.86	6.62	12.88	7.27	6.68	6.60	7.67	7.29	6.83	5.50	7.23	16.21	8.22
CaO	10.11	12.29	8.97	9.00	9.93	11.38	11.63	11.38	11.22	10.92	8.57	8.99	7.11	10.28
Na_2O	2.59	1.15	2.73	1.77	1.84	2.26	2.23	2.14	2.14	2.24	2.26	2.48	1.92	2.32
K_2O	1.21	0.70	1.05	0.83	1.94	0.52	0.26	0.13	0.13	0.18	0.97	1.07	0.63	0.30
P_2O_5	0.41	0.30	0.41	0.62	0.23	0.23	0.23	0.27	0.22	0.23	0.19	0.17	0.16	0.21
Vol.	1.82	4.14	2.20	2.30	2.28	2.00	2.06	1.25	1.04	0.83	1.10	1.11	3.66	1.27
Sum	99.79	99.31	99.83	99.27	99.68	99.62	99.69	99.54	99.61	99.45	99.43	99.63	99.65	99.71
ICP-MS-Lab.	OSU	OSU	*GCI	OSU	OSU	OSU	OSU	OSU	OSU	OSU	OSU	OSU	OSU	OSU
Rb	18.95	13.84	13	12.21	19.36	10.06	6.29	0.70	1.67	3.03	14.22	22.60	15.24	4.61
Sr	484	2301	555	678	331	414	358	289	262	262	211	213	174	252
Y	26.91	22.38	29	45.16	25.85	26.19	25.30	31.29	28.07	31.23	21.91	23.16	20.16	27.20
Zr	238	160	235	552	132	132	128	181	150	164	127	131	112	143
Nb	25.8	17.1	25	30.3	9.0	8.6	8.5	11.6	8.4	8.9	5.5	5.3	6.8	7.2
Ba	332	716	364	225	88	89	72	55	42	48	260	199	89	109
La	28.174	17.707	31	33.650	9.376	9.558	9.148	11.690	8.884	9.206	11.217	11.863	7.577	11.874
Ce	65.310	43.203	70	89.938	24.069	24.326	23.420	30.522	23.929	25.398	25.397	27.086	19.735	29.272
Pr	8.807	6.104	–	13.635	3.614	3.689	3.449	4.642	3.613	3.966	3.496	3.642	2.891	4.176
Nd	37.562	27.803	42	65.692	17.298	17.298	16.473	21.948	18.108	19.309	15.210	16.357	13.601	19.409
Sm	8.123	6.771	–	16.132	4.682	4.801	4.522	5.919	5.110	5.749	3.988	4.109	3.900	4.982
Eu	2.561	2.233	–	4.780	1.599	1.645	1.599	1.978	1.661	1.919	1.323	1.380	1.251	1.666
Gd	8.195	7.002	–	15.182	4.998	5.121	4.700	6.288	5.413	5.989	4.601	4.806	4.119	5.358
Tb	1.110	0.918	–	2.095	0.835	0.841	0.785	1.030	0.905	1.009	0.669	0.716	0.669	0.892
Dy	5.378	4.648	–	9.698	4.404	4.613	4.272	5.507	4.945	5.601	3.885	4.164	3.650	4.864
Ho	0.983	0.823	–	1.700	0.922	0.933	0.895	1.092	1.000	1.091	0.804	0.803	0.731	0.984
Er	2.345	2.003	–	3.869	2.261	2.334	2.259	2.714	2.577	2.806	2.053	2.104	1.927	2.474
Tm	0.316	0.266	–	0.488	0.343	0.353	0.333	0.395	0.365	0.420	0.297	0.298	0.272	0.344
Yb	1.748	1.435	–	2.798	1.950	1.994	1.979	2.246	2.185	2.430	1.689	1.772	1.555	2.113
Lu	0.266	0.216	–	0.363	0.285	0.298	0.276	0.338	0.312	0.357	0.272	0.254	0.231	0.311
Hf	6.004	4.110	–	12.823	3.390	3.301	3.314	4.464	3.571	4.170	3.219	3.274	2.614	3.522
Ta	1.815	1.259	–	2.185	0.648	0.644	0.632	0.872	0.693	0.739	0.434	0.418	0.531	0.563
Pb	5.381	2.361	7	3.607	1.217	1.244	1.101	1.565	1.302	1.291	3.615	3.481	1.240	2.659
Th	2.501	1.450	2.8	2.479	0.652	0.649	0.596	0.931	0.670	0.642	1.182	1.301	0.757	1.421
U	0.646	0.316	–	0.976	0.214	0.176	0.182	0.283	0.253	0.214	0.291	0.276	0.198	0.322
Ga	–	–	27	–	–	–	–	–	–	–	–	–	–	–
TiO_2 (wt%)	–	–	–	–	–	–	–	–	–	–	–	–	–	–
MnO (wt%)	–	–	–	–	–	–	–	–	–	–	–	–	–	–
$^{87}Sr/^{86}Sr_M$	0.705565			0.703915	0.703710	0.703690	0.703508	0.703577	0.703487	0.703336		0.709256	0.705193	0.706777
(±2SE error)	0.000008			0.000008	0.000008	0.000008	0.000006	0.000011	0.000014	0.000006		0.000013	0.000008	0.000007
$^{87}Sr/^{86}Sr_I$	0.705468			0.703874	0.703578	0.703635	0.703468	0.703572	0.703473	0.703310		0.709016	0.704995	0.706736

U1-X, lava flow no. X in Urbjerget 1; U2-X, lava flow no. X in Urbjerget 2; 1982-X, lava flow no. X in 1982 Nunatak 1; UF, Urbjerget Formation; MLF, Milne Land Formation; PAWBF, Prinsen af Wales Bjerge Formation; L., High-Ti, lower high-Ti flow; L.T., Basalt, lower tholeiitic basalt; U.T., Basalt, upper tholeiitic basalt. U., High-Ti, upper high-Ti flow; A., Basalt, alkaline basalt; OSU, Oregon State University; *, XRF data; GCI, Geological Institute, University of Copenhagen; $^{87}Sr/^{86}Sr_M$, measured isotopic value, $^{87}Sr/^{86}Sr_I$, initial isotopic value at 60 (old flows) and 55 Ma (other than old flows).
NBS987 Sr standard averaged to 0.710248 ± 0.000002 over the time of Sr-analysis.

Geochemical compositions alone define some lava flow suites with coherent characteristics (Figs 7, 8 & 9). However, for a complete distinction between individual suites, stratigraphic level of occurrence must be included. A distinct flow suite is the 'high-Ti flows'. They are tholeiitic basalts (with one alkaline exception, Fig. 7) to picrites with TiO_2 contents of 5 to 6 wt%. No other tholeiitic basalts in East Greenland with similar MgO-contents reach such high TiO_2 concentrations, and we have been unable to find matching compositions in other flood basalt provinces. The 'high-Ti

436472	436476	436478	436479	436480	421701	421706	421712	421721	421724	421725	421730	421732	421740	421742
U1-52	U1-55	U1-60	U1-61	U1-62	U2-1	U2-4	U2-8	U2-13	U2-15	U2-16	U2-20	U2-22	U2-30	U2-32
MLF	MLF	MLF	MLF	MLF	MLF	MLF	MLF	MLF	MLF	MLF	MLF	MLF	MLF	MLF
U.T.	U.T.	U.T.	U. High-Ti	U.T.	L.T.	L.T.	High-Si	High-Si	U.T.	U.T.	U.T.	U.T.	U.T.	U.T.
Basalt	Basalt	Basalt		Basalt	Basalt	Basalt			Basalt	Basalt	Basalt	Basalt	Basalt	Basalt
49.22	48.50	48.61	47.83	49.25	49.15	48.57	52.75	53.68	49.73	49.38	50.01	48.84	49.18	48.73
2.64	3.30	2.92	4.04	2.88	2.39	2.55	1.76	1.80	2.11	3.27	2.34	2.20	2.70	3.30
13.71	12.84	13.44	9.12	14.00	13.97	14.13	13.89	13.54	14.02	12.64	14.23	13.44	14.27	13.67
3.59	3.79	4.51	9.36	4.43	4.17	3.96	5.24	2.46	6.69	4.47	7.35	4.52	13.14	5.43
8.52	10.18	8.49	3.09	9.00	7.97	7.46	4.98	7.90	4.00	9.32	3.68	6.71	0.41	8.08
0.18	0.22	0.18	0.16	0.20	0.17	0.40	0.14	0.16	0.13	0.21	0.14	0.16	0.16	0.20
7.09	6.41	6.76	8.04	5.65	7.15	7.05	6.40	6.44	7.78	6.29	6.67	8.77	5.49	6.11
10.84	10.21	10.48	8.52	10.25	11.08	11.22	9.59	9.31	10.53	9.56	9.97	9.88	10.91	9.90
2.34	2.45	2.49	1.31	2.61	2.18	2.25	2.31	2.54	2.12	2.53	2.26	1.88	2.28	2.52
0.18	0.19	0.24	4.68	0.38	0.16	0.19	0.63	0.91	0.57	0.43	1.14	0.61	0.34	0.24
0.23	0.32	0.28	0.47	0.28	0.22	0.24	0.18	0.20	0.20	0.34	0.23	0.21	0.21	0.31
1.21	1.39	1.26	2.79	1.03	1.31	1.59	1.59	0.84	1.78	1.21	1.37	2.07	0.57	0.83
99.75	99.79	99.65	99.41	99.95	99.93	99.61	99.47	99.77	99.66	99.63	99.38	99.29	99.65	99.33
OSU	OSU	OSU	OSU	OSU	Durham	Durham	Durham	Durham	Durham	Durham	Durham	Durham	Durham	Durham
1.78	1.70	4.34	28.18	3.31	2.30	3.65	13.59	22.43	11.36	11.42	34.37	9.52	4.13	2.24
271	279	275	520	274	289	298	248	229	267	284	276	274	295	309
31.28	39.12	35.43	26.84	35.84	30.62	32.43	25.83	27.06	26.24	41.99	29.74	27.03	32.30	39.98
173	225	193	298	193	155	176	145	161	139	251	159	151	181	224
10.6	14.2	11.7	30.2	12.0	9.8	12.1	7.4	8.1	10.7	17.1	10.5	10.1	12.8	16.6
65	74	66	378	89	59	94	145	223	148	136	117	99	90	92
11.665	14.031	13.066	32.538	12.408	9.959	12.312	13.375	14.952	11.664	18.756	11.971	11.149	12.772	15.403
30.417	37.332	34.155	82.128	33.622	26.053	32.067	30.209	33.553	28.786	46.599	29.446	28.193	32.297	39.795
4.604	5.583	5.197	11.141	4.961	3.949	4.713	4.074	4.475	4.104	6.661	4.288	4.099	4.885	5.906
21.901	26.859	24.460	47.934	23.531	18.920	21.734	17.528	19.227	18.250	29.812	19.071	18.574	22.306	27.259
5.681	7.313	6.780	9.764	6.420	5.771	6.333	4.841	5.317	5.204	8.506	5.540	5.447	6.501	7.861
1.922	2.341	2.147	2.832	2.097	1.983	2.106	1.584	1.633	1.708	2.647	1.895	1.739	2.147	2.507
6.082	7.706	6.998	9.384	6.926	6.159	6.729	5.093	5.534	5.447	8.802	5.857	5.751	7.263	8.613
1.019	1.244	1.167	1.210	1.133	1.033	1.085	0.824	0.884	0.868	1.403	0.942	0.909	1.066	1.292
5.622	6.919	6.401	5.576	6.104	5.723	6.096	4.646	5.083	4.892	7.944	5.441	5.180	6.185	7.389
1.127	1.418	1.312	0.995	1.272	1.097	1.175	0.910	0.996	0.952	1.535	1.062	1.003	1.150	1.410
2.837	3.465	3.245	2.464	3.210	2.747	2.936	2.344	2.473	2.379	3.812	2.685	2.499	2.969	3.653
0.430	0.532	0.468	0.320	0.468	0.411	0.416	0.337	0.369	0.343	0.546	0.391	0.365	0.411	0.513
2.395	3.047	2.762	1.771	2.841	2.356	2.598	2.059	2.246	2.106	3.399	2.322	2.207	2.558	3.145
0.371	0.437	0.412	0.240	0.409	0.370	0.392	0.324	0.345	0.321	0.514	0.363	0.331	0.374	0.454
4.213	5.467	4.767	7.085	4.749	4.097	4.551	3.774	4.249	3.662	6.394	4.147	3.924	4.650	5.739
0.773	1.080	0.917	2.276	0.917	0.699	0.880	0.529	0.543	0.703	1.141	0.709	0.691	1.098	1.191
1.641	2.055	1.843	4.254	1.745	1.585	2.071	3.130	3.617	2.770	3.029	2.345	1.559	1.441	1.678
1.073	1.293	1.102	2.703	1.018	0.733	1.124	1.598	1.787	1.307	1.733	1.177	1.120	1.166	1.320
0.281	0.347	0.351	0.784	0.300	0.212	0.296	0.282	0.314	0.363	0.427	0.298	0.241	0.186	0.345
–	–	–	–	–	21.054	23.048	19.874	19.784	19.704	23.627	21.066	20.099	22.346	23.816
–	–	–	–	–	2.338	2.562	1.742	1.710	1.904	3.145	2.241	2.102	2.702	3.295
–	–	–	–	–	0.176	0.416	0.148	0.162	0.135	0.217	0.147	0.164	0.152	0.198
0.703785	0.703537	0.703496	0.704476	0.703364										
0.000006	0.000006	0.000007	0.000015	0.000009										
0.703770	0.703523	0.703460	0.704354	0.703337										

flows' are also characterized by FeO* of 12 to 13 wt%, high P_2O_5 contents (0.5 to 0.7 wt%), low Al_2O_3 (8 to 9 wt%), CaO/Al_2O_3 between approximately 1.1 and 1.2, low Y/Zr (0.07 to 0.09), low Nb/Zr (0.04 to 0.07), high chondrite-normalized Dy/Yb ratios (2.2 to 2.4) and La/Nb around 1 (Figs 7 & 8). The 'high-Ti flows' can be sub-divided into a lower and an upper suite (see below), where the upper suite is less MgO- and TiO_2-rich (Fig. 7) and have higher Nb/Zr and chondrite-normalized La/Sm ratios (Fig. 8). The one alkaline 'high-Ti flow' is located in the upper suite of 'high-Ti flows';

Table 2. (*continued*)

Sample no.	421746	MG-24	MG-25	MG-27	MG-04	MG-06	MG-07	JG-44	MG-09	MG-10	MG-12	JG-45	MG-16	MG-19
Stratigraphic position	U2-35	1982-2	1982-3	1982-4	1982-7	1982-9	1982-10	1982-12	1982-14	1982-15	1982-17	1982-18	1982-21	1982-23
Formation	MLF	MLF	MLF	MLF	MLF	MLF	MLF	MLF	MLF	MLF	MLF	MLF	PAWBF	PAWBF
Suite	U.T. Basalt	U.T. Basalt	U.T. Basalt	U.T. Basalt	U.T. Basalt	U.T. Basalt	U.T. Basalt	U.T. Basalt	U.T. Basalt	U.T. Basalt	U.T. Basalt	U.T. Basalt	A. Basalt	A. Basalt
SiO_2	49.67	48.55	43.71	49.62	48.83	49.03	49.06	48.48	48.57	47.63	48.08	47.61	48.63	42.96
TiO_2	2.92	3.95	1.17	2.53	3.37	2.95	3.11	3.28	2.16	3.23	2.69	3.54	3.74	5.27
Al_2O_3	13.28	10.20	7.14	14.10	13.03	13.01	12.69	12.83	14.91	13.33	13.44	13.70	13.03	9.26
Fe_2O_3	7.69	7.51	2.17	3.51	3.24	6.80	4.76	5.24	7.34	4.21	6.16	6.77	13.66	6.84
FeO	5.21	4.97	11.73	8.25	10.42	5.90	9.40	9.46	4.20	8.85	6.57	6.54	0.00	7.69
MnO	0.16	0.16	0.19	0.18	0.21	0.16	0.20	0.20	0.16	0.19	0.19	0.20	0.17	0.19
MgO	6.35	7.71	22.69	6.40	5.63	6.39	5.63	5.83	6.16	6.26	7.17	5.84	5.04	6.30
CaO	10.10	10.65	4.75	10.72	9.89	10.25	9.71	9.74	11.10	10.49	10.51	9.79	7.11	11.28
Na_2O	2.45	2.46	1.88	2.37	2.59	2.43	2.50	2.47	2.25	2.42	2.24	2.47	3.97	3.34
K_2O	0.59	0.39	0.34	0.22	0.32	0.45	0.54	0.45	0.39	0.36	0.38	0.37	1.83	1.07
P_2O_5	0.28	0.40	0.12	0.24	0.32	0.27	0.46	0.31	0.21	0.32	0.26	0.33	0.94	0.82
Vol.	0.74	1.59	3.20	0.90	0.82	0.97	1.12	1.61	1.50	1.45	1.08	2.37	0.27	3.39
Sum	99.44	98.54	99.09	99.04	98.67	98.61	99.18	99.90	98.95	98.74	98.77	99.53	98.39	98.41
ICP-MS-Lab.	Durham	Durham	Durham	Durham	Durham	Durham	Durham	Durham	Durham	Durham	Durham	Durham	Durham	Durham
Rb	13.32	3.06	8.50	1.45	5.84	7.20	11.94	8.64	9.04	3.11	5.25	3.75	33.07	48.47
Sr	281	655	85	293	296	280	274	271	290	337	271	363	1071	1364
Y	36.87	28.88	14.20	31.76	40.98	36.32	48.25	40.53	27.93	35.49	32.48	35.09	36.85	30.84
Zr	197	307	77	174	227	195	260	227	145	212	173	254	537	436
Nb	14.4	46.0	5.2	12.1	16.9	14.0	20.9	18.6	11.9	20.4	14.5	24.1	84.6	77.1
Ba	92	216	64	87	93	90	120	105	54	98	82	101	579	482
La	13.710	35.918	5.910	12.086	15.731	13.587	20.081	16.446	10.704	16.893	12.385	17.741	76.175	61.001
Ce	35.338	83.630	14.845	31.352	40.390	35.014	51.167	42.611	27.235	42.375	31.648	44.083	173.632	137.607
Pr	5.200	11.172	2.159	4.603	5.913	5.175	7.518	6.241	3.986	6.069	4.672	6.693	22.334	17.836
Nd	24.062	44.394	9.595	21.151	27.116	23.650	33.962	27.541	18.344	26.927	21.359	29.003	87.079	69.620
Sm	6.946	10.623	2.764	6.121	7.824	6.877	9.459	7.997	5.225	7.328	6.134	8.010	18.051	15.011
Eu	2.265	3.102	0.906	2.008	2.525	2.206	2.871	2.535	1.772	2.391	2.029	2.665	4.941	4.170
Gd	7.690	8.881	2.918	6.598	8.488	7.663	10.334	8.557	5.817	7.889	6.830	8.008	13.858	11.928
Tb	1.163	1.229	0.473	1.024	1.295	1.157	1.553	1.323	0.886	1.148	1.044	1.232	1.679	1.441
Dy	6.764	6.167	2.649	5.786	7.529	6.677	8.865	7.567	5.107	6.610	5.969	6.701	8.152	7.042
Ho	1.284	1.091	0.509	1.132	1.446	1.269	1.710	1.481	0.988	1.253	1.152	1.276	1.365	1.147
Er	3.290	2.521	1.321	2.852	3.710	3.264	4.380	3.723	2.584	3.259	2.978	3.234	3.178	2.649
Tm	0.468	0.346	0.193	0.420	0.519	0.464	0.612	0.557	0.364	0.450	0.429	0.488	0.407	0.328
Yb	2.847	1.988	1.155	2.499	3.221	2.835	3.776	3.349	2.272	2.818	2.600	3.071	2.433	1.943
Lu	0.429	0.285	0.171	0.372	0.470	0.408	0.555	0.499	0.335	0.414	0.386	0.477	0.338	0.262
Hf	5.047	7.656	1.999	4.442	5.838	5.089	6.633	5.842	3.811	5.351	4.409	6.536	12.509	10.221
Ta	1.075	3.011	0.404	0.831	1.163	0.983	1.431	1.295	0.872	1.420	1.021	1.596	5.486	5.122
Pb	1.541	4.593	1.130	1.984	2.060	3.184	2.184	1.946	1.194	1.631	1.196	2.705	5.917	5.916
Th	1.153	3.152	0.597	1.107	1.307	1.147	1.663	1.363	0.901	1.441	1.000	1.680	6.158	5.492
U	0.363	0.802	0.145	0.280	0.365	0.324	0.493	0.412	0.229	0.420	0.293	0.631	1.852	1.541
Ga	22.492	22.457	22.457	22.457	24.375	22.376	23.724	24.250	20.978	22.937	21.763	25.861	27.524	23.908
TiO_2 (wt%)	2.927	4.077	1.217	2.692	3.411	2.963	3.104	3.416	2.273	3.336	2.793	3.594	3.853	5.412
MnO (wt%)	0.159	0.161	0.196	0.192	0.206	0.158	0.199	0.210	0.155	0.193	0.189	0.203	0.171	0.187

$^{87}Sr/^{86}Sr_M$
(±2SE error)
$^{87}Sr^{86}Sr_I$

as mentioned below, it is very altered, and may have attained its alkaline composition through an alteration process.

The 'alkaline basalts' are in many respects similar to the high-Ti flows, although they reach considerably higher TiO_2 concentrations (near 8 wt%), lower SiO_2 (down to 42 wt%), higher FeO* (up to 16 wt%), P_2O_5 (up to 1 wt%) and higher CaO/Al_2O_3 ratios (up to 1.8) (Fig. 7). Nb/Zr ratios are high (0.14 to 0.24), Y/Zr similar to the 'high-Ti flows' (0.06 to 0.09), whereas chondrite-normalized La/Sm and Dy/Yb are both high (2.4 to 3.2, and 2.1 to 2.6, respectively), and La/Nb ratios less than 1 (Fig. 8). Trace element spectra are relatively steep due to high enrichments in large ion lithophile and high field strength elements (Fig. 9).

MG-20 1982-24	MG-22 1982-26	JG-19 1982	JG-20 1982	JG-22 1982	JG-47 1982	JG-49 1982	JG-51 1982	JG-53 1982	JG-55 1982	JG-58 1982	JG-61 1982	JG-65 1982	JG-66 1982	JG-72 1982
PAWBF A. Basalt	PAWBF A. Basalt	PAWBF A. Basalt	PAWBF A. Basalt	PAWBF A. Basalt	PAWBF A. Basalt	PAWBF A. Basalt	PAWBF A. Basalt	PAWBF A. Basalt	PAWBF A. Basalt	PAWBF A. Basalt	PAWBF A. Basalt	PAWBF A. Basalt	PAWBF A. Basalt	PAWBF A. Basalt
43.77	41.66	41.04	43.04	42.62	45.54	45.74	46.94	45.32	46.03	46.34	43.44	44.96	45.32	47.17
5.41	5.91	2.93	5.94	5.35	4.84	4.83	4.06	4.88	4.73	5.24	7.51	5.47	5.42	4.73
8.66	7.59	3.92	8.47	7.05	11.04	10.23	8.93	10.98	11.35	10.59	8.75	8.95	9.04	9.27
7.87	3.90	3.65	6.76	4.78	4.92	4.67	5.34	5.53	4.87	4.63	5.71	5.27	7.28	6.24
6.84	11.13	11.78	8.88	10.85	9.09	9.19	7.50	8.76	9.14	9.22	10.64	10.39	8.33	8.01
0.19	0.20	0.20	0.19	0.20	0.19	0.19	0.17	0.19	0.19	0.18	0.19	0.20	0.19	0.18
7.23	7.83	25.56	7.74	11.71	7.25	7.68	9.84	7.45	7.20	5.71	6.78	7.24	6.90	7.33
11.31	11.67	7.09	11.49	11.22	8.93	9.18	10.24	8.77	8.82	8.99	10.52	10.98	10.59	10.11
2.77	3.09	1.45	2.30	2.51	3.12	3.19	2.83	3.42	3.34	3.98	2.75	2.75	2.70	3.17
1.46	1.34	0.39	1.87	1.04	1.48	1.40	1.32	1.49	1.49	1.69	1.21	1.26	1.60	1.42
0.67	0.84	0.33	0.73	0.61	0.70	0.63	0.50	0.69	0.70	0.63	0.55	0.65	0.67	0.61
2.09	1.89	1.29	2.27	1.72	2.05	2.18	1.68	2.11	1.69	2.17	1.59	1.30	1.23	0.97
98.27	97.05	99.63	99.68	99.66	99.15	99.11	99.35	99.59	99.55	99.72	99.64	99.42	99.27	99.21
Durham	Durham	Durham	Durham	Durham	Durham	Durham	Durham	Durham	Durham	Durham	Durham	Durham	Durham	Durham
29.56	32.56	13.59	40.51	28.36	28.15	26.49	25.96	28.06	29.60	34.13	25.69	25.13	33.39	27.58
861	1016	668	812	894	1019	1044	715	873	907	764	928	1276	892	777
32.36	33.76	14.96	30.33	27.15	30.88	30.20	25.37	30.55	31.42	29.86	26.80	30.00	29.18	26.25
397	473	206	456	369	404	376	329	397	407	408	381	413	433	316
69.6	96.9	44.1	101.2	82.6	70.6	69.2	63.3	69.2	71.5	82.5	76.1	86.2	86.2	72.5
376	397	237	414	303	454	465	338	456	462	429	390	371	426	421
50.986	73.551	31.102	71.858	56.698	55.785	57.846	48.411	55.687	57.227	60.854	52.371	63.788	64.693	55.897
117.188	168.351	70.746	161.716	129.271	129.677	131.403	110.633	129.464	132.999	137.288	121.131	142.893	146.661	125.877
15.434	21.797	9.166	20.547	16.607	17.073	16.915	14.184	17.025	17.392	17.588	15.875	18.138	18.828	16.181
61.578	83.411	34.927	77.784	63.097	66.269	65.105	54.541	65.711	67.365	66.627	61.552	73.698	76.093	65.620
13.793	17.451	7.351	15.793	13.195	13.949	13.691	11.496	13.830	14.185	13.730	13.197	14.130	14.312	12.541
3.919	4.861	2.061	4.440	3.714	3.856	3.839	3.176	3.882	3.941	3.806	3.714	4.038	4.087	3.565
11.278	13.260	5.748	12.206	10.243	10.955	10.988	9.095	10.777	11.062	10.646	10.314	11.669	11.556	10.257
1.433	1.675	0.712	1.517	1.311	1.382	1.378	1.158	1.381	1.408	1.352	1.312	1.404	1.383	1.235
7.036	7.823	3.372	7.083	6.164	6.747	6.708	5.579	6.741	6.837	6.488	6.158	6.862	6.653	5.935
1.182	1.287	0.554	1.154	1.030	1.151	1.140	0.936	1.152	1.172	1.097	1.029	1.125	1.076	0.989
2.691	2.831	1.241	2.547	2.299	2.692	2.603	2.140	2.666	2.714	2.528	2.296	2.583	2.480	2.217
0.347	0.365	0.164	0.337	0.297	0.363	0.354	0.290	0.357	0.367	0.336	0.298	0.325	0.308	0.275
1.982	2.050	0.924	1.870	1.689	2.121	2.039	1.686	2.108	2.140	1.975	1.679	1.864	1.824	1.640
0.268	0.285	0.130	0.268	0.237	0.307	0.290	0.248	0.308	0.311	0.285	0.236	0.258	0.250	0.222
9.426	11.242	4.966	10.871	8.945	9.662	9.110	7.935	9.580	9.742	9.820	9.383	9.941	10.352	8.228
4.748	6.265	2.925	6.607	5.554	4.554	4.503	4.225	4.553	4.733	5.468	5.321	5.909	5.894	5.017
4.562	6.710	2.572	6.279	4.686	4.696	5.805	5.426	5.441	5.461	7.097	6.020	4.726	5.586	5.203
4.718	6.738	2.905	6.793	5.224	4.335	4.549	4.166	4.292	4.383	5.425	4.383	5.845	5.940	4.353
1.052	1.940	0.791	1.422	1.477	1.171	1.229	1.063	1.229	1.232	1.591	1.297	1.646	1.069	0.858
22.089	22.457	22.457	22.457	20.694	24.488	23.404	20.050	23.871	24.383	23.538	22.747	22.990	22.387	21.852
5.689	6.269	3.108	6.207	5.596	5.022	4.938	4.208	4.906	4.823	5.352	7.683	5.652	5.631	4.844
0.192	0.212	0.204	0.193	0.202	0.194	0.190	0.177	0.189	0.193	0.181	0.194	0.197	0.189	0.178

'Tholeiitic basalts' have MgO between 4 and 10 wt%, TiO_2 between 2 and 4 wt%, and SiO_2 between 49 and 52 wt%. They have a wide range of FeO* (10 to 15 wt%), relatively low P_2O_5 contents (0.2 to 0.5 wt%), high Al_2O_3 (13 to 16 wt%) and low CaO/Al_2O_3 ratios (0.7–0.8) (Fig. 7). Y/Zr ratios of the 'tholeiitic basalts' are high (0.14 to 0.20), but Nb/Zr, chondrite-normalized La/Sm and Dy/Yb ratios are low (0.05–0.1, 1–1.6, 1.4–1.7). The 'tholeiitic basalts' are separated into a lower and upper suite (see below), where some flows of the upper suite tend to be more TiO_2-, SiO_2-, FeO* and P_2O_5-rich than flows in the lower suite (Fig. 7). 'Upper tholeiitic basalts' also reach higher Nb/Zr, La/Sm_N and La/Nb ratios than 'lower tholeiitic basalts' (Fig. 8).

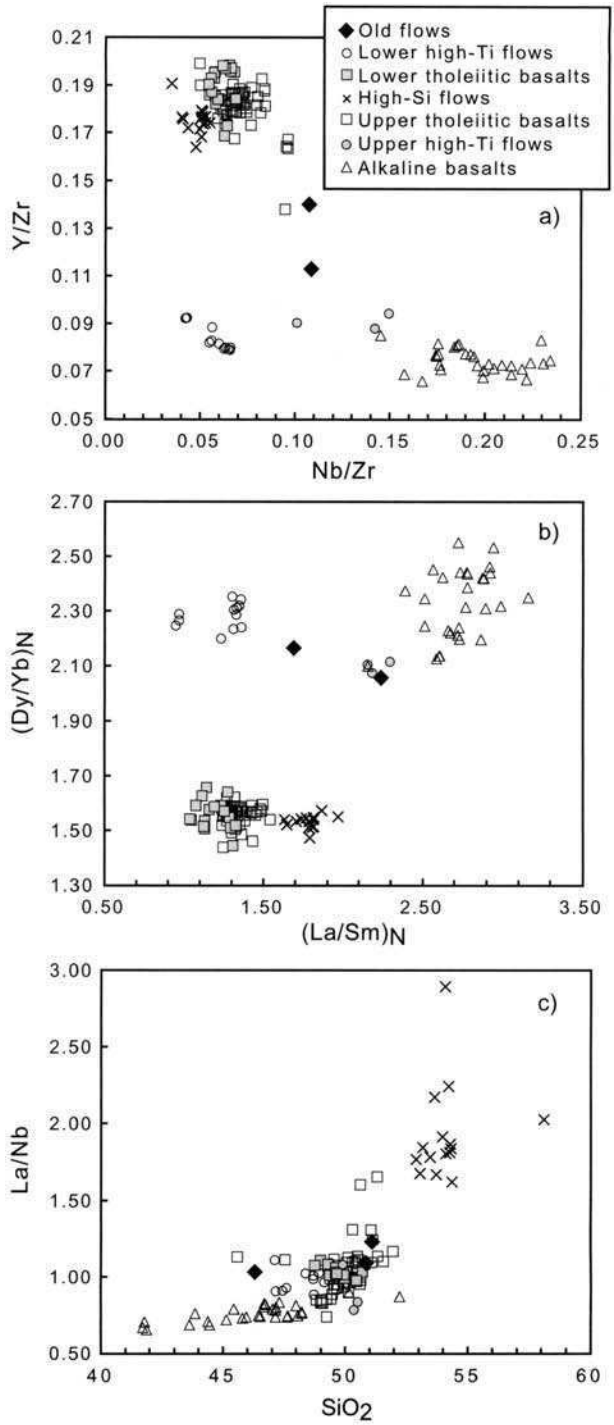

Fig. 8. Selected trace element ratio variations and variation of La/Nb v. SiO_2 of flows from the southern Prinsen af Wales Bjerge region. $(La/Sm)_N$ and $(Dy/Yb)_N$ are La/Sm and Dy/Yb ratios normalized to C1 chondrite of Sun & McDonough (1989).

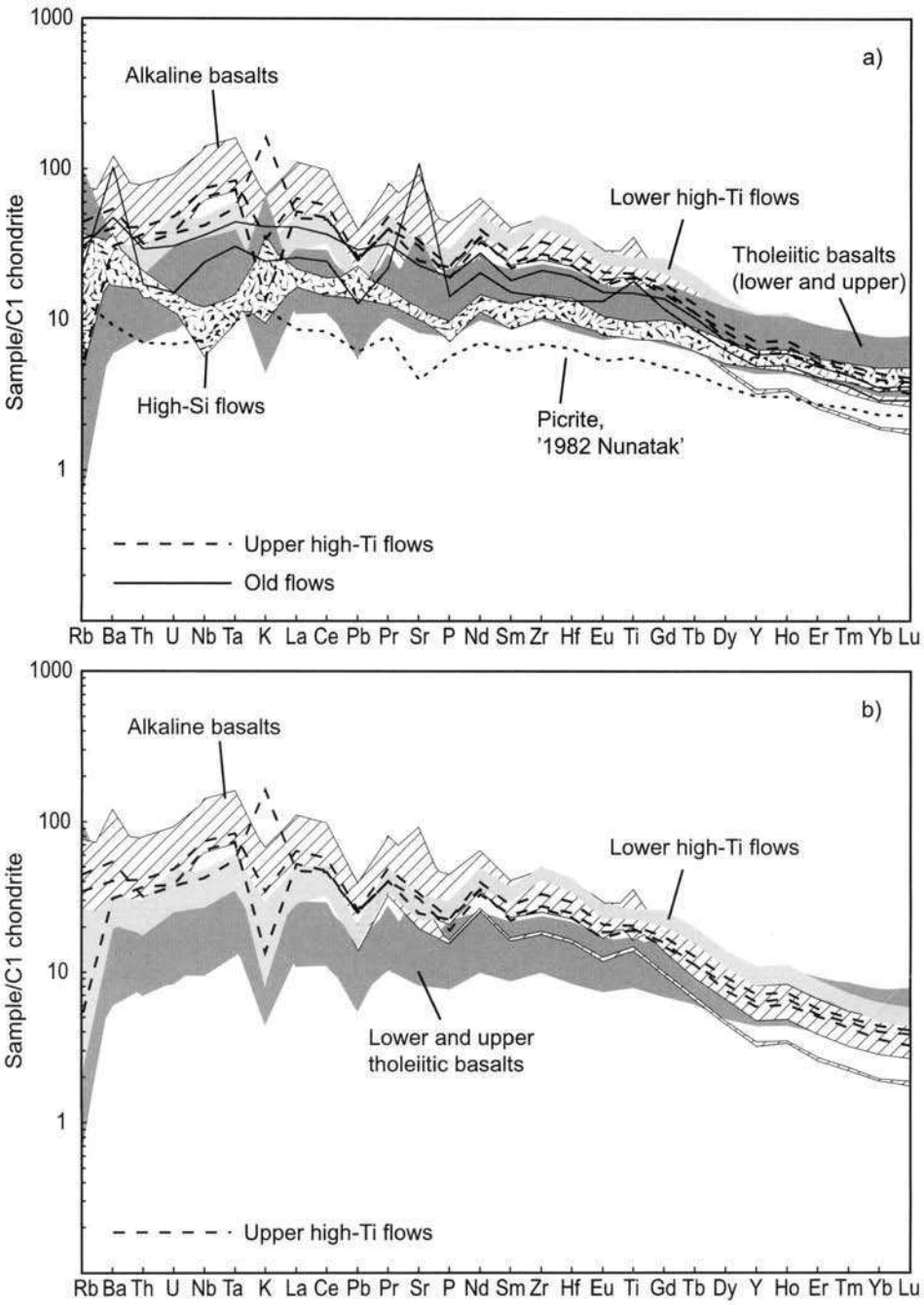

Fig. 9. Trace element spectra of flows from the southern Prinsen af Wales Bjerge. The data are normalized to C1 chondrite of Sun & McDonough (1989).

'High-Si flows' (basaltic andesites and andesite) are in many respects similar to the 'tholeiitic basalts' although the 'high-Si flows' have higher SiO_2 (52 to 58 wt%), lower TiO_2 (1.5 to 2 wt%) and P_2O_5 (0.15 to 0.2 wt%) (Fig. 7), combined with higher La/Sm_N (1.6 to 2) and La/Nb ratios (>1.5) (Fig. 8). Trace element spectra have very distinct Nb–Ta troughs (Fig. 9).

'Old flows' (Figs 7, 8 & 9) tend to have geochemical characteristics intermediate between 'tholeiitic' and 'alkaline basalts'. The suite is not particularly homogeneous, for example SiO_2 vary from 46 to 51 wt%, but the lavas occur in a stratigraphically well-defined succession (see below) and are therefore plotted with one symbol (solid diamonds) in Figures 7 and 8.

Geochemical suites, stratigraphy and correlation in the southern Prinsen af Wales Bjerge

In order to correlate the volcanic sections collected from the southern Prinsen af Wales Bjerge region, successions of lava flows that form distinctive chemical (Figs 7–9) and lithological suites (Figs 4 & 5) have been identified. The suites are listed below, and Table 3 shows the relationship between flow suites and lithostratigraphical formations:

(1) 'Old flows' (in Urbjerget 1);
(2) 'Lower high-Ti flows' (in Urbjerget 1);
(3) 'Lower tholeiitic basalts' (in Urbjerget 1 and Urbjerget 2);
(4) 'High-Si flows' (in Urbjerget 1 and 2);
(5) 'Upper tholeiitic basalts' (in Urbjerget 1, Urbjerget 2 and 1982 Nunatak 1);
(6) 'Upper high-Ti flow' of Urbjerget 1 and high-Ti flows of 1982 Nunatak 1;
(7 'Alkaline basalts' (in 1982 Nunatak 1).

'Old flows' and interbedded sediments

'Old flows' (suite 1) with ages of *c.* 61 Ma (Table 1) are only present at Urbjerget 1 (Figs 5 & 6). The flows are massive, aphyric, 5 to 10 m thick, and constitute a *c.* 30 m thick succession with at least four flows and some poorly exposed intervals. They

Table 3. *Overview of stratigraphy in the southern Prinsen af Wales Bjerge region*

Lithostratigraphy		Geochemical stratigraphy	Exposed sections
Group	Formation	Suites/successions	
Blosseville	Prinsen af Wales Bjerge	7. Alkaline basalts	1982 Nunatak 1
	Milne Land	6. Upper high-Ti flows	Urbjerget 1 and 1982 Nunatak 1
	Milne Land	5. Upper tholeiitic basalts	Urbjerget 1 and 2, 1982 Nunatak 1
	Milne Land	4. High-Si flows	Urbjerget 1 and 2
	Milne Land	3. Lower tholeiitic basalts	Urbjerget 1 and 2
	Milne Land	2. Lower high-Ti flows	Urbjerget 1 and 2
	Urbjerget	1. Old flows	Urbjerget 1

Blosseville Group from Soper *et al.* (1976).

overly a thin black shale of lacustrine origin with plant fossils, and below this is a less than 5 m thick arkosic sandstone with tree limb casts and lenses with black, organic material. This fluviatile sandstone rests unconformably on a banded tonalitic gneiss with amphibolite lenses and massive feldspar segregations. Above the 'old flow' succession is an *c.* 4 m thick volcanogenic finegrained sediment with sparse 3 to 5 cm large rounded clasts of olivine–clinopyroxene–Cr–spinel phyric volcanic rocks, and a strongly altered and SiO_2-veined matrix. The matrix contains subrounded *c.* 0.2–0.7 mm large volcanic rock and crystal fragments of olivine, clinopyroxene, and K-feldspar with cross-hatched twinning (suggesting a low-T origin, probably from the gneiss basement). No drape structures were observed in the matrix above and below clasts and the clasts have no glassy rinds, suggesting that the sediment is a redeposited volcanogenic sediment rather than a pristine tuff. Vitrinite reflectance analysis of the volcanogenic sediment matrix gave a mean value of 0.88% ± 0.07 for 86 counted particles (C. Guvad, pers. comm.) and shows the presence of partially decomposed organic material. The thickness of the succession from top of the tonalitic gneiss to the top of the volcanogenic sediment is *c.* 50 m.

Three of the 'old flows' were analysed for geochemical composition. Two of them have major element compositions fairly similar to the 'tholeiitic basalts' (suites 3 and 5) higher in Urbjerget 1, although with low Al_2O_3 (Table 2). The third flow is relatively TiO_2- and FeO*-rich compared to the 'tholeiitic basalts'. Trace element spectra of old flows tend to be slightly steeper from Ti to Lu than 'tholeiitic basalt' spectra (Fig. 9).

'Lower high-Ti flows' of Urbjerget 1

The 'lower high-Ti flows' (suite 2) are only present in Urbjerget 1, and they have ages close to 56 Ma (Table 1 and Fig. 6, samples 436412 and 436430). The 'high-Ti flow' succession is *c.* 105 m thick and consists of at least 12 olivine ± clinopyroxene-phyric, basaltic to picritic lava flows which are capped by a thin volcaniclastic deposit. Most flows are less than 10 metres thick and compound pahoehoe types, but a couple are 20 to 40 metres thick columnar flows. Interbedded with the flows are black shales and volcanoclastic sandstones containing plant fossils and coal seams. Geochemical characteristics of the 'lower high-Ti flows' are described above. Another somewhat similar succession of 'high-Ti flows' occur at higher stratigraphic levels in Urbjerget 1 and at the base of the 1982 Nunatak 1 (see below).

'Lower tholeiitic basalts' of Urbjerget 1 and Urbjerget 2

'Tholeiitic basalt' is the most abundant flow type of Urbjerget 1, 2 and 1982 Nunatak 1. In Urbjerget 1, the lower succession of 'tholeiitic basalts' (suite 3) starts above the lower 'high-Ti flow' succession and is overlain by a succession of 'high-Si flows' (see below). In Urbjerget 2 'tholeiitic basalts' (suites 3 and 5) form the entire section apart from an interval between *c.* 1560 and 1680 m asl where 'high-Si flows' are present. In 1982 Nunatak 1 'tholeiitic basalts' are found throughout most of the lower portion of gently dipping flows (except from at the very base of 1982 Nunatak 1). At the 1982 Nunatak there is no succession of 'high-Si flows', and the 'tholeiitic basalts' most likely correlate with the 'upper tholeiitic basalts' of Urbjerget 1 and 2 (see below).

The lowermost 'tholeiitic basalts' in Urbjerget 1 is an approximately 20 m thick succession of thin (<5 m thick), columnar and compound aphyric to slightly plagioclase-clinopyroxene phyric flows with 1–2 .vol.% phenocrysts and glomerocrysts, and with up to *c.* 20 vol.% altered glass in the matrix. These flows are overlain by a laterally inhomogeneous 5–15 m thick sediment horizon that varies from shale over silt- and sandstone to pyroclastic deposits. The pyroclastic rocks resemble debris flow deposits and are characterized by a clast assemblage of mudstone and hydrothermally altered basalts. The first lava flows above the sediment horizon are aphyric and very similar to the ones inbetween the 'high-Ti flows' and the debris flow deposit, but from *c.* 1750 m asl some flows are plagioclase-clinopyroxene phyric to glomerophyric (2–7 vol.% phenocrysts) with plagioclase as the predominant phenocryst phase (>90 vol.% of all phenocrysts are plagioclase). One distinct flow near 1800 m asl has a much higher proportion of plagioclase–clinopyroxene glomerocrysts (15–20 vol.%). A volcaniclastic sediment is found at *c.* 1825 m asl, and the columnar jointed 5 to 10 m thick flows above are plagioclase–clinopyroxene or plagioclase–olivine glomerophyric with *c.* 5 to 15 vol.% phenocrysts. A significant part of the section above these flows is covered in talus.

'Tholeiitic basalts' (suite 3) in Urbjerget 2 display variable flow morphology from 5–30 m thick, columnar-jointed flows to thin, vesicular flows. They are phyric to glomerophyric with 0.5 to 5 mm large phenocrysts and glomerocrysts of plagioclase, clinopyroxene and olivine (altered), which form between 2 and 10 vol.% of the rocks. No volcaniclastic sediments were found in this section.

'High-Si flows'

'High-Si flows' (suite 4) are present at Urbjerget 1 and 2, but not at 1982 Nunatak 1, which is consistent with the photogrammetric analysis that indicates the 'high-Si succession' would occur below the lowermost level of exposure at 1982 Nunatak 1. At Urbjerget 1, the 'high-Si flows' are aphyric to slightly olivine-phyric (<5% phenocrysts) basaltic andesites to andesite with intergranular to intersertal groundmass texture of plagioclase, clinopyroxene, FeTi-oxides and altered glass (mesostasis). Occassionally less than 1% clinopyroxene phenocrysts are present. All olivine in the rocks is altered. Phenocrysts are approximately 0.2 to 1 mm, matrix phases are *c.* 0.05 to 0.2 mm or finer-grained. Alteration is patchy, often related to larger volumes of mesostasis.

The Urbjerget 2 succession of 'high-Si flows' is similar to the 'high-Si flows' of Urbjerget 1. However, some of the flows in Urbjerget 2 are olivine + plagioclase phyric, but always with less than about 7 vol.% phenocrysts. At least one flow is orthopyroxene and clinopyroxene phyric with subhedral pyroxene phenocrysts and glomerocrysts; some altered phenocrysts in other flows may also originally have been orthopyroxene. One flow has *c.* 5 vol.% segregations of irregular, rounded, 1 to 7 mm large mesostasis-rich fields with minerals similar to groundmass minerals, but at least twice as large. Some of the 'high-Si flows' also have minor volumes (*c.* 1–3%) of a late, interstitial SiO_2-polymorph which may be secondary. The deduced crystallization sequence for the 'high-Si flows' is (olivine)–plagioclase–(orthopyroxene)–clinopyroxene–FeTi–oxides. In terms of major element composition the 'high-Si flows' from the two sections at Urbjerget are indistinguishable (Fig. 7), but La/Nb ratios tend to be higher in Urbjerget 1 'high-Si flows'.

'Upper tholeiitic basalts' of Urbjerget 1, Urbjerget 2 and 1982 Nunatak 1

The 'upper tholeiitic basalts' at Urbjerget 1 are columnar, 5 to 35 m thick flows, although with short (<10 m) interbedded successions of *c.* 1 m thick, vesicular flows. The lowermost flows are relatively phenocryst-rich with *c.* 10 to 25 vol.% glomerocrysts of either plagioclase–clinopyroxene–olivine or olivine–plagioclase glomerocrysts. After some olivine phyric flows with 3 to 7 vol.% altered olivine phenocrysts and intergranular to intersertal groundmasses occasionally with flow structures, flows again (from *c.* 2100 m asl) become plagioclase–clinopyroxene glomerophyric with 2 to 10 vol.% glomerocrysts. From *c.* 2155 m asl olivine rejoins the phenocryst assemblages, often with strongly elongated crystal habits, and glomerocrysts constitute 3 to 10 vol.% of the rocks but still with plagioclase as the dominating phenocryst phase (>90% of all phenocrysts/glomerocrysts).

At Urbjerget 2, the first flow above the 'high-Si flows' is slightly olivine phyric with *c.* 2 vol.% phenocrysts, and the succession up to *c.* 1820 m asl consists of interspersed olivine phyric (*c.* 5 vol.% phenocrysts), plagioclase + olivine phyric (<7 vol.% phenocrysts) and aphyric flows, all porphyritic flows with 0.1 to 1 mm large phenocrysts. The most abundant matrix phase for all these flows is plagioclase, and groundmass textures are intergranular to intersertal (although all interstitial glass seems to have been altered to mesostasis). Near the top of Urbjerget 2 (*c.* 1850–1890 m asl) some flows have a larger dip (*c.* 40°SW) than the main part of the flows in the section, possibly due to fault-related block rotation. These dipping flows are petrographically and geochemically similar to the flows below and immediately above.

The lowermost 'tholeiitic basalt' at 1982 Nunatak 1 is a 20 m thick picritic flow with more than 15 vol.% olivine phenocrysts. Above is a *c.* 100 m thick succession of plagioclase ± clinopyroxene–olivine glomerophyric flows where glomerocrysts reach up to 1 cm in diameter and comprise *c.* 2 to 10 vol.% of the rocks. The flows above these and up to the base of the variably dipping 'alkaline basalt succession' are aphyric to slightly phyric or glomerophyric with olivine and or plagioclase microphenocrysts.

The chemical compositions of the 'upper tholeiitic basalts' at Urbjerget 1, 2 and 1982 Nunatak 1 are very similar, and collectively also very similar to the 'lower tholeiitic basalts' at Urbjerget 1 and 2 (Fig. 7). The only exception is the picrite at the base of 1982 Nunatak 1. It has MgO near 24 wt% and low TiO_2 and SiO_2 contents because of the high olivine phenocryst volume.

'Upper high-Ti flow' of Urbjerget 1 and 'high-Ti flows' of 1982 Nunatak 1

Near the very top of Urbjerget 1 at *c.* 2200 m asl is a highly altered vesicular slightly olivine phyric Ti-rich flow (Fig. 5). Ti-rich thin scoriaceous aphyric to slightly olphyric flows also occur near the base of 1982 Nunatak 1 at *c.* 1700 m asl. Chemically, and in terms of flow morphology, the 1982 Nunatak 'high-Ti flows' are more similar to the 'upper high-Ti flow' of Urbjerget 1 than the lower 'high-Ti flows' of Urbjerget 1 (Figs 5, 7–9). The 'high-Ti flows' of 1982 Nunatak 1 are succeeded by 'tholeiitic basalts', but no succession of 'high-Si flows' is found above them. This, along with their geochemical compositions, indicates a stratigraphic level similar to the level of the 'upper high-Ti flow' in Urbjerget 1.

'Alkaline basalts'

The southernmost exposure of 'alkaline basalts' is at the 1982 Nunatak from where they extend north and westwards in the Prinsen af Wales Bjerge. At 1982 Nunatak 1 the 'alkaline basalts' are variably dipping and separated from the underlying succession of 'tholeiitic basalt' by a discontinuous red–brown sediment layer, possibly a tuff. The flows in the formation often follow the topography in the underlying lavas, display highly variable flow thicknesses within short distances (Brooks 1979; Hogg 1985; Brooks *et al.* 1996), and there is no systematic variation of flow types. Petrographically they vary from aphyric to strongly olivine ± clinopyroxene phyric flows (Hogg 1985). Photogrammetric and field studies at locations north of 1982 Nunatak have shown that the 'alkaline basalts' become near-concordant with the underlying tholeiitic suites, and that sub-divisions into several suites may be possible. The top of 1982 Nunatak has been identified as an eruption site for the 'alkaline basalts' and tephra and bombs are abundant at this location. Wager (1947) identified another eruption site farther east, and as mentioned above, an additional crater was identified during fieldwork in 1995 (Fig. 4c). Most of the 'alkaline basalts' have SiO_2 lower than 48 wt% and relatively high contents of $Na_2O + K_2O$, which tend to correlate positively with SiO_2 (Fig. 7). Although geochemically similar to the 'lower high-Ti flows' in many respects, the 'alkaline basalts' have higher $Na_2O + K_2O$, Nb/Zr and La/Sm_N (Figs 7 & 8).

Discussion

New stratigraphic, geochemical and age data from the Prinsen af Wales Bjerge are used to argue for the formalization of two new formations, the Urbjerget and the Prinsen af Wales Bjerge Formations, and the stratigraphy of the Blosseville Kyst basalts is for the first time extended into the Prinsen af Wales Bjerge region by the recognition of the Milne Land Formation. The presence of 61 Ma lavas in the Urbjerget Formation, the oldest onshore Palaeogene lavas identified in East Greenland, indicates that the Urbjerget Formation is similar in age to the coastal Lower Basalts at Kangerlussuaq and supports that the earliest volcanism started almost simultaneously over a widespread area in the North Atlantic. Below we discuss the regional significance of the existence and geographical extent of the different formations and relate our new age data to other North Atlantic Palaeogene volcanics and discuss the importance of our data for flood basalt magmatism and plume impact events.

Urbjerget Formation

The 'old flows' of 61 Ma at Urbjerget 1 is a well-constrained rock suite overlain by sediments, and by lavas that are significantly younger (57–55 Ma). Ages of the 'old flows' suggest that their stratigraphical equivalents must be found among the Lower Basalts of the Kangerlussuaq area (Nielsen *et al.* 1981; Fram & Lesher 1997; Hansen & Nielsen 1999), the Nansen Fjord Formation (at Nansen Fjord, see Fig. 1) and the lower series of the Faroese basalts (Larsen *et al.* 1999) (Fig. 3). Larsen *et al.* (1999) showed that the Nansen Fjord Formation and the lower Faroese basalt series have similar ages and chemical compositions. They both have TiO_2/FeO^* ratios lower than

0.25 (Larsen *et al.* 1999), whereas the old flows at Urbjerget have TiO_2/FeO^* ratios above 0.25 for Mg-numbers ($Mg/(Mg + Fe^{2+})$) close to 55. Such compositions are recorded in neither the Nansen Fjord Formation, nor the lower Faroese basalt series (Larsen *et al.* 1999). Lavas with TiO_2/FeO^* ratios and Mg-numbers similar to the Urbjerget 'old flows' are present in the Vandfaldsdalen Formation and Mikis Formation of the Lower Basalts (Nielsen *et al.* 1981; Fram & Lesher 1997; Hansen & Nielsen 1999; T. F. D. Nielsen & C. K. Brooks pers. comm.). Mikis Formation lavas are typically olivine–phyric (Fram & Lesher 1997) whereas the old flows at Urbjerget 1 are aphyric. Nb/Zr ratios of the 'old flows' are also distinctly different from Mikis Formation lavas but similar to Vandfaldsdalen Formation lavas (Fig. 11). This indicates that the Mikis Formation is not identical with the 'old flows' at Urbjerget. It is, however, also difficult to postulate that the 'old flows' at Urbjerget are related to the same volcanic system as the Vandfaldsdalen Formation lavas, mainly because of the large distance (*c.* 80 km) between the two areas of exposure. These considerations lead us to suggest that the lower part of the Urbjerget 1 succession, i.e. the 'old flows' and interbedded sedimentary units, is formalized as a new formation, the Urbjerget Formation. Details of the formation definition are listed in Table 4.

Table 4. *Urbjerget Formation*

General. Lavas from this and the above formation were described by Wager (1947) as fine-grained, non-pophyritic tholeiites. He noted that the lavas either directly overly metamorphic basement, or coarse arkosic sandstone above the metamorphic complex, and he also commented on the irregular surface onto which the lavas were erupted.

Name and type profile. The formation is named after the nunatak Urbjerget in the Prinsen af Wales Bjerge, and Urbjerget 1 (Fig. 2) is the type profile.

Distribution and thickness. The Urbjerget Formation is present in the area from Urbjerget 1 and southwards to the northernmost part of Nordfjord Gletscher at the head of Kangerlussuaq. The thickness at Urbjerget 1 is *c.* 50 m.

Lithology. In the type profile, a thin cover of fluviatile arkosic sandstone with tree limb casts and organic lenses overly banded tonalitic gneiss containing amphibolite lenses and massive feldspar segregations. The sandstone is succeeded by a thin black, lacustrine shale with plant fossils, followed by a *c.* 30 m thick succession of massive, aphyric lava flows which have been dated to *c.* 61 Ma. Above the lava flows is a volcaniclastic sediment.

Chemical compositions of lava flows. Two Urbjerget Formation flows have major element compositions fairly similar to the Milne Land Formation tholeiitic basalts higher in Urbjerget 1, although with low Al_2O_3 (Table 2). A third flow is relatively TiO_2- and FeO*-rich compared to the Milne Land Formation basalts. Trace element spectra of Urbjerget Formation flows tend to be slightly steeper from Ti to Lu than tholeiitic basalt spectra (Fig. 9).

Eruption sites. Eruption sites have not been identified, but the apparent limited areal extent and the relatively thin flows of the Urbjerget Formation may indicate eruption sites close to Urbjerget 1.

Boundaries. The Urbjerget Formation overlies Archaean basement, and is succeeded by the Milne Land Formation. The uppermost part of the Urbjerget Formation is a volcaniclastic sediment with 3 to 5 cm large rounded clasts of volcanic rocks, which is conformably overlain by olivine-phyric high-Ti flows of the Milne Land Formation.

The Milne Land Formation in the Prinsen af Wales Bjerge and the relations to other Milne Land Formation flows

The $^{40}Ar/^{39}Ar$ ages obtained on the lower tholeiitic basalts in Urbjerget 1 indicate they were extruded simultaneously with early plateau basalt lavas, i.e. Milne Land Formation flows (Figs 3 & 6; Table 1). Geochemically, Milne Land Formation basalts are quite distinct. They tend to have high SiO_2 and lower TiO_2/SiO_2 ratios than other plateau basalts with similar TiO_2/FeO^*. In Figures 10 and 11 we plotted Milne Land Formation basalts from the Scoresby Sund, Sortebræ and Nansen Fjord areas with other plateau basalt formations in order to identify Milne Land Formation characteristics and compare them with Prinsen af Wales Bjerge basalts. Figure 10a shows that Milne Land Formation basalts generally have lower FeO* than basalts of the Geikie Plateau Formation. Figures 10b and c show the distinct SiO_2 enrichment of Milne Land Formation relative to Rømer Fjord Formation and Skrænterne Formation basalts with similar TiO_2/FeO^* ratios. The fact that the 'tholeiitic basalts' and 'high-Si flows' of Urbjerget 1, Urbjerget 2 and 1982 Nunatak 1 consistently plot with Milne Land Formation basalts is convincing evidence that they do belong to the Milne Land Formation. This is confirmed by trace element variations shown in Figure 11, where Urbjerget 1, Urbjerget 2 and 1982 Nunatak 1 'tholeiitic basalts' and 'high-Si flows' again plot in the field defined by Milne Land Formation basalts from the Scoresby Sund, Sortebræ area and Nansen Fjord areas. Thus, the geochemical relations support the contention that the tholeiitic basalts and high-Si flow successions in the southern Prinsen af Wales Bjerge region are part of the Milne Land Formation. The ages of the 'lower high-Ti flows' of Urbjerget 1 are indistinguishable from the overlying Milne Land Formation basalts. This indicates either no interval or only a short one between the eruption of the two suites and we therefore assign the succession of 'lower high-Ti flows' to the Milne Land Formation.

One characteristic of the Milne Land Formation is the occurrence of a coherent succession of distinctly Si-enriched flows ($SiO_2 > 53$ wt%), 110 m thick at Nansen Fjord (Larsen *et al.* 1999). Similar flow successions are present in both Urbjerget 1 (at least 55 m of high-Si flows) and Urbjerget 2 (*c.* 120 m of 'high-Si flows') (Fig. 5). Other plateau basalt formations of East Greenland seem to lack such distinct, thick Si-enriched flow successions, although more limited occurrences of high-Si flows are found in, e.g. the Skrænterne Formation (L. M. Larsen pers. comm.; Larsen *et al.* 1989). The 'high-Si flows' have high $(La/Sm)_N$, high La/Nb ratios combined with high SiO_2 contents (Fig. 8), trace element patterns with Nb–Ta troughs (Fig. 9) and very high $^{87}Sr/^{86}Sr$ (0.709016 at 56 Ma sample 436464, Table 2). This suggests that crustal contamination took place during the formation of these rocks and trace element patterns are consistent with what is expected from contamination with East Greenland gneisses, most likely of amphibolite facies type (Hansen & Nielsen 1999). Crustal contamination also provides a reason for the presence of orthopyroxene as a phenocryst phase in high-Si flows at Urbjerget. An increase in silica activity of a basaltic magma due to contamination with felsic melts derived from the gneiss basement will act towards stabilization of orthopyroxene in the final mixing product. In order for the magmas to become crustally contaminated, they must have resided in contact with crustal rocks for a longer period of time than magmas that were erupted as uncontaminated (or less contaminated) 'tholeiitic basalts'. This means that either the magma supply from the mantle slowed down, and/or that the rate of

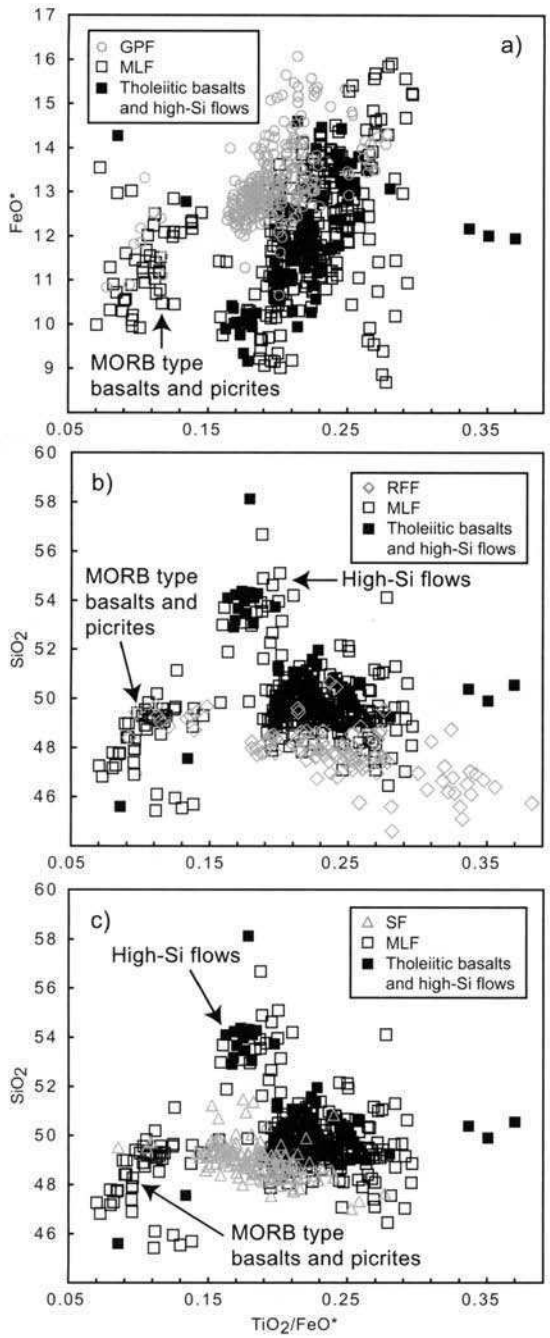

Fig. 10. Major element compositions (in weight %) of Milne Land (MLF), Geikie Plateau (GPF), Rømer Fjord (RFF) and Skrænterne Formation (SF) flows compared with the lower and upper tholeiitic basalts and high-Si flows of the southern Prinsen af Wales Bjerge. Plateau basalt formation data are from the Scoresby Sund area (Larsen *et al.* 1989) Sortebræ (DLC database, O. Stecher pers. comm.) and Nansen Fjord (Larsen *et al.* 1999; L. M. Larsen pers. comm.). Prinsen af Wales Bjerge data are from this study (Table 2).

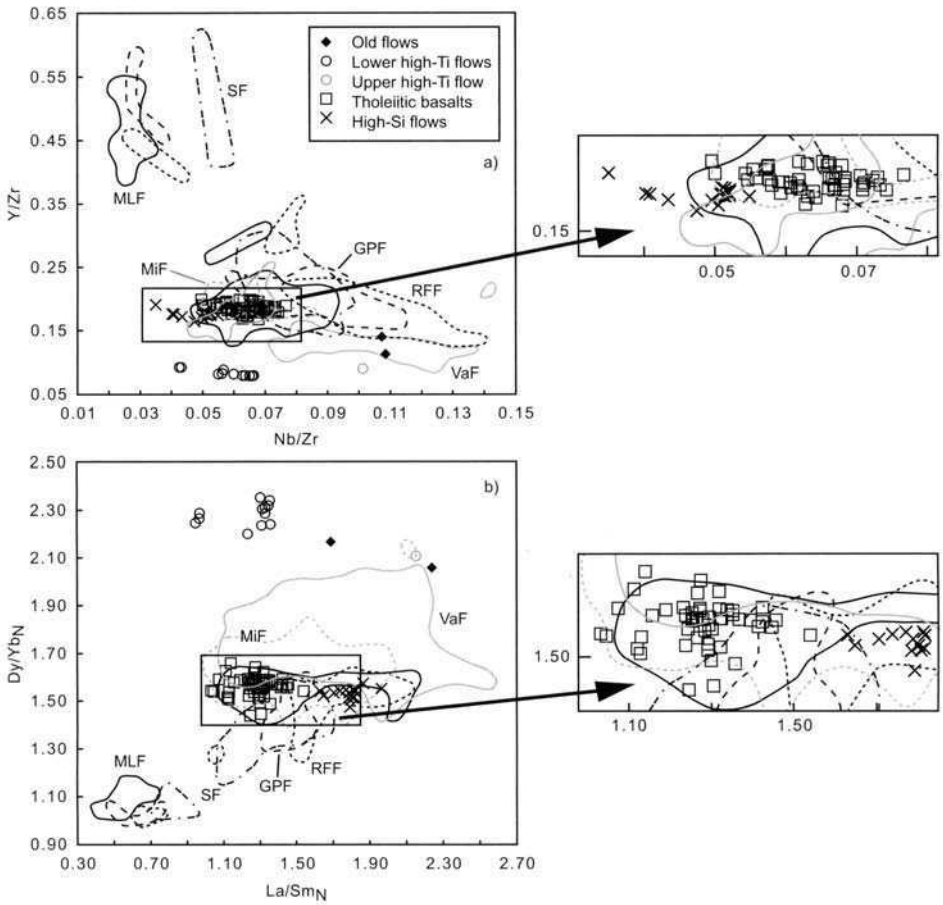

Fig. 11. Trace element compositions of East Greenland flood basalts from the Scoresby Sund and Sortebræ areas compared with the tholeiitic basalts, high-Si, lower high-Ti and old flows of the southern Prinsen af Wales Bjerge. Prinsen af Wales Bjerge data are from this study, others from Larsen *et al.* (1989), Fram & Lesher (1997), Tegner *et al.* (1998*b*), Hansen & Nielsen (1999) plus additional unpublished data for Vandfaldsdalen and Mikis Formation lavas (H. Hansen, T. F. D. Nielsen & C. K. Brooks).

continental rifting episodically decreased. Changes in the rate of continental rifting are very difficult to assess, but Tegner *et al.* (1998*b*) concluded that the mantle potential temperature beneath East Greenland decreased during formation of Milne Land and Geikie Plateau Formation lavas. This suggests that conditions for a regional decline in mantle magma supply were present and this may explain the presence and the geographically widespread nature of the 'high-Si flow' succession in the Milne Land Formation.

Some differences do exist between the Milne Land Formation as exposed in the Scoresby Sund area, in the coastal flood basalt successions along the Blosseville Kyst and in the inland Prinsen af Wales Bjerge successions. For example, Figure 11 shows that no flows in the Prinsen af Wales Bjerge Milne Land Formation overlap with the regional suite of Milne Land Formation basalts which have Y/Zr above *c.* 0.35

and $(Dy/Yb)_N$ lower than *c.* 1.2. These high-Y/Zr and low-$(Dy/Yb)_N$ flows are the MORB-type flows of Larsen *et al.* (1989) and Tegner *et al.* (1998*b*), and they are most abundant in coastal sections (Larsen *et al.* 1999; Nielsen *et al.* 2001; L. M. Larsen pers. comm.). Tegner *et al.* (1998*b*) suggested that the MORB-type basalts require shallower depths of mantle melting and longer melting columns within the mantle than other Milne Land Formation basalts. Another dissimilarity between the inland and coastal Milne Land Formation successions is the presence of the lower and upper 'high-Ti flows' in the inland southern Prinsen af Wales Bjerge (e.g. Figs 5 & 7), and the absence of similar flows in the rest of the East Greenland flood basalt province. The high $(Dy/Yb)_N$ and CaO/Al_2O_3 ratios of the 'high-Ti flows' (Figs 7 & 8) indicate that they were formed by higher pressures of melting than other tholeiitic basalts of the Milne Land Formation (Hansen *et al.* 1998), and they probably also require a unique combination of mantle source regions. The regional variations within the Milne Land Formation, i.e. the absence of MORB-type flows and presence of 'high-Ti flows' in the southern Prinsen af Wales Bjerge, can to some extent be explained by greater proximity to the locus of break-up of coastal flood basalts relative to Prinsen af Wales Bjerge flood basalts. MORB-type flows were not formed in the immediate vicinity of the Prinsen af Wales Bjerge because the lithosphere was never thin enough to allow the shallow mantle melting and long melting columns required to form these magma types (Tegner *et al.* 1998*b*). On the other hand, magmas that gave rise to the 'high-Ti flows' were favoured under the thicker lithosphere in the inland region. MORB-type flows did not flow long distances inland from eruption sites in more coastal areas, and the 'high-Ti flows' never flowed from their inland eruption sites to the coastal areas, possibly due to relatively small flow volumes.

The Milne Land Formation in the Prinsen af Wales Bjerge consists of alternating successions of thin, vesicular pahoehoe flows (each $<c.$ 1 m), and thick ($>c.$ 3 m) sheet flows (this work; Hogg *et al.* 1989). The sheet flows can be followed over several tens of kilometres, whereas the pahoehoe successions seem to be a near-vent facies. The alternation between the different kinds of successions suggests that the location of eruption sites changed during effusion of the flows. Similar changes in flow morphologies are observed in the Milne Land Formation of the Scoresby Sund area (Larsen *et al.* 1989) and at Nansen Fjord (Larsen *et al.* 1999). Small flow volumes in the order of less than 0.3 km^3 and cyclic trace element variations in the tholeiitic basalts of the 1982 Nunatak, which we here have shown belong to the Milne Land Formation, made Hogg *et al.* (1988, 1989) advocate for the presence of small magma chambers during their formation. Flow morphologies and regional compositional differences in the Milne Land Formation throughout central East Greenland strongly supports the view that small magma chambers were also in action outside the Prinsen af Wales Bjerge region. A suite of magnesian basalts to picrites is found at the base of the formation at Nansen Fjord (Larsen *et al.* 1999) at a position corresponding to the 'lower high-Ti flow' suite of Urbjerget 1 (Fig. 5). The geochemical composition of the Urbjerget 'high-Ti flows' is very different from the compositions of the Nansen Fjord suite, but both suites are very Mg-rich. This indicates both the presence of small magma chambers and that the same elevated mantle temperature (required for producing high-magnesian basalts) existed over wide areas. Larsen *et al.* (1989) argued for the existance of crustal magma chambers up to 12 000 km^3 and proposed a sill-like ellipsoid chamber size with dimensions 150 × 30 × 5 km at 10–15 km depth. These dimensions were estimated from the typical 20–60 km^3 flow volumes in the

Scoresby Sund region and by assuming 0.5% of the chamber contents were erupted. Magma chambers of this size have never been imaged by geophysical methods but on the other hand erupted flows have had much lower volumes during the time geophysical imaging techniques have been applied. Magma chamber sizes could well have varied geographically in East Greenland so that larger chambers were present in the Scoresby Sund region were rifting might have been concentrated at the time of extrusion of Milne Land Formation flows (Larsen & Watt 1985), whereas smaller chambers resided in the Prinsen af Wales Bjerge region. Alternatively, the intense rifting and elevated mantle temperatures during flood basalt emplacement may have sustained a high net flux of magma through smaller magma chambers.

Milne Land Formation lavas in general are relatively uniform in composition and distinguishable from other regional plateau basalt formations in East Greenland (Figs 10 & 11). This suggests that the mantle source region for the Milne Land Formation flows was fairly homogeneous. Local compositional variations are caused by mantle melting under variably thick lithosphere, small-scale variations in mantle composition and mixing in small magma chambers, particularly in the Prinsen af Wales Bjerge and southern Blosseville Kyst regions. Potential mantle temperatures were uniform over wide areas, and a decline in mantle potential temperature (Tegner *et al.* 1998*b*) or a decrease in the rate of continental rifting may have favoured prolonged magma storage in crustal magma chambers leading to the formation of 'high-Si flows'.

The Prinsen af Wales Bjerge Formation and the 'missing' plateau basalts

The 'alkaline basalts' in the Prinsen af Wales Bjerge form a unit with a well defined lower boundary to the 'tholeiitic basalts' (e.g. Wager 1947; Hogg 1985; Brown *et al.* 1996), and as shown in Figures 7–9 they are compositionally distinct from other Prinsen af Wales Bjerge lava flows. The abundance of craters built up by 'alkaline basalt' and the presence of basaltic bombs and tephra in the Prinsen af Wales Bjerge suggest that the top of the 'alkaline basalt' suite to a large extent forms the final upper landsurface of the volcanics. However, at least at one locality, 'Lindsay Nunatak', 'tholeiitic basalts' are observed overlying alkaline flows (Nielsen *et al.* 2001). An $^{40}Ar/^{39}Ar$ age determination of the uppermost alkaline flows at 'Lindsay Nunatak' is 52.5 ± 0.3 Ma, which is identical to the 52.7 ± 1.2 Ma age from 'alkaline basalts' in the central Prinsen af Wales Bjerge (age data from Peate *et al.* 2000). This may suggest that alkaline volcanism was short-lived. An alkaline tuff from the Gronau West Nunatak *c.* 100 km ENE of the Prinsen af Wales Bjerge was dated by Heister *et al.* (2001) to 55 ± 0.3 Ma by the $^{40}Ar/^{39}Ar$ method (age reported relative to the flux monitors mentioned in Table 1). The tuff mineralogy indicates a relation to the alkaline Gardiner melanephelinite-carbonatite volcanic complex *c.* 50 km SW of the southern Prinsen af Wales Bjerge (Heister *et al.* 2001). The tuff age is the oldest recorded for onshore alkaline volcanic products in central East Greenland and along with the ages from the Prinsen af Wales Bjerge it indicates that alkaline volcanic activity in this region lasted no more than 2.5 Ma. The Gronau West Nunatak alkaline tuff is found within the Skrænterne Formation and this suggests that the late tholeiitic plateau basalts were extruded while alkaline volcanic activity took place. In the southern Prinsen af Wales Bjerge, however, there are no certain indications of

the presence of other plateau basalt formations than the Milne Land Formation, and the transition from tholeiitic to alkaline flows is abrupt. Farther north tholeiitic and alkaline flows are interbedded in the lower part of the volcanic succession, and the tholeiites seem to be related to plateau basalt formations of Milne Land Formation age or younger (Peate *et al.* in press). The absence of Geikie Plateau, Rømer Fjord and Skrænterne Formations in the southern Prinsen af Wales Bjerge might be explained as a result of local uplift and possibly slight northward kipping initiated during the late stages of Milne Land Formation flow emplacement. Alternatively, the absence of the Geikie Plateau, Rømer Fjord and Skrænterne formations in the southern Prinsen af Wales Bjerge may be due to a more distal location of eruption sites for flows of these formations than of Milne Land Formation eruption sites, or that local topography prevented flows of the missing formations to enter the southern Prinsen af Wales Bjerge.

In accordance with previous authors (e.g. Hogg 1985; Brown *et al.* 1996) we suggest that the succession of 'alkaline basalts' in the Prinsen af Wales Bjerge is considered a separate volcanic formation named Prinsen af Wales Bjerge Formation. We propose that the geographical name of the area (Prinsen af Wales Bjerge) in which the formation is found rather than the partial English translation used by Brown *et al.* (1996) is included in the formation name. However, the 'Prince of Wales Formation' informally used by Brown *et al.* (1996) is identical with the Prinsen af Wales Bjerge Formation. Further details of the Prinsen af Wales Bjerge Formation are listed in Table 5.

Early Palaeogene volcanism in the North Atlantic region

In the North Atlantic region, 62 to 59 Ma lavas and tuffs have been recovered offshore from the SE Greenland margin in ODP Leg 152 (Sinton & Duncan 1998; Werner *et al.* 1998), onshore from the NW British Isles (e.g. Pearson *et al.* 1996; Chambers & Fitton 2000) and West Greenland (Storey *et al.* 1998). Storey *et al.* (1996*a*), Saunders *et al.* (1997) and Tegner *et al.* (1998*a*) suggested that the almost simultaneous outbreak of volcanism within widespread areas of the present North Atlantic region at about 62 to 61 Ma is the result of either plume impact or a sudden burst of plume activity in an existing plume. The *c.* 61 Ma Urbjerget Formation flows in the southern Prinsen af Wales Bjerge are a manifestation of this early plume activity.

There is a considerable age gap from *c.* 61 Ma to *c.* 57 Ma in the lower part of the Urbjerget 1 succession near 69°N. Offshore SE Greenland at 63°N, ages of ODP Leg 152 Lower Series basaltic flows are 61–62 Ma, whereas Upper Series flow ages are 57–58 Ma (Sinton & Duncan 1998). At both locations sedimentary rock units separate the old and the young flows. A volcanogenic sediment at Urbjerget 1 is located at a position corresponding to the 0 m reference level (sediment) in the Nansen Fjord and the coal-bearing horizon in the Faroe Islands volcanic succession (Larsen *et al.* 1999). The two latter sediments both contain partially altered plant remains (Rasmussen & Noe-Nygaard 1969, 1970; Larsen *et al.* 1999), and the presence of vitrinite in the Urbjerget sediment shows plant remains are also present there. This supports the idea that a significant hiatus developed during the early volcanic history of flood basalt deposition in central East Greenland and the Faroe Islands as the $^{40}Ar/^{39}Ar$ age data suggests. The volcanic activity along the East Greenland margin from at

Table 5. *Prinsen af Wales Bjerge Formation*

General. Lavas of this formation were described by Wager (1947), Anwar (1955), Hogg (1985), and Brown *et al.* (1956): Wager (1947) and Anwar (1955) referred to them as the Prinsen af Wales Bjerge Basalts, and Hogg (1985) proposed that the succession should be formalized and given formation status (Prinsen af Wales Formation). Brown *et al.* (1996) used the term Prince of Wales Formation for the basalts but without actually formalizing the term.

Name and type profile. The formation is named after the nunatak mountain range Prinsen af Wales Bjerge (Fig. 1), and the type profile is 1982 Nunatak 1.

Distribution and thickness. The Prinsen af Wales Bjerge Formation is present from 1982 Nunatak in the south from where it extends north and westwards. At 1982 Nunatak it is *c.* 150 m thick. Photogrammetric and field studies at locations north of 1982 Nunatak have shown that the basalts of the Prinsen af Wales Bjerge Formation become near-concordant with the underlying Milne Land Formation (and possibly younger formations further north), and that sub-divisions into several suites may be possible. The flows in the formation often follow the topography in the underlying lavas (Brooks 1979; Hogg 1985; Brooks *et al.* 1996).

Lithology. Flows of the Prinsen af Wales Bjerge Formation at 1982 Nunatak 1 are variably dipping and separated from the underlying succession of tholeiitic basalt by a discontinuous red-brown sediment layer. There is no systematic variation of flow types but petrographically flows vary from aphyric to strongly olivine ± clinopyroxene phyric (Hogg 1985). Flows have been dated to 52.5–52.7 Ma (Peate *et al.* 2000).

Chemical composition. The alkaline basalts of the Prinsen af Wales Bjerge Formation have lower SiO_2 contents and generally steeper trace element spectra than other flows in the southern Prinsen af Wales Bjerge (Figs 7 & 9).

Eruption sites. The top of 1982 Nunatak has been identified as an eruption site for the Prinsen af Wales Bjerge Formation basalts (one is shown in Fig. 2 and 4c), and Wager (1947) identified an eruption site in the eastern part of Prinsen af Wales Bjerge.

Boundaries. The base of the formation is defined at the unconformity between tholeiitic basalts and alkaline basalts at 1982 Nunatak 1. An upper boundary of the formation occurs at 'Lindsay Nunatak', where it is overlain by polymict conglomerates of fluviatile origin and tholeiitic flows (Nielsen *et al.* 2001), but in large areas the uppermost part of the formation constitute the present landsurface.

least 69° to 63°N seems to have declined dramatically in the interval from *c.* 61 Ma to 58 Ma. This pause was succeeded by extrusion of the most voluminous suite of central East Greenland flood basalts (the plateau basalts in Fig. 3), and the Upper Series flows at the palaeo-location of ODP Leg 152. In the British Isles most of the Palaeogene volcanic activity predates 58 Ma (Saunders *et al.* 1997 and references therein), and this is also the case for Palaeogene volcanism in West Greenland (Storey *et al.* 1998). The pause in volcanic activity possibly reflects the time it took from the first batch of hot plume material had dispersed beneath the lithosphere and cooled to such a degree that volcanic activity at the Earth's surface was no longer possible till the next batch of hot plume material arrived and re-activated the volcanism. Later plume pulses would be more difficult to recognize because the lithosphere thinned progressively with time and therefore enhanced mantle upwelling and associated melt production, provided a less severe hindrance for magma passage, and because much of the more recent volcanic products are now below sea level. In the more recent history

of the Icelandic plume variations in trace element ratios and isotopes (e.g., chondrite-normalized La/Sm and Pb-isotopes) of Faroese and Icelandic basalts have been interpreted as consistent with a blob-like plume behaviour (e.g. Schilling & Noe-Nygaard 1974; Hanan & Schilling 1997; Hanan *et al.* 2000).

Conclusions

Two new formal volcanic formations are proposed: the Urbjerget Formation and Prinsen af Wales Bjerge Formation. The Urbjerget Formation consists of intermixed basaltic lava flows and sediments where flows are *c.* 61 Ma and have chemical characteristics similar to the coastal Vandfaldsdalen Formation flows at Kangerlussuaq. At Urbjerget 1 a volcanogenic sediment marks the boundary to a succession of significantly younger (<57 Ma) tholeiitic flows that belong to the Milne Land Formation. The Prinsen af Wales Bjerge Formation consists of mainly alkaline basalts and overly the Milne Land Formation at the 1982 Nunatak.

The Milne Land Formation is present in the southern Prinsen af Wales Bjerge as the only formation of regional extent in East Greenland. Flows from 'missing' plateau basalt formations, i.e. Geikie Plateau, Rømer Fjord and Skrænterne formations, may have been prevented from entering the southern Prinsen af Wales Bjerge due to local uplift of this area, or because eruption sites were located at more distal locations than Milne Land Formation eruption sites, or local topography could have been an obstacle. A geographically widespread succession of crustally contaminated high-Si flows in the Milne Land Formation was probably formed in response to a reduced magma supply from the mantle that favoured magma stalling in crustal chambers, a process possibly promoted by a continuous lowering of potential mantle temperatures suggested by Tegner *et al.* (1998*b*) or by a decrease in the rate of rifting. A suite of tholeiitic high-Ti flows within the Milne Land Formation is unique to the Prinsen af Wales Bjerge region, and equivalents have not been reported from other flood basalt provinces. Local variations in the Milne Land Formation flow compositions can be explained as the result of melting under lithosphere of variable thickness, small-scale variations in mantle composition and mixing in small magma chambers.

The Urbjerget Formation contains the oldest Palaeogene onshore lava flows dated in East Greenland, and the Urbjerget 1 succession has equivalents at Nansen Fjord and in the Faroe Islands. Volcanic rocks with ages of 62 to 58 Ma are found in West Greenland, the British Isles and offshore SE Greenland, and have been interpreted as the result of either plume impact or an early blob arrival in the palaeo-Icelandic plume (Storey *et al.* 1996*a*; Saunders *et al.* 1997; Tegner *et al.* 1998*a*). The pause between the initial phase of volcanism and the phase started by the deposition of Milne Land Formation flows in central East Greenland may approximate the timing between the phase-out of the first and arrival of the second plume pulse.

We thank M. Storey for access to unpublished age data from the East Greenland flood basalts, and C. Meredith and J. A. Pearce for assistance with ICP-MS analysis at Oregon State University and Durham University. R. Frei provided access to isotope laboratory facilities at the University of Copenhagen, and J. Bailey and J. Kystol supplied XRF trace element and major element analyses. L. Heister kindly sent us a manuscript in press, and vitrinite reflectance analysis was performed by C. Guvad. T. F. D. Nielsen elegantly handled East Greenland fieldwork operations in 1995 and 2000, A. Kent and P. Neuhoff assisted in the field,

where Greenlandair helicopter pilots G. Lindmark and M. Hällström provided luxurious inter-nunatak transport. This study was supported by the Danish Lithosphere Centre, which is funded by the Danish National Research Foundation. The Natural Sciences and Engineering Research Council of Canada and the University of Toronto provided funding for JG, MG and JJF. Publication of this paper has been authorized by the Geological Survey of Denmark and Greenland, Copenhagen.

References

ANWAR, Y. M. 1955. Geological investigations in East Greenland, Part V. The petrography of the Prinsen af Wales Bjerge lavas. *Meddelelser om Grønland*, **135**, 1–33.

BROOKS, C. K. 1973. Rifting and doming in southern East Greenland. *Nature*, **244**, 23–25.

BROOKS, C. K. 1979. Geomorphological observations at Kangerdlugssuaq, East Greenland. *Meddelelser om Grønland, Geoscience*, **1**, 1–24.

BROOKS, C. K. AND FIELD PARTIES 1996. The East Greenland volcanic rifted margin – onshore DLC fieldwork. *Bulletin Grønlands Geologiske Undersøgelse*, **172**, 95–102.

BROWN, P. E., EVANS, I. B. & BECKER, S. M. 1996. The Prince of Wales Formation – post-flood basalt alkali volcanism in the Tertiary of East Greenland. *Contributions to Mineralogy and Petrology*, **123**, 424–434.

BROWN, P. E., EVANS, I. B. & BECKER, S. M. 2000. Alkaline basaltic volcanism in the Tertiary of central East Greenland – the Trekantnunatakker. *Transactions of the Royal Society of Edinburgh: Earth Sciences*, **90**, 165–172.

CHAMBERS, L. M. & FITTON, J. G. 2000. Geochemical transitions in the ancestral Iceland plume: evidence from the Isle of Mull Tertiary volcano, Scotland. *Journal of the Geological Society, London*, **157**, 261–263.

DUEHOLM, K. S. & PEDERSEN, A. K. (eds) 1992. Geological analysis and mapping using multi-model photgrammetry. *Grønlands Geologiske Undersøgelse Rapport*, **156**, 1–72.

FRAM, M. S. & LESHER, C. E. 1997. Generation and polybaric differentiation of East Greenland early Tertiary flood basalts. *Journal of Petrology*, **38**, 231–275.

HANAN, B. B., BLICHERT-TOFT, J., KINGSLEY, R. & SCHILLING, J.-G. 2000. Depleted Iceland mantle plume geochemical signature: Artifact of multicomponent mixing? *Geochemistry, Geophysics, Geosystems*, **1**, Paper number 1999G000009, 24.

HANAN, B. B. & SCHILLING, J.-G. 1997. The dynamic evolution of the Iceland mantle plume: the lead isotope perspective. *Earth and Planetary Science Letters*, **151**, 43–60.

HANSEN, H. & NIELSEN, T. F. D. 1999. Crustal contamination in Palaeogene East Greenland flood basalts: plumbing system evolution during continental rifting. *Chemical Geology*, **157**, 89–118.

HANSEN, H., PEDERSEN, A. K., BIRD, D. K., O'DAY, P. & LESHER, C. E. 1998. High-Ti magnesian basalts from the Palaeogene central East Greenland flood basalt province: tholeiitic near-primary magmas formed by high-pressure garnet-lherzolite melting or melts from a unique mantle source? *EOS*, **79**, 1006–1007.

HANSEN, H., REX, D. C., GUISE, P. G. & BROOKS, C. K. 1995. $^{40}Ar/^{39}Ar$ ages on early Tertiary basalts from the Scoresby Sund area, East Greenland. *Newsletters on Stratigraphy*, **32**, 103–116.

HEISTER, L., O'DAY, P. A., BROOKS, C. K., NEUHOFF, P. S. & BIRD, D. K. 2001. Pyroclastic deposits within the East Greenland Tertiary flood basalts. *Journal of the Geological Society, London*, **158**, 269–284.

HOGG, A. J. 1985. *The petrology and geochemistry of the Prinsen af Wales Bjerge, East Greenland.* MSc Thesis, University of Toronto, 1–99.

HOGG, A. J., FAWCETT, J. J., GITTINS, J. & GORTON, M. P. 1988. Cyclical tholeiitic volcanism and associated magma chambers: eruptive mechanisms in E Greenland. *In*: MORTON, A. C. & PARSON, L. M. (eds) *Early Tertiary volcanism and the opening of the NE Atlantic.* Geological Society, London, Special Publications, **39**, 197–200.

HOGG, A. J., FAWCETT, J. J., GITTINS, J. & GORTON, M. P. 1989. Cyclical variation in composition in continental tholeiites of East Greenland. *Canadian Journal of Earth Science*, **26**, 534–543.

HOLM, P. M., HALD, N. & WAAGSTEIN, R. 2001. Geochemical and Pb-Sr-Nd isotopic evidence for separate hot depleted and Iceland plume mantle sources for the Paleogene basalts of the Faroe Islands. *Chemical Geology*, **178**, 95–125.

KARSON, J. A. & BROOKS, C. K. 1999. Structural and magmatic segmentation of the Tertiary East Greenland volcanic rifted margin. *In*: MACNIOCAILL, C. & RYAN, P. D. (eds) *Continental tectonics*. Geological Society, London, Special Publications, **164**, 313–338.

KYSTOL, J. & LARSEN, L. M. 1999. Analytical procedures in the Rock Geochemical Laboratory of the Geological Survey of Denmark and Greenland. *Geology of Greenland Survey Bulletin*, **184**, 59–62.

LARSEN, L. M., WAAGSTEIN, R., PEDERSEN, A. K. & STOREY, M. 1999. Trans-Atlantic correlation of the Palaeogene successions in the Faroe Islands and East Greenland. *Journal of the Geological Society, London*, **156**, 1081–1095.

LARSEN, L. M. & WATT, W. S. 1985. Episodic volcanism during break-up of the North Atlantic: evidence from the East Greenland plateau basalts. *Earth and Planetary Science Letters*, **73**, 105–116.

LARSEN, L. M., WATT, W. S. & WATT, M. 1989. Geology and petrology of the Lower Tertiary plateau basalts of the Scoresby Sund region, East Greenland. *Grønlands Geologiske Undersøgelse Bulletin*, **157**, 1–164.

LE BAS, M. J. 2000. IUGS reclassification of the high-Mg and picritic volcanic rocks. *Journal of Petrology*, **41**, 1467–1470.

LE BAS, M. J., LE MAITRE, R. W. & WOOLLEY, A. R. 1992. The construction of the total alkali-silica classification of volcanic rocks. *Mineralogy and Petrology*, **46**, 1–22.

MAHONEY, J. J. 1987. An isotopic survey of Pacific plateaus: implications for their nature and origin. *In*: KEATING, B. H., FRYER, P., BATIZA, R. & BOEHLERT, G. W. (eds) *Seamounts, Islands, and Atolls*. Geophysical Monograph, **43**, 207–220.

NIELSEN, T. F. D. 1975. Possible mechanism of continental breakup in the North Atlantic. *Nature*, **253**, 182–184.

NIELSEN, T. F. D., HANSEN, H., BROOKS, C. K., LESHER, C. E. & FIELD PARTIES 2001. The East Greenland continental margin, the Prinsen af Wales Bjerge and new Skaergaard intrusion initiatives. *Geological Survey of Greenland, Bulletin*, **189**, 83–98.

NIELSEN, T. F. D., SOPER, N. J., BROOKS, C. K., FALLER, A. M., HIGGINS, A. C. & MATTHEWS, D. W. 1981. The pre-basaltic sediments and the lower lavas at Kangerdlugssuaq, East Greenland. Their stratigraphy, lithology, palaeomagnetism and petrology. *Meddelelser om Grønland, Geoscience*, **6**.

NORRISH, K. & CHAPPELL, B. W. 1977. X-ray fluorescence spectrometry. *In*: ZUSSMAN, J. (ed.) *Physical methods in determinative mineralogy, 2nd edn*. Academic Press, London, 201–272.

PEARSON, D. G., EMELEUS, C. H. & KELLEY, S. P. 1996. Precise $^{40}Ar/^{39}Ar$ age for the initiation of Palaeogene volcanism in the Inner Hebrides and its regional significance. *Journal of the Geological Society, London*, **153**, 815–818.

PEATE, D. W., BAKER, J. A., BLICHERT-TOFT, J., *ET AL.* in press. The Prinsen of Wales Bjerge Formation lavas, East Greenland: the transition from tholeiitic to alkalic magnetism during Palaeogene continental break-up. *Journal of Petrology*, in press.

PEATE, D. W., BROOKS, C. K., BAKER, J. A., BLICHERT-TOFT, J., PEDERSEN, A. K., HANSEN, H., STOREY, M. & MATTEY, 2000. Origin of late-stage alkaline magmatism in the Tertiary East Greenland flood basalt province: the Prinsen af Wales Bjerge in the inland Kangerlussuaq region. *Penrose 2000: Volcanic Rifted margins, London, UK*, Abstract Volume, **67**.

PEDERSEN, A. K., WATT, M., WATT, W. S. & LARSEN, L. M. 1997. Structure and stratigraphy of the Early Tertiary basalts of the Blosseville Kyst, East Greenland. *Journal of the Geological Society, London*, **154**, 565–570.

PYLE, D. G., CHRISTIE, D. M., MAHONEY, J. J. & DUNCAN, R. A. 1995. Geochemistry and geochronology of ancient southeast Indian and southwest Pacific seafloor. *Journal of Geophysical Research*, **100**, 22 261–22 282.

RASMUSSEN, J. & NOE-NYGAARD, A. 1969. Beskrivelse til geologisk kort over Færøerne. *Danmarks Geologiske Undersøgelse 1, Serie* **24**.

RASMUSSEN, J. & NOE-NYGAARD, A. 1970. Geology of the Faroe Islands. *Danmarks Geologiske Undersøgelse 1, Serie* **25**.

RENNE, P. R., DEINO, A. L., WALTER, R. C., TURRIN, B. D., SWISHER, C. C. III, BECKER, T. A., CURTIS, G. H., SHARP, W. D. & JAOUNI, A. R. 1994. Intercalibration of astronomical and radioisotopic time. *Geology*, **22**, 783–786.

SAUNDERS, A. D., FITTON, J. G., KERR, A. C., NORRY, M. J., & KENT, R. W. 1997. The North Atlantic Province. *In*: MAHONEY, J. J. & COFFIN, M. F. (eds) *Large igneous provinces: continental, oceanic, and planetary volcanism*. Geophysical Monograph, **100**, 45–93.

SCHILLING, J.-G. & NOE-NYGAARD, A. 1974. Faroe–Iceland plume: Rare earth evidence. *Earth and Planetary Science Letters*, **24**, 1–14.

SINTON, C. W. & DUNCAN, R. A. 1998. ^{40}Ar–^{39}Ar ages of lavas from the southeast Greenland margin, ODP Leg 152, and the Rockall Plateau, DSDP Leg 81. *In*: SAUNDERS, A. D., LARSEN, H. C. & WISE, S. W. JR. (eds) *Proceedings of the Ocean Drilling Program, Scientific Results*. College Station, Texas, **152**, 387–402.

SOPER, N. J., HIGGINS, A. C., DOWNIE, C., MATTHEWS, D. W. & BROWN, P. E. 1976. Late Cretaceous–early Tertiary stratigraphy of the Kangerdlugssuaq area, east Greenland, and the age of opening of the north-east Atlantic. *Journal of the Geological Society, London*, **132**, 85–104.

STOREY, M., DUNCAN, R. A., LARSEN, H. C., PEDERSEN, A. K., WAAGSTEIN, R., LARSEN, L. M., TEGNER, C. & LESHER, C. E. 1996*a*. Impact and rapid flow of the Iceland plume beneath Greenland at 61 Ma. *EOS*, **77**, 839.

STOREY, M., PEDERSEN, A. K., LARSEN, H. C., LARSEN, L. M., STECHER, O., DUNCAN, R. A., TEGNER, C. & CARLSON, R. W. 1996*b*. Middle Miocene volcanism in East Greenland. *EOS*, **77**, 823.

STOREY, M., DUNCAN, R. A., PEDERSEN, A. K., LARSEN, L. M. & LARSEN, H. C. 1998. $^{40}Ar/^{39}Ar$ geochronology of the West Greenland Tertiary volcanic province. *Earth and Planetary Science Letters*, **160**, 569–586.

SUN, S. S. & MCDONOUGH, W. F. 1989. Chemical and isotopic systematics of oceanic basalts: implications for mantle composition and processes. *In*: SAUNDERS, A. D. & NORRY, M. J. (eds) *Magmatism in Ocean Basins*. Geological Society, London, Special Publications, **42**, 313–345.

TAYLOR, P. N., KALSBEEK, F. & BRIDGWATER, D. 1992. Discrepancies between neodymium, lead and strontium model ages from the Precambrian of southern East Greenland: Evidence for a Proterozoic granulite-facies event affecting Archaean gneisses. *Chemical Geology*, **94**, 281–291.

TEGNER, C. & DUNCAN, R. A. 1999. ^{40}Ar–^{39}Ar chronology for the volcanic history of the southeast Greenland rifted margin. *In*: LARSEN, H. C., DUNCAN, R. A., ALLAN, J. F. & BROOKS, K. (eds) *Proceedings of the Ocean Drilling Program, Scientific Results*. College Station, Texas, **163**, 53–62.

TEGNER, C., DUNCAN, R. A., BERNSTEIN, S., BROOKS, C. K., BIRD, D. K. & STOREY, M. 1998*a*. ^{40}Ar–^{39}Ar geochronology of Tertiary mafic intrusions along the East Greenland rifted margin: Relation to flood basalts and the Iceland hotspot track. *Earth and Planetary Science Letters*, **156**, 75–88.

TEGNER, C., LESHER, C. E., LARSEN, L. M. & WATT, W. S. 1998*b*. Evidence from the rare-earth-element record of mantle melting for cooling of the Tertiary Iceland mantle plume. *Nature*, **395**, 591–594.

TURNER, S. P., PLATT, J. P., GEORGE, R. M. M., KELLY, S. P., PEARSON, D. G. & NOWELL, G. M. 1999. Magmatism associated with orogenic collapses of the Betic-Alboran Domain, SE Spain. *Journal of Petrology*, **40**, 1011–1036.

WAGER, L. R. 1947. Geological investigations in East Greenland, Part IV. The stratigraphy and tectonics of Knud Rasmussens Land and the Kangerdlugssuaq region. *Meddelelser om Grønland*, **134**, 1–64.

WERNER, R., VAN DEN BOGAARD, P., LACASSE, C. & SCMINCKE, H.-U. 1998. Chemical composition, age, and sources of volcaniclastic sediments from Sites 917 and 918. *In*: SAUNDERS, A. D., LARSEN, H. C. & WISE, S. H. (eds) *Proceedings of the Ocean Drilling Program, Scientific Results*. College Station, Texas, **152**, 93–113.

WHITE, R. S. & MCKENZIE, D. 1989. Magmatism at rift zones: the generation of volcanic continental margins and flood basalts. *Journal of Geophysical Research*, **94**, 7685–7729.

K/Ar and $^{39}Ar/^{40}Ar$ whole-rock dating of zeolite facies metamorphosed flood basalts: the upper Paleocene basalts of the Faroe Islands, NE Atlantic

REGIN WAAGSTEIN[1], PHILIP GUISE[2] & DAVID REX[2]

[1] *Geological Survey of Denmark and Greenland, Øster Voldgade 10, DK-1350, København K, Denmark (e-mail: rw@geus.dk)*
[2] *Department of Earth Sciences, University of Leeds, Leeds LS2 9JT, UK*

Abstract: The Paleocene flood basalts of the Faroe Islands form a central part of the North Atlantic Igneous Province, but have proven difficult to date because of very low-grade burial metamorphism in the chabazite–thomsonite to the laumontite zeolite zone. We present 17 replicated K/Ar and 8 Ar/Ar whole-rock analyses of basalts from the >3 km thick lower basalt formation, the age of which has been debated for years. Samples are from the massive core of thick, exposed flows, and two boreholes (Vestmanna-1 and Lopra-1). Six samples are drill cuttings. Extensive microprobe work and mass balance calculations show that roughly 60% of the potassium of the dated basalts resides in plagioclase, interstitial cryptocrystalline rhyolite and smectitic clay, the rest mainly forming thin rims of alkali feldspar on plagioclase. Six basalts fulfil the following criteria: (1) they are almost homogeneous in K and Ar (ages on different splits vary by <4 Ma); (2) the only low-temperature phase present is smectite (saponite ± minor interstratified chlorite–smectite); and (3) max. *c.* 6% of total K occurs in smectite. This smectite replaced metastable interstitial glass during early burial and has a trivial effect on measured ages. The six basalts give mean K/Ar whole-rock ages of 56.5 ± 1.3 to 58.9 ± 1.3 Ma (1σ), which are interpreted as igneous ages consistent with mapped palaeomagnetic reversals and unpublished Ar/Ar dates. They suggest that the oldest drilled lavas erupted at 58.8 ± 0.5 Ma (1σ) in the later part of magnetochron C26r accumulating at >2 km Ma^{-1}, and that the volcanism came to a slow end at 56.4 ± 0.5 Ma in the beginning of chron C24r. The Lower Basalt Formation is overlain by 10 m of coal-bearing sediments and 2 km syn-breakup lavas, deposited in early C24r (>55 Ma).

The remaining 11 basalts are either inhomogeneous, carry >10% of the total K in clay, have C/S > saponite or contain traces of zeolites, secondary quartz, di-octahedral smectite or celadonite as probable indicators of prolonged alteration, and they give low or variable K/Ar ages. The Ar/Ar analyses include five of these poor samples plus three of the first group. They give a plateau age of 55.7 ± 0.9 Ma (1σ) for two exposed flows assigned to chron C25n, but of 60–63 Ma for six drilled lavas assigned to C26r. We argue that the later Ar/Ar ages are too high due to ^{39}Ar recoil loss out of the sample (0–25%) or relocation during irradiation and should be ignored.

The Faroe Islands are situated in the northern part of the Faroe–Rockall Plateau, which forms an extensive, elevated area of sea-floor to the north and west of the

From: JOLLEY, D. W. & BELL, B. R. (eds) *The North Atlantic Igneous Province: Stratigraphy, Tectonic, Volcanic and Magmatic Processes*. Geological Society, London, Special Publications, **197**, 219–252. 0305-8719/02/$15.00

British Isles. The area is separated from the Northwest European continental margin by the Rockall Trough and the Faroe–Shetland Channel. Most of the Faroe–Rockall Plateau is underlain by thick continental crust. The Plateau is almost completely covered with basalts which were erupted in connection with the opening of the NE Atlantic in early Palaeogene time. Most basalts were erupted on dry land but they are now almost completely submerged (Waagstein 1988; Boldreel & Andersen 1994), and land exposures exist only in the Faroe Islands.

The Faroes basaltic succession takes up a central position within the early Tertiary North Atlantic Igneous Province and represents one of the thickest and stratigraphically most complete volcanic sections within the province. Accurate dating of the Faroes basalts is of major importance in establishing the age and duration of the North Atlantic flood basalt volcanism and is pertinent to the understanding of the relationship between volcanism, basin formation and continental rifting processes.

The Faroes flood basalts (Fig. 1) are informally divided into the lower, middle and upper basalt series or formations (Rasmussen & Noe-Nygaard 1969, 1970; Waagstein 1988). They have an exposed thickness of >3 km while an additional 2 km of basalt were sampled in the original Lopra-1 well in 1981 without reaching the base of the lava pile (Fig. 2; Hald & Waagstein 1984; Waagstein *et al.* 1984). The Lopra well was re-entered in 1996 and extended another 1.4 km, but the results of this new drilling are yet to be published. The lower formation is at least 3 km thick and is capped by a thin coal-bearing sediment sequence. The basalt succession of the Faroes has recently been correlated with the basalts in East Greenland which lay less

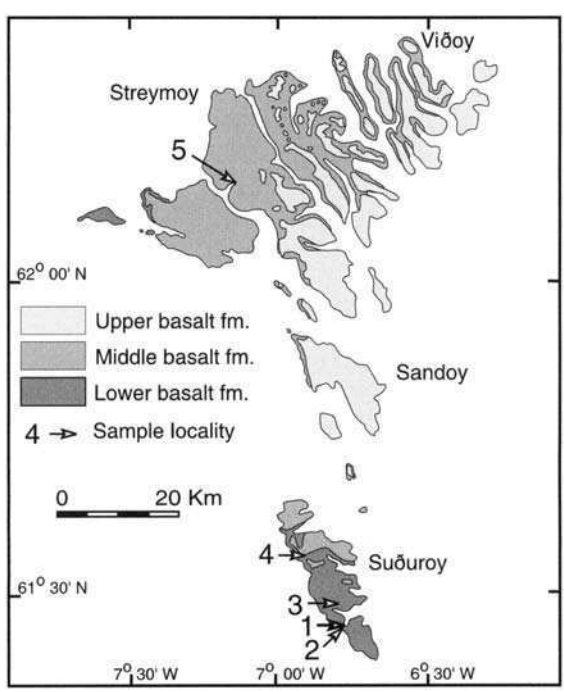

Fig. 1. Geological map of the Faroe Islands showing the areal distribution of the three basalt formations and the location of dated basalts. 1, Lopra-1 well; 2, Kirviskollur mountain; 3, Hvannadalsá river; 4, south entrance of the Hvalba road tunnel; 5, Vestmanna-1 well.

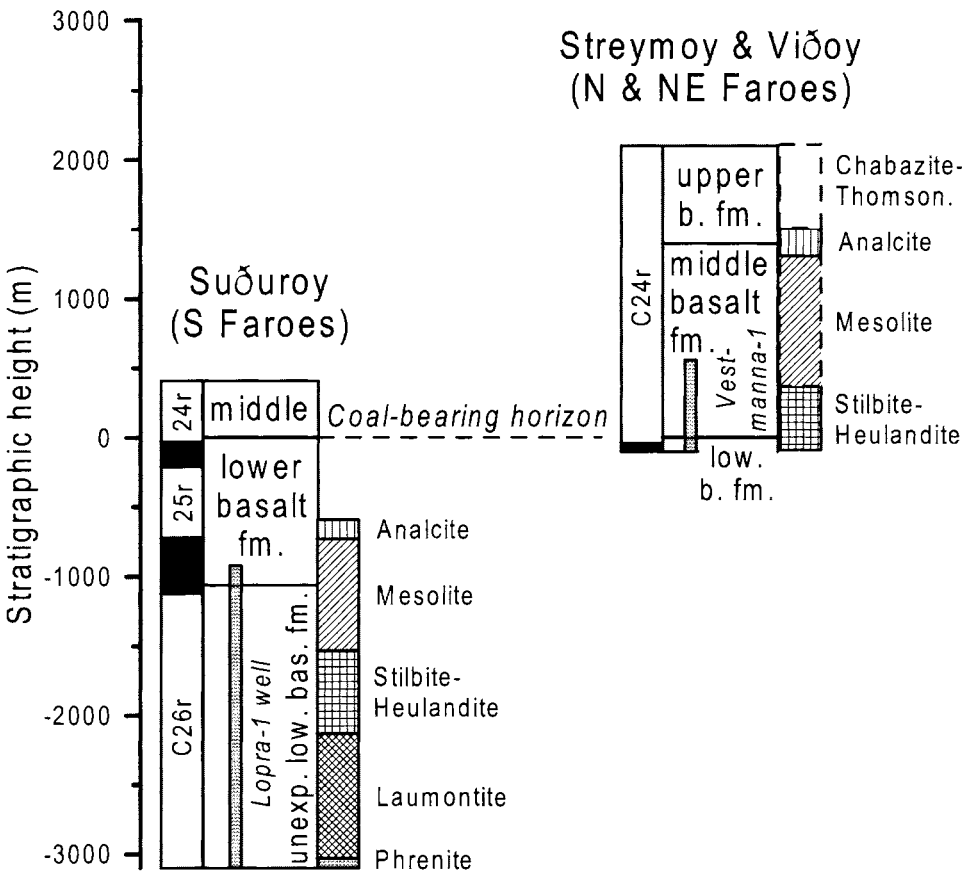

Fig. 2. Palaeomagnetic chronology, lava stratigraphy and zeolite zones of the Faroe Islands. The magnetochrons are from Waagstein (1988). The zeolite distribution is from O. Jørgensen (1984, pers. comm. 2001) and reflects the depth of burial of the lavas. The zeolite zonation for the southern Faroes is based on the Lopra-1 well and nearby mountains (Fig. 1). The partial preservation of the analcime zone suggests <1 km erosion, i.e. the middle and upper basalt formations must have been thin or absent near the southern end of Suðuroy before erosion. In the northern Suðuroy and in the Vestmanna-1 well on Streymoy the lower formation is overlain by middle formation lavas mineralized in the mesolite and stilbite–heulandite zone, respectively (O. Jørgensen pers. comm.), which suggests that the lower formation has been more deeply buried and altered in these areas.

than 100 km N of the Faroes before the opening of the NE Atlantic in late Paleocene (Larsen *et al.* 1999).

The basalts have undergone very low-grade metamorphism during burial as evidenced by the vertical distribution of characteristic zeolite minerals deposited in the porous parts of the lava flows. The zeolites define a number of zeolite zones ranging by depth from the chabazite–thomsonite to the laumontite zone suggesting temperatures from <70°C to >110°C (Neuhoff *et al.* 2000). The spatial distribution of zones indicates that the lower basalt formation has been less deeply buried in the southern than in the northern part of the Faroes (Fig. 2; Jørgensen 1984; Waagstein 1988; Jørgensen pers. comm.).

Due to the low-temperature alteration, the Faroes basalts have been difficult to date, and their age has been the subject of much controversy. Noe-Nygaard (1966) published two K/Ar ages which suggested a Cretaceous age. Shortly after, Tarling & Gale (1968) published a detailed palaeomagnetic and K/Ar study of the entire exposed sequence of the Faroes. They showed that all the basalts were reversely magnetized except for two or three normal intervals within the lower basalt formation. They suspected that many basalts had been affected by argon loss and suggested a minimum age of 50–60 Ma. The measurements of Tarling & Gale (1968) were later re-interpreted by Fitch *et al.* (1978) using K–Ar correlation diagrams. They obtained an apparent age of about 54 Ma for the Faroes basalts and suggested that this was a close estimate of the true average age of the volcanism.

Schoenharting & Abrahamsen (1984) made a detailed palaeomagnetic study of the five existing drillcores of basalt from the lowermost sampled 2 km section of the lower basalt formation. They showed that the basalts were strongly remagnetized and suggested that all the cored basalts had solidified in a reverse earth magnetic field, which they tentatively correlated with magnetochron C24r. Waagstein (1988) refined the magnetostratigraphy of the exposed part of the lower basalt formation on the basis of new field work, correlating the upper and middle formations and the topmost part of the lower formation with C24r, the remaining exposed section of the lower basalts with the magnetochrons C24r to C26n, and most of the drilled section with C26r. Morton *et al.* (1988) likewise assigned the oldest basalts to C26r, but suggested that the lower basalt volcanism ended in C26n. Lund (1983, 1989) identified a non-marine microflora of probable late Paleocene age within the coal-bearing sequence on top of the lower basalt formation and suggested a magneto-chronology similar to that of Waagstein (1988). However, Lund neglected the presence of flows of reverse polarity beneath the coal-bearing horizon (Tarling & Gale 1968; Abrahamsen *et al.* 1984), that were assigned to C24r by Waagstein (1988). Jolley (1997), likewise based on microflora evidence, instead suggested an early Ypresian age for the coal-bearing sequence, and Naylor *et al.* (1999), accepting this age, positioned the coal-bearing sequence slightly above the base of chron C24r as previously done by Waagstein (1988). Naylor *et al.* (1999) further suggested that the 3 km exposed and drilled lower basalt formation formed in pulses from about 63 to 55 Ma ago during chrons C28n to C24r, whereas Ritchie *et al.* (1999) tentatively correlated the same sequence with chrons C27r to C26n with a few flows at the top within C25r (about 62 to 57 Ma) implying a long volcanic pause before the deposition of the Faroes middle and upper basalt formations.

The present paper presents a combined K/Ar and Ar/Ar study of whole-rock basalt samples from the >3 km thick Faroes lower basalt formation. We have dated 17 basalts with the K/Ar method and in addition eight of these with the $^{39}Ar/^{40}Ar$ method. Some preliminary results have been presented in a report of limited circulation (Waagstein 1995) and referred to by Naylor *et al.* (1999, fig. 4) and Ritchie *et al.* (1999). We critically evaluate the two techniques of whole-rock dating and relate our results to the palaeomagnetic polarity shifts observed in the lava sequence.

Samples

K/Ar dating of igneous rocks relies on the assumptions (1) that all radiogenic argon of the magma escaped during crystallization, and (2) that the rock afterwards formed a closed K–Ar system. The crystallization age can then be determined simply from

the amount of radiogenic ^{40}Ar generated from the decay of ^{40}K (half-life 1.25 billion years). While the first assumption is probably fulfilled in extrusive rocks with no telluric phenocrysts (early crystals formed at elevated pressures), the latter one cannot be taken for granted. The presence of zeolites and other secondary minerals shows that the Faroes lavas have been altered by circulating meteoric water during burial, and both potassium and argon may have been mobilized during this process. However, porosity and permeability exert a strong control on the distribution of mafic phyllosilicates and zeolites (Schmidt & Robinson 1997), and in massive basalt the alteration process often seems to have stopped prematurely, presumably because of a sharp decrease in permeability when the few existing pores and fractures became mineralized.

Table 1. *Potassium-bearing phases and secondary minerals in dated basalts*

Sample no.	Depth below top LBF metres	Plagioclase		Alk. f. from K deficit	Interstial rhyolite	Smectite		Vol.% celadonite	Vol.% zeolites	Second quartz	Date used
		Wt%	Alter.	Wt%	Vol.%	Vol.%	Type				
MM11202	−50	47	–	1.7	0.5	2	sap.			tr.	
VM1-625.32	−60	47	(+)	2.1	2	3.8	sap.				×
II-24	−400	43	–	4.6	3	2	sap., C/S				×
II-23	−450	43	–	5.1	2	1.1	sap.				
II-5	−790	47	–	1.3	1	5	C/S, sap.				
RW1981	−810	45	–	3.3	1	1	sap.				×
L1-0337.5	−1260	43	+	6.8	3	7.5	sap.				×
L1-0424x	−1350	47	++	3.0		5	sap.				
L1-0861.7	−1770	45	++	0.7		5	sap., (C/S)			tr.	
L1-1142x	−2060	44	+	4.6		11	sap., (non.)				
L1-1218.5	−2140	45	++	0.0	0.2	4.6	C/S, sap.		0.5		
L1-1266x	−2170	44	+	3.6	1	3	sap.				×
L1-1490x	−2410	44	++	1.9	0.6	8.6	sap.				
L1-1672x	−2570	45	++	3.8	0.5	6	sap., (C/S)				×
L1-1842x	−2750	45	+	3.0		5	sap.				
L1-1922.9	−2850	44	++	3.1		9	sap.	2		tr.	
L1-2177.3	−3100	45	+++	−0.6		8	C/S, sap., bei., (mon.)		1		

Depth = stratigraphic depth below the top of the lower basalt formation (to mid point of sampled lava bed). Wt% plagioclase = an + ab from CIPW norm of whole-rock chemical analysis; alteration of plagioclase is visually estimated from fresh (−) to rather altered (+++). Point counts are made on samples VM1-625.32 (1000 counts), L1-1218.5 (1000 counts) and L1-1490x (363 counts) using transmitted light, 200 × magnification and a 0.6 or 0.3 mm grid (no separate count of plagioclase). Other abundances are visually estimated. 'Alk. f. from K deficit' = wt% alkali feldspar calculated from the difference between K_2O in bulk rock and total K_2O in plagioclase + rhyolite + smectite + celadonite + zeolites. The calculations are based on the concentrations in Table 3, and it is assumed that all components have the same density, that $K_2O = 5\%$ in rhyolite and 7% in alkali feldspar when not measured, and that K_2O in plagioclase is calculated rather than directly measured. Based on microprobe analysis (single identifications in parenthesis) smectite (*senso lato*) is classified into saponite (sap), chlorite/smectite mix layer mineral (C/S), nontronite (non), beidellite (bei) or montmorillionite (mon). The latter three are di-octahedral smectites. The presence of minor (<1%) secondary quartz is indicated by 'tr.'.

Sample list. MM11202: centre of 2nd flow from top of the lower basalt fm., just east of south entrance of Hvalba road tunnel, Suðuroy (232 m a.s.l.); VM1-625.32: core from 625.32 m depth in the Vestmanna-1 well, Streymoy (Waagstein & Hald 1984); II-5, II-23 and II-24: 46 m, 330 m and 355 m a.s.l. in the Hvannadalsá profile, Suðuroy (Rasmussen & Noe-Nygaard 1969; 1970); RW1981: sample RW19810901-01A from east slope of Kirviskollur, Suðuroy, 150 m above sea level; 'L1-': cores and cuttings samples from the Lopra-1 well, Suðuroy; last digits = depth, '×' = cuttings (Hald & Waagstein 1984).

The best chance of finding samples suitable for whole-rock K/Ar dating in very low-grade metamorphosed flood basalt sequences is therefore in massive lava flows. In contrast to the Faroes middle and upper formations, which are dominated by thin-bedded, amygdaloidal compound flows, the lower formation consists of thick flows with an average thickness of 20 m, mostly of simple type with thick, massive cores. They are also richer in K with an average K_2O content of 0.42% (Hald & Waagstein 1984). The 17 samples for dating were all taken from the massive cores of thick flows from the lower formation, preferably with a high K content. They were selected from a much larger collection of basalts used in previous petrographical and geochemical studies of the lava succession (Hald & Waagstein 1984; Waagstein & Hald 1984) and were among those considered most suitable for dating based on mineralogical criteria (Table 1). One is a core sample from the Vestmanna-1 well on Streymoy, the remaining ones are all from the southern island Suðuroy and include five hand specimens from various outcrops and five cores plus six cuttings samples from the Lopra-1 well (Figs 1 & 2). The drill cuttings (*c.* 1 mm) were carefully hand picked in order to avoid cavings detached from the wall of the well at higher levels. The same procedure was used during previous geochemical studies of the drilled basalts and these studies suggest that it is possible to hand pick pure samples of the rock actually drilled (Hald & Waagstein 1984).

Table 2. *Chemical composition of basalts, alkali feldspar and interstitial phases*

Sample phase	II-23 whole rock	L1-1672x whole rock	II-23 alk.f. grdm.	II-23 alk.f. rim	II-23 alk.f.* rim	L1-1672x alk.f.* interstit.	II-23 rhyolite interstit.	L1-1266x rhyolite interstit.	II-23 smectite interstit.	L1-1672x Smectite interstit.
N	1	1	1	1	1	3	8	5	10	7
SiO_2, wt%	48.43	47.84	64.63	66.33	66.22	64.43	76.21 ± 2.83	78.11	45.32 ± 1.70	43.63
TiO_2	3.54	3.01	0.08	0.27	0.33	0.58	0.56 ± 0.19	0.64	0.20 ± 0.21	0.43
Al_2O_3	12.54	12.72	20.81	19.07	17.23	12.75	11.45 ± 2.06	10.87	5.36 ± 0.77	6.50
Fe_2O_3	5.44	6.14								
FeO	10.26	9.40	0.47	0.39	2.01	6.63	1.29 ± 1.28	1.44	25.45 ± 0.85	25.71
MnO	0.22	0.23	0.10	0.00	0.00	0.08	0.04 ± 0.06	0.06	0.06 ± 0.09	0.06
MgO	5.51	5.70	0.08	0.19	0.50	1.35	0.20 ± 0.24	0.44	10.66 ± 1.16	5.19
CaO	9.98	10.55	2.69	0.47	0.42	0.83	0.51 ± 0.14	0.59	1.99 ± 0.19	2.66
Na_2O	2.50	2.68	7.20	5.20	2.96	3.22	2.59 ± 0.73	1.95	0.25 ± 0.15	0.43
K_2O	0.64	0.48	4.21	8.36	9.81	5.74	5.65 ± 1.53	5.81	0.89 ± 0.71	0.89
P_2O_5	0.41	0.30					0.13 ± 0.15	0.04	0.01 ± 0.02	
L.o.i.	0.89	1.17								
Total	100.36	100.22	100.27	100.28	99.48	95.61	98.63	99.95	90.19	85.50
an, mol.%			13.0	2.4	2.4	6.5				
ab			62.8	47.4	30.7	43.3				
or			24.2	50.2	66.9	50.2				

alk.f., alkali feldspar (*, slightly contaminated); grdm., groundmass; interstit., interstitial; N, number of analyses; ±, 1; L.o.i., loss on ignition (corrected for oxidation of iron); an, anorthite; ab, albite; or, orthoclase.

Analyses of minerals and interstitial rhyolite were performed with an energy dispersive equipment from LINK-SYSTEMS mounted on a Jeol 733 superprobe at the Geological Institute, University of Copenhagen. A number of standard minerals were analysed at least twice a day to check the stability of the system. Minor corrections for instrumental drift were later applied using the results on the standard minerals. The spot diameter was about 0.001 mm and the counting time 100 seconds. The specimen was usually moved continuously or in small steps during analysis of smectite or other water-bearing minerals (Table 1). This was done in order to avoid any selective loss of sodium although experiments suggested that this was probably an unnecessary precaution except in the case of some zeolites. Whole-rock analyses are from Hald & Waagstein (1984).

Petrography and mineralogy of the basalts

A detailed study of the petrography and mineralogy of the basalts, including more than 400 electron microprobe analyses, has been conducted in order to map the distribution of potassium in the primary and secondary mineral phases (Waagstein 1995). The basalts are iron–titanium-rich tholeiites (Table 2) mainly composed of plagioclase, clinopyroxene and iron–titanium oxides. Minor olivine was originally present in most, if not all, basalts but is now completely replaced by clay or other secondary minerals. The basalts may contain up to 10% phenocrysts or microphenocrysts of plagioclase and smaller amounts of phenocrysts or microphenocrysts of altered olivine and pyroxene. However, most of the basalts are macroscopically aphyric.

The plagioclase is generally clear and fresh-looking in the basalts from the upper part of the formation, but becomes increasingly clouded with microscopic inclusions and tiny fracture fillings downwards in the Lopra well (Table 1). The inclusions and fracture fillings are much too small to be analysed and form an insignificant part of the host plagioclase. The plagioclase has an anorthite content of An_{88} (sample L1-2177.3) to An_{56} in the centre of phenocrysts or microphenocrysts and of An_{65-20} in the groundmass (Fig. 3). The anorthite content often decreases sharply at the margin of the plagioclase crystals.

Alkali feldspar forms thin rims on the groundmass plagioclase or occurs interstitially in the groundmass, but is rarely sufficiently large to identify with the

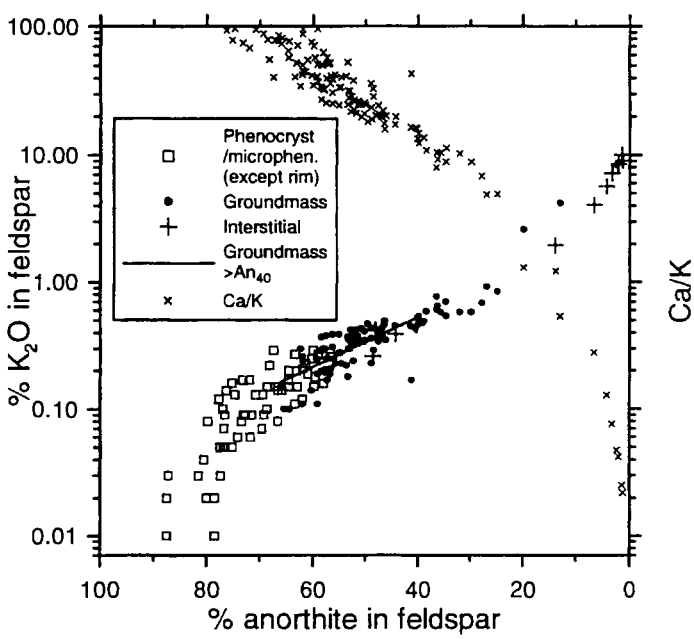

Fig. 3. Wt% K_2O v. anorthite content in plagioclase from basalt lavas in the Faroes lower basalt formation (same samples as in Table 3). All data points with %An > 80 are wave dispersive microprobe analyses, while most points with %An < 80 are by energy dispersion. A linear regression best fit line is shown for groundmass plagioclase with An > 40 and is used in Table 3 for adjustment of measured mean K contents of plagioclase relative to the normative anorthite content of the bulk rock.

microscope. The alkali feldspar has been analysed with the microprobe in four samples (Tables 2 & 3).

The basalts contain up to about 3% of cryptocrystalline rhyolite, which occurs interstitially between the main groundmass minerals and has crystallized from highly fractionated residual melt during the final stage of solidification of the lava. The rhyolite may be identified under the microscope by a distinctly reddish or brownish tint, a turbid appearance and a relatively low refractive index (Fig. 4). The individual crystals are generally too small to be analysed with the microprobe (spatial resolution 0.001 mm). Only in a few cases have pure or almost pure compositions of alkali feldspar (Or_{25-65}) and quartz been obtained, and the remaining analyses represent various combinations of feldspar and quartz, commonly together with some apatite, Fe–Ti-oxides and Fe–Mg silicates. Average bulk compositions of this rhyolite are close to the minimum melt composition of granite, but the scatter among individual

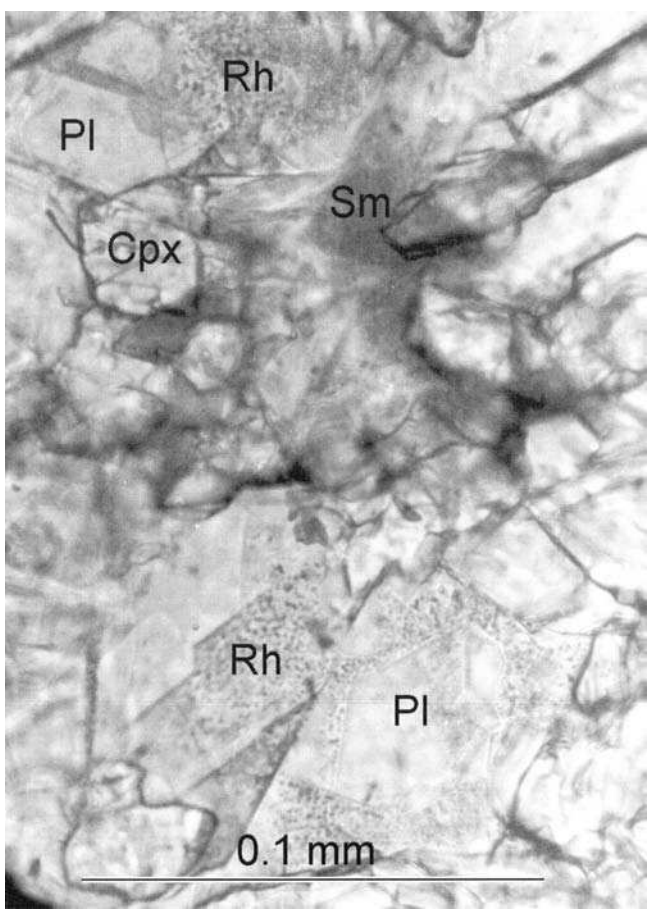

Fig. 4. Microphotograph of thin section of basalt lava RW1981 in transmitted light. In the upper part of the picture dark, translucent smectite (Sm) forms small interstitial areas partly overlapping groundmass clinopyroxene (Cpx) and plagioclase (Pl). In the lower part, a thin wedge of turbid, holocrystalline, interstitial rhyolite (Rh) occurs within the plane of section surrounding and partly overlapping a groundmass grain of clear plagioclase.

spot analyses and totals near 100% suggest that the material is completely crystalline, not glass (Table 2).

The basalts contain between about 1 and 11% smectitic clay (Table 1), which mainly occurs interstitially in the groundmass, but also forms vesicle fillings (amygdales) and replaces olivine and, more rarely, plagioclase. The clay is usually brownish or yellowish and optically slightly anisotropic or almost isotropic. Most of the interstitial smectite has probably formed by low-temperature alteration of primary interstitial glass, but some seems to fill in former interstitial voids. The smectite has been analysed with the microprobe in all dated samples and varies in chemical formula. Most smectite has the composition of saponite, mainly of iron-rich type with $Fe/(Fe+Mg) > 50$ (Table 2), but in six samples some smectite is interstratified chlorite/smectite (C/S) with 10–73% chlorite in the formula, and this clay is probably the dominant one in samples L1-2177.3, II-5 and L1-1218.5. Dioctahedral smectites ('Y' < 4.8 for O = 22) including nontronite, beidellite and Fe–montmorillionite are rare (Table 1). The clay mineralogy seems independent of textural settings although there is a tendency for the smectite that replaces olivine to be more rich in magnesium than interstitial smectite. Other secondary minerals are quartz, zeolites and celadonite which all seem to post-date the smectite. Minor secondary quartz (<1%) occurs in amygdales or replacing olivine in three samples, zeolites (0.5–1%) occur in two samples and celadonite (2%) in one (Table 1). The celadonite is vivid green and contains about 9% K_2O while one of the zeolite minerals in sample L1-2177.3 contains 4–8% K_2O. No attempt has been made to identify zeolites by species.

The modal composition of the basalts is shown in stratigraphic order in Figure 5 using estimated mineral abundances in Table 1. Feldspar and Fe–Ti oxide abundances are from the CIPW norm. Figure 6 shows what fraction of the total K_2O occurs in each rock component, based on the abundances in Figure 5 and the compositions in Table 3. Plagioclase on average contributes about 40%, smectite 10% and rhyolite 8% of the total K_2O of the basalts. This leaves 40% of the K_2O unaccounted for. The residual K_2O has tentatively been assigned to alkali feldspar (Or > An) which forms thin rims on groundmass plagioclase and solitary grains. The calculated amount of alkali feldspar makes up 0–5% of the rock (Table 1) and appears primarily to be a function of the total K_2O of the basalt. An overgrowth of alkali feldspar extending the dimensions of the groundmass plagioclase by a mere 1% would contribute almost 1.5% alkali feldspar to the rock. As most groundmass plagioclase is <0.2 mm long such thin overgrowths would be almost impossible to distinguish optically from sodic plagioclase and they will usually also be too thin for microprobe analysis.

K/Ar dating

Analytical details

Individual K/Ar ages were obtained on up to three different splits of the original sample in order to check sample homogeneity. All results are shown in Table 4 where the various splits are identified with a suffix 'A', 'B' or 'C' related to the time of shipment and analysis. The cores and hand specimens were cut into few-millimetre thick plates by using a diamond saw and any weathering crusts or visible amygdales were carefully removed. The various subsamples were usually taken from different

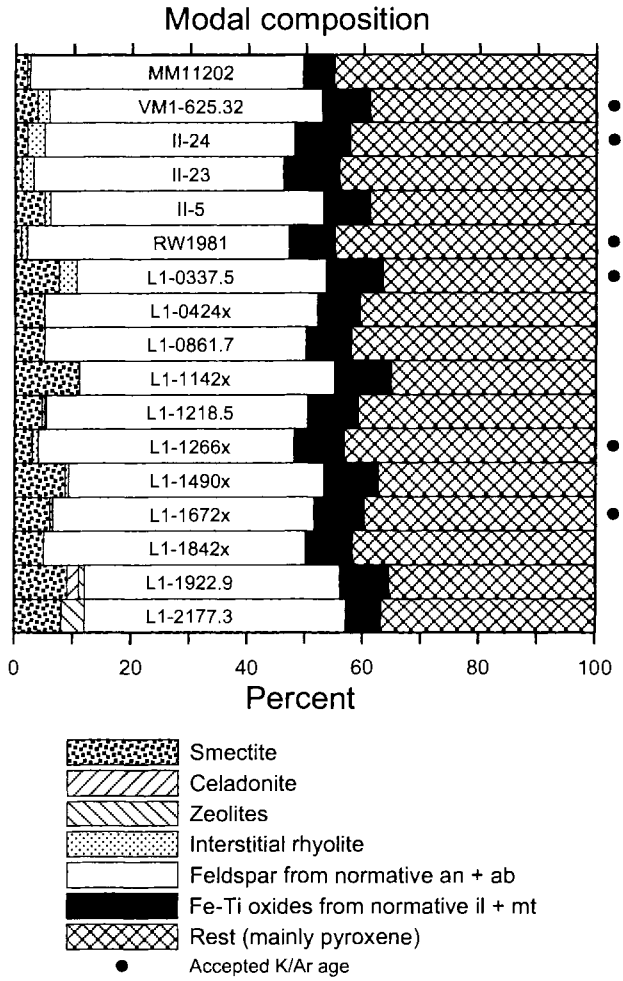

Fig. 5. Modal composition of dated basalts. Abundances of K bearing minerals are from Table 1. Fe–Ti oxides are wt% ilmenite plus magnetite from the CIPW norm assuming $Fe_2O_3/FeO = 0.15$. Pyroxene is taken to make up the rest of the weight of the rock ignoring minor olivine (usually completely altered to smectite) and apatite.

plates. The spacing of subsamples is estimated to be of the order of 1–10 cm. All cuttings subsamples originate from the same cannister of washed and dried cuttings. However, splits 'A' and 'B' are from the same hand picked portion of the sample, while split 'C' was hand picked at a later date. The samples were crushed and sieved and the +90 to −60 or the +90 to −30 size fraction (about 0.17–0.25 mm or 0.17–0.50 mm) was used for both potassium and argon determinations after the removal of all dust by washing. Individual argon determinations were made from 1.0–3.5 g of this size fraction without further crushing. The analytical procedures have been described elsewhere (Rex 1994).

Potassium was determined with an EEL flame photometer in three separate dissolutions of fine rock powder (0.08 g each). The powder was made from the same

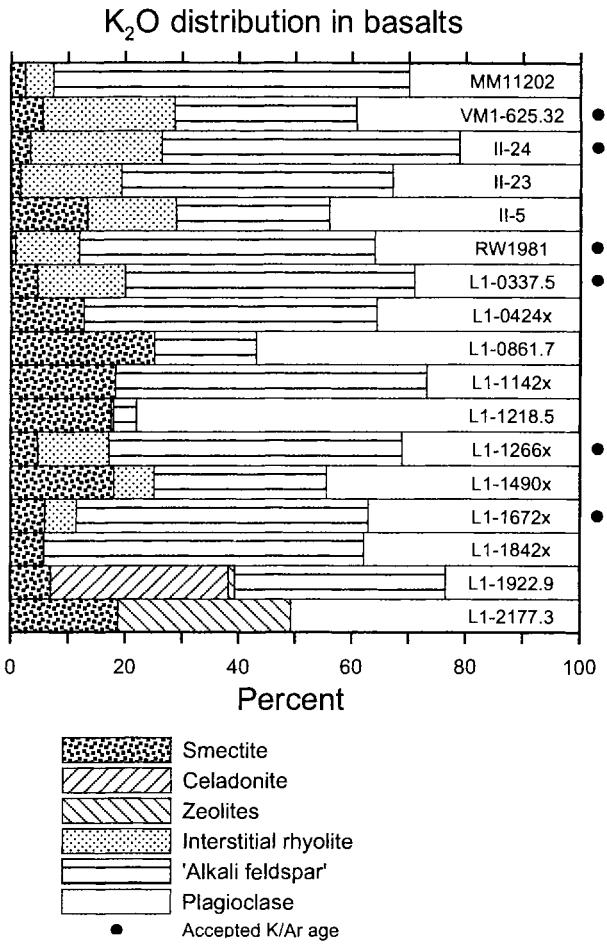

Fig. 6. Distribution of K_2O in dated basalts. The contribution of K_2O from individual mineral phases is computed from estimated abundances in Table 1 and average K_2O contents in Table 3. Mean K_2O in groundmass plagioclase has been adjusted as explained in Table 3. All plagioclase is considered part of the groundmass ignoring the lower K_2O of plagioclase phenocrysts (<10%). Interstitial rhyolite (mainly quartz + alkali feldspar) is assumed to contain 5% K_2O when not analysed. Minor smectite replacing olivine and filling vesicles is very similar to interstitial smectite in composition and the K_2O of interstitial smectite has been used for all smectite. 'Alkali feldspar' is a hypothetical feldspar phase with 7% K_2O which may account for the rest of the K content of the rock after the contribution from plagioclase, interstitial rhyolite, smectite, celadonite and zeolites has been subtracted. Whole-rock K_2O is the mean of 1–3 XRF analyses made at the geochemical lab of the Geological Survey of Denmark and Greenland (except K_2O in VM1-625.32 and MM11202 which are from the present K/Ar analyses).

size fraction that was analysed for Ar. The mean K has an analytical precision of 1% (1σ level) as estimated from individual readings (not shown). The radiogenic argon ($^{40}Ar^*$) determinations were made in duplicate on 15 subsamples (Table 4) from which the precision of single determinations may be estimated at 2.7%. The combined error on individual age results is therefore roughly ±2.9% or ±1.7 Ma (1σ).

Table 3. *Mean wt% K_2O in rocks and potassium-bearing minerals*

	Whole rock	Groundmass plagioclase				Alkali fieldspar	Interstitial rhyolite	Interstitial smectite	
		Measured		Calculated		Measured	Measured	Measured	
Sample no.	K_2O	An	K_2O	An	K_2O	K_2O	K_2O	K_2O	Ca/K
MM11202	0.329	59.3	0.25 (1)	60.7	0.21		3.23 ± 0.97 (2)	0.41 ± 0.11 (4)	5.22
VM1-625.32	0.467	46.1	0.45 ± 0.16 (9)	49.5	0.39		5.40 ± 0.76 (8)	0.68 ± 0.19 (5)	4.50
II-24	0.650	49.4	0.28 ± 0.13 (3)	46.6	0.32	7.46 (1)*	4.99 ± 1.56 (8)	1.09 ± 0.28 (5)	1.25
II-23	0.640	44.4	0.59 ± 0.63 (13)	48.5	0.49	6.09 ± 3.63 (4)	5.65 ± 1.53 (8)	0.96 ± 0.71 (9)	2.08
II-5	0.320	n.a.	n.a.	52.2	0.30		n.a.	0.85 ± 0.56 (6)	4.14
RW1981	0.450	n.a.	n.a.	48.7	0.36		n.a.	0.35 ± 0.08 (6)	5.40
L1-0337.5	0.887	47.1	0.48 ± 0.13 (9)	42.3	0.60	6.79 ± 2.29 (12)	4.54 ± 1.35 (7)	0.54 ± 0.11 (5)	4.81
L1-0424x	0.395	n.a.	n.a.	52.7	0.30			1.00 ± 0.31 (3)	2.51
L1-0861.7	0.237	50.6	0.33 ± 0.21 (11)	52.4	0.30			1.19 ± 0.13 (4)	1.92
L1-1142x	0.590	55.5	0.27 ± 0.10 (7)	49.1	0.36			0.98 ± 1.06 (9)	2.55
L1-1218.5	0.173	53.2	0.28 ± 0.08 (7)	52.0	0.30		n.a.	0.66 ± 0.20 (3)	3.41
L1-1266x	0.465	n.a.	n.a.	50.3	0.33		5.81 ± 1.41 (5)	0.72 ± 0.15 (7)	3.65
L1-1490x	0.425	51.5	0.38 ± 0.12 (5)	48.6	0.43		n.a.	0.89 ± 0.72 (7)	2.99
L1-1672x	0.485	56.2	0.26 ± 0.15 (10)	46.9	0.40	6.55 (1)*	5.34 ± 1.99 (2)	0.48 ± 0.14 (7)	5.29
L1-1842x	0.380	48.8	0.43 (1)	51.3	0.32			0.44 ± 0.13 (4)	6.95
L1-1922.9	0.600	48.0	0.38 ± 0.16 (9)	52.0	0.32			0.47 ± 0.10 (5)	7.55
L1-2177.3	0.173	52.8	0.32 ± 0.25 (4)	59.4	0.24			0.50 ± 0.44 (10)	9.70

All errors are quoted at 1σ level (number of analyses in parenthesis); n.a. not analysed; * contaminated.

An = mol.% anorthite = 100*Ca/(Ca + Na).

Calculated An = molar 100*an/(an + ab) from whole-rock CIPW norm. No whole-rock analysis exists for MM11202 and %An is from another sample of the same flow.

For $N \geq 3$: calculated $K_2O = \exp[\ln(K_2O_{measured}) - 0.045*(An_{calculated} - An_{measured})]$.

For $N < 3$: calculated $K_2O = 3.19*\exp[-0.045*An_{calculated}]$.

K_2O is analysed by microprobe using energy dispersion (Table 1) or wave dispersion (plagioclase in L1-2177.3). Whole-rock K_2O concentrations are based on 1–3 XRF analyses made at the former Geological Survey of Greenland (Hald & Waagstein 1984; Waagstein & Hald 1984 and unpublished), except VM1-625.32 and MM11202, which are from present K/Ar dates (Table 4).

Celadonite in L1-1922.9: 9.35 ± 0.58% K_2O (N = 5); zeolites in L1-1218.5: 0.14 ± 0.11% K_2O (N = 9); zeolites in L1-2177.3: 2.18 ± 2.44% K_2O (N = 18).

Sample inhomogeneity

Nearly all samples have been dated two or more times in order to study the problems associated with sample inhomogeneity and redistribution of K and Ar.

The potassium determinations obtained by flame photometry on 32 subsamples or splits (Table 4) have been compared with the mean of 1–3 XRF (X-ray fluorescence) determinations obtained from major element analysis of the original batch of rock powder used for rock chemistry (Table 3). Linear regression analysis shows no systematic differences between the two analytical methods and suggests that the size fraction used for dating and the part of the sample removed by sieving and washing were similar in potassium content. The only exception is the flame photometric measurement of K in core sample L1-1922.9 which is only 90% of the XRF value, possibly indicating a lower content of green celadonite in the piece of core used for dating (Fig. 6).

Figure 7 is a logarithmic plot of the relative standard deviation on ages v. the deviation on K based on replicate dates of individual samples and outcrops from the Faroes. The replicate dates are from 14 samples from the lower basalt formation

Table 4. *K/Ar dates of basalts from the lower basalt formation, Faroe Islands*

Sample number	Split	Lab no.	K	$^{40}Ar^*$ (STP)	$^{40}Ar^*$	Duplicate ages	Weighted age of splits
			Wt% %σ	10^{-7} cm^3 %σ	Vol.%	Ma 1σ	Ma 1σ
MM11202	A	3378	0.273	5.24	37.4		48.7 ± 1.9
MM11202	B	3699	0.273	5.34	36.7		49.6 ± 2.0
Mean of splits			*0.273 ± 0.0*	*5.29 ± 1.3*	*37.1*		*49.1 ± 1.4*
VM1-625.32	A		0.391	8.50	29.1		55.1 ± 2.8
VM1-625.32	B	3696	0.384	8.63	55.4		56.9 ± 1.4
Mean of splits			*0.388 ± 1.3*	*8.57 ± 1.1*	*42.3*		***56.5 ± 1.3****
II-24	A	3397	0.513	12.11	55.0		59.7 ± 1.5
II-24	B	3722	0.538	12.13	59.2	57.1 ± 1.3	
II-24	B	3751	–	11.94	56.2	56.2 ± 1.4	56.7 ± 1.0
II-24	C	3808	0.540	11.53	55.3	54.1 ± 1.4	
II-24	C	3874	–	12.01	49.1	56.3 ± 1.7	55.0 ± 1.1
Mean of splits			*0.530 ± 2.8*	*11.97 ± 2.1*	*55.0*		***57.1 ± 1.7**†*
II-23	A	3398	0.544	13.82	60.7		64.2 ± 1.4
II-23	B	3733	0.550	12.93	50.3		59.5 ± 1.7
II-23	C	3807	0.554	12.68	71.0	57.9 ± 1.0	
II-23	C	3873	–	12.69	63.4	58.0 ± 1.2	57.9 ± 0.8
Mean of splits			*0.549 ± 0.9*	*13.15 ± 4.5*	*59.4*		*60.5 ± 2.3†*
II-5	A	3396	0.267	5.18	15.8		49.2 ± 4.2
II-5	B	3710	0.266	5.43	18.2		51.8 ± 4.0
Mean of splits			*0.267 ± 0.3*	*5.31 ± 3.3*	*17.0*		*50.6 ± 2.9*
RW1981	A	3377	0.360	7.91	57.5	55.7 ± 1.3	
RW1981	A	3525	–	7.76	42.4	54.6 ± 1.9	55.3 ± 1.1
RW1981	B	3735	0.414	9.64	41.8		58.9 ± 2.1
Mean of splits			*0.387 ± 9.9*	*8.74 ± 14.6*	*45.9*		***57.1 ± 2.5**†*
L1-0337.5	A	2882	0.724	17.27	39.7		60.3 ± 2.3
L1-0337.5	B	3711	0.740	16.92	59.7	57.9 ± 1.3	
L1-0337.5	B	3750	–	16.95	57.1	58.0 ± 1.4	57.9 ± 1.0
Mean of splits			*0.732 ± 1.5*	*17.10 ± 1.4*	*49.1*		***58.3 ± 0.9****
L1-0424x	A	3413	0.306	7.43	47.4	61.4 ± 1.9	
L1-0424x	B	3680	0.299	7.64	55.4	64.6 ± 1.6	63.3 ± 1.2
L1-0424x	C	3827	0.300	7.20	36.1	60.7 ± 2.5	
L1-0424x	C	3862	–	7.38	57.7	62.2 ± 1.5	61.8 ± 1.3
Mean of splits			*0.301 ± 1.3*	*7.41 ± 3.0*	*49.2*		*62.6 ± 0.9*
L1-0861.7	A	2883	0.211	4.52	17.9		54.3 ± 4.3
L1-0861.7	B	3736	0.201	4.19	7.6		52.8 ± 8.3
Mean of splits			*0.206 ± 3.4*	*4.36 ± 5.4*	*12.8*		*54.0 ± 3.8*
L1-1142x	A	3007	0.491	11.27	23.8	58.1 ± 3.6	
L1-1142x	B	3681	0.505	11.23	19.6	56.3 ± 4.1	57.3 ± 2.7
L1-1142x	C	3829	0.500	10.67	43.7	54.1 ± 1.8	
L1-1142x	C	3847	–	10.98	60.4	55.6 ± 1.3	55.1 ± 1.1
Mean of splits			*0.499 ± 1.4*	*11.04 ± 3.1*	*36.9*		*55.4 ± 1.0*
L1-1218.5	A	2884	0.149	3.31	16.7		56.3 ± 4.7
L1-1218.5	C	3815	0.133	3.78	9.5	71.7 ± 9.5	
L1-1218.5	C	3863	–	3.72	8.1	70.6 ± 11.0	71.2 ± 7.0
Mean of splits			*0.141 ± 8.0*	*3.53 ± 8.9*	*12.8*		*63.8 ± 10.6*
L1-1266x	A	3441	0.406	9.50	54.1	59.2 ± 1.6	
L1-1266x	B	3682	0.400	9.11	59.5	57.7 ± 1.3	58.3 ± 1.0
L1-1266x	C	3849	–	9.10	67.4		57.5 ± 1.1
Mean of splits			*0.403 ± 1.1*	*9.20 ± 2.6*	*62.1*		***57.9 ± 0.8****

Table 4. (*continued*)

Sample number	Split	Lab no.	K		$^{40}Ar^*$ (STP)		$^{40}Ar^*$	Duplicate ages	Weighted age of splits
			Wt%	%σ	10^{-7} cm^3	%σ	Vol.%	Ma 1σ	Ma 1σ
L1-1490x	A	3008	0.342		8.45		44.0		62.5 ± 2.1
L1-1490x	C	3828	0.338		7.65		58.3	57.3 ± 1.4	
L1-1490x	C	3848	–		7.47		34.4	56.0 ± 2.4	57.0 ± 1.2
Mean of splits			*0.340*	*± 0.8*	*8.01*	*± 7.9*	*45.2*		*59.7 ± 3.9*†
L1-1672x	A	3006	0.421		9.84		38.9	59.2 ± 2.3	
L1-1672x	B	3693	0.405		9.59		70.3	59.9 ± 1.1	59.8 ± 1.0
L1-1672x	C	3830	0.405		9.22		64.7		57.6 ± 1.2
Mean of splits			*0.409*	*± 2.4*	*9.47*	*± 3.9*	*59.7*		***58.9 ± 1.3****
L1-1842x	A	3442	0.289		7.29		60.3	63.8 ± 1.5	
L1-1842x	B	3694	0.288		6.73		46.0	59.1 ± 1.9	62.0 ± 1.2
L1-1842x	C	3831	0.294		6.21		42.6	53.5 ± 1.9	
L1-1842x	C	3860	–		6.25		49.0	53.9 ± 1.6	53.7 ± 1.2
Mean of splits			*0.291*	*± 1.3*	*6.62*	*± 9.3*	*49.5*		*57.9 ± 5.8*†
L1-1922.9	A	2885	0.448		8.66		42.3		49.1
L1-2177.3	A	2886	0.160		2.38		19.7		37.9

Samples are identified in footnote of Table 1.

Split = split number of original rock or cuttings sample according to time of shipment for analysis. Cuttings samples (identified with an 'x') from splits A and B are from the same hand picking and the results are treated as duplicates.

$^{40}Ar^*10^{-7}$ cm^3 STP = volume of radiogenic Ar at standard temperature and pressure.

^{40}Vol.% $^{40}Ar^*$ = vol.% radiogenic ^{40}Ar of total volume of ^{40}Ar.

For K and Ar the mean and relative std. dev. (%σ) of splits are calculated by giving the same weight to all splits. Duplicate age determinations of splits are averaged according their assigned 1σ errors by weighting then inversely by variance. The age of individual splits are similarly weighted to obtain an average age of the sample in the last column shown in italics (counting duplicates once only). Those considered to represent magmatic crystallization ages are shown in bold and marked '*' (see text). For five samples probability is <15% that the variation of age is solely due to analytical errors (Ludwig 2000). For these samples all splits are weighted equally in the calculation of the mean age and standard error on mean (marked with '†').

(Table 4), two hand specimens from the middle formation (unpublished) and five lava flows from the lower, middle and upper formations (Tarling & Gale 1968). The latter dates were performed on sets of 2–5 mini-cores drilled from the massive part of the flows, usually from an area <1 metre across. Estimated analytical errors are shown at the 2σ level by stippled lines and mean dates with σ > 2% on K or σ > 5.8% on age are considered to reflect an inhomogeneous sample (cuttings, solid rock or outcrop). The calculated errors only give a rough estimate of sample inhomogeneity as most of the mean ages are only based on 2–3 subsamples and none on more than six subsamples. However, the inhomogeneous samples seem to fall on two trends: one of almost constant ages implying co-variation of K and $^{40}Ar^*$ and another one of variable ages implying decoupling of K and $^{40}Ar^*$. The former trend only shows a small increase in the variation of ages with the variation of K and this increase reflects the error associated with the dating method itself, that is that K and Ar are determined on different aliquots of material. The dates may thus be improved by repeating them. The latter trend, on the other hand, suggests a disturbance of the K–Ar system by redistribution of Ar and/or K, and the dates lying on this trend must be considered unreliable.

The K replicates show a standard deviation of max. 10% for the lower formation, but as much as 60% for the middle formation. In both formations the within-sample variation is of similar magnitude as the variation observed between different samples from small outcrops and this suggests that a major part of the variation of K in massive (non-vesicular) lava occurs within a distance of a few centimetres or less. The variation in K (and $^{40}Ar^*$) likely reflects variations in the abundance of alkali feldspar, interstitial rhyolite and secondary minerals replacing interstitial glass and suggests that displacements of residual melt is often taking place at the centimetre-scale during the solidification of lava. This is supported by microscopic observations which show that interstitial material is often irregularly distributed within a thin section. However, residual melt may also migrate over longer distances to form thin horizontal sheets as may be seen in outcrops, especially in the thin flow-units of the Faroes middle basalt formation.

Three cuttings samples seem to be inhomogeneous in either Ar or K. As each split consists of perhaps 500 cuttings the variations are difficult to explain alone by sample taking but suggest differences in the way cuttings were selected during hand picking.

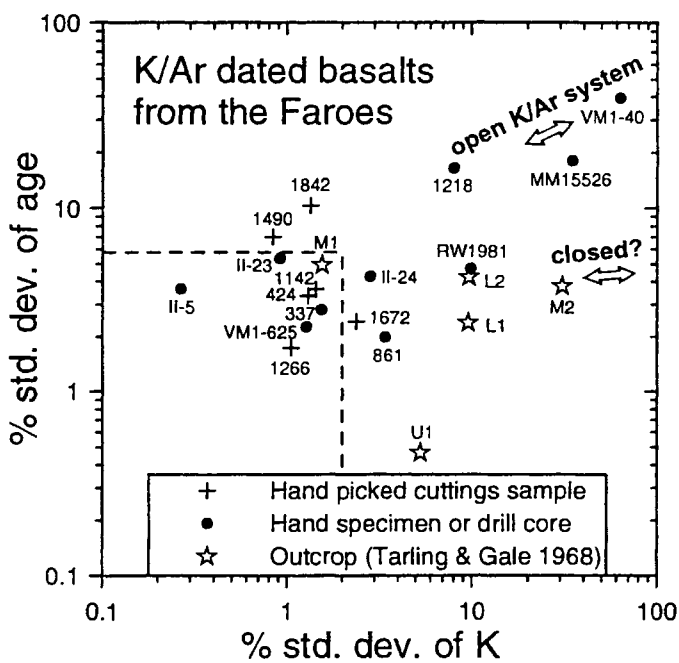

Fig. 7. Percent standard deviation of K and $^{40}Ar^*$ in samples and outcrops calculated from K/Ar analyses of (1) different hand pickings of drill cuttings from the same depth, (2) different subsamples taken from the same hand or core specimen, and (3) different plugs (mini-cores) drilled from the same outcrop. Subsamples are taken <10 cm and plugs presumably <100 cm apart. The plugs are from all three basalt formations and are analysed by Tarling & Gale (1968). Samples VM1-40 and MM15526 are from the middle formation (unpublished). The remaining samples are from the present study (Table 4). Lopra well samples are identified by depths. The analytical precision is about 1% relative on K and 2.6% on $^{40}Ar^*$, and double that deviation (stippled lines) suggests sample inhomogeneity. Double arrows are trends suggesting open and possibly closed K/Ar systems, respectively.

Unfortunately, the problem of sample inhomogeneity has been ignored in most K/Ar studies of basalts.

K/Ar ages

An apparent age has been calculated for each Ar determination, resulting in between two and four ages with associated error estimates for all but two samples (Table 4). Duplicate determinations of the same subsample of solid rock, or the same hand picking of cuttings, have then been converted into a mean age for the subsample by weighting them inversely by variance. Finally, the age of the total sample has been calculated by a similar weighting of subsample ages, or, where the scatter is too large to be explained solely by analytical errors, by simple averaging (see footnote of Table 4).

In Figure 8, the 15 mean K/Ar ages and two single dates are shown versus the fraction of potassium occurring in interstitial clay. The range of subsample ages is shown by vertical bars. The scatter of ages (38–64 Ma) shows that the K–Ar system in many basalts has been affected by alteration, and in order to identify poor dates the samples have been divided in three groups according to the complexity of alteration. All basalts contain saponite clay ± clay of chlorite–smectite mixed layer type (C/S).

Seven basalts (open circles) contain small amounts (max. 2%) of one or more additional low-temperature minerals and/or have C/S as the dominant clay phase. The additional minerals include quartz, zeolites, celadonite and di-octahedral smectite (nontronite, beidellite, montmorillionite). According to Neuhoff *et al.* (1999) celadonite and silica may form before burial and thus predate saponite. However, in the above massive basalts saponite always seems to be the first formed low-temperature mineral. The presence of additional low-temperature phases is therefore an indication of prolonged alteration. The same is the presence of abundant C/S (Neuhoff *et al.* 1999). The basalts give low or variable ages which suggest that they have suffered Ar loss or redistribution of K and Ar, even though several of them are quite fresh-looking.

Four other basalts (circled dots) with saponite and minor C/S as the only low-temperature phases are also likely to give poor ages. Two of these (Nos. III-23 and L1-1842x) give 6–8 million years difference between different splits. This is beyond analytical errors and suggests that K and Ar have been mobilized. The inhomogeneity itself results in a low precision on age, and, if part of the mobilization occurred at a late date, it might have affected the average age of the sample significantly. Two other basalts (Nos. L1-0424x, L1-1490x) have as much as 13–18% of their potassium inventory in interstitial clay, which means that any late process affecting the clay phase may have had a measurable effect on the whole-rock age.

The remaining six basalts (filled circles) all show <4 Ma difference between different splits and contain $<c.6\%$ of their potassium inventory in interstitial saponite ± minor C/S, which are the only low-temperature minerals present. The small amount of clay in these basalts is of little concern. The clay formed mainly from interstitial glass, which is metastable and almost certainly completely replaced during early burial (Neuhoff *et al.* 1999), i.e. before the cessation of the Faroes volcanism. The clay contains much less K than the former glass and, while glass may be diffusive to K and Ar, especially when hydrated, most clay minerals are quite

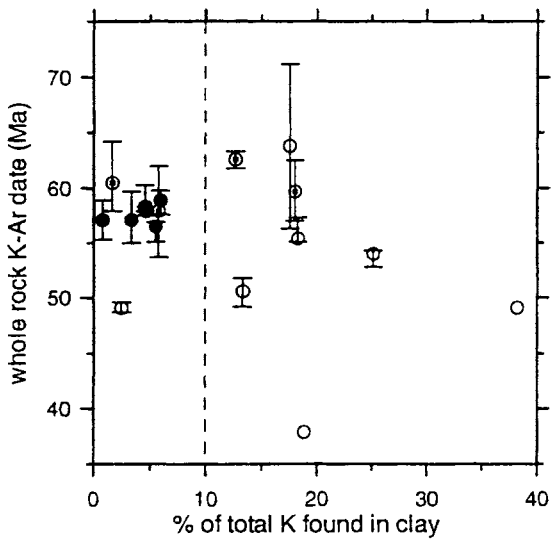

Fig. 8. Whole-rock mean K/Ar dates (Ma) versus the percentage of total K of the rock occurring in clay. Closed circles, homogeneous basalt with <10% of total K in saponite ± minor C/S. Dates are interpreted as magmatic crystallization ages; Circled dots, basalt with >10% of total K in saponite ± minor C/S or with subsample dates differing >4 Ma; Open circles, basalt with complex alterations, i.e. containing saponite ± C/S plus trace amounts of zeolites and/or secondary quartz and/or di-octahedral smectite and/or celadonite. Vertical error bars, total range of subsample dates (Table 4).

retentive of both K and Ar. Besides, in nearly massive basalt lavas like those selected for dating, the formation of clay would tend to impede further alterations by completely filling the few vesicles and fractures present. The ages of the six basalts must therefore reflect their magmatic crystallization ages. This interpretation is supported by the ages themselves which vary only from 56.5 ± 1.3 to 58.9 ± 1.3 Ma (1σ) and roughly increase with depth (Table 4).

All K/Ar mean ages between 50 to 70 Ma are shown versus stratigraphic depth in Figure 9 using the same circular symbols as in Figure 8 with 1σ error bars and with sample number added. Waagstein (1988) suggested that the two normal magnetic polarity intervals within the exposed part of the lava sequence in Suðuroy should be correlated with magnetochrons C25n and C26n, and on the basis of the geomagnetic time-scale he postulated that the duration of the repose periods between the extrusions of individual lava flows became gradually longer towards the top of the Lower Formation. This was suggested by an upward increase of tuffaceous sediments containing minor coal. Using the revised time-scale of Cande & Kent (1995), the ages assigned to the top and bottom of chrons C25n and C26n have been plotted v. stratigraphic depth in Figure 9. The four ages obtained in this way fit almost perfectly a logarithmic curve (thick dashed curve).

A similar logarithmic curve has been fitted to the six accepted K/Ar ages (filled circles) and is shown by a thick full curve in Figure 9. The K/Ar age–depth curve coincides within errors with the palaeomagnetic curve. It is also concordant with an age of 56–59 Ma quoted by Larsen *et al.* (1999) for the Faroes lower formation based on three unpublished Ar/Ar plateau ages of bulk plagioclase and with

an unpublished whole-rock plateau age from the recent deepening of the Lopra well (R. Duncan pers. comm., 2001). This gives further support to the interpretation of the least altered basalts as true geological ages. An extrapolation of the K/Ar curve to the bottom of the Lopra drill hole, i.e. 3100 m below the top of the lower basalt formation, gives an age of 58.8 ± 0.5 Ma (1σ). The same curve gives an age of 56.4 ± 0.5 Ma for the top of the lower basalt formation. This is close to the accepted age of the C24r–C24n reversal of 55.9 Ma (Cande & Kent 1995) that occurs a few flows lower down. However, accepting the reversal chronology, a better estimate can probably be obtained from the palaeomagnetic curve, which give an age of 55.8 ± 0.1 Ma (1σ) for the top of the lower formation (Fig. 9).

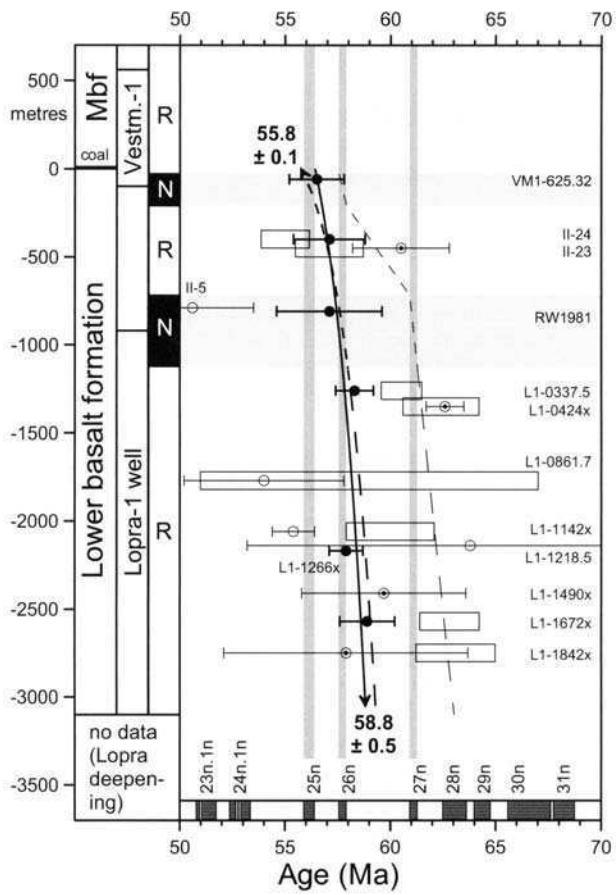

Fig. 9. Age of the Faroes lower basalt formation. K/Ar dates are classified on basis of mineralogical criteria as in Figure 8 using the same circular symbols (error bars, 1 standard error on mean). Thick full curve, logarithmic curve fitted to K/Ar dates interpreted as magmatic crystallization ages (filled circles); Open boxes, Ar/Ar plateau ages of basalt (box width, 1 standard deviation). Thick dashed curve, logarithmic fit assuming that normal polarity intervals are 25n and 26n; Thin dashed curve, broken line fit assuming that normal polarity intervals are 26n and 27n; 1σ errors: 0.5 Ma for upper sample, 0.1 Ma for two lower samples (M. Storey, unpublished). Magnetic polarity zonation at left is from Waagstein (1988). Magnetic timescale at the bottom of the diagram is from Cande & Kent (1995). Preferred ages at the top and base of the 3.1 km section are shown in Ma with 1 standard errors (see text).

Ar/Ar dating

^{40}Ar–^{39}Ar analytical details

Eight samples were analysed for Ar/Ar ages on a portion of the same sieved material as that used for the last batch of K/Ar ages, i.e. split 'B' or 'C'. The analytical details are described in Rex *et al.* (1993). The samples were irradiated at the Petten facility in the Netherlands in three different batches using a fast neutron dose of approximately 5×10^{18} neutron/cm^2 monitored by the inclusion of aliquots of hornblende standards FY12a, HB3gr and MMHb-1, using the ages quoted in Roddick (1983). The Petten 2 irradiation was monitored by 10 FY12a and 12 HB3gr, Petten 3 by 10 FY12a and 10 Hb3gr, and Petten 5 by 10 FY12a, 6 Hb3gr and 5 MMHb-1. Cd shielding was applied during the last irradiation. When calculating the neutron flux (J) for each standard position we use the $^{40}Ar^*/^{40}K$ ratios quoted in Roddick (1983) to provide interlaboratory comparison. The large number of standards spaced along the canister allowed calibration of flux to 0.5–1% (1σ). Errors quoted on the integrated ages take account of this uncertainty but the individual step ages do not. The data differ slightly from those in Waagstein (1995) because we have changed the way in which we extrapolate argon ratios back to the time the gas sample entered the mass spectrometer analysis and because we weight ages of individual steps by their variance instead of by volume.

Ar/Ar ages

The results of the $^{39}Ar/^{40}Ar$ stepwise degassing experiments are presented in Figure 10 and Tables 5 to 7. Age plateaux were picked by the computer program 'Isoplot' of Ludwig (2000) except that we omitted step 8 in II-23 and steps 1–3 in L1-0424x to improve the visual fit. The plateaux consist of 3 to 9 consecutive heating steps yielding similar ages (within 2σ error limits) and comprising 60–100% of the ^{39}Ar released. The same steps give inverse isochron ages similar to the plateau ages, although generally less precise, with no indications of the presence of excess argon. The plateau ages are plotted as boxes against stratigraphic height in Figure 9, the box width indicating estimated analytical errors at the 1σ level.

Samples II-23 and II-24 are from the lower and upper lobe, respectively, of a 100 m thick double flow of high-titanium basalt 370–470 m below the top of the lower basalt formation (loc. 3, Fig. 1). The two samples give a weighted mean age of 55.7 ± 0.9 Ma (1σ error), comparable to 56.8 ± 1.0 Ma for the three accepted K/Ar dates from the exposed succession.

All remaining six samples are from the Lopra well (loc. 1, Fig. 1). They were taken at 337–1842 m depth, or stratigraphically about 1260–2760 m below the top of the lower basalt formation. The plateau ages range from 60.0 ± 2.1 to 63.1 ± 1.8 Ma (ignoring the poor age of 59 ± 8 Ma for L1-0861.7) and show no clear increase with sampling depth. The weighed average of all six drill samples is 61.5 ± 0.7 Ma (1σ), about three million years older than the three accepted K/Ar ages from the same well.

Taking the Ar/Ar ages at face value they seem to partly support the suggestion by Ritchie *et al.* (1999) that the two normal magnetic polarity intervals in the exposed part of the lower formation belong to chrons C26n and C27n. This implies an episodic type of volcanism illustrated by the thin dashed line in Figure 9, which line

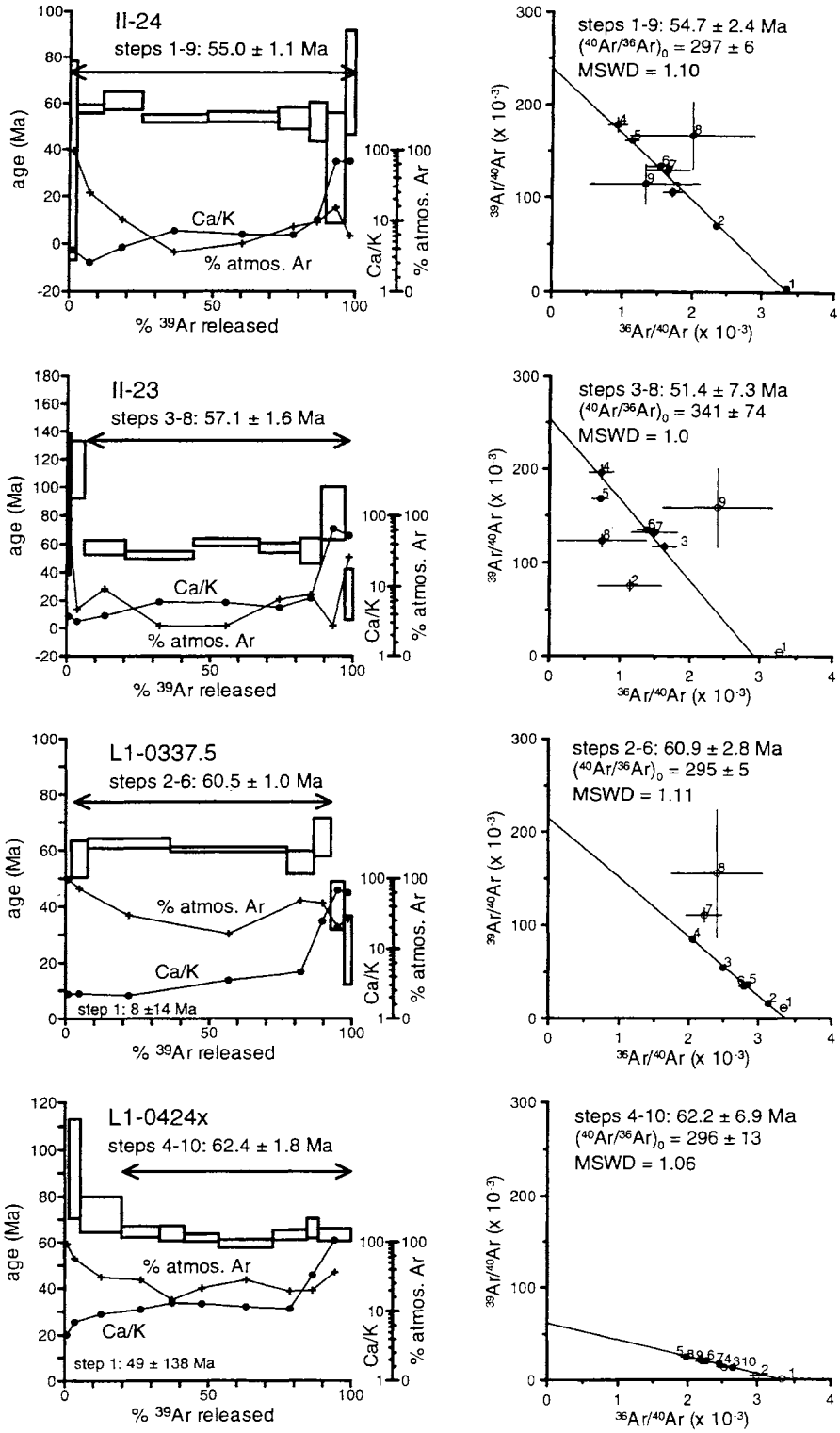

Fig. 10. Ar/Ar step age (left) and inverse isochron diagrams (right) of whole-rock basalts from the Faroes lower basalt formation.

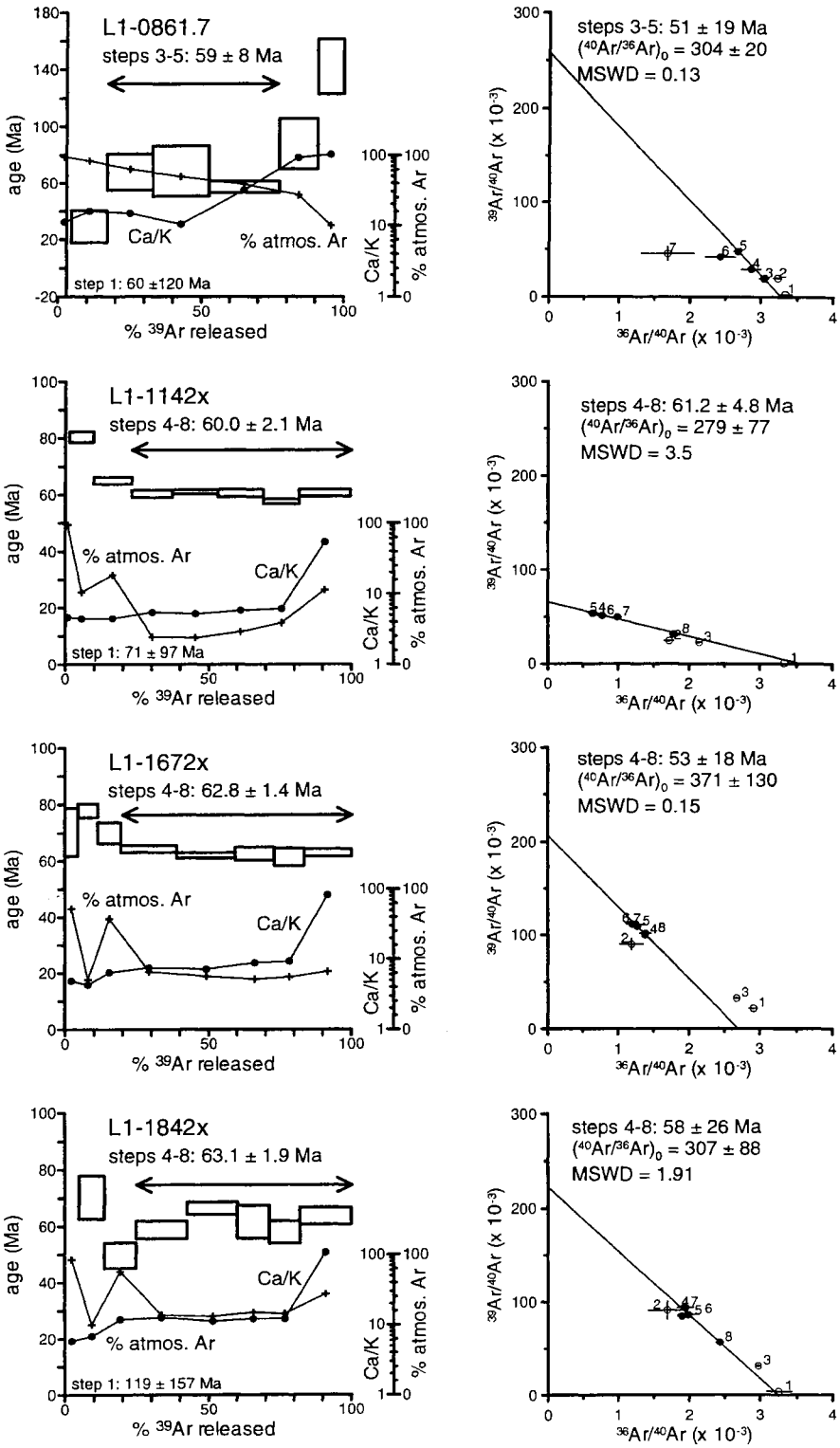

Fig. 10. (*continued*)

Table 5. *Comparisons of XRF, K/Ar and Ar/Ar analytical data*

Sample no.	Split	Depth metres	Wt% K			Ca/K		$^{40}Ar*10^{-7}$ cm^3 STP		Vol.% $^{40}Ar*$	$\frac{^{40}Ar*}{^{39}Ar}$	%σ
			XRF	K/Ar	Ar/Ar	XRF	Ar/Ar	K/Ar	Ar/Ar			
II-24	C	−400	0.540	0.540	0.482§	12.65	12.32	11.77	10.20§	52.2	4.10 ± 2.23	
II-23	C	−450	0.531	0.554	0.538	13.10	11.70	12.69	12.98	67.2	4.68 ± 2.06	
L1-0337.5	B	−1260	0.739	0.740	0.425§	8.89	9.04	16.94	9.68§	58.4	4.40 ± 0.95	
L1-0424x	C	−1350	0.324	0.300	0.288	23.24	22.90	7.29	7.40	46.9	16.77 ± 2.00	
L1-0861.7	B	−1770	0.191	0.201	0.106§	39.15	36.39	4.19	2.92§	7.6	5.35 ± 5.69	
L1-1142x	C	−2060	0.490	0.500	0.477	14.46	14.03	10.83	11.80	52.1	15.61 ± 1.26	
L1-1672x	C	−2570	0.398	0.405	0.429	18.46	19.71	9.22	10.99	64.7	5.95 ± 0.63	
L1-1842x	C	−2750	0.315	0.294	0.312	23.98	28.29	6.23	7.93	45.8	5.00 ± 6.41	
Mean:				0.442	0.382	18.56	18.01	9.90	9.24	49.4	8.12	

Depth, stratigraphic depth below the top of the lower basalt formation (to mid point of sampled lava bed); XRF, whole-rock X-ray fluorescence analysis (from Table 3); Ar/Ar, integrated values from Ar/Ar analysis with 1σ error.

§Absolute argon volumes are probably incorrect. This may be due to erroneous sensitivity values and has no effect on isotopic ratios and thus ages.

Table 6. *Comparisons of K/Ar and Ar/Ar datings (Ma)*

Sample no.	Split	Irradiation	Steps	Temperature °C	$J*10^{-6}$	K/Ar age	Ar/Ar integrated age	Int.-K/Ar	Ar/Ar Plateau age	Ar/Ar isochron age	$(^{40}Ar/^{36}Ar)_0$	MSWD
II-24	C	5	1–9	<125–1235	7377	55.0 ± 1.1*	53.7 ± 1.2	−1.3	55.0 ± 1.1	54.7 ± 2.4	297 ± 6	1.10
II-23	C	5	3–8	565–1150	7357	57.9 ± 0.8	61.0 ± 1.2	3.1	57.1 ± 1.6	51.4 ± 7.3	341 ± 74	1.00
L1-0337.5	B	5	2–6	600–1095	7377	57.9 ± 1.0*	57.7 ± 0.5	−0.2	60.5 ± 1.0	60.9 ± 2.8	295 ± 5	1.11
L1-0424x	C	3	4–10	660–1305	2185	61.8 ± 1.3	64.9 ± 1.3	3.1	62.4 ± 1.8	62.2 ± 6.9	296 ± 13	1.06
L1-0861.7	B	5	3–5	795–1095	7384	52.8 ± 8.3	69.8 ± 3.9	17.0	60 ± 8	51 ± 19	304 ± 20	0.13
L1-1142x	C	3	4–8	700–1320	2261	55.1 ± 1.1	62.6 ± 0.8	7.5	60.0 ± 2.1	61.2 ± 4.8	279 ± 77	3.50
L1-1672x	C	2	4–8	700–1300	6137	57.6 ± 1.2*	64.8 ± 0.4	7.2	62.8 ± 1.4	53 ± 18	371 ± 130	0.15
L1-1842x	C	2	4–8	700–1310	7245	53.7 ± 1.2	64.2 ± 4.1	10.5	63.1 ± 1.9	58 ± 26	307 ± 88	1.91
Mean:						56.5	62.3	5.9	60.1	56.6	311	

Steps, steps included in plateau and isochron ages; Temperature, temperature range of steps included; J, irradiation parameter (irradiation 2: $\sigma = 1\%$; irradiations 3 and 5: $\sigma = 0.5\%$); K/Ar age, K/Ar age of the same split of sample which has been Ar/Ar dated. * denotes that the mean K/Ar age of the sample is considered a magmatic crystallization age; Int.-K/Ar, difference between Ar/Ar integrated age and K/Ar age from same split Ma; MSWD, Mean Square of Weighted Deviates.

All errors quoted at the 1σ level (includes error on J in Ar/Ar ages).

Table 7. *Ar/Ar step heating data, lower basalt formation, Faroe Islands*

Sample no.	Step	T°C	$^{39}Ar_{(K)}$	$^{37}Ar_{(Ca)}$	$^{38}Ar_{(Cl)}$	Ca/K	Cl/K	$\frac{^{40}Ar^*}{^{39}K}$	%atm. Ar	age (Ma)	$\pm\sigma$	% ^{39}Ar	% ^{39}Ar cum.
II-24	1*	465	0.446	0.841	0.032	3.753	0.017	2.705	99.1	35.65	42.58	2.5	2.5
II-24	2*	565	1.658	2.109	0.031	2.531	0.004	4.390	69.3	57.50	1.80	9.2	11.7
II-24	3*	650	2.426	5.045	0.024	4.138	0.003	4.674	50.6	61.16	3.93	13.5	25.2
II-24	4*	730	4.078	14.570	0.038	7.109	0.003	4.073	27.5	53.40	1.73	22.7	47.9
II-24	5*	820	4.452	14.045	0.089	6.278	0.006	4.134	33.4	54.20	2.20	24.8	72.7
II-24	6*	910	1.943	6.037	0.141	6.182	0.021	4.088	45.4	53.60	4.78	10.8	83.5
II-24	7*	1010	1.091	5.585	0.297	10.185	0.076	3.966	48.8	52.03	8.53	6.1	89.6
II-24	8*	1110	1.204	41.075	0.539	67.873	0.128	2.458	59.1	32.43	23.63	6.7	96.3
II-24	9*	1235	0.633	21.739	0.206	68.303	0.094	5.307	39.3	69.29	22.84	3.5	99.8
II-23	1	460	0.243	0.455	0.014	3.723	0.016	6.830	97.0	88.45	50.29	1.2	1.2
II-23	2	565	1.007	1.602	0.019	3.166	0.005	8.743	33.8	112.47	20.43	4.9	6.1
II-23	3*	670	2.930	5.634	0.014	3.826	0.001	4.409	48.3	57.59	5.11	14.3	20.4
II-23	4*	750	4.852	14.606	0.052	5.990	0.003	3.978	21.8	52.04	2.66	23.6	44.0
II-23	5*	840	4.755	13.976	0.061	5.850	0.004	4.687	21.4	61.16	2.55	23.1	67.1
II-23	6*	935	2.953	7.425	0.126	5.003	0.012	4.387	40.8	57.30	3.52	14.4	81.5
II-23	7*	1030	1.517	5.187	0.202	6.805	0.038	4.217	44.2	55.12	9.01	7.4	88.9
II-23	8*	1150	1.698	56.030	0.750	65.678	0.125	6.304	22.0	81.79	18.65	8.3	97.2
II-23	9	1275	0.601	15.896	0.121	52.672	0.057	1.832	70.9	24.15	18.05	2.9	100.1
L1-0337.5	1	600	0.337	0.379	0.008	2.241	0.007	0.613	99.3	8.14	13.54	2.0	2.0
L1-0337.5	2*	695	0.968	1.104	0.007	2.271	0.000	4.346	92.9	56.93	6.50	5.7	7.7
L1-0337.5	3*	790	4.857	5.215	0.025	2.137	0.002	4.778	73.8	62.50	1.76	28.6	36.3
L1-0337.5	4*	900	6.970	12.369	0.067	3.531	0.003	4.606	60.6	60.28	0.85	41.0	77.3
L1-0337.5	5*	990	1.607	3.782	0.056	4.684	0.010	4.246	84.4	55.65	4.12	9.4	86.7
L1-0337.5	6*	1095	1.027	12.729	0.107	24.674	0.030	4.954	82.7	64.75	6.81	6.0	92.7
L1-0337.5	7	1195	0.799	27.589	0.133	68.678	0.047	3.072	65.9	40.42	8.46	4.7	97.4
L1-0337.5	8	1320	0.444	14.103	0.052	63.169	0.033	1.854	71.2	24.51	12.33	2.6	100.0
L1-0424x	1	460	0.084	0.198	0.002	4.673		12.471	98.9	48.50	138.30	1.5	1.5
L1-0424x	2	535	0.230	0.826	0.002	7.145		23.863	88.3	91.70	21.25	4.0	5.5
L1-0424x	3	660	0.822	3.844	0.002	9.302		18.681	74.8	72.17	7.74	14.2	19.7
L1-0424x	4*	730	0.769	4.190	0.002	10.841		16.703	72.7	64.67	2.40	13.3	33.0
L1-0424x	5*	770	0.490	3.274	0.002	13.295		16.491	58.4	63.86	3.27	8.5	41.5
L1-0424x	6*	820	0.705	4.565	0.000	12.891		15.997	66.9	61.98	1.61	12.2	53.7
L1-0424x	7*	920	1.096	6.449	0.007	11.714		15.345	72.6	59.50	1.77	19.0	72.7
L1-0424x	8*	1020	0.680	3.774	0.008	11.043		16.316	64.6	63.20	2.16	11.8	84.5
L1-0424x	9*	1105	0.239	3.992	0.004	33.199		17.091	65.3	66.15	4.29	4.1	88.6
L1-0424x	10*	1305	0.657	35.299	0.010	107.001		16.319	78.3	63.21	2.64	11.4	100.0
L1-0861.7	1	590	0.179	0.993	0.013	11.062	0.020	4.555	98.8	59.68	120.30	4.7	4.7
L1-0861.7	2	795	0.468	3.703	0.005	15.761	0.008	2.198	95.7	29.05	11.48	12.4	17.1
L1-0861.7	3*	900	0.601	4.439	0.012	14.702	0.003	5.188	90.0	67.83	12.80	15.9	33.0
L1-0861.7	4*	995	0.743	3.874	0.045	10.372	0.006	5.247	84.6	68.58	17.94	19.6	52.6
L1-0861.7	5*	1095	0.934	14.763	0.218	31.448	0.017	4.356	79.1	57.11	4.05	24.7	77.3
L1-0861.7	6	1200	0.514	23.793	0.065	92.035	0.065	6.757	71.6	87.84	17.77	13.6	90.9
L1-0861.7	7	1330	0.344	17.621	0.028	102.031	0.035	11.102	49.7	142.15	19.20	9.1	100.0
L1-1142x	1	460	0.143	0.332	0.007	4.639		17.677	98.7	70.70	97.33	1.5	1.5
L1-1142x	2	610	0.773	1.710	0.001	4.400		20.145	50.9	80.36	1.90	8.2	9.7
L1-1142x	3	700	1.266	2.827	0.004	4.442		16.213	63.2	64.95	1.25	13.4	23.1
L1-1142x	4*	770	1.343	3.666	0.003	5.432		15.016	19.3	60.23	1.30	14.2	37.3
L1-1142x	5*	830	1.513	3.930	0.003	5.169		15.198	18.7	60.95	0.75	16.0	53.3
L1-1142x	6*	920	1.514	4.390	0.001	5.771		15.101	22.9	60.57	1.32	16.0	69.3
L1-1142x	7*	1030	1.184	3.629	0.003	6.101		14.329	29.3	57.52	0.90	12.5	81.8
L1-1142x	8*	1320	1.701	46.034	0.012	53.865		15.114	52.6	60.62	1.24	18.0	99.8

Table 7. (*continued*)

Sample no.	Step	T°C	$^{39}Ar_{(K)}$	$^{37}Ar_{(Ca)}$	$^{38}Ar_{(Cl)}$	Ca/K	Cl/K	$\frac{^{40}Ar^*}{^{39}K}$	%atm. Ar	age (Ma)	$\pm\sigma$	% ^{39}Ar	% ^{39}Ar cum.
L1-1672x	1	560	0.885	2.168	0.001	4.876		6.468	86.0	70.23	8.50	4.5	4.5
L1-1672x	2	630	1.329	2.870	0.003	4.296		7.177	35.3	77.76	2.36	6.8	11.3
L1-1672x	3	700	1.569	5.083	0.004	6.446		6.446	78.9	69.99	3.69	8.1	19.4
L1-1672x	4*	775	3.798	14.265	0.002	7.476		5.916	40.9	64.34	1.31	19.5	38.9
L1-1672x	5*	850	3.986	14.372	0.005	7.176		5.698	37.8	62.01	0.98	20.5	59.4
L1-1672x	6*	920	2.664	11.757	0.009	8.782		5.754	35.6	62.61	2.35	13.7	73.1
L1-1672x	7*	1015	2.020	9.330	0.020	9.192		5.641	37.1	61.40	3.21	10.4	83.5
L1-1672x	8*	1300	3.233	133.177	0.106	81.987		5.791	41.1	63.01	1.34	16.6	100.1
L1-1842x	1	525	0.481	1.422	0.003	5.881		9.414	96.4	119.03	156.67	4.9	4.9
L1-1842x	2	625	0.849	2.943	0.002	6.898		5.483	50.1	70.29	7.62	8.7	13.6
L1-1842x	3	700	1.078	6.432	0.003	11.870		3.848	88.0	49.60	4.49	11.0	24.6
L1-1842x	4*	780	1.744	11.076	0.001	12.639		4.566	57.0	58.72	3.19	17.9	42.5
L1-1842x	5*	850	1.721	9.734	0.002	11.256		5.173	56.1	66.38	2.15	17.6	60.1
L1-1842x	6*	925	1.107	6.761	0.004	12.155		4.785	58.8	61.49	5.86	11.3	71.4
L1-1842x	7*	1015	1.034	6.313	0.006	12.152		4.500	57.7	57.88	3.98	10.6	82.0
L1-1842x	8*	1310	1.753	94.177	0.015	106.883		4.963	71.9	63.74	2.99	18.0	100.0

$^{39}Ar_{(K)}$, $^{37}Ar_{(Ca)}$ and $^{38}Ar_{(Cl)}$ in 10^{-9} cm^3 STP units.
* Step included in age plateau.

fits the six Ar/Ar whole-rock datings from the Lopra well but is slightly too old for the dates from the exposed sequence. A better fit may be obtained by assuming that C27n is present above the first core at 337 m in the Lopra well, but there is no supporting evidence of such additional polarity interval. By contrast, both the K/Ar whole-rock dates and Ar/Ar plagioclase dates presented earlier suggest that the Lopra well terminates within chron C26r. The different results obtained by the two dating methods are discussed below.

Discussion

^{39}Ar recoil loss and relocation

Pertinent data on the eight basalts analysed by both the K/Ar and the Ar/Ar dating methods are compared in Tables 5 and 6. The six basalts from the Lopra well may be identified from sample numbers starting with 'L1-' and cuttings samples with the suffix 'x', while three accepted K/Ar mean ages are marked with an '*'. The Ar/Ar integrated ages are calculated by combining the Ar isotope measurements from all heating steps to obtain one single age as when making a one step total fusion experiment. The integrated age is comparable to a K/Ar age except that by Ar/Ar analysis K is analysed by first converting ^{39}K to ^{39}Ar by neutron irradiation in an atomic reactor and then deducing K from the isotopic composition of Ar. Although both methods provide an apparent bulk age, the ages differs by −1 to +17 Ma, and our integrated Ar–Ar ages are, on average, six million years older than the K/Ar ages (Table 6). The Ar/Ar determinations are made on only about 0.1 g of sample, and this means that variations in the K/Ar ratio of the rock at the millimetre-scale will

have a much larger effect on Ar/Ar dates than on K/Ar ages. However, seven samples dated by both methods appear to be either homogeneous or to show a co-variation of K and Ar (Fig. 7). The differences between the integrated Ar/Ar and K/Ar ages are therefore difficult to explain solely by sample inhomogeneity.

An integrated age higher than the K/Ar age may indicate loss of recoiled ^{39}Ar from the sample before the step-heating analysis. It cannot be explained as excess $^{40}Ar^*$ as the K/Ar age would exhibit similarly high ages. Mass balance calculations indicate a ^{39}Ar loss of about 11–24% in the four deepest Lopra samples, while samples II-23 and L1-0424x seem to have experienced minor loss of the order of 5% (Fig. 11). Such uncontrolled leaking of ^{39}Ar is considered to occur mainly in low-temperature minerals, especially in expanding clay minerals like smectite, but possibly also in zeolites. The recoil loss probably occurs during the irradiation of the sample. On step heating these samples, the initial steps will give high apparent ages because $^{39}Ar(K)$ is underestimated. It should be noted that zeolites are absent in the Ar/Ar dated rocks, and in samples L1-1672x and L1-1842x there is too little K in the clay minerals (smectite) to account for the loss (Fig. 11). Even if enough K is present in the smectite it is unlikely that all of the ^{39}Ar generated has been lost, as the mineral tends to be concentrated in large interstitial areas having a low surface/volume ratio. The apparent age of the first heating step is generally <80 Ma (in L1-0861.7 only 25 Ma), these ages which are not excessively higher than the average spectrum ages are hard to reconcile with massive loss of ^{39}Ar from low-temperature phases. Recoil loss from low-temperature minerals can therefore probably only partly explain the high integrated ages. The only other potential source of significant ^{39}Ar loss is alkali feldspar which degasses over a wider range of temperatures than clay minerals and zeolites. Alkali feldspar is a major K host in most rocks (Fig. 6) and must therefore contribute a significant part of radiogenic Ar in the age plateaux. It forms roughly half of the interstitial rhyolite and may be present as microlites in smectite replacing glass; most of it is thought to occur as thin rims on groundmass plagioclase (see the petrography and mineralogy section). Although the alkali feldspar grains and rims are typically less than a few microns wide they are much too thick to cause significant recoil loss because the average recoil distance of ^{39}Ar is only about 0.08 μm (McDougall & Harrison 1999). However, this is only the case if it is a high-temperature feldspar. During slow cooling the first formed feldspar is converted to a low-temperature phase consisting of submicroscopic lamellae of K- and Na-rich feldspar (cryptoperthite) and their interfaces may form rapid diffusion channels for recoiled ^{39}Ar (McDougall & Harrison 1999). The flows (cooling units) of the lower basalt formation have an average thickness of 20 m (Rasmussen & Noe-Nygaard 1969, 1970; Hald & Waagstein 1984) which means that their centres have probably cooled slowly enough so that high temperature alkali feldspar (sanidine) could develop into cryptoperthite as reported in rhyolitic flows (Yund & Chapple 1980). K–Na feldspar intergrowths may also form from the break-down of plagioclase during burial metamorphism, but such intergrowths are likely to be visible under the microscope (and thus having far too widely spaced interfaces to effectively channel recoiled Ar), and they have not been observed in any of the dated basalts. It is noteworthy that the samples which have lost most ^{39}Ar are all from >800 m depth in the Lopra well, and we speculate that the relief of formation pressure may have caused pre-existing microfractures in the borehole samples to open thereby enhancing the diffusion loss of recoiled Ar during later irradiation.

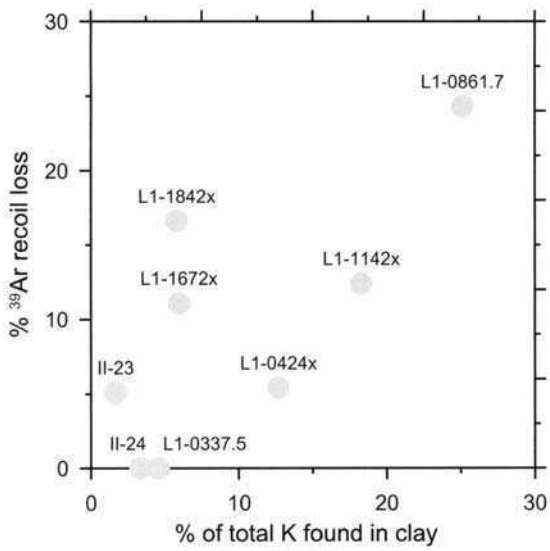

Fig. 11. Percent ^{39}Ar lost by recoil versus the percent of the K in the sample residing in smectite. The recoil loss is calculated from the difference between Ar/Ar integrated age and K/Ar age of the same subsample.

Ar recoil loss may not only explain the high integrated ages but could also be responsible for some of the relatively high plateau ages obtained compared to the accepted K/Ar ages. This makes the interpretation of the Ar/Ar ages uncertain. The samples most likely to give true plateau ages are II-24, II-23, L1-0337.5 and L1-0424x which have integrated ages fairly similar to their K/Ar age. However, recoiled ^{39}Ar is not necessarily lost from the sample but may be relocated into adjacent K-poor mineral phases, and such relocation will not affect the integrated age of the sample. Recoil relocation is generally considered of more concern than recoil loss when dealing with the interpretation of Ar/Ar whole-rock spectra of fine-grained volcanic rocks (cf. Hofmann *et al.* 2000). Potassium mainly resides in alkali-feldspar, sodic plagioclase and clay minerals which release argon at relatively low temperatures, whereas minerals with little or no potassium, like calcic plagioclase and pyroxene, degas at high temperatures (>1000°C judged by the increase in Ca/K ratios). ^{39}Ar recoiled into the latter minerals will therefore result in an overestimate of their ^{39}K content and give low apparent ages at high temperatures. Conversely, the mineral phases supplying the excess ^{39}Ar will give too high ages at lower temperatures. The combined effect of such exchange of ^{39}Ar by recoil often results in decreasing apparent ages with temperature and the true age should probably be found in the last steps just before the degassing of high Ca phases containing excess recoiled ^{39}Ar (Féraud & Courtillot 1994; Hofmann *et al.* 2000). This recoil relocation effect is probably seen in L1-0337.5 where steps 3 to 5 show slightly decreasing ages and increasing Ca/K preceding the degassing of the high Ca phases, while the latter phases give low apparent ages due to ^{39}Ar recoiled into them. If we instead use just steps 4 and 5 for the age calculation we get a lower plateau age of 60.1 ± 0.9 Ma comparable to the mean K/Ar age of 58.3 ± 0.9 Ma. Sample L1-0424x with an integrated age only three million years higher than the K/Ar age shows slightly decreasing

ages in steps 4–7 included in the age plateau. This sample may likewise have been affected by recoil relocation although the high Ca/K steps at the end do not show low ages. The only two Ar/Ar dated samples from the exposed succession have comparable plateau, integrated and K/Ar ages with a difference between the latter two of about −1 and +3 Ma respectively (split C of II-24 and II-23 in Table 6). Unfortunately, neither of them give precise age plateaux, and they may hide non-analytical variations not reflected in the error calculations, which assume only analytical scatter.

The interpretation of the present Ar/Ar isotopic data suggests that whole-rock plateau ages fulfilling standard criteria of acceptance (Dalrymple *et al.* 1980) may in some cases be too high due to recoil processes. The same has recently been suggested for whole-rock dates from the Deccan Traps which often give 1–2 Ma higher ages than plagioclase and amphibole from the same or stratigraphically equivalent lavas or dykes (Hofmann *et al.* 2000). Mineral dates are generally considered more accurate because of the homogeneous composition of samples, which makes it more simple to interpret release spectra. However, suitable minerals for dating are often not available in fine-grained volcanic rocks. Instead, whole-rock dates may sometimes be re-assessed by using more tight constraints on the accepted deviation of apparent ages within a plateau (Féraud & Courtillot 1994; Hofmann *et al.* 2000), although this will often result in questionable plateaux of only 2–3 steps encompassing less than half of the Ar released, or no plateau at all.

The problems with recoil makes it difficult to obtain accurate geological ages from the present Ar/Ar whole-rock measurements. Four samples from the Lopra well give relatively well defined age plateaux of 60–63 Ma but are almost certainly too old due to ^{39}Ar recoil loss or relocation. The two samples from the exposed sequence may be less affected and suggest an age of about 56 Ma for the youngest part of the lower basalt formation, but are unfortunately not very accurate. Our interpretation of the Ar/Ar whole-rock dates suggests that the basalts dated from the Lopra well cannot be older than 61 Ma and that they therefore very probably all erupted during chron C26r (57.1–60.9 Ma).

Choice of samples and methods in whole-rock dating of basalt

The Ar/Ar step-heating method is generally considered superior to the K/Ar method for whole-rock dating of altered rocks. This is because Ar/Ar ages are based on a number of Ar extractions defining an age plateau and isochron, while K/Ar ages are derived from the total amount of K and radiogenic Ar of the sample. However, we have shown above that Ar/Ar ages may be biased due to ^{39}Ar recoil loss or relocation during irradiation. In the investigated basalts the recoil loss is associated with interstitial clay (Fig. 11) and at least one other extremely fine-grained K-bearing phase (most likely invisible cryptoperthite). The loss of ^{39}Ar will tend to give too high Ar/Ar ages. Recoil relocation of ^{39}Ar seems to have a similar effect, but is difficult to quantify. Thus only two basalts low in interstitial clay, but relatively high in interstitial rhyolite matrix, are considered to give igneous ages.

K/Ar whole-rock dating of an igneous rock is based on the assumption that the rock formed a closed K/Ar system since crystallization. Ideally the rock should be completely fresh without any secondary minerals, but this requirement is probably never fulfilled in fine-grained extrusive rocks that have been buried. However, the above Ar/Ar measurements show little evidence of loss or gain of radiogenic ^{40}Ar.

which suggest that slightly altered basalts may give undisturbed K/Ar ages. We have demonstrated (Figs 8 & 9) that consistent ages may be obtained on basalts in which all interstitial glass is altered to saponite ± minor C/S provided that (1) no other low-temperature minerals are present, (2) the clay contains only a small fraction (<10%) of the total K of the rock and (3) that the rock is homogeneous (replicate K/Ar ages differ <4 Ma).

The six basalts giving consistent K/Ar ages are not only poor in clay (former glass), but also contain interstitial rhyolite. Similarly, the only two basalts with reliable Ar/Ar ages are those containing most rhyolite (II-23 and II-24). Although one of these (II-23) is too inhomogeneous for K/Ar dating, it suggests that broadly similar criteria of freshness applies for Ar/Ar dating as for K/Ar dating, except that the former method seems more sensitive to the presence of clay due to recoil effects.

This emphasizes that the selection of samples is more important than the dating method itself. The best samples for dating are from the massive core of thick lava flows with no fractures or with fractures that have been sealed at an early date, and with as much K as possible. Massive cores are often relatively poor in interstitial clay, which replaces glass and represents frozen residual melt. The reduction of melt may be due to slow cooling, which will result in advanced crystallization and eventually formation of interstitial rhyolite instead of glass (a tholeiitic basalt magma with about 50% SiO_2 will gradually change to a rhyolite magma high in SiO_2 by crystal fractionation). However, a paucity of former glass in massive basalt may also result from filter pressing and accumulation of melt into residual veins (Self *et al.* 1997).

The present study demonstrates that it is possible to obtain K/Ar ages from thick, massive lava flows which have been subjected to zeolite facies burial metamorphism. Crystallization ages have thus been obtained even from the deepest zeolite zone, the laumontite zone, where the temperature has exceeded 110°C (Fig. 2; Jørgensen 1984).

It is important as an additional control to date several samples from the same volcanic sequence in order to see if the measured ages correspond (within errors) with the stratigraphic order of the samples. In K/Ar dating, sample inhomogeneity is also of concern, and samples should preferably be analysed in duplicate or triplicate.

The sampling method is less important, and even drill cuttings may be dated, which is very useful because cuttings are often the only material available from commercial wells.

The problems of whole-rock dating of flood basalts may be circumvented by Ar/Ar dating of pure mineral extracts, usually plagioclase phenocrysts. However, this requires that phenocrysts are present, that they are fresh and contain a fair amount of K, but little or no excess argon. The method has been used with success in plagioclase extracted from outcrops and drill cores (Fig. 9; M. Storey unpubl. data), but, as far we are aware, not yet from drill cuttings of basalt.

This study does not include dykes or sills. Faroes dykes and sills consist of almost holocrystalline, relatively fresh basalt, but pose other dating problems because of their intrusive nature, i.e. lack of stratigraphic control and the risk that they contain inherited argon trapped under pressure (McDougall & Harrison 1999).

Age of the Faroes volcanism

Based on the close fit between K/Ar and palaeomagnetic ages we estimate that the 3 km exposed and drilled section of the lower basalt formation range in age from

about 58.8 ± 0.5 Ma to 55.8 ± 0.1 Ma (1σ) (Fig. 9). The Faroes lower basalt formation has been interpreted as a pre-breakup lava sequence and is overlain by a >2 km syn-rift sequence with an age of about 55.5–56 Ma (Larsen *et al.* 1999) formed in the early part of chron C24r during the final breakup of the North Atlantic. The present K/Ar and Ar/Ar dates support previous interpretations that the two normal polarity intervals in the exposed part of the lower basalt formation belong to chron C25n and C26n and that the few reversely magnetized flows at the top belong to C24r (Waagstein 1988). This means that the older cycle of volcanic activity continued until at least 55.9 Ma and that the overlying 10 m-thick coal-bearing sequence therefore must have accumulated in a short period of time (<0.1 Ma?) during the earliest part of chron C24r. This thin sedimentary sequence marks a major shift in the magmatic regime and defines an important regional unconformity. The Faroes lava succession has been correlated in detail with the East Greenland succession where, however, the age of the lower volcanic cycle is less well constrained (Larsen *et al.* 1999). Two major volcanic cycles have also been recognized in Scotland and offshore SE Greenland although the lower cycle of extrusive basaltic volcanism probably ended earlier here than in the Faroes (Hamilton *et al.* 1998; Sinton *et al.* 1998).

The dates also show that the oldest lavas drilled in the Faroes cannot be older than C26r. They therefore do not support the recent correlation of these lavas with C28n or C27r proposed by Naylor *et al.* (1999) and Ritchie *et al.* (1999), respectively. On the contrary, the approximate fit of palaeomagnetic and K/Ar dates to a logarithmic curve (Fig. 9) suggests that the lowermost 2 km of lavas drilled in Suðuroy accumulated at a very high rate, probably in excess of $2\,km\,Ma^{-1}$ High-precision dating work of other flood basalt sequences suggests similar high rates of accumulation (Hamilton *et al.* 1998; Storey *et al.* 1998; Hofmann *et al.* 2000). Although we do not know the total thickness of the volcanics of the major pre-breakup cycle of the Faroes it is quite possible therefore that this cycle first started 59 Ma ago. This is long after the onset of Paleocene volcanism in the British Isles, off SE Greenland and in West Greenland dated at *c.* 62 Ma (Pearson *et al.* 1996; Sinton & Duncan 1998; Storey *et al.* 1998), but at about the time of maximum volcanic activity in Antrim and Skye (Bell & Jolley 1997) and the arrival of the first magmas with an Icelandic mantle plume signature in Mull 58.7 ± 0.3 Ma (1σ) ago (Chambers & Fitton 2000).

There have probably been earlier episodes of volcanic activity in the Faroes region as tuff beds have been reported from the mid-Paleocene Vaila Formation in the Faroe–Shetland basinal area to the SE of the Faroes formed during chron C26r (Knox *et. al.* 1997; Lamers & Carmichael 1999), perhaps starting in C27r (Naylor *et al.* 1999). The Vaila Formation contains deep-water siliciclastic sandstones at several levels, some of which are major hydrocarbon reservoirs. The question is if any of these sandstones have been sourced from the Faroes–Greenland region (Larsen *et al.* 1999), thus setting a lower limit to the start of major volcanism.

Conclusions

By analysing samples from thick, massive basalt flows it may be possible with the K/Ar whole-rock method to date several km thick lava sequences affected by very low-grade burial metamorphism in the chabazite–thomsonite to laumontite zeolite

zones, as demonstrated for the lower basalt formation of the Faroe Islands. Extensive microprobe work and mass balance calculations show that the core of thick, massive flows from the Faroes lower basalt formation has on average 60% of the potassium in groundmass plagioclase, interstitial microcrystalline rhyolite and interstitial smectitic clay, the rest mainly forming thin rims of alkali feldspar on plagioclase. Igneous ages are obtained from basalts almost homogeneous in K and Ar with <6% of the total K in interstitial saponite ± C/S, but no other low-temperature minerals. In contrast, basalts which are inhomogeneous, contain >15% of total K in clay, have abundant C/S or contain traces of zeolites, secondary quartz, di-octahedral smectite or celadonite give low or variable ages of no use. It is paramount to check the homogeneity of the basalts, preferably by replicate dating of different splits or subsamples.

Ar/Ar whole-rock dating is generally considered more accurate than K/Ar dating, but the present study indicates that most of the Ar/Ar analyses are affected by ^{39}Ar recoil loss or relocation which tend to give too high plateau ages. Recoil may affect age plateaux that fulfil normal criteria of acceptance and calls for critical use of whole-rock Ar/Ar dating. Severe recoil problems may be detected by dating the same samples by both the Ar/Ar and K/Ar method, which unfortunately is rarely done.

The K/Ar and Ar/Ar dates considered true crystallization ages agree with unpublished Ar/Ar ages. Together with palaeomagnetic data they indicate that the oldest drilled lavas of the Faroes lower basalt formation started to erupt at a very high rate 58.8 ± 0.5 Ma ago in chron C26r, but that the accumulation rate diminished before the volcanism came to a temporary halt about 55.8 ± 0.1 Ma ago in the beginning of chron C24r. It suggests that the overlying thin coal-bearing sequence formed in a short period of time before the volcanism resumed with the deposition of the middle and upper basalt formations during early C24r.

The senior author thanks Statoil for financial support during a preliminary compilation of some of the data presented here and the Geological Survey of Denmark and Greenland for permission to publish. The microprobe analyses were made with equipment funded by the Danish Natural Science Research Council. The authors thank M. Storey for comments on the Ar/Ar section and S. Kelley for his constructive review and many suggestions for improvements.

References

ABRAHAMSEN, N., SCHOENHARTING, G. & HEINESEN, M. 1984. Palaeomagnetism of the Vestmanna core and magnetic age and evolution of the Faroe Islands. *In*: BERTHELSEN, O., NOE-NYGAARD, A. & RASMUSSEN, J. (eds) *The deep drilling project 1980–1981 in the Faroe Islands*. Føroya Fróðskaparfelag, Tórshavn, 93–108.

BELL, B. R. & JOLLEY, D. W. 1997. Application of palynological data to the chronology of the Palaeogene lava fields of the British Province: implications for magmatic stratigraphy. *Journal of the Geological Society, London*, **154**, 701–708.

BOLDREEL, L. O. & ANDERSEN, M. S. 1994. Tertiary development of the Faroe–Rockall Plateau based on reflection seismic data. *Bulletin of the Geological Society of Denmark*, **41**, 162–180.

CANDE, S. C. & KENT, D. V. 1995. Revised calibration of the geomagnetic polarity time scale for the late Cretaceous and Cenozoic. *Journal of Geophysical Research*, **100**, 6093–6095.

CHAMBERS, L. M. & FITTON, J. G. 2000. Geochemical transitions in the ancestral Iceland plume: evidence from the Isle of Mull Tertiary volcano, Scotland. *Journal of the Geological Society, London*, **157**, 261–263.

DALRYMPLE, G. B., LANPHERE, M. A. & CLAGUE, D. A. 1980. Conventional and $^{40}Ar/^{39}Ar$ K–Ar ages of volcanic rocks from Ojin (Site 430), Nintoku (Site 432), and Suiko (Site 433) seamounts and the chronology of volcanic propagation along the Hawaiian-Emperor Chain. *In*: JACKSON, E. D., KOISUMI, I. *et al.* (eds) *Initial Reports Deep Sea Drilling Project*. U.S. Government Printing Office, Washington, **55**, 659–676.

FÉRAUD, G. & COURTILLOT, V. 1994. Comment on: 'Did Deccan volcanism pre-date the Cretaceous-Tertiary transition?' *Earth and Planetary Science Letters*, **122**, 259–262.

FITCH, F. J., HOOKER, P. J., MILLER, J. A. & BRERETON, N. R. 1978. Glauconite dating of Palaeocene–Eocene rocks from East Kent and the time-scale of Palaeogene volcanism in the North Atlantic region. *Journal of the Geological Society, London*, **135**, 499–512.

HALD, N. & WAAGSTEIN, R. 1984. Lithology and chemistry of 2-km sequence of Lower Tertiary tholeiitic lavas drilled on Suðuroy, Faroe Islands (Lopra-1). *In*: BERTHELSEN, O., NOE-NYGAARD, A. & RASMUSSEN, J. (eds) *The deep drilling project 1980–1981 in the Faroe Islands*. Føroya Fróðskaparfelag, Tórshavn, 15–38.

HAMILTON, M. A., PEARSON, D. G., THOMPSON, R. N., KELLEY, S. P. & EMELEUS, C. H. 1998. Rapid eruption of Skye lavas inferred from precise U–Pb and Ar–Ar dating of the Rum and Cuillin plutonic complexes. *Nature, London*, **394**, 260–263.

HOFMANN, C., FÉRAUD, G. & COURTILLOT, V. 2000. $^{40}Ar/^{39}Ar$ dating of mineral separates and whole rocks from the Western Ghats lava pile: further constraints on duration and age of the Deccan traps. *Earth and Planetary Science Letters*, **180**, 13–27.

JOLLEY, D. W. 1997. Palaeosurface palynofloras of the Skye lava field and the age of the British Tertiary volcanic province. *In*: WIDDOWSON, M. (ed.) *Palaeosurfaces: Recognition, Reconstruction and Palaeoenvironmental interpretation*. Geological Society, London, Special Publications, **120**, 67–94.

JØRGENSEN, O. 1984. Zeolite zones in the basaltic lavas of the Faroe Islands – A quantitative description of the secondary minerals in the deep wells of Vestmanna-1 and Lopra-1. *In*: BERTHELSEN, O., NOE-NYGAARD, A. & RASMUSSEN, J. (eds) *The deep drilling project 1980–1981 in the Faroe Islands*. Føroya Fróðskaparfelag, Tórshavn, 71–91.

KNOX, R. W. O'B., HOLLOWAY, S., KIRBY, G. A. & BAILY, H. E. 1997. *Stratigraphic nomenclature of the UK North West Margin. 2. Early Paleogene Lithostratigraphy and Sequence Stratigraphy*. British Geological Survey, Nottingham.

LAMERS, E. & CARMICHAEL, S. M. M. 1999. The Paleocene deepwater sandstone play West of Shetland. *In*: FLEET, A. J. & BOLDY, S. A. R. (eds) *Petroleum Geology of Northwest Europe: Proceedings of the 5th Conference*. Geological Society, London, 645–659.

LARSEN, L. M., WAAGSTEIN, R., PEDERSEN, A. K. & STOREY, M. 1999. Trans-Atlantic correlation of the Palaeogene volcanic successions in the Faroe Islands and East Greenland. *Journal of the Geological Society, London*, **156**, 1081–1095.

LARSEN, M., HAMBERG, L., OLAUSSEN, S., PREUSS, T. & STEMMERIK, L. 1999. Sandstone wedges of the Cretaceous–Lower Tertiary Kangerlussuaq Basin, East Greenland – outcrop analogues to the offshore North Atlantic. *In*: FLEET, A. J. & BOLDY, S. A. R. (eds) *Petroleum Geology of Northwest Europe: Proceedings of the 5th Conference*. Geological Society, London, 337–348.

LUDWIG, K. R. 2000. *Users manual for Isoplot/Ex version 2.3 – A Geochronological Toolkit for Microsoft Excel*. Berkeley Geochronology Center, Special Publication, **1a**.

LUND, J. 1983. Biostratigraphy of interbasaltic coals from the Faroe Islands. *In*: BOTT, M. H. P., SAXOV, S., TALWANI, M. & THIEDE, J. (eds) *NATO Conference Series, Series IV, Marine Sciences*, Volume 8. Plenum Press, New York, 417–423.

LUND, J. 1989. A late Paleocene non-marine microflora from the interbasaltic coals of the Faroe Islands, North Atlantic. *Bulletin of the Geological Society of Denmark*, **37**, 181–203.

MCDOUGALL, I. & HARRISON, T. M. 1999. *Geochronology and Thermochronology by the $^{40}Ar/^{39}Ar$ Method*, 2nd edition. Oxford University Press, New York.

MORTON, A. C., EVANS, D., HARLAND, R., KING, C. & RITCHIE, D. K. 1988. Volcanic ash in a cored borehole W of the Shetland Islands: evidence for Selandian (late Palaeocene) volcanism in the Faroes region. *In*: MORTON, A. C. & PARSON, L. M. (eds) *Early Tertiary Volcanism and the Opening of the NE Atlantic*. Geological Society, London, Special Publications, **39**, 263–269.

NAYLOR, P. H., BELL, B. R., JOLLEY, D. W., DURNALL, P. & FREDSTED, R. 1999. Palaeogene magmatism in the Faroe–Shetland Basin: influences on uplift history and sedimentation. *In*: FLEET, A. J. & BOLDY, S. A. R. (eds) *Petroleum Geology of Northwest Europe: Proceedings of the 5th Conference*. Geological Society, London, 545–558.

NEUHOFF, P. S., FRIDRIKSSON, T., ARNÓRSSON, S. & BIRD, D. K. 1999. Porosity evolution and mineral paragenesis during low-grade metamorphism of basaltic lavas at Teigarhorn, eastern Iceland. *American Journal of Science*, **299**, 467–501.

NEUHOFF, P. S., FRIDRIKSSON, T. & BIRD, D. K. 2000. Zeolite parageneses in the North Atlantic Igneous Province: Implications for geotectonics and groundwater quality of basaltic crust. *International Geology Review*, **42**, 15–44.

NOE-NYGAARD, A. 1966. The invisible part of the Faroes. *Meddelelser fra dansk Geologisk Forening*, **16**, 191–195.

PEARSON, D. G., EMELEUS, C. H. & KELLEY, S. P. 1996. Precise $^{40}Ar/^{39}Ar$ age for the initiation of Paleogene volcanism in the Innner Hebrides and its regional significance. *Journal of the Geological Society, London*, **153**, 815–818.

RASMUSSEN, J. & NOE-NYGAARD, A. 1969. Beskrivelse til geologisk kort over Færøerne i målestok 1: 50.000 [English summary]. *Danmarks Geologiske Undersøgelse, 11th Series*, **24**.

RASMUSSEN, J. & NOE-NYGAARD, A. 1970. Geology of the Faroe Islands. *Danmarks Geologiske Undersøgelse, 11th Series*, **25**.

REX, D. C. 1994. K–Ar age determinations of samples from Leg 134. *In*: GREENE, H. G., COLLOT, J.-Y., STOKKING, L. B. *ET AL.* (eds) *Proceedings of the Ocean Drilling Program, Scientific Results, 104*. Ocean Drilling Program, College Station, Texas.

REX, D. C., GUISE, P. G. & WARTHO, J.-A. 1993. Disturbed ^{40}Ar–^{39}Ar spectra from hornblendes: Thermal loss or contamination. *Chemical Geology*, **103**, 271–281.

RITCHIE, J. D., GATLIFF, R. W. & RICHARDS, P. C. 1999. Early Tertiary magmatism in the offshore NW UK margin and surrounds. *In*: FLEET, A. J. & BOLDY, S. A. R. (eds) *Petroleum Geology of Northwest Europe: Proceedings of the 5th Conference*. Geological Society, London, 573–584.

RODDICK, J. C. 1983. High precision intercalibration of ^{40}Ar–^{39}Ar standards. *Geochimica et Cosmochimica Acta*, **47**, 887–898.

SCHMIDT, S. T. & ROBINSON, D. 1997. Metamorphic grade and porosity and permeability controls on mafic phyllosilicate distributions in a regional zeolite to greenschist facies transition of the North Shore Volcanic Group, Minnesota. *Geological Society America Bulletin*, **109**, 683–697.

SHOENHARTING, G. & ABRAHAMSEN, N. 1984. Magnetic investigations on cores from the Lopra-1 drillhole, Faroe Islands. *In*: BERTHELSEN, O., NOE-NYGAARD, A. & RASMUSSEN, J. (eds) *The deep drilling project 1980–1981 in the Faroe Islands*. Føroya Fróðskaparfelag, Tórshavn, 109–114.

SELF, S., THORDARSON, T. & KESZTHELYI, L. 1997. Emplacement of continental flood basalt lava flows. *In*: MAHONEY, J. J. & COFFIN, M. F. (eds) *Large Igneous Provinces: Continental, Oceanic, and Planetary Flood Volcanism*. Geophysical Monograph **100**, 381–410.

SINTON, C. W. & DUNCAN, R. A. 1998. ^{40}Ar–^{39}Ar ages of lavas from the southwest Greenland margin, ODP Leg 152, and the Rockall Plateau, DSDP Leg 81. *In*: SAUNDERS, A. D., LARSEN, H. C. & WISE, S. W. JR. (eds) *Proceedings of the Ocean Drilling Program, Scientific Results, 152*. Ocean Drilling Program, College Station, Texas, 387–402.

SINTON, C. W., HITCHEN, K. & DUNCAN, R. A. 1998. ^{40}Ar–^{39}Ar geochronology of silicic and basic volcanic rocks on the margins of the North Atlantic. *Geological Magazine*, **135**, 161–170.

STOREY, M., DUNCAN, R. A., PEDERSEN, A. K., LARSEN, L. M. & LARSEN, H. C. 1998. $^{40}Ar/^{39}Ar$ geochronology of the West Greenland Tertiary volcanic province. *Earth and Planetary Science Letters*, **160**, 569–586.

TARLING, D. H. & GALE, N. H. 1968. Isotopic dating and palaeomagnetic polarity in the Faroe Islands. *Nature, London*, **218**, 1043–1044.

WAAGSTEIN, R. 1988. Structure, composition and age of the Faroe basalt plateau. *In:* MORTON, A. C. & PARSON, L. M. (eds) *Early Tertiary Volcanism and the Opening of the NE Atlantic*. Geological Society, London, Special Publications, **39**, 225–238.

WAAGSTEIN, R. 1995. Radiometric dating of the basalts in and around the Lopra-1 well, Faroe Islands. *DGU Service report.* Ministry of the Environment, Geological Survey of Denmark, Copenhagen, **42-1995**.

WAAGSTEIN, R. & HALD, N. 1984. Structure and petrography of a 660 m lava sequence from the Vestmanna-1 drill hole, lower and middle basalt series, Faroe Islands. *In*: BERTHELSEN, O., NOE-NYGAARD, A. & RASMUSSEN, J. (eds) *The deep drilling project 1980–1981 in the Faroe Islands.* Føroya Fróðskaparfelag, Tórshavn, 39–65.

WAAGSTEIN, R., HALD, N. JØRGENSEN, O., NIELSEN, P. H., NOE-NYGAARD, A., RASMUSSEN, J. & SCHÖNHARTING, G. 1984. Deep drilling on the Faroe Islands. *Bulletin of the Geological Society of Denmark*, **32**, 133–138.

YUND, R. A. & CHAPPLE, W. M. 1980. Thermal histories of two lava flows estimated from cryptoperthite lamellar spacings. *American Mineralogist*, **65**, 438–443.

The stratigraphy, environment of eruption and age of the Faroes Lava Group, NE Atlantic Ocean

DAVID ELLIS[1], BRIAN R. BELL[2], DAVID W. JOLLEY[3] & MICHELLE O'CALLAGHAN[1]

[1] *StatoilFoeroyene a.s, Statoil House, 11a Regent Street, London SW1Y 4ST, UK (e-mail: DDAEL@statoil.com)*
[2] *Division of Earth Sciences, University of Glasgow, Gregory Building, Lilybank Gardens, Glasgow G12 8QQ, UK*
[3] *Centre for Palynology, Department of Animal & Plant Sciences, University of Sheffield, Sheffield S1 3JD, UK*

Abstract: Palaeogene volcanism on the NW margin of the Faroe–Shetland Basin is represented by the Faroes Lava Group, within an age range of 57.5–60.56 Ma. The volcanic sequence comprises >1000 m of basaltic volcaniclastic rocks deposited in estuarine or marginal lagoons, overlain by three laterally-extensive formations of subaerial facies basaltic lavas: Lower, *c.* 3250 m; Middle, *c.* 1400 m; Upper, at least 900 m (top not preserved). The Lower and Upper formations comprise high-volume sheet flows, commonly with ferrallitized tops, interbedded with reddened, thin, fluvial claystone and basaltic siltstone deposits. Laterally-impersistent coals occur within the Lower Lava Formation. The Coal-bearing Formation (*c.* 20 m) was deposited in an overbank floodplain environment during an hiatus in the volcanism between the Lower and Middle formations. The Volcaniclastic Sandstone Sequence comprises hydroclastic and pyroclastic deposits which post-date the Coal-bearing Formation and represent a return to volcanism, prior to the eruption of the Middle Lava Formation which is mainly characterized by inflated pahoehoe flows. The onshore sequence of the Faroes Lava Group can be correlated with basaltic flows within the Faroe–Shetland Basin, where lavas in Well 205/9-1 are interpreted to be of Lower Lava Formation affinity, possibly erupted from a local vent system. Seismic and gravity mapping and modelling suggest that the offshore extension of the Lower Lava Formation, together with the oldest part of the Middle Lava Formation, comprise subaqueous hyaloclastites deposited in a prograding Gilbert-type lava delta system. The youngest part of the Middle Lava Formation and all of the Upper Lava Formation occur as subaerial facies lavas within the basin.

The Faroe Islands, located in the NE Atlantic Ocean approximately midway between NW Europe and Iceland, comprise a remnant of the originally extensive flood basalt lava field which was erupted during the Palaeogene in response to the arrival of the proto-Icelandic Plume and the development of the North Atlantic volcanic rift margin (Fig. 1). After impacting the stretched continental crust below central Greenland during the earliest Paleocene (Danian, *c.* 65–63 Ma), the mantle plume initially caused thermal doming, before breaching lithospheric thin spots with upwelling magma producing surface volcanism and the emplacement of shallow-level sills

From: JOLLEY, D. W. & BELL, B. R. (eds) *The North Atlantic Igneous Province: Stratigraphy, Tectonic, Volcanic and Magmatic Processes*. Geological Society, London, Special Publications, **197**, 253–269. 0305-8719/02/$15.00

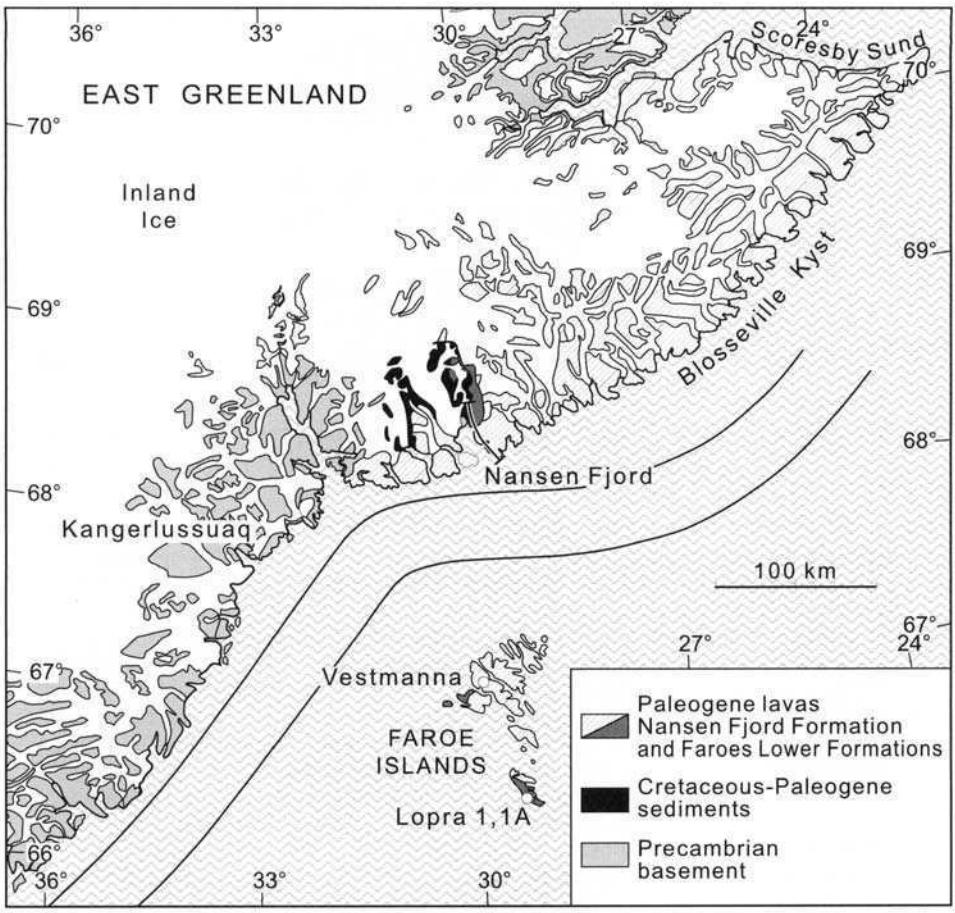

Fig. 1. Palaeogene plate reconstruction (pre-Anomaly 24) for the NE Atlantic, indicating the pre-drift location of the Faroes Block relative to East Greenland (after Larsen *et al.* 1999).

and intrusive complexes (White & McKenzie 1989; Naylor *et al.* 1999). This contribution summarizes the stratigraphy, environments of eruption and biostratigraphic age of the Palaeogene volcanic rocks of the onshore and offshore Faroes Lava Group.

Restoring the North Atlantic to early anomaly 24r time (i.e. before the commencement of ocean floor spreading in the early Ypresian), it is evident that the Faroes Block and associated volcanic rocks have a close association with the flood lava sequence of the Kangerlussuaq–Nansen Fjord area, East Greenland (Larsen *et al.* 1999). It is likely that the separation was less than 100 km, and possibly as little as 60 km. No convincing major feeder systems or vents capable of sourcing the relatively large volume eruptions represented by the Faroes lavas have been recognized on the Faroe Islands and it is concluded that the majority of the fissure eruption sites were close to the heavily intruded Paleocene volcanic sequence in East Greenland.

Volcanic activity culminated with the eruption of the Balder Tuff(s), a thick and extremely widespread sequence of reworked and altered basaltic volcaniclastic deposits sourced from the rift subsequent to plate separation and initiation of sea floor

spreading (Naylor *et al.* 1999). After thermal contraction of the plume (Saunders *et al.* 1997), magmatism was restricted to the active rift. The Faroe–Shetland Basin subsequently underwent significant subsidence during the Eocene.

Geochemical analysis of Faroes lavas indicates predominantly tholeiitic basalt compositions, ranging from magnesian picrites to ferrobasalts (Waagstein 1988). The silica content of the majority of the flows is <48 wt%, indicating they are mantle-derived magmas that did not undergo significant ponding in the crust in substantial magma chambers. A few flows with higher silica values (52–55 wt%) and high initial $^{87}Sr/^{86}Sr$ ratios indicate some interaction (contamination) with crust.

It is possible to clearly distinguish the three main lava formations (defined below) geochemically, in particular on plots of FeO/MgO v. TiO_2/FeO. Lower Lava Formation flows contain relatively low concentrations of titanium, are silica-oversaturated and have distinctive light rare-earth-element (LREE)-enriched compositions, whereas Middle Lava Formation flows are predominantly Mg-rich tholeiites enriched in titanium and the LREE. Towards the top of the Middle Lava Formation and throughout the Upper Lava Formation (with increasing frequency, up sequence) are flows with Mid-Ocean Ridge Basalt (MORB) compositions and thoroughly LREE-depleted signatures.

Stratigraphy of the Faroes Lava Group

The total proven thickness of the volcanic sequence of the Faroes Lava Group is estimated at *c.* 6500–7000 m (Fig. 2), consisting of *c.* 3000 m above sea level, i.e. exposed on the Faroe Islands and covering an area of *c.* 1400 km^2, together with *c.* 3565 m proven in the Lopra-1 and 1A wells (2178 m drilled in 1981 and a further 1387 m drilled in 1996, respectively). All of the lavas are of tholeiitic affinity (Waagstein 1988), indicative of relatively voluminous mantle melting. The majority of the flows exposed on the Faroe Islands (i.e. the uppermost 3000 m) were erupted into a subaerial environment, whereas the section within the Lopra 1 & 1A wells can be subdivided into subaerial facies flows overlying subaqueous facies volcaniclastic deposits. Figure 2 summarizes the distribution and stratigraphic relationships of the main formations of the (onshore) lava pile.

Lower Lava Formation

The Lower Lava Formation (LLF) crops out on the islands of Suduroy, Mykines and Vagar, has an estimated thickness (at outcrop) of at least 900 m, and comprises aphyric, high-volume sheet flows with average thicknesses of *c.* 20 m. A further *c.* 2550 m of LLF flows are interpreted from the Lopra 1/1A stratigraphic test well (see below).

There is very little evidence for any significant topographic relief (palaeohighs) on the LLF lava field during its development: where seen, such features are of the order of a few metres, typically comprising mound-like areas around which subsequent lavas have flowed. Individual lavas up to *c.* 70 m in thickness are noted, for example within the *c.* 500 m thick sequence exposed on Beinisvord on the west coast of south Suduroy. This particular flow may be traced laterally for several kilometres, both along strike and down dip, implying an eruption volume of at least 1 km^3, and perhaps considerably more in that no appreciable thinning of the flow is evident.

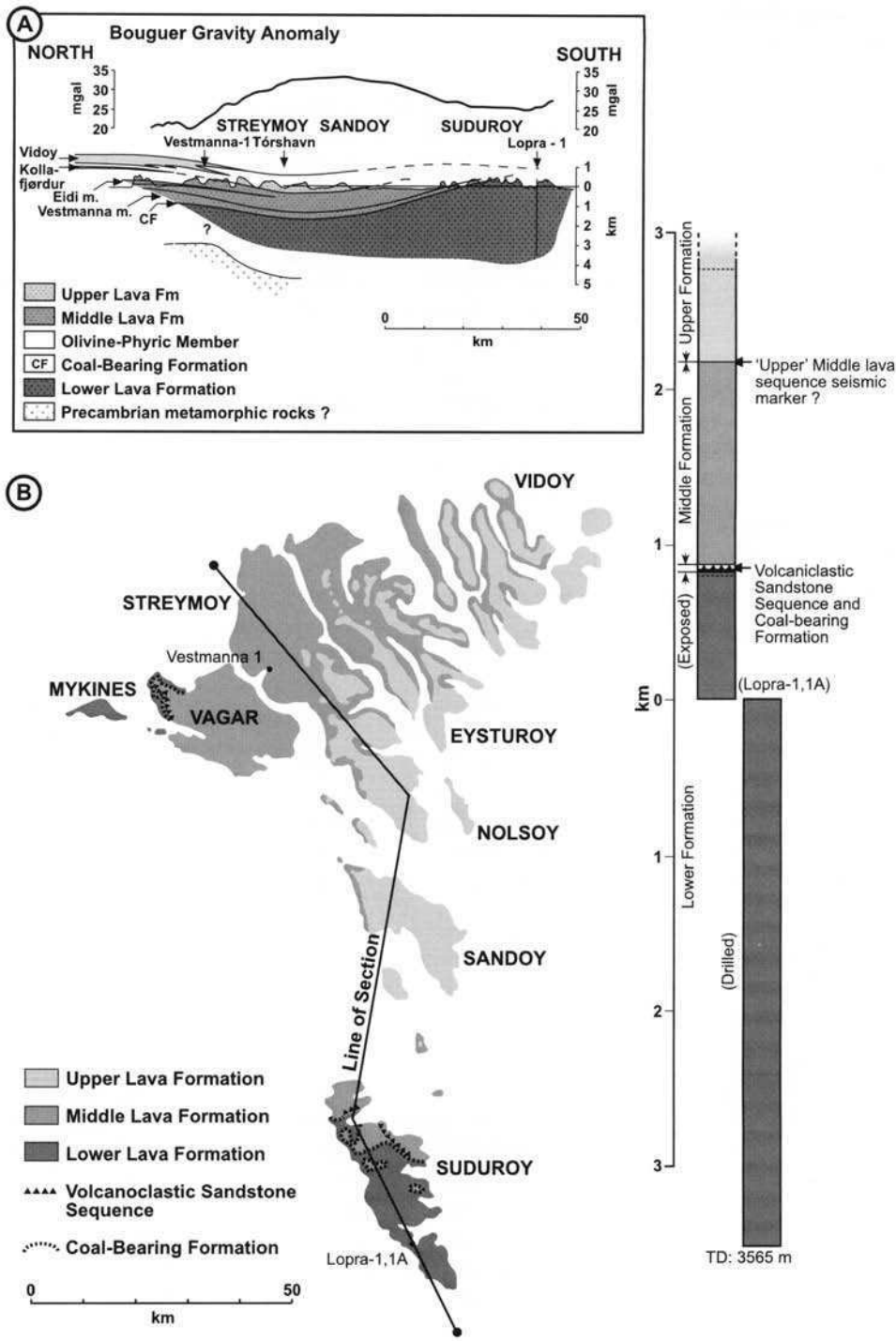

Fig. 2. Geological map, section and stratigraphic column for the Faroes Lava Group (after Waagstein 1988).

Reddened (ferrallitized) tops to flows are relatively common, indicating hiatuses in the volcanic activity during which subaerial weathering and soil formation took place, commonly with the establishment of a forest vegetation. Land surface temperatures in the late Paleocene to early Eocene reached a maximum around the initiation of eruption of the LLF, cooling throughout the remainder of the eruption interval of the lava field. This global warm phase, the Late Paleocene Thermal Maximum (LPTM), initiated a warm temperate climate in the region, resulting in rapid weathering of exposed lava surfaces. In addition to flow-top soil development, there are thin (up to a few tens of centimetres thick), laterally discontinuous coals interbedded with the lavas on the islands of Mykines and Suduroy, implying the existence of small, locally-developed swamps during hiatuses in the volcanism. These coals and associated sediments yield a palynoflora dominated by *Inaperturopollenites hiatus* (swamp cypresses and *Metasequoia*), *Caryapollenites veripites* (Juglandaceae; hickories), *Monocolpopollenites tranquilus* (Ginkgo), and *Momipites* species with occurrences of *Striatricolporites* sp. (Anacardiaceae – cashews & mangos). This flora appears to have been widespread across the NE Atlantic margin at this time and has been recorded as far south as the London–Paris Basin (Jolley *et al.* 2002), enabling us to attribute dates to the LLF of 57.5–60.56 Ma based on isotopic dates in correlative rocks (Jolley *et al.* 2002). The palynofloral assemblage of these coals is typical of swamp and floodplain facies with *Tricolpites hians*-producers occurring along watercourses and the *Caryapollenites* and *Momipites* species as colonizers at the margins of lakes and newly formed swamp areas (Wing & Hickey 1984).

Interlava sedimentation was not restricted to swamp facies. Also preserved are fluvial claystone–siltstone deposits, containing both glassy (now partially palagonitized) basaltic material (shards and rounded fragments) and sand-size grains and pebbles of crystalline basalt, which may be traced laterally for significant distances (typically >1 km). Sediment transport by river systems developed over a gently inclined land surface, with drainage, in general, from west to east. Typically, the lava flows overlying sedimentary deposits have crudely developed prismatic jointing and pillow-like (bulbous) loading and bulldozing/ploughing structures, implying that the these deposits were not fully lithified by the time volcanism recommenced. Towards the top of the LLF, between Kolheyggjur and Frodba on the east side of Suduroy, there are distinctive columnar-jointed lavas with colonnades and entablatures, typical of flows which have been erupted either over a wet substrate or into shallow water.

Lopra Sequence

The Lopra Sequence (LS) is defined from the interpretation of side-wall core (SWC) and ditch-cutting (DC) samples, together with down-well log data and palynological analysis of selected composite ditch cuttings for the Lopra 1/1A wells (see also Hald & Waagstein 1984).

Statoil, with its access to the Lopra 1/1A well samples, has evaluated the following stratigraphy (Fig. 3):

(i) 0 m to 2550 m: low SGR (Spectroscopy Gamma Ray), variable NPHI (Neutron Porosity) and high variable RHOB (bulk density): most likely dominated by subaerial facies lavas. However, palynofloral data from this interval shows that this basal part of the LLF was erupted into an environment with standing freshwater

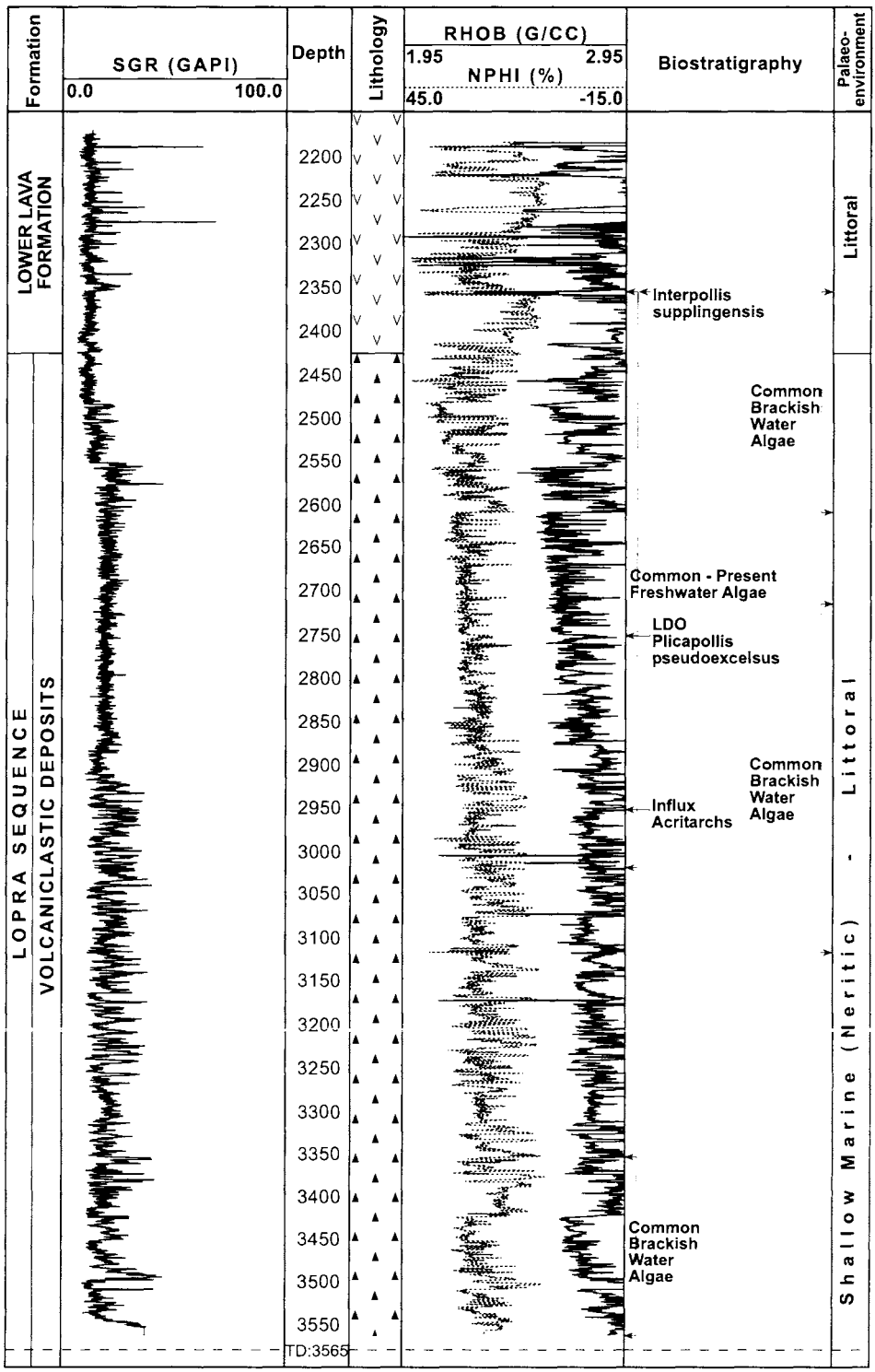

Fig. 3. Log for the Lopra stratigraphic test well, Suduroy, Faroe Islands.

bodies. The sediments from this interval contain common *Botryococcus braunii* and *Leiosphaera* spp. with *Pterospermella* spp. and fragmentary dinocysts which together charaterize freshwater estuaries or marginal lagoons.

(ii) 2550 m to 2900 m: moderate SGR; less variable NPHI; moderate variable RHOB: these volcaniclastic rocks were emplaced into a neritic to estuarine environment, which sourced the same palynoflora as the overlying dominantly lava sequence. These palynofloras provide some age correlative information. The occurrence of *Plicapollis pseudoexcelsus* and *Interpollis supplingensis* are indicative of sediments younger than the uppermost Lamba Formation in the Faroe–Shetland Basin, an age which accords well with the abundance of *Leiosphaera* spp. in these sediments.

(iii) 2900 m to 3565 m: very variable high SGR; moderate variable NPHI; high variable RHOB: a mixture of volcaniclastic rocks and ?invasive lavas/sills emplaced into a neritic to estuarine environment.

One of the main objectives of the oil industry-funded deepening of the Lopra well was to ascertain the nature of the crust below the lava pile. Unfortunately, it was known prior to the well deepening that the depth to 'basement' (i.e. to the base of the volcanic sequence) was most likely in excess of 3500 m below sea level (e.g. Palmason 1965). Based upon the estimated thicknesses of lavas, in particular the LLF, it is likely that the sequence below Lopra on Suduroy is the result of eruption of material into a significant depression in the pre-lava topography, within a Palaeogene sediment trap which existed prior to the volcanic activity.

Coal-bearing Formation

There is a stratigraphical break of uncertain, but possibly short duration between the LLF and the overlying Coal-bearing Formation (CF). This is best evidenced by the shift in 'depocentre' between the two units on Suduroy. In part this may be due to the infilling of palaeogeographical low areas by the ponded lava flows at the top of the LLF.

The Coal-bearing Formation (CF) varies in thickness between 10 m and 20 m and crops out on Suduroy, Vagar and Mykines, comprising two coal beds (the lower up to 1.5 m thick, the upper 30 cm thick), interlayered with carbonaceous claystones, siltstones and cross-bedded sandstone deposits. The detritus within the clastic deposits consists of shards of basaltic glass (palagonitized to varying degrees), together with crystalline basaltic material derived exclusively from the underlying lava pile. The occurrence of *Schizosporis* species (*Spirogyra* cysts) recovered from a spherulitic carbonate deposit indicates that small ephemeral lakes developed on the drainage surface.

The palynoflora of this sequence has been reported by Lund (1988), and is further detailed here. This is the most diverse pollen flora within the Faroes Lava Group, dominated by *Inaperturopollenites hiatus*, *Caryapollenites circulus*, *C. triangulus* and *C. veripites*, with abundant occurrences of *Momipites* species and *Pityosporites* spp. Other taxa represented include common *Sciadopityspollenties serratus* and occurrences of *Phaseoidites stanleyii* and *Montanapollis* spp. This association is seen in offshore wells at the base of Flett Formation F2 (Jolley 1997; Naylor *et al.* 1999). The palynoflora, gross sediment distribution pattern, lithologies and internal structure of the CF indicate deposition in an overbank floodplain environment with extensive peat swamps and small lakes.

Volcaniclastic Sandstone Sequence

This sequence (the VSS), referred to as the Tuff-Agglomerate Zone by Rasmussen & Noe-Nygaard (1970), is a complex assemblage of channelized clastic and volcaniclastic deposits (up to a few tens of metres thick) comprising material ranging from silt grade through to coarse rudaceous accumulations with boulders several tens of centimetres across. It crops out on Suduroy and Vagar in a relatively narrow, NW-trending corridor. In places, the uppermost part of the VSS is strongly reddened (ferrallitized) and is also complicated by the presence of irregular, sill-like intrusions. Locally, primary accumulations of basaltic scoria and spatter are preserved, indicative of local vent sites (Swanson *et al.* 1975). A detailed interpretation of the VSS will be published elsewhere (S. Passey pers. comm.).

Middle Lava Formation

The Middle Lava Formation (MLF) has an estimated thickness of *c.* 1400 m and consists, predominantly, of thin, plagioclase-phyric, compound flow units, with abundant vesicle zones now filled with various (amygdale) minerals. On Vagar, the Vestmanna 1 well (Fig. 1) penetrated *c.* 660 m of MLF flows (Waagstein 1988). Two distinct olivine–phyric members are identified: (a) the *Vestmanna Member* (*c.* 450 m thick) of olivine–phyric basalt lavas, comprising twelve separate flow 'groups'; and, (b) the *Eidi Member* (*c.* 100 m thick) of olivine–phyric basalt lavas, located *c.* 600 m below the top of the MLF.

Within the MLF there are many units that preserve characteristics of inflated pahoehoe flows (Self *et al.* 1996, 1997): sub-horizontal vesicle/amygdale-rich and -poor sheets (all outcrops), pahoehoe tongues and lobes (e.g. at Vidareidi, north Vidoy), and lava tubes (e.g. the sea cliffs of Frodbiarbotnur, east of Tvoroyri, east Suduroy). These low viscosity flows would have been erupted slowly from moderate-sized vents (possibly >100 m across). To date, other than the vent-associated basaltic scoria and spatter within the VSS (see above), the eruption sites of MLF flows have not been recognized.

Red interflow claystone–siltstone and sandstone deposits are thinner than in the LLF, and are concentrated towards the top of the MLF. The frequency of the initially small, but rapid, eruptions does not appear to have allowed the establishment of fluvial systems. However, a change in eruptive style in the upper part of the MLF resulted in localized alluvial channels with sandstone–shale sequences which are commonly rubified. Around Eidi on Eysturoy, these deposits preserve a palynoflora dominated by *Inaperturopollenites hiatus* (*Metasequoia*) with *Retitricolpites* species (a riparian plant?), *Monocolpopollenites tranquilus* (*Ginkgo*) and bryophyte spores (*Stereisporites* spp.). This association is characteristic of floras within fluvial systems cutting through areas of vegetated flow tops. It lacks the characteristic swamp species of the earlier floras of the LLF and CF. No age diagnostic taxa are recorded within this impoverished flora.

Upper Lava Formation

The Upper Lava Formation (ULF) is at least 900 m thick and is composed of thick (on average *c.* 10 m), simple (i.e. non-compound) flows intercalated with thin

crystal- and glass-rich tuffs, together with reddened claystones and volcaniclastic siltstones and sandstones. The thickest sedimentary sequence crops out at Flesin a Hosmol on the west side of Nolsoy, where several metres of reddened claystones and sandstones occur interbedded with thin basalt sheets. The lower 3 m of strata is composed of alternating beds of claystone and coarse sandstones/grits, and is overlain by a brecciated amygdaloidal lava. Above this is a further 6 m of siltstones, with some minor coarse sand- to grit-grade beds at the base. The terrestrial palynoflora recovered from these beds is dominated by *Inaperturopollenites hiatus* (*Taxodium*/*Metasequoia*), and is typical of the flowtop vegetation throughout the lava field. In addition to this material there are occurrences of *Leiosphaeridia* spp, *Pediastrum bifidites* and scolecodonts, all typical of shallow fresh to brackish water in an estuarine and marginal marine setting. These data help to constrain the altitude of the lava field to being at, or near, sea level during this time. Further confirmation of the altitude of the ULF lava field is derived from the thick sedimentary unit at Dalur on Sandoy. Here, at least 5 m of sandy claystones and siltstones contain a similar *I. hiatus*-dominated palynoflora to that seen at Nolsoy. In association with this assemblage are specimens of *Impletosphaeridium densicomatum* and *Spiniferites ramosus* subsp. *ramosus*, both common Palaeogene dinocysts. These taxa again indicate a shallow marine environment, probably more saline than that at Nolsoy. These data, when compared to the ULF palynofloras from Leynavatn on the island of Streymoy, which yield the freshwater algae *Botryococcus braunii*, indicate a low-lying lava field with ephemeral lakes and shallow marine embayments.

Hollow cylindrical structures occur within a few lavas, for example at Kirkja on Fugloy, and at Sundshalsur on Streymoy, and are interpreted as tree moulds. In the latter case, the moulds appear to be of small branches or trunks preserved immediately above weakly cross-laminated fluviatile sandstones and siltstones which have been colonized by vegetation, evident from the common rhizolith structures replaced by heamatite, giving the rock a mottled appearance. Nearby, during roadbuilding, a well preserved specimen of *Metaseqoiua occidentalis* foligae was recovered (Rasmussen 1990), representing what was the dominant taxon on the vegetated flow tops, marginal to the fluvial system.

The ULF flows are predominantly plagioclase-phyric in the central part of the Faroe Islands (e.g. Sandoy). At the base of the Formation, in the NE part of the Faroe Islands, aphyric and olivine-phyric flows are more common and define the Kollafjordur and Vidoy members (Waagstein 1988).

The original thickness of the ULF can only be estimated. On Sandoy and Vidoy, the uppermost flows have vesicles that are devoid of amygdale minerals, which implies that they have not been subjected to substantial burial by a significant thickness of younger lavas (Rasmussen & Noe-Nygaard 1970; Waagstein 1988). Thus, perhaps, only a few hundreds of metres of the ULF have been lost by erosion since Paleocene times. Furthermore, the amygdale mineral assemblages within the lavas of the Lopra 1 well imply that they too have not been buried significantly and, consequently, that the MLF and ULF did not constitute appreciable sequences in the Suduroy (i.e. southern Faroe Islands) area. Thinning of the MLF and ULF towards the south is implied, suggesting that the rate of subsidence was greater further north and that the distribution and thickness of the lava sequences was strongly influenced by the eruption rate of the lavas and by the subsidence history of the entire lava pile.

Interpretation of the offshore volcanic sequence

To date, only one offshore well (205/9-1) within the Faroe–Shetland Basin has penetrated lavas (see below). However, seismic interpretation and isochore mapping of the entire volcanic sequence within the western part of the Faroe–Shetland Basin indicates a general thinning to the SE, away from the Faroe Islands from an offshore interpreted maximum vertical thickness of 2–3 km, to less than 50 m in UK waters (Fig. 4). The offshore seismic sequence is divided into three major units based on interpretations of seismic character and mapping of major bounding surfaces within the sequences, where major progradations are marked by significant onlap surfaces.

The picture is complicated by mapping of two significant volcanic 'thicks' or lobes, one SE of Suduroy, bounded by the Judd and Westray NW-trending transfer zones, and one due east of the Faroe Islands, bounded by the Victory and Clair transfer zones (Figs 4 & 5). These are interpreted to represent the sites of prograding 'Gilbert type' hyaloclastite deltas (Smythe *et al.* 1983; Kiorboe 1999).

Gravity mapping and modelling suggest that the major linear 'reverse' polarity feature immediately NW of the East Faroe High (Fig. 4) represents the limit of progradation of the LLF (which was erupted predominantly during a reversal of the Earth's magnetic field). Loss of this feature to the SW and NE and its coincidence with the interpreted lava delta lobes suggests significant smearing out of the signature, possibly by greater basinward flow.

Palynological data acquired from (onshore) Faroe Islands exposures (see above) indicate that the palaeo-land surface was at a low altitude (sub 300 m) during the final eruptive phases of the ULF, and was relatively flat. Transferring this knowledge offshore, we can flatten the seismic volcanic sequence and demonstrate further major volcanic progradations during late Middle and Upper formations times (Figs 4 & 5). The latter progradation was laterally far-ranging, predominantly involving subaerial facies (MORB-type?) lavas, extending across the Faroe–Shetland Basin (Figs 6 & 7). This is in contrast to the hyaloclastite deposition of the LLF and MLF materials into waters interpreted to vary between 150 m and 500 m in depth (based on interpreted delta foreset heights, Fig. 5).

The Faroe–Shetland Escarpment, which merges into the Victory Transfer Zone, has a distinct seismic character, with a high amplitude top truncating underlying inclined reflectors (Boldreel & Andersen 1994). The latter are interpreted to represent progradational hyaloclastite MLF-equivalent clinoforms (Kiorboe 1999) which are then overlain by subaerial facies MLF? and ULF flows (cf. Smythe *et al.* 1983; Ritchie *et al.* 1999) (Figs 6 & 7).

Well 205/9-1

Hydrocarbon exploration Well 205/9-1 (Figs 5 & 6) penetrates *c.* 70 m thickness of basaltic rocks. Given the relatively poor quality of the seismic data available to tie this well back (towards the NW) into the main offshore (Faroes) volcanic sequence, we prefer to refer to the 205/9-1 lavas as being of Faroes association, with the possibility that they were erupted from a discrete, relatively local vent system.

The palynofloras recovered from immediately beneath and between the lava flows of Well 205/9-1 have a particular diagnostic character that is seen over a wide geographical area. They are dominated by aquatic and aquatic-marginal pollen and spore

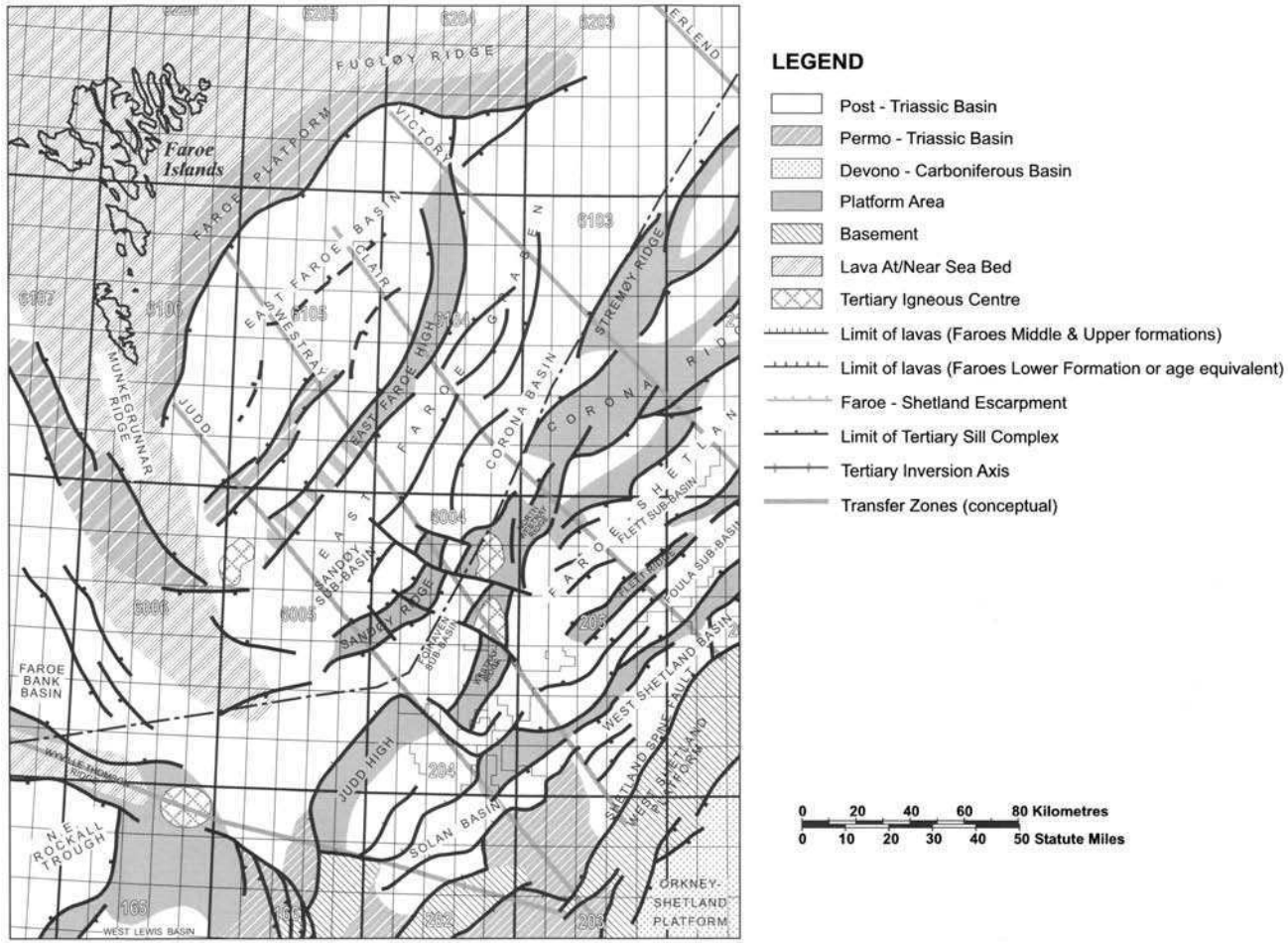

Fig. 4. Offshore geological map indicating pre-Palaeogene geological units, the likely distribution of Lower, Middle and Upper lava formations, the East Faroe High, and transfer zones.

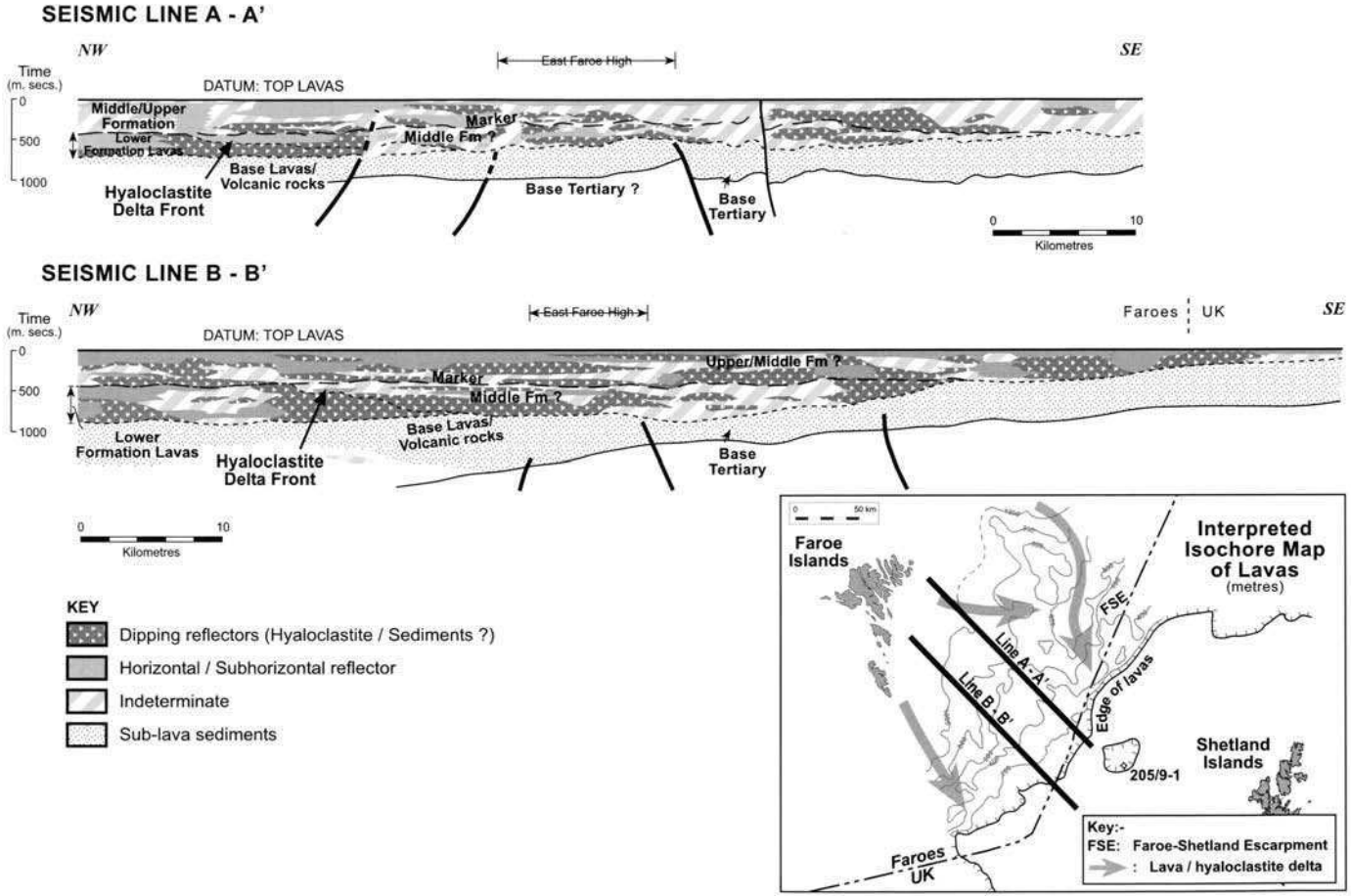

Fig. 5. Seismic interpretation (line drawing) of selected dip lines of the offshore Faroes Lava Group illustrating the nature and distribution of the volcanic sequence. Sections flattened on an assumed horizontal top Upper Lava Formation surface.

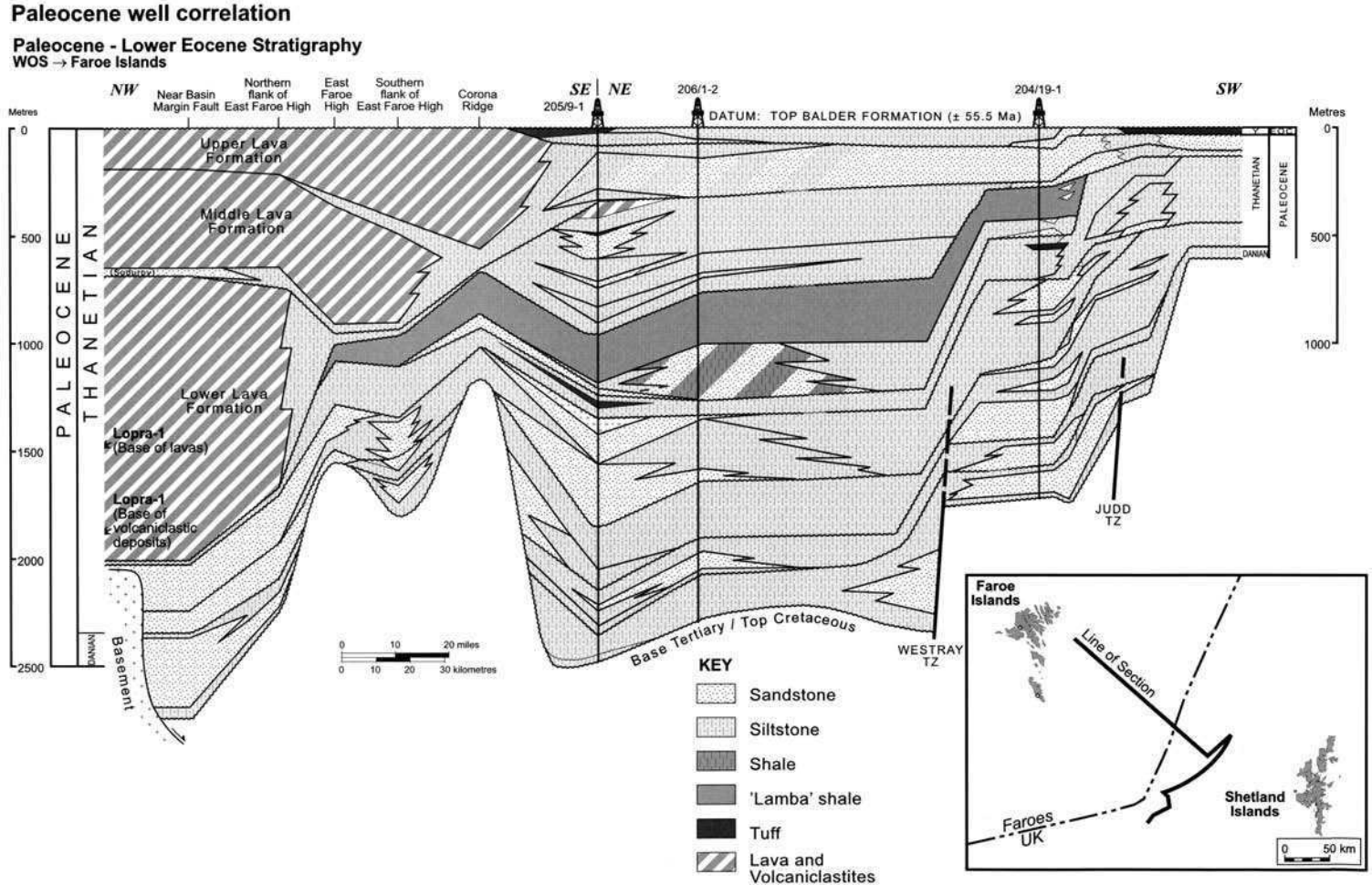

Fig. 6. Proposed correlation from the Faroe Islands, SE into the Faroe–Shetland Basin.

taxa, including *Sparganiaceaepollenites* species (bullrushes) and *Azolla* massulae (floating water fern) occurring with abundant *Carayapollenites veripites* and *Platycaryapollenites platycaryoides* (both associated with primary colonisation of wetlands), common *Intratriporopollenites microreticulatus* (?limes) and frequent *Monocolpopollenites tranquilus* (*Ginkgo*). This aquatic and swamp community is comparable to the assemblages recovered from the LLF coals on Suduroy and Mykines. It is also identical to the assemblages seen in the uppermost basaltic lavas of the Erlend Volcano lava field (Jolley & Bell 2002), and to the palynofloras of the upper Woolwich Formation, and upper Formation de Varengiville of the London–Paris Basin (Ellison *et al.* 1994). This correlation is re-enforced by the presence of common *Apectodinium* species in the uppermost units of the lava interval. These include *A. homomorphum* and *A. augustum*, which are characteristic of strata immediately above Chron 25n in NW Europe, (Ellison *et al.* 1996), and the occurrence of which has been related to migration subsequent to the Late Paleocene Thermal Maximum by Bujak & Brinkhuis (1998).

Summary

The *c.* 3000 m exposed section of the Faroes Lava Group (FLG) on the Faroe Islands (Fig. 2) is divisible into three lava-dominated units, the Lower (LLF, *c.* 700 m), Middle (MLF, *c.* 1400 m) and Upper (ULF, >900 m) lava formations (cf. Rasmussen & Noe-Nygaard 1970). A further 3565 m of volcanic rocks occur in the onshore Lopra 1/1A stratigraphic test well (Fig. 3). Within this well, the uppermost 2550 m of strata are interpreted as the lowermost part of the LLF. The underlying 350 m thick interval, 2550 m–2900 m, is composed of basaltic volcaniclastic rocks, which overlie a 665 m thick sequence (2900 m–3565 m) of interbedded basaltic volcaniclastic rocks and ?invasive lavas/sills. Thus, estimated total thicknesses for the three formations are: Lower: 3250 m; Middle: 1400 m; and, Upper: at least 900 m (top not preserved) (Fig. 2). The age of the FLG has been refined by detailed analysis of the palynoflora of the Coal-bearing Formation (CBF) and intra LLF sedimentary strata, yielding an age range of 57.5–60.56 Ma.

The LLF and ULF comprise subaerial facies, high volume, sheet flows, interbedded with reddened, thin, laterally extensive, fluvial claystone–siltstone deposits composed exclusively of basaltic debris. Ferrallitized tops to flows, indicative of surface oxidation between eruptions, are relatively common. Ephemeral swamps developed in Lower Lava Formation times, as attested by thin, laterally-impersistent coals.

During an hiatus in the volcanism between the LLF and the MLF, the Coal-bearing Formation (CBF) (*c.* 20 m thick) was deposited in an overbank floodplain environment with extensive peat swamps and small lakes. The Volcaniclastic Sandstone Sequence (VSS) post-dates these coal-bearing strata and marks a return to volcanism, predominantly hydroclastic and pyroclastic, before the effusion of MLF flows.

The MLF comprises inflated pahoehoe flows, with well-developed tongues and lobes, together with lava tubes which acted as conduits during construction of this sequence of vesiculated subaerial lavas. Reddened tops are much less common than in the LLF.

The majority of the sequence of rocks below the LLF flows within the Lopra 1/1A well (from 2550 m to the bottom of the well at 3565 m) are interpreted as being of

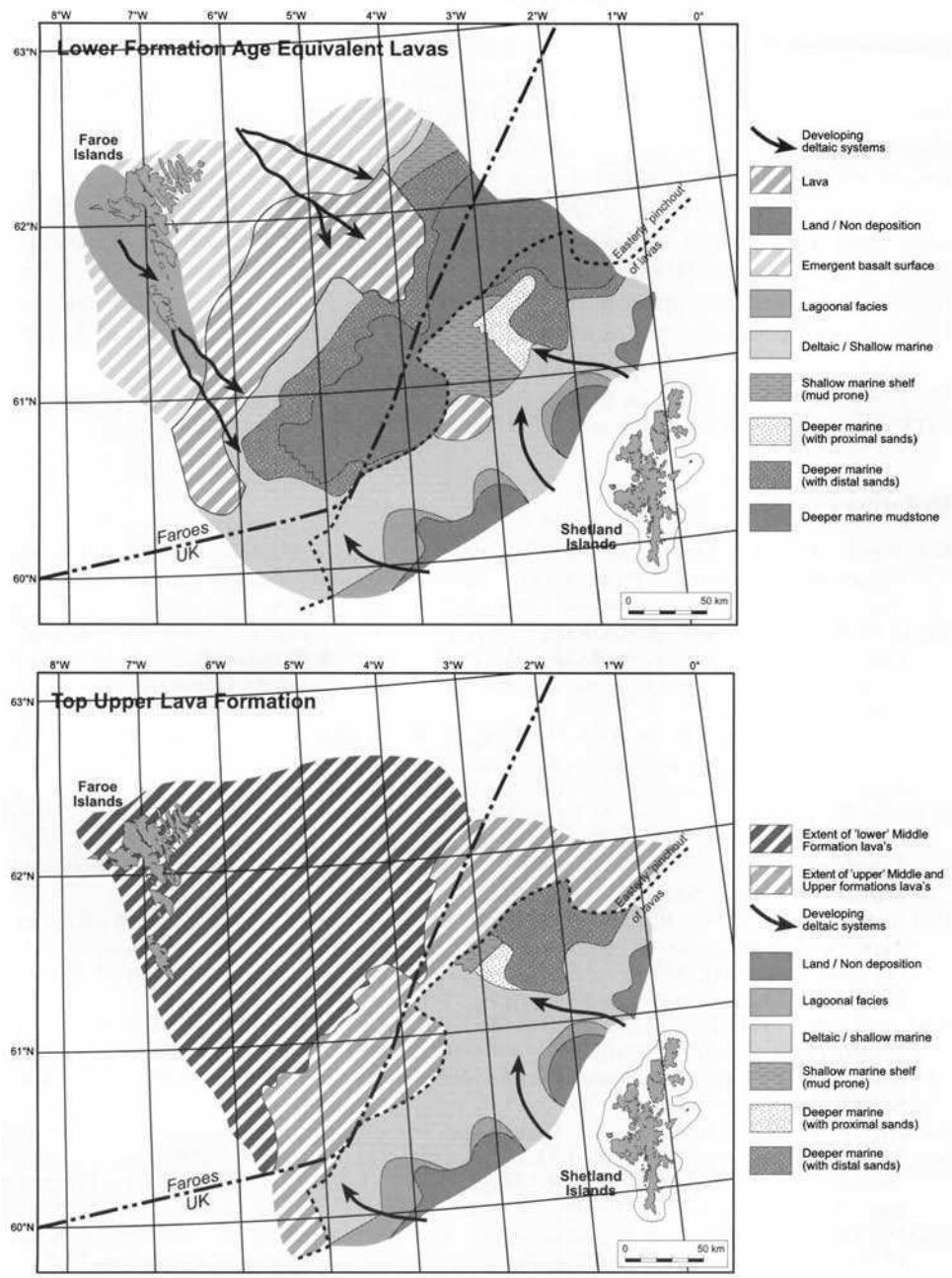

Fig. 7. Palaeogeographic maps for the Faroe–Shetland Basin during Lower and end Upper formation times.

volcaniclastic origin, emplaced into a neritic to estuarine environment. This suggests that the pre-volcanic landscape had a significant topographic relief, possible with a NW-trending structural control parallel to the offshore transfer zones of the Faroe–Shetland Basin (FSB).

Larsen *et al.* (1999) demonstrated a clear correlation between the Faroes Lava Group and the thick lava sequences of East Greenland. We continue this correlation into Faroe–Shetland Basin (Figs 6 & 7) and conclude that the lavas encountered in Well 205/9-1 (Figs 5 & 6) are of Lower Lava Formation affinity, although possibly erupted from a local vent system. Seismic mapping, together with gravity mapping and modelling suggest that the Lower Lava Formation extends into the Faroe–Shetland Basin as subaqueous hyaloclastites, but only as far as the East Faroe High. The lower part of the Middle Lava Formation is also represented by hyaloclastites, which extend SE into the basin, beyond the limit of the Lower Lava Formation hyaloclastites. The upper part of the Middle Lava Formation, together with the Upper Lava Formation, are represented by subaerial facies lavas within the basin.

We thank Statoil Foeroyene a.s, Phillips Petroleum Europe Exploration Ltd., Enterprise Oil Exploration Ltd and Veba Oil & Gas UK Ltd for permission to publish this paper.

References

BOLDREEL, O. & ANDERSEN, M. S. 1993. Late Palaeocene to Miocene compression in the Faroes–Rockall area. *In*: PARKER, J. R. (ed.) *Petroleum Geology of Northwest Europe: Proceedings of the 4th Conference*. Geological Society, London, 1025–1034.

BUJAK, J. & BRINKHUIS, H. 1998. Global warming and dinocyst changes across the Paleocene/Eocene Epoch boundary. *In*: AUBRY, M.-P., LUCAS, S. & BERGGREN, W. A. (eds) *Late Paleocene–Early Eocene Climatic and Biotic Evolution*. Columbia University Press, New York, 277–295.

ELLISON, R. A., KNOX, R. W. O'B., JOLLEY, D. W. & KING, C. 1994. A revision of the lithostratigraphical classification of the early Palaeogene strata of the London Basin and East Anglia. *Proceedings of the Geologists' Association*, **105**, 187–197.

ELLISON, R. A., ALI, J. R., HINE, N. M. & JOLLEY, D. W. 1996. Recognition of chron C25n in the upper Paleocene Upnor Formation of the London Basin. *In*: KNOX, R. W. O'B., CORFIELD, R. & DUNAY, R. E. (eds) *Correlation of the Early Palaeogene in Northwest Europe*. Geological Society, London, Special Publications, **101**, 185–193.

HALD, N. & WAAGSTEIN, R. 1984. Lithology and chemistry of a 2-km sequence of Lower Tertiary tholeiitic lavas drilled on Suduroy, Faroe Islands (Lopra-1). *In*: BERTHELSEN, O., NOE-NYGAARD, A. & RASMUSSEN, J. (eds) *The Deep Drilling Project 1980–1981 in the Faroe Islands*. Foroya Frodskaparfelag, Torshavn, 15–38.

JOLLEY, D. W. 1997. Palaeosurface palynofloras of the Skye lava field and the age of the British Teriary volcanic province. *In*: WIDDOWSON, M. (ed.) *Palaeosurfaces: Recognition, Reconstruction and Palaeoenvironmental Interpretation*. Geological Society, London. Special Publications, **120**, 67–94.

JOLLEY, D. W. & BELL, B. R. 2002. Genesis and age of the Erlend Volcano, NE Atlantic Margin. *In*: JOLLEY, D. W. & BELL, B. R. (eds) *The North Atlantic Igneous Province: Stratigraphy, Tectonic, Volcanic and Magmatic Processes*. Geological Society, London, Special Publications, **197**, 95–109.

JOLLEY, D. W., CLARKE, B. & KELLEY, S. 2002. Evidence for the association between rifting of the North Atlantic and the Late Paleocene Thermal maximum. *Geology*, **30**, 7–10.

KIORBOE, L. 1999. Stratigraphic relationships of the Lower Tertiary of the Faroe Basalt Plateau and the Faroe-Shetland Basin. *In*: FLEET, A. J. & BOLDY, S. A. R. (eds) *Petroleum Geology of Northwest Europe: Proceedings of the 5th Conference*. Geological Society, London, 559–572.

KNOX, R. W. O'B. & HOLLOWAY, S. 1992. *Lithostratigraphic nomenclature of the UK North Sea. 1. Palaeogene of the Central and Northern North Sea*. UKOOA, London, 1–133.

LARSEN, L. M., WAAGSTEIN, R., PEDERSEN, A. K. & STOREY, M. 1999. Trans-Atlantic correlation of the Palaeogene volcanic successions in the Faroe Islands and East Greenland. *Journal of the Geological Society, London*, **156**, 1081–1095.

LUND, J. 1988. A late Paleocene non-marine microflora from interbasaltic coals of the Faroe Islands, North Atlantic. *Bulletin of the Geological Society of Denmark*, **37**, 181–203.

NAYLOR, H. P., BELL, B. R., JOLLEY, D. W., DURNALL, P. & FREDSTED, R. P. 1999. Palaeogene magmatism in the Faroe–Shetland Basin: influences on uplift history and sedimentation. *In*: FLEET, A. J. & BOLDY, S. A. R. (eds) *Petroleum Geology of Northwest Europe: Proceedings of the 5th Conference*. Geological Society, London, 545–558.

PALMASON, G. 1965. Seismic refraction measurements of the basalt lavas of the Faroe Islands. *Tectonophysics*, **2**, 475–482.

RASMUSSEN, J. 1990. *The Origin of the Faroe Islands*. Danmarks Geologiske Undersogelse, Copenhagen.

RASMUSSEN, J. & NOE-NYGAARD, A. 1970. *Geology of the Faroe Islands*. Danmarks Geologiske Undersogelse 1. Serie, **25**.

RITCHIE, J. D., GATLIFF, R. W. & RICHARDS, P. C. 1999. Early Tertiary magmatism in the offshore NW UK margin and surrounds. *In*: FLEET, A. J. & BOLDY, S. A. R. (eds) *Petroleum Geology of Northwest Europe: Proceedings of the 5th Conference*. Geological Society, London, 573–584.

SAUNDERS, A. D., FITTON, J. G., KERR, A. C., NORRY, M. J. & KENT, R. W. 1997. The North Atlantic Igneous Province. *In*: MAHONEY, J. J. & COFFIN, M. L. (eds) *Large Igneous Provinces*. American Geophysical Union, Geophysical Monographs, **100,** 45–93.

SCHRODER, T. 1992. A palynological zonation for the Paleocene of the North Sea Basin. *Journal of Micropalaeontology*, **11**, 113–126.

SELF, S., THORDARSON, T., KESZTHELYI, L., WALKER, G. P. L., HON, K. & MURPHY, M. T. 1996. A new model for the emplacement of Columbia River basalts as large inflated pahoehoe lava flow fields. *Geophysical Research Letters*, **23,** 2689–2692.

SELF, S., THORDARSON, T. & KESZTHELYI, L. 1997. Emplacement of Continental Flood Basalt Lava Flows. *In*: MAHONEY, J. J. & COFFIN, M. L. (eds) *Large Igneous Provinces*. American Geophysical Union, Geophysical Monographs, **100**, 381–410.

SMYTHE, D. K., CHALMERS, J. A., SKUCE, A. G., DOBINSON, A. & MOULD, A. S. 1983. Early opening history of the North Atlantic – I. Structure and Origin of the Faroe–Shetland Escarpment. *Geophysical Journal of the Royal Astronomical Society*, **72,** 373–398.

SWANSON, D. T., WRIGHT, T. & HELZ, R. 1975. Linear vent systems and estimated rates of magma production and eruption of the Yakima basalt on the Columbia Plateau. *American Journal of Science*, **275**, 877–905.

WAAGSTEIN, R. 1988. Structure, composition and age of the Faroe basalt plateau. *In*: MORTON, A. C. & PARSON, L. M. (eds) *Early Tertiary Volcanism and the opening of the NE Atlantic*. Geological Society, London, Special Publications, **39**, 225–238.

WHITE, R. S. & MCKENZIE, D. P. 1989. Magmatism at rift zones: the generation of volcanic continental margins and flood basalts. *Journal of Geophysical Research*, **94**, 7685–7729.

WING, S. L. & HICKEY, L. J. 1984. The *Platycarya* perplex and the evolution of the Juglandaceae. *American Journal of Botany*, **71**, 388–411.

This page intentionally left blank

The properties, morphology and distribution of igneous sills: modelling, borehole data and 3D seismic from the Faroe–Shetland area

JOHN R. SMALLWOOD[1] & JENNY MARESH[2]

[1] *Amerada Hess Ltd., 33 Grosvenor Place, London SW1X 7HY, UK (e-mail: john.smallwood@hess.com)*

[2] *Bullard Laboratories, Madingley Road, Cambridge CB3 0EZ, UK*

Abstract: An extensive suite of igneous sills, collectively known as the Faroe–Shetland Sill Complex, has been intruded into the Cretaceous and Tertiary sedimentary section of the Faroe–Shetland Channel area. These sills have been imaged offshore by three-dimensional (3D) reflection seismic surveys and penetrated by several exploration boreholes. Data from wireline log measurements in these boreholes allow us to characterize the physical properties of the sills and their thermal aureoles. The borehole data has been compiled to produce new empirical relationships between sonic velocity and density, and between compressional and shear sonic velocities within the sills. These relationships are used to assist in calculation of synthetic seismic traces for sills intruded into sedimentary section, in order to calibrate the seismic response of the sills as observed in field data. This paper describes how the seismic amplitude response of the sills can be used to predict sill thickness where there is some nearby well control, and use this technique to estimate the volume of one well-imaged sill penetrated by Well 205/10-2b. Since the sills have a high impedance contrast with their host rocks, they return strong seismic reflections. 3D seismic survey data allow mapping of the morphology of the sills with a high level of confidence, although in some instances disruption of the downgoing seismic wavefield causes the seismic imaging of deeper sills and other structures to be very poor. Examples of sub-circular and dish-shapes sills, and also semi-conical and sheet-like intrusions, which are highly discordant are shown. The introduction of intrusive rocks can play an important role in the subsequent development of the sedimentary system. An example is shown in which differential compaction or soft sediment deformation around and above the sills appears to have controlled deposition of a reservoir quality sand body. The positioning of the sills within sedimentary basins is discussed, by constructing a simple model in which pressure support of magma from a crustal magma chamber provides the hydrostatic head of magma required for intrusion at shallow levels. This model is made semi-quantitative using a simple equation relating rock densities to intrusion depth, calibrated to observations from the Faroe–Shetland area. The model predicts that sills can be intruded at shallower levels in the sedimentary section above basement highs, which agrees with observations detailed in this paper.

The Faroe–Shetland Channel lies between the Shetland Isles and the Faroe Islands, forming a section of the NW European continental margin (Fig. 1). The development of the area has been punctuated by a series of tectonic events including major rifting

From: JOLLEY, D. W. & BELL, B. R. (eds) *The North Atlantic Igneous Province: Stratigraphy, Tectonic, Volcanic and Magmatic Processes*. Geological Society, London, Special Publications, **197**, 271–306. 0305-8719/02/$15.00

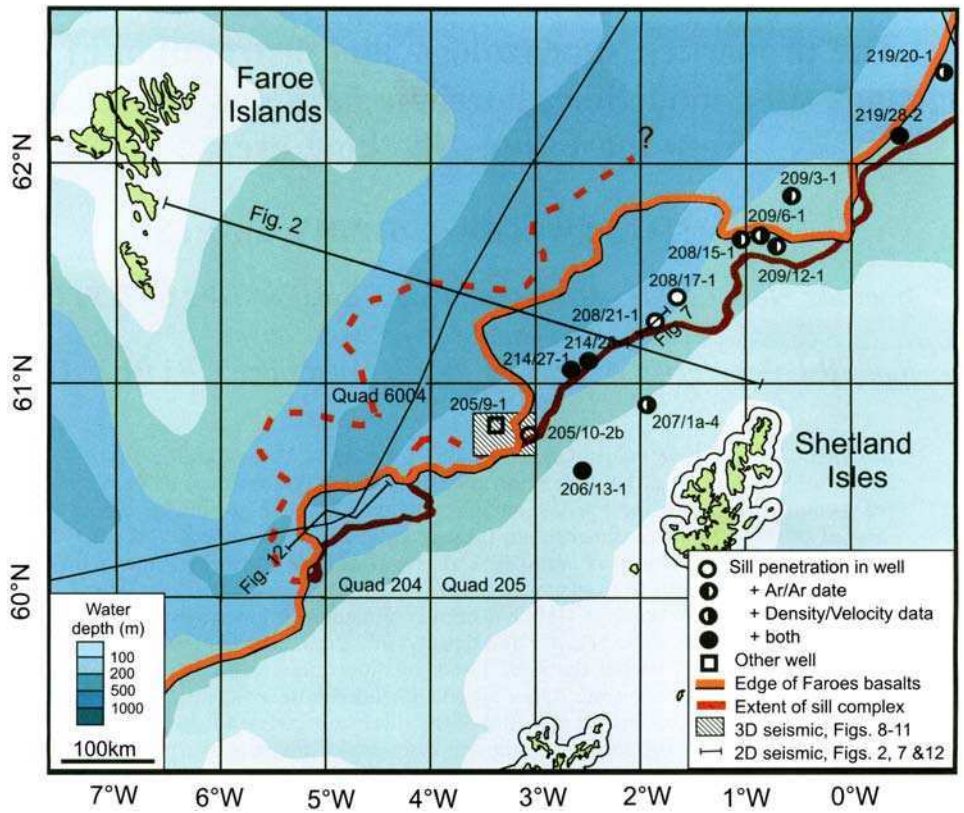

Fig. 1. Faroe–Shetland Channel area with bathymetry shaded. Location of the Faroe–Shetland Sill Complex is outlined in red. The northwestern edge of the sill complex (dashed) is uncertain due to the deterioration of seismic quality beneath the Faroes basalts (outlined in orange). Some well penetrations of sills are marked with circles. Line locations of Figures 2, 7 & 12 shown. Area of 3D seismic in Quad 205 (Fig. 9) is hatched.

during the Permo-Triassic, possibly the Jurassic, the Cretaceous and the Paleocene (Dean *et al.* 1999). Compressional episodes between the late Paleocene and the Miocene have also affected the development of the region (Boldreel & Anderson 1993).

The architecture of the sedimentary basin has been extensively mapped using seismic reflection profiles, and the crust has been probed with seismic refraction and reflection data. The crust beneath the centre of the Faroe–Shetland Channel has been thinned such that the crust-mantle boundary (Moho) lies at less than 20 km depth (Fig. 2) (Bott & Smith 1984; Richardson *et al.* 1999).

The development of the Faroe–Shetland Channel has been strongly influenced by the magmatic events of the North Atlantic Tertiary Igneous Province. The extrusive magmatism which commenced around 61 Ma includes the 'lava pile' of flood basalts, which cover the Faroe Islands and an extensive area of the region now beneath the Faroe–Shetland Channel (Figs 1 & 2). The flood basalts, created at the time of break-up between the Faroe Islands and east Greenland, extend over 250 000 km^2 (Waagstein 1988, L. M. Larsen *et al.* 1999), at least 40 000 km^2 of which lie in the Faroe–Shetland Channel area (Naylor *et al.* 1999).

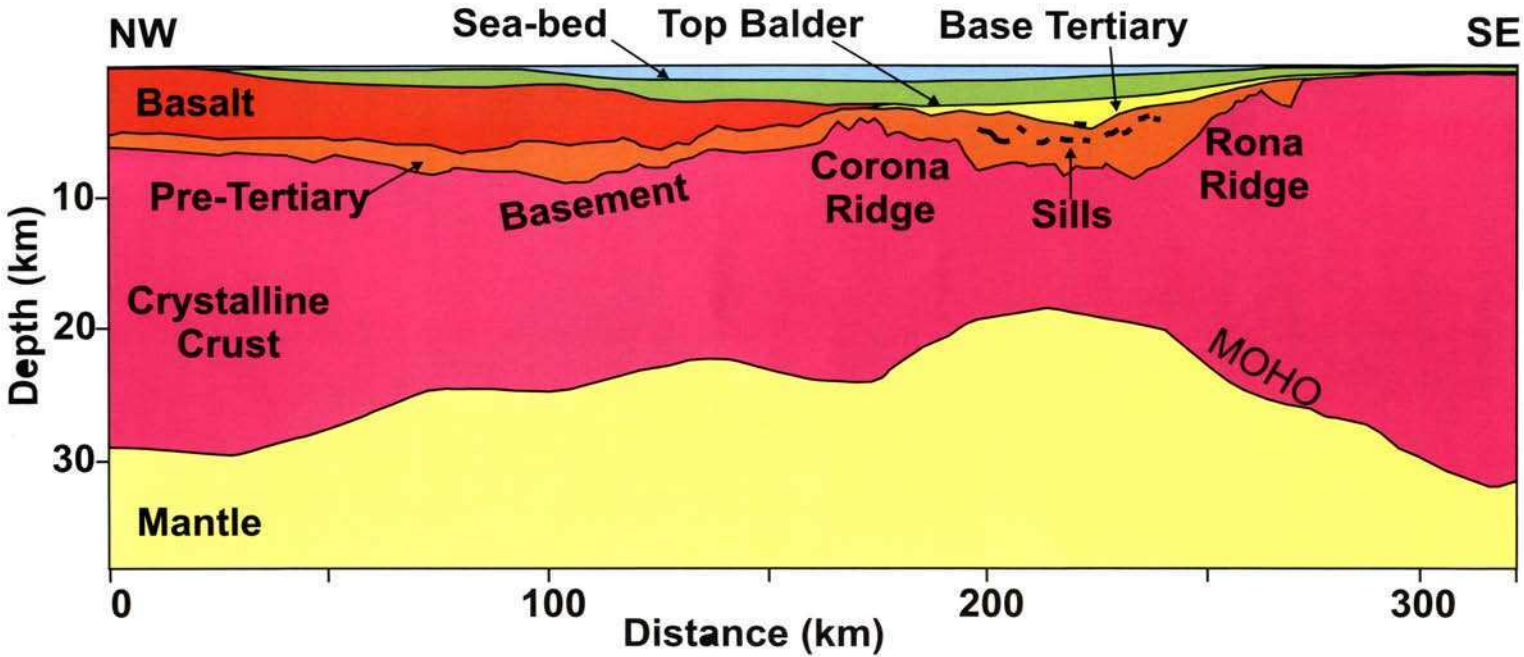

Fig. 2. Cross-section of the Faroe–Shetland Channel (see Fig. 1 for profile location). Profile is based on the British Institutions Reflection Profiling Syndicate (BIRPS) deep seismic reflection line 'FAST' (Faroes and Shetlands Transect) and potential field modelling (Smallwood *et al.* 2001). The Faroe–Shetland Sill Complex is located in the section of the basin with the most highly attenuated crustal section.

The Faroe–Shetland area is also characterized by an extensive suite of intrusive igneous rocks, both central igneous complexes and small-scale bodies (Naylor *et al.* 1999). In this paper the properties, morphology and distribution of the areally extensive intrusive igneous sills in the Faroe–Shetland Channel area are discussed. In the central part of the Faroe–Shetland Channel, the uppermost sills lie mainly within the Mesozoic section, although a few lie within the lowest part of the Paleocene (Fig. 2). In Quads 6004 and 204 in the southern part of the Faroe–Shetland Channel area, however, the uppermost sills are more commonly in the Lower Paleocene section (Lamers & Carmichael 1999). The age of the host rocks to the intrusions places a stratigraphic maximum age on the sill intrusion, since by definition sills are introduced into existing section.

Gibb & Kanaris-Sotiriou (1988) referred to the sills collectively as the 'Faroe–Shetland Sill Complex', and used data from earlier workers' 2D seismic mapping to delineate the SE edge of the main complex, although some sills lie outside this boundary (Fig. 1). Several boreholes or wells have penetrated igneous sills in the UK West of Shetland hydrocarbon exploration area (Fig. 1). Work on samples from several of these sill borehole penetrations has defined the petrology and geochemistry of the sills (Gibb & Kanaris-Sotiriou 1988). Petrographically, the sills are dolerites or olivine dolerites, with modal mineralogy indicating that they are olivine tholeiites. In major and trace element chemistry the sills are significantly different to the Lower and Middle Formation lavas of the Faroes (Waagstein 1988) but they closely resemble the Faroes Upper Formation lavas. The light rare earth elements are not strongly depleted in the sills, causing them to be classified as 'T-type' Mid Ocean Ridge Basalt (MORB), transitional between normal 'N-type' and enriched (plume) 'E-type' MORB.

Radiometric dating has been undertaken on several samples of the sills. Figure 3 summarizes the most reliable ages quoted by Ritchie & Hitchen (1996). Although radiometric dates range from 63.5 Ma (early Paleocene) to 48 Ma (late Eocene) (Hitchen & Ritchie 1993), most of the reliable dates cluster around the 55–53 Ma interval (early Eocene). The late Cretaceous sills in Well 219/28-2 are chemically distinct from the Tertiary sills in the same well, and so are considered to represent a separate phase of igneous activity in the basin (Gibb & Kanaris-Sotiriou 1988). No radiometric dates have yet been published for the sills in Quads 6004 and 204.

In the first part of this paper, new compilations of data are used to document the physical characteristics of sills where they have been sampled in exploration boreholes. These characteristics are used to calibrate the seismic imaging of sills by providing new relationships between elastic properties, and by constructing synthetic seismograms for a range of sill thicknesses. The synthetic seismogram modelling is used to show how the seismic response of sills can be used to predict sill thickness, where there is some borehole calibration.

In the second part of the paper the observations that can be made from field seismic surveys across the sills in the Faroe–Shetland area are discussed. Gibb & Kanaris-Sotiriou (1988) commented that 'the lateral dimensions of the individual sills are unknown'. The paper aims to address this knowledge gap by use of three-dimensional (3D) seismic data, from which the dimensions and morphology of the sills can be determined. The 3D seismic data give a view of sill size and geometry with coverage and detail that is not normally achievable by surface geological mapping, as the host-rock section is still present and the sills are complete. This paper uses an

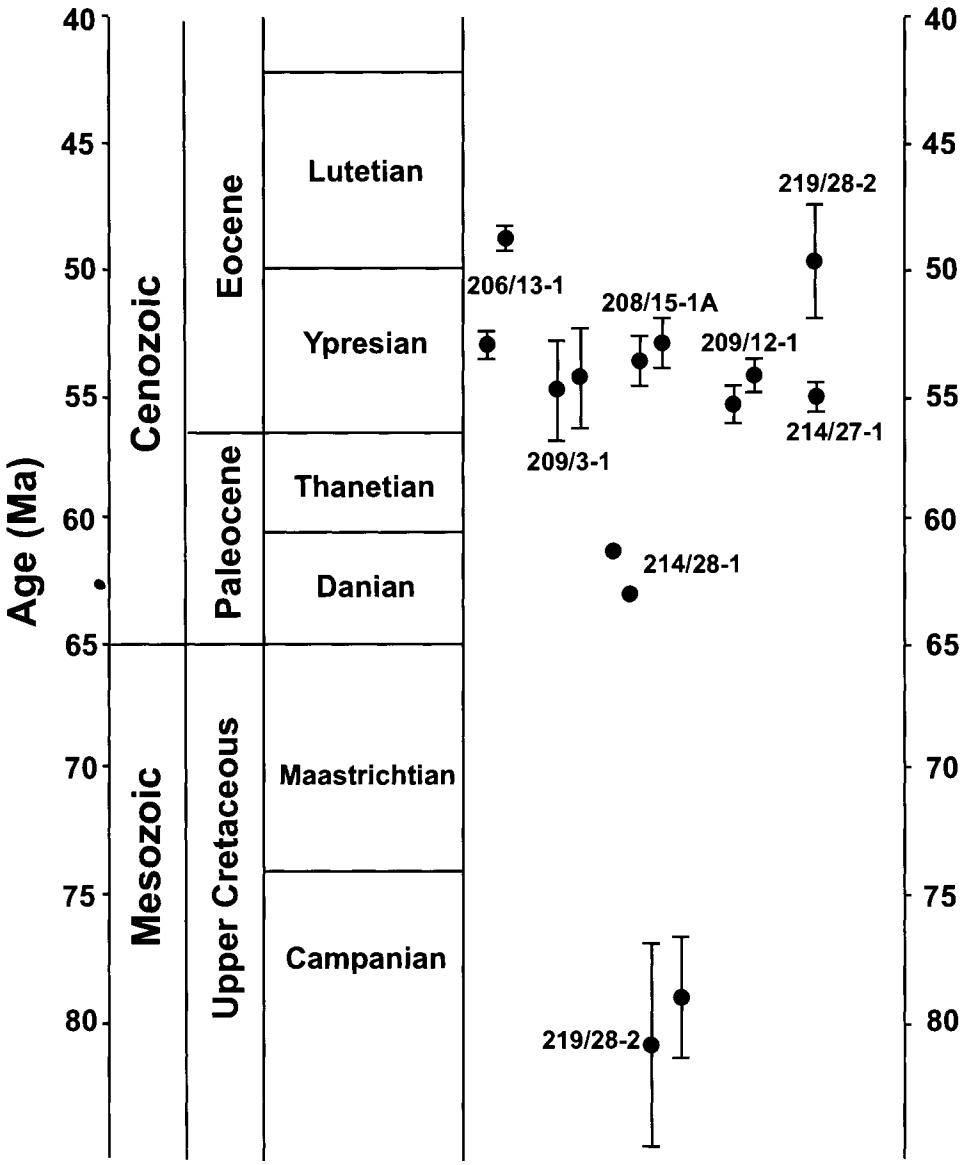

Fig. 3. Summary of reliable sill radiometric dates, from Hitchen & Ritchie (1993) and Ritchie & Hitchen (1996).

example in which sills appear to have controlled the depositional extent of a deep-water gravity flow sand body by inflation of the sea-floor during intrusion.

Thirdly, this new knowledge from the mapping of the sills is used to discuss the distribution of sills within the sedimentary basin setting. In particular, a simple mathematical model is used to discuss the control on the vertical position of the intrusion of sills within the sedimentary section. This model predicts that sills will be intruded at shallower levels above basement highs, which is observed in this area.

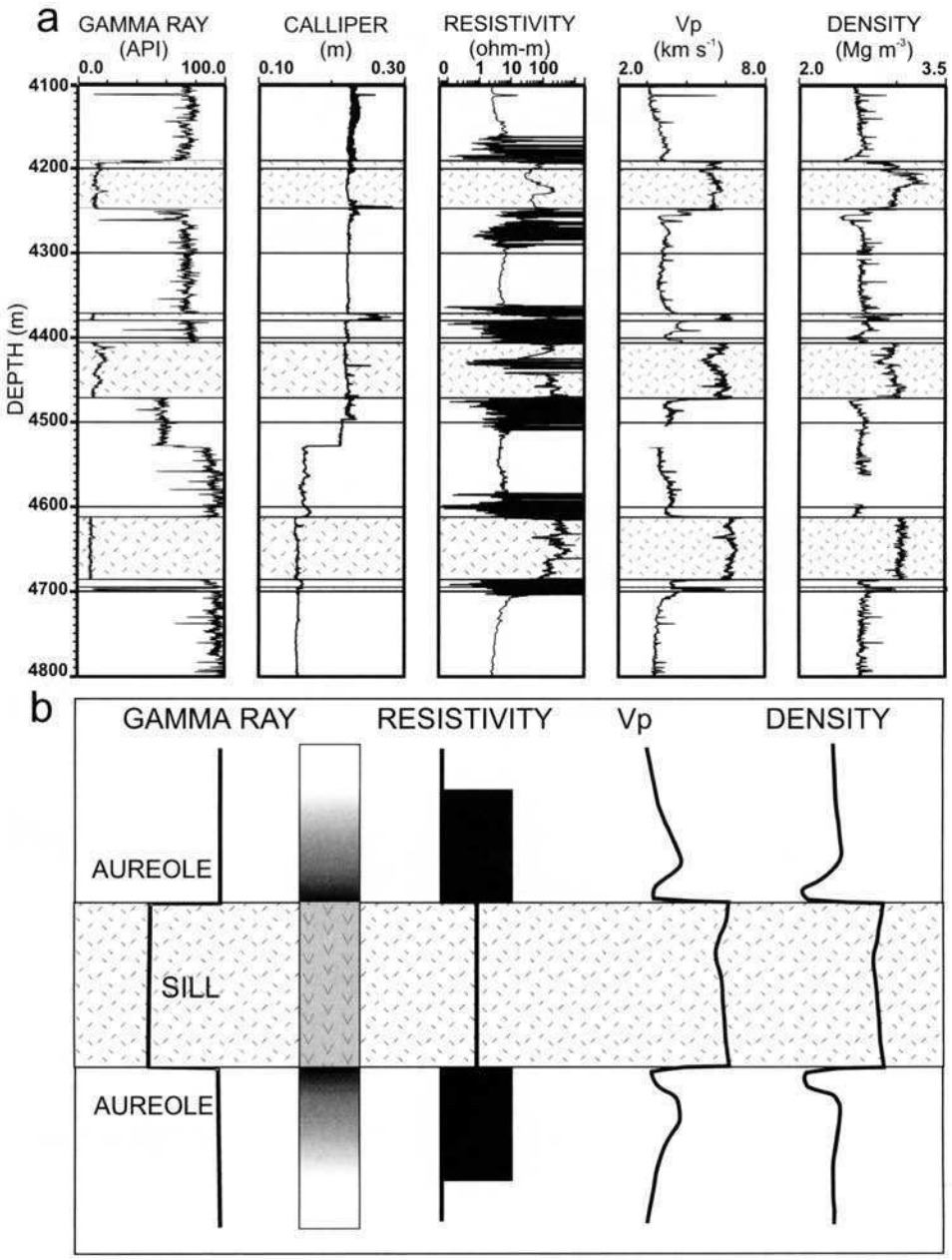

Fig. 4. (**a**) Wireline log response around sills. This example is taken from Well 219/20-1 and shows variations in gamma ray log, caliper log (borehole diameter), resistivity log, sonic velocity (derived from sonic slowness log) and density log through three significant sills each around 60 m thick. (**b**) Schematic summary of log responses.

Physical characteristics of sills: Wireline log response

Rock property measurements are made in exploration wells using tools which return data continuously to the surface as they are suspended from a wire and run down the borehole. The data are often plotted out as a continuous curve against depth in the ground, leading to the term 'wireline logs' for such data (Figs 4–6). The data shown in Figure 4 are examples of the downhole wireline log response of an intruded section of shale, from Well 219/20-1. The section of the well from 4100 m to 4800 m depth penetrated three major doleritic sills, each of around 60 m thickness, and two minor sills which are just resolvable, given the 0.15 m sampling interval of the log data.

Perhaps the most common wireline log, normally used to distinguish between sands and shales, is the natural radioactivity or Gamma Ray (GR) log. Each sill is characterized by an abrupt drop in the Gamma Ray log, reflecting the relatively low proportion of radioactive elements uranium, thorium and potassium in sills compared with that in the surrounding shales.

The caliper tool (Fig. 4) measures the internal diameter of the borehole and is used to indicate hole condition. Normally, soft or friable formations have a tendency to crumble and collapse into the borehole ('washout'), and the caliper log measures a larger borehole diameter than the drilled 'gauge' over such sections. In contrast, the borehole usually maintains its gauge through hard and competent formations. The caliper log in Figure 4 shows that the borehole is in good condition through the three major sills, in both the 0.22 m ($8\frac{1}{2}''$) and 0.15 m (6″) hole sections, above and below 4530 m, respectively. However, the caliper log shows that one of the minor sills, at 4370 m depth, has suffered from significant washouts, with the borehole diameter up from 0.22 m to 0.27 m. Similar washouts have been observed in other sills elsewhere in the Faroe–Shetland Channel, for sills up to 35 m in thickness. It is proposed that in these cases, brittle deformation or cooling fractures in the sill are exploited, and spalling occurs into the borehole.

The sills in Well 219/20-1 have density and compressional sonic velocity (Vp) properties typical of such doleritic intrusions. The density values (2.8–3.1 $Mg\,m^{-3}$) and compressional sonic velocities (5.5–6.5 $km\,s^{-1}$) are high relative not only to the country rock shales in this well, but also to the majority of sediments (Fig. 4). Sonic velocities are not constant through the major sills, but often have a weak tendency to decrease (by 0.1–0.2 $km\,s^{-1}$) from the margins towards the centre. Some sill density logs share this log pattern (e.g. Fig. 6). These changes are attributed to the variation of phenocrysts, vesicles and flow fabrics from the cores of the sills to those of the margins. Francis (1982) noted that most sills of 50 m or more in thickness show similar profiles, in that they often have coarse pegmatite zones one-third the way down from the upper contact. Gibb & Kanaris-Sotiriou (1988) commented, without giving specifics, that internal differentiation was observed in cores of the sills from Wells 219/20-1 and 208/21-1.

During and after intrusion, the host rocks adjacent to igneous sills are subjected to contact metamorphism, both above and below each sill. The thermal aureoles are not seen on the GR log, as any mineralogical changes during metamorphism do not significantly affect the composition of the rock. While intrusions have high electrical resistivity values relative to the background host shales, high electrical resistivities, and large variations in resistivity, are often recorded from the thermal aureole region (Fig. 4). These correspond to the recorded occurrence of mineralization, such as

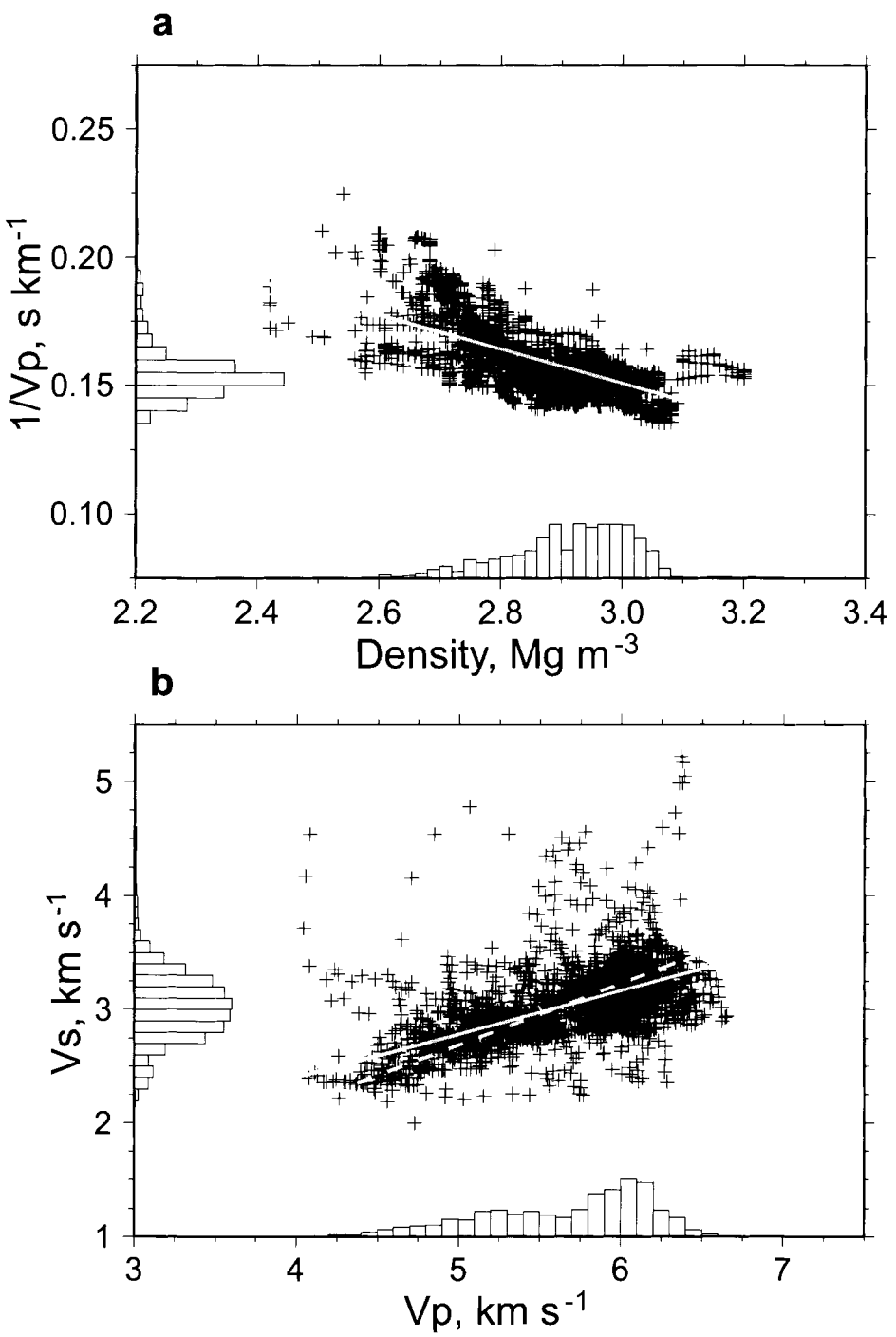

Fig. 5. Compilations of wireline log data for sills. Histograms on the axes show the distribution of data points. (**a**) Compressional sonic velocity and density data (crosses) from well logs over a cumulative 1230 m thickness of sills in the UK West of Shetland area. (**b**) Compressional sonic (V_p) and shear sonic (V_s) velocity data (crosses) from well logs over a cumulative 360 m of sills. The solid line is the best-fit straight line to the data, the dashed line shows the best fit line for a constant V_p/V_s ratio (see text for details).

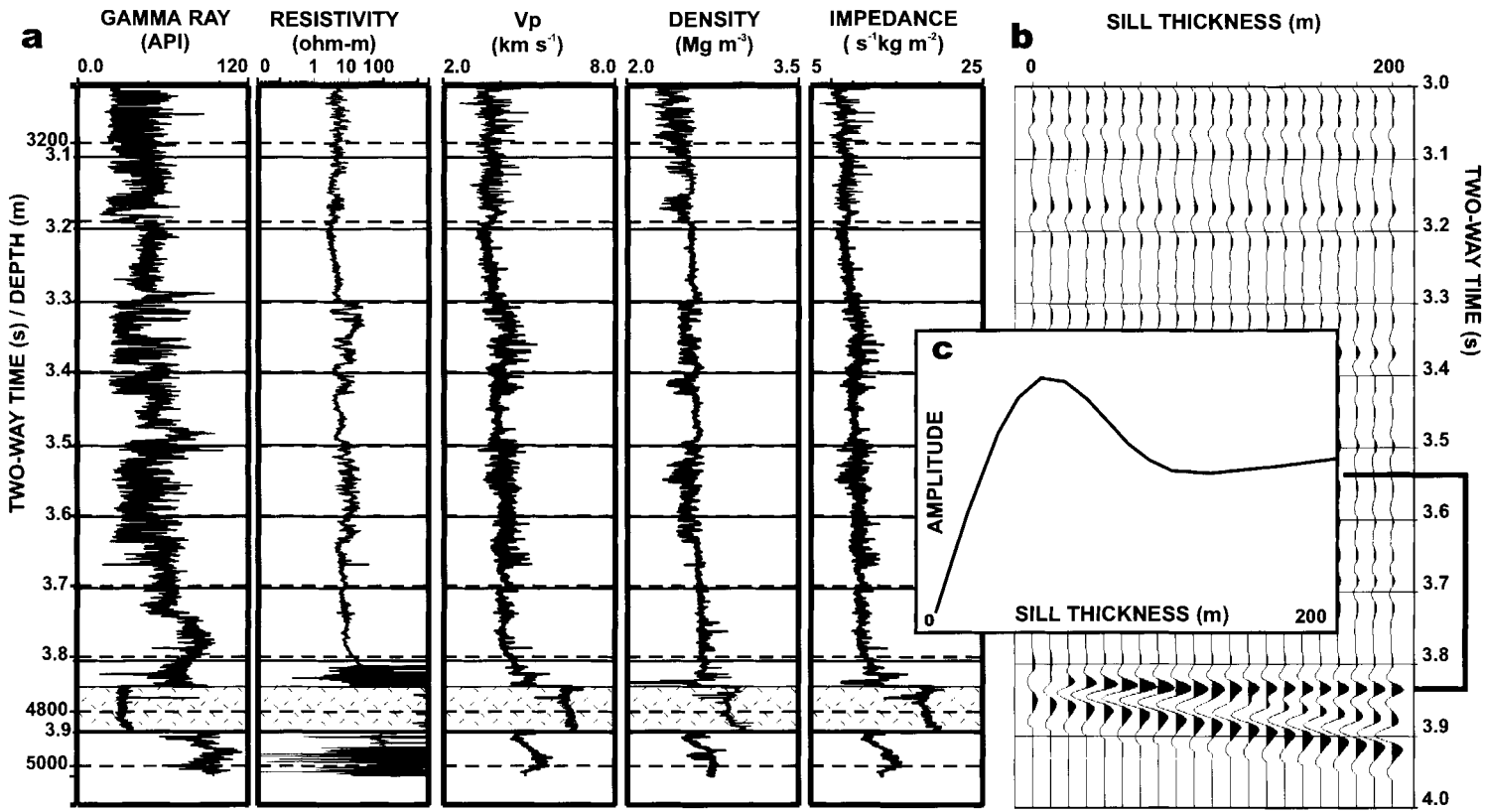

Fig. 6. (**a**) Wireline log suite from Well 214/27-1, which penetrated a 180 m thick sill at depth 4690 m. Solid two-way time lines shown at 0.1 s intervals, dashed depth lines at 200 m intervals, almost conicident with the time lines as the velocity is *c.* 4 km s^{-1}. The gamma ray, sonic velocity, density and resistivity log curves show the same characteristics as those in Figure 3. (**b**) Synthetic seismogram traces for stacked data based on well logs in (a), with a model sill at 4690 m depth having thickness varying from zero (left) to 200 m (right) in thickness. A 26 Hz Ricker wavelet was used. The polarity of the traces shown is such that a positive impedance contrast in the model well log results in a trace excursion to the right (a black peak) in the seismogram. (**c**) Relative seismic amplitude for top sill reflector, showing the tuning maximum amplitude at 60 m thickness.

pyrite, in the hornfels contact metamorphic zones in the wells. Such mineralization can also be observed in the field, for example in the Kangerlussuaq basin of East Greenland (e.g. M. Larsen *et al.* 1999, Locality 3), where several sills are flanked above and below by notable pyrite mineralization.

The compressional sonic velocity, as recorded by the down-borehole tools, increases towards each sill, with the exception of the region adjacent to each sill contact. This immediately adjacent region has a somewhat lower sonic velocity than both the sill and the more distal part of the aureole (Fig. 4b). Planke *et al.* (1999) noted this wireline log response, and attributed it to the presence of fracturing adjacent to the sill. This interpretation is supported by this paper, with the display of complementary density data (Fig. 4), which also show a decrease immediately adjacent to each major sill. For the 60 m thick sills in Well 219/20-1, the distance over which the density and sonic responses are affected by this fracturing is approximately 20 m above and below each sill. The 0.25 $Mg\,m^{-3}$ decrease in density adjacent to the sill at 4185 m (Fig. 4) represents a fracture porosity of 16%. There appear to be slight washouts immediately adjacent to the sill contacts in the shale sections, perhaps caused by disaggregation of these fractured intervals of baked shale. The two thinner sills (Fig. 4, at depths of 4370 m and 4700 m) do not appear to share the characteristic of a local depression in sonic and density responses, perhaps being too thin and fast-cooled to exert a fracture-inducing thermal or hydrothermal circulation influence.

Acoustic and elastic properties of sills

The product of the compressional sonic velocity and density of a material is its acoustic impedance. Since both the density and compressional sonic velocity of sills are high, relative to the majority of sediments, there is generally a large impedance contrast across the interface between each sill and its host rock. This, in turn, means that the sills have a prominent expression on reflection seismic data (Planke *et al.* 1999).

To understand the expression of the sills in seismic data, it is helpful to compare the field seismic data with modelled synthetic seismograms. To compute a normal incidence synthetic seismogram for a sill, velocity and density profiles are required. Compressional sonic velocity and density wireline data has been compiled from a cumulative 1200 m of sill thickness (Fig. 5). Mean compressional sonic sill velocity from these data is $6.50 \pm 0.41\ km\,s^{-1}$ and mean sill density is $2.91 \pm 0.11\ Mg\,m^{-3}$.

It can be helpful to have an empirical relationship between sonic velocity and density, as on occasion only one type of data are available, and an estimate of the other property is required. Such a relationship can be used, for example, when gravity modelling in a basin for which seismic stacking velocities are available, or for estimating impedance values for computation of a normal incidence synthetic seismogram for which only one log type is available. The best-fit straight line through our sill data compilation takes the form

$$\frac{1}{V_p} = -6.25 \times 10^{-2}\rho + 0.3375 \quad (1)$$

where V_p is the compressional sonic velocity in $km\,s^{-1}$ and ρ is the density in $Mg\,m^{-3}$. This relationship is appropriate for a range of density from 2.5 to 3.1 $Mg\,m^{-3}$ or compressional sonic velocities from 4.8 to 7.0 $km\,s^{-1}$.

To extend to a calculation of a full offset synthetic seismogram, which can then be stacked and legitimately compared to stacked seismic data, shear velocity (V_s) values are also required. The shear velocity parameter enables calculation of the variation in seismic reflection coefficients with angle. Shear sonic velocity data are acquired less often than compressional sonic velocity, but the data in Figure 5b are a compilation from a cumulative 360 m of vertical section through forty sills in the region. The best-fit straight line to the data has the form

$$V_s = 0.3818V_p + 0.8727 \quad (1)$$

where V_p is the compressional sonic velocity in $km\,s^{-1}$ and V_s is the shear sonic velocity in $km\,s^{-1}$. This relationship is appropriate for a range of compressional sonic velocities from 4.8 to 7.0 $km\,s^{-1}$. An alternative straight line (Fig. 5b) for the most appropriate single V_p/V_s ratio gives a V_p/V_s of 1.86 ± 0.08, alternatively expressed as a Poisson's ratio of 0.28 ± 0.1.

Shear wave velocity data for sills are scarce in the literature, but published V_p/V_s relationships for similar lithologies include Hamilton (1978) ($V_s = 0.531 + 0.2077V_p + 0.0374V_p^2$, for laboratory-measured mid-ocean ridge basalt specimens), Planke & Cambray (1998) ($V_p/V_s = 1.8 - 2.0$ for wireline-logged flood basalts, SE Greenland) and Smallwood *et al.* (1999) ($V_p/V_s = 1.78 \pm 0.03$, from wide-angle seismic data, mainly flood basalts but also some intrusive rocks, Faroe–Iceland Ridge). The new estimate, given in this paper, shows that sills have a similar Poisson's ratio to extrusive rocks of similar composition.

Modelling seismic reflections from sills

In order to calibrate and understand the seismic response of sills, a series of models have been created to introduce a sill of varying thickness into a sedimentary section. This modelling exercise is used to demonstrate that the seismic response of the sills can be used to predict their thickness, when the thickness of the sill is below approximately 60 m.

The series of 20 models constructed within this paper each include a sill with a thickness varying from 0 to 200 m, substituted into the well logs from Well 214/28-1 at the position of a real sill (4690 m depth, Fig. 6a). For each model, full offset synthetic seismograms were calculated, using the newly determined ratio of $V_p/V_s = 1.86$ for the sill and a 26 Hz Ricker wavelet. The gathers were stacked and are shown as single traces, one for each of the 20 models, there being an increment of 10 m in sill thickness between each stacked seismic trace shown (Fig. 6b). The polarity of the traces shown is such that a positive impedance contrast in the model well log results in a trace excursion to the right (a black peak) in the seismogram.

Where the sill is less than approximately 15 m in thickness, the amplitude of the top sill reflection is comparable to, or smaller than, those of the reflections in the seismogram which originate from sedimentary lithology contrasts. This demonstrates that thin sills will be below seismic resolution, and will not be clear on seismic data. The modelling also demonstrates that with larger sill thicknesses, the sill seismic reflection becomes the dominant event in the seismic data.

Interference between the top and base sill reflections causes the amplitude of the sill reflection to increase linearly up to a thickness of 60 m (Fig. 6c). For larger sill

thicknesses the reflection amplitude stabilizes at a lower value, proportional to the reflection coefficient of a half-space of sill material. The seismic 'tuning' response, that this paper highlights for sills, allows prediction of sill thickness away from a borehole penetration, as the seismic amplitude is proportional to the thickness of the sill up to the point of maximum tuning. As with any seismic tuning response, the thickness at which the maximum amplitude is observed is inversely proportional to the frequency of the seismic data.

Seismic imaging in areas affected by sills: discussion

Seismic imaging of sedimentary basins containing crystalline igneous rocks provides a series of challenges. There are several fundamental effects on the seismic wavefield as it is incident on intrusions, such as reduced energy transmission, intrinsic attenuation, interference effects, refraction and scattering. In addition, some conventional seismic acquisition and processing techniques are not best suited to imaging in these areas.

High reflection coefficients at the top surface of the igneous bodies reduce energy penetration. Multiplying the mean sill sonic velocity of $6.5 \pm 0.4\,\mathrm{km\,s^{-1}}$ and the sill density of $2.9 \pm 0.1\,\mathrm{Mg\,m^{-3}}$ given above suggests a mean sill acoustic impedance of $19\,000 \pm 2000\,\mathrm{Mg\,m^{-2}\,s^{-1}}$. At a depth of 3000 m below sea-bed in the Faroe–Shetland Channel area, the mean shale sonic velocity is $3.3 \pm 0.2\,\mathrm{km\,s^{-1}}$ and the mean shale density is $2.55 \pm 0.05\,\mathrm{Mg\,m^{-3}}$. These values suggest that typical shale acoustic impedance is $8500 \pm 700\,\mathrm{Mg\,m^{-2}\,s^{-1}}$. Together, these impedances combine to give a typical acoustic reflection coefficient of 0.41 for a sill intruded into shale. This is equivalent to a significant reduction (17%) in the energy of transmitted seismic waves at normal incidence. The borehole penetrations of the sill complex commonly include series of vertically stacked sills. Such stacks compound the reduction in seismic energy penetration, which can hinder attempts to image underlying structure, in a similar manner to that observed in sequences of basalt lavas.

While the intrinsic seismic attenuation of basaltic material is estimated to be equivalent to a Q-factor of 100 (Smallwood *et al.* 1998), there may be a higher overall effective attenuation rate within igneous complexes due to scattering and anelastic losses etc. As discussed above, the high impedance of the sills almost always results in a 'hard' seismic response from their top surface. However, certain stacking patterns of sills will cause seismic interference effects which may produce apparent 'soft' events. The production of these misleading events may be exacerbated by the attenuation of the various frequency components of the seismic wavefield as it passes through the sill complex. High velocity basaltic material tends to preferentially absorb the higher frequencies in the incident wavelet (Fliedner & White 2001). There will also be a complex interaction of primary reflections and inter-layer or peg-leg multiples which may be difficult to remove from the data, and these will hinder imaging of underlying structure.

Using the typical velocities given above for sills and shales suggests that seismic refraction will occur along the sills at incident angles of just 31°, within the range of many marine seismic reflection surveys, particularly those with long hydrophone streamers. These refracted events may cause difficulties in processing raw seismic data if appropriate mutes are not applied and refracted energy is included in the final

reflection stack. A further seismic processing effect damaging to imaging nearby to sills is that the indiscriminate application of an automatic gain control (AGC). The AGC operator equalises gain differentially down the seismic trace, with the aim of enhancing weak reflections. This process will reduce the gain on sections of the trace which include very strong events, so weak reflections near a strong sill reflection may become virtually invisible in the final dataset. Sedimentary reflections near sill complexes may therefore be more easily traced on seismic datasets without AGC applied.

The difficulties in processing and the low energy penetration through the sills mean that the quality of seismic reflection data can often be very poor below the uppermost sill reflector. While the uppermost sill in a particular area may be well-imaged, it can be difficult to discern possible underlying intrusive rocks. For example, below the top sills in Well 208/21-1, several more were penetrated, which are not well-imaged on seismic sections (Fig. 7). In such areas, a better estimate of the overall volume of intrusive material may come from potential field modelling. Both Ashcroft *et al.* (1999) and Smallwood *et al.* (2001) included a significant interval of sill-impregnated section in crustal models across the most highly extended part of the basin to satisfy the observed gravity field.

It is also worth noting that conventional seismic reflection acquisition geometries and standard processing techniques are not designed to image vertical or very steep structures, precluding the imaging of vertical feeder dykes that may be present. Similarly, imaging of steep sill limbs is more difficult than the imaging of flat-lying sections of intrusions. It is also sometimes difficult to distinguish between steep sill edges, as mapped in the field, for example in the Jurassic Karoo Province (Chevallier

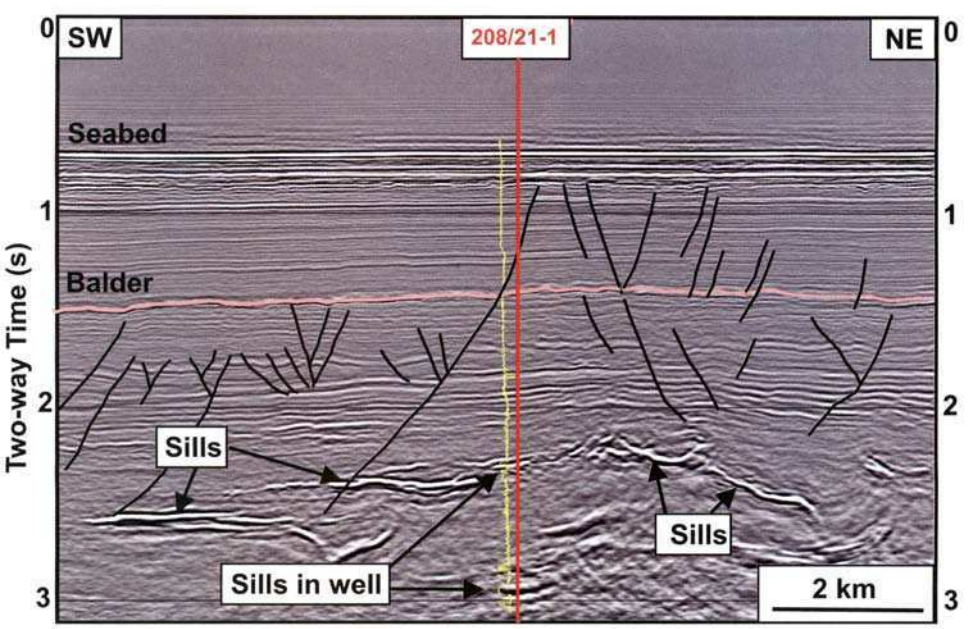

Fig. 7. Example seismic line through Well 208/21-1 location of line shown in Figure 1. The well penetrated several sills (indicated by low GR response log which is displayed adjacent to the well bore). Frequency content and image quality is degraded beneath the uppermost tier of sills.

& Woodford 1999) and migration 'smiles' (e.g. NE end of Fig.7, 2.75 s Two-way time). Diffractions from sills require careful seismic migration if a sharp image of the edges is to be achieved.

It is a tribute to the advances in seismic acquisition and processing technology and expertise over the last decade that, in spite of these unfavourable conditions when attempting to produce images in areas affected by sill intrusion, excellent data can now be obtained in the Faroe–Shetland area (contrast images in this paper with Fig. 2b of Gibb & Kanaris-Sotiriou 1988). This paper is, therefore, able to use recent seismic data to constrain the geometries, vertical and lateral positions of sills within the basin.

Example of sill morphology

To show an example of the use of 3D stacked seismic data in examining sill morphology, one well-imaged sill has been chosen, which has been penetrated by exploration Well 205/10-2b (Figs 8 & 11). The bright seismic reflection, 4 km across and lying at 3 s two-way time (marked 'Sill B' on Fig. 8) corresponds to the depth of 2840 m below sea level (water depth of 447m) at which the well penetrated a 48 m thick dolerite sill within Campanian shales. Unfortunately, attempts to date this sill using radiometric techniques were unsuccessful (Hitchen & Ritchie 1993).

On seismic data the reflection from the sill has a distinct lateral extent, where, as we have shown above, the sill must have a thickness greater than 10–15 m (Fig. 8).

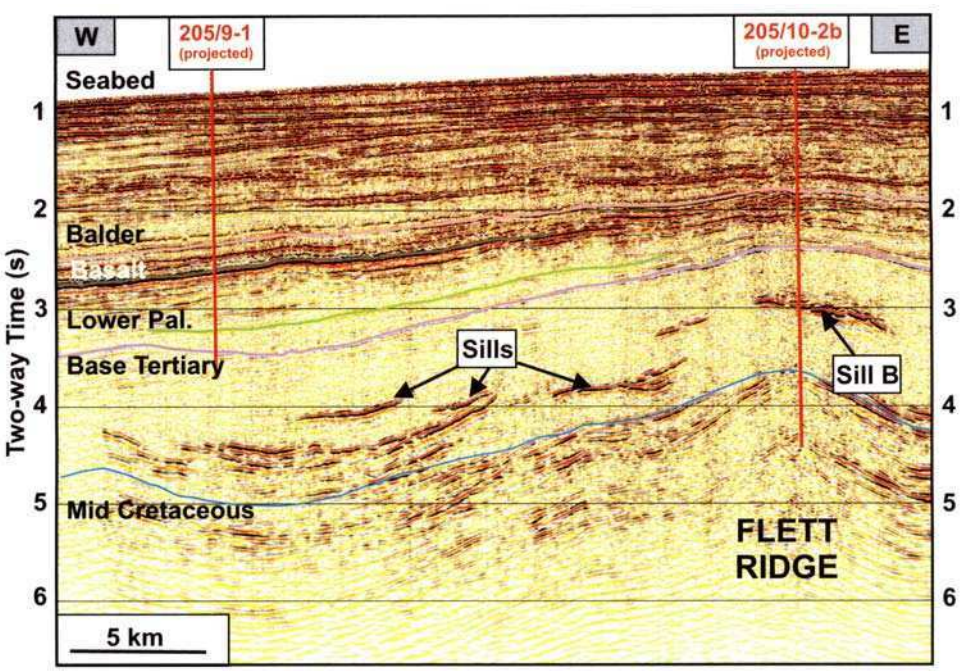

Fig. 8. Seismic line through 'Sill B' in the Flett Ridge area (with location of line shown in Figure 9). Line shows suite of sills over Flett Ridge and in depocentre to the west. Projected borehole traces of wells 205/9-1 and 205/10-2b dashed.

Although impossible to image a possible lateral continuation of the sill below seismic resolution, the sharp cut-off at the edges of the sill suggests that the sill is tabular in form.

Sill B is the shallowest of a small suite of sills, centred in the depocentre to the west of Well 205/10-2b and south of Well 205/9-1 (Figs 8 & 9a). This suite of sills lies below the 'Base Tertiary' seismic marker that is tied into 205/10-2b and other nearby wells (Fig. 8). These sills are mostly of similar dimensions to Sill B (4–5 km across) and are saucer-like in form, with a gentle upward concave shape. Several of the sills are nested, with smaller saucers within the larger underlying ones. From local well control the host rock is thought to be a section of monotonous shales, leaving these sills with little local structural variation to cause complications in their geometry.

The dominant frequencies of the seismic data at the depth of the sill are 20–26 Hz (Fig. 8), and it is impossible to discern separate seismic reflections for the top and the base of the sill, such as those modelled in Figure 5. A seismic pick has been made on the main seismic reflection 'peak' from the top of Sill B and shows three attributes of the seismic pick in Figure 9.

The two-way time structure of Sill B (Fig. 9b) approximates the depth structure since when the water column is included, the overburden has an overall seismic velocity of approximately 2 km s^{-1}. The sill measures 3–4 km in a NE–SW direction and 4 km from NW–SE. Overall present-day dip is to the north, with the shallowest part being a small area to the south of the sill. The areas of steepest dip are the southern corner, where Sill B is at its shallowest, and in the east and west of the sill, towards the lower sides.

The dip map (Fig. 9c) shows the difference in the two-way time to the pick on adjacent seismic traces, and is scaled in ms m^{-1}. This attribute of the sill pick highlights the structural fabric of the sill. The dominant trend of sharp discontinuities in the sill surface is NE–SW, with a subsidiary N–S trend evident in the western part of the sill. The structural offsets of Sill B may be caused by post-intrusion faulting or have been primary offsets in the geometry of the intrusion, such as the fingering described by Pollard *et al.* (1975). While 'steps' may be seen in a sill profile along an outcrop or on a single seismic line (e.g. Fig. 8), the map of Sill B shows that 'throw' across each of the offsets varies along the length of the discontinuity and decreases to zero in each example seen. Thus this sill remains a single, connected intrusive body. From individual seismic sections alone it is difficult to discern whether the sill has been faulted or whether the offset is a primary feature of the intrusion geometry. There is no faulting discernible in the surrounding seismic reflectors (Fig. 8) although this is not unambiguously diagnostic as the immediately surrounding reflectors are rather weak. A three-dimensional view of the sill (Fig. 10) shows, however, that the traces of some of the offsets bend through 90° over a distance of about 1 km. This geometry is unlikely to be associated with a normal fault, and therefore the offset is interpreted to be part of the primary intrusion geometry. However, the relationship between sills and faults is probably best addressed with outcrop studies in which small-scale local intrusion and deformation fabrics can be investigated.

The amplitude of the reflection from the sill (Fig. 9d) shows the strength of returned seismic energy from the sill. The lobate pattern of the reflections from this sill explains the informal name proposed for Sill B: the 'Brain sill'. As discussed above, reflection amplitude will vary with elastic rock properties of the sill and its country-rock host and the sill thickness. Secondary considerations are seismic

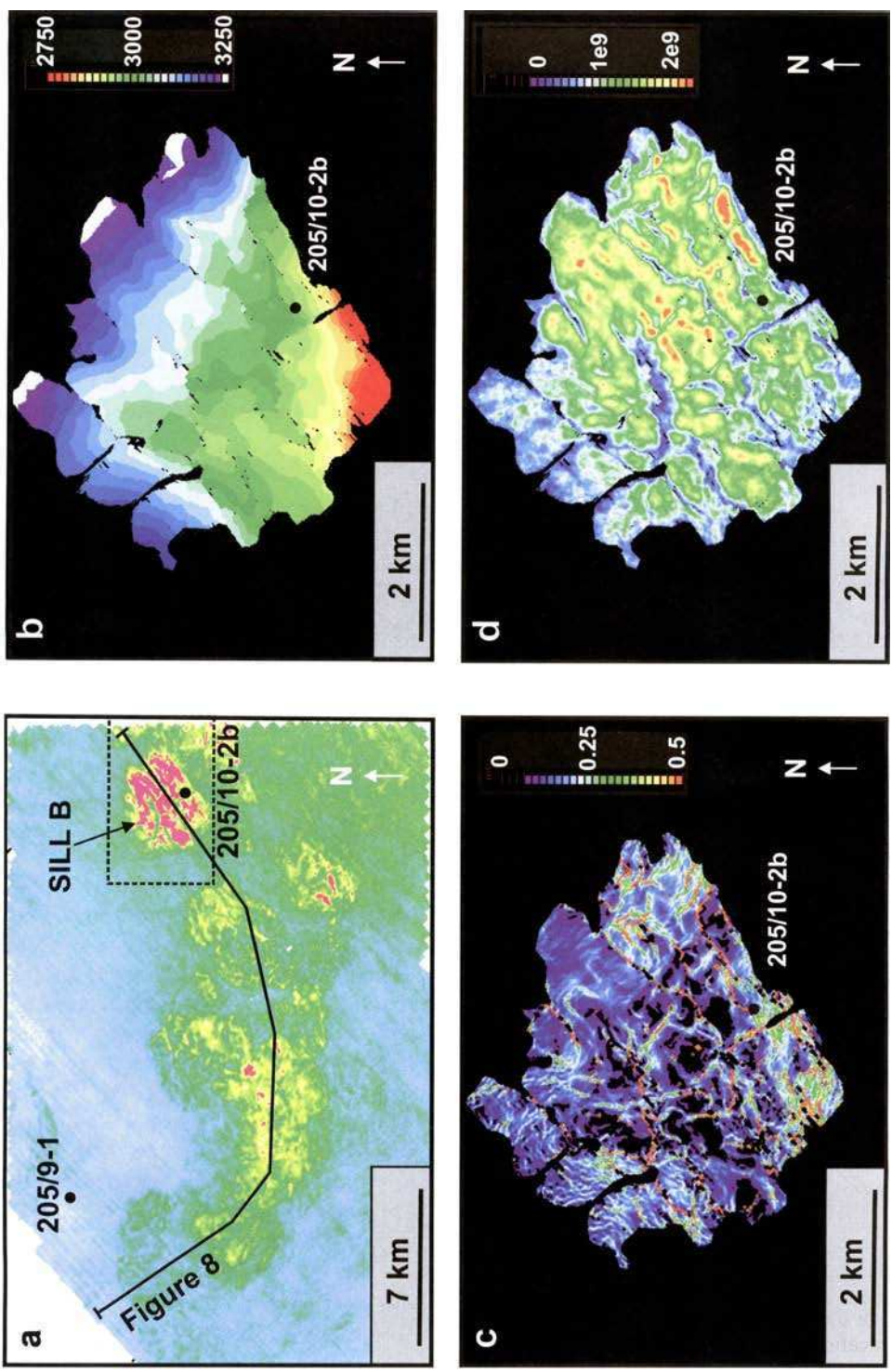
a
205/9-1
SILL B
205/10-2b
Figure 8
N
7 km
b
2750
3000
3250
205/10-2b
N
2 km
c
0
0.25
0.5
205/10-2b
N
2 km
d
0
1e9
2e9
205/10-2b
N
2 km

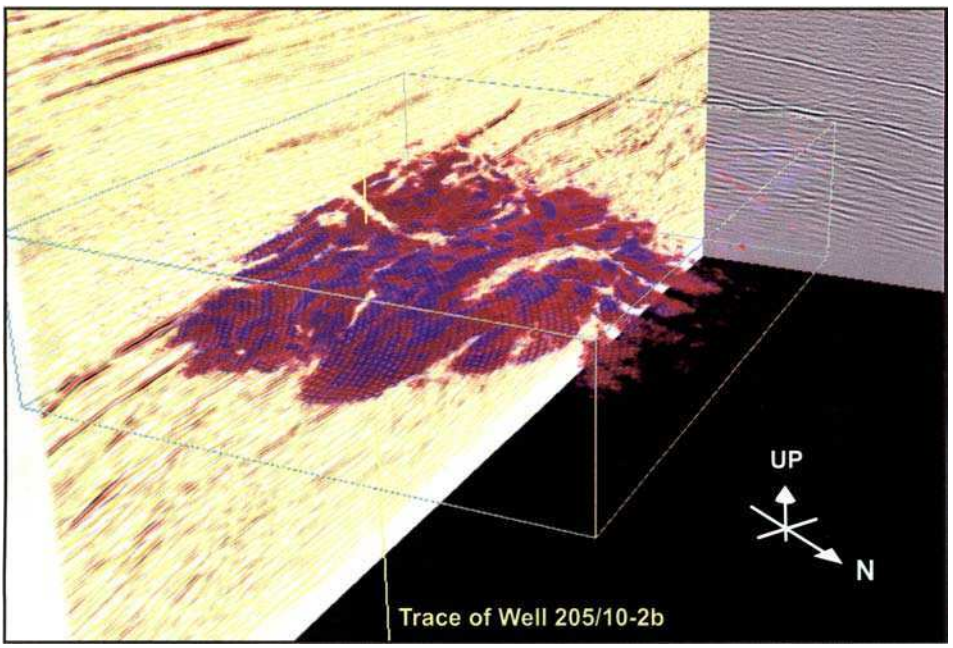

Fig. 10. Example of 3D visualization of Sill B (Figs 8 & 9). The opacity of the seismic volume has been adjusted until only the strongest reflections remain, leaving the sill.

processing effects and possible lateral changes in overburden. Considering the areas where this sill has a relative seismic reflection strength in the stacked data greater than a value of 1×10^9, the area of the sill is $10.0\,km^2$. As shown above, the amplitude of the reflection of the sill is proportional to the thickness of the sill where other factors remain constant and the sill is below the maximum tuning thickness. Using the known thickness of the sill at the well location (48 m) to calibrate the amplitudes, and assuming no lateral lithological variation, gives an estimate of the volume of the sill as $0.45\,km^3$.

The morphology of sills can perhaps be understood most easily by using a combination of the seismic reflection amplitude information and the structural form of the sill visualized in three dimensions on a workstation, where the data can be viewed in any orientation (e.g. Fig. 10). The continuity of the sill reflector can be traced out and the relative magnitude of the structural offsets running across the intrusion can be examined. The NW and SW edges of the sill, and to a lesser extent the NE edge are characterized by a lobate structure on a 500–1000 m scale. It is tentatively suggested that if this sill was sourced from a feeder dyke, such a dyke would be oriented NE–SW, parallel to the structural grain of the intrusion. Such a

Fig. 9. Maps of attributes extracted from 3D seismic data. (**a**) Mean amplitude between Base Tertiary and Mid-Cretaceous reflectors as marked in Figure 8. Brighter (warm) colours show the locations of the sills. Location of area shown in Figure 1. The dashed box shows the location of maps (b), (c) and (d). (**b**) Two-way time to the top sill reflector, in ms. (**c**) Dip of the top sill reflector, in $ms\,m^{-1}$. (**d**) Reflection amplitude from the top sill reflector. Amplitude scale arbitrary.

dyke may have been located towards the southeastern part of the sill, with the intrusion periphery being controlled rather abruptly to the SE (tectonically?) but with magma fingering out into a lobate structure to the northwest.

Although at present day the sill dips mainly to the north and east, at least part of this dip has been imposed by post-intrusion subsidence. Original dip can be approximated by flattening a seismic horizon contemporaneous with the time of intrusion, which brings this sill closer to the horizontal. Ideally, compaction of the sediments should be taken into account, in which case the dip change will be slightly more pronounced as the downdip, deeper sediments are usually more compacted in their present-day positions.

The effect of the sill intrusion on sedimentation

Although the sill intrusion process introduces material beneath the seafloor, it may affect subsequent sedimentary processes operating at the surface. During the early Paleocene, sedimentary deposits were accumulating in a deep-water setting in the area (Lamers & Carmichael 1999). While pelagic fall-out in deep-water areas is insensitive to the topography of the sea-floor, gravity-driven clastic depositional processes are highly sensitive to variations in substrate gradient. A small gradient change can affect the flow regime sufficiently to cause dumping of significant quantities of the load of an incident turbidite flow (e.g. Kneller 1996). Since, as discussed below, the pressure in the intruding sill may be sufficient to overcome the prevailing lithostatic pressure at the depth of intrusion, the creation of accommodation space by the sill may result in localized uplift of the seafloor above the sill. Evidence that sills can create space for themselves by elevating the overlying section is commonly observed in the field (e.g. Macgregor & Macgregor 1936). Seafloor topography so created will act as a submarine obstacle to turbidite flows and contribute to controls on deposition.

Deepwater Lower Paleocene turbiditic sands in Well 205/9-1 have been correlated with a seismic reflector extending 8 km to the south of the well (Fig. 11). The seismic amplitude of the sand reflection has been calibrated with other wells in the locality and the high amplitudes are interpreted to reflect the presence and extent of the sand body. Although the initial impression of the geometry of the amplitude map may be of a sand lobe sourced from the S–SE, the anisotropy of magnetic susceptibility from core samples of the massive sands (Hailwood & Ding 1995) in the well suggests that these sands were sourced from the NW.

The mean amplitude map for the upper Cretaceous interval shows the location of the bright reflectors interpreted to be sills underlying the area (Figs 8 & 11). The complementary geometry of the embayment in the sill complex and the southward oriented sand tongue is suggestive of a genetic link. Slight inflation and topography introduced at the seafloor by the intrusion of the sills may have shaped a depression within which the deepwater sands ponded.

Sill morphologies in three dimensions

While Sill B has a fairly equant aspect ratio in plan view, there is a wide variety of sill morphologies in the region, which is illustrated using sills mapped on 3D seismic data to the north of the Judd High in Quads 204 and 6004 (Figs 12 & 13). The upper parts of these sills lie above the Base Tertiary and within the 'T10' to 'T20' Paleocene

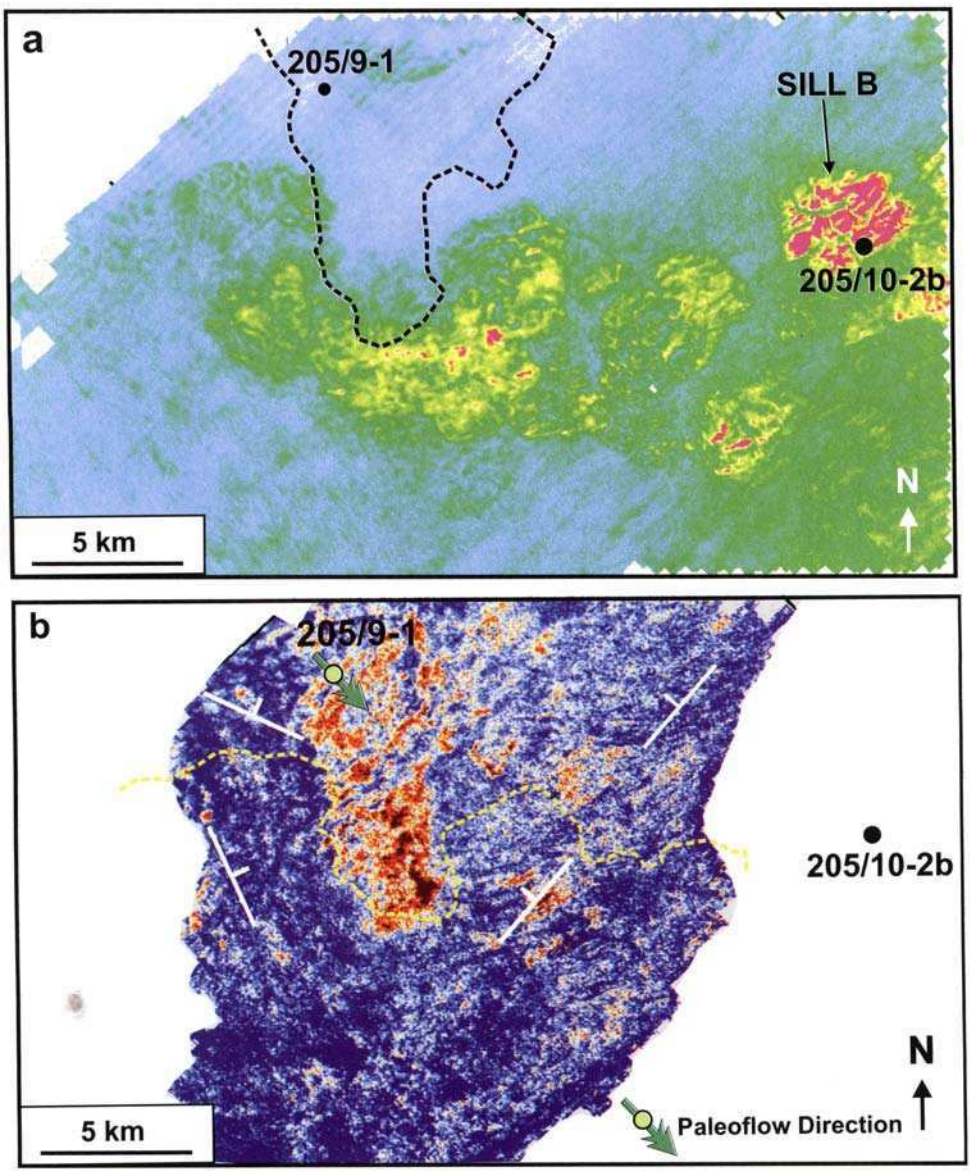

Fig. 11. Maps of attributes extracted from 3D seismic data. Area of maps shown in Figure 1. (**a**) Root mean square amplitude between Base Tertiary and Mid-Cretaceous reflectors as marked in Figure 8. Brighter (warm) colours show the locations of the sills. Location of Wells 205/9 and 205/10-2b marked. Dashed line shows extent of bright amplitudes from a lower Paleocene reflector interpreted to show extent of the turbiditic sand package shown in Figure 11(b). (**b**) Amplitude from a lower Paleocene reflector, calibrated to the 205/9 well and interpreted to show the extent of a turbiditic sand package. Dashed line shows the northern edge of the sill swarm highlighted by the display in Figure 11(a). Dip indicators (white) show shape of basin at lower Paleocene level. The paleoflow direction measured in these sands in the well is indicated with an arrow.

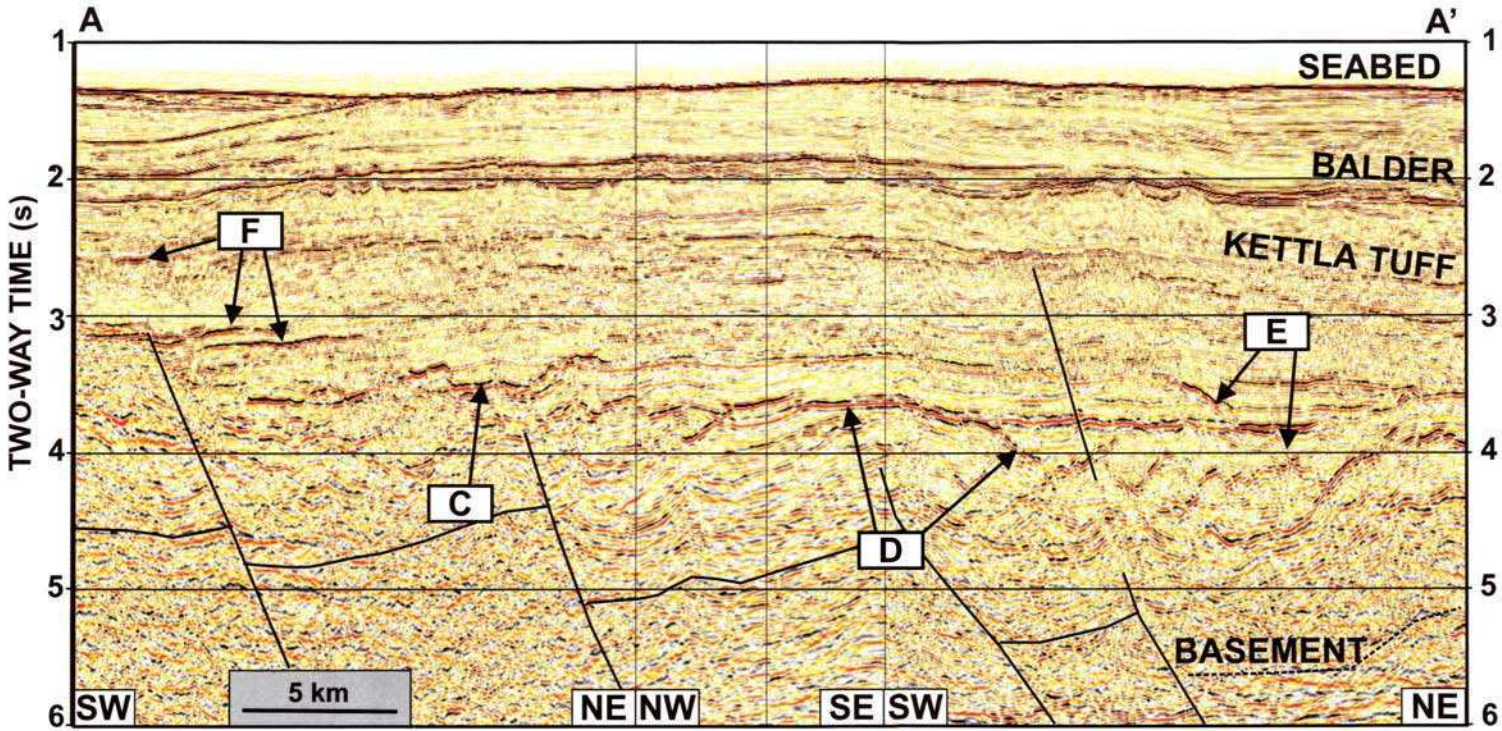

Fig. 12. Seismic line through Sills C, D & E in the Quads 204/6004 area (location of line shown in Figures 1 & 13). Line shows plate-like and trumpet-like sills within Lower Paleocene section. Image quality deteriorates to the southwest under the 'T34' volcanic rocks (marked 'F').

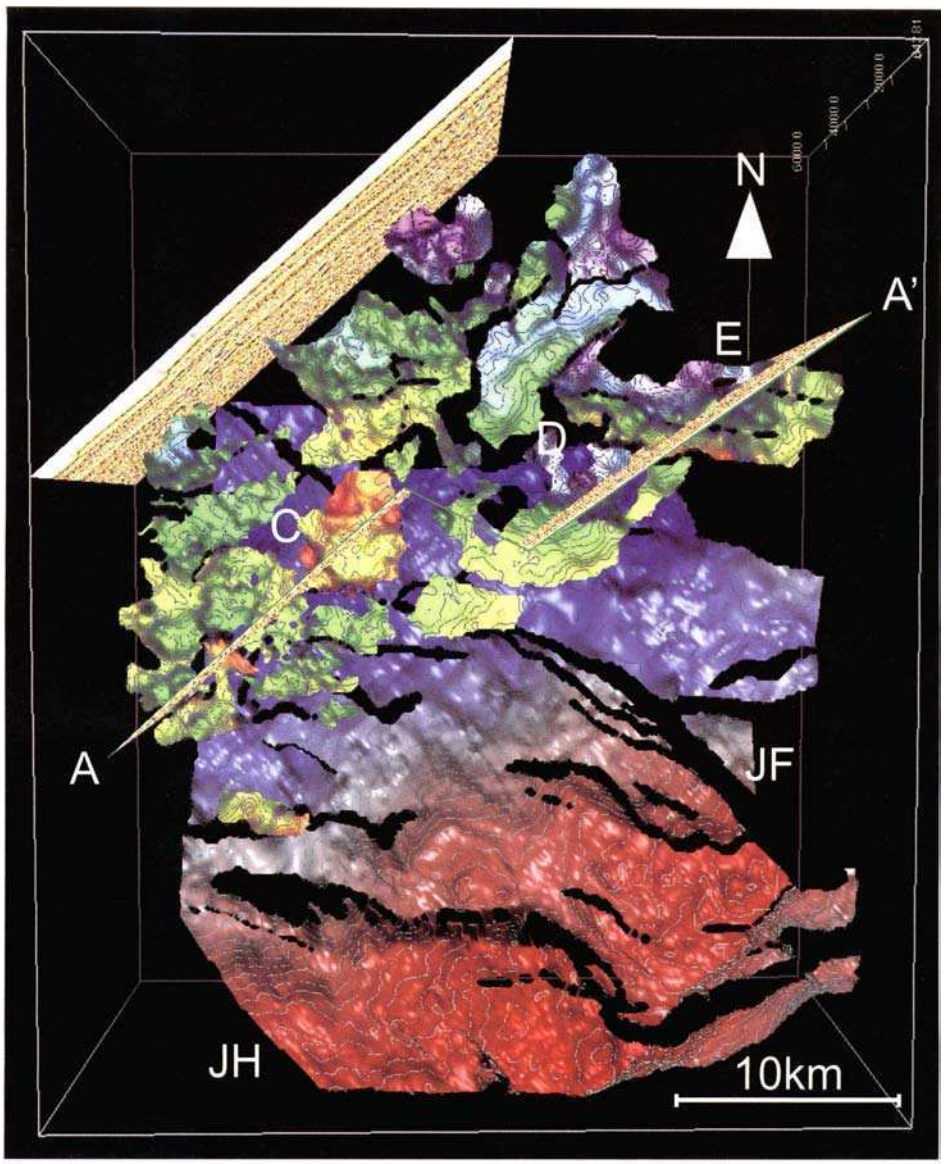

Fig. 13. Three-dimensional visualisation of the sills in the Quads 204/6004 area. The visualisation box extends from 0 s to 6 s two-way time. JH, Judd High; JF, Judd Fault. The basement surface is coloured red (shallow) to blue (deep) and dips to the north. Major faults appear as gaps in the surface. The sills are coloured such that warm colours are shallow and cool colours are deeper. Seismic line A-A′ is shown in Figure 12. Sills C, D and E from Figure 12 are marked.

intervals of Ebdon *et al.* (1995). The seismic event marked 'C' in Figures 12 & 13 is unambiguously caused by an igneous intrusive, as the event cross-cuts pre-existing stratigraphy and has a 'hard' (black) seismic response. This intrusive body, referred to here as Sill C, is approximately circular in plan view (Fig. 13) and has the form of a deep plate with a wide, flat rim. The central bowl of Sill C is 3.3 km across N–S and

5.3 km across E–W, and the rim, 150–200 m above it, generally 0.5 to 1 km across, but the rim extends a distance of 3.5 km to the north. This geometrical structure is similar to the sills mapped in the Karoo Province by Chevallier & Woodford (1999) who argued that this form of sill is usually fed from a ring dyke. Such a dyke cannot be imaged clearly in these data, although the data do show a small disruption in the centre of the floor of the bowl, elongated in a N–S direction, which can be interpreted to be a central feeder point for the sill (Fig. 12).

The interpretation of the deeper structure of the basin shows Sill C, one of the shallowest sills in the basin, overlying a major basement high, where the Judd Fault intersects a major NE/SW fault trend. Sill B (Fig. 8), which overlies the Flett Ridge basement high, is also the shallowest sill in its area. The link between high-level sills and underlying basement highs is an important observation when considering the processes controlling sill intrusion (see later discussions).

To the NE of Sill C, where the basement deepens below approximately 6 km depth, the geometry of the intrusions changes to a form often viewed as a 'V'-shape in section view (Fig. 12). Sill D is one such intrusive body. When mapped out from the 3D data, the sill has a northern section which forms a half-trumpet shape, but the intrusion flattens out to the south, where a more conformable limb covers an area of approximately 50 km^2 (Fig. 13). Sill E, further NE again (Fig. 12), forms a strong cross-cutting geometry in section view and forms a sheet with approximately 1 km of vertical relief in a distance of 5 km, or an average dip angle of about 12°. This sheet dips north for its most part, and includes two major steeper ramps which are not well-imaged due to their steepness (gaps on Fig. 13, Sill E). These ramps run E–W, parallel to an important series of faults that were active in the early Paleocene and dissect the Suilven, Foinaven and Schiehallion oil fields (Lamers & Carmichael 1999). The data are consistent with the sill intrusion in this area being coincident with that dated further north, and it appears that the Paleocene faulting, which largely ceased by 'T36' times (Ebdon *et al.* 1995) has controlled the final geometry of Sill E. Although the sill appears to have exploited the Paleocene faults, it has not followed one single fault plane exclusively, as E–W striking Paleocene fault planes in this area dip north at approximately 45°. The eastern part of sheet intrusion 'D' curves around to dip west, and the overall shape of the intrusive is that of half an ellipsoidal trumpet (Fig. 12).

The seismic imaging deteriorates to the southeast below the 'hard' bright reflectors in the 'T34' (Ebden *et al.* 1995), marked 'F' on Figure 12. These reflectors are interpreted to originate from volcanic sheets, although these sheets are probably older than the sills in this area, as it is assumed that these sills share the earliest Eocene age of those radiometrically dated to the north.

Distribution of the sill complex within the basin

The eastern and southeastern extents of the sill complex are relatively well-known (see citations in Gibb & Kanaris-Sotiriou 1988), but since an extensive area now within the Faroe–Shetland Channel area was covered by flood basalt lavas in the Paleocene, the underlying stratigraphy and any sills within it are increasingly poorly imaged in seismic data to the W and NW. The northwestern limit of the Faroe–Shetland Sill Complex is therefore highly uncertain. This paper proposes the speculative limit to the main part of the sill complex shown in Figure 1. This limit is based

on seismic observations, including long-offset migrations (Fliedner & White 2001), understanding of the location of the early Paleocene rift basins, the overall crustal thinning (Smallwood *et al.* 2001) (Fig. 2), and a mirror image of the southeastern limit with respect to the basin boundaries.

The British Institutions Reflection Profiling Syndicate (BIRPS) deep seismic reflection line 'FAST' (Faroes and Shetlands Transect) profile shows that where the crust has been thinned by the greatest extent (around 200 km on Fig. 2), the crystalline crust has a thickness of approximately 10 km. Crustal thicknesses of 27–32 km are found in the surrounding regions of northern Scotland, the Hebridean shelf, Ireland, the North Sea, Irish Sea and Rockall Bank (Richardson *et al.* 1999, fig 10). Assuming that the original crustal thickness is the average of these, at 30 km, a maximum crustal stretching factor (beta factor) of 3.3 is found under the Faroe–Shetland Channel on the FAST profile. The Faroe–Shetland Sill Complex is located in the region in which the crust has been thinned to the greatest extent. By inference, the location of the sill complex appears to have been focussed into the area with the most major rifting and lithospheric thinning. However, the intrusion of the sill complex (Fig. 3) was not coincident with any known extensional faulting in the Faroe–Shetland Basin. The melt for the sills must therefore have been generated either by the introduction of material with elevated potential temperatures below the litho-sphere, or else have been channelled laterally from the region to the east where continental breakup was approaching completion (Smallwood & White 2002). The tuff-prone earliest Eocene Balder Formation, approximately coeval with the main period of sill intrusion (Ritchie & Hitchen 1996), marks the major period of regional lowstand between the highstands of the Lower Paleocene and the Lower Eocene. This regional lowstand is considered to be due to transient uplift, attributed to dynamic support from the Iceland mantle plume (e.g. Clift *et al.* 1995). The arrival of this abnormally hot asthenospheric mantle, beneath the lithosphere still thinned after Cretaceous and Paleocene rifting, is likely to have provided the melt for the intrusions in the centre of the basin.

Qualitatively, sill intrusion appears to be most intense where the basin is segmented by the NW–SE transfer zones that run perpendicular to the main axis of the Faroe–Shetland Basin (Rumph *et al.* 1993). However, the quantification of the volume of intrusive material and its relationship to the transfer zones requires further investigation, perhaps when the next generation of seismic data allows better resolution of stacked sills.

Modelling of the controls on sill complex distribution

Exhumed basins containing sills are commonly missing the youngest part of their stratigraphy due to erosion following the subaerial exposure of the basin. When sills are mapped in outcrop, therefore, the overburden present at the time of sill intrusion is usually absent. While outcrop data provide some unique opportunities to study sills, an important advantage of using seismic data is that the overburden is much more likely to be preserved. This paper builds on seismic mapping of the sills in the Faroe–Shetland area to discuss the vertical distribution of sills within a sedimentary basin setting. The depth at which the sills are observed within the seismic data is not the same as the depth at which they intruded. Subsequent sedimentation, changes in

water depth and compaction of the overburden mean that the sills are generally deeper now than at the time of intrusion. To determine the original intrusion depth, compensation must be made for this younger section and the compaction of the overburden.

Firstly, two cases are described in which it is possible to estimate the depth of overburden at the time of intrusion, from contemporary volcanic rocks observed in the seismic data, or where sills have been radiometrically dated. This paper then goes on to develop a model that can be applied where neither of these constraints are available, enabling estimation of the thickness of overburden above a sill at the time of its intrusion.

Estimating the depth of sill intrusion

In some areas on the Atlantic margin, there is evidence in the seismic data for the position of the sea-bed at the time of intrusion. For example, if, as tentatively suggested, the sill intrusion shown in Figures 8 & 9 did control the extent of the sand body of Figure 11, then an opportunity arises for an estimate to be made of the depth at which the sills were intruded. From biostratigraphic analysis of Well 205/9-1 and seismic interpretation, the sand body is placed within the Paleocene 'T35' to lower 'T36' sequence of Ebdon *et al.* (1995). Sonic velocities from nearby wells have been used to depth convert the 'T36' and the sill seismic reflection times, and then corrected this section for compaction. By this method, the shallowest sill in the complex, Sill B, over the Flett Ridge, is estimated to have intruded 1000 m below the sea-bed, while the lower sills to the west are estimated to have been 1500–2000 m below sea-bed at the time of intrusion.

In other areas, the sills appear to be associated with concurrent extrusive features. For instance, a truncated volcano or 'guyot' has been mapped at Base Tertiary and coincident Top Balder in block 206/12, with nearby sills present in Upper Cretaceous shales. If it can be demonstrated that such extrusive bodies are contemporaneous with a particular sill, then an estimate of the sill's depth below the seafloor at the time of intrusion can be made using the same technique as used above.

Alternatively, if a reliable radiometric date has been established for a sill, then a depth of intrusion is straightforward to estimate. This estimate can be made by stripping off the sedimentary section that is younger than the intrusion, and then applying a decompaction estimate to the remaining section that was present and overlying the sill at the time of intrusion. For example, the hornfels immediately below the sill at 4045–4225 m below sea-bed in Well 214/27-1 has been dated as 55 ± 0.6 Ma. This age corresponds to the age of deposition of the Balder Formation (Lower Eocene). In the well, the Balder Formation was penetrated at a depth of 1645 m below sea-bed. Subtracting this 1645 m of post-Balder sedimentary section leaves 2400 m of Paleocene sedimentary section in place at present day between the sill and the paleo-sea-bed. Decompaction of this 2400 m Paleocene section, using Sclater & Christie's (1980) method and parameters for shaley sand, suggests a thickness of 2900 m of sediments present above the sill at the time of intrusion. Coals within the Balder Formation are interpreted to indicate near-sea-level conditions within the Upper Balder Formation, therefore the sill was intruded approximately 2900 m below sea level. Although it is not believed that there has been significant

erosion anywhere in the Paleocene section in this area, the method will yield a minimum depth estimate in areas where erosion has taken place.

The methods described above for estimating intrusion depth cannot be used where sills are observed on seismic data but are without local radiometric dating or means of determining contemporary sea-bed position, and an independent method is required. The intrusion of sills is a complex process influenced by many factors such as magma supply, magma density and viscosity, stress regime, host rock lithology and deformation history. However, in order to obtain some insights into the controls on the vertical intrusion level of sills, this paper presents a simplification of the natural system by considering the vertical pressure distribution in a one-dimensional model. Underlying this model are very old ideas cited by Bradley (1965), although in this paper the ideas of the base-crustal magma chamber (White & McKenzie 1989; England 1992), local measurements of the crust (Smallwood *et al.* 2001) and the sill overburden from seismic data are added. This model is then extended into two dimensions to consider the variation in intrusion level across a model sedimentary basin.

A one-dimensional pressure model

One possible starting assumption for a model of sill intrusion would be that the sills intrude at a level of neutral buoyancy. To pursue this approach, densities of intruding magma and host rocks must be known. Estimates of basaltic magma density lie around 2.65 $Mg\,m^{-3}$ (Bradley 1965). This figure might decrease by a few percent with volatile content in the magma, but will increase by as much as 0.1 $Mg\,m^{-3}$ if denser olivine or pyroxene phenocrysts are present. Using exploration well wireline log data, the density values of shales close to sills are examined, but outside their thermal aureoles. These present-day shale densities are, almost universally, lower than the 2.65 $Mg\,m^3$ thought to be representative of a basaltic magma. This observation demonstrates that it is highly unlikely that the sills were intruded at a level of neutral buoyancy, particularly since the shale densities have been increased by compaction since the time of sill intrusion. The sills must require pressure support in order to have capability to intrude the sedimentary section at the levels observed.

A more fruitful approach is to assume that the sill intrusion depth is determined by such a pressure control, with support for the intruding sill from the lithostatic pressure confining a magma chamber supplying the melt (Fig. 14). This approach stems from Holmes (1944), and was discussed by Bradley (1965). A simple pressure balance can be written

$$P_{\text{chamber}} - \rho_{\text{magma}} gh + R = P_{\text{sill}} \tag{2}$$

where P_{chamber} is the pressure in the magma chamber, ρ_{magma} is magma density, g is the gravitational constant, h is the height change between the chamber and the sill (Fig. 14) and P_{sill} is the pressure in the sill. The ρgh term represents the gravitational loss of head in the feeder dyke. One additional factor, R, has been included to account for the strength of the rocks being intruded, which must be overcome by the pressure of the intruding magma. Bradley (1965) argued that pressure loss due to friction during intrusion would be negligible.

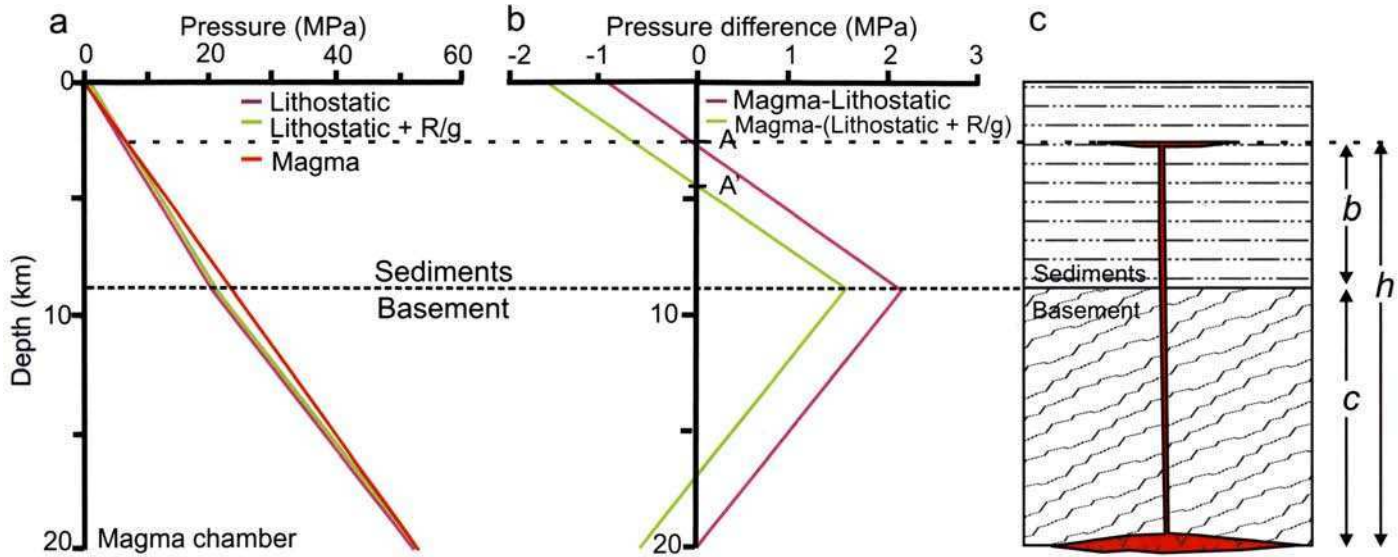

Fig. 14. (**a**) Lithostatic and hydrostatic magma column pressure profiles. Model shows a sediment column (thickness b) of constant density over a crystalline crust (thickness c) of constant density. (**b**) Pressure difference between magma and lithostatic for weak (maroon) and strong (green) wall rocks. (**c**) Diagrammatic representation of sill intruding with the maximum possible magma column height (h) for weak wall rocks.

This paper adds further simplifying assumptions in order to develop this approach: that the magma chamber is within or at the base of the crust, that the magma pressure in the chamber is lithostatic (i.e. the pressure in the magma chamber is controlled by the weight of the overburden); and also that the magma pressure in the sill is the lithostatic pressure at the intrusion level (i.e. the pressure in the sill balances the load of the overburden). If simplified further, to assign a constant density, ρ_{seds}, to the sedimentary section and a constant density, ρ_{crust}, to the crystalline crust then the pressures can be written

$$P_{chamber} = \rho_{seds} g b + \rho_{crust} g c \quad \text{and} \tag{3}$$

$$P_{sill} = \rho_{seds} g (b + c - h) \tag{4}$$

where b is the thickness of the sedimentary basin and c is the thickness of crystalline crust above the magma chamber (see Fig. 14).

Substituting Equations 3 and 4 into Equation 2, the pressure balance equation becomes

$$h = \frac{c(\rho_{crust} - \rho_{seds}) - (R/g)}{(\rho_{magma} - \rho_{seds})} \tag{5}$$

This equation is a rephrasing of the starting assumptions that the height of magma column that can be supported, h, depends on the density contrast between the crystalline basement and the sedimentary section, that between the magma and the sedimentary section and the depth of the magma chamber. The term corresponding to the overburden to the sills cancels out and therefore if assumptions are correct, then the overburden is not a factor controlling intrusion depth according to this scheme. This suggestion contrasts with that of Mudge (1968) who suggested overburden to the sill was an important factor in controlling sill intrusion depth. The cancelling out of the overburden term also has the effect that subsequent burial of the sill does not have to be taken into account when using the equation, as long as there has been no crustal thinning since intrusion. In the Faroe–Shetland Channel area, there is little evidence of post-Paleocene rifting (Dean *et al.* 1999), thus satisfying this condition.

Calibration of the model from observations in the area

It is possible to calibrate the intrusion pressure balance equation (Equation 5) using sills imaged from the FAST line (Fig. 2), making the further assumption that the magma chamber was at the base of the crust. Justification for this assumption comes from the recognition of magmatic underplating at the base of the crust, identified remotely by its high seismic velocities and density (e.g. Smallwood *et al.* 1999). The lower crustal underplating is assumed to represent the cumulates from magma chambers associated with the upper crustal magmatism (Clift 1999). The density of melt rising from the mantle is mid-way between that of the mantle and that of the crust and so the rising melt is likely to be trapped at the base of the crust (White & McKenzie 1989; England 1992).

From the FAST line (Fig. 2), the crystalline crustal thickness, c, is 10.5 km, and the height between base crust and sill complex, h, is 14.5 km. It is possible to estimate densities from the seismic velocities using published velocity–density relationships (referenced by Smallwood *et al.* 1999). Taking sediment density (ρ_{seds}) to be

2.3 $Mg\,m^{-3}$, crystalline crustal density (ρ_{crust}) to be 2.85 $Mg\,m^{-3}$, and magma density (ρ_{magma}) to be 2.65 $Mg\,m^{-3}$ (Bradley 1965) gives the rock 'strength' term R/g (in pressure units) to be 0.9 MPa.

The graphical form of Equation 5 is given in Figure 14, which shows the variation of pressure with depth for a conceptual basin, full of sediments (9 km) and with 11 km of igneous crust. The relationship between the pressure in the intruding magma and that of the lithological column is highlighted by taking the differential pressure (Fig. 14b), an approach used by Williams & McBirney (1979). It is favourable for sills to intrude anywhere within the region where the pressure in the magma is greater than the lithostatic confining pressure. While differential pressure is greatest at the interface between the basement and the sedimentary section (Williams & McBirney's 'optimum level for sill emplacement'), the pressure from a deep magma chamber can support the magma column as high as level A in Figure 14. The exact level at which lateral intrusion occurs will be strongly influenced by local factors, such as variations in the lithological column giving steps in the pressure–depth profile, variations in the ease of creating accommodation space (e.g. by local compaction) and variations in ease of fracturing.

Francis (1982) commented that for the sills in Scotland and northeast England, there was 'no evidence to show that any particular lithology had any influence in determining preferred horizons of intrusion'. In the Kangerlussuaq Basin of East Greenland, which is believed to be the counterpart of the Faroes section of the eastern Atlantic margin, igneous sills within the Cretaceous and Paleocene section are largely associated with sand-rich sections within overall shale-prone successions (M. Larsen *et al.* 1999, fig. 9). In contrast, many of the sills penetrated by the wells in the Faroe–Shetland Channel are within dominantly shaley sequences. Changes in density between geological units will give inflections or local maxima in the pressure–depth profile that may encourage intrusion at those particular levels. Sands and shales have different compaction-depth trends, and if a sill is to create space for itself by local compaction of the sediments, then this difference may control the ease with which the sill may intrude into each lithology. Considering compaction only, at greater depths it is likely to be preferable for the sills to intrude coarser-grained section, but finer-grained sediments will become easier to intrude closer to the seabed. As magma is forced higher within a basin, however, lithological considerations may be secondary when a particular zone of weakness may provide an interface (with sufficiently low R/g) to be exploited by the intrusion before the maximum possible height of the intrusion is reached.

Extending the model into two dimensions

The intrusion pressure equation can also be used to gain insight into the distribution of sill complexes laterally within a sedimentary basin as the crustal thickness and thickness of basin fill varies. Figure 15 shows a schematic basin in isostatic equilibrium, which is filled with sediments, together with the line predicted by the intrusion pressure equation to indicate the height to which sills may be intruded from a base-crustal magma chamber. In simple terms, the top of the sill complex is predicted to follow the basement up towards the basin margin, as is observed to be the case for the Faroe–Shetland Channel area (Fig. 2).

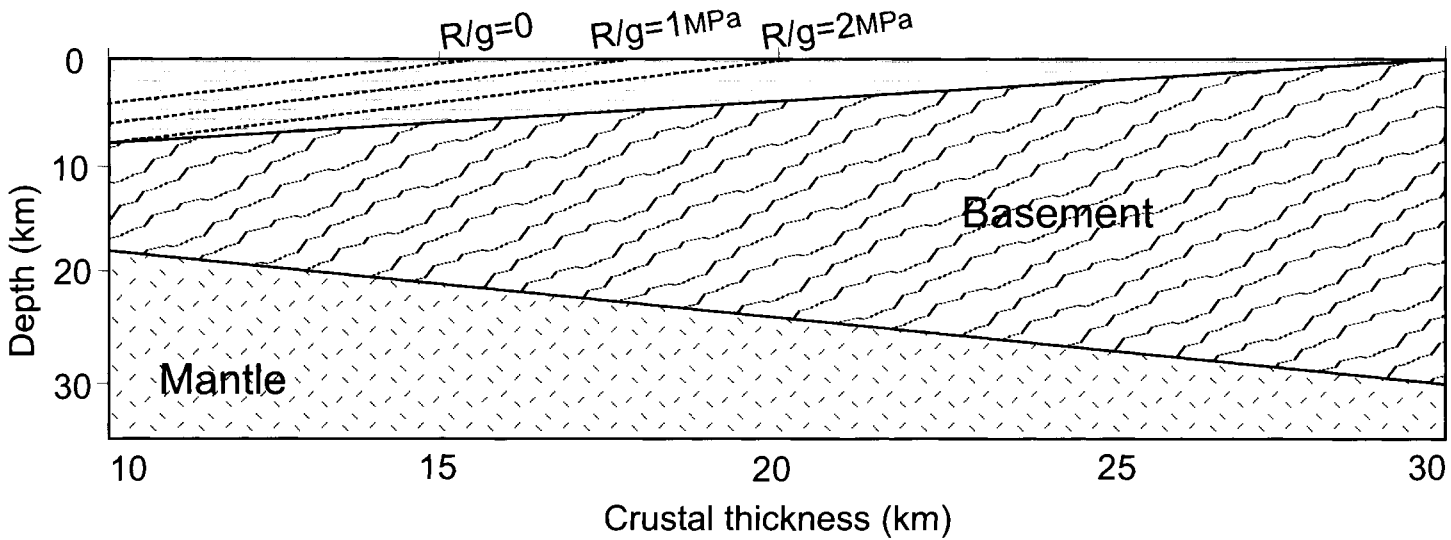

Fig. 15. Conceptual basin cross-section showing maximum height of sill intrusion given assumptions discussed in the text, varying crustal thickness and a rock strength (R/g) ranging up to 2 MPa.

If the rock 'strength' term (R/g) in Equation 5 is increased, then the highest sill intrusion depth will be less shallow, as more of the supporting pressure has to be used to fracture the host rock. If the densities of sedimentary section are allowed to vary with depth, then the gradient of the line showing highest sill intrusion level will vary accordingly, although to first order the shape will remain the same. Lateral changes in density, such as bunching of the isobars toward the basin margin, will tend to encourage the sills to migrate upwards parallel to the surfaces of equal pressure, as observed, for instance in Sill E (Fig. 13). This phenomenon is simply the intrusion of sills perpendicular to the least compressive stress vector.

Figure 16a shows a sill that has intruded laterally below level A, overcoming the rock strength at level B. This sill then has sufficient pressure support to step structurally up within the basin, continually overcoming the rock strength to the maximum height of level A. These steps tend to occur at local maxima in the differential pressure curve or levels of lithologic weakness, perhaps caused by lower pressure near faults, which the sills may tend to follow (such as Sill E, Fig. 13). If the rock strength decreases upwards, or simply acts as a threshold to be overcome once, then the intrusion may be able to reach as high as level A. As described above, if supporting pressure is sufficient, then the magma column may be able to reach the surface.

Figure 16b shows the situation in which the magma supply is exhausted or the conduit closed beneath the sill. With the pressure support removed, the magma within the sedimentary section will not be able to rise further. If still fluid, the magma will tend to descend, perhaps to level C, the highest level now sustainable in weak rocks ($R/g = 0$) or level C′, the highest level now sustainable in strong rocks. If the magma conduit is further truncated, stranding the magma within the sedimentary section, then the sill will evolve towards a position of hydrostatic equilibrium unless it freezes before it is able to achieve this or is prevented by the rock strength (Francis 1982). If fluid flow conditions permit (weak rocks) then the magma may descend towards the level of neutral buoyancy around the level of top basement.

Testing and predicting from the model

Where an alternative method is available to estimate the depth below surface of the sill intrusion, it is possible to check the pressure balance equation. This depth is estimated as 2.9 km for the 214/27-1 sill using its radiometric age. Using the same mean densities as above for magma, crystalline crust and sedimentary section, the same rock strength factor, and a crustal thickness estimate of 13 km from projecting the well onto the line of Figure 2 returns the value of 3.2 km from the model. The two methods are in very good agreement.

In qualitative terms the main prediction of the model is that where the basement is high then the sills will be able to intrude at shallower levels (Fig. 15). This prediction is supported by the high emplacement of sills over basement highs in Figures 8 and 12. Gibb & Kanaris-Sotiriou (1988) comment that, in the area they considered, the sills lie at higher stratigraphic levels to the NW. This increase in height to the NW reflects the presence of the underlying Corona Ridge (Fig. 2; Dean *et al.* 1999), although this basement high could not be seen on the seismic data they show due to imaging problems. The model, demonstrated in this paper, is further supported by the presence of sills intruded at extremely high levels over the high basement in the east

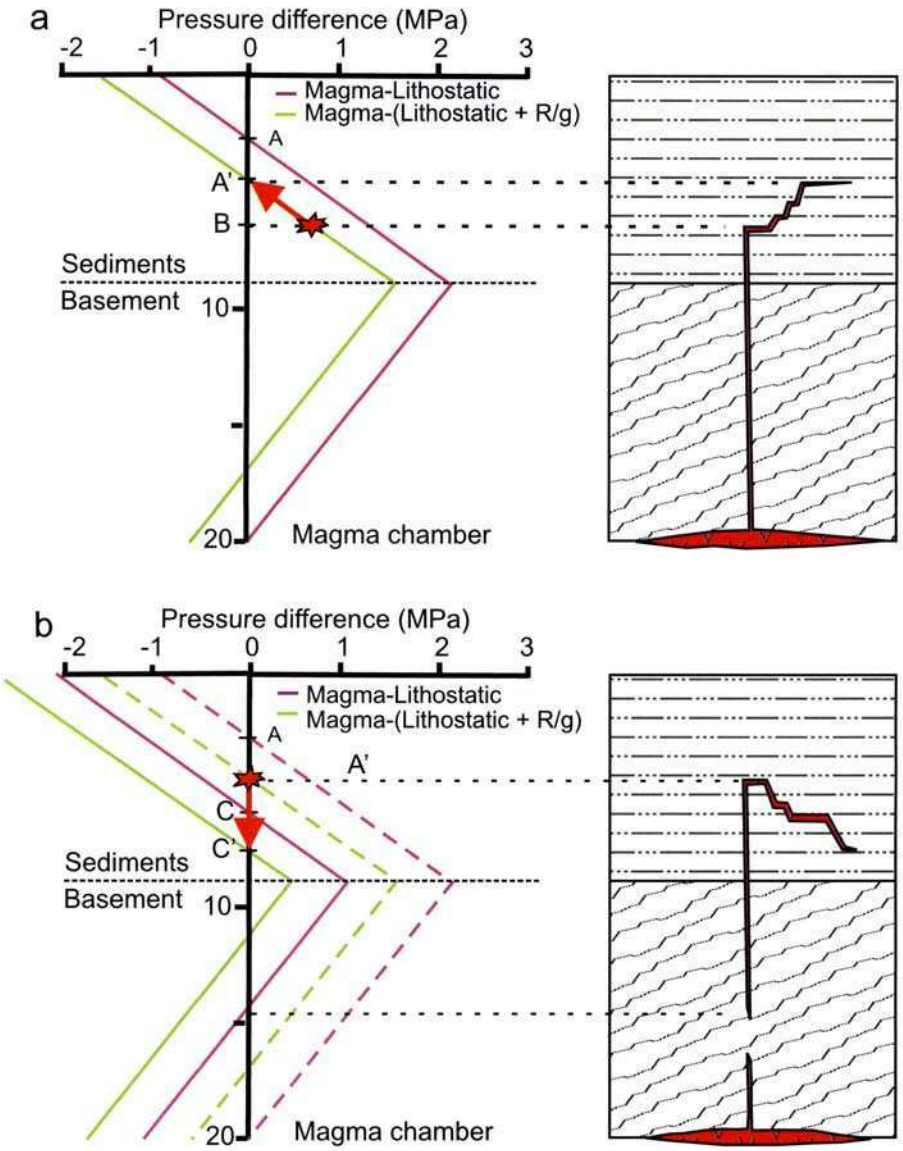

Fig. 16. (**a**) Pressure difference between magma and lithostatic for weak (maroon) and strong (green) wall rocks (same basin structure as Figure 14). An intruding sill overcomes the wall strength at level B and has sufficient pressure support from the magma chamber to climb as high as level A′. (**b**) Dashed lines show pressure difference between magma and lithostatic for weak (maroon) and strong (green) wall rocks with magma supplied from the base of the crust, same basin structure as Figure 14. An intruding sill overcomes the wall strength at level A′ (the highest sustainable level in this example) but conduit discontinuity removes pressure support, pressure profiles assume form shown by solid lines, and the intrusion descends in the basin to a new highest sustainable level (C′ for strong wall rocks).

of the basin: there are only a few hundred metres depth between the sills in the area around Rona Ridge wells 206/13-1 and 207/1a-4 (Figs 1 & 2) and the Top Balder seismic pick in that area.

The intercept of the lines showing highest sill intrusion level with the surface (Fig. 15) notionally indicate the point at which the pressure from a base-crustal magma chamber can support an extrusive process. However, as crust becomes thicker towards the basin margin the likelihood of a magma supply being able to support a continuous feeder system decreases, and so the grading of sill complex into an extrusive complex is likely to be the exception rather than the rule for the quantities of magma involved. The concept, though, is to be supported by the observation of extrusive centres at the basin margins rather than in the basin centre, for example the 'guyot' mentioned above over the Rona Ridge in Block 206/12. On a bigger scale, the occurrence of the flood basalt lavas from feeder vents around the present-day Faroe islands and the Western Isles rather than from the thickest parts of Mesozoic and Paleocene basins can be explained in the same way.

The main application for Equation 5 is to understand the level at which sills may be able to intrude given a particular pressure profile and crustal thickness. Additionally, in the same way that we calibrated the intrusion pressure equation (Equation 5) to determine the effective 'R/g' rock strength term, the equation can be rearranged to estimate any other one unknown. For example, if the R/g term is taken to be constant with depth, and the distance between sill and basement (h–c) can be determined from seismic data, then depth to the magma chamber (a proxy for crustal thickness as suggested above?) can be estimated. For example, above we estimated that Sill B in Well 205/10-2b, presently 2.8 km below sea-bed, was intruded a depth of 1.0 km below the sea-bed. This well penetrated to a depth of 5731 m in Cretaceous sediments, and beneath this we estimate basement to lie at around 6.5 km depth below sea-bed. Using these figures, h–c is 5.5 km, and rearranging Equation 5 to solve for c, using the same values as above for densities and rock strength, gives an estimate of 16 km of crystalline crust over the magma chamber (crustal thickness?). Such a value seems reasonable compared to the along-strike crustal model of Figure 2.

Alternatively, if sills of known age are mapped in a basin where the crustal thickness is known and densities can be estimated, then the depth to basement could be estimated (England pers. comm.).

Since in formulating the pressure balance equation, the overburden term cancels out, the observation of sills does not, unfortunately, allow any statement to be made about the water depth at the time of intrusion. Perhaps the suggestion of the independence of sill intrusion from water depth is a worthwhile result in itself.

Conclusions

The Faroe–Shetland Sill Complex is an excellent natural laboratory in which to study igneous sills since there is extensive seismic and some well data available. This paper shows the typical wireline log response of sills and their thermal aureoles, which are developed around the thicker sills. The sills have low Gamma Ray (GR) response compared to that of shales, but the thermal aureoles flanking the sills are not seen on the GR log, as any mineralogical changes during metamorphism do not affect the composition of the rock. However, high and rapidly fluctuating resistivity

readings often characterise the thermal aureole, which we attribute to the contact metamorphism. The sills have high densities and sonic velocities relative to their host sediments. On both the velocity and the density logs the aureoles show 'swells' towards the sills, but readings decrease immediately adjacent to the sills, which we attribute to local fracturing both above and below the intrusions. The caliper log shows that thin sills (particularly) sometimes collapse into the borehole, which are attributed to disaggregation of the sill along fractures as the confining pressure is released by the drilling process.

The sills form prominent seismic reflectors due to their high acoustic and elastic impedances. The seismic response of the sills has been calibrated by compiling exploration well wireline log data, creating new empirical velocity–density and compressional–shear velocity relationships. The relationships allow any of the elastic properties to be estimated from any one of the other two, and the new V_p/V_s estimate shows that sills have a similar Poisson's ratio to that of extrusive rocks of similar composition. These relationships can aid particularly in the construction of synthetic seismograms where one data type has not been acquired in a borehole. Within this paper, synthetic seismograms have been calculated for a range of sill thicknesses and show how the seismic amplitude 'tuning' response for sills varies with sill thickness.

Examples of seismic data over sills, in particular focussing on one well-imaged sill in the Quad 205 area, which we call 'Sill B' are shown. Mapping from 3D seismic data indicates that this sill is 3–4 km across, has a lobate geometry along its edges and is dissected by a series of offsets, which this paper argues are of primary intrusive origin. The demonstration of the seismic 'tuning' effect for sills is used together with the amplitude response of the sill to estimate the volume of this intrusion at 0.45 km^3.

The introduction of intrusive rocks can play an important role in the subsequent development of the sedimentary system. This paper uses an example from Quad 205, in which inflation of the seafloor above the sills appears to have controlled deposition of a reservoir quality sand body. Screening sill complexes for similar geometries and timing relationships may prove a worthwhile activity for hydrocarbon exploration.

Sill geometry is particularly well imaged in the Quad 204/6004 area. This paper has described deep plate-shaped and trumpet-shaped intrusions, which have been mapped on 3D seismic data. Some of the sills appear to have exploited pre-existing Paleocene faults during their intrusion.

The distribution of the sill complex within the basin has also been discussed, with reference to a model of pressure support of magma from a crustal magma chamber. In particular, a simple equation relating rock densities to intrusion depth gives insight into some of the controls affecting the intrusion process and gives a framework in which to set observed geometries of the sill complex. This intrusion pressure equation has also been used to discuss the height of intrusions relative to the crustal thickness of the basin. One important prediction of the model is that sills will be intruded at the shallowest levels over basement highs and at the basin margins, which agrees with qualitative observations. The model described in this paper has been tested quantitatively against sills for which estimates have been made of the depth of intrusion by alternative methods, and the figures returned are consistent with the predictions of the model. The simplicity of the model allows the effect of the individual parameters to be considered. However, the model presented here is a gross simplification of a complex natural system, and as such could be refined in several ways,

including consideration of any zones of overpressure in the basin, variations in density through the basin and a more detailed treatment of the process by which the sill fractures the host rock.

The seismic data are shown by kind permission of Veritas DGC (Fig. 12), Chevron and Kerr-McGee (Figs 8–11). The FAST line (Fig. 2) was acquired and processed under the auspices of BIRPS on behalf of a consortium consisting of Amerada Hess, Amoco, Conoco, Mobil and Shell. Our attention was drawn to the idea of pressure support from a crustal magma chamber by Richard England in a paper presented at the Geological Society in 1998. Michael Tate identified the 'guyot' in 206/12. We thank Sverre Planke, Bob White, Richard England and Amerada Hess' Atlantic Margin team for their input and Mike Widdowson and an anonymous reviewer for their helpful comments. The opinions and interpretations expressed herein are not necessarily those of Amerada Hess Ltd., its partners or any other organization mentioned. Department of Earth Sciences contribution 6540.

References

ASHCROFT, W. A., HURST, A. & MORGAN, C. J. 1999. Reconciling gravity and seismic data in the Faroe–Shetland Basin, West of Shetland. *In*: FLEET, A. J. & BOLDY, S. A. R. (eds) *Petroleum Geology of Northwest Europe: Proceedings of the 5th Conference*. Geological Society, London, 595–600.

BOLDREEL, L. O. & ANDERSON, M. S. 1993. Late Paleocene to Miocene compression in the Faroe–Rockall area. *In*: PARKER, J. R. (ed.) *Petroleum Geology of Northwest Europe: Proceedings of the 4th Conference*. Geological Society, London, 1025–1034.

BOTT, M. H. P. & SMITH, P. J. 1984. Crustal structure of the Faroe–Shetland Channel. *Geophysical Journal of the Royal Astronomical Society*, **76**, 383–398.

BRADLEY, J. 1965. Intrusion of Major Dolerite Sills. *Transactions of the Royal Society of New Zealand*, **3**, 27–54.

CHEVALLIER, L. & WOODFORD, A. 1999. Morpho-tectonics and mechanism of emplacement of the dolerite ring and sills of the western Karoo, South Africa. *South African Journal of Geology*, **102**, 43–52.

CLIFT, P. D. 1999. The thermal impact of Paleocene magmatic underplating in the Faroe–Shetland–Rockall region. *In*: FLEET, A. J. & BOLDY, S. A. R. (eds) *Petroleum Geology of Northwest Europe: Proceedings of the 5th Conference*. Geological Society, London, 585–593.

CLIFT, P. D., TURNER, J. & OCEAN DRILLING PROGRAM LEG 152 SCIENTIFIC PARTY 1995. Dynamic support by the Icelandic plume and vertical tectonics of the northeast Atlantic continental margins. *Journal of Geophysical Research*, **100**, 24 473–24 486.

DEAN, K., MCLACHLAN, K. & CHAMBERS, A. 1999. Rifting and development of the Faroe–Shetland Basin. *In*: FLEET, A. J. & BOLDY, S. A. R. (eds) *Petroleum Geology of Northwest Europe: Proceedings of the 5th Conference*. Geological Society, London, 533–544.

EBDON, C. C., GRANGER, P. J., JOHNSON, H. D. & EVANS, A. M. 1995. Early Tertiary evolution and sequence stratigraphy of the Faroe–Shetland Basin: implications for hydrocarbon prospectivity. *In*: SCRUTTON, R. A., STOKER, M. S., SHIMMIELD, G. B. & TUDHOPE, A. W. (eds) *The Tectonics, Sedimentation and Palaeoceanography of the North Atlantic Region*. Geological Society, London, Special Publications, **90**, 51–69.

ENGLAND, R. W. 1992. The role of Palaeocene magmatism in the tectonic evolution of the Sea of Hebrides Basin: implications for basin evolution on the NW Seaboard. *In*: PARNELL, J. (ed.) *Basins on the Atlantic Seaboard: Petroleum Geology, Sedimentology and Basin Evolution*. Geological Society, London, Special Publications, **62**, 163–174.

FLEIDNER, M. & WHITE, R. S. 2001. Sub-basalt imaging in the Faroe–Shetland Basin with large-offset data, *First Break*, **19**, 247–252.

FRANCIS, E. H. 1982. Emplacement mechanism of late Carboniferous tholeiite sills in Northern Britain. *Journal of the Geological Society, London*, **139**, 1–20.

GIBB, F. G. F. & KANARIS-SOTIRIOU, R. 1988. The geochemistry and origin of the Faroe–Shetland sill complex. *In*: MORTON, A. C. & PARSON, L. M. (eds) *Early Tertiary Volcanism and the Opening of the NE Atlantic*. Geological Society, London, Special Publications, **39**, 241–252.

HAILWOOD, E. A. & DING, F. 1995. Palaeomagnetic re-orientation of cores and the magnetic fabric of hydrocarbon reservoir sands. *In*: TURNER, P. & TURNER, A. (eds) *Palaeomagnetic Applications in Hydrocarbon Exploration and Production*. Geological Society, London, Special Publications, **98**, 245–258.

HAMILTON, E. L. 1978. Sound velocity-density relations in sea-floor sediments and rocks. *Journal of the Acoustical Society of America*, **63**, 366–377.

HITCHEN, K. & RITCHIE, J. D. 1993. New K–Ar ages, and a provisional chronology, for the offshore part of the British Tertiary Igneous Province. *Scottish Journal of Geology*, **29**, 73–85.

HOLMES, A. 1944. *Principles of Physical Geology*, Nelson, London, 532.

KNELLER, B. 1995. Beyond the turbidite paradigm: Physical models for deposition of turbidites and their implications for reservoir prediction. *In*: HARTLEY, A. J. & PROSSER, D. J. (eds) *Characterization of Deep Marine Clastic Sequences*. Geological Society, London, Special Publications, **94**, 31–49.

LAMERS, E. & CARMICHAEL, S. M. M. 1999. The Paleocene deepwater sandstone play West of Shetland. *In*: FLEET, A. J. & BOLDY, S. A. R. (eds) *Petroleum Geology of Northwest Europe: Proceedings of the 5th Conference*. Geological Society, London, 645–659.

LARSEN, L. M., WAAGSTEIN, R., PEDERSEN, A. K. & STOREY, M. 1999. Trans-Atlantic correlation of the Palaeogene volcanic successions in the Faroe Islands and east Greenland. *Journal of the Geological Society, London*, **156**, 1081–1095.

LARSEN, M., HAMBURG, L., OLAUSSEN, S, NORGAARD-PEDERSEN, N. & STEMMERIK, L. 1999. Basin evolution in Southern East Greenland: An outcrop analog for Cretaceous–Paleogene Basins on the North Atlantic Volcanic margins. *Bulletin of the American Association of Petroleum Geologists*, **83**, 1236–1261.

MACGREGOR, M. & MACGREGOR, A. G. 1936. *The Midland Valley of Scotland*. British Regional Geology, Institute Geological Sciences, HMSO.

MUDGE, M. R. 1968. Depth control of some concordant intrusions. *Bulletin of the Geological Society of America*, **79**, 315–332.

NAYLOR, P. H., BELL, B. R., JOLLEY, D. W., DURNALL, P. & FREDSTED, R. 1999. Palaeogene magmatism in the Faroe–Shetland Basin: influences on uplift history and sedimentation. *In*: FLEET, A. J. & BOLDY, S. A. R. (eds) *Petroleum Geology of Northwest Europe: Proceedings of the 5th Conference*. Geological Society, London, 545–558.

PLANKE, S. & CAMBRAY, H. 1998. Seismic properties of flood basalts from Hole 918A downhole data, Southeast Greenland Volcanic margin. *In*: SAUNDERS, A. D., LARSEN, H. C. & WISE, S. W. JR. (eds) *Proceedings of the Ocean Drilling Program, Scientific Results*. College Station, Texas, **152**.

PLANKE, S., ALVESTAD, E. & ELDHOLM, O. 1999. Seismic characteristics of basaltic extrusive and intrusive rocks. *The Leading Edge*, **18**, 342–348.

POLLARD, D. D., MULLER, O. H. & DOCKSTADER, D. R. 1975. The form and growth of fingered sheet intrusions, *Bulletin of the Geological Society of America*, **86**, 351–363.

RICHARDSON, K. R., WHITE, R. S., ENGLAND, R. W. & FRUEHN, J. 1999. Crustal structure east of the Faroe Islands: mapping sub-basalt sediments using wide-angle seismic data. *Petroleum Geoscience*, **5**, 161–172.

RITCHIE, J. D. & HITCHEN, K. 1996. Early Paleogene offshore igneous activity to the northwest of the UK and its relationship to the North Atlantic Igneous Province. *In*: KNOX, R. B. O'B., CORFIELD, R. M. & DUNAY, R. E. (eds) *Correlation of the Early Paleogene in Northwest Europe*. Geological Society, London, Special Publications, **101**, 63–78.

RUMPH, B., REEVES, C. M., ORANGE, V. G. & ROBINSON, D. L. 1993. Structuring and transfer zones in the Faroe Basin in a regional context. *In*: PARKER, J. R. (ed.) *Petroleum Geology of Northwest Europe: Proceedings of the 4th Conference*. Geological Society, London, 999–1009.

SCLATER, J. G. & CHRISTIE, P. A. F. 1980. Continental stretching: an explanation of the post Mid-Cretaceous subsidence of the central North Sea basin. *Journal of Geophysical Research*, **85**, 3711–3793.

SMALLWOOD, J. R. & WHITE, R. S. 2002. Ridge-plume interaction in the North Atlantic. *In*: JOLLEY, D. W. & BELL, B. R. (eds) *The North Atlantic igneous province: stratigraphy, tectonics, volcanic and magmatic processes*. Geological Society, London, Special Publications, **197**, 000–000.

SMALLWOOD, J. R., WHITE, R. S. & STAPLES, R. K. 1998. Deep crustal reflections under Reydarfjordur, eastern Iceland: Crustal accretion above the Iceland mantle plume. *Geophysical Journal International*, **134**, 277–290.

SMALLWOOD, J. R., STAPLES, R. K., RICHARDSON, K. R., WHITE, R. S. & THE FIRE WORKING GROUP 1999. Crust formed above the Iceland mantle plume: from continental rift to oceanic spreading center. *Journal of Geophysical Research*, **104**, 22 885–22 902.

SMALLWOOD, J. R., TOWNS, M. J. & WHITE, R. S. 2001. The structure of the Faroe–Shetland Trough from integrated deep seismic and potential field modelling. *Journal of the Geological Society, London*, **158**, 409–412.

WAAGSTEIN, R. 1988. Structure, composition and age of the Faroe basalt platform. *In*: MORTON, A. C. & PARSON, L. M. (eds) *Early Tertiary Volcanism and the Opening of the NE Atlantic*. Geological Society, London, Special Publications, **39**, 225–238.

WHITE, R. S. & MCKENZIE, D. P. 1989. Magmatism at rift zones: the generation of volcanic continental margins and flood basalts. *Journal of Geophysical Research*, **94**, 7865–7729.

WILLIAMS, H. & MCBIRNEY, A. R. 1979. *Volcanology*, Freeman, Cooper & Co., San Francisco, 397.

On the emplacement of sill complexes: evidence from the Faroe–Shetland Basin

BRIAN BELL[1] & HELEN BUTCHER[2]

[1] *Division of Earth Sciences, University of Glasgow, Gregory Building, Lilybank Gardens, Glasgow G12 8QQ, UK (e-mail: bbell@earthsci.gla.ac.uk)*

[2] *Statoil (UK) Ltd., Statoil House, 11a Regent Street, London SW1Y 4ST, UK*

Abstract: The North Faroe–Shetland Basin (NFSB) Sill Complex is of late Paleocene/earliest Eocene age and was emplaced within Cretaceous and Paleocene sedimentary rocks, in places to depths as shallow as a few hundred metres below the contemporaneous basin floor. Intersections of the Complex occur in exploration wells drilled by the oil industry and indicate tholeiitic basaltic compositions. High quality 3D seismic data, obtained during hydrocarbon exploration along the NE Atlantic Margin, provide a unique view of an uneroded suite of these sheet-like intrusions in UK Quadrants 218 and 219 and indicate the multi-centred nature of the NFSB Sill Complex, with upward-fingering terminations from broad bowl-shaped foci of intrusion. Where the intrusion depth is very shallow, depending upon the host lithology, sill emplacement has lead to the development of structures on the contemporaneous basin floor interpreted as submarine hyaloclastite-dominated vents, up to *c.* 2 km across and with heights of up to *c.* 100 m. Where intrusion depth is greater, 'seismic chimney' structures are interpreted as the fluid-escape feeders of sedimentary-hydrothermal mounds. Subsequent differential compaction of sedimentary sections, with and without shallow-emplaced sills, has given rise to distinctive 'eye' structures, as seen in seismic sections.

Some of the largest and short-lived magmatic events involve the emplacement of basic sill complexes into upper crustal sedimentary rocks (Walker 1993). Prior to continental break-up and the formation of new ocean basins, voluminous sequences of (predominantly) subaerial facies basaltic (flood) lavas are erupted into areas of rifted continental crust. Accompanying these volcanic episodes, the subjacent rift sedimentary sequences are injected by suites of sills, commonly achieving volumes rivalling those of the extrusive rocks.

Our understanding of the geometry, and consequently mechanism of emplacement, of such sills is, to a large extent, based upon observations of exhumed sill complexes (for example: the Midland Valley of Scotland Carboniferous sills (Francis 1982); the Western Karoo Jurassic sills, South Africa (Chevallier & Woodford (1999)), together with theoretical arguments concerning factors which control the geometry (Francis 1982), mechanism (Pollard *et al.* 1975) and depth (Bradley 1965) of emplacement.

From: JOLLEY, D. W. & BELL, B. R. (eds) *The North Atlantic Igneous Province: Stratigraphy, Tectonic, Volcanic and Magmatic Processes*. Geological Society, London, Special Publications, **197**, 307–329. 0305-8719/02/$15.00

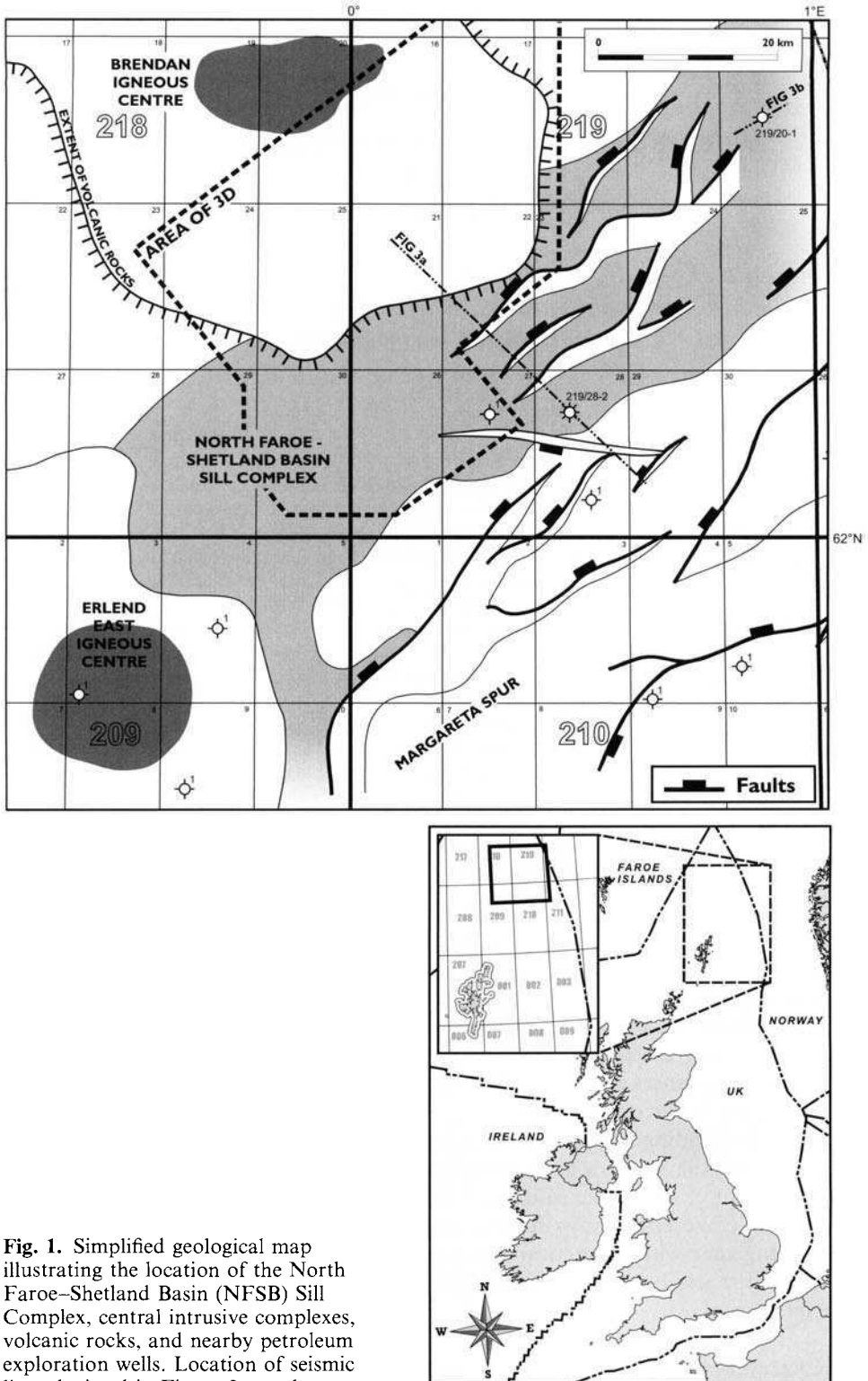

Fig. 1. Simplified geological map illustrating the location of the North Faroe–Shetland Basin (NFSB) Sill Complex, central intrusive complexes, volcanic rocks, and nearby petroleum exploration wells. Location of seismic lines depicted in Figure 3 are also indicated.

This contribution discusses what can be learned about the architecture of sill complexes from 3D seismic surveys. Recently acquired datasets resulting from hydrocarbon exploration programmes in the Faroe–Shetland Basin on the NE Atlantic Margin (Fig. 1) allow us to image suites of sills and associated phenomena which have not been subjected to subsequent erosion and, therefore, where the uppermost intrusive phenomena and related extrusive products are preserved. Exploration wells have intersected several of these intrusions within the Faroe–Shetland Basin. Petrographical and geochemical studies show that they are typically olivine tholeiites which have a transitional (T) mid-ocean ridge basalt (MORB) composition (Gibb *et al.* 1986; Gibb & Kanaris-Sotiriou 1988). Lavas of similar composition occur within the Upper Formation of the Faroes Lava Group (Waagstein 1988).

Specifically, we examine the following features of sill complexes: (i) their geometries, in particular at the highest structural levels, typically not seen in exhumed examples due to erosion; (ii) the nature of any contemporaneous surface (extrusive) products, i.e. a vent facies; and, (iii) the effects on compaction histories of host strata, together with sediments deposited after sill emplacement.

Wireline log and seismic response of sills

Basic sills are typically emplaced into host basinal sedimentary sequences which, due to their differing rock properties, produce a significant acoustic impedance contrast (where acoustic impedance is the product of the velocity and density of the different rocks). Sills are composed of relatively dense crystalline rock (2.75–3 $Mg\,m^{-3}$) that has a sonic velocity in excess of 5000 $m\,s^{-1}$. Host sedimentary rocks, typically claystones (shales) and sandstones, have significantly lower densities and sonic velocities: $<2.5\,Mg\,m^{-3}$ and $<3000\,m\,s^{-1}$, respectively.

Data collected in exploration wells by wireline logging tools capture certain (sometimes more subtle) variations in a number of rock properties. In summary, rock property contrasts between sills and host rocks include (Fig. 2):

(i) gamma ray logs measure the amount of radioactive material (K, U, Th) within lithologies. The contrast between a sill and typical argillaceous host rocks is particularly marked, with the former showing a consistent reduced response (35–45 api);

(ii) electrical resistivity within sills is typically very variable (1000–2000 ohm m), although substantially higher than that of the host sedimentary rocks. In some instances, the immediately underlying and overlying thermally indurated (aureole) host rocks may have high values due to the development of secondary (hydrothermal) minerals such as magnetite and pyrite;

(iii) sonic velocity is typically relatively constant and high within sills (typically 50–60 $\mu sec\,ft^{-1}$), in contrast to the response from the host rocks. The uppermost and lowermost portions of sills may have slightly reduced values of sonic velo-city due to the presence of gas cavities (typically with amygdale mineral infills), together with close-spaced fractures which formed during and subsequent to crystallization and cooling. Locally, within the host rocks, the effects of fracturing (lowering velocities) and growth of metamorphic minerals (increasing velocities) may be evident;

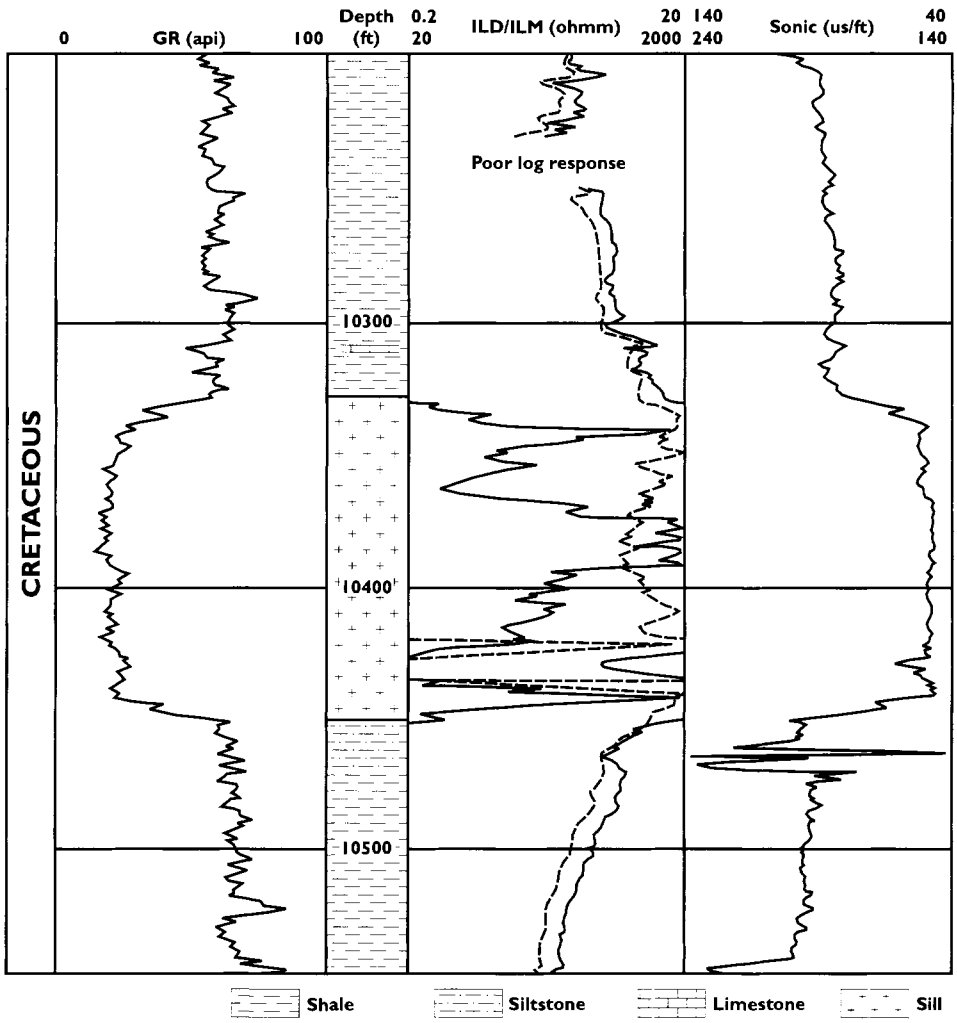

Fig. 2. Petrophysical log response of a basic sill and various host rock sedimentary lithologies in Well 219/28-2/2Z.

(iv) high rock density is relatively constant throughout the thickness of sills and contrasts with lower values for the host rocks; the effects of gas cavities and fractures in sills, and fracturing in the host rocks adjacent to sills, may cause a localized reduction in density, similar to the sonic response described in (iii), above.

As explained above, sills typically have a very distinctive seismic expression due to their acoustic impedance contrast with the host lithology. Indeed, it can be observed from seismic modelling that sills of about 30 m thickness show the highest amplitude on seismic sections. This is a result of constructive interference (tuning), at typical seismic frequencies, of the seismic events caused by the top and base of the sill.

In sills of greater thickness, the top and base of the event should be identifiable. However, it is often difficult to interpret whether an observed seismic event results from one sill or a stacked package of sills.

Although the lithology contrast between sills and host rocks permits their imaging in some detail, the efficient reflection of seismic energy from the top surface of the shallowest sill in a vertical sequence of intrusions means that those at deeper levels receive less energy and, consequently, are less well-imaged. Similarly, where sills occur below significant thicknesses of basaltic lavas, as is typical of the Faroe–Shetland Basin (Figs 1 & 3) and volcanic provinces worldwide, then significant imaging problems occur. Such imaging problems are exacerbated when the top volcanic surface is irregular or rugose, leading to significant scattering of seismic energy. Imaging of vertical or very steeply inclined surfaces is not a strength of seismic investigations and, therefore, fault planes and vertical (feeder) dykes possibly associated with sills are all but invisible. Other problems associated with imaging sills, including the generation of seismic time migration 'smiles' resulting from the selection of too low stacking velocities, are discussed by Smallwood & Maresh (2002).

The geometry of sills and sill complexes

Dimensions. Sills are typically relatively planar sheets of fine- to coarse-grained igneous rock, most commonly of basic composition. Individual sheets or leaves of a complex can achieve thicknesses of several tens of metres, and in exceptional cases several hundreds of metres (Stose & Lewis 1916). Each sheet or leaf is commonly the result of a single pulse of magma, although multiple intrusions are also recognized (Walker 1969).

Aggregate thicknesses of sills within sedimentary sequences can be in excess of 1000 m, with estimated (preserved) volumes of 2×10^5 km^3 (du Toit 1920). The aspect ratio (length parameter : thickness) of sills is commonly 2000 : 1, or greater, similar to that of continental flood lavas.

Relationships with host strata. Transgressive ('step-and-stair') relationships (both vertical and lateral) with host strata are relatively common (Carey 1958), sometimes using pre-existing faults. Construction of so-called isostrats, surfaces connecting the surface of a sill where it is in contact with the same stratigraphic datum, suggests inverted cone or saucer-like geometries (Carey 1958; Francis 1982) with relatively flat lower parts.

The study of Francis (1982) recognized that sills commonly thicken towards their lowest structural level, although post-intrusion subsidence has been suggested as a cause for certain intrusion geometries (Petraske *et al.* 1978). However, Francis (1982) concluded that such an effect is relatively minor for the Carboniferous sills of northern Britain, Furthermore, Francis (1982) was able to clearly demonstrate that for the main Midland Valley Sill, the saucer-shaped base of the intrusion follows the same axis as that of the host sedimentary basin sequence. Thus, there is clear evidence for causal links between sill location and geometry, and the overall disposition of the host strata.

Where evidence is preserved, it appears that sills become more inclined (relative to the dip of the host strata and a horizontal datum) and thinner towards their

upward terminations, and in some instances ultimately dying out in en echelon lenses (Grapes *et al.* 1972). The formation of these lenses may be attributed to tension fractures propagating in the host strata as the magma is emplaced (Bradley 1965; Grapes *et al.* 1972). Exhumed sills in areas with irregular topographic relief typically define annular geometries with inwardly inclined dips (Francis 1982; Chevallier & Woodford 1999).

Studies of eroded sill complexes (Francis 1982) suggest that the intensity of intrusion is greatest in the sedimentary rocks directly above 'highs' in the crystalline basement, diminishing up-section; however, it is not always possible to confirm this observation from seismic data due to the masking effect of the uppermost sills. Seismic data from the study area (see below) also suggest that the extent of a sill complex may ultimately be limited by the presence of up-faulted 'basement' blocks, acting as a barrier to further lateral migration.

Local soft sediment deformation is common where the host strata are under-compacted (Duffield *et al.* 1986). Intrusion of hot basaltic magma into such pore fluid-rich sediments may lead to fluidization of the sediments and the formation of mixed rocks, peperites, along sill margins. Einsele *et al.* (1980) proposed that the volumetric loss of pore fluid from such sediments may approximately balance the volume of sill material introduced.

Mechanism(s) of emplacement of sills

Most models of sill emplacement have several common elements, and are concerned with the 'magma-static' relationship between a (static) column of magma fed from depth and the density profile of the crustal rocks through which it has risen. Typically, the density (ρ) of crustal lithologies, especially within a sedimentary sequence, decreases with decreasing depth. Furthermore, load pressure, σ_z, decreases with decreasing depth. Consequently, there is a 'critical' depth where the least principal stress is vertical (and not horizontal, as is the case at deeper levels in the crust, where σ_z is relatively large). It is at (and above) this critical depth, where magma can be emplaced into the crust as near-horizontal sheets, perpendicular to σ_z. This model was explored by Roberts (1970) with respect to the relative stresses during the emplacement of dykes, sills and plugs. In summary, when $\sigma_z \gg \sigma_x$, dykes are formed, whereas when $\sigma_z \ll \sigma_x$, then sills are formed. At very shallow depths, where both σ_z and σ_x are low, then cylindrical, pipe-like structures will form.

Bradley (1965) proposed a model for sill emplacement whereby intrusion occurs along an equipotential surface, where the magma pressure balances the load pressure (σ_z) plus the tensile strength of the rocks; thus, sills will be intruded at relatively shallow levels where there are topographic lows and at greater depths where there are topographic highs. Hence, the depth of emplacement of sills mirror-images (and is not co-planar with) that of the contemporaneous land surface (or sea bed).

In order that magma is able to migrate upwards through low density sedimentary materials in the upper crust with a typical tensile strength of *c.* 5×10^7 Pa, it is necessary to have an additional driving pressure. Williams & McBirney (1979) suggested that this pressure difference (essentially a pressure head sufficient to overcome the strength of the wall rocks and thus permit lateral intrusion) be sufficient to raise magma to a height in excess of 2 km above the Earth's surface. Francis (1982)

concluded that this column height may be greater than this estimate. Mudge (1968) concluded that the optimum depth of emplacement for sills is *c.* 1 to 2 km, implying that the typical (excess) magma pressure is sufficient to 'lift' such an overburden.

North Faroe–Shetland Basin Sill Complex

The North Faroe–Shetland Basin (NFSB) Sill Complex extends over a *c.* 25 km wide tract trending NE–SW, some 150 km north of the Shetland Islands, to the north of the Shetland Platform, and stretching from the northern limit of the Faroe–Shetland Basin into the SW part of the Møre Basin (Fig. 1). At depth, the area is dominated by the positive expression of the Palaeogene Brendan Igneous Centre and associated volcanic escarpment to the NW, and the Palaeogene Erlend igneous centres to the south and SW.

Large volumes of volcanic rocks were extruded along the NE Atlantic Margin during the late Paleocene/early Eocene, as part of the onset of ocean floor spreading in the NE Atlantic Ocean and proximity to the proto-Icelandic plume. Contemporaneous with, or immediately subsequent to, the voluminous outpouring of basaltic lava flows, the subjacent Cretaceous and Palaeogene sedimentary strata were pervasively intruded by basic magmas in the form of sill complexes. Exploration wells drilled in this area during the 1980s in the search for hydrocarbons mainly targeted structural highs; however, some of them encountered sills and, furthermore, have proven that the Paleocene and Cretaceous sequences, into which they are intruded, are dominated by claystone lithologies. It is largely due to the fine-grained, homogeneous nature of the host rocks that the detailed geometry of the NFSB Sill Complex can be observed on 3D seismic data.

The NFSB Sill Complex has not been eroded subsequent to its emplacement and currently lies buried to depths between 2 and 6 km (Fig. 3). 3D seismic data provide high spatial and vertical resolution to image the geometric relationships of the sills throughout the majority of their depth profiles. The uppermost portion of the sill complex, the vent facies, is interpreted to have developed on the contemporaneous basin floor and is covered by marine strata of early Eocene age.

The NFSB Sill Complex has been intersected by several wells, including Well 219/28-2 which penetrated two intrusions within Cretaceous sedimentary rocks located near to the SE limit of the sill complex and close to the 3D seismic data discussed in this contribution (Fig. 3). Further to the NE, Well 219/20-1 encountered *c.* 18 sills ranging from 5 to 75 m in thickness within rocks of late Cretaceous age (Figs 1 & 3). In both of these wells the sills can be described as tholeiitic olivine dolerites and show wireline log characteristics as described earlier.

From knowledge of the geology derived from well control, together in combination with observations from the seismic data, the depth of intrusion of sills is typically relatively shallow, from a few kilometres down to shallow depths of cover. Smallwood & Maresh (2002) presented an argument for the depth of cover for Faroe–Shetland Basin sills based upon the assumption that the level of emplacement was controlled by the magma pressure necessary to intrude the sedimentary section in which they now occur. They concluded that, for a 9 km thickness of sedimentary material overlying a basement with an assumed magma reservoir at a depth of 20 km, sills should be emplaced at a depth of *c.* 6 km, possibly rising by some form

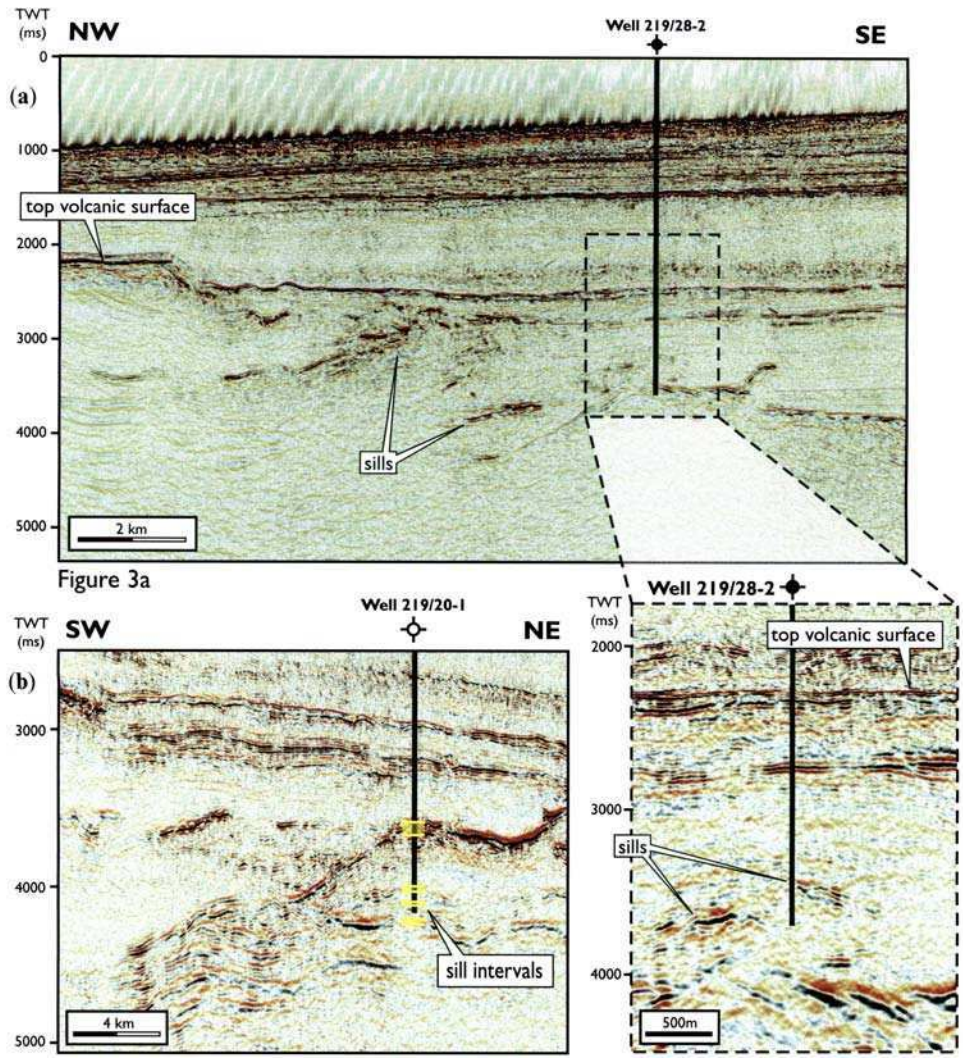

Fig. 3. Seismic (2D) line across the volcanic rocks SE of the Brendan Igneous Centre, through Cretaceous and Paleocene strata containing intrusions of the NFSB Sill Complex. The sills produce strong reflections, although the seismic reflection response of deeper sills is masked by shallower intrusions or by volcanic rocks (where overlying). Inserts show detail from the section intersected by Wells 219/28-2 and 219/20-1.

of step-and-stair migration, to depths of *c.* 4 km. The location of the sill transgressions may be controlled by low pressure points in the vicinity of faults (cf. Smallwood & Maresh 2002). Downward transgression may occur when magma has risen to its shallowest possible level and then supply is stopped, thereby removing the pressure support. The magma would then descend to a level where it can be supported by strong (i.e. lithified) sedimentary rocks, or even to the base of the sedimentary sequence (i.e. top basement).

Age of NFSB sills

The sills described in this contribution have not been dated directly by any radiometric (isotopic) technique. However, sills from elsewhere in the Faroe–Shetland Basin have been isotopically dated, yielding a somewhat enigmatic broad age spectrum from early Palaeocene through to middle Eocene (summarized by Ritchie & Hitchen 1996). Many of these age data have been obtained by the K–Ar technique, considered less reliable for basaltic igneous rocks, and have significant errors attached to them due to the typically altered nature of the analysed material. However, a relatively short duration for their intrusion is preferred, at around the latest Paleocene/earliest Eocene, on the basis of more reliable Ar–Ar data, together with biostratigraphic age data from the youngest strata which they invade (Naylor *et al.* 1999; Davies *et al.* 2002). On the Faroe Islands, one of the three main sills is of similar MORB-type composition (Hald & Waagstein 1991). This sill invades, and therefore post-dates, Middle and Upper formation flows of the Faroes Lava Group, further suggesting an age of *c.* 54.5 Ma (Naylor *et al.* 1999). Indirect dating of the NFSB Sill Complex, based on the argument that the identified vent facies developed at or close to the contemporaneous basin floor, supports an earliest Eocene age.

Sill architecture

The overall geometry of the NFSB Sill Complex, apparent from 3D seismic data, can best be described by analogy with the branches on one side of a 'fir tree', appearing to be most laterally extensive with depth. Figures 4–6 contain visualizations of the three discrete suites of intrusions identified as forming the sill complex, where the transparency of the seismic volume dataset has been adjusted such that only the reflections caused by the sills are visible. The shallowest sills occur closest to the volcanic escarpment SE of the Brendan Igneous Centre (Figs 1 & 3). The disposition of the deepest sills is obscured by the overlying (i.e. shallower) intrusions and limited in visibility by the extent of the 3D seismic data volume. The shallowest level within the sedimentary sequence which has been intruded by the sills is correlated from nearby wells (Quads 219 and 220) as being of late Palaeocene/Eocene age. The overlying horizon, identified as a reasonably strong, continuous seismic marker (Figs 3–6), is marked by a number of circular and elliptical features which appear to have formed positive structures on the basin floor, and which were subsequently mantled by Lower Eocene marine shales.

Individual sills show a spoon- or saucer-shaped geometry. Our investigation of NFSB sills suggests that three genetically-related suites, or sill clusters, may be defined.

Sill Suite 1. Consists of lateral, elongated sills which are predominantly concordant with the host sedimentary rocks over most of their length, ending in upward-angled 'terminations', where the sills thin and cross-cut the host strata (Fig. 4). These sills are currently buried between 3 and 5 km below the sea bed and are preferentially entrained within the Cretaceous sedimentary section which nearby well control reveals to be of fairly homogeneous claystone lithology. Sill Suite 1 is located towards the SE limit of the NFSB Sill Complex and is orientated parallel with the basement structural grain, trending away from the Erlend Transfer Zone to the NE. The

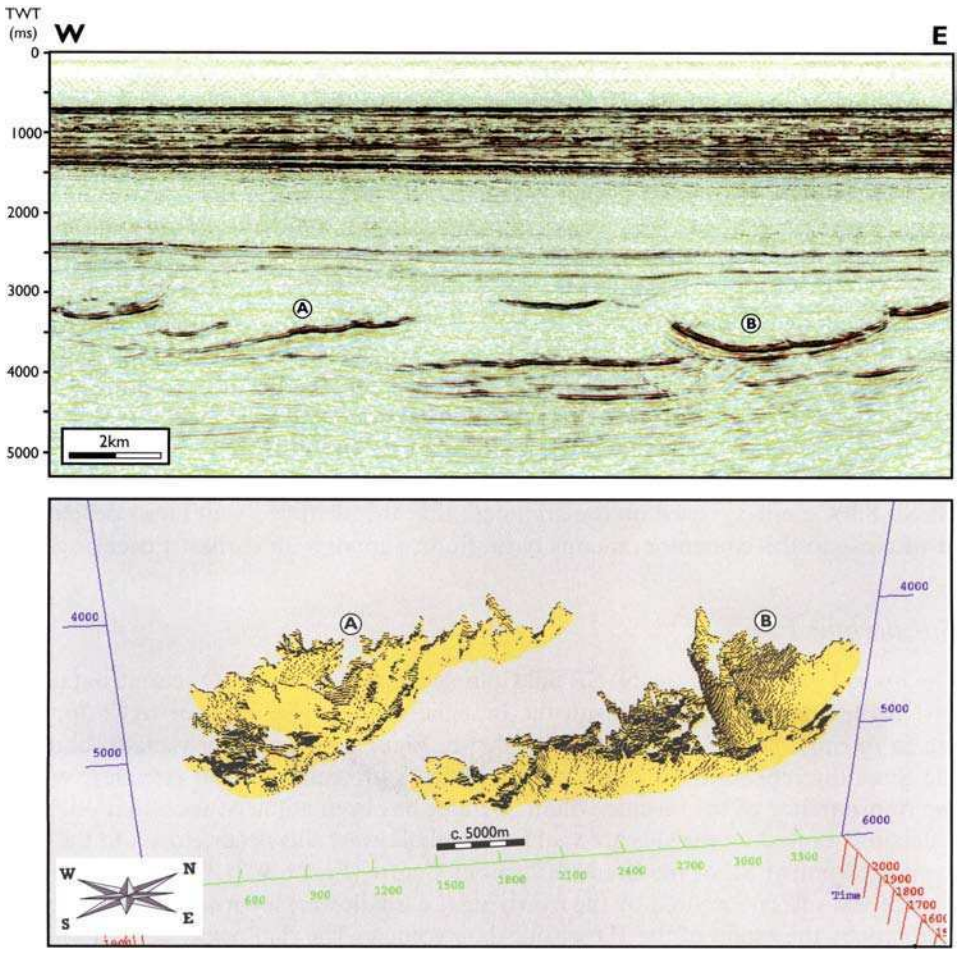

Fig. 4. Visualization of Suite 1 sills. Scale varies in this perspective.

general elongate geometry of these sills suggests that they are largely constrained within fault blocks, with the significant upward-angled 'terminations' interpreted to occur proximal to fault planes. However, independent identification of fault planes from seismic data within the Cretaceous strata is contentious due to the limited reflectivity within this sedimentary unit.

As far as can be identified from the seismic data, the lateral extent or length of the deepest, spoon-shaped sills, is *c.* 17 km, with a 'diameter' of *c.* 6.5 km. The lowermost sill identified has a total areal extent of *c.* 90 km^2 and an apparent 'thickness' up to 200 m, although the low frequency and hence resolution of the seismic data limits the accuracy of this figure in reflecting one sill as opposed to a series of closely associated, sub-parallel sills. Where the sills occur shallower in the section their lateral extent diminishes, with the shallower sills averaging 9 km in length and 6 km across.

The spoon- or saucer-shaped geometry of the sills shows upward-angled 'terminations' at typical angles of 20 to 25°, even following detailed depth conversion. Only the very longest sills show evidence of local downward transgression. Where

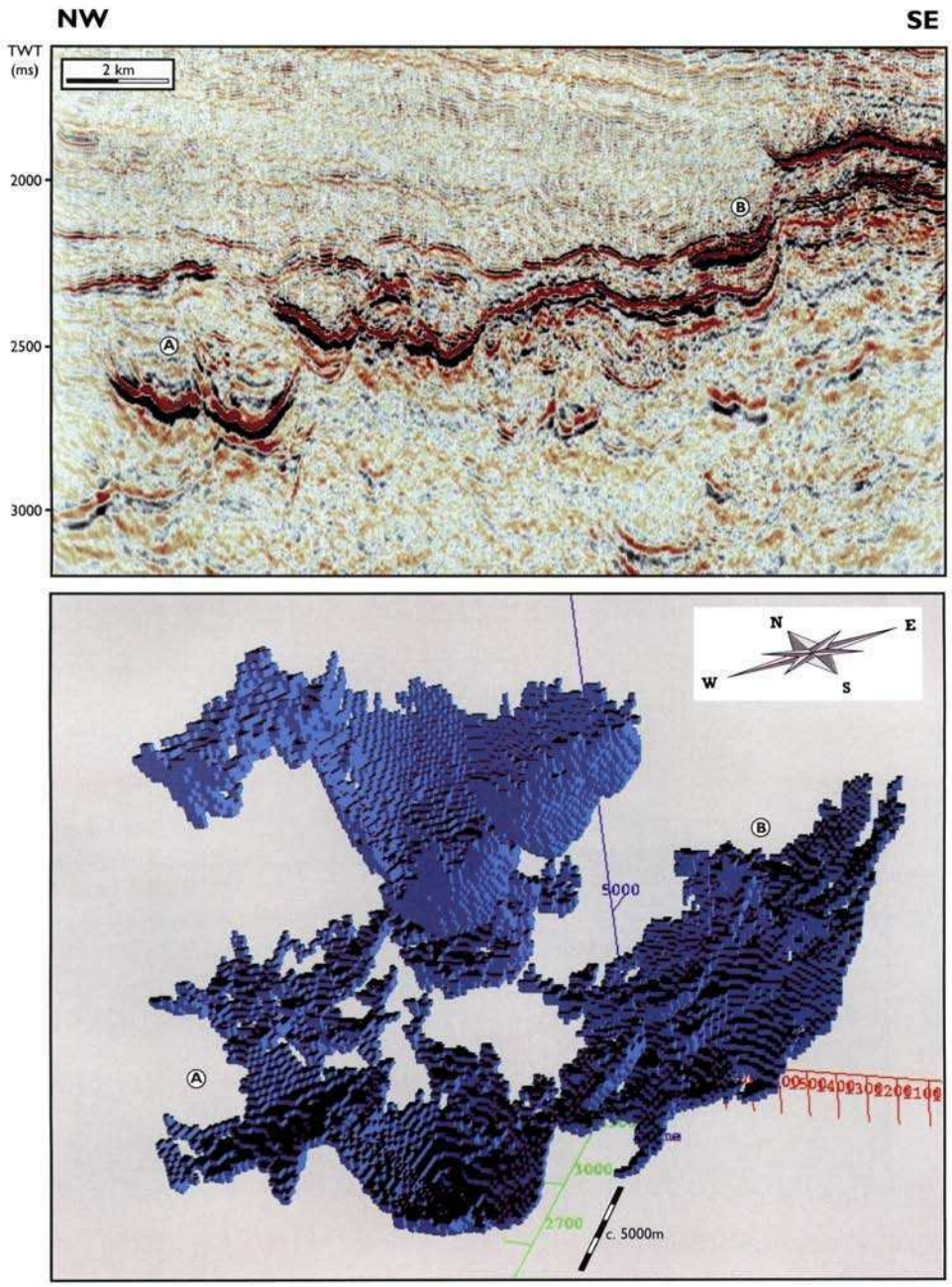

Fig. 5. Visualization of Suite 2 sills. Scale varies in this perspective.

this occurs it is commonly about half way along the length of the sill and appears to correspond with areas of sill thickening.

At the northeastern limit of the most significant and deepest spoon-shaped sill, a further saucer-shaped sill can be seen sited above and within the bowl of the spoon.

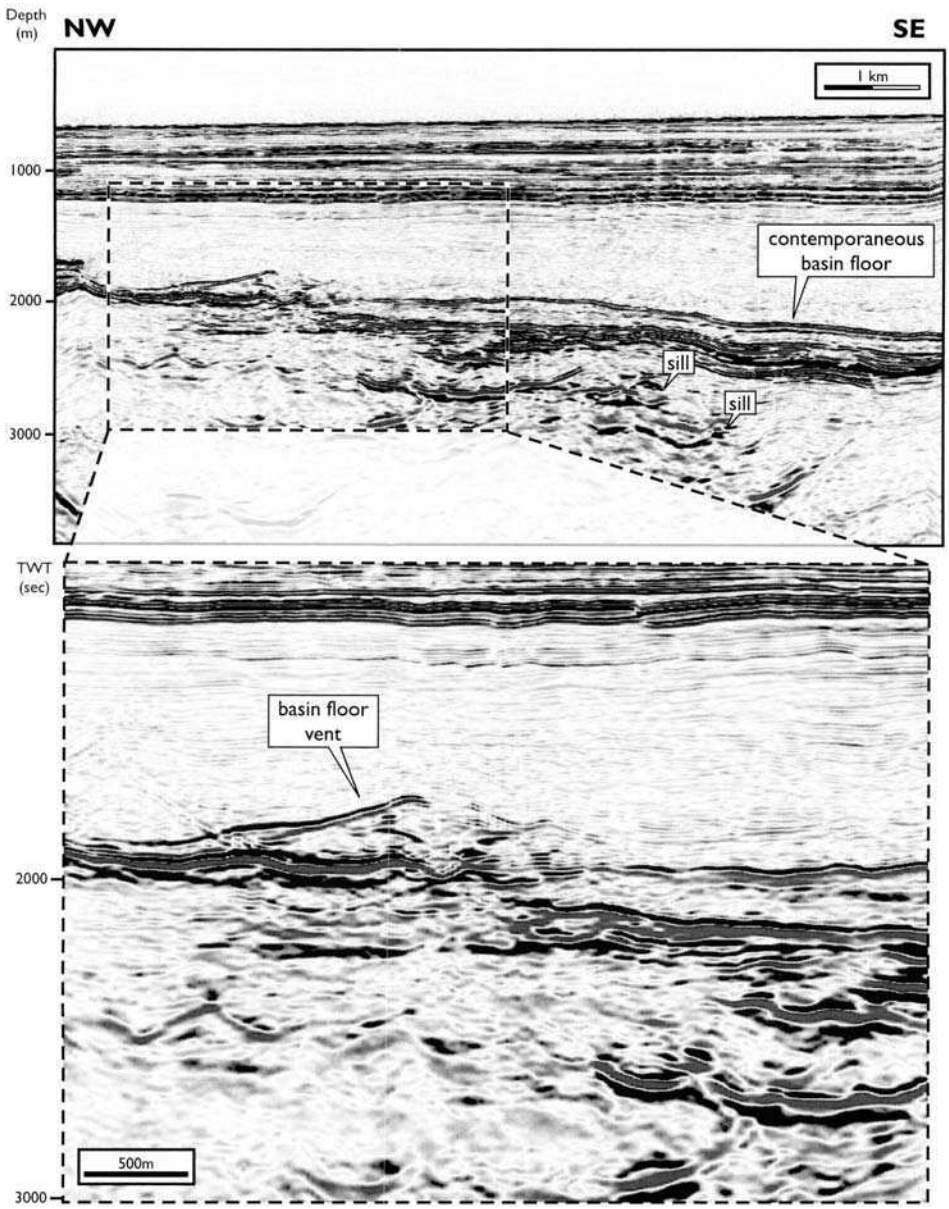

Fig. 6. Visualization of Suite 3 sills.

This saucer-shaped sill has thin, upward-angled, transgressive, finger-like 'terminations' which can, in places, be correlated with the location of small mound or vent-like features on the horizon interpreted as the contemporaneous basin floor at the time of intrusion (cf. Davies *et al.* 2002). The mounds appear to be locally preferentially orientated in a north–south direction and are variable in size, although commonly with a height of *c.* 30 m (but up to 100 m) and diameter of *c.* 500 m. The nature of the vent products is discussed further below, either involving the eruption of

magma and producing mounds of pillowed lava and/or hyaloclastite (volcanic breccia), or the development of 'explosion' breccias and remoblized volcano-sedimentary accumulations caused by the expulsion of pore water.

The upward-angled 'terminations' of certain sills can be as much as 1200 m below an associated mound. Commonly, vertical 'seismic chimneys' of disrupted reflections, including local amplitude brights, can be observed rising vertically from the tips of the 'terminations' to the mounds. These chimneys can be compared with known gas chimneys (Cole *et al.* 2000) and hence are interpreted to represent focussed zones of vertical fluid migration.

Sill Suite 2. Currently buried between 1.5 and 4 km below the sea bed, this suite of sills is dominated at depth by stacked, slightly ovoid, saucer-shaped intrusions with diameters of 3 to 5 km, being individually slightly more elongate in a north–south direction (Fig. 5). The upward-angled 'terminations' around the rim of the saucer rise some 500 m at a steadily increasing angle, ranging from *c.* 15° to near vertical. The uppermost 'terminations' appear to feed laterally into a system of interlocking cuspate sills. The 'root' of Sill Suite 2 is unclear; however, connections can be established with an area of very strong amplitudes, towards the edge of the 3D dataset, indicating a 'source' or upward migration path from the SW.

These interlocking, shallow, cuspate intrusions underlie an area which has a domed appearance on the seismic data, with dimensions of 3 km by 8 km, and a height of up to 300 m at late Paleocene horizons. The relief on this structure was established by the earliest Eocene. Several similar domed features have been identified along the SW margin of the 3D seismic volume, on trend with the postulated location of the Erlend Transfer Zone. In cross-section this feature shows a characteristic 'eye' structure which is interpreted to be, in part, a function of subsequent differential compaction (see below). It is considered that the vertically-dominated geometry of the sill complex may be indicative of a particularly hot and voluminous intrusive event which was able to overcome the prevailing stress regime, allowing large volumes of magma to be intruded to a shallow level in the sedimentary section. The high water content of these sediments resulted in hydrothermal alteration and hence early inter-grain cement formation (Einsele *et al.* 1980). An upward-angled sill can be observed to rise from an estimated paleo-depth of *c.* 3 km, through the base of the uppermost saucer-shaped sill, to within *c.* 500 m of the basin floor paleosurface. At this point the sill intrudes parallel to host rock bedding, within the confines of the sill.

Sill Suite 3. Comprises the uppermost branches of the 'fir tree' and is dominated by a significant number of short, laterally-feeding sills which step vertically upwards through the shallow section and are currently buried to depths ranging from 4 km to 2 km below sea bed (Fig. 6). The uppermost units of Sill Suite 3 are considered to have been emplaced as shallow as *c.* 200 m below the contemporaneous basin floor. Locally, this sill suite has been entrained within an interval interpreted to contain Paleocene claystones, together with volcaniclastic deposits derived through erosion of a volcanic sequence SE of Brendan's Dome, to create a laterally extensive sequence, locally dominated by strong seismic amplitudes. Individual sills range in dimension from 1200 m to 3200 m and in thickness up to *c.* 60 m, but are most likely to be dominated by thinner, stacked sills, particularly those around 30 m in thickness

or less. There is evidence that these sills may originate from NW of the area, although their individual visible areal extent and complex cross-cutting geometry make it less easy to determine their source.

Locally, steeply-inclined, cross-cutting sills feed into and through the interpreted volcaniclastic sequence, contributing towards the formation of the 'eyes' (as seen in seismic sections) and in some instances, vents. These sills are *c.* 600 m wide and elongate (*c.* 3 km) in a south-easterly direction. One saucer-shaped sill has a diameter of *c.* 2 km and shows a characteristic 'eye' structure forming a 'mirror image' to the top of the overlying volcaniclastic sequence. Although of limited number in comparison with the mounds associated with Sill Suite 1, these mounds can have significant dimensions, reaching a height of *c.* 180 m and a diameter of *c.* 1600 m. The origin of the cross-cutting sills is obscured by their proximity to the Brendan's Dome volcanic escarpment.

In addition, there are examples of intrusions which reach the base of the volcaniclastic package, form a saucer-shaped sill, then appear to continue downwards with respect to the host strata bedding. Seismic data suggests that these are either very thick sills or multiple intrusions following the path of earlier sills.

Extrusive facies. The internal geometries of the largest mounds are discernable from the 3D seismic dataset and suggest that they are constructional, rather than the product of some form of erosional event. When viewed on (horizontal) time-slices (Fig. 7), the mounds typically have circular or elliptical shapes, being up to *c.* 2 km across and with heights of >100 m. On seismic plan views, the mounds display distinctive 'onion-ring' geometries (Fig. 8). In the vicinity of the crest of a mound, the layers which define the ring-like reflections dip outwards at shallow angles, typically <15°, towards the margin of the mound. With increasing distance from the crest, the dip angle diminishes, reaching *c.* 4° around the margins of mounds.

The clear spatial and temporal links between the mounds and the underlying sills suggest that the two features are genetically associated. Typically, the mounds have formed directly above the steeply-inclined 'terminations' or leading edges of the sills, where they tend towards more discordant, dyke-like orientations, discordant to the host strata (Fig. 8). Furthermore, the geometry and internal structure of the mounds indicate that they developed on the contemporaneous basin floor as vents and their survival and seismic character suggest that they are composed of material considerably harder and denser that the overlying and subjacent claystones. Thus, we can confidently link the timing of sill intrusion with vent development and argue that their spatial link points towards a lithologic link.

The most obvious lithology for the vent products is dense basaltic rock, either pillowed lava if the water depth was sufficient to suppress degassing (vesiculation) of the magma, or hyaloclastite if brecciation took place in shallower water. Eruption rate can also influence whether brecciation/fragmentation does or does not occur, with high rates favouring submarine fountaining of magma and associated fragmentation. Fragmental vent products have been reported from modern ocean basins such as the Juan de Fuca Ridge (Embly & Chadwick 1994) using various imaging techniques (sidescan sonar, seabeam data) and sampling programmes. Similar materials have been recorded from eruptions in shallow water (Planke *et al.* 2000). Palaeogene analogues are recognized from the Nuussuaq Basin, central West Greenland (Pedersen *et al.* 1993).

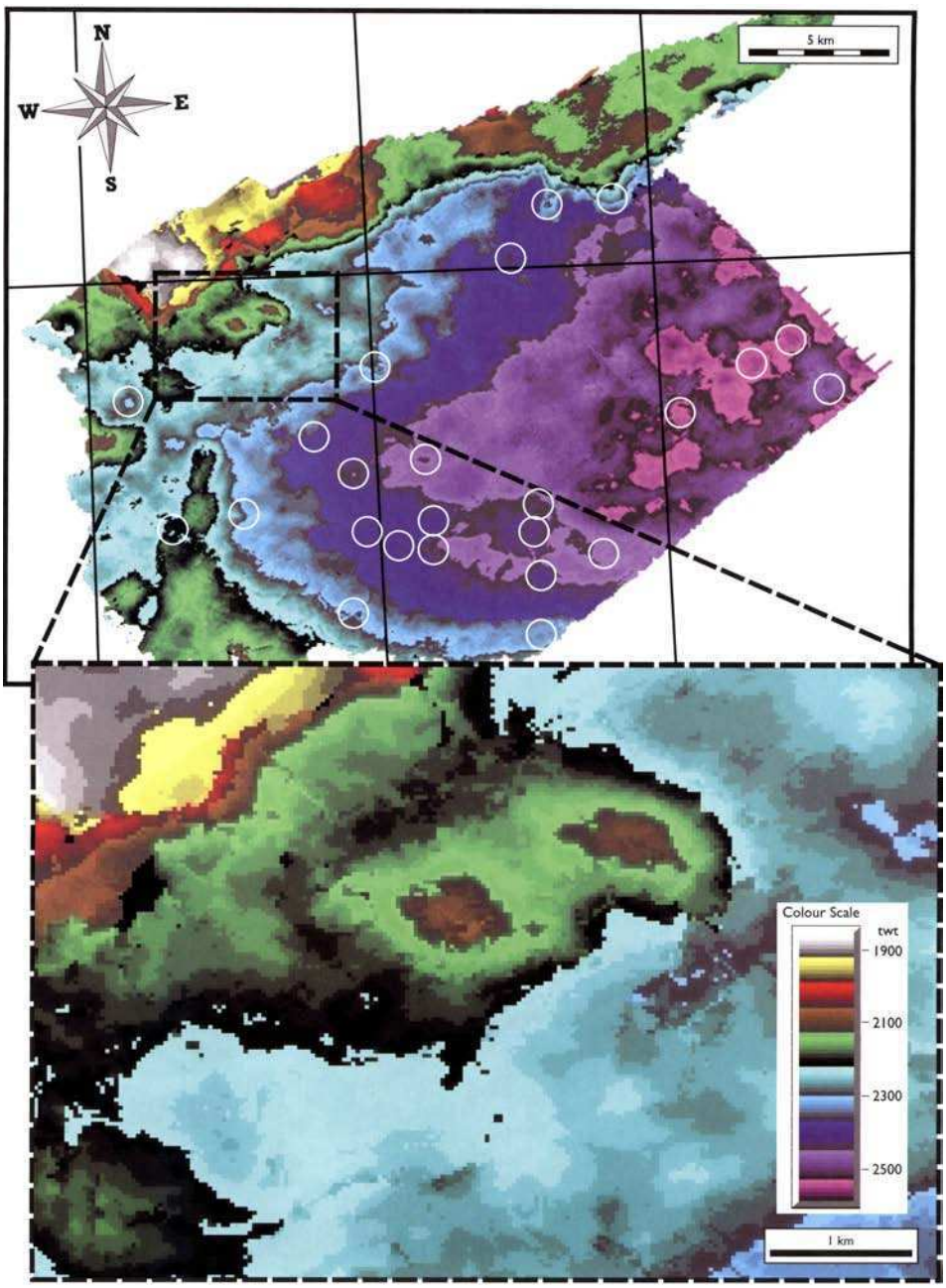

Fig. 7. Paleocene two-way-time (TWT) map illustrating the nature and distribution of basin floor vents (circled) associated with the sill complex.

In many instances there are well-developed 'seismic chimneys' of distorted reflectors linking the terminations of deeper-level sills with smaller mound-like structures, again developed on the horizon interpreted as the contemporaneous basin floor (Fig. 9). We interpret such chimneys to be the result of vertical fluid migration,

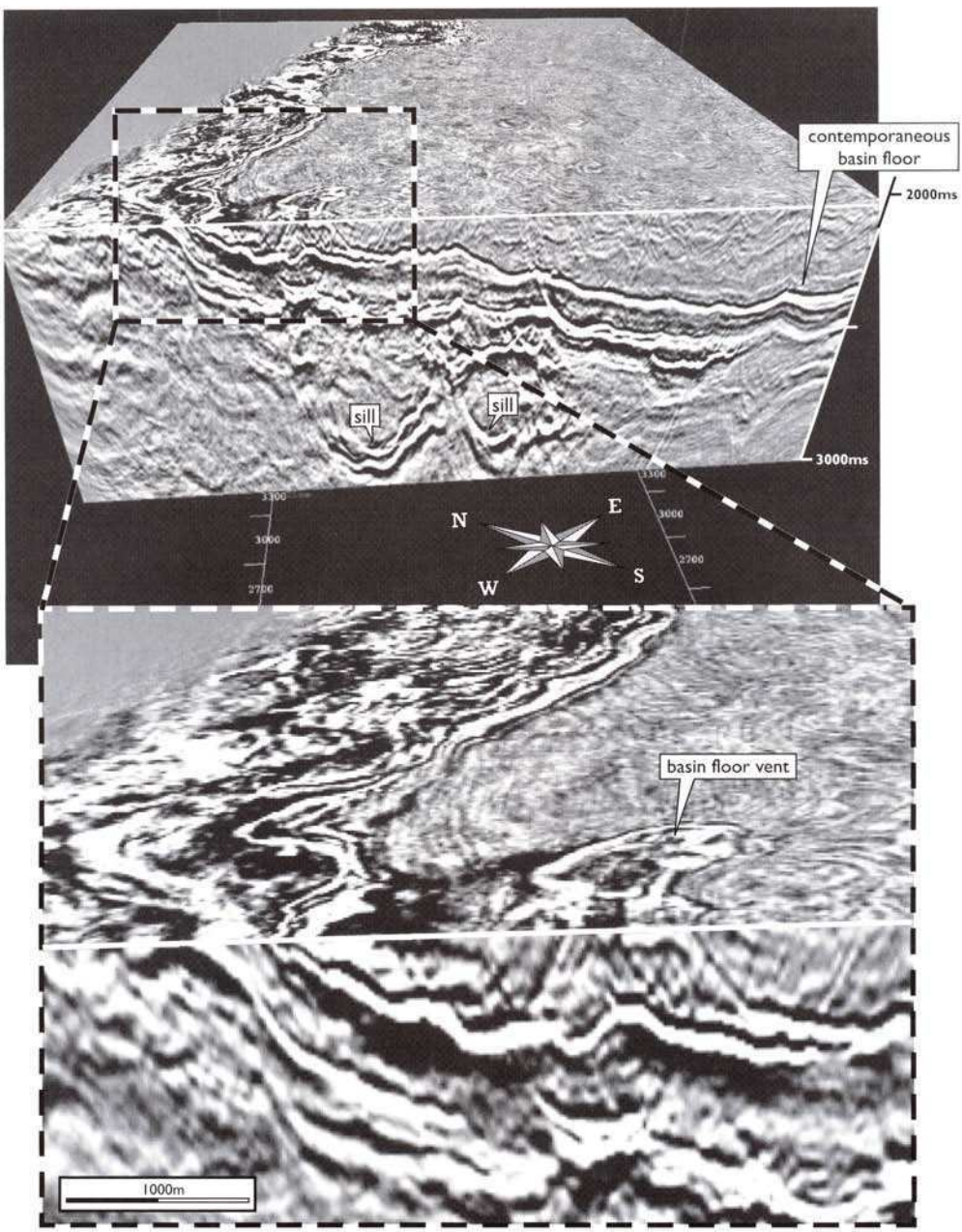

Fig. 8. Perspective block diagram illustrating the seismic response and spatial link between shallow-emplaced sills and associated vents. Scale varies in this perspective.

concurring with the study of Einsele *et al.* (1980) which determined that the volume of pore fluid expelled from weakly-lithified strata during the emplacement of sills would be approximately equal to the volume of magma. The deep level of sill emplacement suppressed the venting of true magmatic products onto the basin floor.

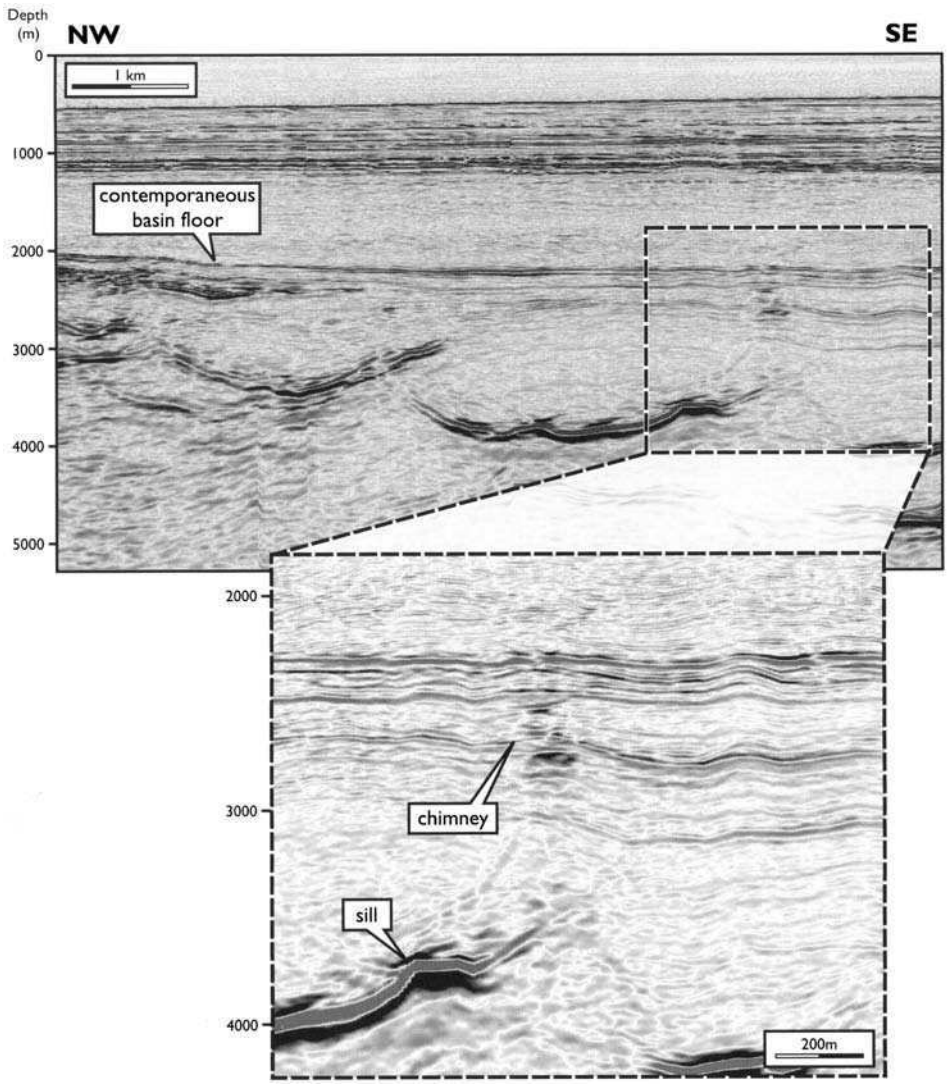

Fig. 9. Suite 1 sills and associated 'seismic chimneys', interpreted as fluid escape and sediment remobilization phenomena, possibly resulting in small vent-like accumulations of sedimentary breccia on the basin floor.

Hence, we propose that the mound-like features associated with these phreatic fluid expulsion structures are more likely to be composed of various forms of mobilized, heavily-cemented clastic materials, ranging from breccia through to silt grade material. A component of these clastic products may be primary magmatic material, most likely vesiculated glassy basalt. Such materials have been described from clastic intrusions and associated mudflow breccias which formed when Jurassic dolerite sills intruded porous and permeable Permian-Triassic strata in the Allan Hills Region, Antarctica (Grapes *et al.* 1972). Steam-driven remobilization of sedimentary material resulted in 'sedimentary' products expelled upwards, and commonly onto the Earth's surface. Similar materials have been described from: Jurassic (Karroo) sills in South

Africa (Gevers 1928; Thorarinsson 1951); shallow Pliocene intrusions of the Navajo-Hopi Region, SW USA (Williams 1936); and, Carboniferous dolerite pipes in central Scotland (Francis 1972).

Consequently, we suggest that the mounds observed within the area of the NFSB Sill Complex are basin floor (submarine) volcanic vents, built up either by pulsed eruptions of basaltic magma from shallow-emplaced sills, or 'sedimentary' vents caused by fluid-entrainment and upward expulsion of clastic material from deeper-level sills.

Davies *et al.* (2002) proposed a four-stage model for similar vents further south within the basin: (i) extension and faulting of basin floor strata; (ii) mantling of the faulted strata by marine claystones; (iii) emplacement of sills, either concordant to bedding, or within the low stress environment of faults, the latter permitting magma to migrate upwards to very shallow levels; and, (iv) breaching of magma from the leading edges of the sills to the contemporaneous basin floor and the formation of vents. Subsequent marine sedimentation led to the preservation of the vents in a near-pristine state.

Origin of 'eye' structures

A consequence of the shallow emplacement of sills is that the compaction history of the host strata will be locally distorted. The local presence of dense, relatively rigid slabs of non-compressible dolerite within undercompacted strata will lead to

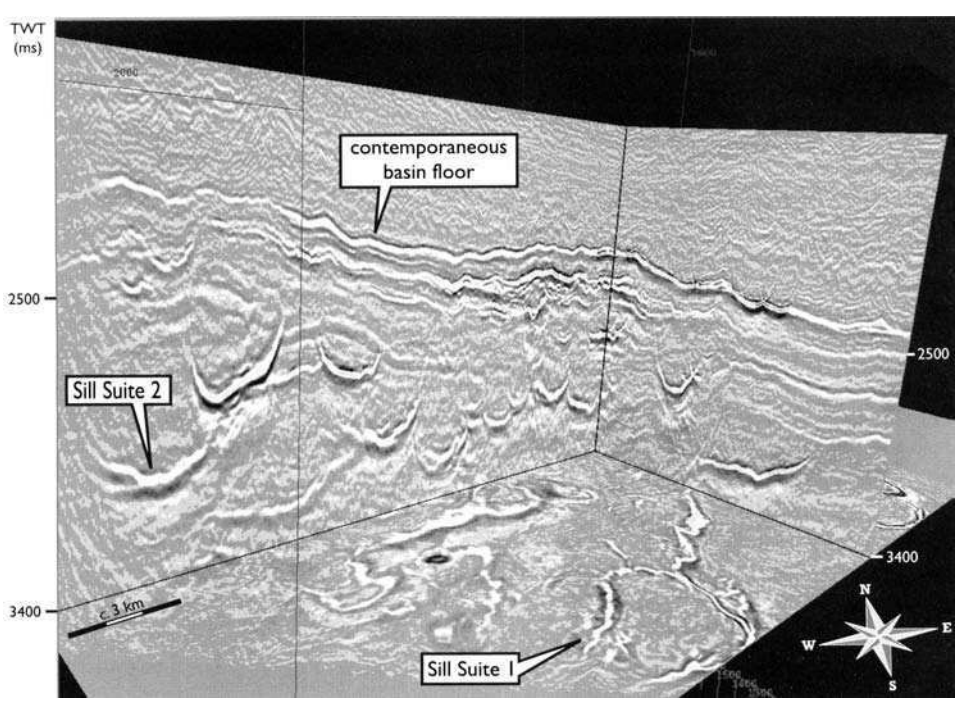

Fig. 10. Perspective visualization of shallow-emplaced sills on two orthogonal arbitrary lines and a time-slice surface, illustrating relief on the surface interpreted as the contemporaneous basin floor.

differential uplift/subsidence (possibly aided by faulting) on the basin floor, typically by an amount comparable to the net thickness of the sill(s). Futhermore, a thickness of host strata approximately equal to that of the sill, both above and below the intrusion, will be subjected to porosity reduction at the time of intrusion, due to thermally-driven fluid advection-expulsion, thus further distorting the compaction profile.

One possible outcome of such shallow sill intrusion will be the development of a compaction-induced topography on the basin floor (Fig. 10). Smallwood & Maresh (2002) have explored the role played by shallow-emplaced sills in the Faroe–Shetland Basin in the area around Well 205/9-1 and concluded that the disposition of onlapping deepwater turbiditic sands is such that they were deposited within the more compacted basin floor lows which fringed the basin floor high generated by shallow sill intrusion. The complementary nature of shallow-emplaced sills flanked by sediment-filled basin floor palaeo-lows is highly suggestive of a cause-and-effect relationship.

The aggregate thickness of sills emplaced within the uppermost kilometre of strata in the NFSB is locally in excess of 100 m (see above), implying that basin floor topographic relief of a similar magnitude developed at this time. Younger strata, predominantly Lower Eocene shales, mantle these highs, with the topographic relief fading out upwards over a depth interval of several hundreds of metres. Figure 10 illustrates the spatial link between these shallow-emplaced sills and the general topographic high on the contemporaneous basin floor within the NFSB.

Conclusions

A new perspective on the geometry and formation of sill complexes can be obtained from the analysis of high quality 3D seismic data. Rather than being limited to a

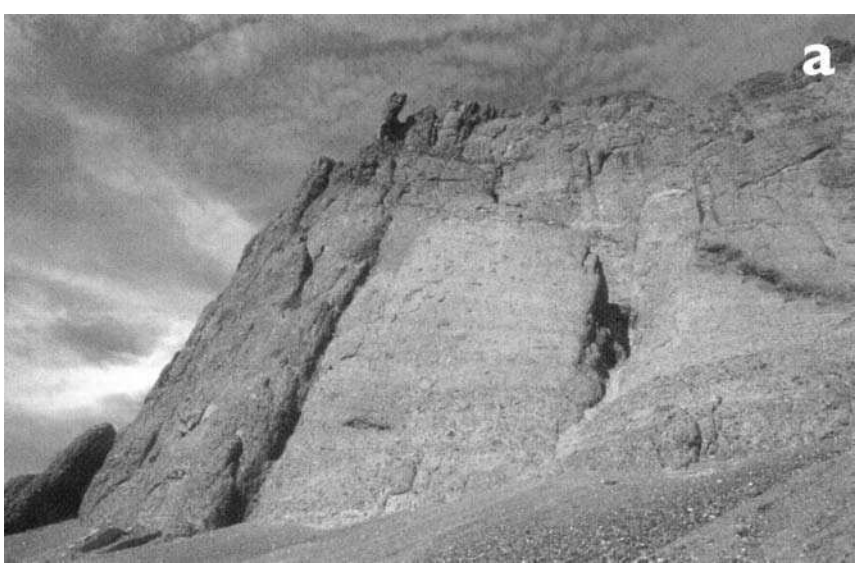

Fig. 11. (**a**) Field view of a hyaloclastite deposit illustrating the crudely bedded nature of these subaqueous volcanic breccias; (**b**) detail of (**a**), showing the heterogeneous nature of hyaloclastites; (**c**) Field view of a subaqueous pillowed lava vent. All views from the Paleocene volcanic sequence of the Nuussuaq Basin, central West Greenland.

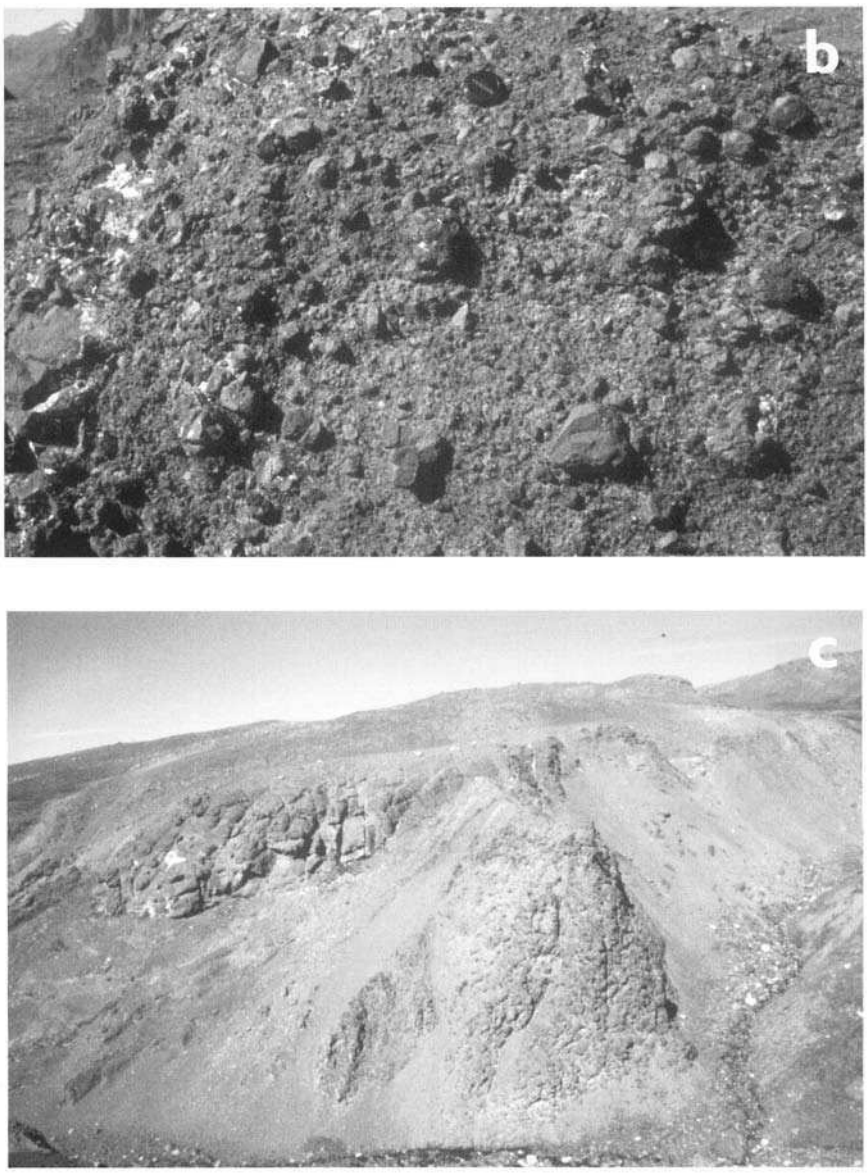

Fig. 11. (*continued*)

number of typically two-dimensional views, typical of field exposures, seismic data permit depth relationships to be examined in detail. Furthermore, because post-intrusion erosion has not occurred, the links between shallow intrusion and extrusive activity associated with sill complexes may also be interrogated. Post-intrusion differential compaction of basinal sequences gives rise to distinctive 'eye' structures, only clearly discernible at the seismic scale.

Within the North Faroe–Shetland Basin three discrete suites of tholeiitic basaltic sills are recognized:

Suite 1. laterally elongate, possibly structurally controlled and therefore defining fault orientations; 'spoon-shaped' and concordant with host strata; upward-angled terminations and associated vent facies;

Suite 2. stacked, 'saucer-shaped' intrusions, commonly cross-cutting; fed upwards into interlocking cuspate clusters; uppermost sills characteristically underlie (basin floor) highs or 'domes' ('eye' structures);

Suite 3. vertically- and laterally-stacked intrusions; appear to be preferentially emplaced to shallow depths and associated with a vent facies.

An extrusive facies to the NFSB Sill Complex is recognized as forming volcanic vents on the contemporaneous basin floor. These vents are typically circular or elliptical in plan view, up to 2 km across, although commonly only a few hundreds of metres across, and with heights above the basin floor in excess of 100 m. The organized internal structure and strong reflections of these vents indicates that they are composed of a similarly dense, hard lithology to that of the sills, which we suggest is hyaloclastite (a coarse basaltic breccia) with or without pillowed (i.e. subaqueous) lava (Fig. 11). There is a clear spatial link between the location of vents and the

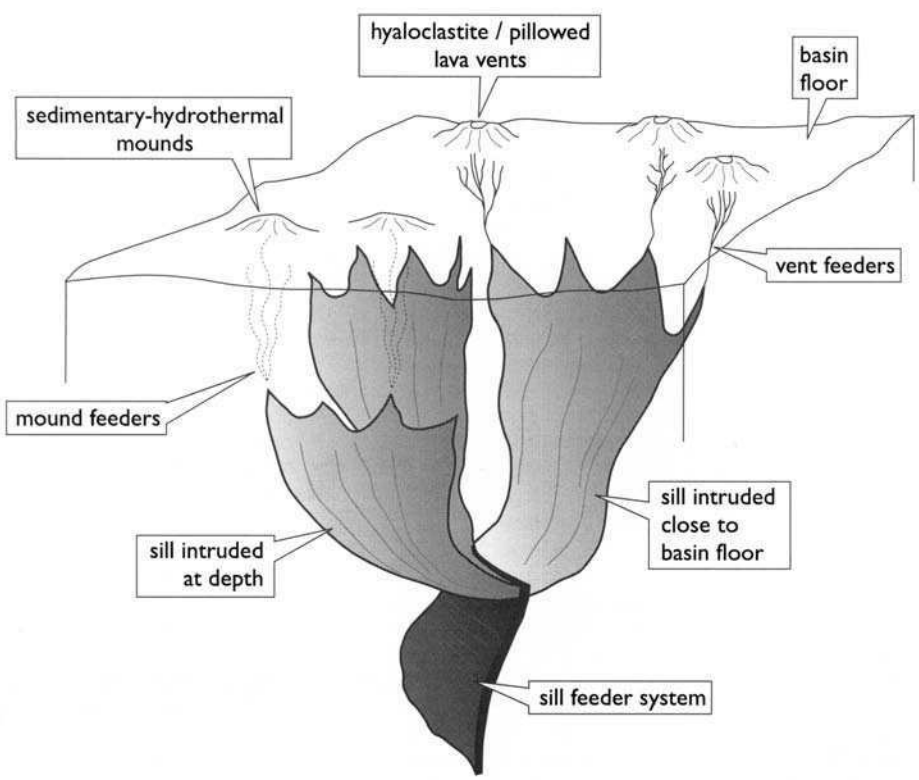

Fig. 12. Cartoon illustrating possible relationships between feeder dykes, sills and vents in the North Faroe–Shetland Basin.

steeply-inclined leading edges of subjacent sills, which we interpret as evidence that where sills have penetrated to within a few hundreds of metres of the contemporaneous basin floor, then extrusive activity may occur (Fig. 12).

'Seismic chimneys' which have developed from the margins of deeper-emplaced sills can be traced upwards to the contemporaneous basin floor. We prefer a model involving vertical fluid expulsion and migration to explain these structures. Small associated vent-like features are interpreted as remobilized, heavily-cemented clastic deposits, transported upwards during steam-dominated fluid expulsion.

One consequence of the shallow emplacement of sills into under-compacted, pore fluid-rich strata involves the differential compaction of sections which contain thick, dense, relatively rigid slabs of non-compressible dolerite, relative to sections which do not contain sills. The concave-up geometry of the sill, when combined with the concave-down form of the basin floor and overlying (mantling) strata, leads to distinctive 'eye'-shaped structures when viewed in seismic sections. Sedimentation within the peripheral lows around the basin floor domes caused by the sills may lead to the development of stratigraphic traps. This potential role of sills as a cause of structural and stratigraphic trap formation is intriguing and, as far as we are aware, has not been fully explored and may merit further investigation.

We thank Statoil (UK) Limited, ExxonMobil International Limited and Enterprise Oil plc for permission to publish this paper. We are also grateful to TGS-Nopec for permission to publish the seismic data shown in Figure 3.

References

BRADLEY, J. 1965. Intrusion of major dolerite sills. *Transactions of the Royal Society of New Zealand*, **3**, 27–55.

CAREY, S. W. 1958. The isostrat, a new technique for the analysis of the structure of the Tasmanian dolerite. *In*: *Dolerite: a symposium*. University of Tasmania, Hobart, 130–164.

CHEVALLIER, L. & WOODFORD, A. 1999. Morpho-tectonics and mechanism of emplacement of the dolerite rings and sills of the western Karoo, South Africa. *South African Journal of Geology*, **102**, 43–54.

COLE, D., STEWART, S. & CARTWRIGHT, J. A. 2000. Giant irregular pockmarks from the Eocene of the North Sea. *Marine and Petroleum Geology*, **17**, 673–689.

DAVIES, R., BELL, B. R., CARTWRIGHT, J. A. & SHOULDERS, S. 2002. Three-dimensional seismic imaging of Palaeogene dike-fed submarine volcanoes from the northeast Atlantic margin. *Geology*, **30**, 223–226.

DUFFIELD, W. A., BACON, C. R. & DELANEY, P. T. 1986. Deformation of poorly consolidated sediment during shallow emplacement of a basalt sill, Caso Range, California. *Bulletin of Volcanology*, **48**, 97–107.

DU TOIT, A. L. 1920. The Karoo dolerites – a study in hypabyssal intrusion. *Transactions of the Geological Society of South Africa*, **23**, 1–42.

EINSELE, G. & 18 OTHERS. 1980. Intrusion of basaltic sills into highly porous sediments, and resulting hydrothermal activity. *Nature*, **283**, 441–445.

EINSELE, G. 1985. Basaltic sill-sediment complexes in young spreading centers: Genesis and significance. *Geology*, **13**, 249–252.

EMBLY, R. W. & CHADWICK, W. W. (1994). Volcanic and hydrothermal processes associated with a recent phase of seafloor spreading at the northern Cleft segment: Juan de Fuca Ridge. *Journal of Geophysical Research*, **99B**, 4741–4760.

FRANCIS, E. H. 1971. Bedding in Scottish (Fifeshire) tuff pipes and its relevance to maars and calderas. *Bulletin Volcanologique*, **34**, 697–712.

FRANCIS, E. H. 1982. Magma and sediment-I Emplacement mechanism of late Carboniferous tholeiite sills in northern Britain. *Journal of the Geological Society, London*, **139**, 1–20.

GEVERS, T. W. 1928. The volcanic vents of the Western Stormberg. *Transactions of the Geological Society of South Africa*, **31**, 43–62.

GIBB, F. G. F. & KANARIS-SOTIRIOU, R. 1988. The geochemistry and origin of the Faroe–Shetland sill complex. *In*: MORTON, A. C. & PARSON, L. M. (eds) *Early Tertiary Volcanism and the Opening of the NE Atlantic*. Geological Society, London, Special Publications, **39**, 241–252.

GIBB, F. G. F., KANARIS-SOTIRIOU, R. & NEVES, R. 1986. A new Tertiary sill complex of mid-ocean ridge basalt type NNE of the Shetland Isles: a preliminary report. *Transactions of the Royal Society of Edinburgh: Earth Sciences*, **77**, 223–230.

GRAPES, R. H., REID, D. L. & MCPHERSON, J. G. 1972. Shallow dolerite intrusion and phreatic eruption in the Allan Hills region, Antarctica. *New Zealand Journal of Geology and Geophysics*, **17**, 563–577.

HALD, N. & WAAGSTEIN, R. 1991. The dykes and sills of the Early Tertiary Faroe Island basalt plateau. *Transactions of the Royal Society of Edinburgh: Earth Sciences*, **82**, 373–388.

HOTZ, P. E. 1952. Form of diabase sheets in southeastern Pennsylvania. *American Journal of Science*, **250**, 375–388.

MUDGE, M. R. 1968. Depth Control of some concordant intrusions. *Bulletin of the Geological Society of America*, **79**, 315–332.

NAYLOR, P. H., BELL, B. R., JOLLEY, D. W., DURNALL, P. & FREDSTED, R. 1999. Palaeogene magmatism in the Faroe–Shetland Basin: influences on uplift history and sedimentation. *In*: FLEET, A. J. & BOLDY, S. A. R. (eds) *Petroleum Geology of Northwest Europe: Proceedings of the 5th Conference*. Geological Society, London, 545–558.

PEDERSEN, A. K., LARSEN, L. M. & DUEHOLM, A. K. 1993. *Geological section along the south coast of Nuussuaq, central west Greenland*. 1:20000 coloured geological sheet. The Geological Survey of Greenland, Copenhagen.

PETRASKE, A. K., HODGE, D. S. & SHAW, R. 1978. Mechanics of emplacement of basic intrusions. *Tectonophysics*, **46**, 41–63.

PLANKE, S., SYMONDS, P. A., ALVESTAD, E. & SKOGSEID, J. 2000. Seismic volcanostratigraphy of large-volume basaltic extrusive complexes on rifted margins. *Journal of Geophysical Research*, **105**, 19335–19351.

POLLARD, D. D., MULLER, O. H. & DOCKSTADER, D. R. 1975. The form and growth of fingered sheet intrusions. *Bulletin of the Geological Society of America*, **86**, 351–363.

RITCHIE, J. D. & HITCHEN, K. 1996. Early Paleogene offshore igneous activity in the northwest of the UK and its relationship to the North Atlantic Igneous Province. *In*: KNOX, R. W. O'B., CORFIELD, R. M. & DUNAY, R. E. (eds) *Correlation of the Early Paleogene in Northwest Europe*. Geological Society, London, Special Publications, **101**, 63–78.

ROBERTS, J. L. 1970. The intrusion of magma into brittle rocks. *In*: NEWALL, G. & RAST, N. (eds) Mechanism of igneous intrusion. *Journal of Geology*, Special Issue **2**, 287–338.

SMALLWOOD, J. R. & MARESH, J. 2002. The intrusion of igneous sills in the Faroe–Shetland Channel. *In*: JOLLEY, D. W. & BELL, B. R. (eds) *The North Atlantic Igneous Province: Stratigraphy, Tectonic, Volcanic and Magmatic Processes*. Geological Society, London, Special Publications, **197**, 271–306.

STOSE, G. W. & LEWIS, J. V. 1916. Triassic igneous rocks in the vicinity of Gettysburg, Pennsylvania. *Bulletin of the Geological Society of America*, **27**, 623–643.

THORARINSSON, S. 1951. Laxarglijufur and Laxarhraun. *Museum of Natural History, Reykjavik. Miscellaneous Paper*, **2**, 1–84.

WAAGSTEIN, R. 1988. Structure, composition and age of the Faroe basalt plateau. *In*: MORTON, A. C. & PARSON, L. M. (eds) *Early Tertiary Volcanism and the Opening of the NE Atlantic*. Geological Society, London, Special Publications, **39**, 225–238.

WALKER, G. P. L. 1993. Basaltic-volcano systems. *In*: PRICHARD, H. M., ALABASTER, T., HARRIS, N. B. W. & NEARY, C. R. (eds) *Magmatic processes and plate tectonics*. Geological Society, London, Special Publications, **76**, 3–38.

WALKER, K. R. 1969. The Palisades Sill, New Jersey: a reinvestigation. Special Paper of the Geological Society of America, **111**, 178.

WILLIAMS, H. 1936. Najajo-Hopi Pliocene volcanoes. *Geological Society of America Bulletin*, **47**, 111–171.

WILLIAMS, H. & MCBIRNEY, A. R. 1979. *Volcanology*. Freeman, Cooper & Co., San Francisco.

This page intentionally left blank

Index

Page numbers in *italic* refer to illustrations, those in **bold** type to tables